The University of Sheffield

Biosorption of selected heavy metal ions and methylene blue from aqueous solution using chemically treated *Luffa cylindrica*

A thesis submitted for the degree of Doctor of Philosophy to the Chemical and Biological Engineering Department, the University of Sheffield, Sheffield, UK

By

Akanimo Udo Emene

July, 2018

Dedication

Dedicated to my two sons, Akan and Unwana Emem Amba, and my late father Engr. Emene Udo Emene.

Abstract

The production of industrial wastewater is a threat to the environment when it contains heavy metals and organic pollutants that are above the World Health Organisation (WHO) requirement levels expected in all waters. A lot of this pollution comes from industrial activities. Conventional methods, such as chemical precipitation and reverse osmosis, had been utilized to treat these wastewaters but due to the challenges of creating more waste in the form of sludge, high cost and the need to remove pollutants to lower levels, new methods are needed to treat industrial wastewaters. Wastewater treatment by biosorption, a low cost and efficient process, is an economically viable option for industries. The utilisation of this treatment process has not been fully implemented due to the complex and not fully understood nature of the biosorption systems. To optimise the process is to choose a suitable adsorbent and to study the parameters that influence the adsorption design system.

Some of the most detrimental heavy metal ions found in industrial wastewater are lead, zinc and cadmium. These heavy metal ions cause many health problems and are of great environmental concern. A chemically modified (alkali or acid treated) adsorbent, *Luffa cylindrica (L. cylindrica)*, with a high affinity for heavy metals, was used to adsorb heavy metal ions from aqueous environmental solution under various experimental conditions. The potential use of *L. cylindrica* to successfully remove an organic pollutant, methylene blue (MB), a cationic dye, from aqueous solution was investigated. The *L. cylindrica*, when chemically treated with 4% NaOH and 4% HCl shows an increased amount of ion exchange functionality and structural change, thereby enhancing the adsorption capacity. Experimental factors of adsorption time, initial metal ion concentration, ionic strength and pH of solution were studied for the different pollutants both alone and in mixed solutions. The experimental data were analysed with kinetic and isotherm models. From the FT-IR spectra, protonated hydroxyl and carboxyl functional groups was observed. The adsorption of lead, zinc, cadmium ions and MB onto chemically treated *L. cylindrica* material was investigated in both batch and column experiments. Adsorption isotherm models, Langmuir, Freundlich, two-site Langmuir, Temkin, Dubinin-Radushkevich and Sips; Thomas and Yoon-Nelson models were utilized in understanding the adsorption mechanism and the ability of the adsorption system evaluated.

The maximum adsorption capacity is 24.9mg/g, 8.8mg/g & 37.0mg/g for lead, cadmium and zinc respectively as described by the Langmuir isotherm and the maximum percentage uptake (efficiency) is 96.4%, 60.7% & 77.6% respectively. The equilibrium data for MB was well represented by the Freundlich isotherm model, and supported by the Temkin model, which showed a highly heterogeneous nature of the adsorption. A significant difference of adsorption

capacity occurred under dark and light conditions. The maximum adsorption uptake reached within 60 minutes was at 99% adsorption efficiency for methylene blue concentrations of 5-40 mg/L. Using the Excel SOLVER, the best fit model was found for each metal ions adsorption onto the *L. cylindrica*. The kinetics of the biosorption process was studied. A pseudo second order model shows a good correlation fit for all heavy metals ions and MB adsorption. In agreement with the literature, the optimum condition for the maximum adsorption capacity for lead, cadmium, zinc and MB occurs at pH 5, 7, 6 & 7 respectively at room temperature. These studies show that heavy metal ions and methylene blue were found to bind differently to the two active binding sites of the heterogeneous surface of the *L. cylindrica.* The multiple adsorption system differs from the single adsorption system and an alteration of these systems would optimise the adsorption process. The cost evaluation attempted to show a feasible adsorption process for developing countries. An understanding of the use of *Luffa cylindrica* for the removal of pollutants from industrial wastewater will improve the commercial application of adsorption processes in their treatment.

Acknowledgement

I would like to express my sincere gratitude and appreciation to all whom have supported me in making this work a success:

I am grateful to Niger Delta Development Commission for the awarded scholarship and the given opportunity to carry out this research in a prestigious University.

I am beyond words to express my gratitude to my supervisor, Dr. Robert Edyvean for his great sense of direction, expertise, experience and assisting me in overcoming the challenges of this research work.

I also thank my second supervisor, Dr. Mark D. Ogden for his input and constructive feedback.

I express my thanks to the Kroto Research Institute, Groundwater Protection and Restoration Group, Andrew Fairburn and Gabriella Kakonyi, Professor Zimmerman's group, Dr. MacGregor's group, the Materials and Science Engineering group, Beverley Lane, Dr. Esther Karunakaran, Dr. Alan Dunbar, the Separation & Nuclear Chemical Engineering Research (SNUCER) group, Mark Jones, Keith Penny; and the mechanical and electrical workshop group of the Department of the Chemical and Biological Engineering, of The University of Sheffield.

I extend my heartfelt appreciation to my mother, Mrs Ebenge Udo Emene, my family and friends for their assistance, love and support.

TABLE OF CONTENTS

List of figures

List of tables

CHAPTER ONE

1.0 Introduction

Water is the most valuable natural resource existing on earth and it is undeniably important to sustain its quality for the existence of life. An important source of pollution detrimental to the water environment (ground and surface water), human health and the ecosystem is industrial wastewater from industries such as electroplating, wood processing, petroleum refining, textile production, paper manufacture, leather processing, solvent distillation, etc. In the past century, large amounts of industrial wastewater have been released into rivers, lakes and coastal areas (Vijayaraghavan & Yun, 2008; Shi, 2013; Adewumi and Oguntuase, 2016). These frequently contain organic and inorganic pollutants, in the form of toxic heavy metals and organic compounds (Aksu , 2005; Kurniawan *et al.,* 2006; Kim *et al.,* 2014; Boudechiche *et al.,* 2016). The heavy metals include zinc, cadmium, chromium, nickel, lead and copper. Some of the organic pollutants are dyes such as methylene blue and orange dye which cause damage to the aquatic ecosystem (Shi, 2013; Dahri *et al*., 2015). In developing countries, heavy metals such as zinc, cadmium and lead are found in amounts that exceed the WHO recommended maximum concentration requirements. Therefore, the enforcement of adequate sustainable treatment methods for effluents is required to reduce environmental impact (Kurniawan *et al*., 2006; Anyakora *et al.,* 2011).

Different conventional treatment techniques, have been developed to decrease the amount of wastewater produced and also to enhance the quality of the effluent, such as chemical precipitation, flotation, membrane filtration, ion exchange, biodegradation, electrolysis, photocatalysis and electrochemical removal. However, these methods are considered not economically feasible and some significant disadvantages are the production of toxic sludge (requiring additional waste treatment), high energy demand and insufficient removal of the

metals (Kurniawan *et al*., 2006; Barakat, 2011; Kapur & Mondal, 2014; Mohammed *et al*., 2014; Boudechiche *et al* .,2016).

An environmentally friendly, water and energy saving process is needed. It must be efficient, effective, widely available and compatible with most treatment applications. The different types of industrial wastewater, the combination of various pollutants and their characteristics, determine the specific design of treatment for the particular type of effluent produced (Shi, 2013).

Biosorption is the best alternative method with good potential to act as a replacement for conventional treatment methods. It is the passive uptake of pollutants by biological materials or materials derived from biological sources. These materials are called biosorbents and the material used will determine how efficient and economical the treatment process can be. The biosorption mechanisms is low cost and rapid with potential for modification for higher efficiency and has a high uptake capacity due to the ability to bind a large variety of ions. Also, they can be regenerated and re-used (Vijayaraghavan & Yun, 2008; Rangabhashiyam *et al*., 2014). Biosorption technology is a complex process and the uncertainty about the mechanisms delayed its commercialisation. Also, the increase in cost as regards to the manipulation or enhancement of the biosorptive capacity and concerns about the environmental issues around the disposal of pollutant-loaded biosorbents have delayed and limited implementation (Fomina & Gadd, 2014). The biosorption process involves ion exchange, complexation and coordination (Han *et al*., 2006; Naeem *et al*., 2009; He & Chen, 2014). It involves the exchange of ions and bonding of the ions to chemically active sites during the adsorption process. Many biological materials have been investigated for their use as biosorbents such as sawdust, chitin, algae, fungi, rice, chestnut shell, tea waste, wild fruit bodies of mushroom, seaweed, etc. (Nasuha *et al*., 2010; Taty-Costodes et *al*., 2003; Liu & Lee, 2014a; Boldizsar Nagy *et al*., 2014; Salazar-rabago *et al*., 2017) .

Luffa cylindrica (loofa) is a low cost and widely available adsorbent derived from a biological source and is a good candidate for an efficient and economical alternative adsorbent for use in biosorption technology. Loofa is a lignocellulose material having a high affinity for heavy metal ions and other pollutants in aqueous solution. It is a sustainable natural resource material that is produced in many countries as a waste and also utilised as a domestic product. The loofa fruit is commonly grown in India, Brazil, China, Japan and Central America and has a cultivation history in the tropical countries of Africa (Mazali & Alves, 2005; Oboh et al., 2009; Ahmad & Haseeb, 2015). In some of these countries, they are grown as a feed for poultry and also as a vitamin supplement for aqua feeds. The fibrous residues of the fruit (mature fruit) are used in producing gourds and loofa sponges, after which it is regarded as a waste material. It has a fibrous vascular system, large surface area and it is highly porous in nature. Being cellulose based it has potential for modification and its surface is negatively charged when in contact with water (Ghali *et al*., 2009; Oboh & Aluyor, 2009; Siqueira *et al*., 2010; Ajuru & Nmom, 2017). The application of loofa for biosorption was utilised by Iqbal and Edyvean (2007) to remove lead ions from aqueous solution. The loofa was used as an immobilising agent for fungal biomass, white rot basidiomycete *Phanerochaete chrysosporium* prior to its use in efficiently adsorbing Pb(II) from aqueous solution (Iqbal & Edyvean, 2007). Also, Saueprasearsit *et al*. (2010) utilised the alkali modified loofa to adsorb lead ions from aqueous solution. An efficient removal was achieved at 82.7% at 40^{o}C (Saueprasearsit et al., 2010). Yu *et al.* (2013) utilised chemical grafted loofa to efficiently adsorb cationic dyes, such as basic magenta and methylene, from aqueous solution. As compared with the unmodified loofa utilised, the maximum uptake capacity was increased by 73% (Yu *et al*. 2013). The successful treatment of contaminated waters with a potential biosorbent, loofa, will minimise waste, enhance the recirculation of water, provide the reuse of chemicals and heavy metals via recovery and regeneration (Mohsen & Jaber, 2002).

The novel step in this thesis will be an attempt to further explain the mechanism of biosorption through the ion exchange and complexation binding capacity of the biosorption of lead, cadmium and zinc metal ions onto chemically modified loofa; to ascertain the functional groups

involved in the process and the degree of contribution of both ion exchange and complexation mechanisms. The measurement of the metal binding capacity of loofa will further explain the percentage adsorption by ion exchange or complexation as regards to change in experimental parameters. The extent of ion exchange capacity will be investigated, the availability of binding sites highlighted, and the extent and stability of the metal complexes (speciation of metal ions) investigated. The research aim of this thesis is to produce an effective low cost and economical biosorption system for wastewater treatment in developing countries while reducing waste. The objective is to produce an efficient biosorbent that undergoes simple modification and is readily available in developing countries. This will answer the question on how this modified loofa can sufficiently remove the selected pollutants found in wastewater produced from industries in developing countries.

A review of the literature on the global issue of wastewater, it's pollution potential and treatment will be covered in chapter one, together with more specific coverage of the biosorption system, paying particular attention to loofa and its potential use for the uptake of toxic heavy metal ions and organic pollutants. The experimental set-up, materials and methods are explained in chapter two. There then follows a series of chapters describing the results obtained. Chapter three covers the characterisation of the loofa. Chapter four highlights the mechanism of the uptake of lead ions from aqueous solution under different experimental conditions using batch studies. Chapters five and six, give a similar coverage as in chapter four, but for the analysis of zinc and cadmium ions respectively. Chapter seven, highlights the uptake mechanism of methylene blue (as a representative of an organic pollutant compound) from aqueous solution under various experimental conditions. Also, when methylene blue is co-adsorbed with either lead, zinc or cadmium. Chapter eight, describes the uptake mechanisms in mixed metal ion solutions under different experimental conditions. Chapter nine, focuses on the column studies of the mechanism of all previously discussed heavy metals' experimental batch results. Chapter ten explains the ion exchange mechanism of lead ions in aqueous solution. Chapter eleven, emphasises on the accuracy and similarity of the different equipment used in

metal ion analysis. Chapter twelve gives a general discussion of the research findings and highlights the industrial and economic impact of loofa utilisation in a developing country such as Nigeria. Conclusions on the use of loofa for biosorption studies, its regeneration and reuse and how loofa compares to other biosorbents are discussed in chapter thirteen. This chapter also reports on the possible mechanisms for the disposal of metal and organic pollutant loaded loofa and recommendations for future work. The thesis report concludes with references and appendices.

1.1 Literature review

1.1.1 Wastewater and pollution

A global drive to tackle environmental issues and ensure the sustainability of our environment is paramount when making worldwide decisions. The world is linked and integrated by technology where issues in one part of the world, in various countries, affect others in the other part of the world. Understanding areas of environmental contamination and how it affects countries can be considered a global issue.

The continent of Africa is faced with environmental pollution and global attention needs to be focused on the sustainable and efficient wastewater management in this area. Nigeria, the largest and fastest growing economy and population in Africa, is an example why a decrease in environmental contamination needs to be prioritised (Okunola *et al.*, 2008; Adewumi and Oguntuase, 2016).

Industrialisation and agricultural activities have led to an increase in the amount of wastewater containing toxic pollutants being released into the environment. The inadequate treatment of this waste results in a disastrous outcome to the environment. While this research is focused on environmental concerns in Nigeria, it is also applicable to the worldwide problem of environmental contamination (Bhatnagar & Minocha, 2006; Fan *et al.*, 2014; Adewumi and Oguntuase, 2016). Table 1.1 shows the concentration of heavy metal ions, lead, zinc and

cadmium, present in the environment in different countries. The exposure of these heavy metal ions to different areas of the environment is highlighted in the evaluation report section of the table.

Table 1.1: Table of the amount of heavy metal ions (mg/L) present in the environment in various countries.

Country	**Zinc**	**Lead**	**Cadmium**	**Evaluation report- references**
India	15	0.1	0.06	Permissible limits found in the environment (Singh *et al*., 2011)
China	0.14	0.05	3.1E04	Concentration found in soil environment (Zhao *et al*., 2010)
Pakistan	1E03 – 0.60	0.20 – 2.00	0.30 -0.90	Concentration found in sewage and canal water (Mussarat *et al*., 2007)
Nigeria	0.07 -1.67	0.09 – 0.22	3E03 – 0.45	Concentration found in underground waters (Ayenimo *et al*., 2005; Ehi-Eromosele & Okiei, 2012; Gimba *et al*., 2015)
United Kingdom	n/a	0.16	3E03	Concentration found in soil environment, average amount

				at industrial sites and drinking water (Defra UK, 2002; Vincent & Passant, 2006; Gordon *et al*., 2008)

Acceptable limits for drinking water for heavy metals such as cadmium, lead and zinc recommended by the World Health Organisation are 0.003mg/L, 0.01mg/L and ≤ 3mg/L respectively (Gordon *et al*., 2008). Water quality is reduced when harmful unwanted substances, such as heavy metal ions and organic pollutants, are released into it. The quality of water in Nigeria is affected by the socio-economic development of the country. To determine the influence of pollutants on water quality, the concentrations and sources of anthropogenic pollutants need to be identified (Namieśnik & Rabajczyk, 2010; Sangi *et al*., 2008; Ameta *et al*., 2013).

1.1.2 Treatment processes and methods

Many conventional treatment techniques have been developed to treat wastewater containing heavy metal ions that are detrimental to health and the environment. Some examples are membrane separation, ion exchange, chemical precipitation, flotation, coagulation-flocculation and electrolytic recovery. These technologies have downsides to their usage such as corrosion of electrodes for electrolytic recovery, non-selectivity for ion exchange, chemical sludge production for chemical precipitation etc., and they are collectively expensive and all have high energy consumption (Kurniawan *et al*., 2006; Park *et al*., 2010**;** Barakat, 2011**;** Mancy *et al*., 2013)**.** Some examples of these conventional treatment systems are the ion exchange and adsorption treatment process which requires an ion exchange resin and activated carbon, as an adsorbents, respectively. This is an efficient but a costly approach to wastewater treatment system (Nagy *et al*., 2014; Arshadi *et al*., 2014; Srivastava *et al*., 2015). Research on these treatment methods are highlighted below:

A chemical coagulation and precipitation treatment is used to remove zinc, cadmium, manganese and magnesium ions from wastewaters. This is carried out at an elevated pH range at 8.5 - 11 which zinc and cadmium hydroxides are formed and the coagulated particles sediment out (Charerntanyarak, 1999). A sorptive floatation treatment used to remove anionic pollutants from wastewater has been adapted to give a highly efficient removal of cationic heavy metal ions but require high amounts of energy (heat) in the process (Lazaridis *et al*., 2001; Doyle & Liu, 2003; Kurniawan *et al*., 2006)**.** Ion exchange, using zeolite as an ion exchanger, has been used to treat wastewaters with heavy metals such as zinc and cadmium at pH 6. This was done by exchange of the ions by cations and possible speciation of free zinc ions and hydroxides of cadmium. The use of the synthetic zeolite produces precipitates on the material (Álvarez-Ayuso *et al*., 2003). A membrane separation treatment method with the use of water–soluble chitosan has been used to remove divalent heavy metal ions by forming metal chitosan aggregate complexes in the pH range of 3.5 -9.5 (Juang & Shiau, 2000; Kurniawan *et al*., 2006). The adsorption process of lead ions using *Enteromorpha prolifera* modified by zinc chloride activation, and the use of high temperature, showed a high adsorption capacity removal (Li *et al*., 2010). An electro dialysis treatment method with the application of an electric voltage at 10V has been utilised to remove lead achieving high separation at 99.9% (Gherasim *et al*., 2014).

Organic pollutants, which exist in large quantities, have also been found to contaminate waters. They are equally dangerous and detrimental to health and the environment (Aksu, 2005; Zhou *et al*., 2014). The photocatalytic degradation of organic pollutants has been researched by many authors and utilised to remove methylene blue from industrial effluent (Rahman *et al*., 2012; Ameta *et al*., 2013). At a light intensity of 50mW/cm^2 and pH at 9.5, the cationic form of methylene blue (MB^+) was removed from aqueous solution which was at an optimal efficiency (Ameta *et al*., 2013).

The many advantages of the adsorption method, such as low operating cost, high efficiency in detoxifying heavy metals that have lower concentrations and wide availability of low cost

adsorbents, have led to its use as an effective and economically attractive alternative to the conventional treatment technologies. Research in this area has shown the adsorption process to be able to remove dissolved heavy metal ions and other pollutants from industrial wastewater. Environmental factors such as pH, pollutant initial concentration, temperature, contact time, adsorbent dosage and ionic strength, have been studied and shown to have an effect on the treatment process. Some of the types of materials that were used to demonstrate the effects of these various parameters are rice husk, saw dust, coconut husk, papaya seeds, peanut hull, olive pomace and yellow passion fruit waste. (Rafatullah *et al*., 2010 ; Vijayaraghavan & Yun, 2008; Park *et al*., 2010; Ali *et al*., 2012 ; Mancy *et al*., 2013**;** Liu & Lee, 2014; He & Chen, 2014)**.**

The key is to find a sustainable treatment method that can provide a high binding capacity to pollutants and also utilises an adsorbent that is readily available. Since this method is required to be utilised over a long term period, a zero waste target, which encourages the reuse and recycling of the spent adsorbents, is sought after. Other advantages of the adsorption treatment method are reduced energy usage, low operational cost and, thus, economic attractiveness (Huang *et al*., 2007; Barakat, 2011; Gouamid *et al*., 2013).

1.1.3 Adsorption systems

Adsorption involves the interaction between pollutants and adsorbents to treat wastewater (Yang & Volesky, 1999). The key factor in an effective treatment process is to choose a suitable adsorbent, that meets the criteria of being widely available and cheap.

A variety of mechanisms can be involved in the process of biosorption, where certain types of biomass materials have the ability to bind, by complexation and ion exchange, and separate particular metal ions and other molecules from an aqueous phase, (Volesky & Holan, 1995). The two most important performance factors in the biosorption system, are the rates and quantities of biosorption. These are controlled by interaction between the solute in solution and the surface sites of the biomass material (Liu & Lee, 2014b). Some factors that affect the binding

mechanism in the biosorption system are the chemical nature of the pollutants (speciation, size and ionic charge), the specific properties and preparation, type of biomass material (chemical state of the sites, number of available sites, its affinity for pollutants), the environmental factors and the occurrence of the competing complexes in the solution. The quantities of pollutants that can be removed by a biosorbent depends on the kinetics at equilibrium and also on the surface properties of the biosorbent (Volesky, 2003; Aksu, 2005; Park *et al*., 2010). Tsai and Chen (2010) reported the adsorption of malachite green onto *Chlorella* based biomass. This finding implied an ion exchange mechanism between the biomass surface and the cationic dye. (Tsai & Chen, 2010). The successful utilisation of biosorption systems in the uptake of pollutants have been reported by many researchers (Sari & Tuzen, 2008a; Sari & Tuzen, 2008b; Lesmana *et al*., 2009; Yang *et al*., 2012; Edris *et al*., 2012; Njoku, 2014; Gimenez *et al*., 2014). Figure 1.1 shows the batch system adsorption process and Figure 1.2 shows an adsorption system for a packed bed column.

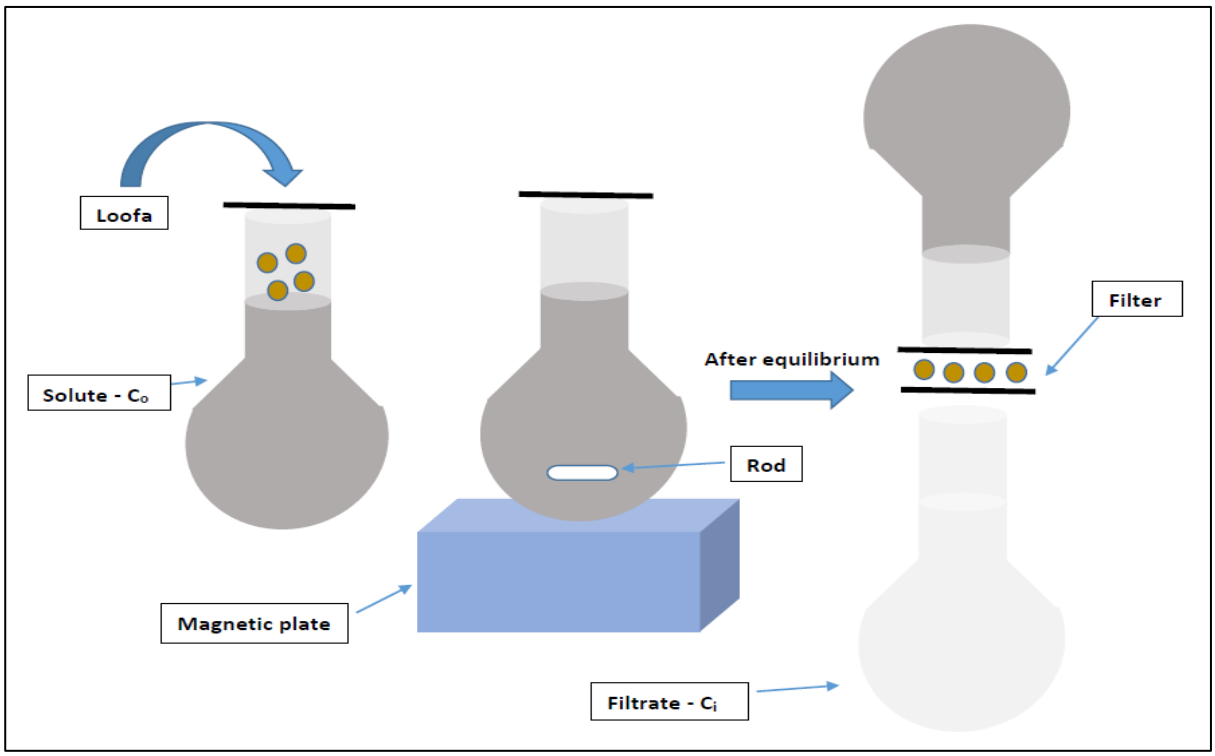

Figure 1.1: Batch process of an adsorption system

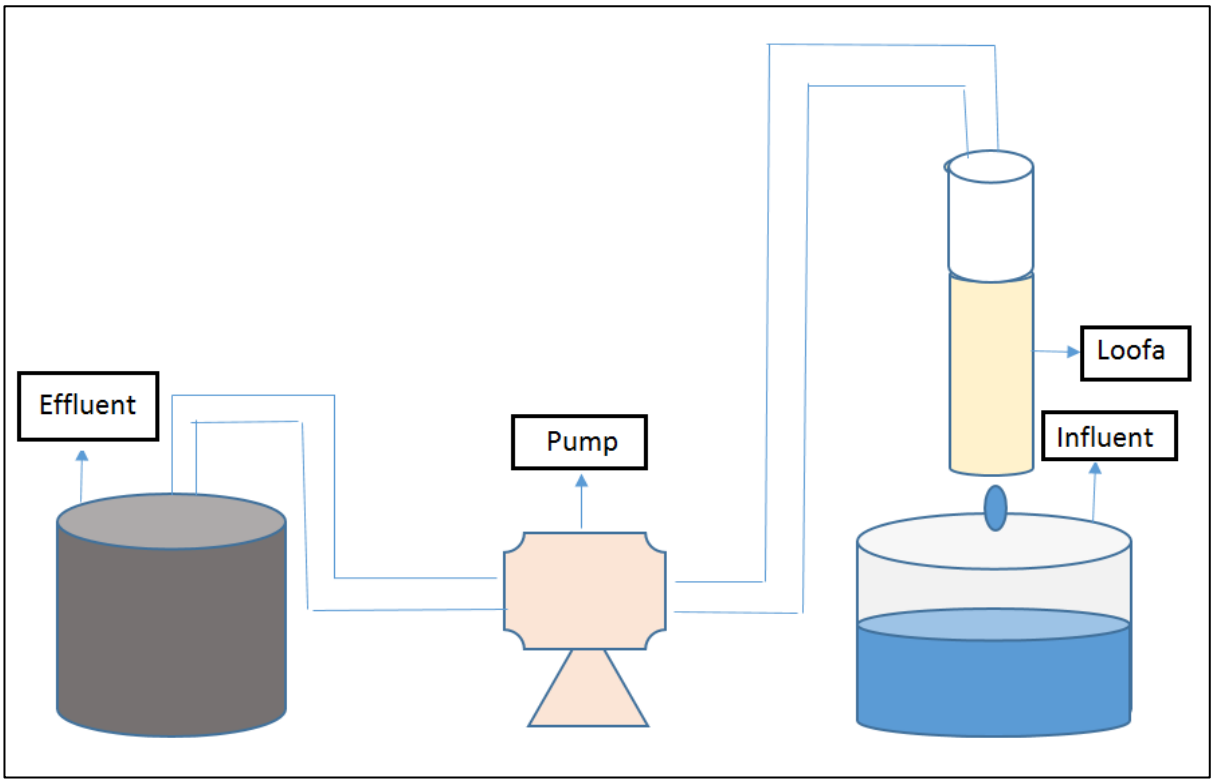

Figure 1.2: Packed-bed column process of an adsorption system

In the design of a biosorption system, experimental factors, such as flow rate, column size and particle size affect the optimal performance of the biosorption process. The difference in the maximum adsorption capacity and solid diffusion coefficient depend on flow rate (Vassillis, 2000). Minimum contact between the adsorbent and adsorbate in the biosorption system decreases the adsorption capacity. However, in the adsorbate-adsorbent system the understanding of the adsorption-desorption reaction step is essential because this determines the biosorption set-up process (Xu *et al*., 2013).

1.1.4 Desorption systems

The potential to desorb the adsorbed pollutants from the adsorbent and to reuse the adsorbent or to recapture the pollutant for further processing is an important aspect of a sustainable treatment process. This is referred to as recovery of the pollutants and regeneration of the biosorbent. Desorption studies detect damage to the biosorbent and also changes in the binding strength of the adsorption system. The behavioural pattern of desorption depends on the

porous nature of the biosorbent. This desorption system, which is the removal of adsorbed ions from the adsorbent, leads to a decreased affinity between the solute and biosorbent. The efficiency of the desorption steps are assessed by the adsorption-desorption cycles (Kapur & Mondal, 2014; Abdolali *et al*., 2015). After equilibrium has been reached, saturation occurs thereby leading to a reverse mechanism process (desorption) which is observed as a change in pH which indicates the presence of the hydronium ions into solution. There is a change in pH because the metal ions released back from the adsorbent into solution leads to the removal of the hydronium ions due to exchange of ions (Gongden *et al*., 2016). However, many researchers have utilised eluents during the desorption process (Iqbal & Edyvean, 2004; Mancy *et al*., 2013; Munoz *et al*., 2006; Shi *et al*., 2014; Kapur & Mondal, 2014; Abdolali *et al*., 2015).

1.1.5 Adsorbents

Adsorbents are materials that remove adsorbate ions from aqueous systems and they need to meet the criteria of being sustainable materials. The low-cost, mass production and easily available properties of adsorbents, which are key properties, meet the principles of sustainability. A number of biomass materials (biosorbents) had been investigated over the years. Waste materials from different sources are ideal candidates for the adsorption process. Sharma and Tiwari (2016) utilised cheap raw materials, *Sapindus* seed hull and *Camelina*, two agricultural wastes, obtained from India, to produce low-cost adsorbents for methylene blue. The adsorbent was treated with sulphuric acid and heated to 200^{o}C for 24h. At pH 7, 12% and 99.38% of methylene blue were adsorbed for *Sapindus* seed hull and *Camelina* respectively. The functional groups present on the surface played a significant role in the adsorption of methylene blue (Sharma & Tiwari, 2016). Asuquo and Martin (2016) utilised agricultural residues (sweet potato peels) as an adsorbent for the removal of cadmium. The functional groups on the surface of the adsorbent, which facilitate adsorption possesses a 58.7% carbon and 32.9% oxygen content. The adsorbent was effective for cadmium ion removal from aqueous systems (Asuquo & Martin, 2016). Silkworms' faeces obtained from Egypt, were utilised to obtain high adsorption

capacity of cadmium and methylene blue. They contain approximately 90% organic matter and were pre-treated with chemical agents at 60^{o}C (ElShafei *et al*., 2014). Unmodified tea waste was reported by Nasuha *et al*. (2010) as a low-cost adsorbent to effectively remove methylene blue at a maximum adsorption capacity of 147mg/g. Other low -cost adsorbents such as activated carbon, bentonite, blast furnace slag and fly ash have been utilised to adsorb zinc and lead ions (Mishra and Patel, 2009). For maximum adsorption capacity of lead and zinc were in the range of 4.98 - 6.68mg/g and 5.82 - 11.24mg/g respectively. Saber-Samandari *et al*. (2014) reported the ability of enhanced chitosan to adsorb both lead ions and cationic dye. The chitosan was modified via micro-emulsion technique and it showed a 60% regeneration efficiency (Saber-Samandari *et al*., 2014). Low cost adsorbents, waste materials such as saw dust, fruit wastes, seaweed, fertilizer wastes and coconut shell have been reported by Ali *et al* (2012) to remove organic pollutants from polluted waters. However, these were utilized in an activated form (prepared at high temperatures) due to their high percentage of carbon content. Ali *et al*. (2012) utilised algae activated carbon and prepared it in a two stage process by carbonization at high temperature followed by using oxidant at elevated temperatures to effectively remove lead and zinc ions ranging from 80 – 99.9% (Ali *et al*., 2012). However, activated carbon materials cannot be regarded as low cost adsorbents since their preparation costs make them less cost effective compared to agricultural, industrial and natural wastes (Bhatnagar & Minocha, 2006). Fungal biomass, from *Rhizomucor pusillus*, was used for the adsorption of coloured pollutants from effluent which showed an effective removal capacity of 90% (Christov *et al*., 1999). The growth of the fungi had to be monitored to ensure its optimum capacity in the removal process (Christov *et al*., 1999). As a result of the scope of study, this adsorbent was not adopted in the removal of heavy metal ions from effluent. Dahri *et al*. (2015) reported the use of the branches and twigs (needles) of *Casuarina equisetifolia*, a sustainable lignocellulose plant found in Australia, as an adsorbent for the removal of methylene blue. This effectively removed 93% of methylene blue from aqueous solution at a particle size of less than 355mm (Dahri *et al*., 2015). Mazmanci and Unyayar (2005) reported the use of loofa immobilised *Funalia trogii* for the removal of reactive

black 5 dye. This adsorption process achieved a 99% removal capacity (Mazmanci & Ünyayar, 2005). Loofa immobilised microalgae was reported by Akhtar *et al*. (2003) for the removal of heavy metal ions. Effective removal of cadmium at 97.9% was achieved (Akhtar *et al*., 2003).

Loofa*, Luffa cylindrica and Luffa acutangula species,* is a vegetable that belongs to a sub-tropical plant. It can be found in many countries in Africa, Asia and America. However, it can be grown in many parts of the world in greenhouses or temperate regions with warm summer temperatures and long cultivation seasons free of frost (Oboh *et al*., 2013).

Figure 1.3: A green and unripe; and a brown and ripe loofa fruit. Photo by Claude Adjanahoun, 2011. Department of Bioresource Engineering, McGill University.

The loofa fruit is commonly grown as a feed for poultry and also as a vitamin supplement for aqua feeds. The fibrous residue of the fruit (mature fruit) is used in producing gourds and loofa sponges, after which it is regarded as a waste material. The smooth and cylindrical shaped fruit is about 12cm long, the flesh of which is a sponge-like material that is comprised of a reticulate matrix consisting of various fibrous interwoven cords. These cords are composed of fibrils which are resinous lignocellulose material comprising of 55-90% cellulose, 10-23% lignin, 8-22%

hemicellulose (the exact proportions depending on factors such as plant origin, weather conditions, nature of soil, etc.). It is this inner part of the fruit which, when dried, forms the typical loofa sponge that has been employed for centuries as a sponge or scrubber for washing (Laidani, 2012; Ajuru & Nmom, 2017). Loofa is a commercially viable and environmentally friendly biomaterial that can be recycled (Shen *et al*., 2012; Ye *et al*., 2013). The high hydrophilicity of the lignocellulose loofa fibers is attributed to the interaction between the hydroxyl groups of the components of the fiber and water molecules. *Luffa acutangula* grown as a cheap vegetable, but regarded as waste, is found in India while *Luffa cylindrica* grown primarily for sponge production, is found in Africa. It comprises of functional groups, both hydroxyl and carboxyl, on its surface that bind to the metal ions during the adsorption process. It has a carbon and oxygen content of 57.5% and 42.5% respectively (Hussain *et al*., 2013; Ahmad & Haseeb, 2015). Cationic metal ions and pollutants are attracted to the anionic loofa structure (Oboh & Aluyor, 2009; Merdan *et al*., 2012). Umpuch *et al*. (2011) reported *Luffa cylindrica* charcoal (prepared by burning at a temperature of 500^{o}C) to have an efficient adsorption capacity for lead ions. Activated carbon derived from loofa, was found to be effective at adsorbing reactive orange dye from aqueous solutions by Abdelwahab (2008). Untreated *Luffa acutangula* was utilised as an adsorbent for the adsorption of lead ions from aqueous solution by Ahmad and Haseeb (2015). Oboh *et al*. (2016) & (2013) utilised loofa (*Luffa cylindrica*) as an adsorbent to remove zinc and copper ions from aqueous systems (Oboh *et al*., 2013; Oboh *et al*., 2016). The preparation of the adsorbent was a mixture of loofa seeds and sponges with a high percentage of carbon (79.33% by weight) and was not chemically treated. A chemical modified loofa was shown to have a 60% increase in the adsorption capacity of methylene blue dye as compared to the unmodified loofa (Chi *et al*., 2013). However, the preparation of the modified loofa required increased temperature and continuous stirring of the loofa in the required chemicals. Shahidi *et al.* (2016) successfully utilised unmodified *Luffa cylindrica* to remove cadmium ions from aqueous solution (Shahidi *et al*., 2016). Boudechiche *et al*. (2015) successfully utilised unmodified loofa in the removal of methylene blue cationic dye from

aqueous solution (Boudechiche *et al*., 2016). Alkali treated *Luffa cylindrica* was used to adsorb lead ions from synthetic wastewater (Saueprasearsit *et al.*, 2010). Figure 1.4 shows a longitudinal and transversal view of dried loofa material. Figure 1.5 shows the chemical structure of loofa.

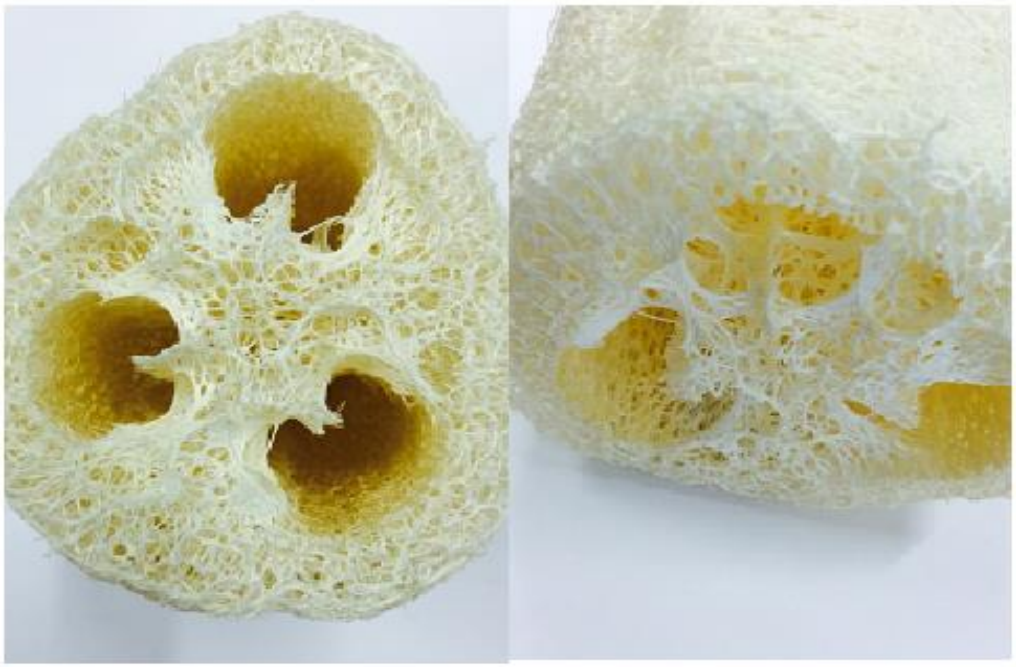

Figure 1.4: Cross sectional area of dried loofa (Luffa cylindrica) fruit.

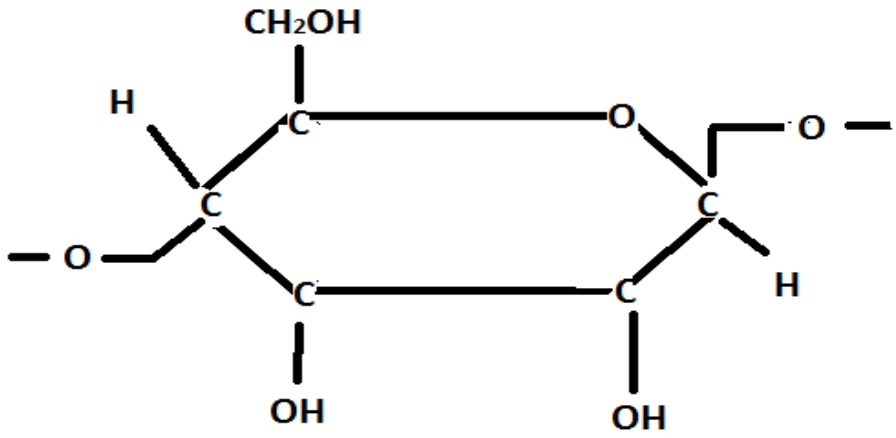

Figure 1.5: Chemical structure of loofa (a cellulosic compound).

Loofa acts as a good adsorbent material, and modification of the loofa shows an enhanced removal ability. Some of the modifications were by simple chemical graft method done by Yu et al. (2013) which showed an increase in the adsorption of methylene blue and basic magenta in a 60.6 - 73.4% range; and by alkali treatment method done by Saueprasearsit et al. (2010) which increased the adsorption capacity of lead ions by 12.2%. A low-cost spent adsorbent is required to be disposed of without being regarded as more waste for the environment. It is essential to ensure environmentally safe options have been adopted to dispose of the metal loaded spent biomass. However, the reuse of this material will be an added advantage as potential adsorbent for a sustainable adsorption process which includes recovery of the metal pollutant.

This study utilised loofa, *Luffa cylindrica* species, a low-cost adsorbent which was chemically modified with alkali at room temperature with no additional energy consumption. This study focuses on the understanding of the mechanism of heavy metal ion and organic pollutants adsorption by loofa. This report suggests that, as loofa material is widely available in tropical and sub-tropical countries and is economical to produce. Indeed, enhancement of its adsorption properties by chemical treatment could be beneficial for wastewater treatment. However, in order to enhance the adsorptive properties of the loofa material, it is essential to have an understanding of the surface mechanisms involved in the retention of pollutants.

1.1.6 Effect of surface chemistry

Surface chemistry is the dominant factor in adsorption. The proportion of acidic or basic groups on the surface of adsorbents determine the effectiveness of the adsorption of the pollutant ions. Surface chemistry determines the ion exchange capacities of the adsorbents, the zeta potential, indicative measure of the electrokinetic properties of a dispersion, as it relates to the change in pH; the ability of the adsorbent to be modified by adsorptive factors or chemical reactions, the swelling that occurs in water and the bonding between the adsorbent surfaces and adsorbate (Bach, 2007). Bhatnagar *et al*. (2013) have listed the various modification treatments used to enhance the surface chemistry of activated carbon which in turn improves the adsorptive

capacity (Bhatnagar *et al*., 2013). Altenor *et al*. (2009) used chemically activated carbon which increased the presence of basic groups on the surface, enhancing the surface properties and therefore improving its ion exchange potential (Altenor, *et al*., 2009). Derakhshan *et al*. (2013) improved the adsorptive capacity of pumice by acid treatment (Derakhshan *et al*., 2013). The modification of the surface of the adsorbent enhances its affinity to heavy metal ions during the adsorption process. Surface modification with NaOH treatment, increases the number of pores on the fiber surface and removes impurities from the fiber surface. It also changes the chemical composition on the fiber surface which further leads to increase in its adsorption capacity (Oushabi *et al*., 2017). Equation 1 below is the alkali treatment surface reaction of loofa with NaOH (Williams *et al*., 2011):

$$ROH + \ Na^{+}OH^{-} \ \rightarrow \ RO^{-}Na^{+} + H_2O \qquad (1)$$

1.1.7 Heavy metal ions

Heavy metals are the most persistent pollutants and they vary in their levels in the different parts of water bodies (Namieśnik & Rabajczyk, 2010). Heavy metals such as chromium, cadmium, zinc, lead etc. are discharged into the environment from industries such as textile, fertilizer, plastic, ceramic and glass manufacturing, mining, electroplating, and metallurgical processes (Barakat, 2011; Montazer-Rahmati *et al*., 2011). Heavy metals occur in several forms: as free ion (most toxic to living organisms), ion bound to different ligands (formation of complex compounds), and as the precipitated compounds. Complex factors are responsible for these forms of division, which are the chemical properties of the metal and the formation of the ion compounds (Namieśnik & Rabajczyk, 2010). Cadmium and lead are two of the toxic heavy metals which have major health detrimental impacts on man, animals and aquatic life. Zinc an essential element is also harmful to humans, plants and the environment in either excess or too little amounts. Due to the similarity between cadmium and zinc (2^{+} valence state), cadmium can substitute for zinc in enzymes and proteins (Gupta & Rastogi, 2008; Gongden *et al*., 2016; Wuana & Okieimen, 2011). Some of the heavy metal ions found in surface water in Lagos, Nigeria are

zinc, cadmium, lead and nickel (Yahaya *et al*., 2012). In the United Kingdom, arsenic, cadmium, lead and nickel are found in roadside soil and industrial sites (Defra UK, 2002). The chemical similarity between some of these metal ions leads to their competition for active sites in the adsorption process (Ayenimo *et al*., 2005).

1.1.8 Adsorption of heavy metals

Adsorption of heavy metal occurs when the metal ions and adsorbent interact. Heavy metal ions are charged solutes and their removal from an aqueous system depends on the ratio of the metal ion to the total number of ions present in aqueous solution. The physical interactions that occur in solution depend on how dilute the metal ions are in solution (metal bound versus weight ratio) is and also on the presence of other ions in solution (Kim, 2003; Borbely & Nagy, 2009; Liu & Lee, 2014). Lasheen *et al*. (2012) reported an increase in the dilution factor of the metal ions in solution to lead to an increase in the distribution ratio (as metal ion concentration decreases) (Lasheen *et al*., 2012). The heavy metal ions were effectively removed at a range from 81 – 99.5%. Particle size of the adsorbent also affects the adsorption of the heavy metal ions. A smaller particle size of biosorbent gives a higher adsorption capacity which can be related to a larger surface area (Amuda *et al*., 2007; Filatova *et al*., 2016). Saueprasearsit *et al*. (2010) reported the utilisation of 250 - 600µm loofa particles to successfully adsorb lead ions from aqueous solution (Saueprasearsit *et al*., 2010).

The adsorption process of heavy metal ions involves two important processes, complexation and ion exchange. Complexation occurs when the metal ion, which acts as a central group, makes close contact with the functional groups on the biosorbent. An inner sphere complex occurs when the central group and ligands directly contact the surface complex if one or more water molecules are interposed between the surface ligand and the central group. Inner sphere complexes involve either ionic or covalent bonding or a combination of both; and are more stable than the outer sphere complexes. This type of complexation is slower than outer -sphere complexation. It is often irreversible and weakly influenced by ionic strength. The

process takes into account the binding capacity of the biosorbent with heavy metals through the exchange of hydrogen ions with metal ions in solution or by the formation of metal ion complexes (donation of an electron pair from the functional groups (Lesmana *et al*., 2009). Outer-sphere complexation, on the other hand, is a rapid reversible process. Albadarin *et al*. (2013) reports bonding of biomaterials with chromium which leads to colour change due to complexation (Albadarin *et al*., 2013). Ionic strength affects the adsorption of ions when ion exchange occurs. This involves electrostatic attraction and forms weaker complexes compared to inner-sphere complexes. Equation 2 below shows the possible complexation that occurs on the surface of an adsorbent (Adewuyi & Pereira, 2017):

$$2(ROH) + M(OH)_2 \rightarrow (ROH)_2 + M(OH)_2 \quad (2)$$

Functional groups of the adsorbent are key contributors in the metal ion complexation and ion exchange processes. Ion exchange mechanism is explained by the exchange of ions in an aqueous system. Equation 3 & 4 below represent the ion exchange mechanism that occurs on the surface of adsorbent (Adewuyi & Pereira, 2017:

$$2(ROH) + M^2 \rightarrow 2(RO)M + 2H^+ \quad (3)$$

$$ROH + M(OH)^+ \rightarrow (RO)M(OH) + H^+ \quad (4)$$

Fras *et al*. (2000) explained that it is of great importance to determine the quantity of accessible groups on an adsorbent in order to ascertain ion exchange capacity. He reported that, in cellulose biomaterials, ion exchange capacities are linked to carboxyl groups which act as sources of ion exchangers (Fras *et al*., 2000). Ion exchange is thought to be the most relevant process of removal of heavy metal ions (Holmberg, 2006; Fan *et al*., 2014; Abdolali *et al*., 2016). The efficiency of adsorption of heavy metal ions is determined by the kinetics at equilibrium (Saber-Samandari *et al*., 2014).

Factors, such as the dilution factor of the metal ions, particle size of adsorbent and mechanism processes, that affect the adsorption of heavy metal ions onto to an adsorbent play an important role in determining the process mechanism that occurs.

The biosorption mechanism indicates chelating, ion exchange, complexation of metal ions with functional groups and release of hydronium ions into aqueous solution (Abdolali *et al*., 2016). It takes into account the binding capacity of the biosorbent with heavy metal through the exchange of hydrogen ions with metal ions in solution or by the formation of metal ion complexes (donation of an electron pair from the functional groups (Lesmana *et al*., 2009). It involves both passive and active mechanisms, which begins with the transfer of metal ions to the surface of the biosorbent material. The initial uptake of metals in biosorption is a result of passive mechanisms. They are rapid and reversible; hence they are associated with the biosorbent surface. These processes are mainly physical adsorption, ion exchange and chemisorption.

Passive biosorption occurs as an exchange of heavy metal ions for counter ions bound to weak acidic groups, such as carboxyl, hydroxyl or amino, found in polysaccharides attached to the cell wall. The next process is a much slower, irreversible, metal binding processes involving surface precipitation, redox reactions, covalent bonding or crystallization on the cell surface (Munoz *et al*., 2006).

Some researchers had reported the uptake of Cu^{2+} ions to be as a result of active groups such as hydroxyl and carboxyl groups. Argun *et al*. (2007) reported copper ions to be bound by the O^{2-} ions present on the active sites of oak sawdust. Guiza (2017) reported copper ion adsorption by orange peel at a pH of 5. This explains the low uptake of copper ions at low pH values and uptake (amount adsorbed) increased with increase in pH. Other researchers reported the adsorption process of Pb^{2+} to be due to the functional groups of carboxyl, amine, and hydroxyl groups present on the surface of the biomass (Oboh *et al*., 2009).

Ion exchange and hydrogen bonding induced the adsorption process of heavy metal ions by sawdust (Liu & Lee, 2014; Blázquez *et al*., 2014; Guiza, 2017). Saber-Samanderi *et al*. (2014) report divalent metal ions to be removed from aqueous solutions by modified chitosan via monolayer chemisorption via the involvement of functional groups (Saber-Samandari *et al*., 2014). Lee *et al*. (2002) reported the uptake mechanism of metal ions to depend on the functional groups on the biosorbent surface and the metal solution chemistry (Lee *et al*., 2002). Nagy *et al*. (2014) reported the uptake of cadmium ions to involve the carboxyl, hydroxyl, amine and two amide groups and also stated that the hydroxylated complexes of cadmium are formed at a high pH (B. Nagy et al., 2014). Arshadi *et al*. (2014) attributed the low adsorption capacity of cadmium ions and other heavy metals onto barley straw in acidic medium, to partial protonation of the functional groups and competition between the metal ions and hydrogen ions in solution for the active sites (Arshadi *et al*., 2014). This then determines the uptake mechanism. The results from Ouyang *et al*. (2014) show that the amount of sodium chloride could significantly affect the uptake efficiency of lead ion adsorption by peanut shells (Ouyang *et al*., 2014). These reports focus on the bonding of heavy metals ions by the functional groups present on the adsorbent. These factors will determine the prioritisation and optimisation of the adsorption process of heavy metal ions. However, the charged metal ions in aqueous solution, depending on the solution pH, exist as different species.

1.1.9 Metal speciation in aqueous solution

Chemical speciation is described as a process to identify and quantify the different species, phases and forms found in a material (Cai *et al*., 2007). Species of metal depend on pH and the presence of ligands such as hydroxides, carbonates etc. Metal ions are known to form complexes with complexing agents or ligands released from industrial activities. The solubility and mobility of metal ions in ground and surface waters are increased by metal complexing. For example, the total lead ion concentration is given based on the amount of free lead ions and lead complexes.

Therefore, the greater the amount of lead ions that are complexed, the lower the concentration of the free lead ions in solution. These metal complexes are then transported and mobilised in environmental and biological systems. The metal complex species that are kinetically and thermodynamically stable determine the environmental and biological impact of such metal complexes (Fernando, 1995). Complexes of great concern are those formed by some of the heavier elements in the periodic table, such as cadmium, mercury, lead, arsenic etc.

The kinetic and thermodynamic stability of these heavy metal complexes and the occurrence of the forms of the individual species determine their bioavailability and toxicity. Identification of the speciation of these elements by critically assessing their thermodynamic and kinetic stability is a major problem for environmentalists and toxicologists. The evaluation of the toxicity of an element, synergistic or antagonistic effects with respect to other elements, and positive or negative effects on the functionality of living things, depends on the occurrence of its species. For the determination of relative concentrations of heavy elements in the environment, information on the thermodynamic and rate constants are essential. A database of constants of metal complex formation found in the environment is available (Luo & Millero, 2007). One of the steps in determining the total trace element concentration is to know the speciation of the elements present in complex environmental and biological samples as a function of time to ensure steps are taken to preserve the integrity of the sample (Fernando, 1995). The binding patterns of the metal complexes are dependent on the metal speciation at a certain pH range (speciation diagrams) (Han *et al*., 2006).

Lasheen and Ammar (2009) report that cadmium and zinc in wastewater sludges exist in various chemical forms which exist in metal fractions such as exchangeable; bound to carbonates, bound to iron and manganese oxides; organic and sulfide; and residual (Lasheen & Ammar, 2009). Escudero *et al*. (2013) report the different species of lead ions occur at various pH values (Escudero *et al*., 2013). Naeem *et al*. (2009) state that the adsorption of lead ions in aqueous

solution is influenced by their speciation. They also report that singly charged ($PbOH^+$) ion is more easily adsorbed than the doubly charged M^{2+} due to the steric hindrance. Derakhshan *et al*. (2013) show that solution pH has an effect on the speciation of pollutants in aqueous solution. This is supported by Chowdbury and Saha (2012). Albadarin *et al*. (2013) also show the importance of speciation of chromium in aqueous solution and the effect on its uptake onto waste biomaterials (Chowdhury & Saha, 2012; Albadarin *et al*., 2013). The bioavailability of heavy metals in soil environment depends on their speciation which is reported to determine the effectiveness of different treatments (Hernandez-Soriano & Jimenez-Lopez, 2012). Information on the speciation of the heavy metal ions helps in understanding the adsorption process and can be used to optimise the solution conditions for improved retention efficiency. Therefore, speciation and exchange of the heavy metal ions involved in the mechanism process were determined. Also, the understanding of the mechanism of organic pollutants, such as methylene blue, helps to maximise the adsorption process of mixed pollutants in the adsorption system.

1.1.10 Mechanism for adsorption of methylene blue

Methylene blue (MB) ($C_{16}H_{18}N_3SCl$) is a basic dye that has a cationic form and has been used over the years as a model for the adsorption of organic pollutants from aqueous solution. It is a natural oxidizing agent, exhibits stability when exposed to sunlight and resists biodegradation (Fan *et al*., 2014). Figure 1.6 shows the structure of methylene blue.

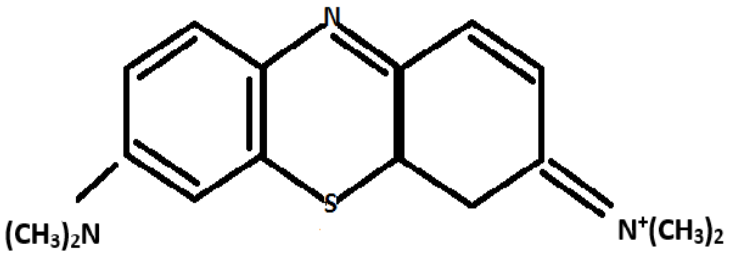

Figure 1.6: Structural formula of methylene blue

Kavitha and Namasivayam (2007) found the adsorption of MB by coir to be favoured at a high pH due to the presence of OH^- ions and also reported the presence of positively charged surface sites on the coir at pH of 2. As the pH increased, the negatively charged sites increase, as a result of deprotonation. Han *et al*. (2007) using leaves from the pheonix tree for the adsorption of MB found that the negative charge on the leaf surface enhances the adsorption of MB. The excess H^+ ions, present at low pH, compete with the cationic dye ions for adsorption sites under acidic conditions, hence reducing MB adsorption. According to Weng and Pan (2007), the negatively charged surface of spent activated clay, when the solution was pH>pHpzc, promoted the adsorption of MB. This supported the report by Han *et al*. (2007) and the argument was based on the reactions of the acid and base on the surface groups controlling the pH dependent charges present at the adsorbent edges which was responsible for the degree of adsorption. Oliveira *et al* (2008) explained a low uptake of MB to be due to the competing excess protons under acidic conditions and also reported the adsorbent to become negatively charged at pH>pHpzc (range of 4.3 -4.5), enhancing the electrostatic attraction between the MB cationic dye and the surface of coffee husks. These studies showed the prominent role of pH in the adsorption process. Barka *et al*. (2011) studied the adsorption of MB by *Scolymus hispanicus*. These studies showed the isoelectric point of the adsorbent to be about pH 5.2. However, at pH < 5.2, the repulsion forces between the MB molecules and the adsorbent surface is due to the positively charged surfaces of the adsorbent. At pH > 5.2, the ligands such as carboxyl, phosphoryl, sulfhydryl, and hydroxyl, become negatively charged thereby enhancing MB adsorption. Derakhshan *et al*. (2013) explained that electrostatic attraction occurs during adsorption of MB onto pumice (Derakhshan *et al*., 2013). Demir *et al*. (2008) explained the MB concentration overrides the influence of medium temperature in the adsorption onto loofa (Demir *et al*., 2008).

Other dye studies predominately exhibited ion exchange adsorption mechanisms. Some by chemisorption and others by physiosorption (MB on montmorillonite clay). An example of chemisorption involves valence forces through the exchange and sharing of electrons between

the adsorbent and adsorbate ions as covalent forces (Asuquo & Martin, 2016). Also, Fan *et al*. (2014) reported the presence of MB in solution to have an antagonistic effect on the adsorption of copper ions (Fan *et al*., 2014). Saber-Samnadari *et al*. (2014) reported the adsorption of lead ions to be influenced by the presence of MB ions. However, there is an ion-dipole interaction between MB and OH^- groups of the adsorbents (Samiey & Ashoori, 2012; Saber-Samandari *et al*., 2014). Derakhshan *et al*. (2013) utilised pumice for methylene blue and at an equilibrium time of 120mins.

In summary, all studies have reported the effect of pH on adsorption behaviour because of the pressure of competing protons and ions for the surface charged sites on the adsorbent. The key functional groups such as proteins, polysaccharides and lipids (possess affinity for the adsorbate), were identified via FTIR studies. However, for FTIR studies dry samples are used and this may lead to altered results as there are the possibility of reactions occurring during the drying and pre-treatment steps (Han *et al*., 2006; Liu & Lee, 2014).

Additional understanding of the adsorption process of the organic dye was achieved by utilising an absorbance plot technique to determine adsorption capacity.

1.1.11 Absorbance vs. concentration

An absorbance versus concentration calibration curve is needed to determine the unknown concentration of organic pollutants present in aqueous solution. The different absorbance at known concentrations is used to plot a graph. Tsai and Chen (2010) mentioned the utilisation of a calibration curve of absorbance versus concentration at different values to ascertain the adsorbed concentration of malachite green in solution (Tsai & Chen, 2010).

At constant temperature, after the derivation of the concentration values, the adsorption mechanism process was further studied by use of various models.

1.1.12 Isotherm modelling

The extent to which the adsorption mechanism of a metal ion fits to a model is determined by the correlation coefficients obtained. Analysis of the isotherms can provide some partial information on the microscopic properties of the surface (Brouers, 2014). Langmuir and Freundlich models were utilised by Mamatha *et al*. (2012) to describe the mechanism of lead adsorption onto tree bark (Mamatha et al., 2012a). These two models were successfully utilised by Areco *et al*. (2012) for the adsorption of heavy metals onto green alga (Areco *et al*., 2012). Many researchers have utilised various isotherm models to predict the adsorption mechanisms, including the Langmuir, Freundlich, Dubini-Radushkevich, Sips and Temkin models (Ho *et al*., 2002; Brinza *et al*., 2007; Abdelwahab, 2008; Oboh *et al*., 2009; Foo & Hameed, 2010; Nagy *et al*., 2014; Arshadi *et al*., 2014; Tang *et al*., 2014; Brouers & Al-musawi, 2015).

The suitability fit of the adsorption process to these models assist in understanding the behavioural patterns of the uptake mechanism. The kinetics of the adsorption process helps in the optimisation of pollutant removal. Therefore, the kinetic models is useful in predicting the suitability of each model best.

1.1.13 Kinetic modelling

One of the essential parameters to apply in an economical wastewater treatment plant is the rate of adsorption (Gongden *et al*., 2016). In order to produce a kinetic model that explains the adsorption process of metal ions, an understanding of the stages involved in the adsorption process by the adsorbent are essential. Three important aspects of the adsorption processes are (Hui *et al*., 2005):

- The transfer of solute from the bulk solution to the surface of the biosorbent.
- The transfer of solute from the biosorbent surface to the active sites.
- The interactions of the solute with available sites on both the external and internal surfaces of the sorbent.

Pseudo first order models have been widely used due to simplicity and these are based on the sorption of the solid phase from a liquid phase. The pseudo first order (PFO) model is appropriate for the initial adsorption rate and therefore cannot be applied to the entire range of contact time. The most cases, the PFO model is only suitable for the initial contact time of 20-30 minutes, and not for the whole range of adsorption. The linear plot, described by the PFO equation, occurs approximately in the first 30 minutes, and beyond this point, the experimental and theoretical data does not adequately fit. Also, the uptake capacity (q_e) values obtained from PFO model is not equal to the experimental q_e obtained from the data. This further explains the inability of the PFO model to fit the kinetic adsorption data (Tran *et al*., 2017). Pseudo second order (PSO) is superior to the pseudo first order kinetics as it shows the interaction of adsorbent-adsorbate through their valency forces and relates to chemisorption mechanism. The whole range of the kinetic adsorption process are represented by the PSO model and also, the q_e values are close to the obtained experimental q_e values. This shows the (Lesmana *et al*., 2009; Febrianto *et al*., 2009; Guerrero-Coronilla *et al*., 2015; Derakhshan *et al*., 2013). It reflects the whole kinetic adsorption process as compared to pseudo first order model that only explains the initial rate of adsorption (Plazinski *et al*., 2009; Olu-owolabi & Unuabonah, 2010). Many researchers successfully utilised the pseudo second order model to describe the kinetic (reaction pathway) adsorption of pollutants onto various biosorbents (Oboh *et al*., 2009 ; Doss & Kodolikar, 2012; Plazinski *et al*., 2013; Arshadi *et al*., 2014; Ye *et al*., 2013; Shi *et al*., 2014; Tang *et al*., 2014).

The intra particle diffusion model is utilised to explain the intraparticle diffusion effect. This effect explains the solute transfer from the adsorbent particle surface to the intra particle active sites via sorption. The reason why the straight line is not from the origin, shown in Figure 1.7, is explained by the difference in the rate of mass transfer in the initial and final step of adsorption and this is attributed to more than one mechanism of diffusion involved. Nagy *et al*. (2014) utilised the intraparticle diffusion model for the adsorption of cadmium (Plazinski et al., 2013; Nagy et al., 2014). Abdelwahab (2008) utilised this model to evaluate the removal of reactive orange dye by loofa activated carbon (Abdelwahab, 2008).

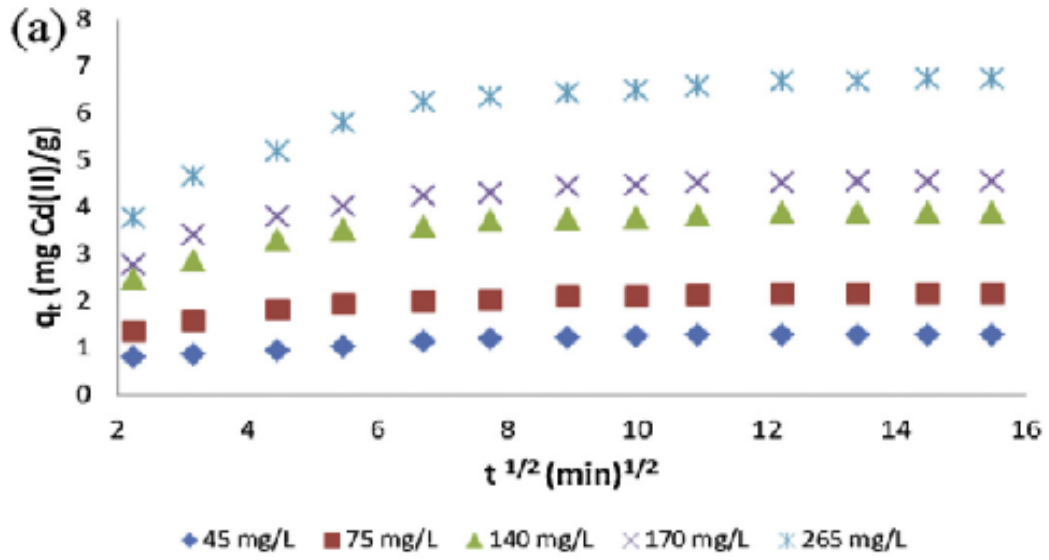

Figure 1.7: (a) Plot of intra-particle diffusion model for Cd(II) biosorption using A. bisporus based biocomposite; C_i = 45-265mg/L, 2g biomass, d = 4mm, 296K, pH 5.6, 700rpm (Nagy *et al*., 2014).

The Elovich kinetic model describes the sorption on highly heterogeneous sorbents. The satisfactorily application of the Elovich model provides information on the chemisorption process that occurs in biosorption and the initial sorption rate (α-mg/g/min) and the desorption constant (*b* - g/mg) relate to the extent of surface coverage and activation energy for chemisorption respectively (Madala *et al*., 2013). This was utilised by Altinisik *et al*. (2010) to explain the adsorption kinetics of basic dye onto loofa (Altinişik *et al*., 2010). Mamatha *et al*. (2012) described lead adsorption onto tree bark by the Elovich kinetic model (Mamatha *et al*., 2012a).

Each kinetic model is supposed to depict the pattern of adsorption behaviour that attempts to understand the adsorption process of heavy metal ions and organic pollutants onto adsorbents, and provide the basis for interpreting the experimental data. In order to apply these models, it is essential to carefully define the experimental parameters used in the measurements.

1.1.14 Hypothesis and Objectives

Hypothesis:

- That the loofa adsorbent shows a stronger binding affinity for metal ions and methylene blue after modification by treatment with alkali. The change of its characteristics should show as multiple binding energies during the adsorption process which improves the adsorption capacity.
- That the removal of pollutants, such as lead, cadmium, and zinc ions; and methylene blue from aqueous solution (together as a model of wastewater effluent) can be effected by an environmentally safe and easily modified loofa adsorbent.
- That experimental conditions that affect the adsorption capacity of the pollutants onto loofa can be changed to optimise the adsorption mechanisms of pollutants.
- That the adsorption mechanism of the pollutants onto loofa are classed as both ion exchange and complexation in varying percentages.
- That the Loofa biosorbent can be used an alternative adsorbent for the removal of pollutants from wastewater.

Objectives:

- To investigate the modification with alkali of loofa biosorbent and how this modification affects the structural characteristics, active surface functional groups, surface area, pore size, binding energies and efficiency in the removal of the selected metal ions and methylene blue.
- To optimise the adsorption of the pollutants by altering the experimental conditions that affect the adsorption onto the loofa.
- To investigate the adsorption mechanism of the loofa adsorbent by differentiating the involvement of ion exchange and complexation.

- To investigate the adsorption capacity performance of alkali treated loofa for the removal of the pollutants in both batch and column studies.
- To compare the modified loofa adsorbent with reported data on other biosorbents used in wastewater treatment processes.

CHAPTER TWO

2.0 Materials and methods

2.1 Introduction

This chapter details the experimental procedures used in the adsorption studies of the heavy metals and MB with *Luffa cylindrica* (loofa) as the adsorbent. Section 2.2 describes the preparation of the loofa, the difficulties encountered prior to its successful utilisation and the problems that occurred prior to the adsorption studies and experimental analysis.

In section 2.3 and 2.4, the treatment and characterisation of the loofa is explained. Section 2.5 outlines how the stock solutions were prepared and section 2.6 describes the equipment used in the filtrate analysis. Section 2.7 & 2.8 gives the experimental procedure of the batch and column adsorption processes, the models and calculations used to obtain the results. Section 2.9 describes the two step procedures in the ion exchange mechanism process.

2.2 Experimental procedures prior to analysis

This section describes the problems overcome in the processing of the loofa for use in the described experiments. These issues are highlighted in order to assist in the design of future experiments.

2.2.1 Preparation of loofa

Loofa is a hard but not brittle plant material with a high tensile strength.

- **Cutting of loofa**

The loofa was cut on a band saw into small pieces of different shapes. This approach was used after the use of a sharp knife could only cut through some parts of the loofa with much difficulty.

- **Sections of loofa**

It was firstly cut into cube sizes but it this shape could not be used because there was contact obstruction with the magnetic rod for the batch experiments. The internal and external parts of the loofa was then ground prior to adsorption studies but the core part of the loofa could not be ground due to its very tough nature and was not utilised in the experiments.

- **Grinding of loofa**

- **Mortar and pestle**

The loofa material was cut into bits and placed in a mortar. A pestle was used in an attempt to crush it but it was not possible due to the need of more contact and strength needed to crush to particle size.

- **Portable blender**

The cube size cut loofa was placed in a blender hub and approximately 3g was ground within 2h. This was because after a few minutes of grinding, the blender had to be switched off and allowed to cool down in order to minimise damage to the equipment. The core section of the loofa was not ground to particle size because there was no contact between it and the blades of the blender.

- **Ball mill**

A Retsch model PM100 Ball Mill was utilised in an attempt to crush the dried loofa. The contact made with the balls of the mill could only flatten the loofa and this had little effect in breaking up the material.

- **Milling machine**

A milling machine was found to be better for breaking up the dried loofa. A Retsch Mill, model SM100, was used in grinding the internal and external parts of the loofa into particles. The

toughest part (core) could not be ground. The small pieces of loofa were fed through the hopper of the Mill and passed through a 2mm sieve and collected.

- **Weighing of loofa**

The loofa was weighed on a balance using a weighing boat. The values were measured with accuracy to 4 decimal places as displayed on the balance screen. The use of a metallic or ceramic weighing boat is favoured due to the static force attraction of the loofa to the plastic material which made it more difficult to release loofa into the aqueous solution.

- **Sieving of loofa**

The loofa was sieved to between 1-2mm using a mechanical Retsch AS200 sieving equipment.

- **Filtering of loofa**

The loofa was separated from the aqueous phase after the adsorption experiments by a 90mm diameter Whatman filter paper Grade 1 to obtain the filtrate and adsorbate loaded loofa. The filtered out loofa was used for further characterisation.

2.2.2 Adsorption studies

- Over a period of time, lead, cadmium and zinc ions attach to the walls of the glass containers in which the aqueous solutions are stored. They were shown to have decreased by 38.8%, 12.5% and 62% respectively in 3 months. Samples prepared the same day have a 5% decrease in metal ion concentration in 24 hours. Therefore, the metal ions stock solution was prepared and utilised on the same day.

- The metal ion stock solution was found not to be 100% preserved in the refrigerator (-2^0C) or by 1% acidification by nitric acid. Therefore, once acidified by 1% nitric acid, the samples were immediately analysed by the ICP-MS, ICP-OES and AAS.

- Using the ICP-MS, the metal levels in some samples could not be detected if the dilution factor was high or low. This means that if the metal ion diluted sample concentration

was higher or lower than the ICP-MS concentration detection limit then the metal level could be detected. The relative standard deviation gives a clear depiction of the accuracy of the instrument. If the accuracy was above 5% then the results could not be considered accurate. The range of concentration was expected to be exact and within the limit of the calibration curve of each metal ion element. All diluted samples were ensured to be within the set range of the ICP-MS calibration concentration values.

- The dilution of the metal ion samples, prior to analysis, was carried out by using a Flow Gravimetric Diluter.

- Loofa – metal ion samples at the end of the adsorption experiments (loofa in metal ion solution) showed in a 5-10% decrease in adsorption capacity at a low pH of 3 and a 5-10% increase at a pH of 5 after being stored over a duration period of 7 days. This shows that adsorption and desorption process occurs in a non-agitated state. The pH values of the batch metal ion solutions with the metal loaded loofa, were not consistent and could not be accurately recorded.

2.3 Loofa treatment

2.3.1 Preparation of NaOH and HCl treated loofa

The dried fruit of loofa (the loofa sponge) were purchased in the United Kingdom from a local retailer. The whitish yellow fibres were washed several times with deionised water to remove surface impurities and seeds, then alkali treated by soaking in 4% 0.1M NaOH at room temperature for 1h. This procedure was repeated for acid treated loofa. The untreated dried fruit loofa was then acid treated by soaking in 4% 0.1M HCl at room temperature for 1h. The loofa was repeatedly washed in deionised water until the pH was neutral, and then oven dried at 90 °C for 24h.The dried samples were ground and sieved to a 1mm particle size fraction and stored until required.

2.4 Loofa characterisation

2.4.1 pHpzc determination

50ml of 0.01M NaCl solution was introduced into 250ml Erlenmeyer flasks and 0.5g of loofa added to each of them. The pH value of each solution was adjusted in a range of 2 - 12 by addition of 0.1M HCl or NaOH solutions. Each flask was agitated for 48h and the final solution pH measured by a pH meter. A graph curve was plotted of the final pH against initial pH. The point of intersection of the curve was taken as the pHpzc (Banerjee & Chattopadhyaya, 2013).

2.4.2 SEM coupled with EDX preparation

Dried samples of loofa were placed on a metal stub and coated with a thin layer of gold by an Agar Sputter Coater Model 108. This was mounted and analysed by an Analytical Scanning Electron Microscope (SEM) (Model JOEL JSM- 6010LA) coupled with energy dispersive X-ray (EDX) operating at an accelerating voltage of 10kV and at a magnification setting of x550 SS60.It was used for microscopic examination of the loofa samples.

2.4.3 Fourier Transform Infra-red spectroscopy (FT-IR)

50mg of dried loofa (< 250µm thickness) were prepared for ATR- FTIR analysis. Measurements were made in transmittance mode using a spectral resolution of $4cm^{-1}$ by 256 scans and approximately 150 seconds per step across the range $4000cm^{-1}$ to 650 cm^{-1} using a Nicolet 6700 FTIR Spectrometer. Before analysing the sample, a reference (zero) spectrum is acquired which is later subtracted from the raw spectra data to obtain the actual spectra of the sample.

2.4.4 CHNS analysis

Dried samples of loofa were analysed for CHNS using the Elementar Vario MICRO Cube CHN/S Elemental Analyser which uses a combustion method in a pure oxygen environment to convert the accurately weighed sample into the simple gases CO_2, H_2O, N_2 and SO_2. After reduction through pure copper this mixture of gases was then separated using an adsorption column. The

resultant gases were measured as a function of their thermal conductivity. The elements, carbon and hydrogen were determined in percentage with a 0.3% limit of detection. The oxygen content was calculated as the difference from 100%.

2.4.5 BET analysis

The surface area of each sample of loofa was determined from nitrogen adsorption at 77.2K in the range of relative pressure (p/p^0) of 0.05 – 1 by using a Micromeritics 3Flex instrument. The samples were degassed at 150°C for 24 hours. A three-parameter non-linear fitting procedure was used and the loofa samples were subjected to a 99-point BET surface analysis and full adsorption isotherms were collected for all samples. The conventional single point method of relative pressure was used.

2.4.6 TGA analysis

The thermal stability of untreated and treated loofa was determined using a Perkin Elmer Thermo Gravimetric Analyser (TGA 4000). Samples were scanned between 40 – 800°C at a rate of 50°C/min (held for 10 min at 150°C) at under a nitrogen atmosphere.

2.4.7 Water adsorption measurements

Use of humidity chambers (desiccators). The equation below was used:

$$MC = \frac{m - m_d}{m} \times 100\% \quad (1)$$

Where MC = the moisture content, m = the mass after exposure to humidity and m_d is the dry mass (Bismarck *et al.*, 2002).

2.5 Preparation of stock solutions

2.5.1 Reagents and stock solutions

All chemicals utilised were of analytical grade. The stock solution, 1 g/L of Pb (II), Cd(II) and Zn(II) were prepared by dissolving $PbCl_2$, Cd $(NO_3)_2$ and $ZnSO_4$ salt respectively, obtained from Sigma-

Aldrich, United Kingdom, in deionised water. The desired concentrations were obtained by diluting the stock solution to set concentrations, varying from 50 to 200mg/L. Solutions of 0.1 M HCl and 0.1M NaOH were used to alter the solution pH.

2.5.2 Methylene blue solution

The stock solution, 1g/L of methylene blue was prepared by dissolving methylene blue dye powder, obtained from Sigma- Aldrich, United Kingdom, in deionised water. The desired concentrations were obtained by diluting the stock solution to set concentrations, varying from 5 to 40 mg/L. Solutions of 0.1 M HCl and 0.1M NaOH were used to alter the solution pH.

2.5.3 Mixed metal solution

A stock solution of mixed metal solution was prepared by mixing stock solutions of each metal ion solution, lead, cadmium and zinc in the desired ratio of concentration. The desired concentrations were obtained by diluting the stock solution to set concentrations, varying from 5 – 100 mg/L. Solutions of 0.1M HCl and 0.1M NaOH were used to alter the solution pH.

Table 2.1: The experimental parameters of mixed metal solutions.

Mixed metal ions	**Total concentration (mg/L)**	**pH**	**Ratio**
Pb , Zn, Cd	50	5	3:6:1
Zn, Pb, Cd	70	6	3:4:1
Cd, Pb , Zn	100	7	2:1:6

2.5.4 Metal and dye solution

A stock solution of a 1:1 ratio was prepared by mixing stock solution of each desired metal ion solution and methylene blue solution. The desired concentrations were obtained by diluting the

stock solution to a set concentration of 50mg/L. Solutions of 0.1 M HCl and 0.1M NaOH were used to alter the solution pH.

2.6 Metal determination

2.6.1 ICP-MS

The supernatant liquid, after being filtered using a 540 Hardened Ashless Diameter 90mm Whatman filter, was diluted and placed in a tube rack. The ICP-MS detects atomic mass units of ion in the mass region 3-250 Dalton. The ICP-OES was also used to analyse the diluted supernatant samples by passing them through an emission spectrophotometer (Thermo Scientific iCAP 6000 series Inductively Coupled Plasma Optical Emission Spectrometry (ICP-OES) and the level of ions present detected. Also, the supernatant samples were measured by a fully PC-controlled AAS using an air-acetylene flame (Anaylst 200/400 Spectrometer PerkinElmer) with automated lamp selection features. Blank samples were used throughout the analysis procedure after every 5 samples to ensure the accuracy of the results.

All metal ion and mixed metal ion concentrations were analysed using this equipment. Each 5ml sample was acidified with 50µl of nitric acid. Extra care was exercised to prevent contamination and preserve the samples for the specific analyses. The calibration blank was a solution of deionised water with 50µl nitric acid. A method blank having the same volume of acidified water as for the metal solution samples underwent the same complete procedure for the analysis.

2.6.4 UV-Vis Spectrophotometer

The filtrate of the methylene blue solution and a zero blank of deionised water were placed in different compartments of the spectrophotometer equipment and the wavelength scan between 300 – 700nm at concentrations of 5 - 40mg/L of methylene blue solutions, exposed to different light intensity and experimental conditions in order to obtain the optimum wavelength for the measurements.

2.6.5 Spectrophotometer

Firstly, the equipment was calibrated by a zero blank of deionised water. The methylene blue solution was then placed in cuvettes and measured at an optimum wavelength of 668nm, which gives optimum absorbance of methylene blue (Tsai and Chen, 2010), by a Spectrophotometer (Spectronic ™ 200E Thermo Scientific Version 4.04i). The absorbance values were displayed on the screen. A calibration curve was generated by the using the interpolation function of Wolfram Mathematica 10.2. The concentration was determined by the calibration curve of absorbance versus concentration.

2.7 Batch adsorption studies

All batch adsorption experiments were carried out as single contacts with the contact of 1g of 1mm sieve size loofa with 200 mL of aqueous solution. Experiments were carried out at desired metal ion, methylene blue or mixed concentrations of 5 - 200mg/L, each at pH values of 3, 4, 5, 6, 7, 8 and 9. The treated loofa and aqueous feed were continuously mixed at an agitation speed of 200rpm for a period of 24 hrs for metal ion adsorption, 90 mins for methylene blue dye solutions and 24hrs for mixed solutions at room temperature (21 °C) on a magnetic stirrer. Experiments were studied under additional temperatures of 35°C, 45°C and 55°C. Adsorption capacity was determined using the following equation:

$$q_e = \left(\frac{C_i - C_e}{C_e}\right) \times \frac{V}{m} \qquad (2)$$

where q_e is the weighted distribution of the filtrate, where C_i is the initial aqueous activity of the filtrate before contact and C_e is the aqueous activity of the filtrate after equilibration. V is the volume of the aqueous phase (mL) and m is the mass of the loofa (g). The percentage removal was determined by difference (using eqn. 2), the concentrations of the metal ions were determined by ICP-MS and the methylene blue concentrations and adsorption spectra of methylene blue, as a function of absorbance versus wavelength, were determined by using the

Spectrophotometer and UV-Vis Spectrophotometer Model UV-10 UV-Vis Thermo Fisher Scientific 180VA respectively.

The percentage removal of the metal ions from aqueous solution was calculated by using the equation below:

$$E\% = \frac{C_i - C_e}{C_i} \times 100 \quad (3)$$

where C_i is the initial metal concentration before contact and C_e is the concentration of the metal ion in the aqueous phase after contact with the loofa. pH measurements for solutions were determined using a silver/silver chloride reference electrode, from Hanna Instruments, calibrated at pH 4 and 7 using buffers. Error was determined by triplicate measurement in aqueous feed solution concentrations prior to contact.

2.7.1 Light intensity studies

Additional batch adsorption studies were carried out under different light intensities, 0.17 and 820 lux for methylene blue solutions. Experiments were carried out at a concentration of 10mg/L at pH 7. The treated loofa (ATLC) and methylene blue were continuously mixed for a period of 90 mins for methylene blue dye solutions at room temperature (21 °C) on a magnetic stirrer. The absorbance of the residual dye solutions was analysed using a Spectrophotometer.

2.7.2 Determination of loading behaviour

All loading isotherms were carried out as single contacts with the contact of 1 g of treated loofa (ATLC) with 200 mL of aqueous feed. The ATLC and aqueous feed were continuously mixed for a period of 24 hrs at room temperature (21°C). The data were fitted to the following models: Langmuir, two-site Langmuir, Temkin, Freundlich, Sips and Dubinin-Radushkevich (Foo & Hameed, 2010), equations (4) – (8). A widely researched and commonly used two parameter fitting model, was used to determine the closeness of fit(Chen, 2015; Özkaya, 2006). The fitting

was carried out by using linear regression and by non-linear least squares analysis using excel SOLVER and Graphpad (Arshadi *et al*., 2014). The equations are as shown below:

Langmuir

$$q_e = \frac{K_L C_e}{1+a_L C_e} \quad (4)$$

The monolayer saturation capacity, q_m (g L^{-1}_{wsr}), was calculated from the Langmuir equation using equation (4):

$$K_L = q_m a_L \quad (5)$$

Two site Langmuir

$$q_e = \frac{Q_1 b_1 C_e}{1 + b_1 C_e} + \frac{Q_2 b_2 C_e}{1 + b_2 C_e} \quad (6)$$

where:

a_L = Langmuir isotherm constant

b_1 = Two site Langmuir constant

K_L = Langmuir isotherm constant

Freundlich

$$q_e = K_f C_e^{\frac{1}{n_F}} \quad (7)$$

where:

k_f = Freundlich isotherm constant

n_F = adsorption intensity indicator

Dubinin-Radushkevich

$$q_e = q_D \exp(-B_D \left[RTln\left(1 + \frac{1}{C_e}\right)\right]^2) \quad (8)$$

The mean free energy of sorption, E, was calculated using equation (9).

$$E = \frac{1}{\sqrt{2B_D}} \quad (9)$$

where:

B_D = Dubinin-Radushkevich isotherm constant

q_D = Dubinin-Radushkevich isotherm constant (mol g^{-1})

T = Absolute temperature (°K)

Temkin

$$q_e = \frac{RT}{b_T} ln(A_T C_e) \quad (10)$$

where:

A_T = Temkin isotherm constant

b_T = Temkin isotherm constant

R = Universal gas constant (8.314 J mol^{-1} $°K^{-1}$)

Sips

$$\beta_s \ln(C_e) = -In \left[\frac{k_s}{q_e}\right] + In\,(a_s) \quad (11)$$

where:

a_s = Sips constant

Flory-Huggins

$$\frac{\theta}{C_o} = K_{FH}(1-\theta)^{n_{FH}} \quad (12)$$

where:

K_{FH} = Flory-Huggins isotherm equilibrium constant (L/g)

C_e =Solution phase metal ion concentration at equilibrium ($mol \cdot L^{-1}$)

q_e = Solid phase metal ion concentration at equilibrium ($mol \cdot g^{-1}$)

Error in the isotherm constants was calculated from the linearized form of the model using the SOLVER calculated values using the deviations of the experimental data from this best fit line.

2.7.3 Thermodynamics

The change in enthalpy of the adsorption process was calculated by using the equation below:

$$\Delta G = -RTIn\ K_D \quad (13)$$

where:

R= Universal gas constant (8.314J/mol)

T = Temperature

K_D = Distribution coefficient

2.7.4 Determination of the kinetics of extraction

Batch kinetics was determined by the contact of 1 g of ATLC with 200 mL of aqueous simulant feed. The ATLC and aqueous feed were continuously mixed for a period of 24 hrs at 21 °C and 5 mL samples were extracted at set time intervals. The data was fitted using a linear fit of pseudo first and second order models which do not take into account the mechanism of the reaction.

The Pseudo-first-order kinetic model (Lagergren's rate equation)(Foo & Hameed, 2010) is given as:

$$ln(q_e - q_t) = ln(q_e) - k_1 t \quad (14)$$

where k_1 = pseudo first order reaction constant (hr^{-1}).

The linear form of the pseudo-second-order kinetic model (Yang *et al*., 2014) is as follows:

$$\frac{t}{q_t} = \frac{1}{k_2 {q_e}^2} + \frac{1}{q_e} t \quad (15)$$

where k_2 = pseudo second order reaction constant (hr^{-1}).

The non-linear form for the pseudo second-order kinetics is given below:

$$q_t = \frac{k_2 q_e^2 t}{1 + k_2 q_e t} \quad (16)$$

The non-linear form was fitted using the minimization of the sum of square errors (SSE) using SOLVER (Yang *et al*., 2014). The $t_{1/2}$ was calculated using the relationship:

$$t_{1/2} = \frac{1}{k_2 q_e} \quad (17)$$

The initial sorption rate h_0 (Foo & Hameed, 2010) is given by:

$$h_0 = k {q_e}^2 \quad (18)$$

Film and pore diffusion

$$t_{1/2} = 0.03 \frac{{r_0}^2}{D_p} \quad (19)$$

Where D_p is the pore diffusion coefficient

$$t_{1/2} = 0.23 \frac{r_0 \, \partial}{D_f} \times \frac{\bar{C}}{C} \quad (20)$$

where D_f is the film diffusion coefficient.

The equation (19) was used to calculate the ore and film diffusion coefficient to determine the rate controlling step of the sorption process.

The Boyd model confirms the external mass transfer as the rate limiting step of the sorption process.

Boyd model

$$Bt = -0.4977 - \ln(1-F) \quad (21)$$

Intraparticle diffusion model assumes that the adsorbate diffuses into the interior of the adsorbent and attributes the process to the square root of time ($t^{1/2}$) rather than time (t).

$$q_t = K_{id} t^{1/2} + C \quad (22)$$

where q_t is amount of ions adsorbed at time t (mg/g), K_{id} is the intraparticle diffusion constant ($m/g/min^{1/2}$) and C is the intercept which is a constant related to the thickness of the boundary layer.

2.7.5 Determination of ionic strength

All batch experiments were carried out as single contacts with the contact of 250 mg of 1 mm sieve size ATLC with 50ml of NaCl (0.1 M, 0.5 M and 1 M) and 50 mg/L metal ion solution (50:50 ratio). The ATLC and binary solution were continuously mixed for a period of 24hrs at pH 5 at room temperature (21°C) on a magnetic stirrer. The adsorption uptake capacity and percentage removal were determined using equation (1) and (2) and the concentrations of both metal ions and Na^+ were analysed by the ICP-MS.

2.8 Determination of zeta potential

The electrophoretic mobility technique was conducted to measure the zeta potential by using two different pieces of equipment, a Malvern Zetasizer Nano Instrument and a NanoBrooks ZetaPALS instrument. 0.1% concentration of loofa (>150µm<1mm) in 0.01M/L NaCl aqueous

solution was stirred continuously with a magnetic stirrer. As desired, the pH was adjusted by addition of 0.1M of HCl and 0.1M NaOH over a range of pH 2-10. The pH of the sample solution was measured before each measurement. The samples were loaded into a capillary cell and measurements were performed at room temperature (21^{o}C). All experiments were carried out in triplicate (Kim & Lawler, 2005; Yukselen & Kaya, 2003).

2.9 Column adsorption studies

Fixed bed column studies were carried out using a plastic column of 2.1cm diameter and 15cm length, which was packed with 2g of loofa of varying particle size range between 1 - 2mm. Before the treated loofa (ATLC) was placed in the column, the bottom was layered with a flat cotton wool and glass beads to prevent the loss of any of the loofa and to ensure uniform outflow. A bed height of 5.5cm and a column height of 9cm (15ml column) was used and the solution was introduced into the column by a peristaltic pump (Econo TM Gradient Pump BIO-RAD) at flow rates of 0.5, 1.5 and 2mL/min. The column was first washed with deionised water before loading with the metal ions aqueous solution. The metal ion solutions were loaded in a down-flow mode at flow rates of 2mL/min and 0.5mL/min; and at a concentration of 50mg/L, at pH 5 and at room temperature (21^{o}C). The effluent samples were collected at specific intervals by a Model 2110 Fraction Collector, using 13 x100mm tubes with 9mL capacity which were ¾ full and analysed for residual metal ion concentration by using the ICP-MS. The experimental column set up was terminated when saturation (600ml) of the column was reached (figure 1.2) (Nwabanne & Igbokwe, 2012;Shahidi *et al*., 2016). The breakthrough curve determines the mass transfer zone and it is calculated by plotting a graph of effluent – influent ratios versus time of adsorption.

- Scale –up approach

The following equations were used to calculate the parameters for a pilot plant:

Filtration rate (FR)

$$FR = \frac{Q}{A} \quad (23)$$

where:

Q is the flow rate and A is the cross- sectional area (A) which is calculated as below:

$$A = \frac{\pi d^2}{4} \quad (24)$$

where:

d is the diameter of the column.

Area of the packed column

$$\frac{Q}{FR} \quad (25)$$

Empty bed contact time (EBCT)

$$\tau = \frac{V}{Q} \quad (26)$$

where:

V is the volume of the bed and Q is the flow rate.

Height of the packed column (H)

$$H = \tau \times FR \quad (27)$$

Mass of loofa required

$$M = V \times D \quad (28)$$

where:

D is the packed bed loofa density and V is the volume of the packed bed column calculated as below:

$$V = A \times H \quad (29)$$

where:

H is the height of the column.

q_e measured as

$$q_e = \frac{V_{TC}}{M} \quad (30)$$

where:

M is the mass of the loofa in the pilot column and V_{TC} is the total capacity volume which is calculated as shown below:

$$V_{TC} = V_E \times t \quad (31)$$

where:

V_E is the volume at exhaustion and t is the time to reach exhaustion.

Breakthrough time (B_t)

$$= \frac{A_c}{A_{lr}} \quad (32)$$

where:

A_c is the amount consumed and A_{lr} is the pollutant ion loading rate

Volume of treated effluent

$$= V \times B_t \quad (33)$$

Model kinetic approach was used to investigate the column performance (Okewale *et al*., 2015; Nwabanne, & Igbokwe, 2012) as shown below:

Thomas model

$$\frac{C}{Co} = \frac{1}{1+exp\frac{K_1}{Q}(q_0 M - C_0 V)} \quad (34)$$

The Thomas model predicts that the rate of adsorption is controlled by the surface reaction and ignores the intraparticle mass transfer resistance and the external film resistance.

Yoon-Nelson model

$$\frac{C}{Co} = \frac{1}{1+exp[K(\tau-t)]} \quad (35)$$

where:

C= Effluent solute concentration

Co = Influent solute concentration

K_1/K = rate constant, q_o = maximum solid-phase concentration of the sorbed solute

M = mass of the adsorbent

V = throughput volume

Q = flow rate

τ = Empty bed contact time

The Yoon-Nelson model is based on the assumption that the rate of decrease in the probability of adsorption for each adsorbate molecule is proportional to the probability of adsorbate adsorption and the probability of adsorbate breakthrough on the adsorbent (Nwabanne & Igbokwe, 2012).

These two models of column kinetic approach, were used to analyse the column performance, here the equations represent the non-linear equation. The regression coefficients were used as an indication of fit. The parameter values such as constants were not obtained from the linear plot (using linear equations) because the reason for using the models were not to compare the

experimental parameters to determine which is better and how best one parameter affect the adsorption (as this was set at constant flow rate, bed height etc.) but to determine the performance of the column testing.

2.9.1 Desorption and regeneration

After loading the column with metal ions solution, it was rinsed with deionised water to remove any unbound metal ions and then 0.1M HCl was introduced as an eluent with a down flow through the column at constant flow rate of 1mL/min and by the same procedure as the adsorption process. Once the column was regenerated, it was reused for five adsorption-desorption cycles.

The regeneration efficiency was calculated by using the equation below:

$$RE\% = \frac{q_{rc}}{q_{ac}} X\ 100 \quad (36)$$

where:

q_{rc} (mg/g) is the adsorptive capacity of the regenerated column and q_{ac} (mg/g) is the adsorptive capacity of the adsorbent after each cycle.

2.10 Ion exchange capacity

Step 1: A single contact of 1g of 1mm sieve size loofa was mixed with 100 mL of aqueous solution of 0.1M NaOH using a magnetic stirrer for 24hrs. Then the filtered loofa was rinsed off with deionised water until neutral pH and then contacted with 100ml of aqueous solution of 0.1M HCl and mixed for 24hrs. After which the filtered loofa was used for further batch adsorption experiments.

Step 2: The filtered loofa from step 1 was mixed with 1M NaCl for 24hrs, sufficient time for exchange of ions in the solution. Then the filtrate solution obtained, after the contact time of exchange of ions, was titrated against 0.1M NaOH. The pH was then recorded at each point (Harland, 1994).

CHAPTER THREE

3.0 CHARACTERISATION OF LOOFA

3.1 Introduction

This chapter gives an overview of the characterisation of *Luffa cylindrica* (loofa) used for all experimental analysis. It describes the functional groups, elemental composition, thermal stability, morphology and surface charge at point zero of the loofa. Also, the determination of the surface characteristics, pore size measurements and the reaction of loofa in water is discussed.

3.2 FT-IR spectra

Figure 3.1 shows the FT-IR spectra of treated and untreated loofa. The treated loofa is distinguished between NaOH treated and HCL treated. The predominant functional groups that have been altered, as a result of treatment, and the peak intensities are shown at wavelengths between the ranges of 800 – 1800cm^{-1} and 2600 – 3600cm^{-1}. Figure 3.2 gives a clear depiction of the regions that have been altered after NaOH treatment. This indicates an increase or decrease in the peak intensity. Table 3.1 shows the changes in the percentage transmittance at different regions and their corresponding shift as it occurs at different functional groups after NaOH treatment. A clear depiction of the altered peak intensities after HCl treatment is shown in Figure 3.3. Also, as shown in table 3.1, the depicted values after HCl treatment are shown in Table 3.2. Figure 3.4 shows the difference in the number of scans suitable to obtain an FT-IR spectrum for loofa. The elemental composition of loofa under various conditions is recorded in Table 3.3.

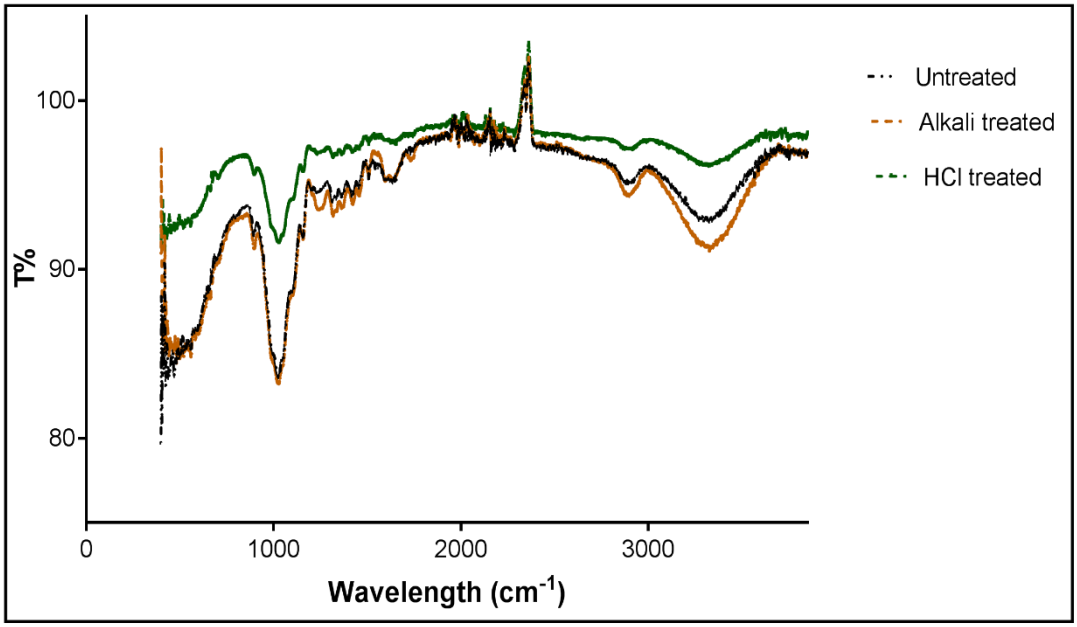

Figure 3.1: FT-IR spectra of 4% NaOH treated, 4% HCl treated and untreated loofa showing T% versus wavelength.

Table 3.1: FTIR spectra results at specific regions of absorbance showing the change in T% and range of wavelength (4% NaOH treated).

Region	ΔT%	Corresponding absorbance
1265cm^{-1}-1460cm^{-} ^{1}(fingerprint region)	+0.6 - +1.1	O-H bending
1735cm^{-1}	+0.6	C-O stretching
2890cm^{-1}	+0.8	C-H stretching
3340cm^{-1}	+1.6	O-H bonding

Table 3.2: FTIR spectra results at specific regions of absorbance showing the change in T% and range of wavelength (4% HCl treated).

Region	ΔT%	Corresponding absorbance
1265cm^{-1}-1460cm^{-1}(fingerprint region)	-8.0	O-H bending
1735cm^{-1}	-2.5	C-O stretching
2895cm^{-1}	-2.0	C-H stretching
3354cm^{-1}	-3.3	O-H bonding

The fingerprint region (this is the region attributed to the unique molecular structure of the lignocellullosic material) assists in identifying the vibrational intensities of the functional groups. As shown in Figure 3.1, prominent IR absorbances occur between 800cm^{-1} and 3600cm^{-1}. Changes in the peak intensity of the adsorption bands, which indicate characteristic functional groups, were observed at various points following the alkali and acid treatment of the loofa. The majority of the characteristic adsorption bands were changed (Table 3.1 and 3.2) (Liu *et al*., 2015). In agreement with previously reported data, a decrease or increase in the peak intensities indicates a change in the binding energy (Boudechiche *et al*., 2016; Saueprasearsit, 2010; Vilar *et al*., 2009; Lasheen *et al*., 2012). A reduction of the peak at 1735cm^{-1} is attributed to the disappearance of the hemicellulose and lignin contents (Jayamani *et al*., 2014). The stretching of hydrogen bonds on the carboxyl groups is shown in the 3400cm^{-1} region (Jayamani *et al*., 2014).

The use of an alkali solution in the treatment of loofa leads to a brighter appearance of the loofa fibers. There was an observed release of a yellow colour into the aqueous solution. This is the breakdown of the lignin molecule attributed to the removal of lignin from the loofa material. The OH^+ ion, which is a strong electrophilic agent, produced from NaOH aqueous solution reacts

with the lignin to aid the process of delignification (Watkins *et al*., 2014; Ghali *et al*., 2011). Also, it has been reported in the literature that the removal of lignin enhances adsorption.

As shown in Figure 3.1, changes in the peak intensity leads to the disappearance of prominent IR absorbances. The effect of HCl treatment shows a band shift from 1033cm^{-1} to 1018cm^{-1} which indicates the disappearance of lignin (Ahmad and Haseeb, 2015). The peak at 3330cm^{-1} shows the presence of carboxyl groups. An increase in the peak intensity with HCl treatment is observed at 1033cm^{-1} and 3354cm^{-1}. This is attributed to C-O stretching and intermolecular and bonded O-H bonds respectively (Williams and Fleming, 2008).

Based on the fingerprint region, the spectra bands represent a cellulosic material. The frequency of the mid rid range region of the FT-IR is indicated by 4000cm^{-1} to 625cm^{-1} and having a frequency $3.8 \times 10^{14} - 1.2 \times 10^{14}$ respectively. However, the change in peak intensities, as a result of shift in the bands, leads to the change in frequency and this attributes to a stronger hydrogen bond with a lower frequency. As compared with the three FT-IR spectra, NaOH treated loofa (Figure 3.1) has the lowest frequency (3313cm^{-1}) when compared to HCl treated and untreated loofa. The strong hydrogen bonds give rise to strong adsorption (Banerjee and Chattopadhyaya, 2013; Agrawal, 2014).

The characterisation of loofa shows that dominant functional groups have been altered and this change has an effect on the adsorption mechanism.

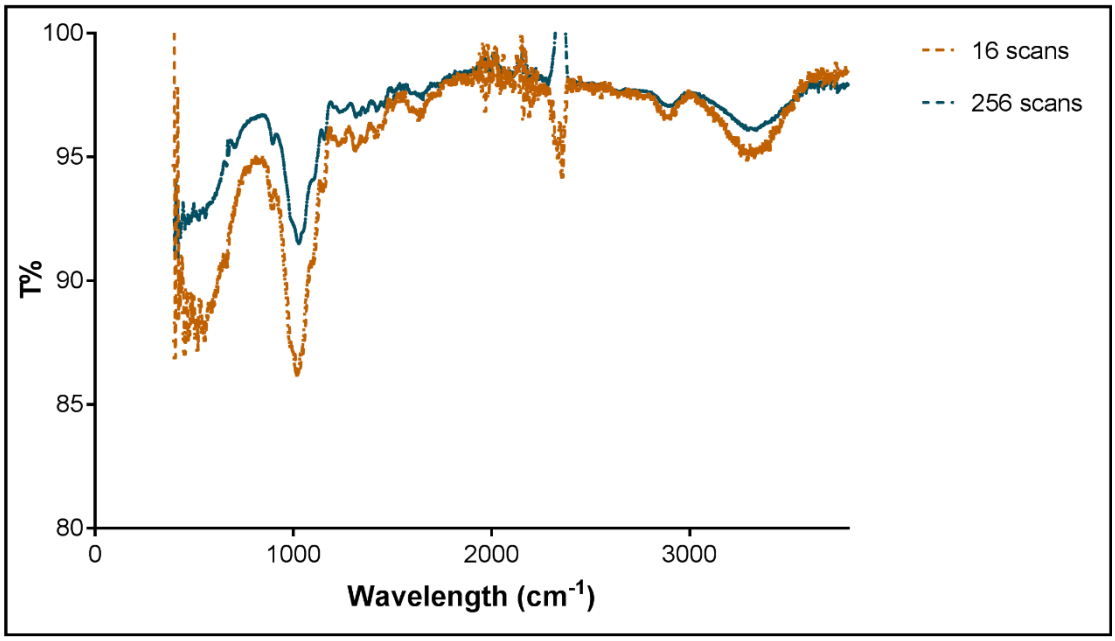

Figure 3.2: Difference in the scan numbers utilised for FT-IR analysis of HCl treated loofa.

The scan number and resolution factor of the FT-IR can be altered in the analysis. The multiple scan numbers required to analyse the loofa sample are averaged. The more the scan numbers the closer the value to actual value. However, there is a slight difference in the FT-IR spectra that occurs as regards to scan numbers as shown in Figure 3.2.

In Figure 3.2, smoother line graphs are shown at 256 scans than at 16 scans of the FT-IR analysis spectrum. The more number of scans gives a value that is closer to the expected value as this is an averaged value. The prominent functional groups found between 800 – 1000cm^{-1} and 3000 – 3400cm^{-1} can be seen to have a well-defined peak at both 16 and 256 scans (Tullin and Amand, 2000). Also, at 2350cm^{-1}, a strong band of CO_2 is observed, the single-to-noise ratio (SNR) is improved when averaging the larger scan number of 256. Therefore, a 16 scans FT-IR analysis was also sufficient for the loofa samples because the dominant functional groups (adsorption peaks) of the *Luffa cylindrica*, were observed under this number of experimental scans. The functional groups on the loofa indicate its elemental composition.

3.3 CHNS analysis

CHNS analysis shows the presence of carbon and hydrogen with no detectable presence of nitrogen and sulphur. Table 3 shows the loofa to be mainly composed of carbon, hydrogen and oxygen. This is known to be the main composition of lignocellulose materials as reported by previous researchers (Leyva-Ramos *et al*., 2005).

The amount of carbon in the loofa decreased from 43.80% to 42.97% when treated with 4% NaOH. Hydrogen, on the other hand, increased from 6.32% to 6.54%. For HCl treated loofa, the carbon content increased to 43.89% with also an increase in the hydrogen content by 0.96%. The highest amount of carbon was for HCl treated loofa followed by ion exchange capacity loofa. This exchange of hydrogen ions on the loofa showed a decrease in the hydrogen ion content from 6.19% to 3.68% and an increase in the amount of carbon from 43.1% to 43.8%. However, this confirms the presence of cellulose with a range of 40 - 44% carbon content (Suhas *et al*., 2016). A change in the amount of oxygen had occurred, this is known to alter the adsorption process as it is known that the surface characteristics of loofa is based on the functional groups present (Bach, 2007). The composition of loofa in weight percentage under different conditions are shown in Table 3.3 below:

Table 3.3: Elemental composition of treated and untreated loofa

Luffa cylindrica	Carbon %	Hydrogen %	Oxygen %	O/C ratio
Untreated	43.10	6.19	50.71	1.18
NaOH treated	42.97	6.54	50.49	1.18
HCL treated	43.89	6.25	49.85	1.14
IEX-HCL	43.79	3.68	52.53	1.20

Table 3.3 shows that the same O/C ratio was found on both the untreated and NaOH treated loofa. The lowest amount was for the HCl treated loofa. All forms of loofa had over 40% of carbon content, which is expected for carbonaceous materials (usually ranging from 40 to 90%) and which are highly porous and possess an extended inter particulate surface area that aids adsorption (Altenor *et al*., 2009; Ali *et al*., 2012). However, the highest amount of hydrogen content was found in the NaOH treated loofa which aids in the exchange of cations for a better adsorption mechanism. As compared to untreated loofa, NaOH treated loofa shows a 0.3% decrease in the carbon content having a higher surface area (Correa *et al*., 2017). This shows the importance of the surface characteristics of the loofa in the adsorption process.

3.4 SEM analysis

The structural surface of the loofa before and after treatment was analysed by the scanning electron microscope. The morphology of the untreated loofa as shown in figure 3.5 appears dry and flaky with many loose particles on the surface. The morphology of the NaOH treated loofa, on the other hand, appeared to be broken up with few loose particles on the surface. This may be as a result of exposure of the pores for further adsorption (Ghali *et al*., 2009; Merdan *et al*., 2012; Lindino *et al*., 2014).

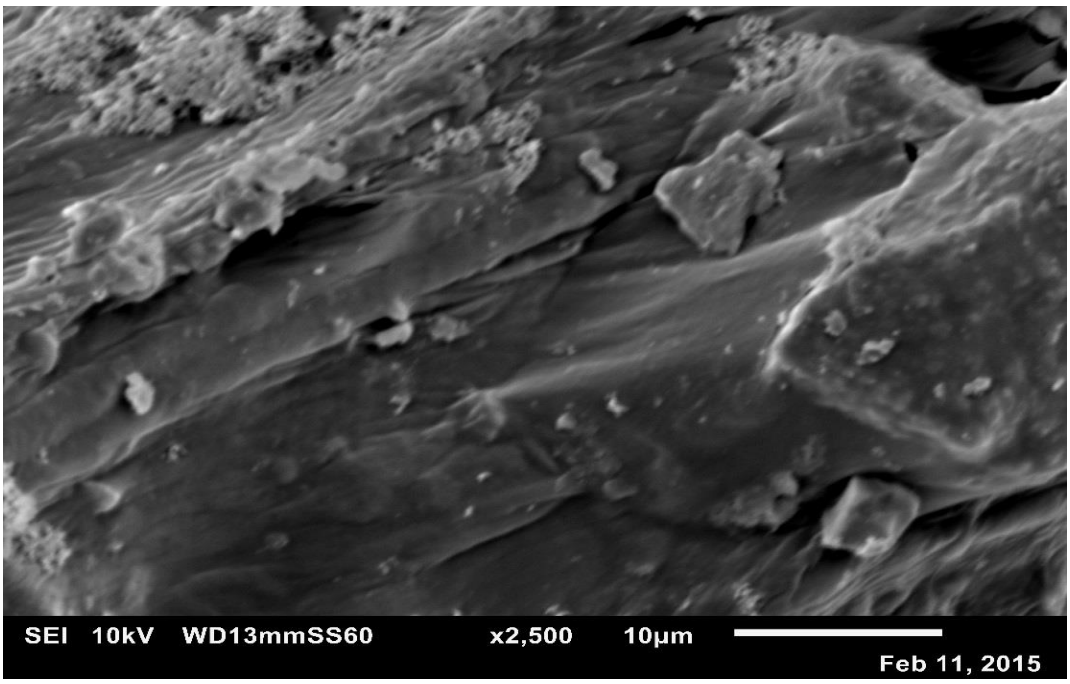

Figure 3.3: Surface morphology of untreated loofa (raw loofa)

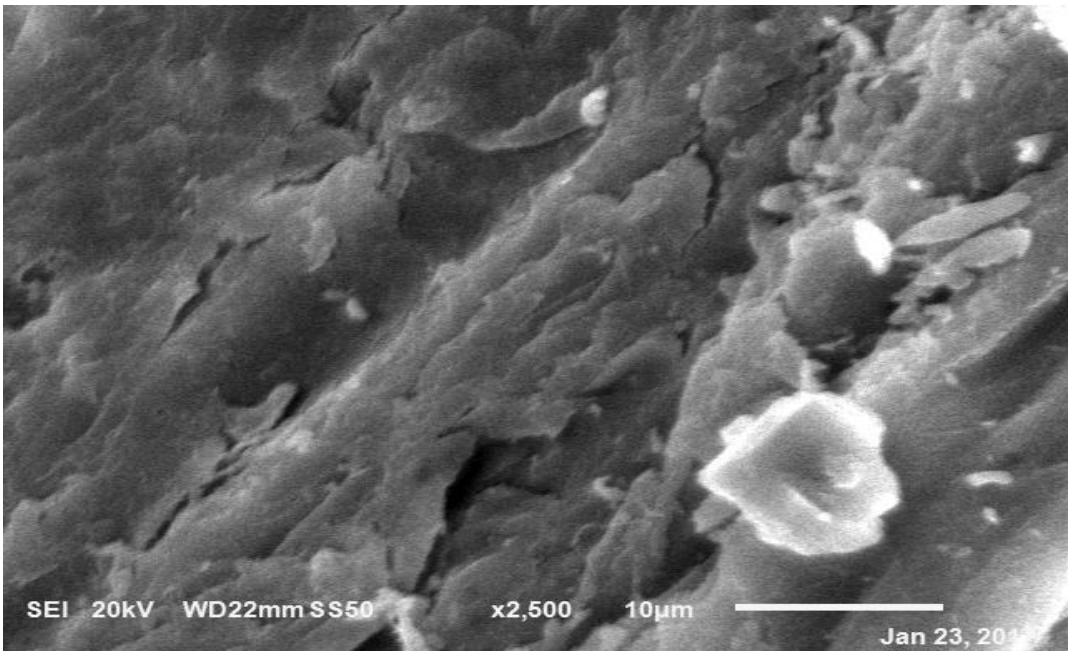

Figure 3.4: Surface morphology of treated loofa (4% NaOH).

Figures 3.3 and 3.4 show the modification of the surface morphology and change in characteristics of the loofa. A layered surface is observed after treatment for possible penetration and improvement in the adhesion capacity. However, alkali treatment of fibers is known to increase moisture uptake (Ghali *et al*., 2011). Apart from the surface characteristics,

the presence of charged functional groups can aid adsorption as a result of electrostatic interactions.

3.5 pHpzc values

The salt addition method was used to obtain the pHpzc values. Altenor *et al*. (2009) used the salt addition method for particle size ranging from 0.4 – 1mm**.** Mahmood *et al*. (2011), compared the salt addition method to other methods such as mass titration and fast titration and found it to be close in detection range. As compared to other methods used by previous researchers, the salt addition method has been successfully used to determine the pHpzc. The pHpzc, which is the point of intersection of graph plot ΔpH versus initial pH, was at approximately pH 6.1 for untreated loofa and pH 7.2 for the alkali treated loofa (figure 3.5 & 3.6). At a lower pH than the pH_{pzc}, the surface is predominantly positive charged and at a higher pH than pH_{pzc}, the surface is negatively charged. Such a situation determines the effect of electrostatic attraction between the adsorbate species and the adsorbent surface charge (Iqbal *et al*., 2009; Altenor *et al*., 2009; Mahmood *et al*., 2011; Esan *et al*., 2014; Khosravi *et al*., 2014).

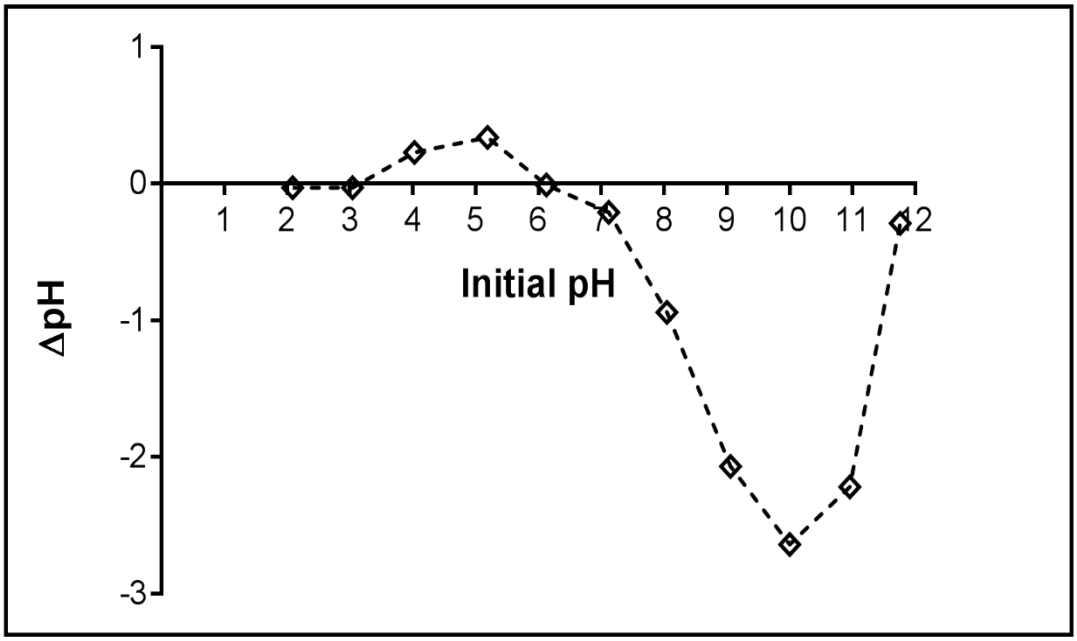

Figure 3.5: Plot of the determination of the pHpzc of untreated loofa

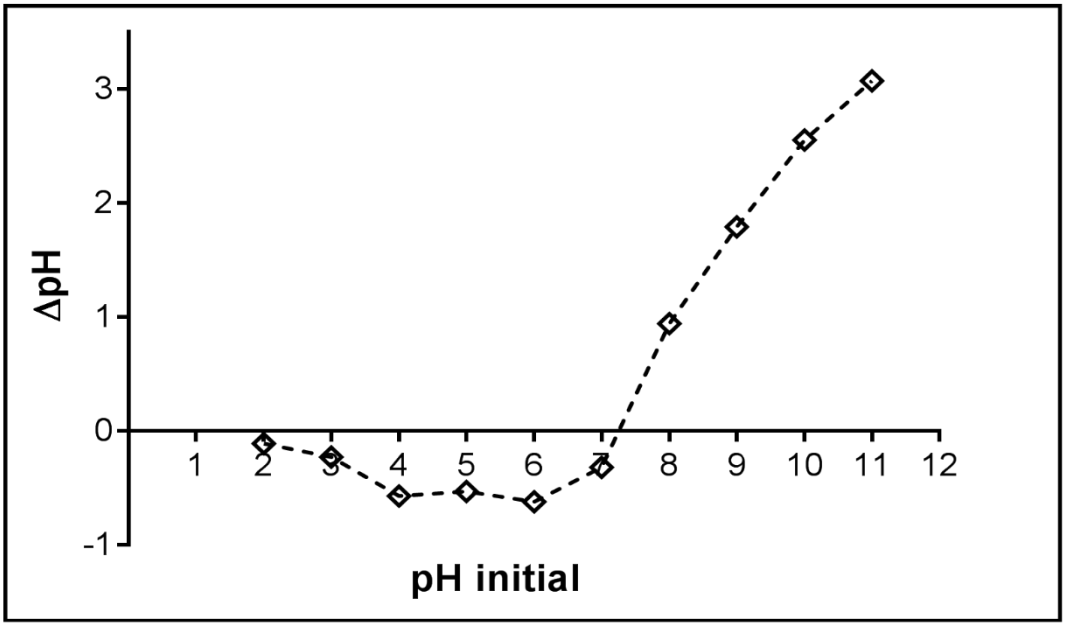

Figure 3.6: Plot of the determination of the pHpzc of alkali treated loofa

3.6 Zeta potential of loofa

The zeta potential determines the surface charge on the loofa. The dissociation of the carboxyl groups on the loofa, when dispersed in water, gives an overall negative charge on the loofa

surface. The change in the pH will determine its effect on the zeta potential. For the zeta potential (ζ) experimental analysis, the solution pH was altered at different points to determine a ζ at a range of pH values. When the pH is low, it tends to cause the colloids in the system to coagulate and form more visible particles in solution (Kim & Lawler, 2005).

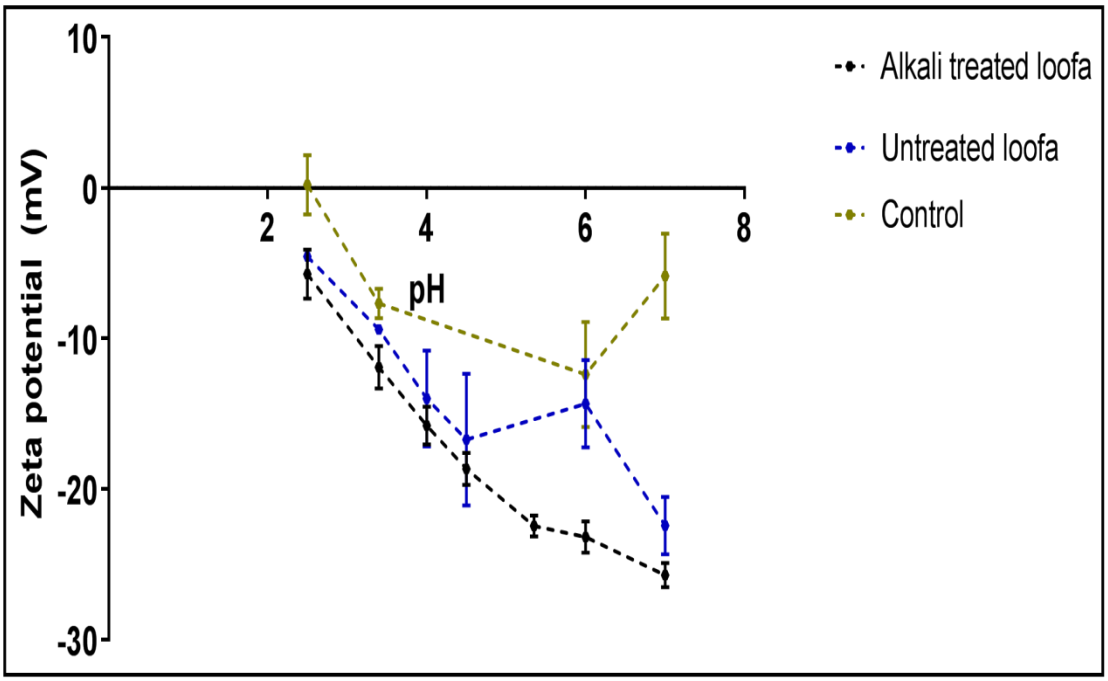

Figure 3.7: The mean zeta potential of untreated and alkali treated loofa under constant ionic strength (10mM): Effect of pH change (ZetaPALS instrument). Data from 3 replicate measurements.

Figure 3.7 shows a decrease in the zeta potential when the loofa was alkali treated. The magnitude of the negative zeta potential of the alkali treated loofa increases as pH increases, which suggests a potential stability for metal ion adsorption. This change is explained by the change in the loofa structure after modification (Stana-Kleinschek *et al*., 2002; Adewuyi & Pereira, 2017). Figure 3.8, analysed by a different instrument, also shows a decrease in the zeta potential of loofa when alkali treated. It supports the results described in figure 3.7, that depicts a negatively charged loofa surface.

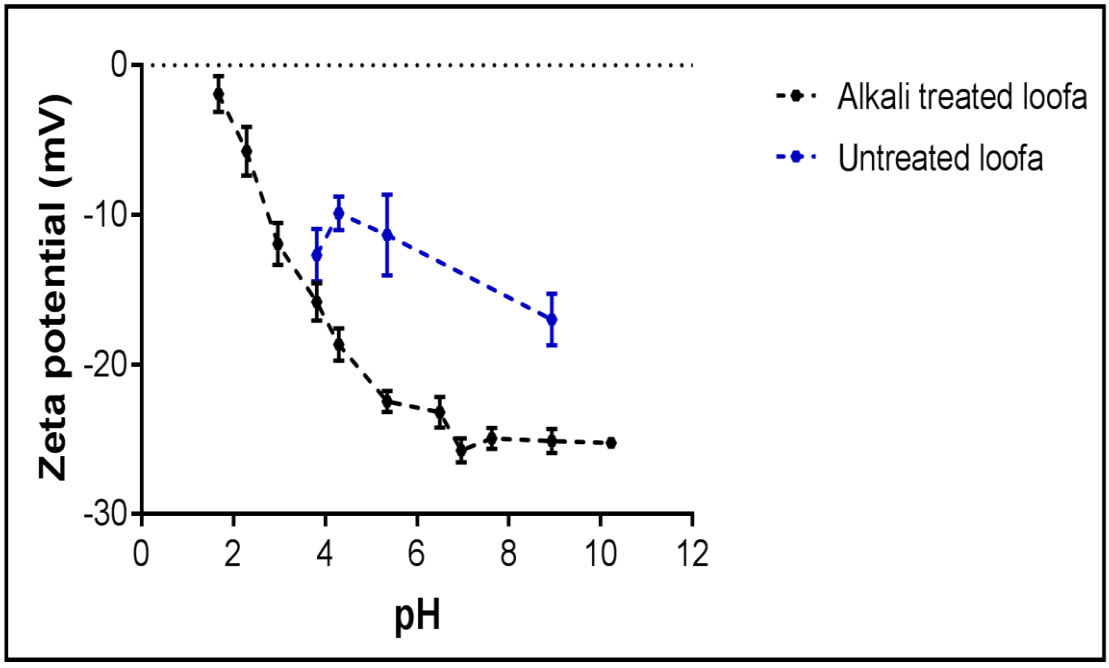

Figure 3.8: The mean zeta potential of untreated and alkali treated loofa under constant ionic strength (10mM): Effect of pH change (Malvern instrument). Data from 3 replicate measurements.

A negative charge on the surface of a cellulose material occurs when it is dissolved in aqueous solution. The positivity and negativity of a surface charge depends on the solution pH. The isoelectric point occurs when the net charge of the particles is zero (Kim & Lawler, 2005). However, an isoelectric point was not observed (Figure 3.7 & 3.8). The zeta potential values are lowered once protonation occurs. This shows that the pH has a great impact on the zeta potential (Smith *et al*., 2017). The homogeneity of the loofa in the aqueous solution is difficult to obtain but the validity of the results as compared to the control shows that loofa particles of nano sizes were not dissolved in the solution prior to analysis. Stana-Kleinschek *et al*. (2002) reported the use of the streaming potential technique to determine the zeta potential measurements of cellulosic materials. Although a different technique, electrophoretic mobility technique, was used in this analysis, the results were similar to the effect caused by the changes in solution pH on the zeta potential measurements (Stana-Kleinschek *et al*., 2002) .

3.7 Pore size distribution of loofa

This gives the total surface area of the loofa based on the mass covered by the analysis of the sample. The pore size distribution was measured from the values obtained and the presence of mesopores, micropores and macropores were determined (Figure 3.9 – 3.13). The TGA curve analysis is described in Figure 3.14 and the weight loss percentage based on the thermal degradation process of loofa is shown in Table 3.4. Further information of loofa in aqueous solution is explained.

3.8 BET results

Several methods were utilised for the BET analysis technique but a suitable method that gave the most consistent surface area results was adopted. The temperatures and degassing time interval and the resulting BET specific surface area determined are shown in Table 3.4.

The BET surface area is explained as the surface area per gram of loofa, therefore, the specific surface area of loofa was calculated by dividing by the mass of loofa utilised. This was done to determine the actual surface area of the loofa used for analysis. Further calculations were done to determine the BET specific area of loofa utilised in further experiments.

Table 3.4: Temperature and degassing time interval for BET surface area measurements on 4% NaOH treated loofa.

Time interval	*1hr*	*2hrs*	*24hrs*	
Temperature	*40°C*	*120°C*	*120°C*	*150°C*
BET surface area	*14.322m²/g*	*32.647m²/g*	*20.644m²/g*	*43.096m²/g*
BET specific surface area	*4.324m²*	*4.463m²*	*4.992m²*	*6.995m²*

The temperatures, degassing time intervals, and the resulting BET specific surface area determined are shown in Table 3.4. However, increasing the temperature too much will degrade the material and at a 180^{o}C, it was noticed that the loofa had turned from yellowish brown to light brown, indicating some degradation. The maximum temperature was therefore set at 150^{o}C at 24hrs.

The BET analysis was performed on an untreated loofa sample mass 0.227g to give a BET surface area of 25.322m^2/g. Specific BET surface area was calculated to be 5.748m^2. For the NaOH treated loofa of mass 0.162g, a BET surface area of 43.096m^2/g was determined and the BET specific surface area calculated at 6.995m^2. The HCl treated loofa sample of mass 0.235g, had a BET surface area of 27.465m^2/g and a calculated specific BET surface area of 6.454m^2. The BET analysis was carried out on approximately 0.2g of loofa (under all three conditions).

Table 3.5: BET surface area and total pore volume of the untreated and treated loofa.

Data	*Untreated*	*NaOH treated*	*HCl treated*
BET surface area	*25.322m^2/g*	*43.096m^2/g*	*27.465m^2/g*
BET specific surface area	*5.748m^2*	*6.995m^2*	*6.454m^2*
Total pore volume	*0.012cm^3/g*	*0.017cm^3/g*	*0.012cm^3/g*
Δ in pore volume (at 2nm)	*0%*	*33.0%*	*8.9%*

Specific BET surface area for both untreated and treated loofa are low which attributes to a small number of macroporous structures present on the surface of the loofa (Oboh *et al*., 2013;Oboh

et al., 2016). The surface characteristics of the NaOH treated loofa at a specific BET surface area of 6.982m^2 was higher than the untreated at 5.748m^2. The HCl treated loofa has a specific BET surface area at 6.454m^2, which is higher than the untreated loofa but lower than the NaOH treated loofa. There was a change in the specific surface area of NaOH treated loofa which shows a 21.5% increase as compared to HCl treated loofa with a 12.3% surface area increase (Feng and Guo, 2012; Gimenez *et al*., 2014). The largest BET surface area was attributed to the NaOH treated loofa.

The adsorption potential pressure increase is shown in Figure 3.11 (quantity absorbed versus relative pressure for untreated loofa) and the formation of monolayer adsorption is observed. The monolayer adsorption is between the range of 0.05 – 0.3 p/p^0. A multilayer formation occurs above a pressure range of over 0.3.

The external surface area at 36.61m^2/g indicates the area where multilayer occurs and a volume of mesopores are present, which shows the absence of micropores, indicated by a negative value. The micropores had been filled at a p/p^o range below 0.3, therefore the micropores did not contribute to further multilayer adsorption (Shields *et al*., 2004). The external surface area for HCl treated and NaOH treated loofa is 34.765m^2/g and 50.930m^2/g respectively. Shown in the data analysed, the volume of micropores present in the external surface area, of both treated loofa, are represented by a negative value. This means that the micropores had been filled up at this stage of adsorption and was not involved in the further multilayer adsorption. A similar plot of the adsorption isotherm of the untreated loofa shown in Figure 3.9 is reported for NaOH and HCl treated loofa (Figures 3.10 & 3.11).

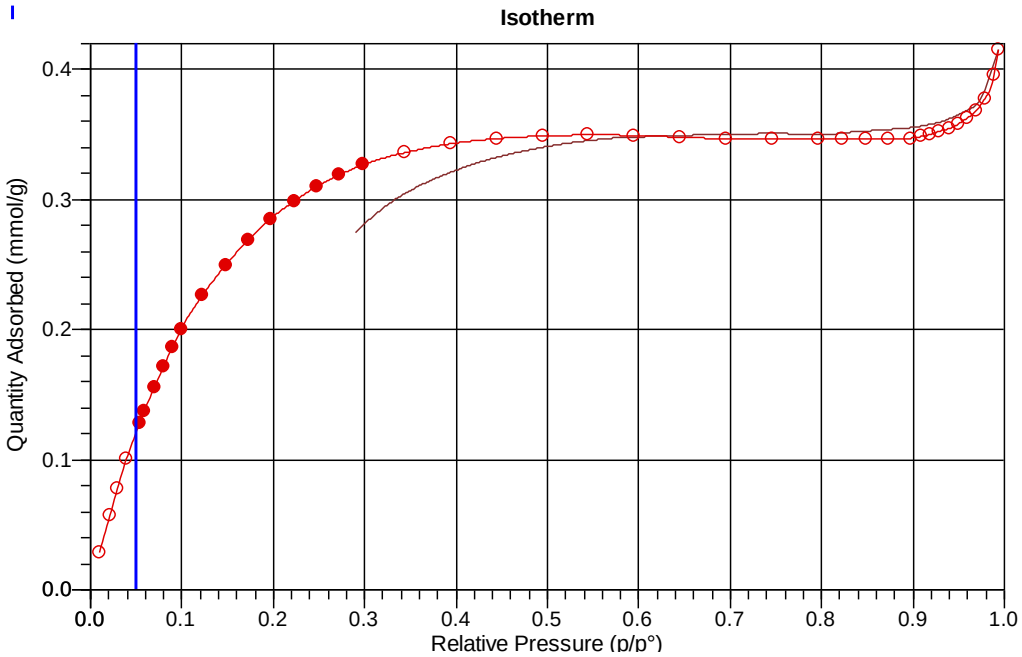

Figure 3.9: Adsorption isotherm of untreated loofa showing the quantity absorbed onto the pores versus the relative pressure (Monolayer complete adsorption between 0.05 – 0.3).

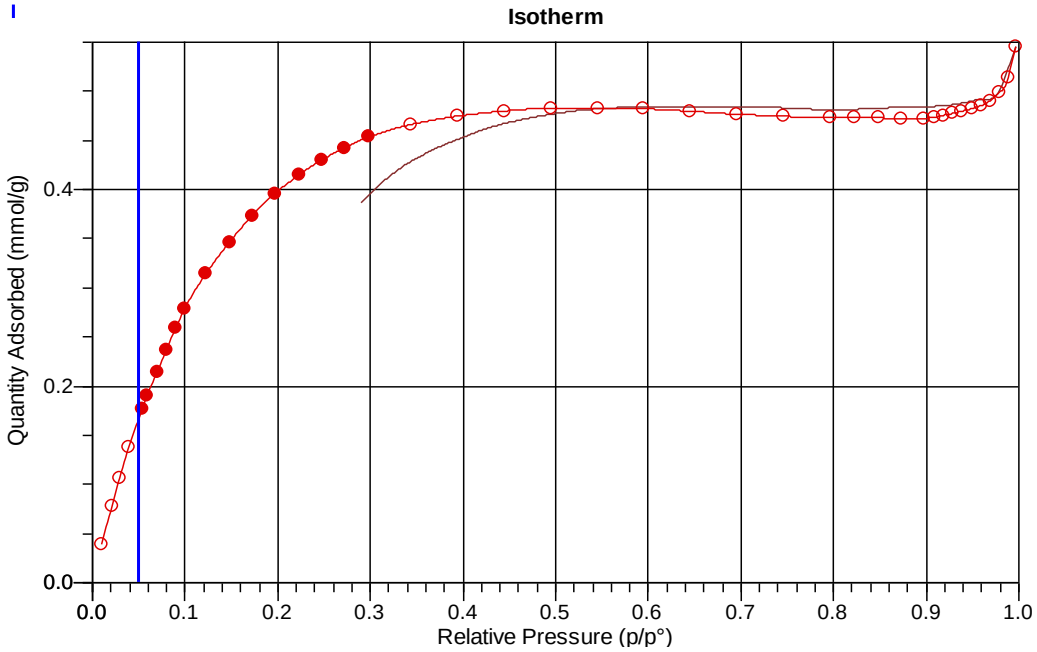

Figure 3.10: Adsorption isotherm of NaOH treated loofa showing the quantity absorbed onto the pores versus the relative pressure (Monolayer complete adsorption between 0.05 – 0.3)

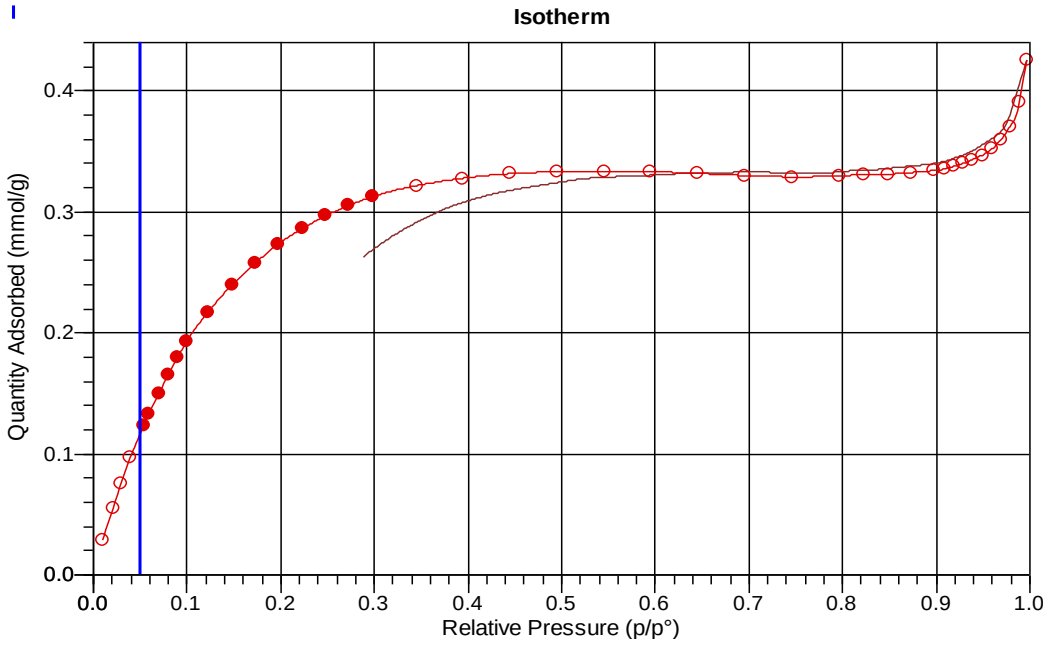

Figure 3.11: Adsorption isotherm of HCl treated loofa showing the quantity absorbed onto the pores versus the relative pressure (Monolayer complete adsorption between 0.05 – 0.3).

The difference in the nitrogen adsorption capacity at a single point pressure of 0.3 can be seen in Figures 3.9, 3.10 & 3.11. The highest adsorption capacity is 0.442mmol/g for NaOH

treated loofa which means that there is a higher number of adsorption surface sites present on the NaOH treated loofa than in the untreated or HCl treated loofa.

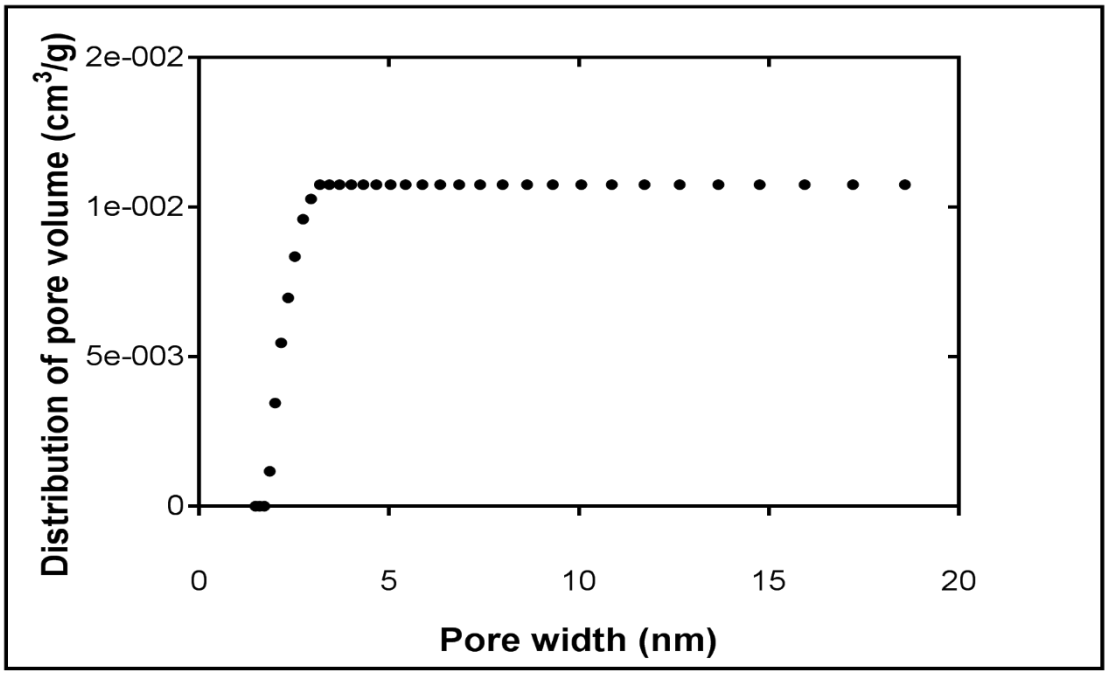

Figure 3.12: The distribution of pore volume in untreated loofa.

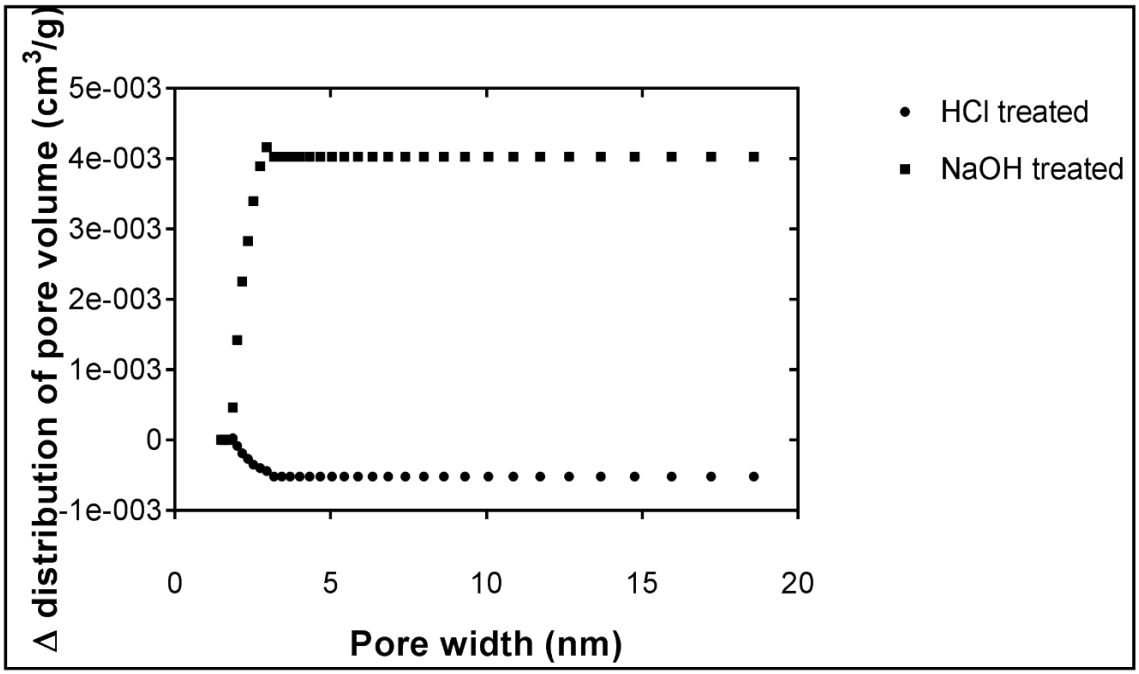

Figure 3.13: The difference in the distribution of pore volume between NaOH and HCl treated loofa with reference to the untreated loofa.

A change in the pore volume between the range of 0.7 – 20 nm attributes to the presence of micropores and mesopores for the loofa (Occelli *et al*., 2003; Pavan *et al*., 2008). BJH adsorption cumulative volume of pores between 10 -70nm and the BJH desorption cumulative volume of pores between 5- 50nm show the presence of mesopores. Figure 3.13 shows a decrease in the pore volume for HCl treated loofa, as compared to the untreated loofa, and when compared to NaOH treated loofa. The loss of pore volume may be a result of hydrogen ions deposited on the pore walls. For the NaOH treated loofa, an increase in the pore volume, as compared to the untreated loofa, was observed. The increase in pore volume is attributed to the collapse of larger mesopores, thereby creating available pores in the loofa for possible adsorption (Occelli *et al*., 2003).

Table 3.5 shows the values of BET surface area, total pore volume and percentage change in the pore volume at an average pore size of 2nm for untreated, NaOH and HCl treated loofa (control material – untreated loofa).

Alkali treatment shows a higher crystallinity index of loofa fibres. Its modification with 4% NaOH bestows additional functionality of OH^- groups added onto the surface area of the loofa (Ghali *et al*., 2009 ; Saueprasearsit *et al*., 2010; Tong *et al*., 2014). The BET results indicate an enhancement in the crystalline structure of treated loofa and the highest enhancement is observed in the NaOH treated loofa, thereby leading to a better adsorptive capacity.

The pore size distribution shown in Tables 3.6 and 3.7 indicates the effect of varying treatment methods on the pore dimensions of the loofa. Tables 3.6 and 3.7 also highlight a predominantly mesoporous structure.

Table 3.6: Pore volume distribution found under different treatment conditions of the loofa.

Untreated loofa	***Description***	***Result***
BJH adsorption cumulative volume	*Pore width range 4 - 100nm*	*0.0010cm^3/g*
BJH desorption cumulative volume	*Pore width range 4 – 100nm*	*0.0022cm^3/g*
NaOH treated loofa	***Description***	***Result***
BJH adsorption cumulative volume	*Pore width range 4 - 100nm*	*0.0007cm^3/g*
BJH desorption cumulative volume	*Pore width range 4 – 100nm*	*0.0014cm^3/g*
HCl treated loofa	***Description***	***Result***
BJH adsorption cumulative volume	*Pore width range 4 - 100nm*	*0.0014cm^3/g*
BJH desorption cumulative volume	*Pore width range 4 – 100nm*	*0.0027cm^3/g*

Table 3.7: Pore size distribution under measurements of different treatment conditions of loofa.

Untreated loofa	***Description***	***Result***
BJH adsorption average pore width	*By 4V/A. Adsorption cumulative pore surface area*	*39.86nm*
BJH desorption average pore width	*By 4V/A. Desorption cumulative pore surface are*	*11.52nm*
NaOH treated loofa	***Description***	***Result***
BJH adsorption average pore width	*By 4V/A. Adsorption cumulative pore surface area*	*35.31nm*
BJH desorption average pore width	*By 4V/A. Desorption cumulative pore surface are*	*15.76nm*
HCl treated loofa	***Description***	***Results***
BJH adsorption average pore width	*By 4V/A. Adsorption cumulative pore surface area*	*33.40nm*

BJH desorption average pore width	*By 4V/A. Desorption cumulative pore surface are*	*14.56nm*

3.9 TGA analysis

The TGA (ThermoGravimetric Analysis) curve reveals the mass loss percentage of the loofa *(Luffa cylindrica*) with temperature. The three stages of the thermal degradation that occur are shown in Figure 3.14, the initial stage is attributed to water loss via evaporation, the second stage is the degradation of the components of the loofa and final stage is where the degraded volatile products and gaseous products formed are removed. This degradation process as seen by the TGA curve is in agreement with literature (Saw *et al*., 2013; Watkins *et al*., 2014; Tanobe *et al*., 2014 **;** Jayamani *et al*., 2014; Amali *et al*., 2014; Ali *et al*., 2016 ; Parida *et al*., 2016). A homogeneous pattern during thermal decomposition is observed in all three conditions of the loofa (similar profile). It can be seen in Figure 3.14, that there is approximately a 4.5% loss of mass for untreated, 7% for NaOH treated and 5% for HCl treated loofa between 200 - 400^{o}C. The huge weight loss that is measured between 250 to 420^{o}C corresponds to degradation of amorphous cellulose and this is about 75% of the total weight of loofa. The thermal decomposition of cellulose for the untreated loofa occurred at 388^{o}C as compared to both treated loofa at a temperature range of 410^{o}C to 420^{o}C. This shows an increase the thermal stability indicating a higher temperature required for both treated loofa. This temperature shift is due to the alkali and acid treatment. Table 3.8 shows the thermal degradation of each sample within the temperature range of 40^{o}C to 800^{o}C.

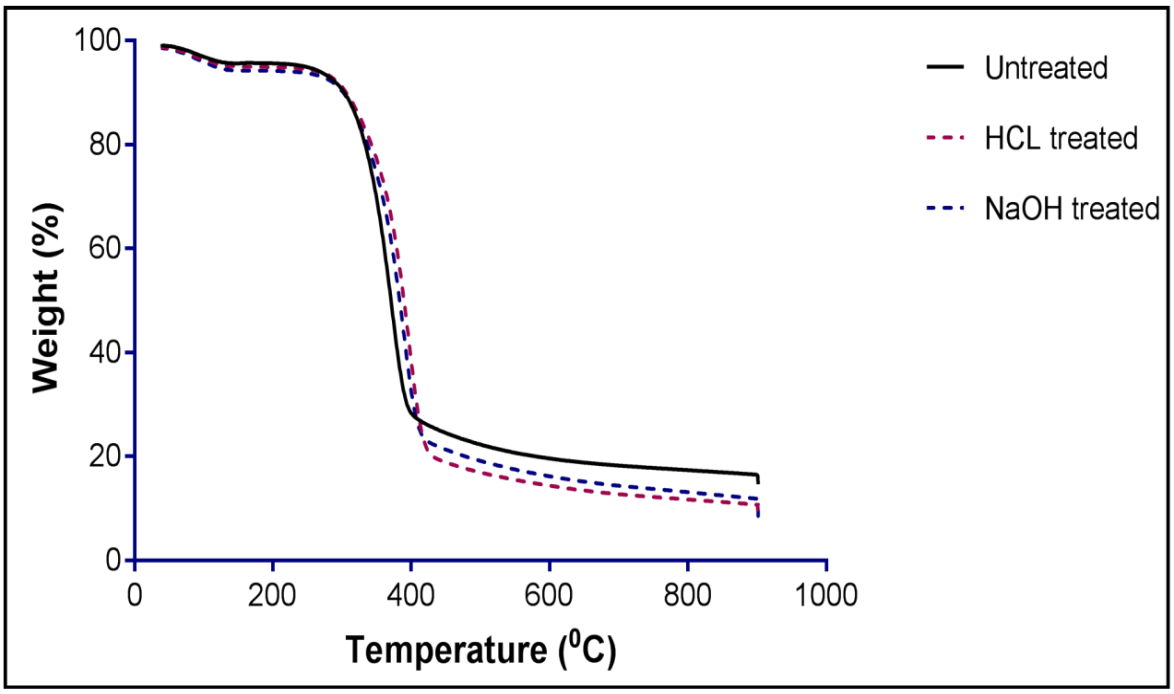

Figure 3.14: TGA curve of untreated and treated loofa under nitrogen atmosphere at 50°C/min.

Table 3.8: Percentage loss after TGA analysis of loofa under different conditions in the temperature range of 40 – 800°C.
(Initial stage – 40 – 200°C; Second stage – 250 -450°C; Final stage – 450 – 900°C).

	Weight loss (%)		
Samples	Initial stage	Second stage	Final stage
Untreated	4.5	70	9
NaOH treated	7.0	72	10
HCl treated	5.0	74	11.5

NaOH treated loofa has the highest percentage weight loss due to less water being evaporated. This shows that a lower quantity of water was retained during the treatment process. Due to a reduced ability of the loofa to absorb water molecules from the surrounding environment, a lower percentage of water loss/ higher percentage of mass loss is seen in both treated loofa as compared to untreated loofa (Jayamani *et al.*, 2014).

A change in the sample composition shows a slight increase in temperature needed to decompose the loofa cellulose material in the range of 250-450^{o}C. This is explained by a higher crystalline structure indicating the absence of more non-cellulosic materials. At the final stage of thermal degradation, a range of 9 – 12% weight loss is shown for all three conditions of the loofa and a higher thermal stability was shown for both treated loofa (Ouajai & Shanks, 2005).

3.10 LFC in aqueous – water effect

Loofa has a highly polar character that is hydrophilic in nature. In the development of a durable composite adsorbent material, the high moisture adsorption and swelling of the loofa fibers is a major restriction and could act as a hindrance in optimum technological use (Bismarck *et al*., 2002). However, loofa does not rot after months of being in contact with aqueous solutions (wet state). Most of the adsorbed water in the loofa can be removed by drying in an oven at 90^{o}C after 24h prior to use in the adsorption studies. The water uptake capacity was measured at 0.04% (equation 1). The water uptake capacity is in competition with the accessibility of the ζ - potential to the surface functional groups present on the loofa**.** However, the more hydrophobic the solid surface of the loofa becomes, as a result of the exposure to the functional groups, the less hydrophilic sites are available therefore the less favourable the water adsorption factor affects the adsorption mechanism (Bismarck *et al*., 2002).

CHAPTER FOUR

4.0 LEAD ADSORPTION MECHANISM

4.1 Introduction

This chapter describes the effect of different experimental conditions on the adsorption of lead ions onto *Luffa cylindrica* (loofa). The batch experiment results obtained when changes in pH, initial lead ion concentration, loofa dosage, temperature and ionic strength on the biosorption of lead were investigated, are reported in section 4.2. The Pb^{2+} speciation diagram, kinetic and isotherm models used to investigate the biosorption of lead ions by loofa are also discussed in this chapter. This covers the mechanism of adsorption and how the effect of the varying experimental conditions alters the adsorption process.

4.2 Batch experiments

4.2.1 pH effect

Lead uptake increases with pH. Using equations (1) and (2) (Chapter two), the trend effect of pH is shown in Figures 4.1, 4.2, 4.3 and 4.4. The speciation diagram is shown in Figure 4.5. Figure 4.6 gives FT-IR spectra comparison between NaOH treated loofa without Pb and Pb-loaded loofa at pH 5 and pH 6. The effect of the calculated Sips constant from equation (9) (Chapter two) to change in pH is shown in Figure 4.7. Figure 4.8 shows the distribution ratio obtained at different pH values. Figure 4.9 shows the difference in pH at equilibrium compared to the initial pH.

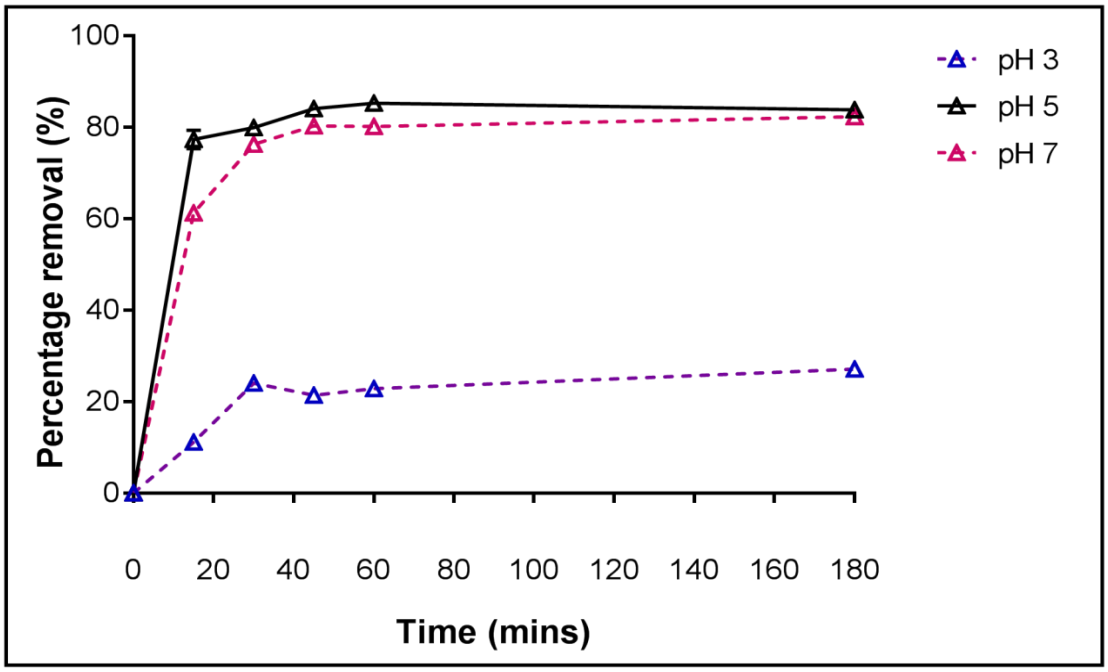

Figure 4.1: Percentage removal of lead ions with change in time after 3hrs at pH range 3-7; lead ion concentration: 50mg/L; agitation speed: 200rpm; at 21°C, 3h contact time, 5g/L dosage of alkali treated loofa. Data from 3 replicate measurements.

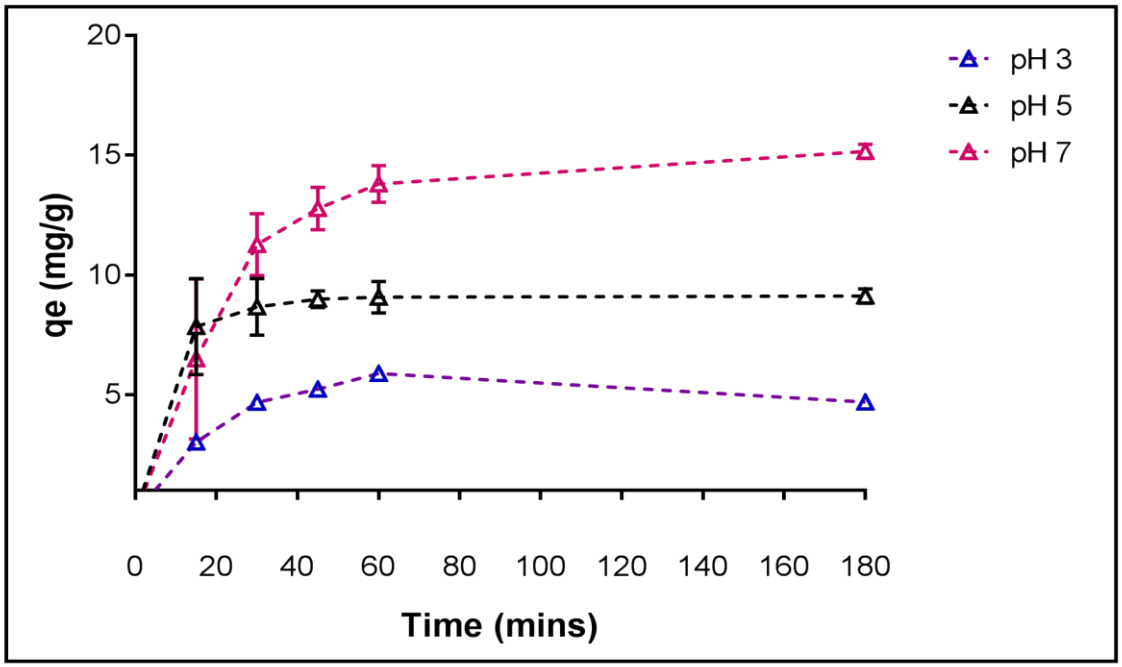

Figure 4.2: Uptake capacity of lead ions with change in time after 3hrs at pH range 3-7; lead ion concentration: 50mg/L; agitation speed: 200rpm; at 21°C, 3h contact time, 5g/L dosage of untreated loofa. Data from 3 replicate measurements.

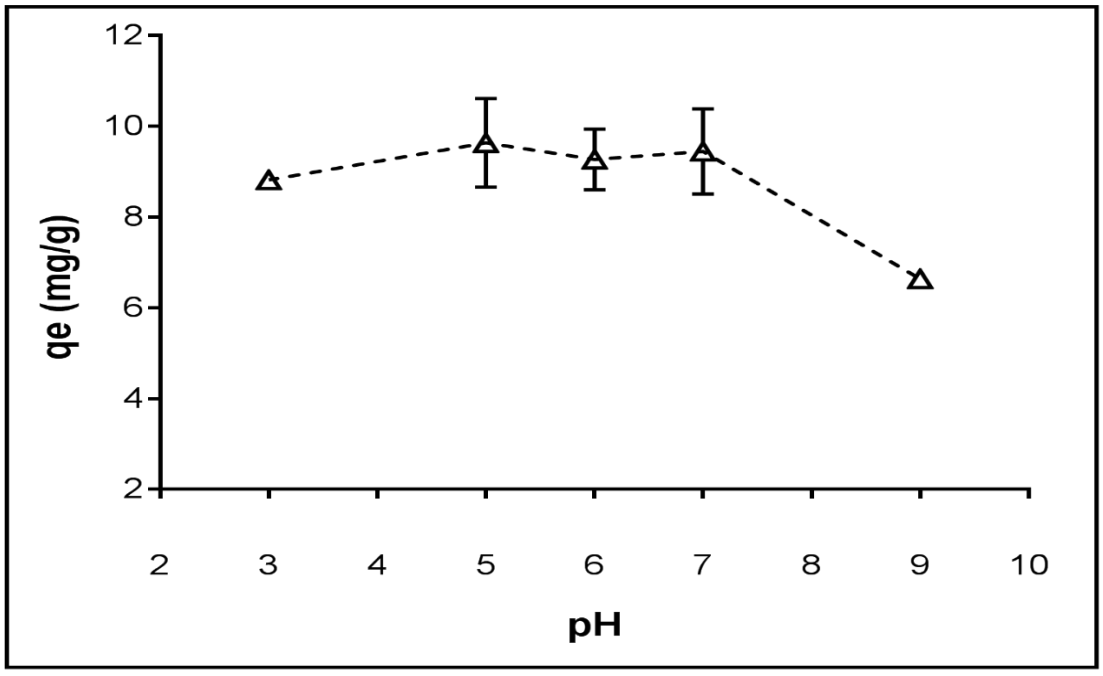

Figure 4.3: Uptake capacity of lead ions with change in pH after 24hrs; lead ion concentration: 50mg/L; agitation speed: 200rpm; at 21°C, 24h contact time, 5g/L dosage of alkali treated loofa. Data from 3 replicate measurements.

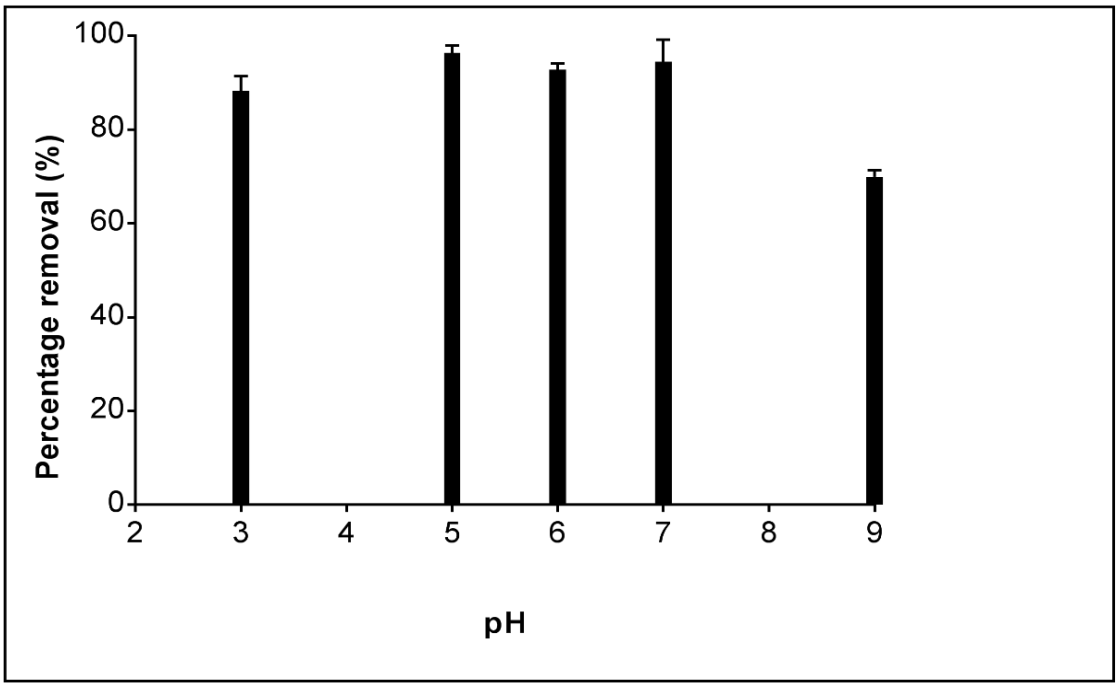

Figure 4.4: Percentage removal of lead ions with change in pH after 24hrs at pH range 3-9; lead ion concentration: 50mg/L; agitation speed: 200rpm; at 21^{o}C, 24h contact time, 5g/L dosage of alkali treated loofa. Data from 3 replicate measurements.

At low pH the weakly acidic nature of the active sites and the competition of hydrogen ions with the lead gives an 8.8mg/g uptake capacity but as deprotonation occurs and as the pH increases to 5, the uptake capacity increases by 9.2% with 96.4% lead ion removal to 9.6mg/g. Further pH increase leads to a reduction in the uptake capacity. As shown in Figure 4.4, the percentage removal decreased by 26.5% when the pH increased to pH 9 due to the hydroxylation of the lead ions in aqueous solution (Pagnanelli *et al*., 2003; Saeed *et al*., 2009; Fan *et al*., 2014).

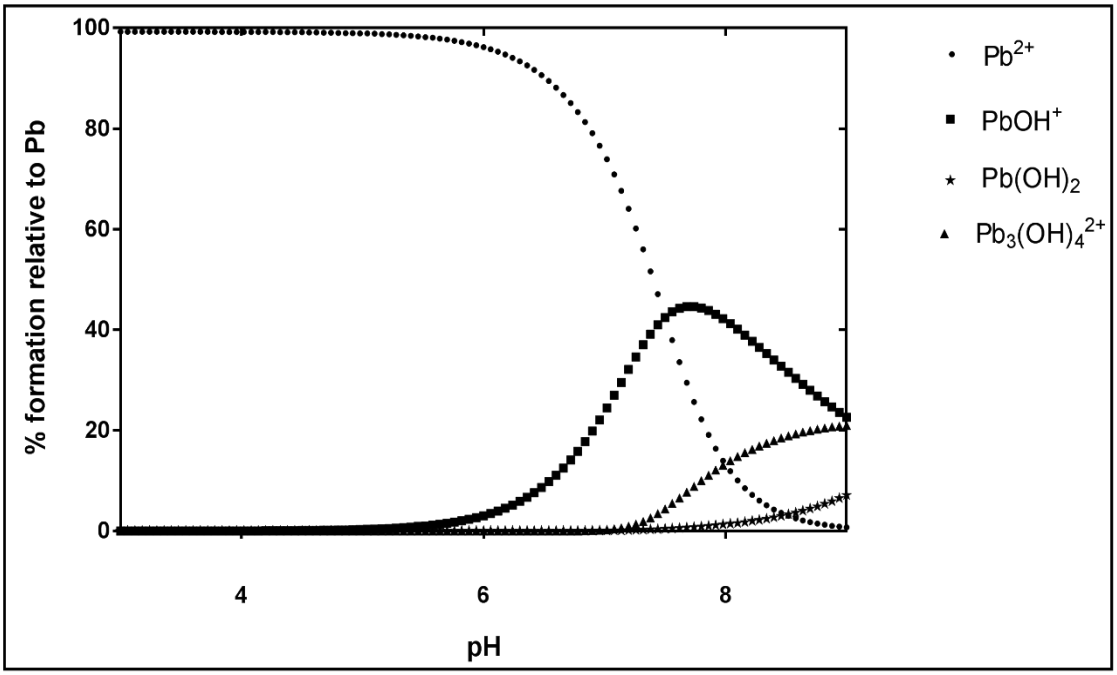

Figure 4.5: Speciation diagram of lead chloride ions in aqueous solution at different pH at 21^{o}C showing the predominant species at pH 5 is Pb^{2+}.

At pH 5, lead is present in the solution as free ions, as pH increases lead hydroxide complexes are formed and the concentration of ions decrease sharply between pH 6-8. The complexes Pb $(OH)_2$, $PbOH^+$ and $Pb_3(OH)_4^{2+}$ occur in alkaline medium and shows a maximum of 40% of hydroxylated Pb as it relates to free Pb ions. Respectively, the attachment of lead ions onto the surface of loofa was highest at a pH of 5 and this indicates that the speciation of lead ions is free lead ions. Furthermore, the adsorption of lead ions at over pH 7 indicates hydroxylation of the lead ions and therefore a reduction the adsorption capacity of free lead ions to be adsorbed on the surface. The presence of free lead ions is decreased as the pH increases to 6 and then to 9. The Pb^{2+} ions are the dominant species on the loofa at pH 5 (Smith and Martell, 2004; Sangi *et al*., 2008; Iqbal *et al*., 2009; Altinisik *et al*., 2010; Feng *et al*., 2011; Dubey *et al*., 2012; Yusoff *et al*., 2014; Ahmad *et al*., 2015).

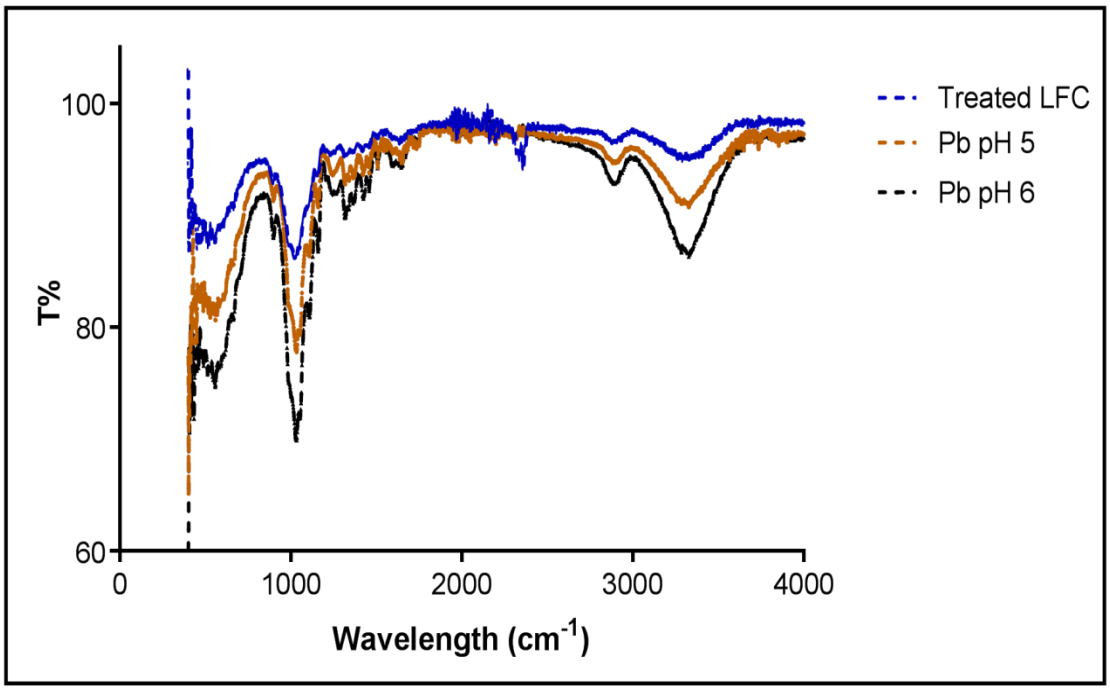

Figure 4.6: T% versus wavelength FT-IR spectra of 4% NaOH treated loofa before exposure to Pb, Pb-loaded loofa at pH 5 and Pb loaded loofa at pH 6 (lead ion concentration: 50mg/L; agitation speed: 200rpm; at 21°C,24h contact time, 5g/L dosage of alkali treated loofa).

Figure 4.6 shows the changes in peak intensity of specific characteristic functional groups on the loofa, wavelengths between 1050 – 1065cm^{-1} are attributed to O-H bending, 2900 -2950cm^{-1} to C-H stretching and 3330 - 3340 cm^{-1} to O-H bonding. The peak intensities correspond to a change in binding energy as adsorption occurs. The broad band in the 3545 -3050cm^{-1} range indicates strong intramolecular hydrogen bonds that give rise to strong adsorption. Furthermore, the FT-IR spectra decreases in transmittance at pH 5 which indicates further adsorption of lead ions on the loofa (Whittaker, 2000; Jayamani *et al*., 2014).

With a pH_{pzc} value of 7.2, adsorption decreases when pH < pH_{pzc} and when pH > pH_{pzc}, adsorption increases. At pH < $pH_{pzc,}$ there is the competitive effects of the hydronium ions and the electrostatic repulsion that occurs between the positively charged loofa surface and the lead cations in solution. The bond of the negatively charged ions present on the loofa surface, when pH > pH_{pzc}, and the metal cations in solution formed due to electrostatic attraction influence the adsorption process. Due to hydroxylation over pH 7, a decrease in adsorption is expected as the

concentration of available charged lead species decreases. Maximum adsorption occurs at pH 5 and there is a decrease in adsorption, as shown in Figure 4.3, over the pH range of 5 to 9. The involvement of electrostatic attraction forms weaker complexes compared to inner-sphere complexes (Holmberg, 2006; Liu and Lee, 2014). This further explains the effect of the ion exchange effect during the adsorption acts is the dominant factor in the adsorption of lead ion onto alkali treated loofa. For the untreated loofa, the pH_{pzc} is at 6.1. At pH > pH_{pzc}, due to electrostatic attraction, adsorption increases and the maximum adsorption is seen to occur at pH 7 (Figure 4.2). A further increase in the pH is then expected to lead to a reduced adsorption capacity because of the hydroxylation of the lead ions present in aqueous solution. Furthermore, apart from the ion exchange mechanism, the formed bond due to electrostatic attraction and reduced competitive effect of the hydronium ions plays a dominant role that influences the lead adsorption on untreated loofa.

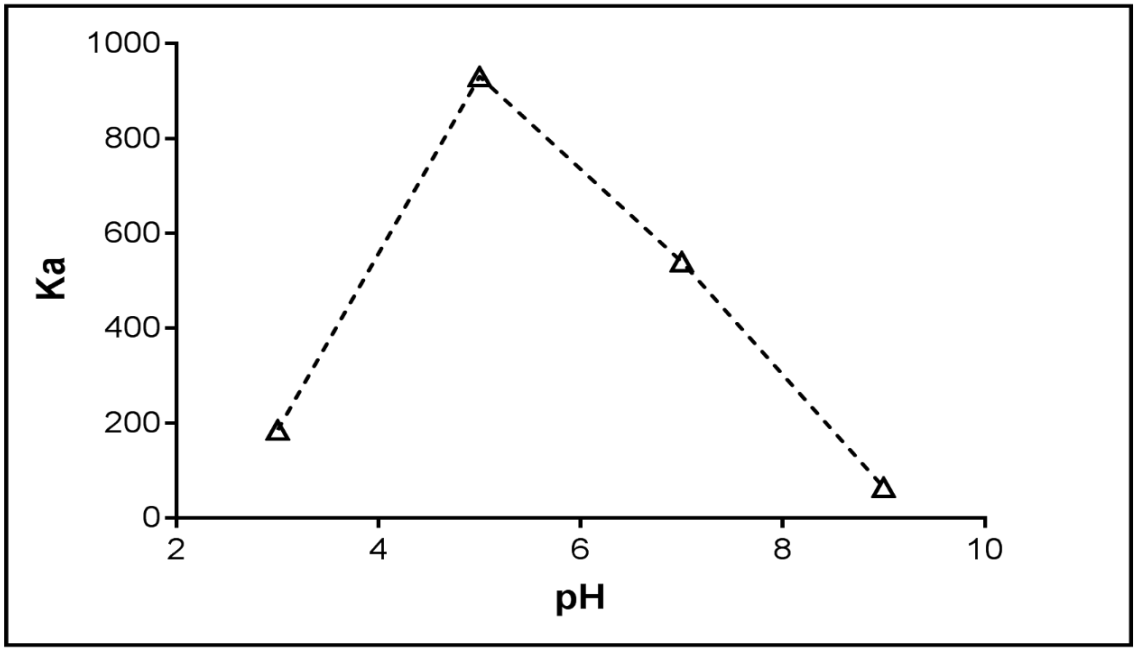

Figure 4.7: Sips isotherm constant values (K_a) versus change in pH which shows the binding constant, K_a, of the alkali treated loofa and lead ions.

As shown in Figure 4.7, the relationship between K_a constant values of the Sips isotherm model, calculated from equation 9 in Chapter two, and pH shows a decrease in K_a as pH increases. The

optimum pH for adsorption of lead onto alkali treated loofa was found to be at pH 5. At lower pH values, the surface active sites would be more positively charged thereby showing an electrostatic repulsion towards the positively charged lead ions**.** This shows a reduced affinity for the available binding sites. As the pH increases from pH 5, the K_a constant decreases as hydroxylation and precipitation occur which results in a decrease in affinity for surface sites. An exchange of ions occurs at the different solution pH values (Jeppu and Clement, 2012).

In agreement with previously reported data, solution pH is the most important controlling factor in the adsorption of heavy metals ion from aqueous solution (Saeed *et al*., 2009; Montazer-Rahmati *et al*., 2011). Metal speciation of lead ions (Figure 4.5), specific functional groups on the loofa and the exchange of ions present in solution (Figure 4.6 & 4.7) are shown as the predominant adsorbent characteristics in the adsorption process.

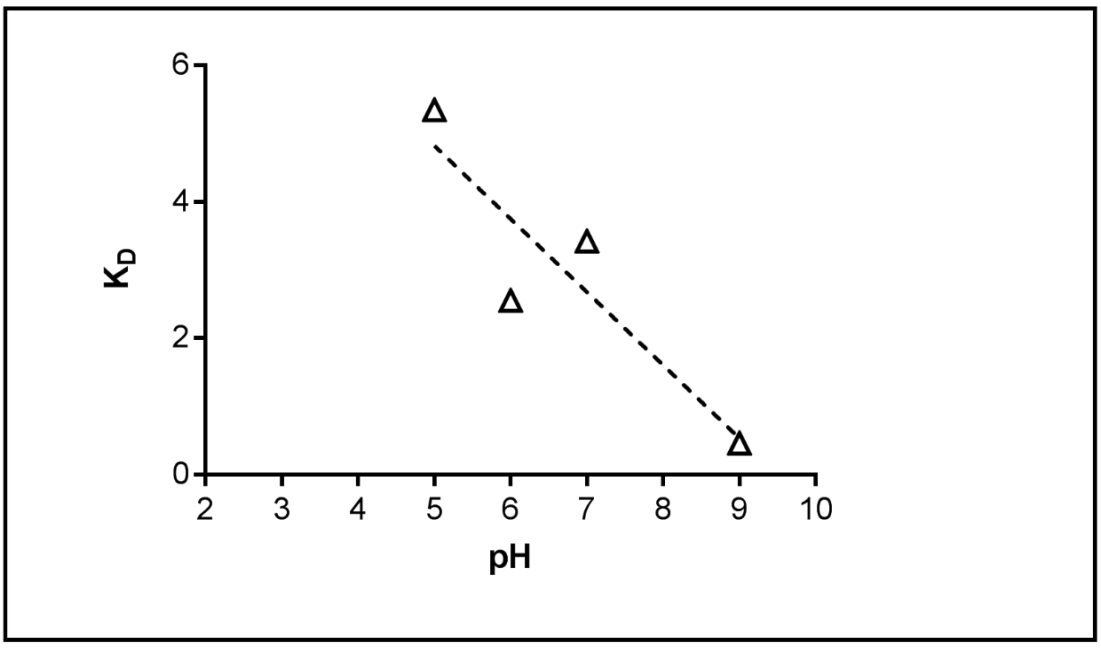

Figure 4.8: Distribution ratio (K_D) versus pH at equilibrium at pH range 5-9; lead ion concentration: 50mg/L; agitation speed: 200rpm; at 21^oC, 24h contact time, 5g/L dosage of alkali treated loofa.

The distribution ratio decreases as the pH increases reaching a lowest point at pH 9 (Figure 4.8). The strength of bonding of loofa to lead ions is shown by the K_D values which indicate distribution ratio of lead ions in solution. At a pH of 7 and above, lead hydrolysis occurs which

leads to a weak lead chelation. This change in speciation affects the adsorption efficiency. The distribution ratio also falls with decreasing pH below 5. The highest distribution ratio at pH 5 depicts a strong lead chelation and enhanced adsorption efficiency compared to other pH values. The adsorption increases from pH 3 to 5 and then decreases from pH 6 to 9 (Ahamed *et al*., 2010; Zhao *et al*., 2016).

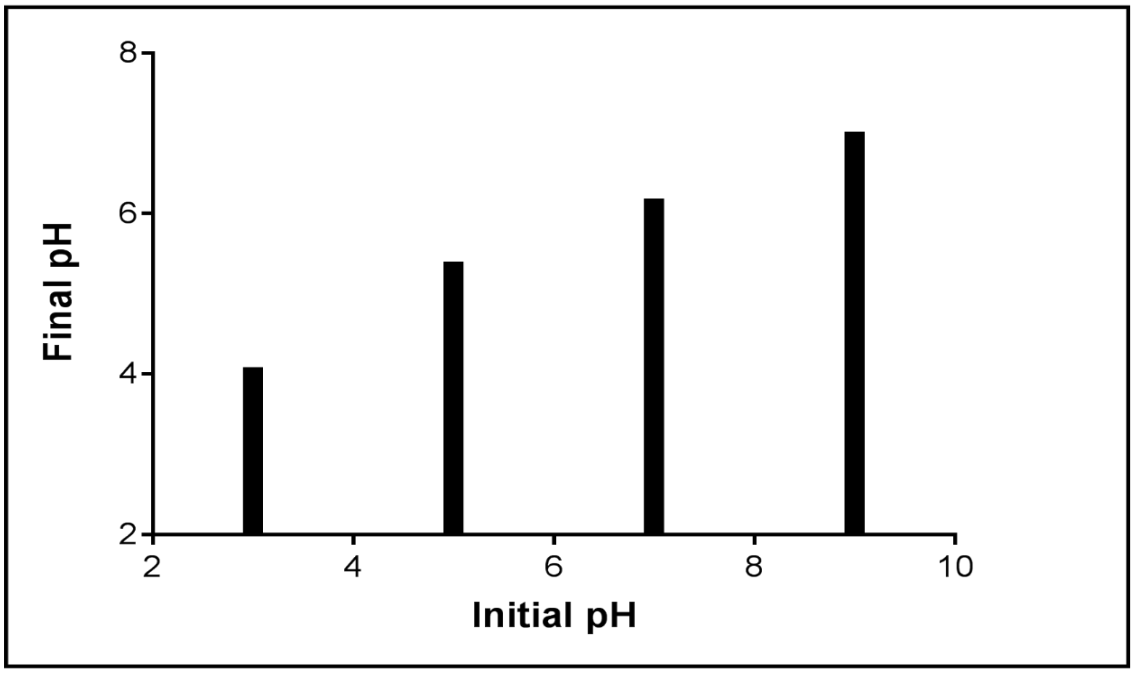

Figure 4.9: Final pH versus initial pH of lead solution after equilibrium during batch studies at pH range 3-9; lead ion concentration: 50mg/L; agitation speed: 200rpm; at 21^{o}C, 24h contact time, 5g/L dosage of alkali treated loofa.

Figure 4.9 shows change in the final pH versus initial pH of lead solution at equilibrium for different initial pH values. At pH 3, hydrogen ions and lead ions are competing for active sites on the loofa in an acidic condition. This changes the pH from 3 to 4 after adsorption. At an optimal pH of 5, the maximum amount of lead ions adsorbed onto the loofa equals the maximum number of hydronium ions present in the aqueous solution. This also remains in an acidic medium and the pH remains almost constant throughout the experimental procedure. An increase in pH results in the formation of hydroxylated lead ions which are then precipitated out of solution (Sangi *et al*., 2008; Nasef *et al*., 2010; Doss and Kodolikar, 2012; Abdolali *et al*., 2016).

4.2.2 Concentration effect

Figure 4.10 and 4.11 shows the trend of lead ion adsorption at different initial concentrations. As the initial concentration is increased, the lead ion adsorption increases over time. An increase in lead ion adsorption is observed at equilibrium as the initial concentration increases (figure 4.11). The metal uptake capacity is increased from 9.6mg/g to 23.4mg/g as the initial concentration of lead ions is increased from 50 – 200mg/L.

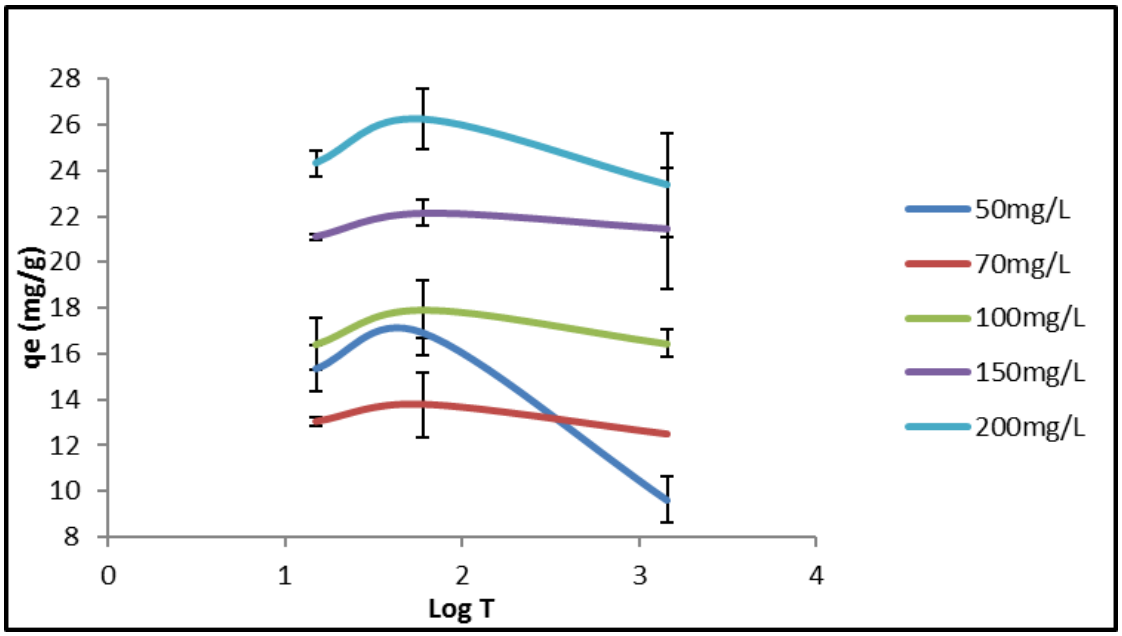

Figure 4.10: Uptake capacity of lead ions (qe) with change in time after 24hrs at pH 5; lead ion concentration ranges of 50 – 200mg/L; agitation speed: 200rpm; at 21°C, 24h contact time (represented by the log of time in mins [Log T]), 5g/L alkali treated loofa dosage. Data from 3 replicate measurements.

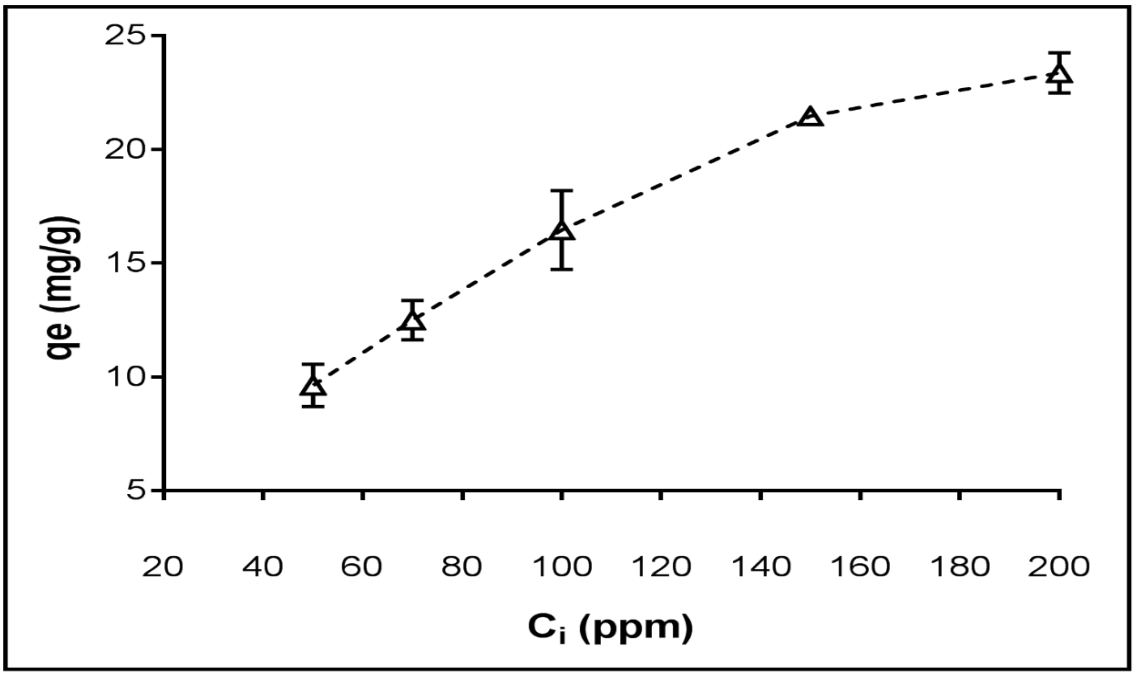

Figure 4.11: Uptake capacity of lead ions (qe) with change in initial concentration after 24hrs at pH 5; lead ion concentration ranges of 50 – 200mg/L; agitation speed: 200rpm; at 21^{o}C, 24h contact time, 5g/L alkali treated loofa dosage. Data from 3 replicate measurements.

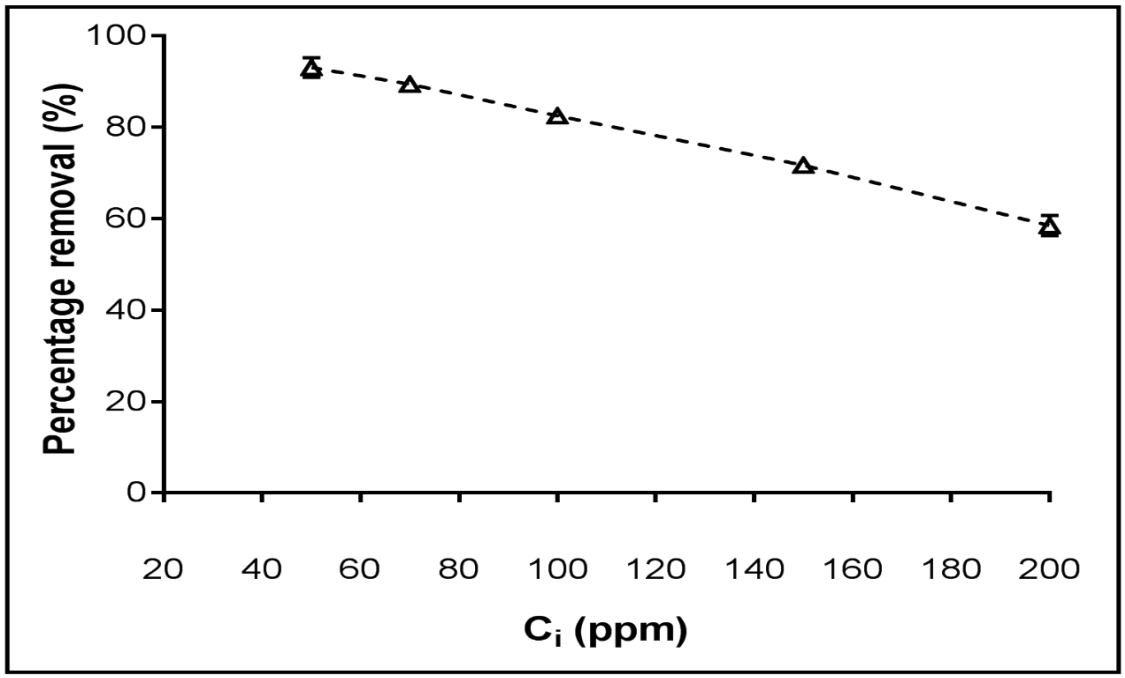

Figure 4.12: Percentage removal of lead ion with change in initial concentration after 24hrs at pH 5; lead ion concentration ranges of 50-200mg/L; agitation speed: 200rpm; at 21°C, 24h contact time, 5g/L alkali treated loofa dosage. Data from 3 replicate measurements.

The percentage removal efficiency decreases when the initial concentration increases as shown in figure 4.12. There is a high amount of vacant sites available for lead ion binding at a low concentration of 50mg/L, giving a 93% removal efficiency. As the initial concentration increases, the binding sites become occupied (saturation occurs) and therefore decreases the uptake efficiency of the lead ions on the loofa. Figure 4.12 shows that there is a decrease of 37.2% when the initial lead ion concentration is increased to 200mg/L. In agreement with previous literature, the initial concentration of heavy metal ions is shown to have an effect on the adsorption process (El-Sikaily *et al*., 2007; Yusoff *et al*., 2014).

4.2.3 Loofa loading effect

Here, the effect of the varying loofa loadings on lead ion adsorption was investigated. Figure 4.13 shows the change in the percentage removal capacity over time.

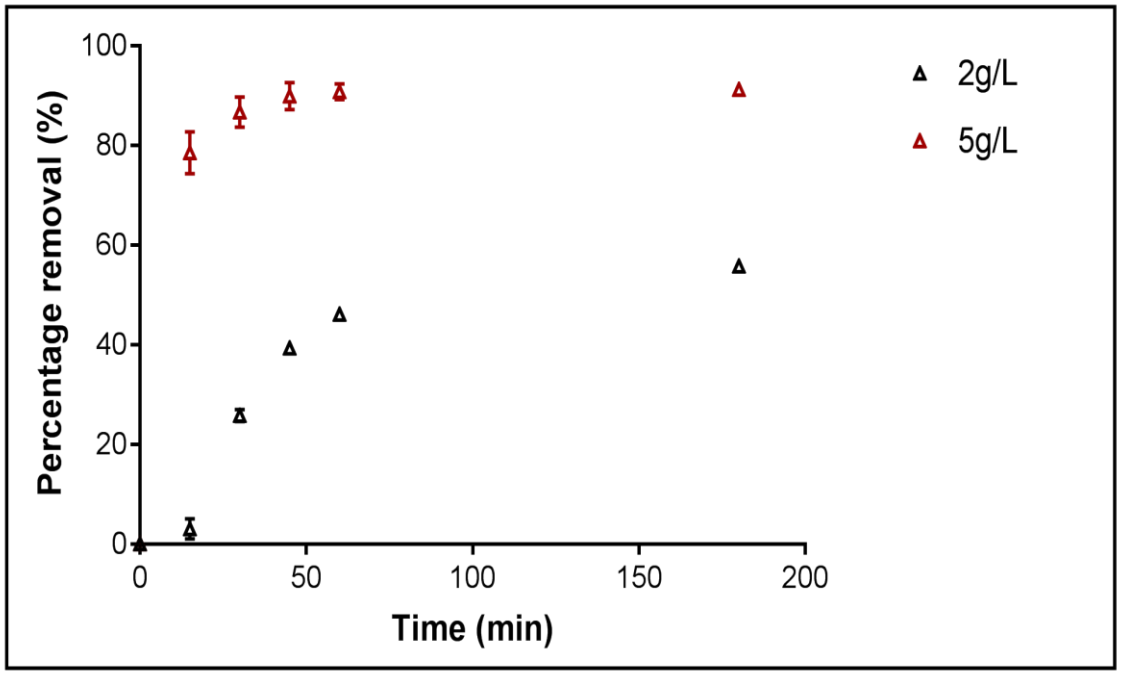

Figure 4.13: Percentage removal of lead ion with change in time after 3hrs at pH 5; lead ion concentration 50 mg/L; agitation speed: 200rpm; at 21°C, 3h contact time, 2g/L & 5g/L alkali treated loofa dosage. Data from 3 replicate measurements.

The removal capacity increases when the loofa loading is increased from 2g/L to 5g/L. This implies that the number of binding active sites available for biosorption increased which leads to more surface area present with an increase in the loofa loading. After 3hrs, the percentage removal was increased from 50% to 90% when the loofa concentration increases to 5g/L. As shown in figure 4.13, a 60% increase in loofa dosage leads to a 40% increase in percentage removal of lead ions from aqueous solution. Having more than doubled the binding sites (amount of loofa), the increase in the uptake removal has not achieved 100% removal possibly due to the fact that some lead ion is being released back into the solution during the adsorption process. The BET specific surface area of the lead loaded loofa was 18.80m^2/g (loading capacity of 5g/L), a pore volume of 0.007cm^3/g (within a pore width range of 1.7 – 300 nm) and an average pore size of 2.1nm. This shows a decrease in the surface area sites available on the loofa for adsorption, indicating adsorption of lead ions had occurred on the surface pores as compared to the unused loofa (without adsorption of lead ions), having a BET specific surface area of 43.09m^2/g, a pore volume of 0.017cm^3/g. The loss of pore volume occurs as a result of

lead ion deposition within the pores (Occelli *et al*., 2003). The uptake of lead ions can be attributed predominantly to mesopores (an average pore size of 2.1nm indicates the presence of mesopores). The deposition of lead ions on the pores of the loofa leads to a reduced pore volume per gram on the surface area. Furthermore, the low surface area and low pore size, which may lead to a lower uptake capacity for the lead ions, shows that the adsorption process cannot solely be physiosorption but depends more widely on the chemical properties of the adsorption process. This is supported by the low R^2 value of the intra particle diffusion model (Figure 4.27), which shows that the adsorption is not solely controlled by mesopores (Altenor *et al*., 2009; Khosravi *et al*., 2014).

In agreement with previous researchers, the loading capacity of biosorbents play an important role in the adsorption process (Tsai and Chen, 2010; Jeyanthi and Dhinakaran, 2012).

4.2.4 Temperature

Figures 4.14 and 4.15 show the trend of uptake removal of lead ions from aqueous solution at varying temperatures.

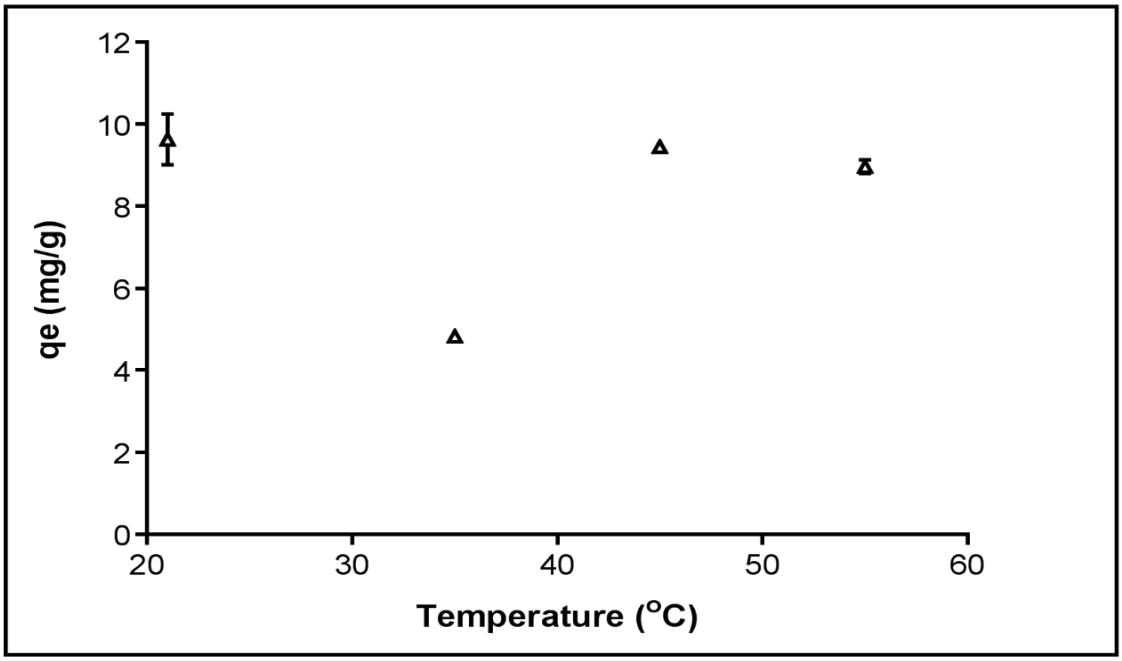

Figure 4.14: Uptake capacity of lead ions (qe) with change in time after 24hrs at pH 5; lead ion concentration 50 mg/L; agitation speed: 200rpm; at 21, 35, 45 & 55°C, 24h contact time, 5g/L alkali treated loofa dosage. Data from 3 replicate measurements.

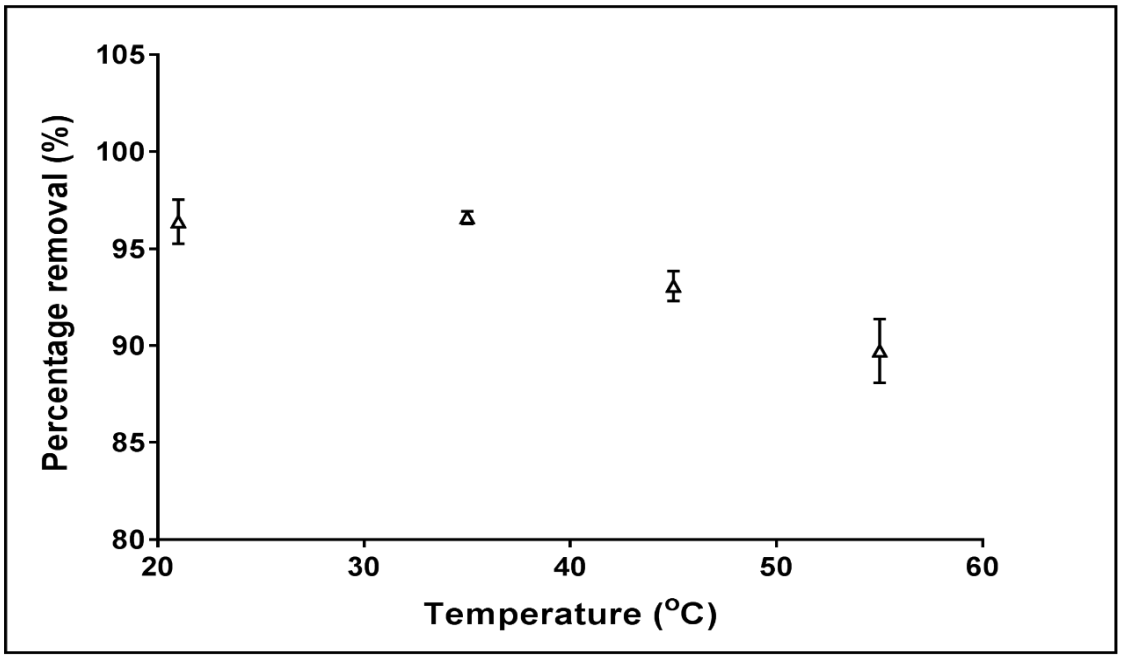

Figure 4.15: Percentage removal of lead ions with change in time after 24hrs at pH 5; lead ion concentration 50 mg/L; agitation speed: 200rpm; at 21,35,45 & 55°C, 24h contact time, 5g/L alkali treated loofa dosage. Data from 3 replicate measurements.

In Figure 4.15, the percentage removal capacity of lead ions from aqueous solution is decreased as the temperature increases. This indicates a negative impact of temperature on lead ion adsorption. Temperature appears to affect the biosorption process to a lesser extent within a temperature range from 21^{o}C to 45^{o}C. A further increase in temperature also shows a further decrease to 90%. This implies an exothermic reaction process (Sari and Tuzen, 2008; Fan *et al*., 2014). This effect of temperature is consistent with the presence of physical adsorption features of the lead ion adsorption process (Li *et al*., 2004). The damage of the actives sites as a result of a rise in temperature could be the reason for decreased adsorption of lead ions. The optimum temperature utilised is room temperature (21^{o}C).

4.2.5 Ionic strength

Salinity effects the stability constants of metal ions in solution which affects the speciation of the metals (Luo & Millero, 2007). Therefore, information on the effect of ionic strength on the adsorption process is needed. Figure 4.16 to 4.23 show the trend in the percentage removal capacity of lead ions from aqueous solution and the effect of ionic strength of the aqueous solution. The maximum adsorption shown to occur in a mixed aqueous solution of lead ions and NaCl when the mixed concentration is in a 1: 1 ratio. Also, the comparison of the percentage uptake of lead ion alone in solution (previous results), the NaCl uptake and mixed lead and NaCl aqueous solution is shown.

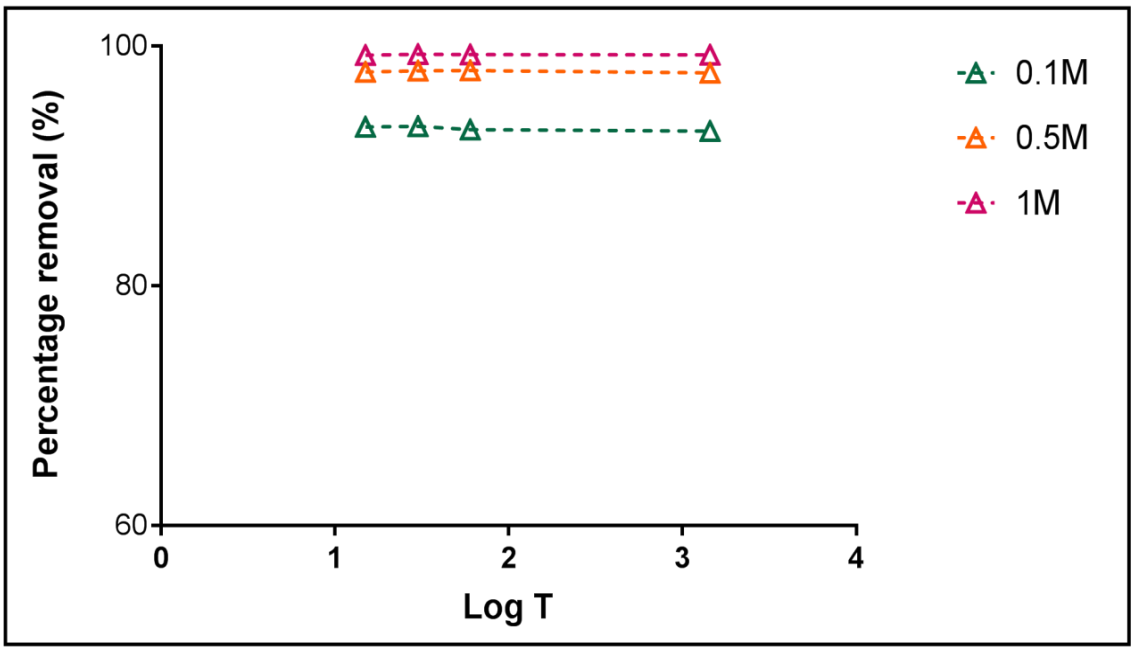

Figure 4.16: Percentage removal of NaCl in aqueous solution; agitation speed: 200rpm; at 21^{0}C, at pH 5, 24h contact time (represented by the log of time in mins [Log T]), 5g/L alkali treated loofa dosage.

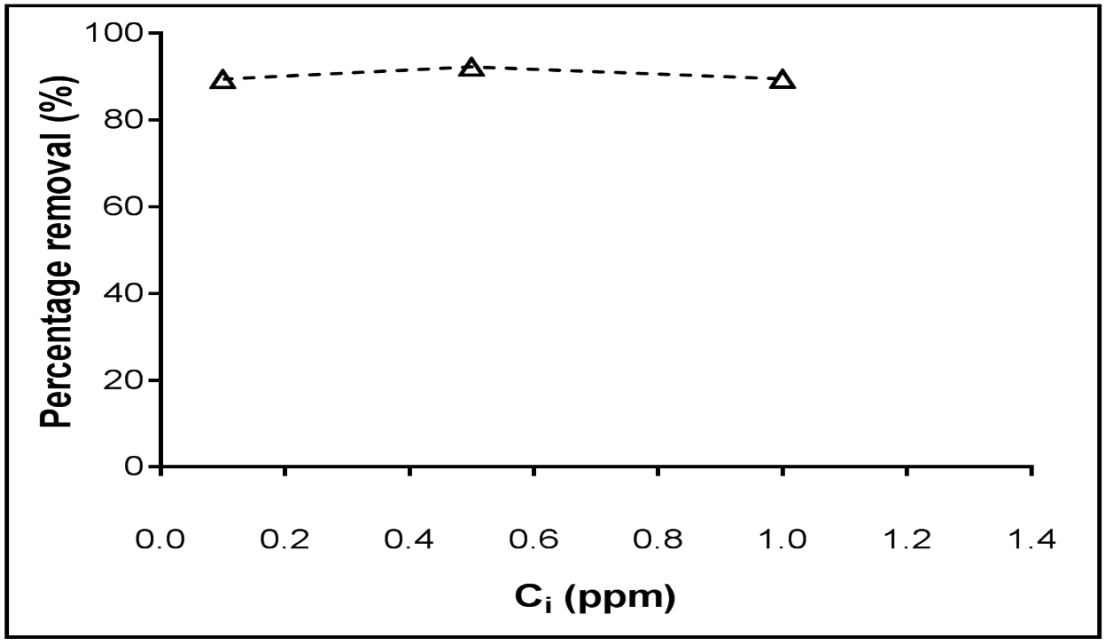

Figure 4.17: Percentage removal of lead ions with change in NaCl concentration in mixed solution after 24hrs; lead ion concentration: 50mg/L; agitation speed: 200rpm; at 21^{o}C, at pH 5,24h contact time, 5g/L alkali treated loofa dosage.

The adsorption of lead ions decreased with increase in ionic strength.

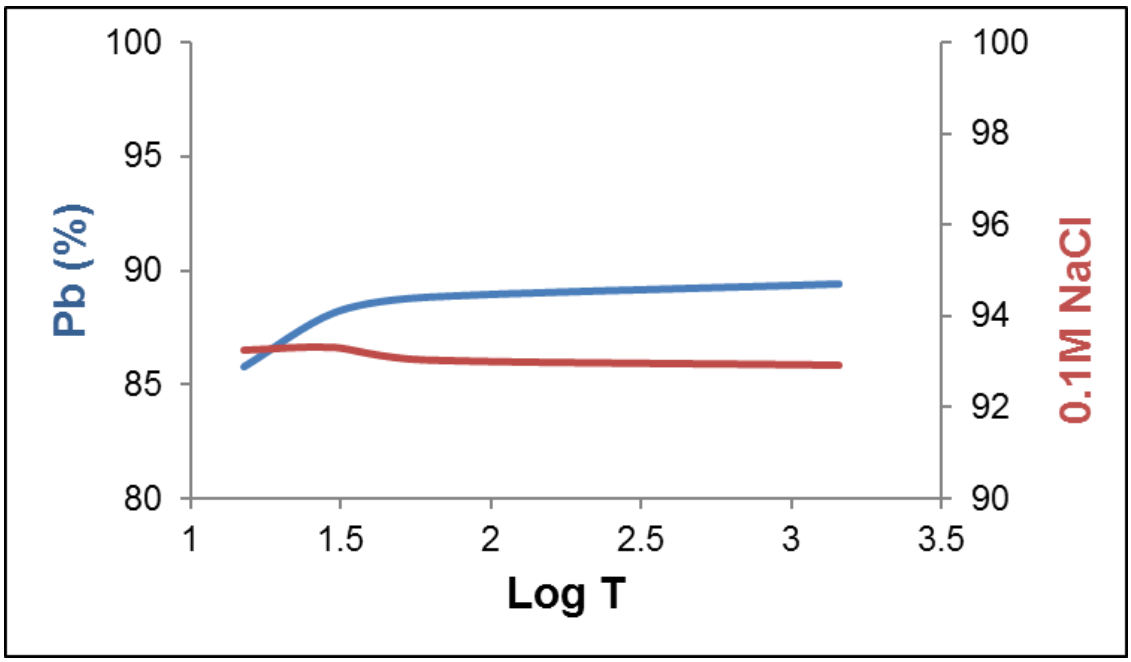

Figure 4.18: Comparison of percentage removal of lead ions and 0.1M NaCl in mixed solution after 24hrs; lead ion concentration: 50mg/L; agitation speed: 200rpm; at 21°C, at pH 5,24h contact time, 5g/L alkali treated loofa dosage; Log T represent Log time.

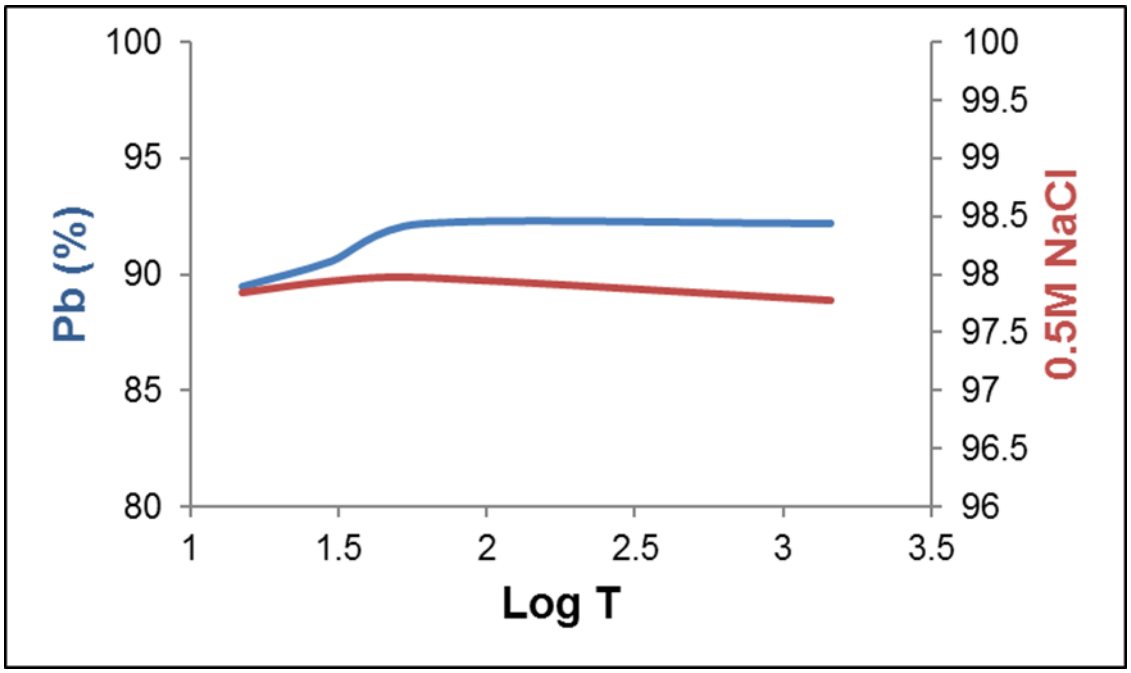

Figure 4.19: Comparison of percentage removal of lead ions and 0.5M NaCl in mixed solution after 24hrs; lead ion concentration: 50mg/L; agitation speed: 200rpm; at 21°C, at pH 5,24h contact time, 5g/L alkali treated loofa dosage; Log T represent Log time.

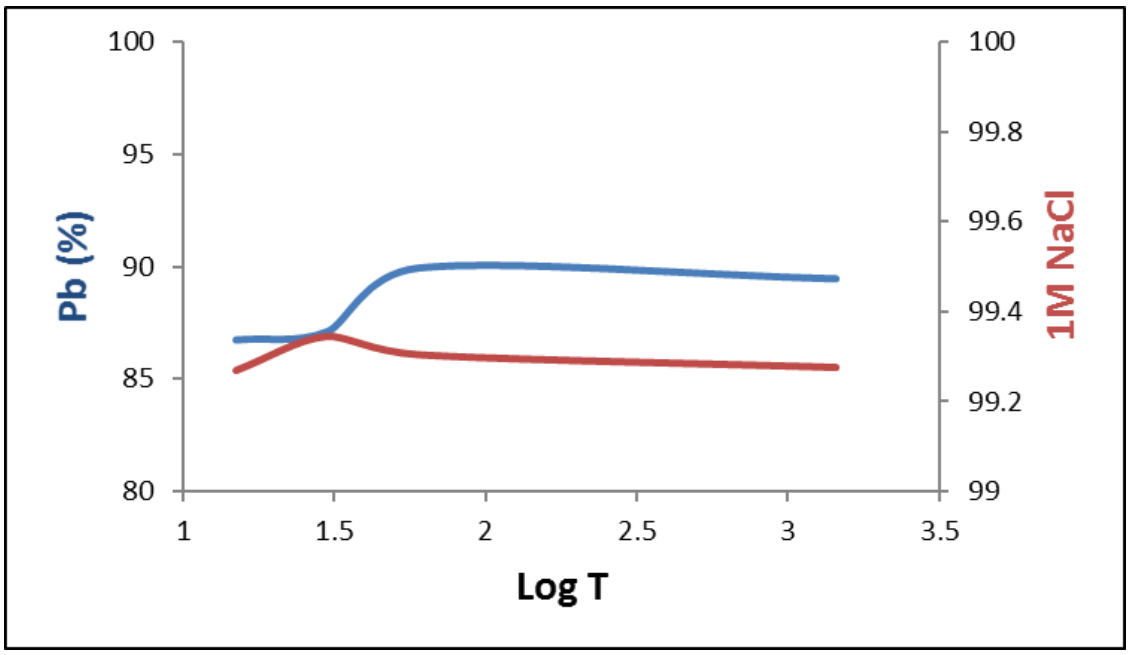

Figure 4.20: Comparison of percentage removal of lead ions and 1M NaCl in mixed solution after 24hrs; lead ion concentration: 50mg/L; agitation speed: 200rpm; at 21^{o}C, at pH 5,24h contact time, 5g/L alkali treated loofa dosage; Log T represent log time.

Figure 4.18, 4.19 & 4.20 show the difference in the percentage removal of lead ion and NaCl concentrations from mixed aqueous solution over time. There is an initial increase in percentage removal for both lead ions and NaCl. However, after 60 mins the percentage removal of lead ions remains fairly constant and that of NaCl tends to decrease. This shows that saturation occur leading to no further adsorption of either lead ions or NaCl at different concentrations.

The uptake of lead ions and the percentage removal is shown to increase and then remain fairly constant due to the ionic strength which enhances the aggregation of carbon nanomaterials on the loofa surface. The ionic strength decreases over time. The adsorption sites are reduced and adsorption affinity decreases over time (Zhao *et al*., 2016).

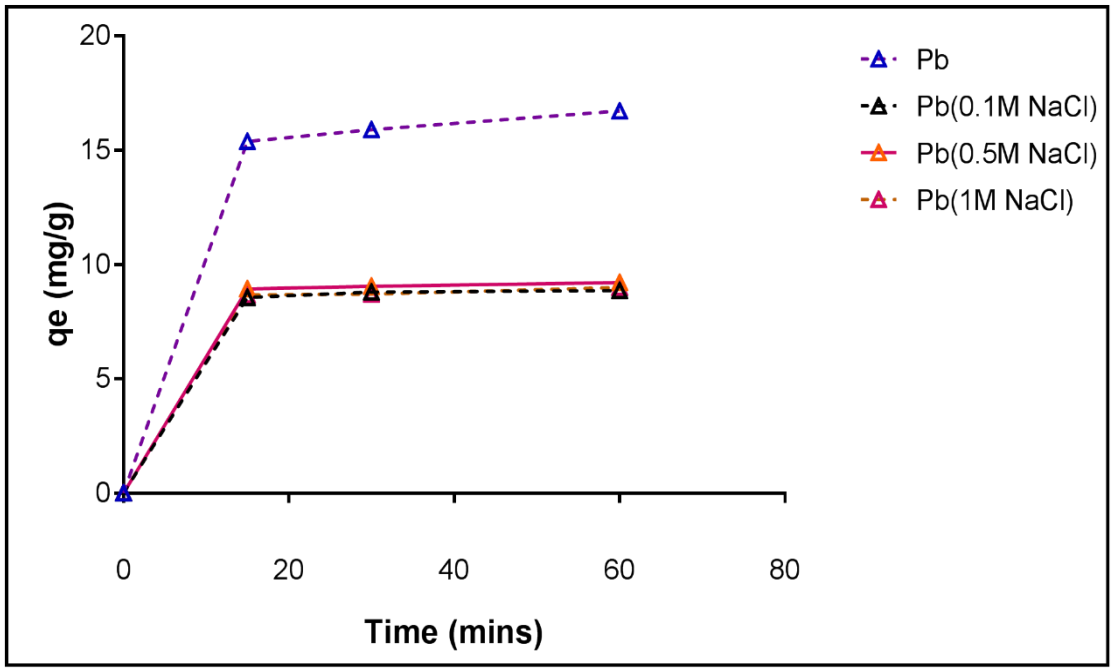

Figure 4.21: Uptake capacity of lead ions (qe) with change in NaCl concentration over time; lead ion concentration: 50mg/L; agitation speed: 200rpm; at 21°C, at pH 5,1h contact time, 5g/L alkali treated loofa dosage.

Figure 4.21 shows the trend of adsorption capacity over time. Lead uptake remains fairly constant after 15minutes. The uptake of lead is similar for the various concentrations (0.1M, 0.5M & 1M) of NaCl all of which are lower than a solution with no added NaCl.

The effect of ionic strength on the surface charge results in the increased presence of ionic forms. This could result in repulsion of lead ions thereby decreasing adsorption. Further increase in the ionic strength shows no effect on the lead uptake from aqueous solution because saturation has occurred on the surface adsorption sites therefore there are no more available sites for sodium uptake.

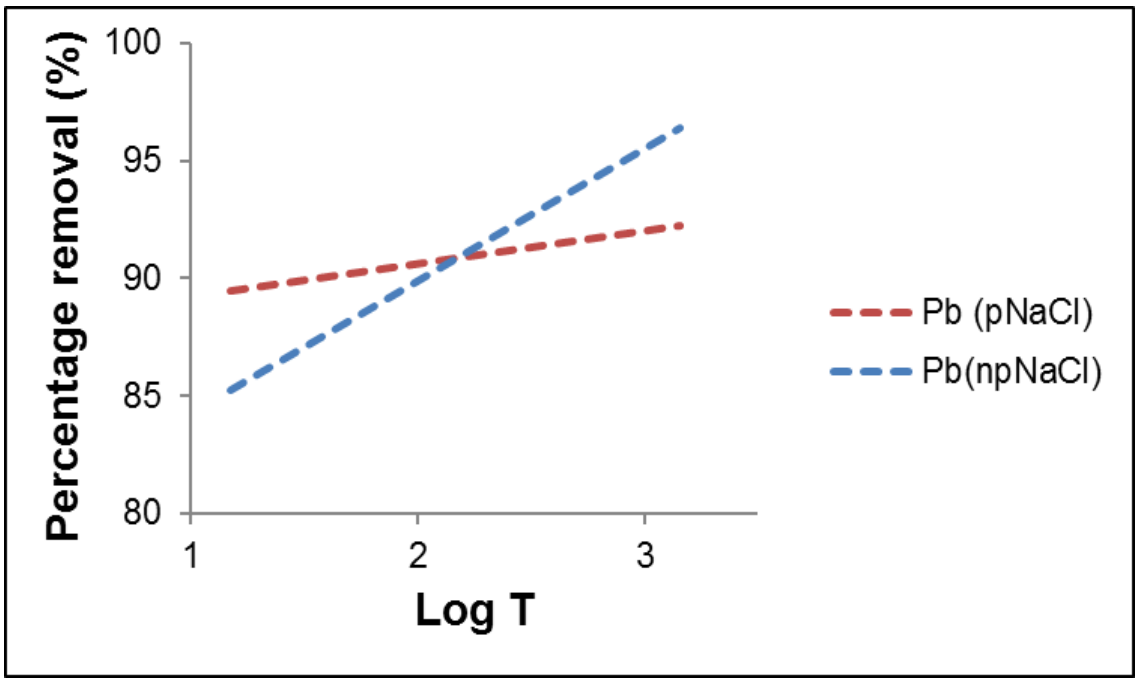

Figure 4.22: Percentage removal of lead ion in the presence of 0.5M NaCl (pNaCl) and not in the presence of NaCl (npNaCl); lead ion concentration: 50mg/L; agitation speed: 200rpm; at 21^{0}C, 24h contact time, 5g/L alkali treated loofa dosage.

Figure 4.22 shows the highest affinity to loofa leading to maximum adsorption with no NaCl.

An alteration in the ionic strength, by introducing sodium chloride, reduces the percentage removal of lead ions (causes limitation in the adsorption process of Pb^{2+} ions) on the loofa. The effect of ionic strength as a function of the addition of 0.5M NaCl is a dual effect of Na^+ and Cl^- ions. The tendency of Cl^- ions to form complexes with Pb^{2+} , decreasing the concentration of Pb^{2+} ions in solution by forming $PbCl_2$ and making it less soluble, allows for Na^+ ions to compete with remaining Pb^{2+} ions in solution for the active sites (Volesky, 2003). Therefore, the uptake capacity of Pb^{2+} ions onto the loofa is reduced. Furthermore, the hydrated ionic radius of Na^+ ions is less than that of lead ions; therefore, the removal of Na^+ ions from solution and its exchange for ions is easier than Pb^{2+} ions. Therefore, Na^+ occupies the active sites on the loofa which limits the surface sites available for the adsorption of Pb^{2+} ions (Saeed *et al*., 2009; Arshadi *et al*., 2014). An overall decrease of about 4% is found in the uptake capacity of lead ions in the presence of 0.5M NaCl as compared to that in the absence of NaCl. The influence of Na^+ ions on the uptake of lead ions can be explained by lead ions being electrostatically and covalently

bound, because of the electronegativity of the lead ions, to loofa by forming both inner and outer sphere complexes (Holmberg, 2006). Therefore, ionic strength shows a little effect on the Pb^{2+} ion adsorption on loofa (about 4.2% reduction in the initial adsorption capacity of Pb^{2+} uptake) *(Sangi et al*., 2008; Ouyang *et al*., 2014; Yang *et al*., 2014). This shows an inner sphere sorption mechanism.

The results show that the presence of Na^{+} and Cl^{-} produces an overall negative effect on the uptake efficiency of Pb^{2+} ions.

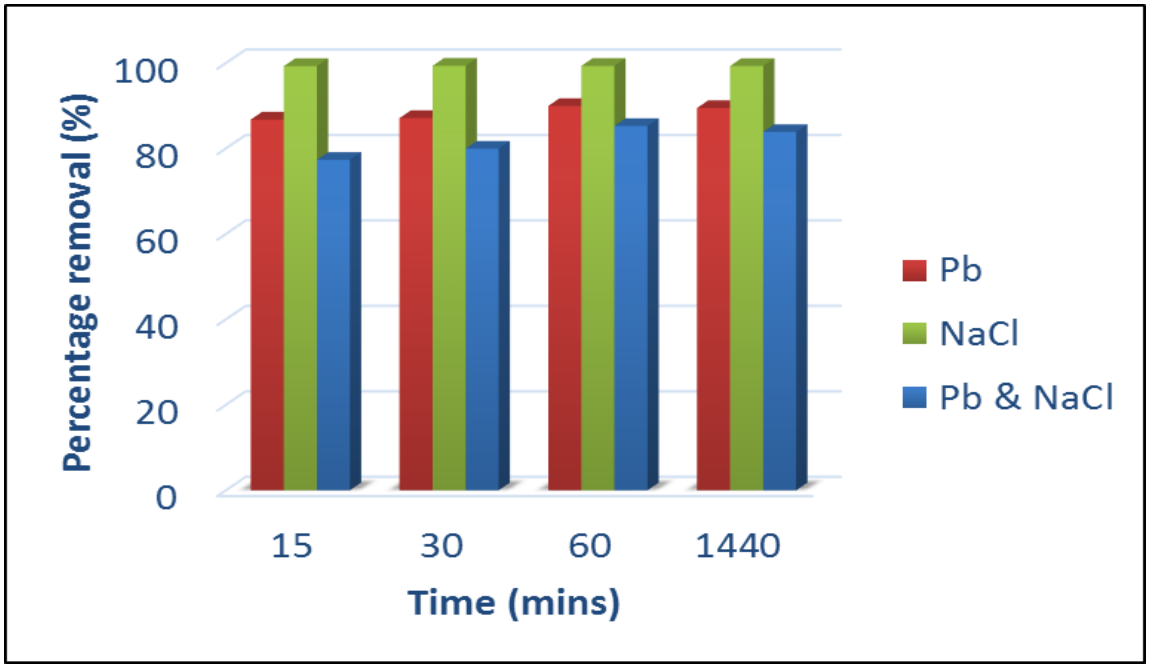

Figure 4.23: Percentage removal of lead ions in solutions containing 0.5M NaCl and mixed aqueous solution of both after 24hrs; lead ion concentration: 50mg/L; agitation speed: 200rpm; at 21°C, at pH 5, 5g/L alkali treated loofa dosage.

4.2.6 Kinetic modeling

The rate controlling step of the adsorption mechanism depends on the kinetics of the system. Figure 4.24 to 4.27 show the kinetic models utilised to determine the rate controlling step such as mass transfer and chemical reaction processes. The correlation coefficients of each model is depicted in the plots and the best fit shown.

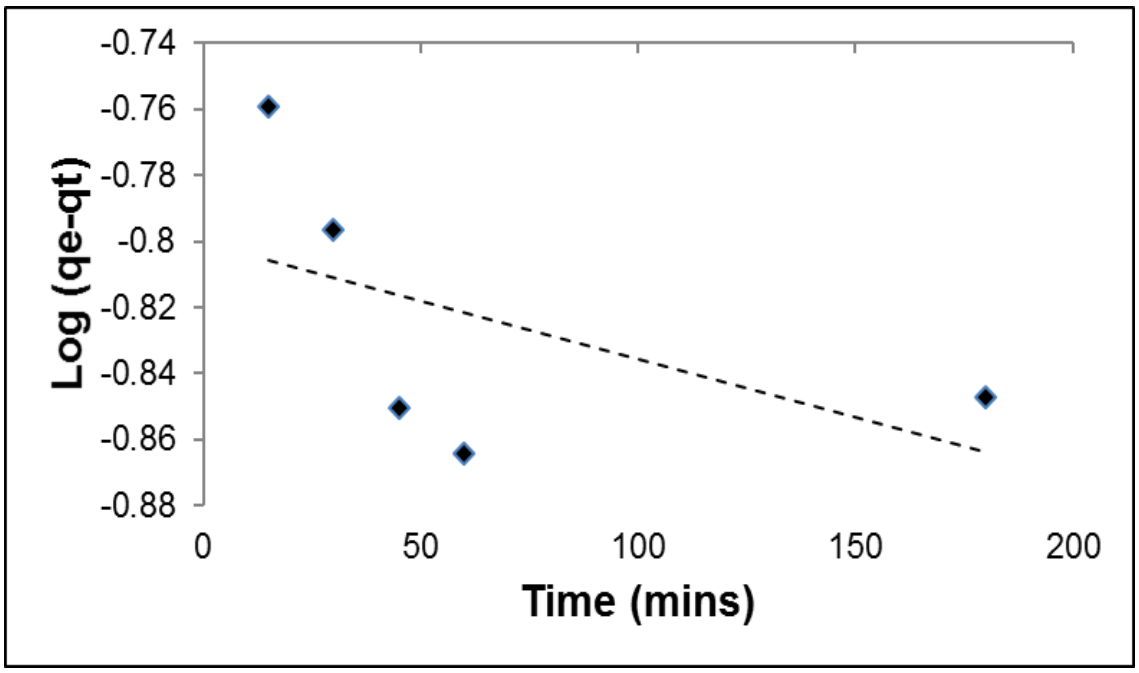

Figure 4.24: Pseudo first order (PFO) kinetic model at pH 5; lead ion concentration 50 mg/L; agitation speed: 200rpm; at 21°C, 24h contact time, 5g/L alkali treated loofa dosage (R^2 = 0.2776). PFO model fit shown by dashed line.

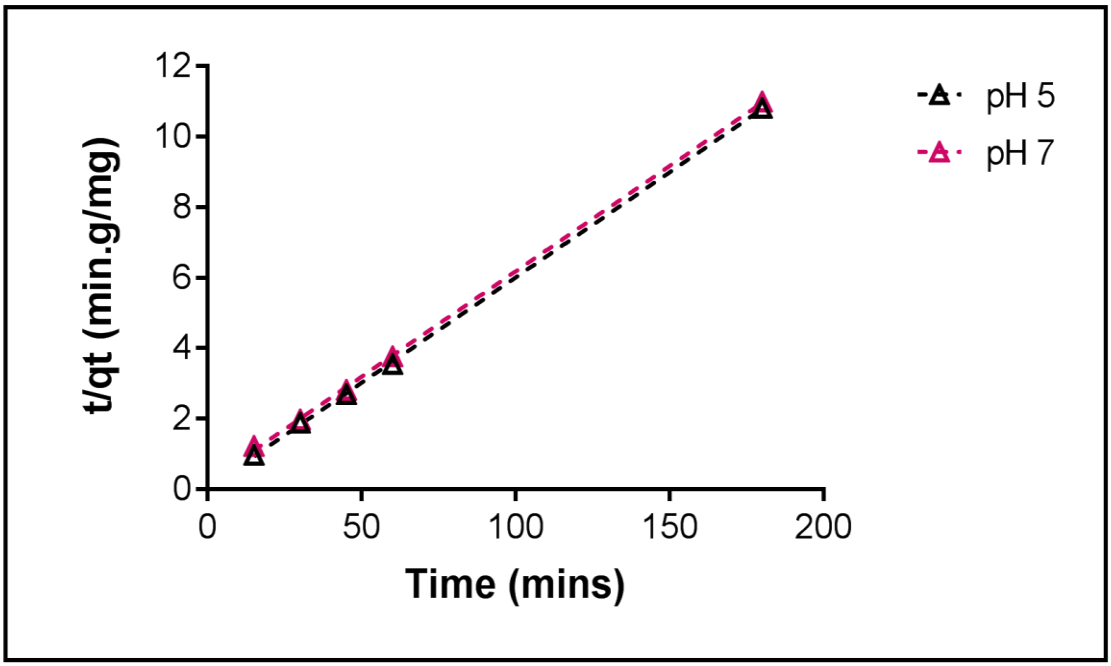

Figure 4.25: Pseudo second order (PSO) kinetic model at pH 5 and pH 7; lead ion concentration 50 mg/L; agitation speed: 200rpm; at 21°C, 24h contact time, 5g/L alkali treated loofa dosage. PSO model fit shown by dashed line.

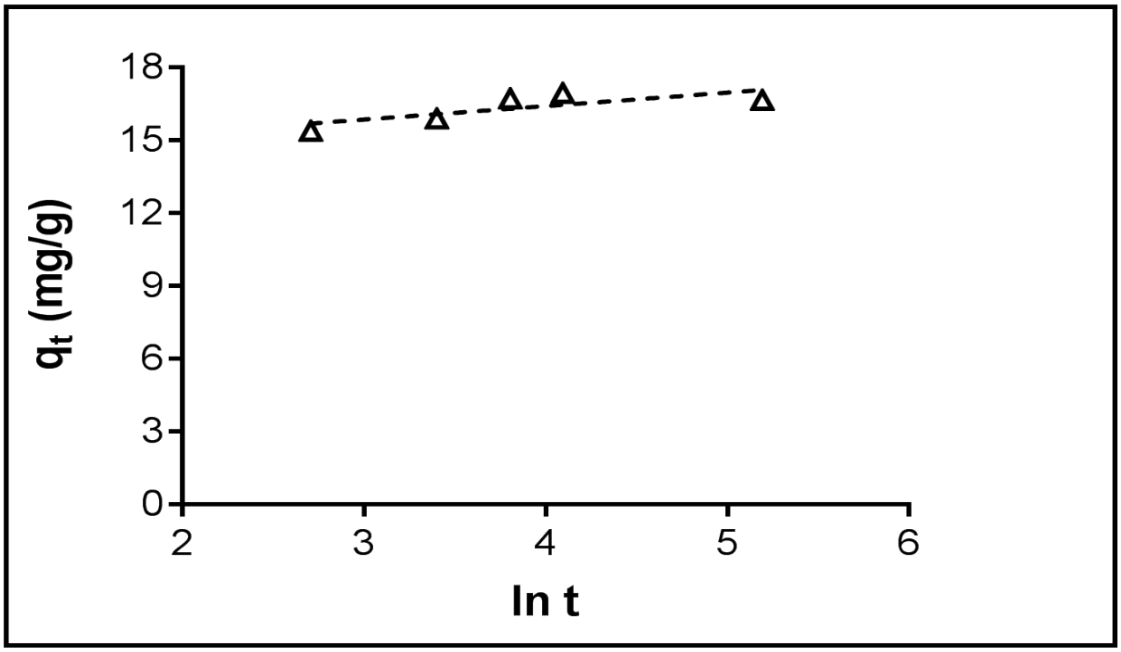

Figure 4.26: Elovich kinetic model at pH 5; lead ion concentration 50 mg/L; agitation speed: 200rpm; at 21^{o}C, 24h contact time, 5g/L alkali treated loofa dosage (R^2 = 0.594). Elovich model fit shown by dashed line.

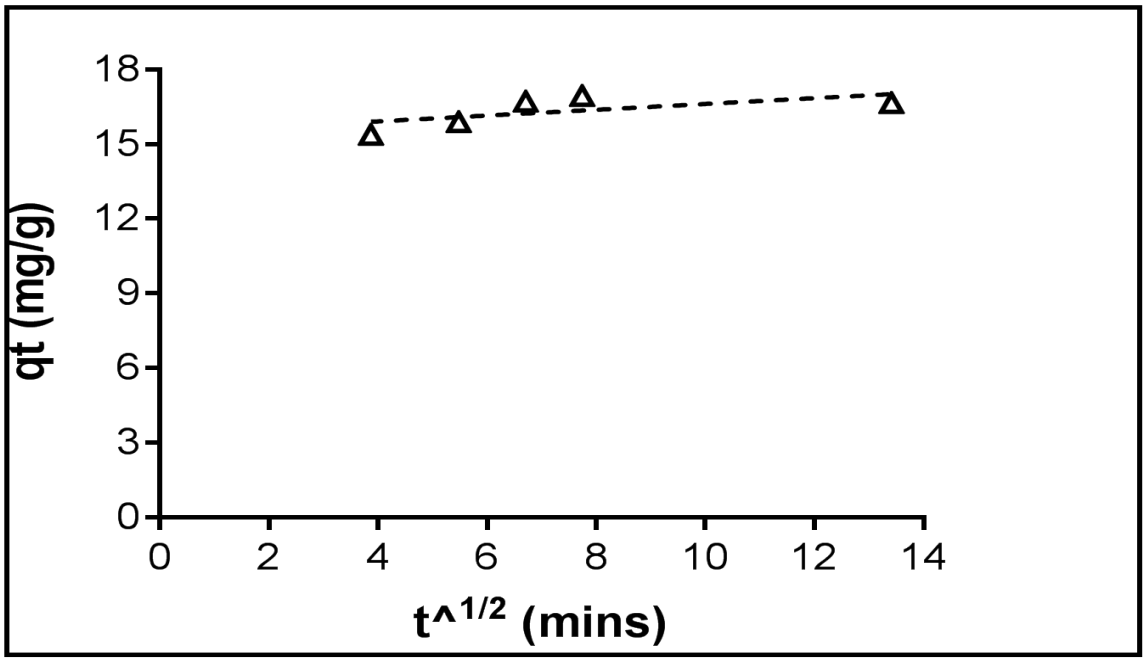

Figure 4.27: Intraparticle diffusion (IntraP) model at pH 5; lead ion concentration 50 mg/L; agitation speed: 200rpm; at 21°C, 24h contact time, 5g/L alkali treated loofa dosage (R^2 = 0.412). IntraP model fit shown by dashed line.

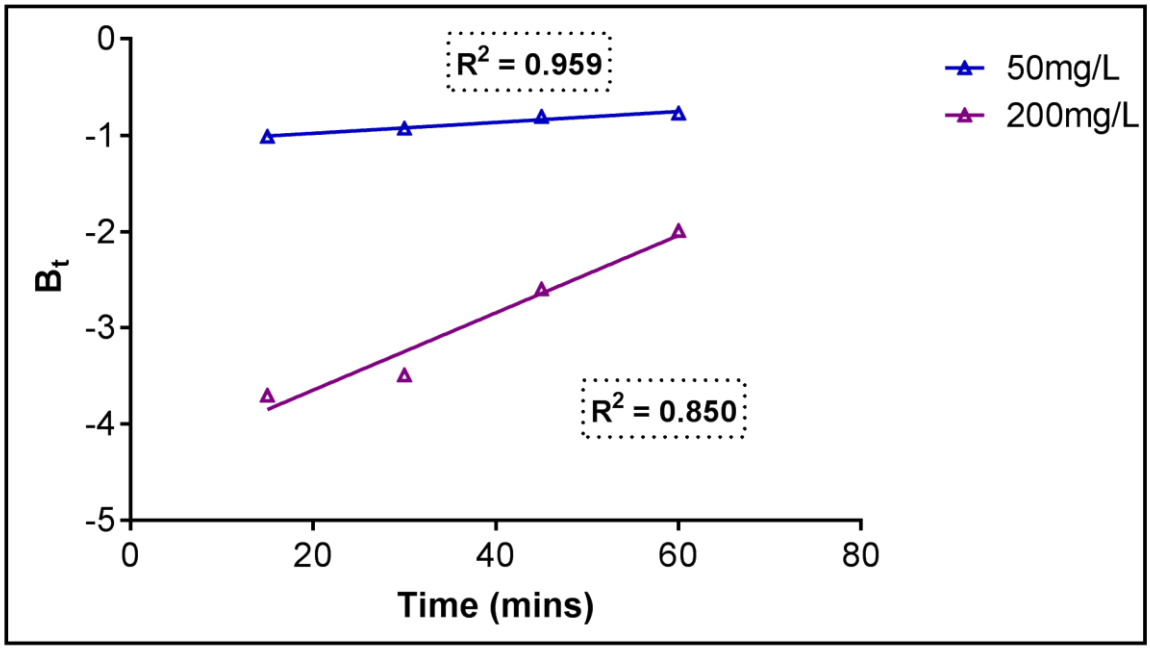

Figure 4.28: Boyd model at pH 5; lead ion concentration 50 mg/L & 200mg/L; agitation speed: 200rpm; at 21°C, 24h contact time, 5g/L alkali treated dosage. Boyd model fit shown by line.

Table 4.1: Pseudo second order kinetic parameters for non-linear regression.

50mg/L	NSD	R^2	RMSE	SSE	X^2
Pseudo second order	**0.030**	**0.998**	**6E-05**	**0.283**	**0.019**

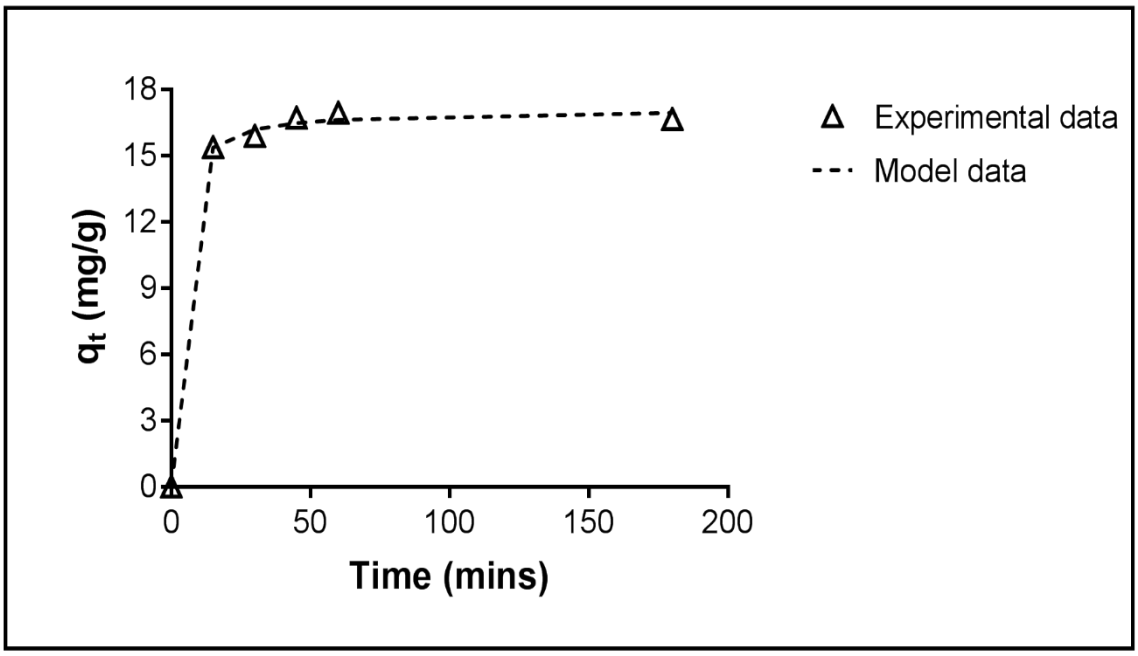

Figure 4.29: Pseudo second order (PSO) kinetic model using non-linear regression. PSO model fit shown by dashed line.

Table 4.2: Pseudo second order kinetic model parameters for linear regression.

Concentration (mg/L)	**qe**	**h**	**k_2**
50	16.778	23.041	0.022
100	18.587	7.868	0.023
150	22.573	20.325	0.040
200	27.100	11.834	0.016

A pseudo second order kinetic model shows the best fit for the lead adsorption on loofa. The correlation coefficient values are 0.99 with a low standard error value. The results fitted the pseudo-second order better than the pseudo first order model (Figure 4.25) indicating the involvement of two species in the sorption process of metal ions. Pseudo second order models best describe the adsorption of divalent metal ions (Vilar *et al.,* 2009).

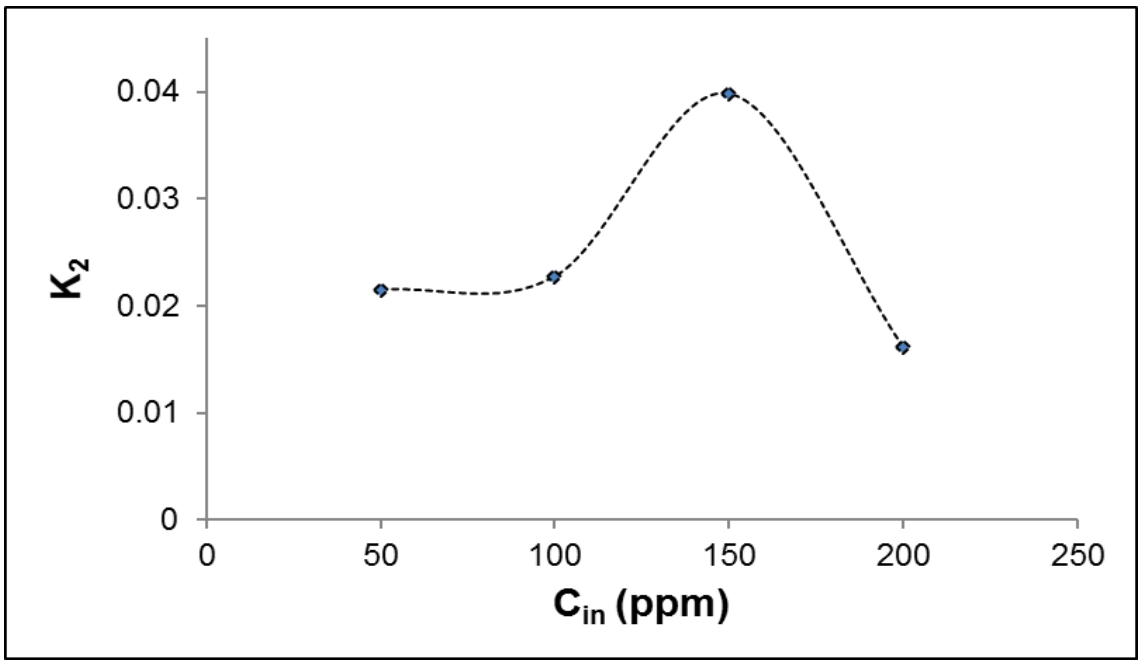

Figure 4.30: K_2 (pseudo second order constant) vs. initial metal ion concentration (50 - 200mg/L)

The pseudo second order rate constant (k_2) increases as concentration increases till it reaches a peak (Figure 4.30). This shows that the uptake rate is decreased and resistance in the mesopores is increased, until equilibrium is reached (Chi *et al*., 2013). This may be attributed to change in the ratio of binding interactions. The maximum adsorption capacity of the experimental values was very close in value to the model qe values as shown in Table 4.2. As initial concentration increases, K_2 decreases but as shown in Figure 4.30, the increase in initial concentration results in an increase in K_2 and after an optimum value had been reached, a decrease in K_2 was seen as concentration further increased. This implies that other experimental factors, not solely diffusion, play an important role in the kinetic process of adsorption. Also, this further explains the relationship between the number of available binding sites and the rate of adsorption since availability of sites is related to the initial concentration of metal ions and the time at which equilibrium adsorption capacity is reached (Plazinski *et al*., 2009). The rate controlling step could be determined solely on the above kinetic parameters, therefore further parameters where utilised to explain the adsorption mechanism.

In the intra particle diffusion model, shown in the Figure 4.27, the intercept was not equal to zero, therefore the rate controlling step is shown to be a complex mechanism and not the only rate limiting step. It involves a range of diffusive resistance (Yu *et al*., 2013; Madala *et al*., 2013; Abdelwahab and Amin, 2013).

The adsorption mechanism as expressed by boyd model in Figure 4.28 emphasizes film diffusion and not intraparticle diffusion mechanism. Boyd kinetic model expression, which determines the mechanism of adsorption kinetics, was utilized in differentiating between film and intraparticle diffusion (Banerjee & Chattopadhyaya, 2013; Madala *et al*., 2013). The results, in figure 4.28, show a linear relationship with a correlation coefficient of 0.959 at 50mg/L and 0.850 at 200mg/L. As the concentration increases the correlation coefficient decreases. This shows that the further away the values are from linearity, the higher the pore diffusion coefficient, which gives an indication that the rate controlling step is not governed by pore diffusion. This can possibly be explained as being film diffusion at lower concentrations. Therefore, the initial stages have film diffusion as the rate-controlling step and particle diffusion as the diffusion path increases (Kumar, 2003). This then suggests an adsorption process with a rate controlling step to be film diffusion.

Table 4.3: Pore diffusion coefficient (Dp) values at different uptake capacities (qe) at pH 5.

qe (mg/g)	Dp (cm^2/s)
15.375	1.239E-05
15.891	8.763E-06
16.716	7.155E-06
16.949	6.196E-06
16.664	3.577E-06

The values of pore diffusion are shown in table 4.3 to be between 10^{-5} - 10^{-7} which shows that pore diffusion is not the rate-determining step. This supports the Boyd model plot (Figure 4.28) with film diffusion model as the rate controlling step (Karthikeyan *et al*., 2010).

Rapid adsorption occurs in the first 15 minutes of the adsorption process. This is governed by the external diffusion, the transport of lead ions unto the external surface of the loofa. As the process proceeds, a slow process of adsorption occurs until equilibrium is reached. This is governed by internal diffusion which is the film diffusion kinetic mechanism. The process of lead adsorption on loofa is a complex mechanism governed by the transport process of external and internal diffusion.

4.2.7 Isotherm modeling

Two and three parameter isotherm models were used to best predict the mechanism behaviour of lead adsorption. Figure 4.31 to 4.35 show the different isotherm fitting models utilised using non-linear regression. Two-site Langmuir isotherm model indicates the best fit for the lead adsorption unto loofa with a correlation coefficient of 0.98.

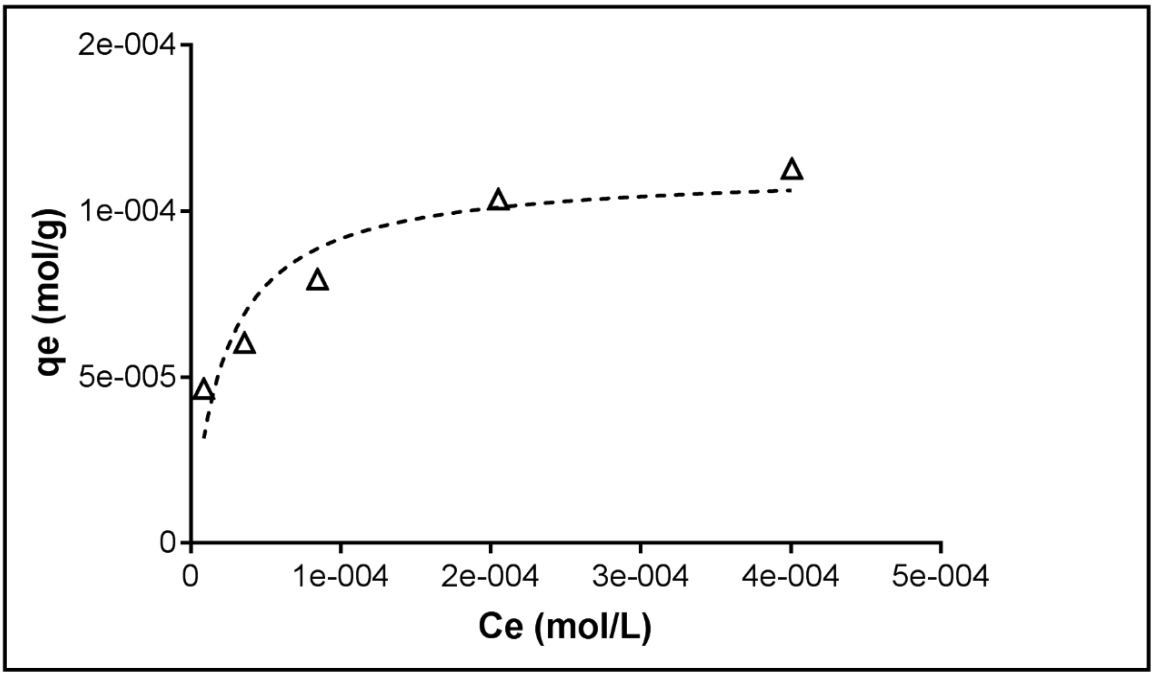

Figure 4.31: Lead isotherm from pH 5.0 ± 0.1 at 21 °C at 24 hr. contact time. Langmuir model fit shown by the dashed line.

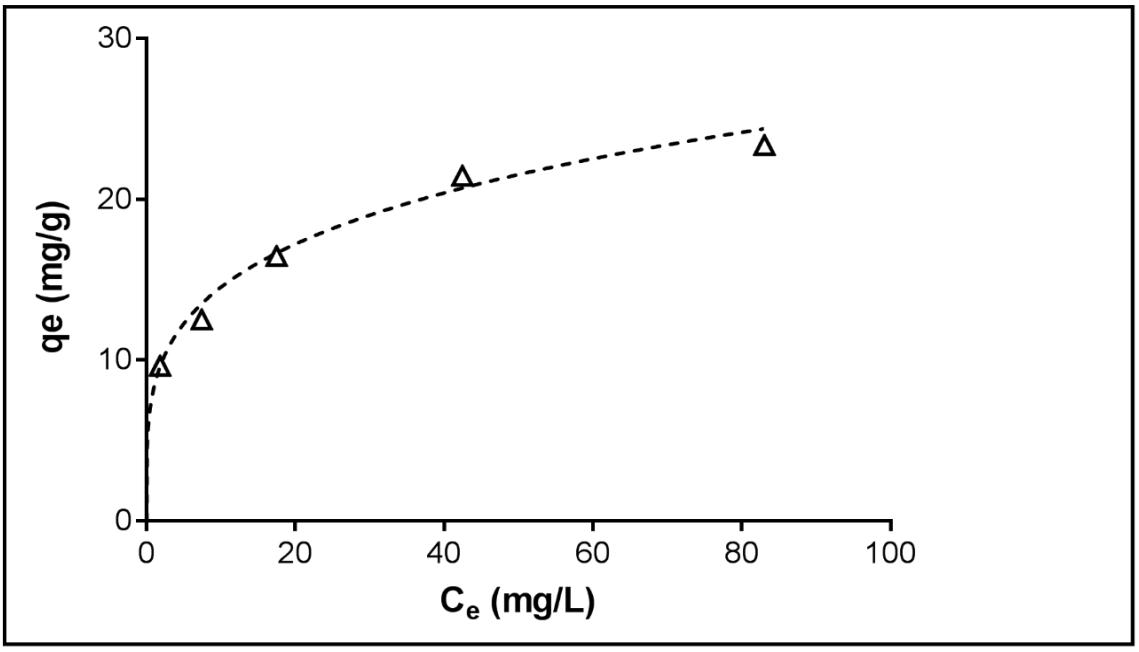

Figure 4.32: Lead isotherm from pH 5.0 ± 0.1 at 21 °C for 24 hr. contact time. Freundlich model fit shown by the dashed line.

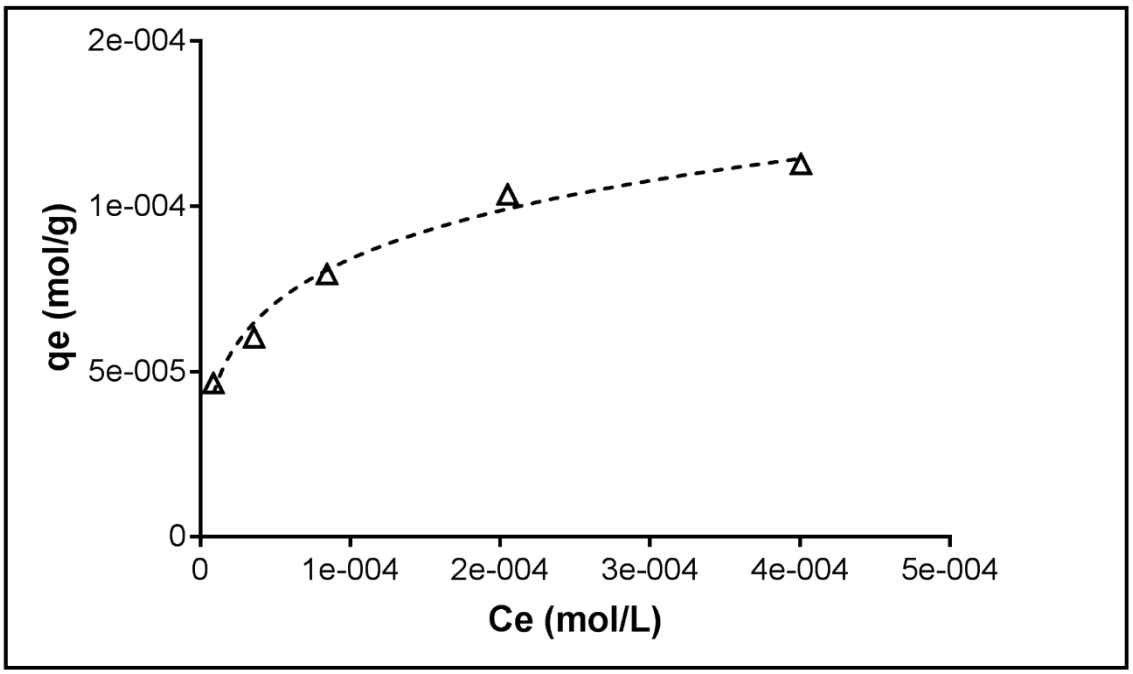

Figure 4.33: Lead isotherm from pH 5.0 ± 0.1 at 21 °C for 24 hr. contact time. Dubinin-Radushkevich model fit shown by the dashed line.

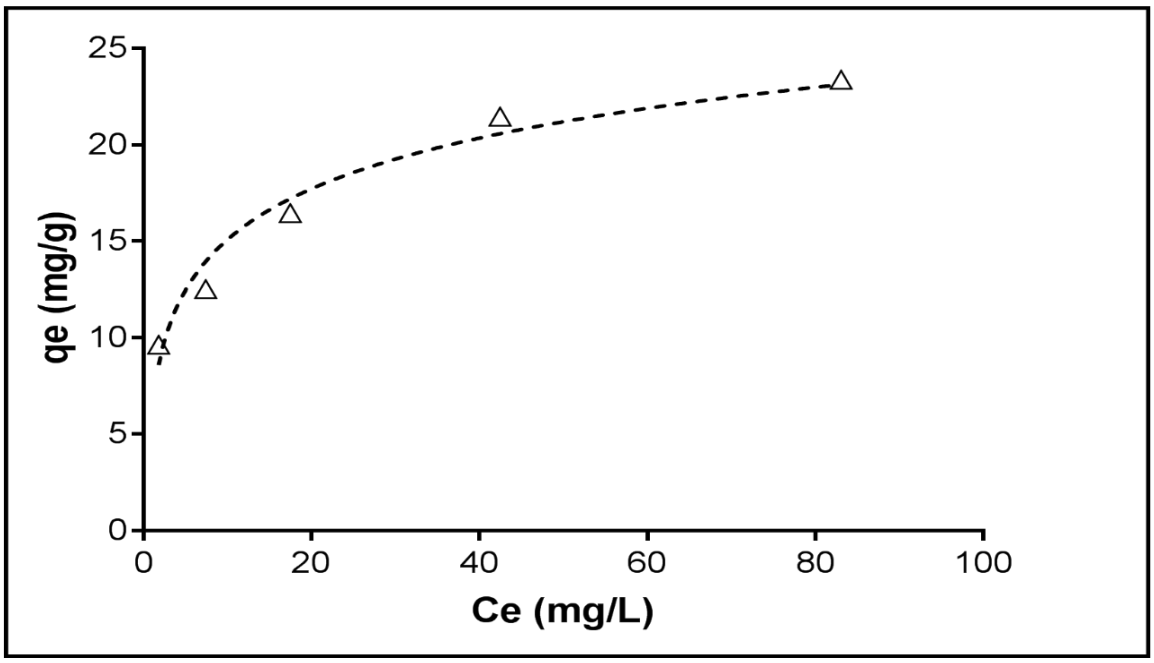

Figure 4.34: Lead isotherm from pH 5.0 ± 0.1 at 21 °C for 24 hr. contact time. Temkin model fit shown by the dashed line.

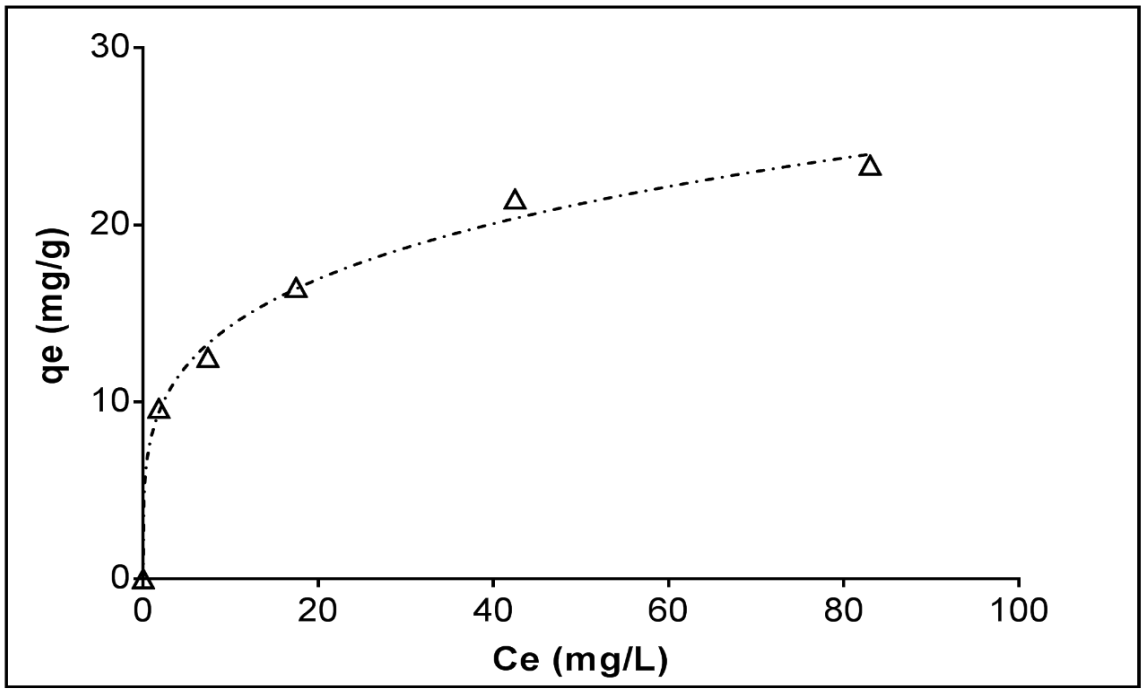

Figure 4.35: Lead isotherm from pH 5.0 ± 0.1 at 21 °C for 24 hr. contact time. Sips model fit shown by the dashed line.

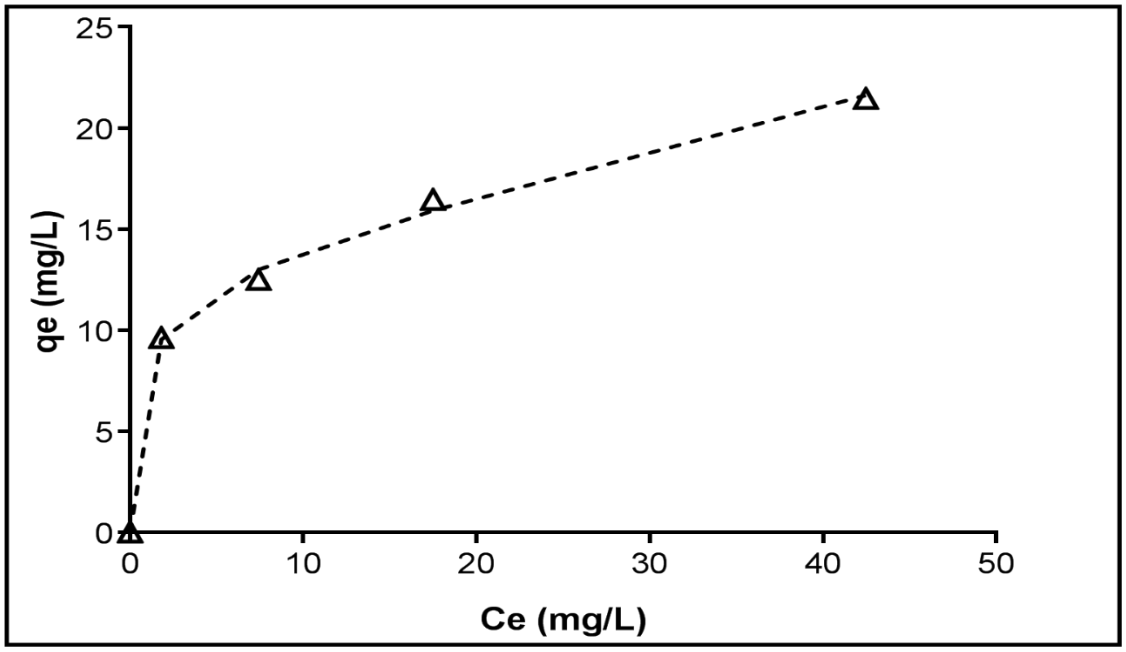

Figure 4.36: Lead isotherm from pH 5.0 ± 0.1 at 21 °C for 24 hr. contact time. Two-site Langmuir model fit shown by the dashed line. (R^2 = 0.984; 0.975).

Table 4.4: Correlation coefficient of isotherm models' fit.

Isotherm models	**R^2**
Langmuir	0.861
Freundlich	0.980
Dubinin-Radushkevich	0.983
Temkin	0.966
Sips	0.983
Flory - Huggins	0.888
Two-site Langmuir	0.985; 0.975

The relationship between the equilibrium concentration and adsorption capacity is depicted in Figures 4.31 to 4.35. Figure 4.31 shows a gradual increase in uptake capacity to a point where there is no significant change. This is a monolayer adsorption behavioural pattern. At low concentration, the specific sites on the adsorbent adsorb the lead ions and as lead ion concentration increases the sites become saturated, shown by no further increase in the loofa loading of lead ions. The adsorption behaviour of lead ions fitted the isotherm models, Two-site Langmuir > Sips > Dubinin-Radushkevich > Freundlich > Langmuir >Temkin. Two-site Langmuir was shown to give the best fit with a R^2 value of 0.985; 0.975. The Langmuir maximum loading capacity was 24.876mg/g having a K_L value of 0.160L/mg and R_L value of 0.099 which indicates a favourable adsorption process. The K_L values relate to a higher binding energy of adsorption will leads higher adsorption capacity (Madala *et al*., 2013; Ahmad & Haseeb, 2015; Li *et al*., 2008). Freundlich isotherm constants, K_f and n (8.27 and 4.09) are indicators of the adsorption capacity and adsorption intensity respectively (Mamatha et al., 2012a). The lead ion biosorption behaviour of loofa was termed favourable adsorption with a Freundlich constant, n, greater than

unity (Chowdhury & Saha, 2012). The interaction between the adsorbate and adsorbent as described by a Freundlich model shows favourable adsorption that is not restricted to monolayer formation (Figure 4.32) The value of 1/n at 0.244 measures the surface heterogeneity which becomes more heterogeneous with a value closer to 1 (Foo & Hameed, 2010). The Sips model is a combined form of the Langmuir and Freundlich models which predicts heterogeneous adsorption systems. The Temkin adsorption potential (binding constant), 5.309L/mg, depicts a higher value than the range between 0.77 – 1.5, which shows a higher loofa-lead ion potential (Rahman and Sathasivam, 2015). The Two-site Langmuir model indicates that there are two different sites available for adsorption of the lead ions.

The E value (12.910kJ/mol) obtained from equation (7) is in the range of 8-16kJ/moles which shows a chemisorption ion exchange process (Mamatha *et al*., 2012 ; Chowdhury & Saha, 2012).

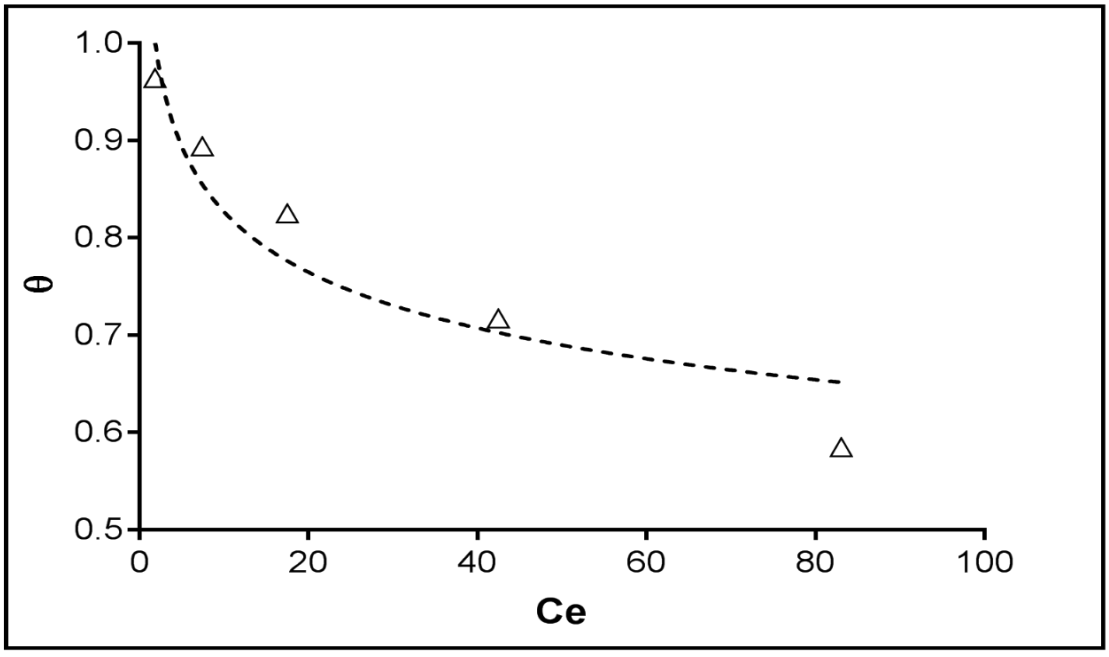

Figure 4.37: Lead isotherm from pH 5.0 ± 0.1 at 21 °C for 24 hr. contact time. Flory-Huggins model fit shown by the dashed line.

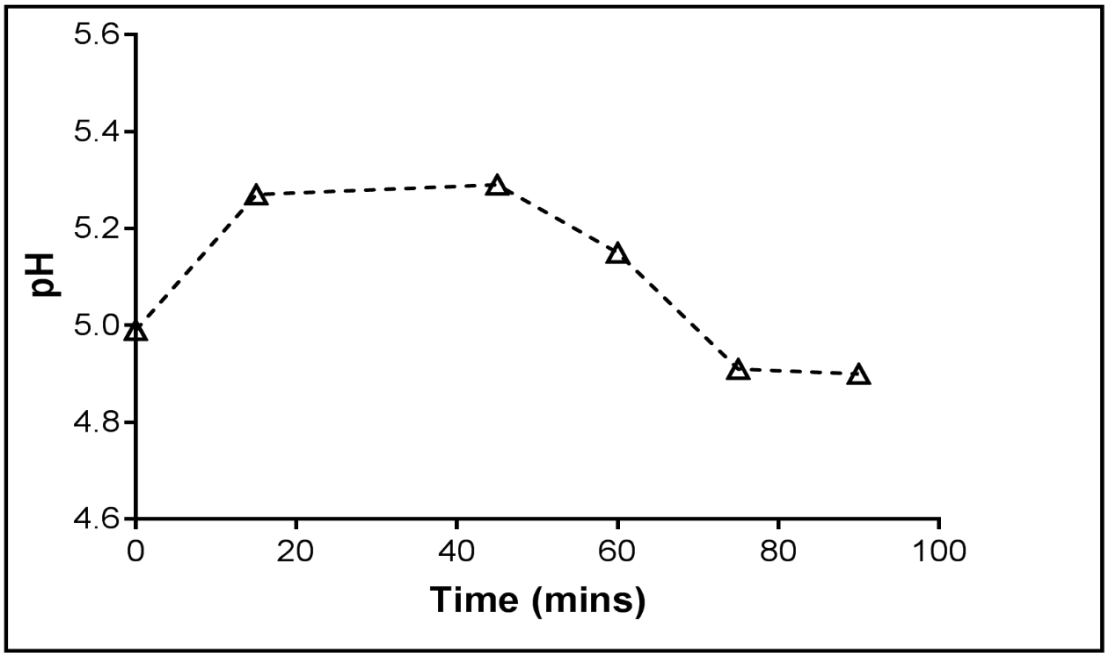

Figure 4.38: Change of solution pH over time at pH 5; lead ion concentration 100 mg/L; agitation speed: 200rpm; at 21^{o}C, 90 mins contact time, 5g/L alkali treated loofa dosage.

During the initial lead sorption process onto loofa at 15 mins (Figure 4.38), the pH value is shown to increase until 45 mins and then decrease afterwards. This supports the presence of a heterogeneous surface on the loofa which explains complexation at the initial adsorption stage and then ion exchange. At an initial pH, complexation tends to occur as the pH is increased by 5%. Over time, the pH slightly reduces as a result of the release of hydronium ions during the adsorption process. The initial rapid increase and gradual increase over time is shown as the pH changes.

4.2.8 Thermodynamics study

The thermodynamic parameters, obtained from a plot of Ink versus 1/T (Figure 4.39), shows its dependence on the utilised loofa. The results, shown in Figure 4.14 and 4.15, support the exothermic reaction of the lead adsorption process. Measurements were carried at 21^{o}C, 45^{o}C and 55^{o}C, and adsorption efficiency decreased with increase in temperature (Figure 4.14) The negative effect of temperature on the adsorption of lead ions therefore shows that increase in temperature favours desorption of lead ions from the loofa. This could be explained by the outer

sphere bonding of the lead ions which easily become unstable by application of thermal movements. This confirms that the uptake of lead ions was influenced negatively by increase in temperature and agrees with a number of authors who report that the adsorption of lead ions by different adsorbents decreases as temperature increases (Li *et al*., 2004, Brinza *et al*., 2007, Sari and Tuzen, 2008, Dahri *et al*., 2015).

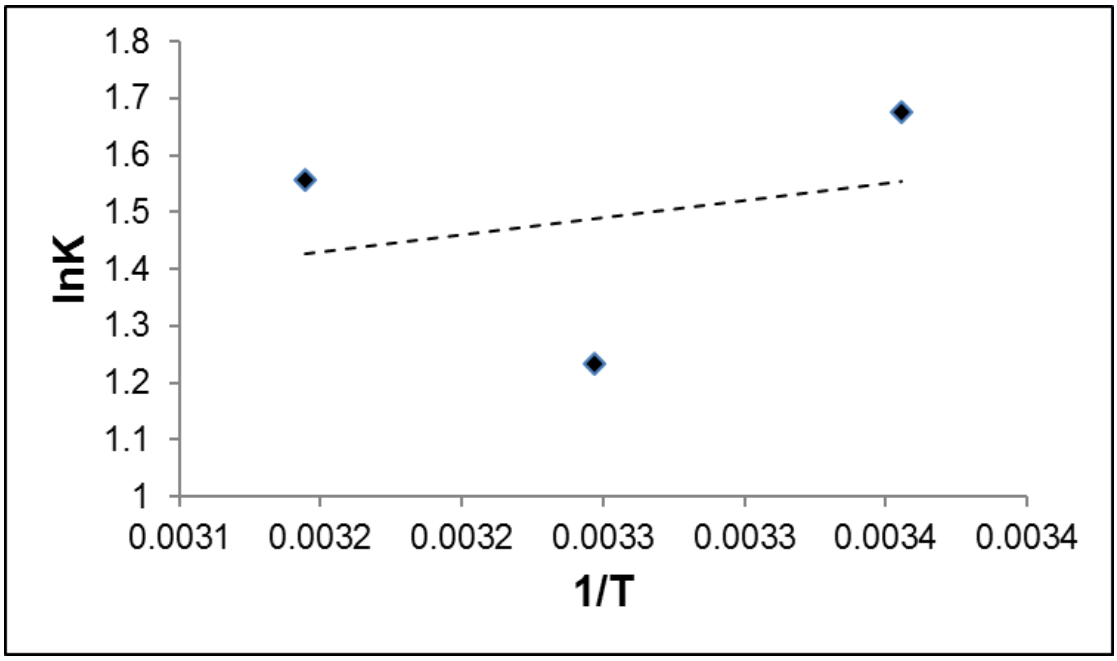

Figure 4.39: Estimation of thermodynamic parameters showing a plot of $\ln K_D$ versus 1/T.

The thermodynamic behaviour of lead adsorption onto loofa was described by the obtained ΔG, ΔS & ΔH values. The negative value of ΔG (Gibb free energy) (-4.2kJ/mol, -3.2kJ/mol & -4.1kJ/mol) at each temperature (298K, 308K & 318K) shows the thermodynamic feasibility and spontaneous nature of the adsorption process. The spread of the data points is an indicator of the inverse of the temperatures in Kelvin. The measured values ΔS and ΔH (-3.9kJ/mol &-5.0kJ/mol) were both negative which identifies an exothermic reaction (Liu and Lee, 2014). The ΔS (entropy change) determines the randomness at the solid/solution interface. The negative value obtained for ΔS shows a decrease in the randomness. The values of ΔG support the results from the D-R isotherm model that indicate chemisorption.

CHAPTER FIVE

5.0 ZINC BIOSORPTION MECHANISM

5.1 Introduction

This chapter discusses the speciation of zinc in aqueous solution and describes the effect of different experimental conditions on the adsorption of zinc ions onto *Luffa cylindrica* (loofa). The batch experimental results obtained when changes in pH, initial zinc ion concentration, loofa dosage, temperature and ionic strength on the biosorption of zinc were investigated are reported in section 5.2. Kinetic and isotherm models used to investigate the biosorption of zinc ions are also covered in this Chapter.

5.2 Batch experiments

The speciation of zinc depends on the pH of the solution as shown in the speciation plot (Figure 5.1 & 5.2). Solution pH is a dominant factor that affects the adsorption of metal ions from aqueous solution and the adsorption of zinc is shown to be a function of solution pH. The effect of pH on the adsorption of zinc is summarised below in Figures 5.3 – 5.6. Using equation (1) and (2) (Chapter 2), the uptake capacity and percentage removal was calculated and plotted against pH. Figure 5.7 shows the FT-IR spectra of zinc loaded loofa as compared to the alkali treated loofa. Figure 5.8 shows the influence of pH on the distribution ratio.

5.2.1 Zinc Speciation at different pH values

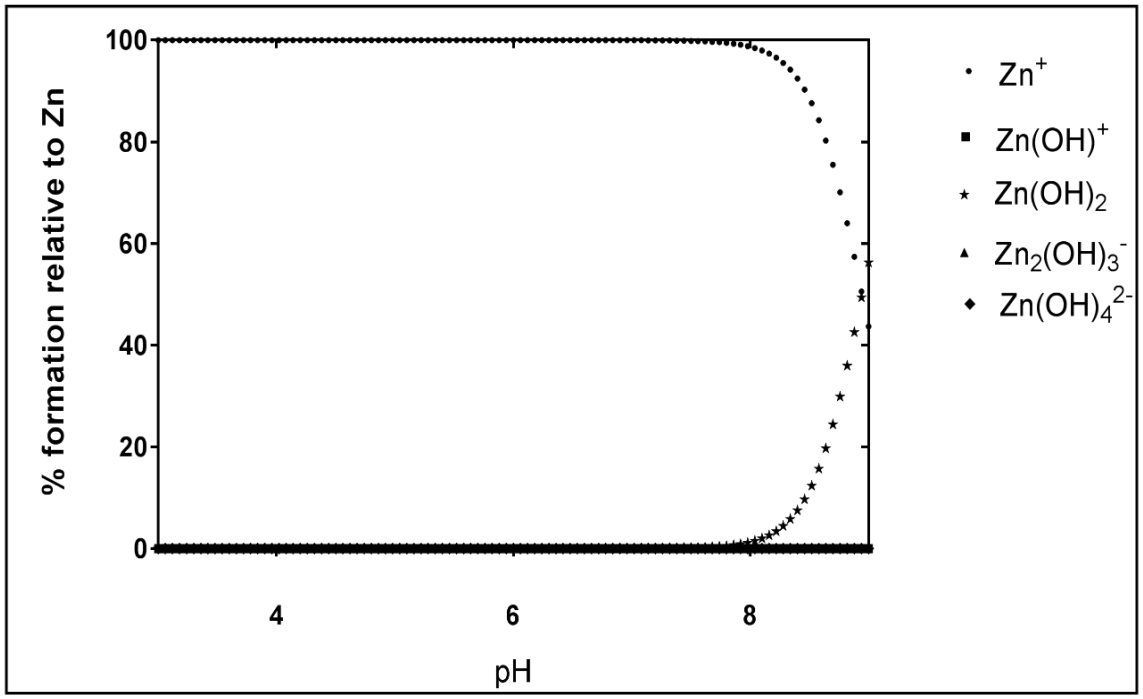

Figure 5.1: Speciation diagram of zinc ions in aqueous solution between pH 3 – 9 at 21°C. (Ekberg & Brown, 2016).

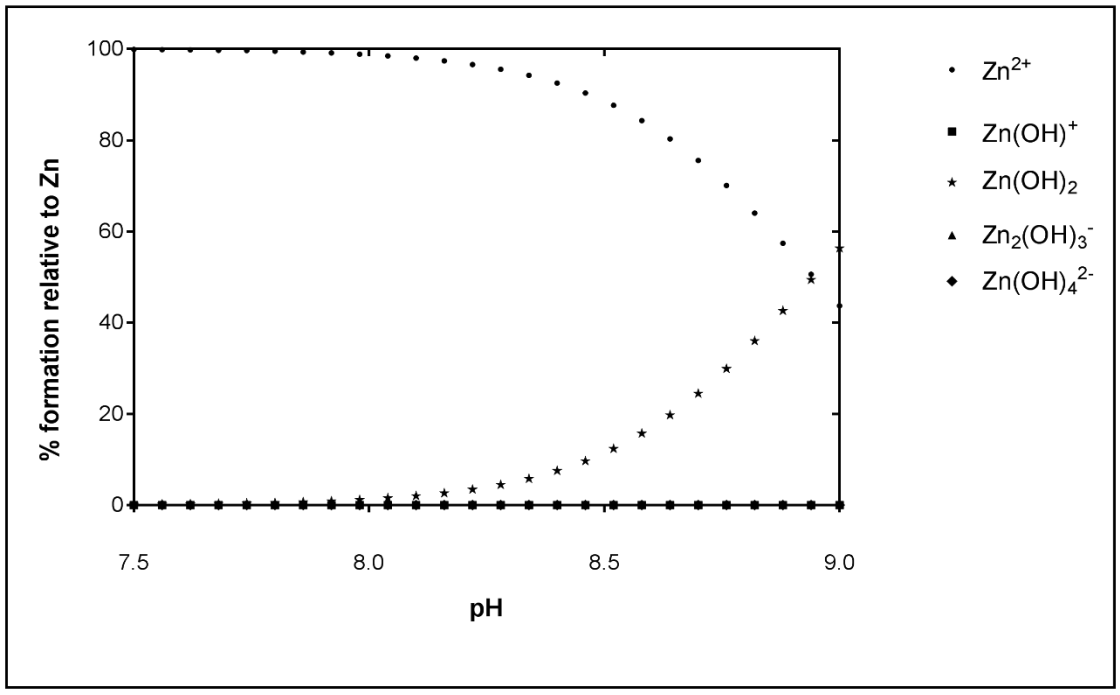

Figure 5.2: Speciation diagram of zinc ions in aqueous solution between pH 7.5 – 9 at 21°C. (Ekberg & Brown, 2016).

Figure 5.1 shows the speciation of zinc ions attached to the loofa surface. At a pH range of 3 – 9, the free zinc ions have a 100% dominance while there is little or no formation of zinc hydroxides on the loofa surface over a pH range of 3 -8. As the pH is increased, the formation of Zn $(OH)_2$ pH greater than 8. An enlarged plot is shown in Figure 5.2 at a pH range of 7.5 – 9.

5.2.2 pH effect

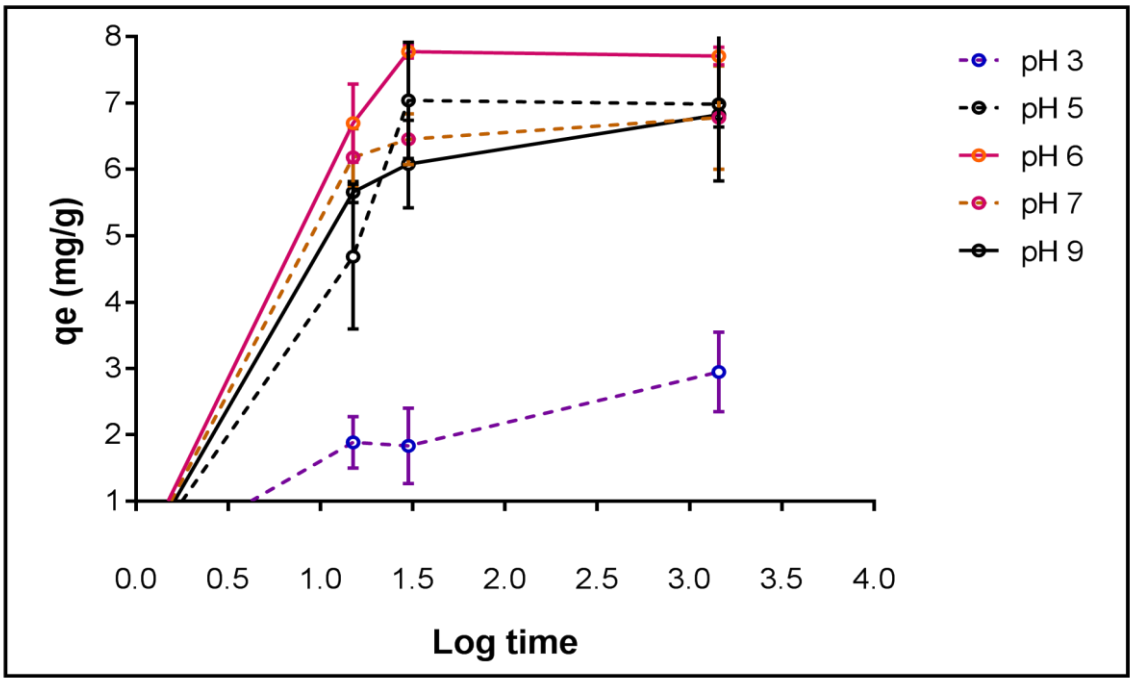

Figure 5.3: Uptake capacity (qe) of zinc ions with change in time (Log T in mins) after 24hrs at pH 3,5,7 and 9; zinc ion concentration: 50mg/L; agitation speed: 200rpm; at 21^{o}C, 24h contact time, 5g/L alkali treated loofa dosage. Data from 3 replicate measurements.

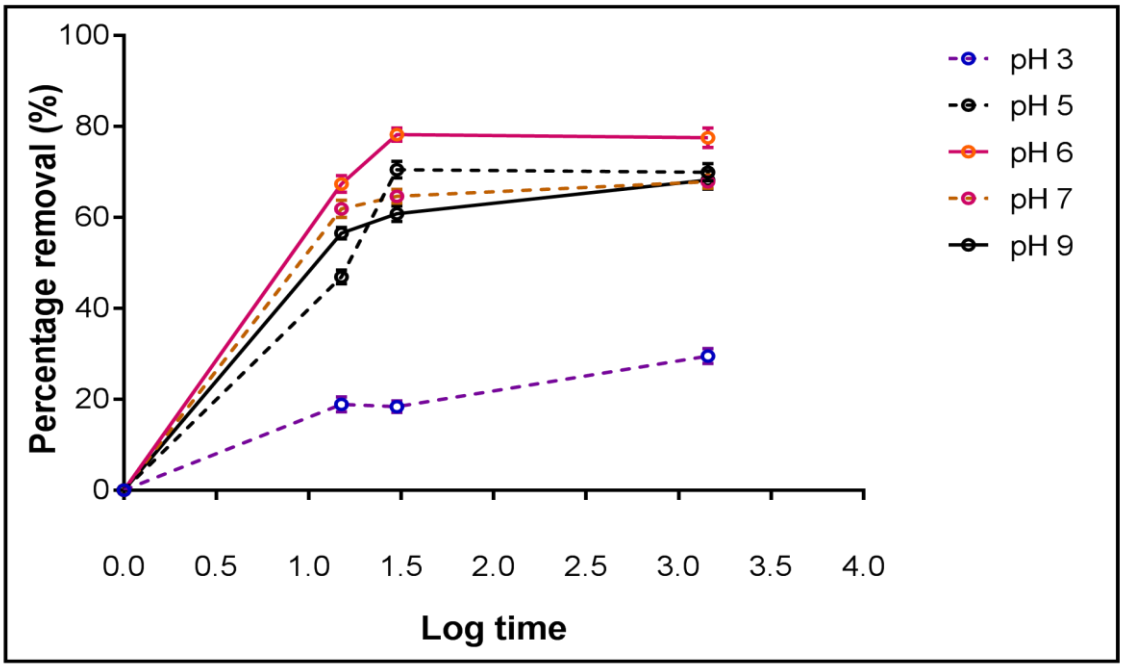

Figure 5.4: Percentage removal of zinc ion with change in time (Log T in mins) after 24hrs at pH 3, 5, 7 and9; zinc ion concentration: 50mg/L; agitation speed: 200rpm; at 21^{o}C,3h contact time, 5g/L dosage of alkali treated loofa. Data from 3 replicate measurements.

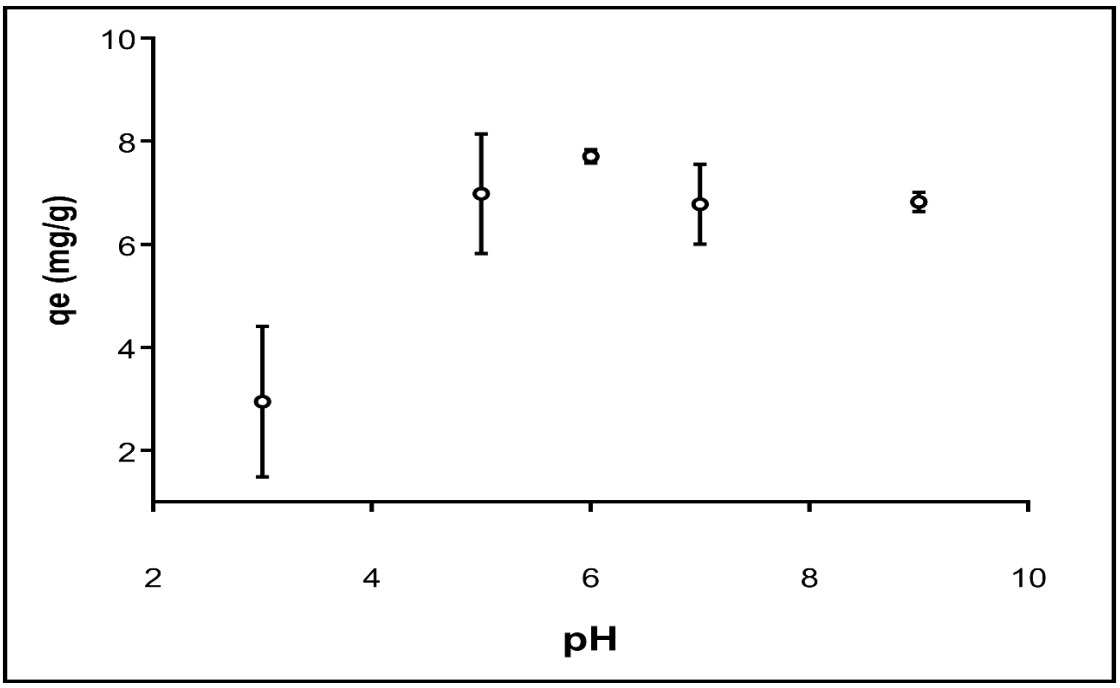

Figure 5.5: Zinc uptake capacity (qe) with change in pH after 24hrs; zinc ion concentration: 50mg/L; agitation speed: 200rpm; at 21^{o}C,24h contact time, 5g/L dosage of alkali treated loofa. Data from 3 replicate measurements.

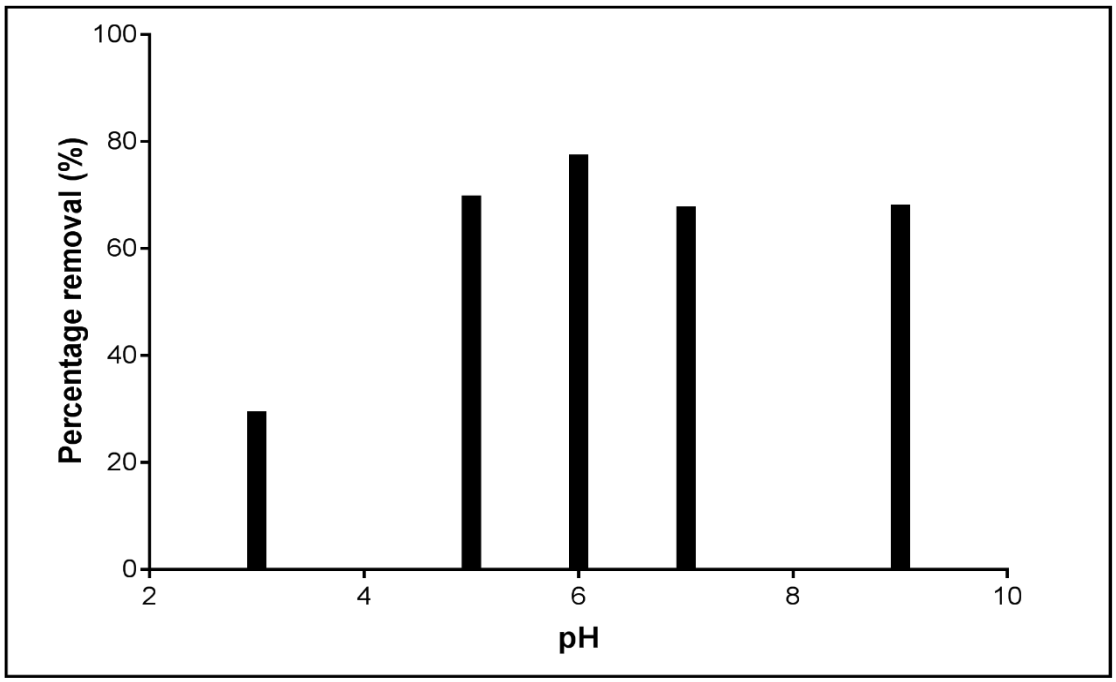

Figure 5.6: Percentage removal (E%) of zinc ions with pH after 24hrs at pH 3,5,6,7 and 9; zinc ion concentration: 50mg/L; agitation speed: 200rpm; at 21^{o}C, 24h contact time, 5g/L dosage of alkali treated loofa.

Figures 5.3-5.6 show that the maximum uptake capacity of zinc ions on loofa is at a pH of 6 (6.98mg/g). At a pH of 3, an uptake capacity of 2.95mg/g was measured. This low uptake capacity is explained by the competition between the H^+ and Zn^{2+} ions present in the solution. As the pH increases, the functional groups on the loofa surface are protonated and the amount of hydronium ions present in solution decreases thereby leading to a maximum uptake capacity of 6.98mg/g at pH 6 (figure 5.5) (Iqbal & Edyvean, 2004; Areco *et al*., 2012). Any further increase in pH causes the uptake capacity to decrease. This is not only attributed to lower hydrogen ion competition but also because of the more weakly acidic properties of the active sites on the adsorbent (deprotonation occurs) (Pagnanelli *et al*., 2003).

As shown in Figure 5.1 & 5.2, the dominant speciation of zinc are the free zinc ions present in the acidic medium up to a pH of 8. As the medium becomes alkaline in nature, the presence of the free zinc ions decreases.

Over a pH of 8, the presence of hydroxylated zinc ions is increased leading to a lower percentage removal of 68.2% (Figure 5.6). The reduction in percentage removal (9.3%) between pH 6 to 9 shows the dominant factor that affects the adsorption of zinc is the competition of hydrogen ions present in solution as compared to the hydroxylation of the zinc ions that lead to precipitation in solution. The metal uptake capacity is more importantly correlated between the metal acidic property than the specific functional groups of the surface of the adsorbent (Pagnanelli *et al*., 2003).

5.2.3 FT-IR spectra

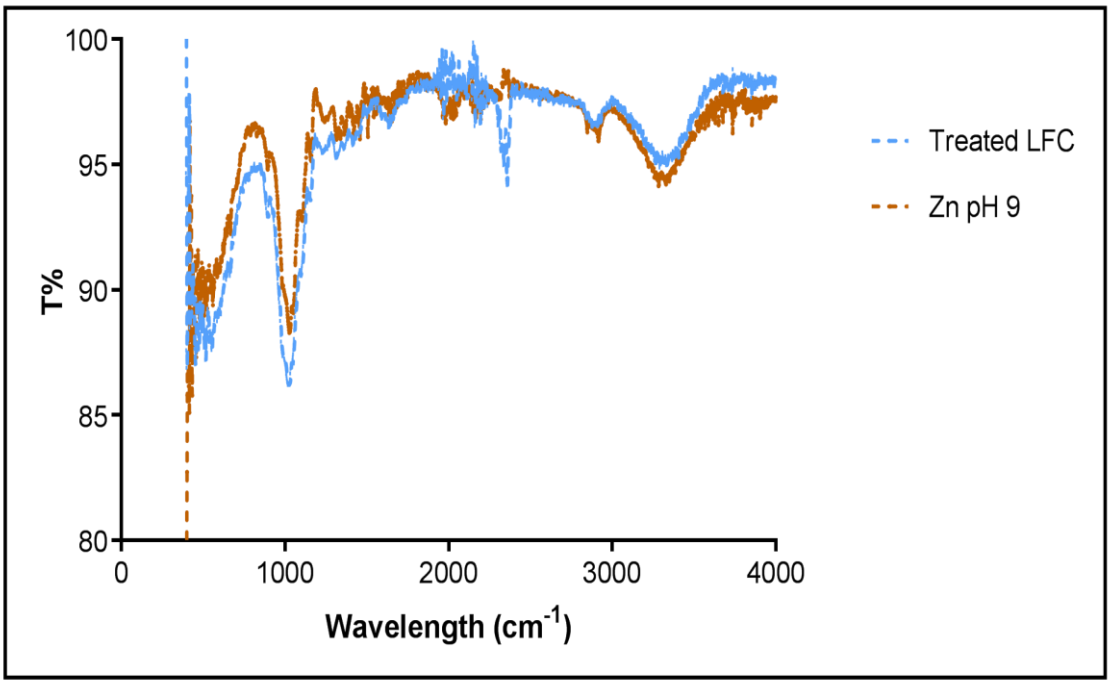

Figure 5.7: T% (transmittance percentage) versus wavelength FT-IR spectra of 4% NaOH treated loofa before exposure to Zn and Zn-loaded loofa at pH 9 (zinc ion concentration: 50mg/L; agitation speed: 200rpm; at 21°C, 24h contact time, 5g/L alkali loofa dosage).

Figure 5.7 shows the changes in peak intensity of specific functional groups on the loofa that occur at wavelengths between 1000 – 1500cm^{-1}. These are attributed to O-H bonding. No change is seen between 2900 -2950cm^{-1} which is attributed to C-H bonding. At 3330 - 3340 cm^{-1}, the broad band is associated with O-H stretching where O-H bonding occurs (Altinişik *et al*., 2010; Olu-owolabi & Unuabonah, 2010) The peak intensities correspond to the change in binding energy as adsorption occurs. Furthermore, the FT-IR spectra increases in transmittance, this change indicates adsorption of zinc ions on the loofa. The changes that occur on the functional group of the loofa surface are indicated by the FT-IR spectra.

At pH > pH_{pzc} (pH_{pzc} = 7.2) due to electrostatic attraction, adsorption is expected to increase but the maximum adsorption is seen to occur at pH 6 (Figure 5.5). And further increase in the pH leads to a reduced adsorption capacity because of the hydroxylation of the lead ions present in

aqueous solution. Furthermore, the formed bonds due to electrostatic attraction and reduced competitive effect of the hydronium ions is the dominant factor that influences zinc adsorption on alkali treated loofa.

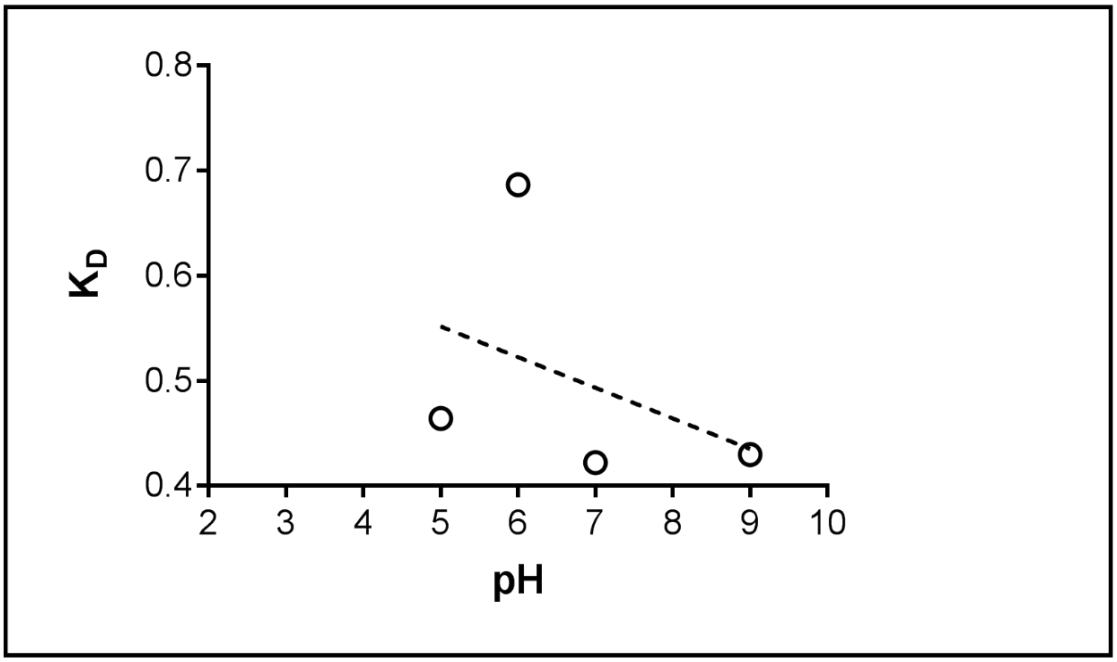

Figure 5.8: Distribution ratio (K_D) versus pH at equilibrium at pH range 5-9; zinc ion concentration: 50mg/L; agitation speed: 200rpm; at 21^oC, 24h contact time, 5g/L alkali treated loofa dosage.

Figure 5.8 shows a high distribution ratio value of 0.7 at an optimum pH of 6. This describes a strong chelation metal bond being formed as compared to bonds formed at the different pH values (Ahamed *et al.,* 2010; Zhao *et al*., 2016).

5.2.4 Concentration effect

Figure 5.9 – 5.11 show the uptake capacity of zinc ions adsorbed onto loofa at different initial concentrations. As the initial concentration is increased, the zinc ion adsorption increases over time. At equilibrium, the uptake capacity is observed to have reached an optimum value as shown in Figures 5.8 and 5.9. The percentage removal of zinc ions increased from 77.55% at 50mg/L to 86% at 70mg/L. No increase was observed with a further increase to 100mg/L (Figure 5.11).

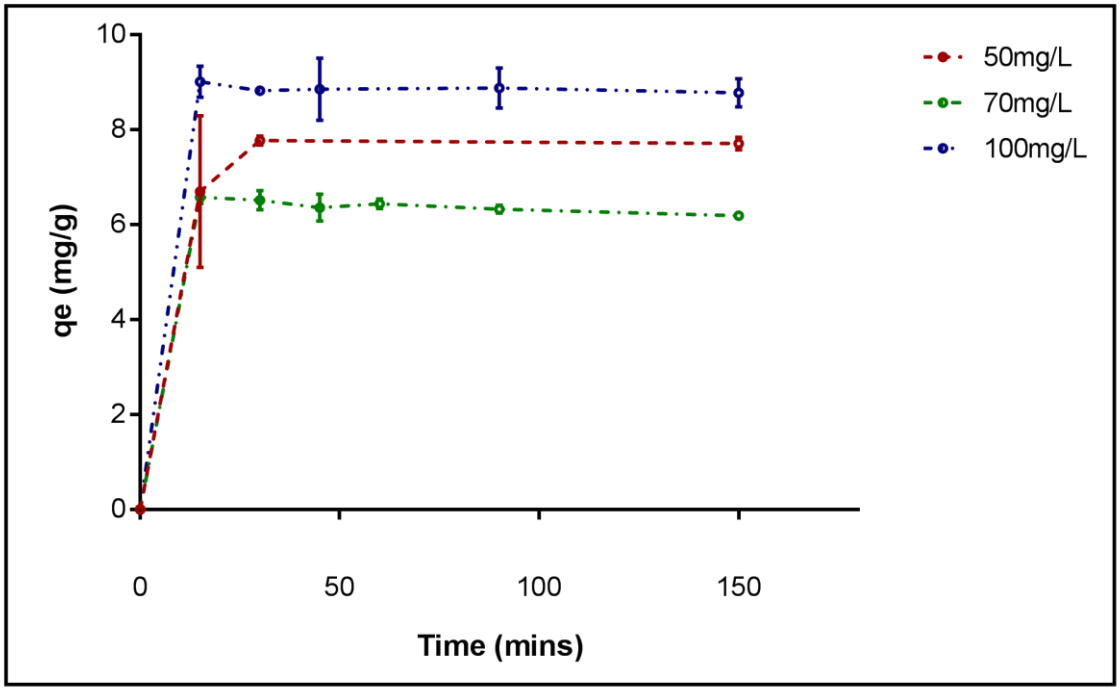

Figure 5.9: Uptake capacity (qe) of zinc ions with time over 2.5hrs at pH 6; zinc ion concentration ranges of 50 – 100mg/L; agitation speed: 200rpm; at 21°C,2.5h contact time, 5g/L alkali treated loofa dosage. Data from 3 replicate measurements.

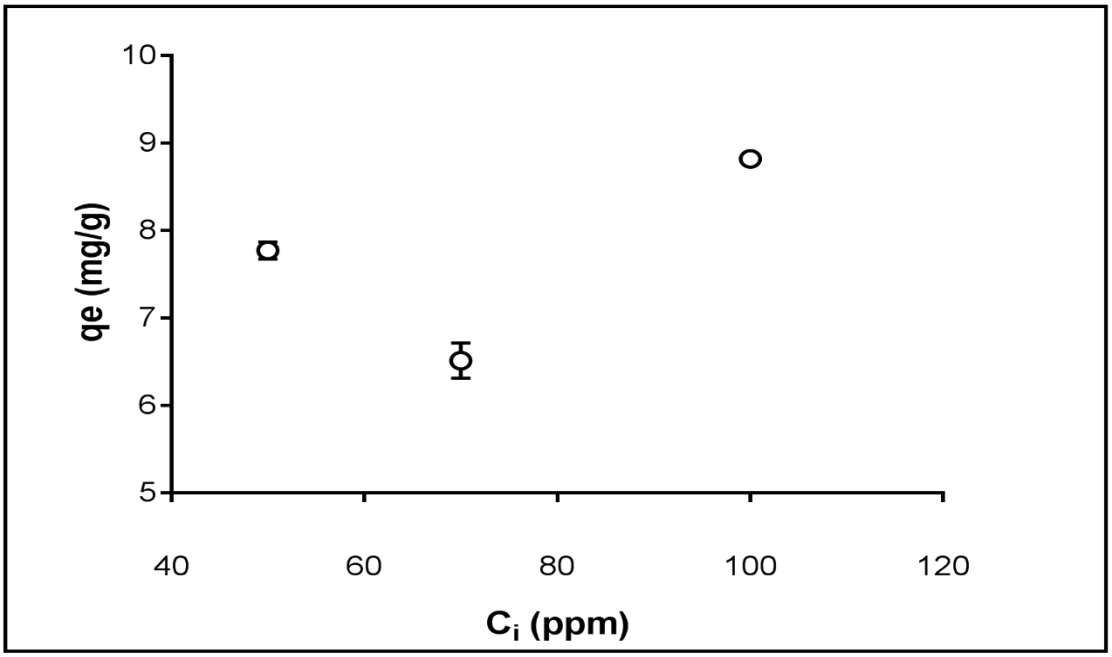

Figure 5.10: Uptake capacity (qe) of zinc ions at different initial concentrations (C_i) after 2.5hrs at pH 6; zinc ion concentration ranges of 50 – 100mg/L; agitation speed: 200rpm; at 21°C,2.5h contact time, 5g/L alkali treated loofa dosage. Data from 3 replicate measurements.

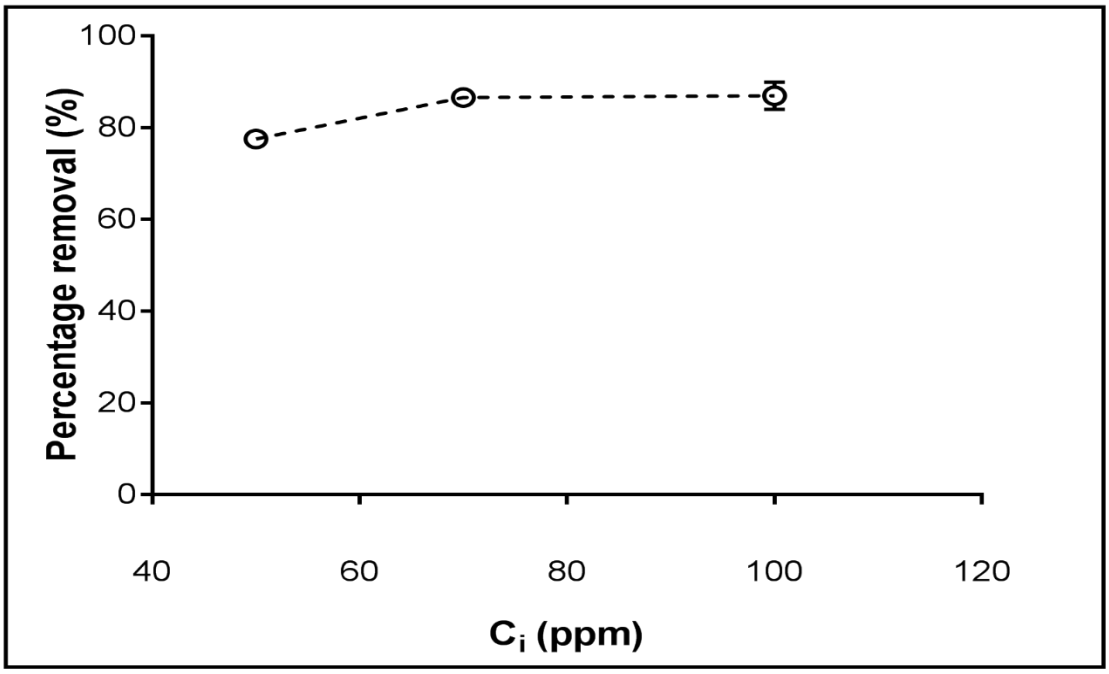

Figure 5.11: Percentage removal of zinc ions at different initial concentrations (C_i) after 2.5hrs at pH 6; zinc ion concentration ranges of 50-100mg/L; agitation speed: 200rpm; at 21^{o}C,2.5h contact time, 5g/L alkali treated loofa dosage. Data from 3 replicate measurements.

At low concentrations, the zinc ions are adsorbed at specific sites and at increased concentrations, the specific sites are saturated and the exchange sites are occupied, eventually leading to no significant increase in the adsorption of the zinc ions (Pagnanelli *et al*., 2003).

5.2.5 Loofa dosage – The highest amount of 5g/L was used to run all experiments as this was previously shown (in chapter 4) to have the best adsorptive capacity.

5.2.6 Temperature – Temperature was observed to have a negative effect on the lead adsorption by loofa (Chapter 4). This binding process for zinc is similar to that of lead (divalent metal ion), therefore a similar effect of temperature is predicted for zinc ion adsorption. The nature and structure of the loofa which is influenced by experimental factors such as solution pH and initial metal ion concentration as shown in chapter 4, supports the literature report by Šoštari *et al*., 2016. Sostari *et al*. (2016) shows lead adsorption by raw corn silk to be an endothermic reaction with optimum pH of 5 which is favourable at higher temperatures (Amer *et al*., 2015; Šoštari *et al*., 2016; Drweesh *et al*., 2016). Therefore, any damage of the active sites of the loofa as a result of a rise in temperature could be the reason for decreased adsorption of lead ions and such would also be expected for zinc adsorption. However, the optimum temperature is expected to be at room temperature (21^{o}C).

5.2.7 Ionic strength

The effect of ionic strength of the aqueous solution on the adsorption of zinc ions onto loofa is depicted in Figure 5.12 – 5.18. The competition for active sites on the loofa in a mixed concentration of aqueous solution (zinc ions and NaCl – 1:1 ratio) is described. Also, the comparison of the percentage removal of zinc ions alone and the mixed zinc and NaCl solutions is shown.

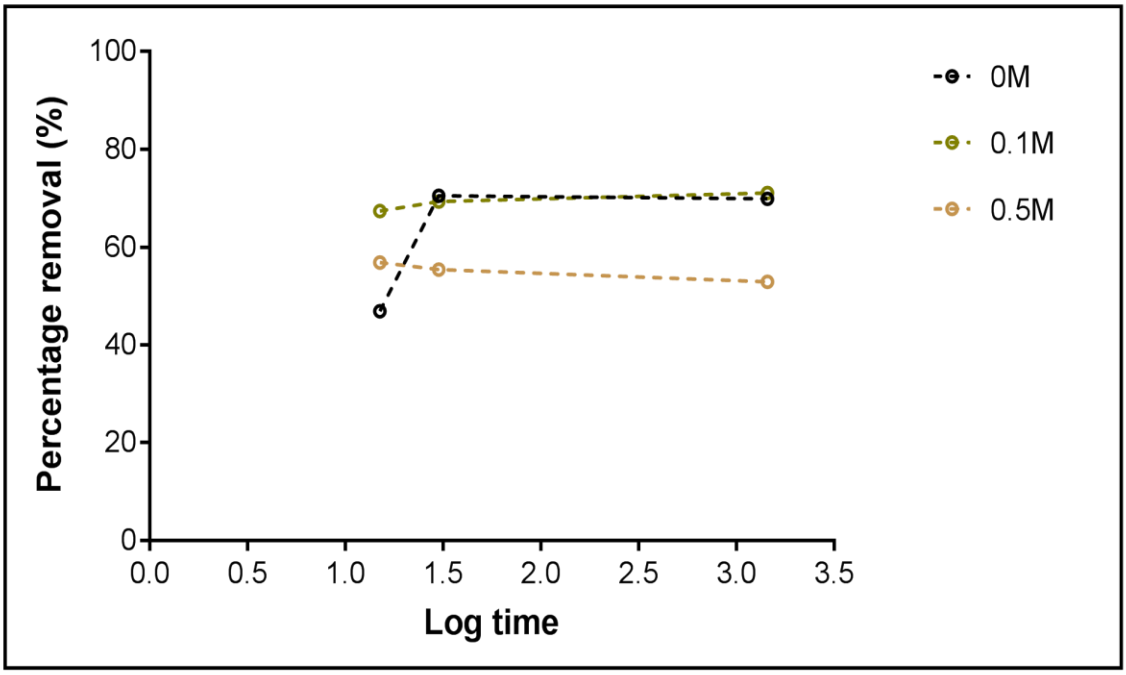

Figure 5.12: Percentage removal (E%) of zinc against time (Log time in mins) in the presence of NaCl in aqueous solution; agitation speed: 200rpm; at 21^{0}C, at pH 5, 24h contact time 5g/L alkali treated loofa dosage.

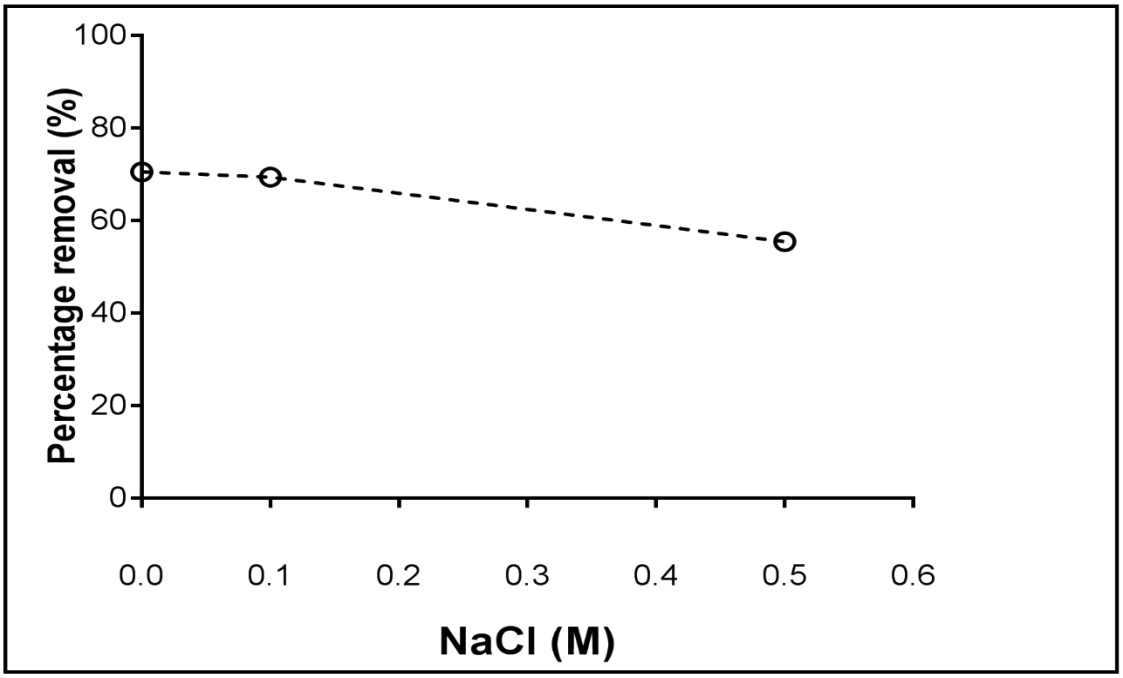

Figure 5.13: Percentage removal of zinc ion with change in NaCl concentration after 24hrs; zinc ion concentration: 50mg/L; agitation speed: 200rpm; at 21^{o}C, at pH 5,24h contact time, 5g/L alkali treated loofa dosage.

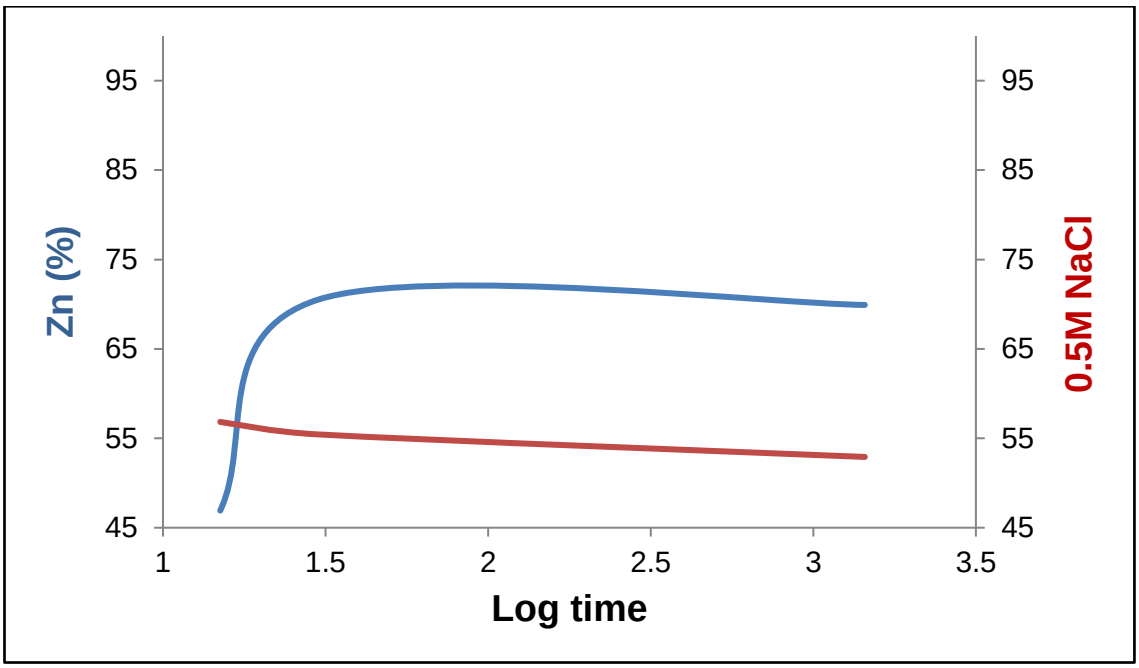

Figure 5.14: Comparison of percentage removal of zinc ions and 0.5M NaCl after 24hrs (Log time in mins); zinc ion concentration: 50mg/L; agitation speed: 200rpm; at 21^{o}C, at pH 5,24h contact time, 5g/L alkali treated loofa dosage.

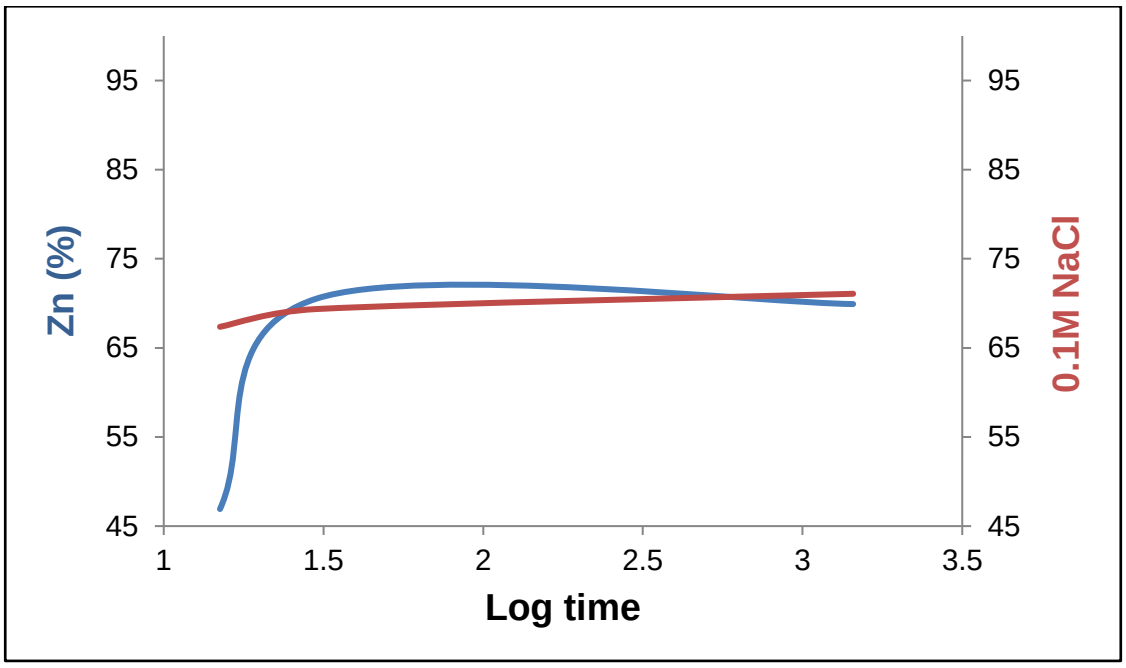

Figure 5.15: Comparison of percentage removal of zinc ions and 0.1M NaCl after 24hrs (Log time in mins); zinc ion concentration: 50mg/L; agitation speed: 200rpm; at 21°C, at pH 5,24h contact time, 5g/L alkali treated loofa dosage

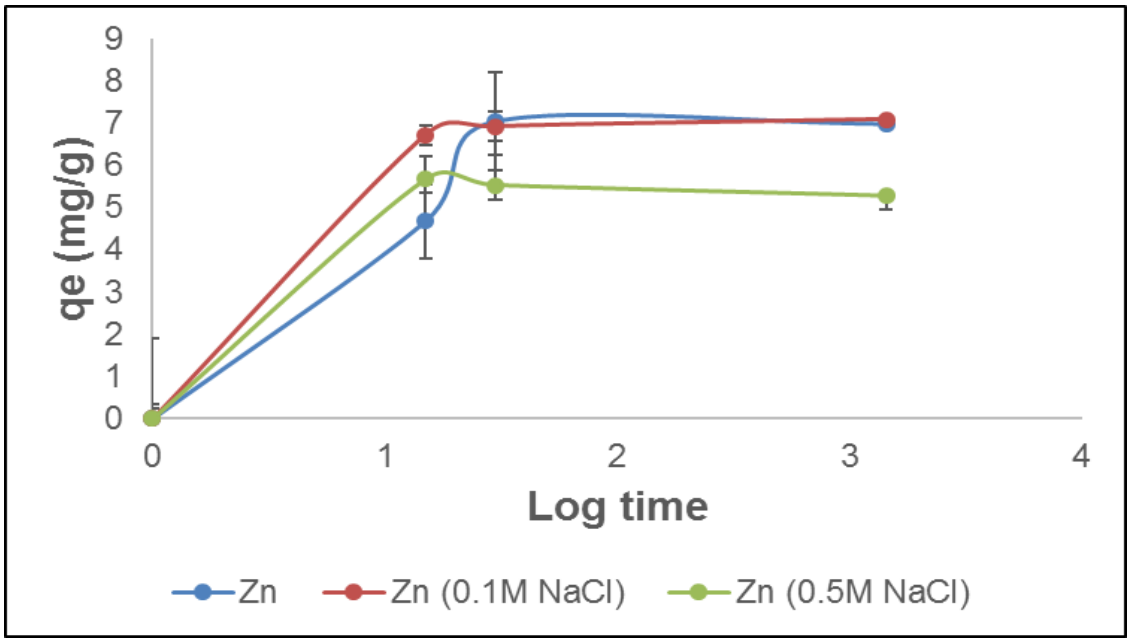

Figure 5.16: Uptake capacity (qe) of zinc ions with change in NaCl concentration over time (Log time in mins); lead ion concentration: 50mg/L; agitation speed: 200rpm; at 21°C, at pH 5, 24h contact time, 5g/L alkali treated loofa dosage. Data from 3 replicate measurements.

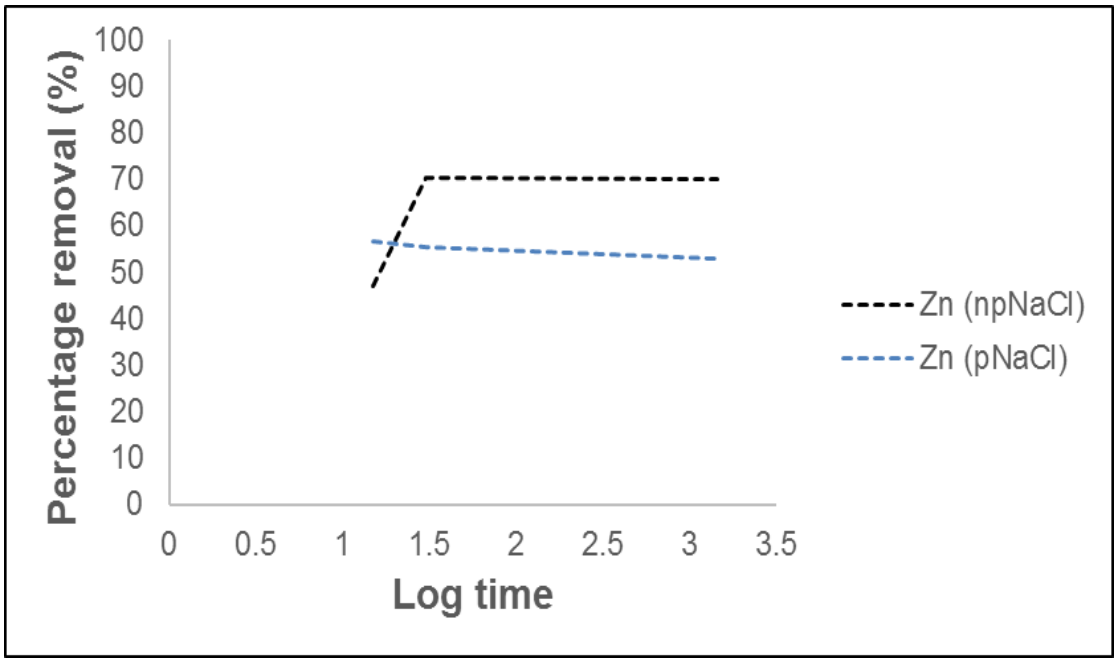

Figure 5.17: Percentage removal of zinc ions in the presence of (pNaCl) and absence (npNaCl) of 0.5M NaCl (Log time in mins); zinc ion concentration: 50mg/L; agitation speed: 200rpm; at 21^{0}C, 24h contact time, 5g/L alkali treated loofa dosage.

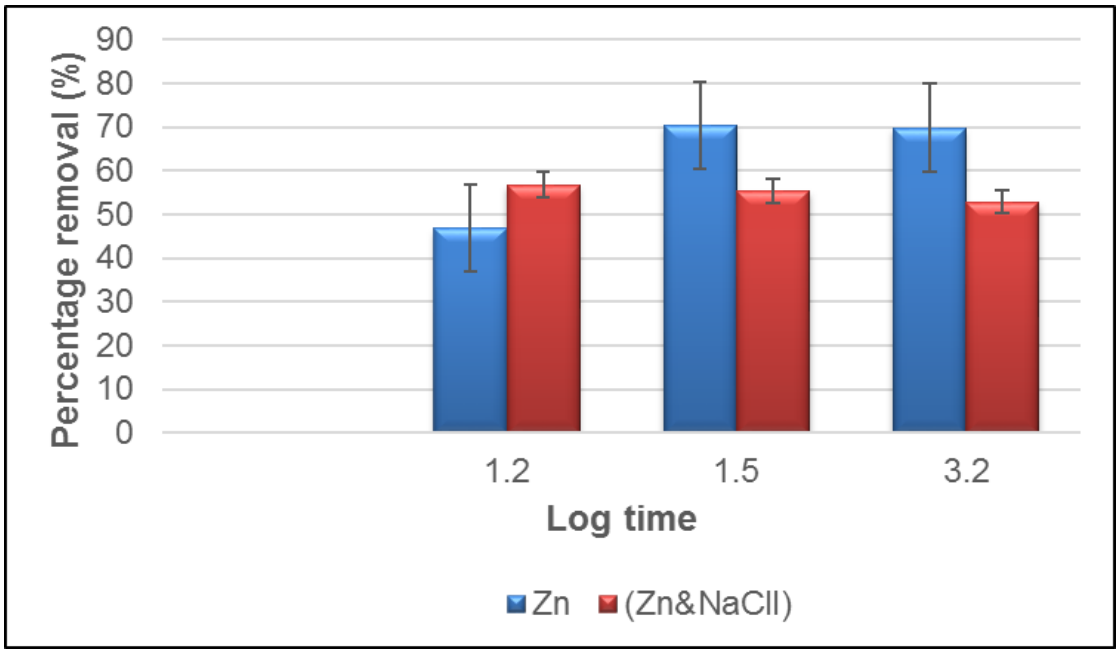

Figure 5.18: Percentage removal of zinc ions, 0.5M NaCl and mixed aqueous solution of both after 24hrs (Log time in mins); zinc ion concentration: 50mg/L; agitation speed: 200rpm; at 21^{o}C, at pH 5, 5g/L alkali treated loofa dosage. Data from 3 replicate measurements.

As shown in Figures 5.12 – 5.16, as the NaCl concentration is increased, the uptake capacity of the zinc ions is decreased. The initial concentration of NaCl at 0.1M and 0.5M is shown to have an effect on zinc adsorption by approximately 1% and 25% reduction respectively (Figure 5.13). The effect of the ionic strength at the different concentrations is shown to occur rapidly after 15mins (Figure 5.14 – 5.17). This could be due to the rapid enhancement of aggregation of carbon nanomaterials on the loofa surface thereby leading to reduced adsorption active sites which decreases the adsorption affinity over time (Zhao *et al*., 2016).

Once sodium chloride is introduced into the aqueous solution, the effect of ionic strength on the surface charge of the loofa leads to an increase in the presence of ionic forms thereby decreasing zinc ion adsorption. A further increase in ionic strength increases the effect on zinc ion uptake over time. Further discussion on the effect of sodium ions on divalent ions in solution is described in Chapter 4.

5.2.7 Kinetic modelling

The kinetics of an adsorption system determines the rate controlling step of the adsorption mechanism. Figure 5.19 – 5.25 show the kinetic models utilised to determine the rate controlling step of the adsorption process. The kinetic plots are calculated for a range of different pH values. The best fit model (pseudo second order) values are shown in Table 5.2. A non-linear regression fitting was done for the pseudo second order model (Figure 5.26) and the effect of the pseudo second rate constant as regards to change in initial concentration is described in Figure 5.27.

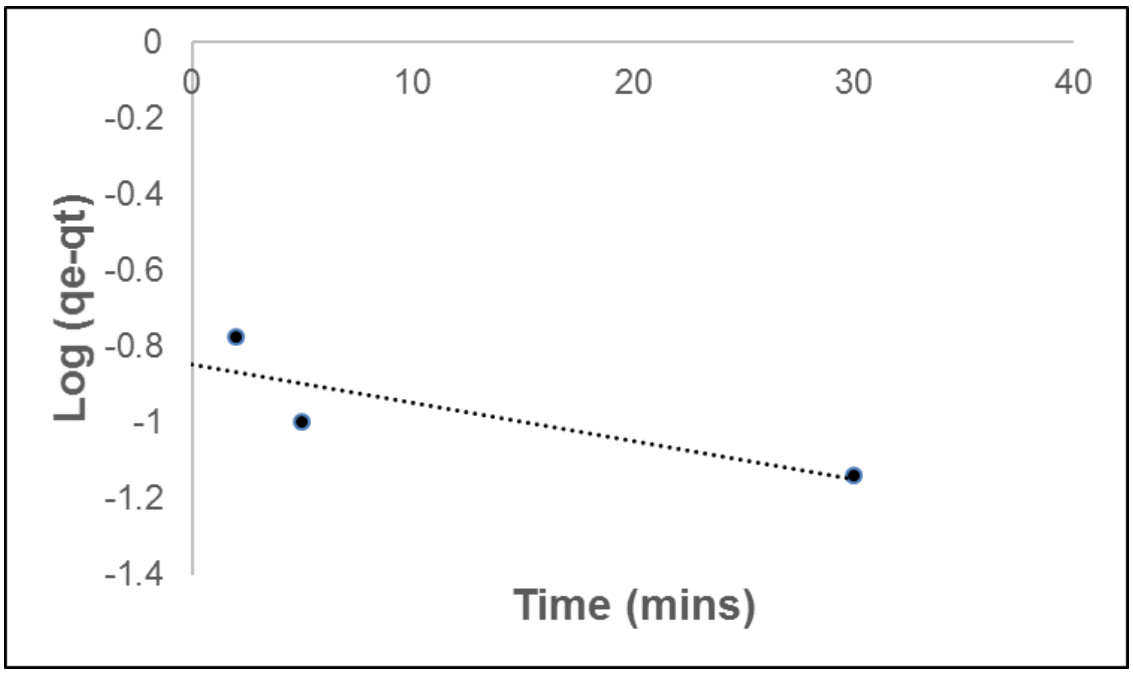

Figure 5.19: Pseudo first order (PFO) kinetic model at pH 6; zinc ion concentration 70 mg/L; agitation speed: 200rpm; at 21°C, 0.5h contact time, 5g/L alkali treated loofa dosage (R^2 = 0.99). PFO model fit shown by the dashed line.

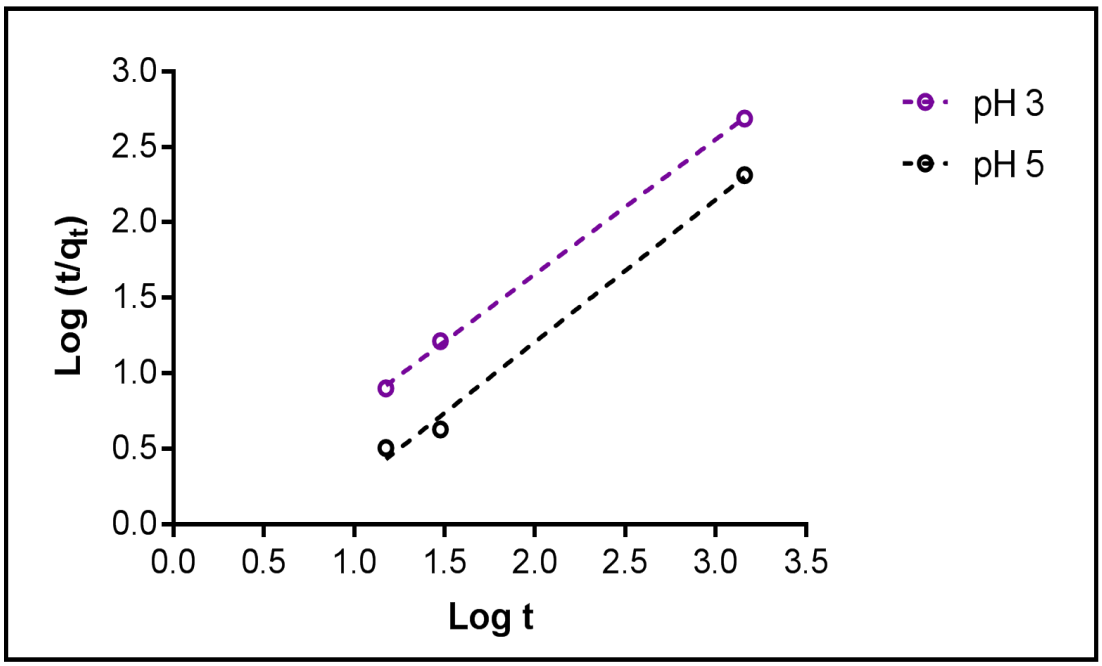

Figure 5.20: Pseudo second order (PSO) kinetic model at pH 3 and pH 5 (Log t is Log time in mins); zinc ion concentration 70 mg/L; agitation speed: 200rpm; at 21°C, 24h contact time, 5g/L alkali treated loofa dosage. PSO model fit shown by the dashed line.

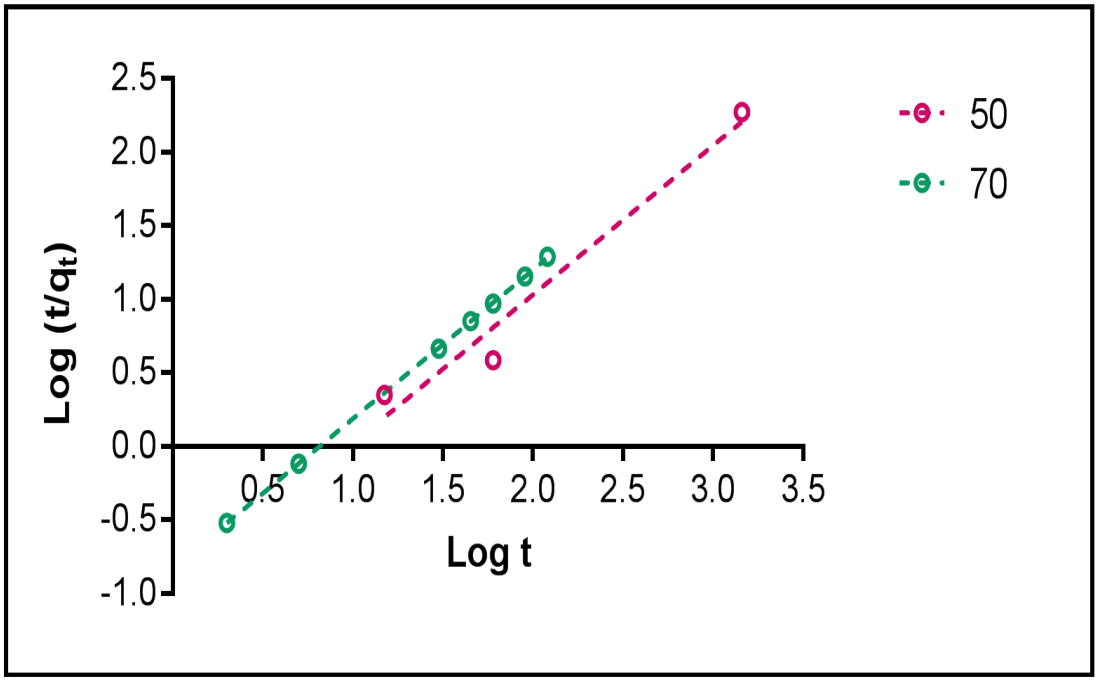

Figure 5.21: Pseudo second order (PSO) kinetic model at pH 6; zinc ion concentration 50 & 70 mg/L; agitation speed: 200rpm; at 21°C, 24h contact time, 5g/L alkali treated loofa dosage. PSO model fit shown by the dashed line.

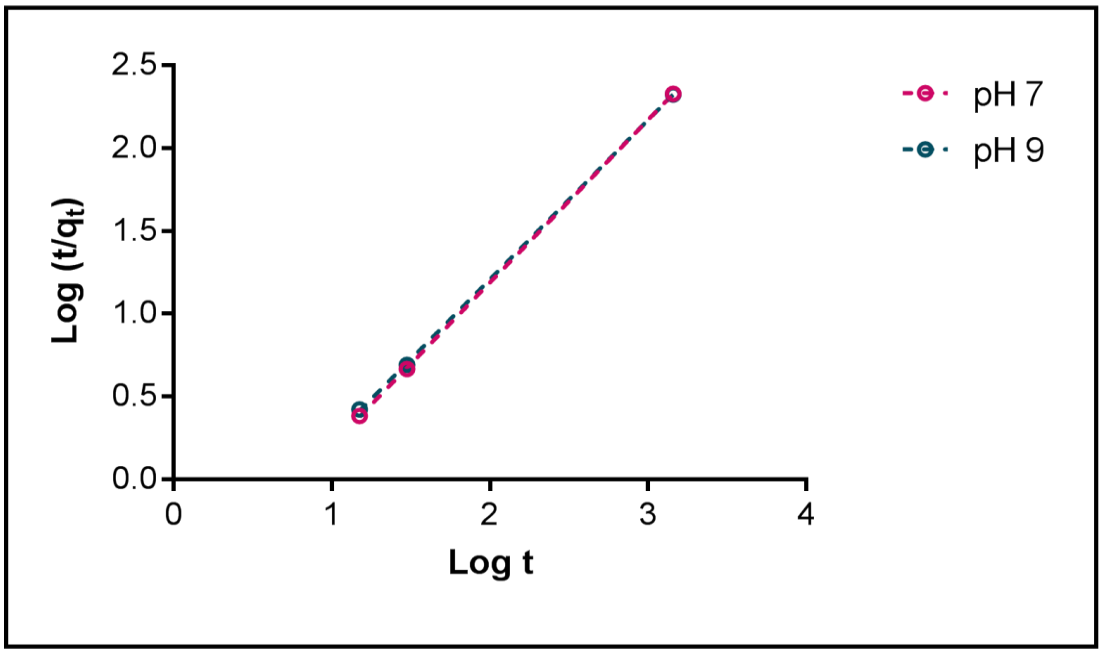

Figure 5.22: Pseudo second order (PSO) kinetic model at pH 7 and pH 9; zinc ion concentration 50 mg/L; agitation speed: 200rpm; at 21°C, 24h contact time, 5g/L alkali treated loofa dosage. PSO model fit shown by the dashed line.

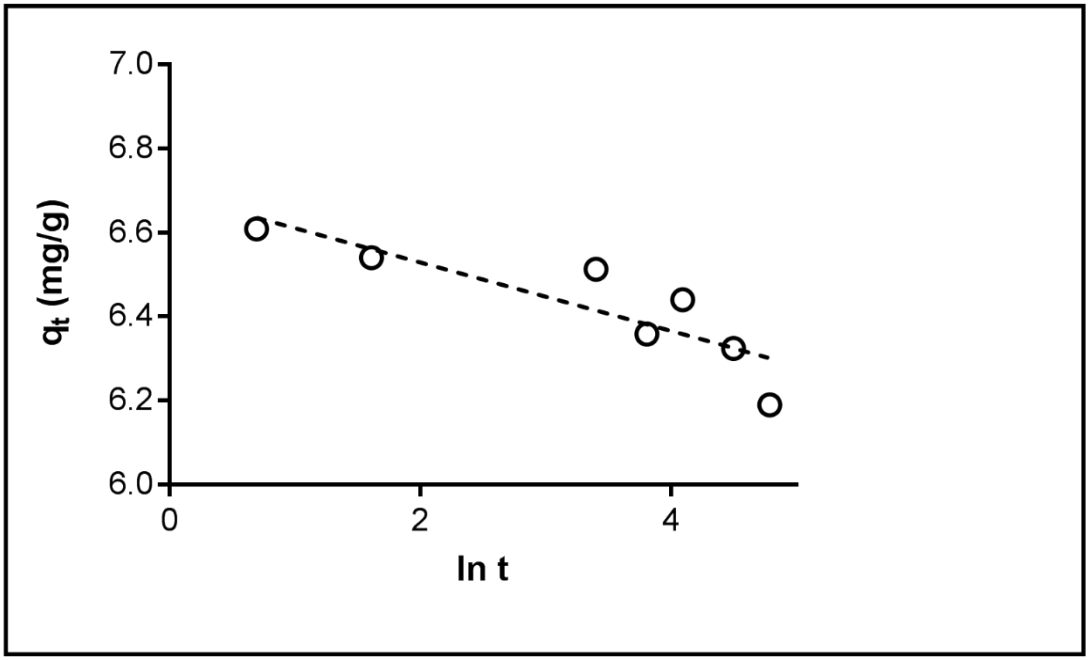

Figure 5:23: Elovich kinetic model at pH 6; zinc ion concentration 70 mg/L; agitation speed: 200rpm; at 21^{o}C, 2h contact time, 5g/L alkali treated loofa dosage. Elovich model fit shown by the dashed line.

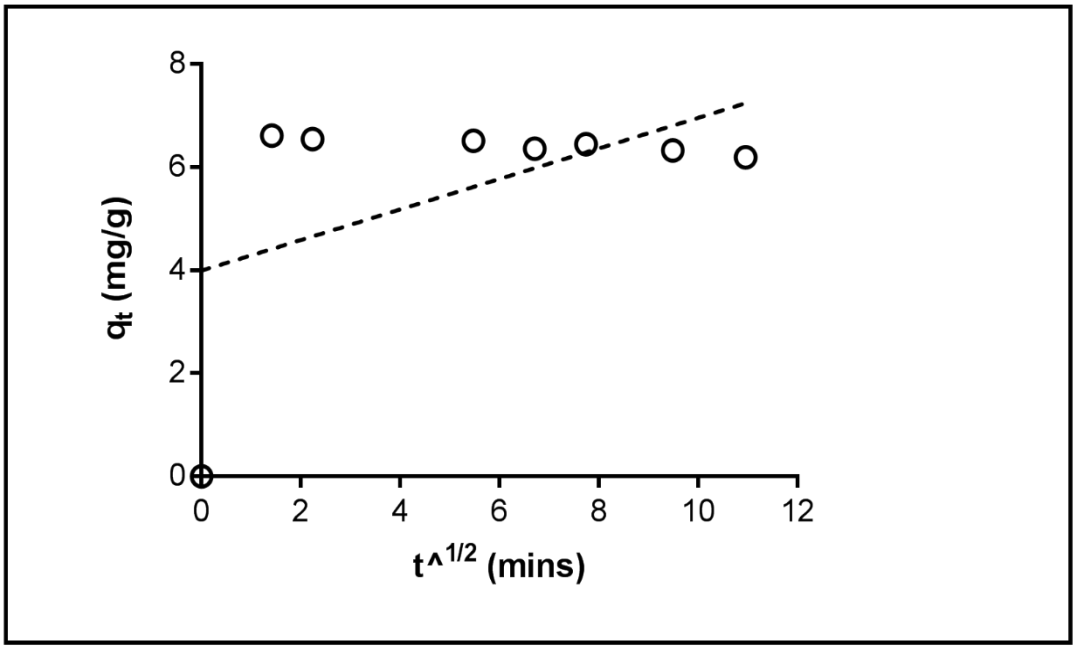

Figure 5.24: Intraparticle diffusion (IntraP) model at pH 6; zinc ion concentration 70 mg/L; agitation speed: 200rpm; at 21^{o}C, 2h contact time, 5g/L alkali treated loofa dosage. IntraP model fit shown by the dashed line.

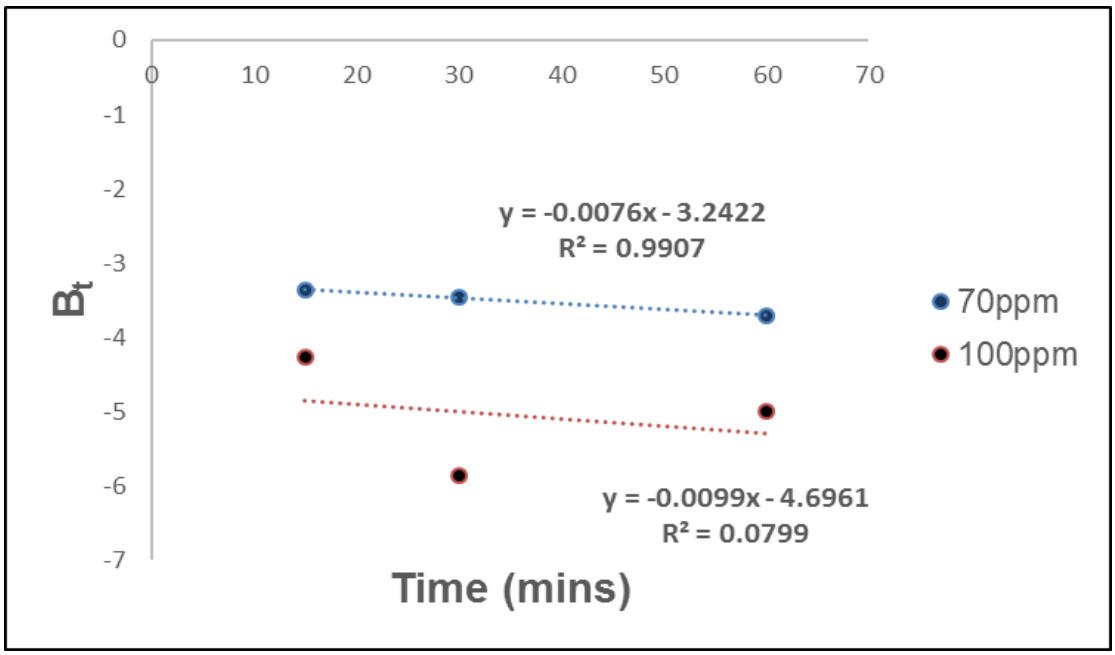

Figure 5.25: Boyd model at pH 6; zinc ion concentration 70 mg/L & 100mg/L; agitation speed: 200rpm; at 21°C, 1h contact time, 5g/L alkali treated loofa dosage. Boyd model fit shown by the dashed line.

Table 5.2: Pseudo second order kinetic model parameters for linear regression.

pH	qe_2	h	k_2	R^2
2	1.119	7.663	0.104	1.000
5	1.060	1.477	0.602	0.994
6	1.020	1.205	0.798	0.999
7	1.018	1.288	0.749	1.000
9	1.039	1.393	0.665	1.000

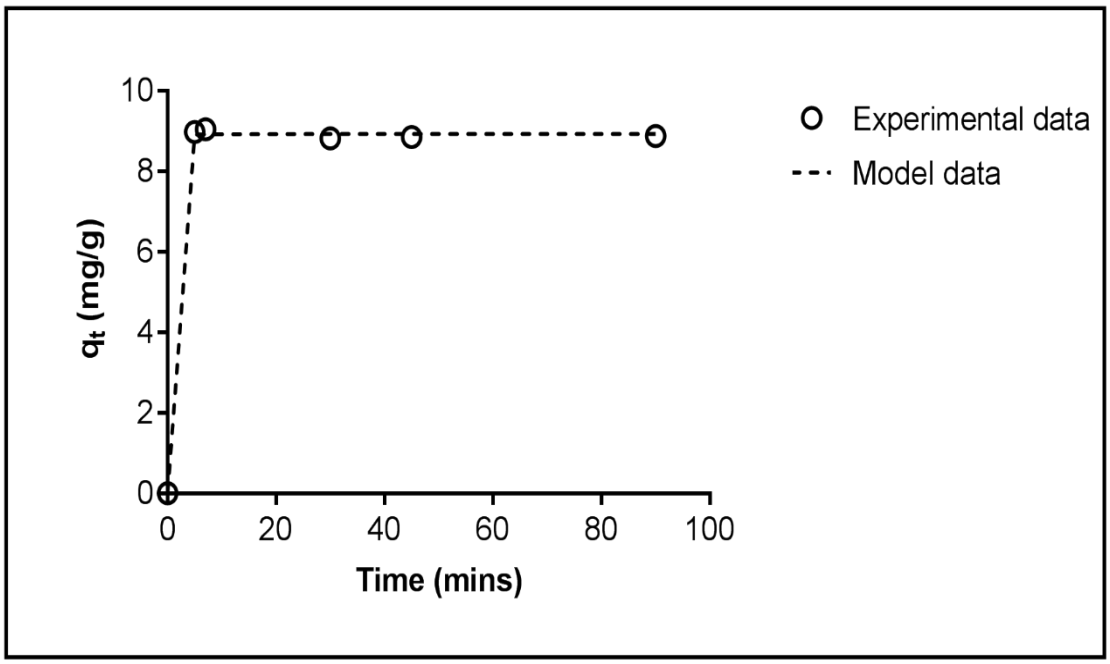

Figure 5.26: Pseudo second order (PSO) kinetic model using non-linear regression. PSO model fit shown by the dashed line.

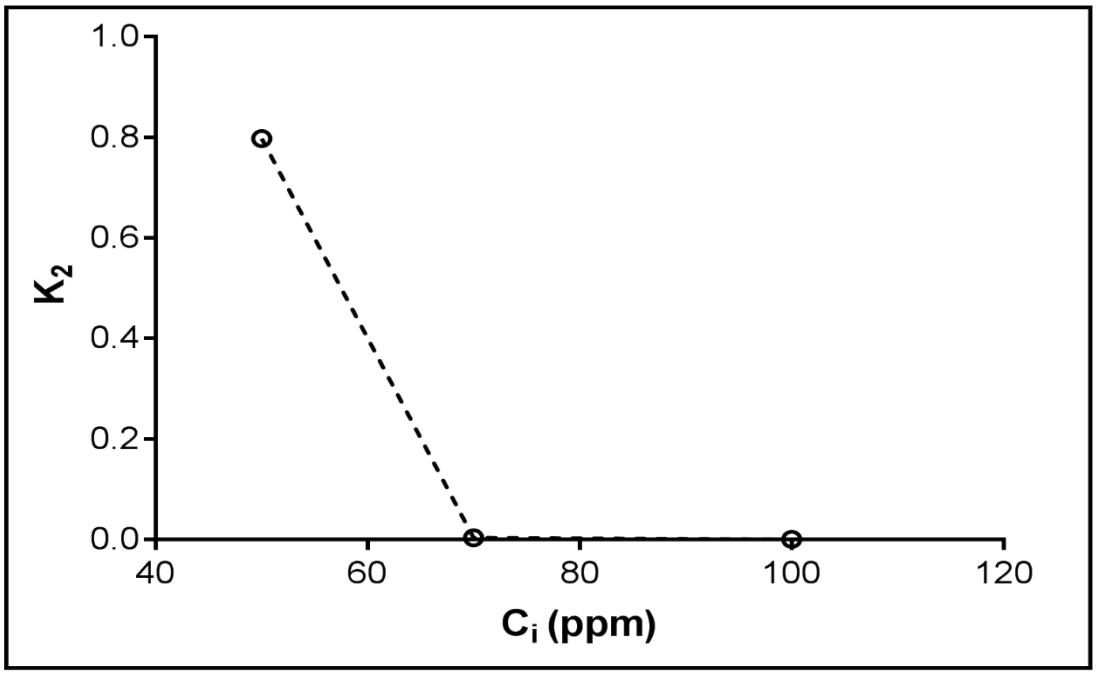

Figure 5.27: K_2 (pseudo second order constant) vs. initial zinc ion concentration (50 - 100mg/L)

A pseudo second order model was shown to have the best fit. The correlation coefficients (0.994 – 1) at different pH values are shown in Table 5.2. The results in Figure 5.25 show a linear

relationship with a correlation coefficient of 0.991 at 70mg/L and no fit at 100mg/L. As the concentration increases the correlation coefficient decreases. This shows that the further away the values are from linearity, the higher the pore diffusion coefficient, which gives an indication that the rate controlling step is not governed by pore diffusion but by film diffusion (Banerjee & Chattopadhyaya, 2013).

The intra-particle diffusion model, shown in Figure 5.24, gives an intercept not equal to zero, therefore the rate controlling step is shown to be a complex mechanism (Chi *et al*., 2013). The driving force of mass transfer of the metal ions between the biosorbent phase and solution, is increased as the initial concentration increases thereby the uptake of metal ions is increased (Nagy *et al.*, 2014). As initial concentration increases, K_2 decreases as shown in Figure 5.27. The K_2 value obtained from mixed solution of NaCl with zinc ions is 0.012 and this, as shown in Figure 5.15 – 5.18, decreases the uptake capacity and percentage removal of zinc ions from aqueous solution. Therefore, zinc adsorption is decreased. The kinetic constant decreases as diffusion rate increases due to no diffusion resistance in the micropores. This implies that other experimental factors, not solely diffusion, play an important role in the kinetic process of adsorption (Chi *et al*., 2013).

5.2.8 Isotherm modelling

A three parameter isotherm model was used to best predict the mechanism behaviour of zinc adsorption.

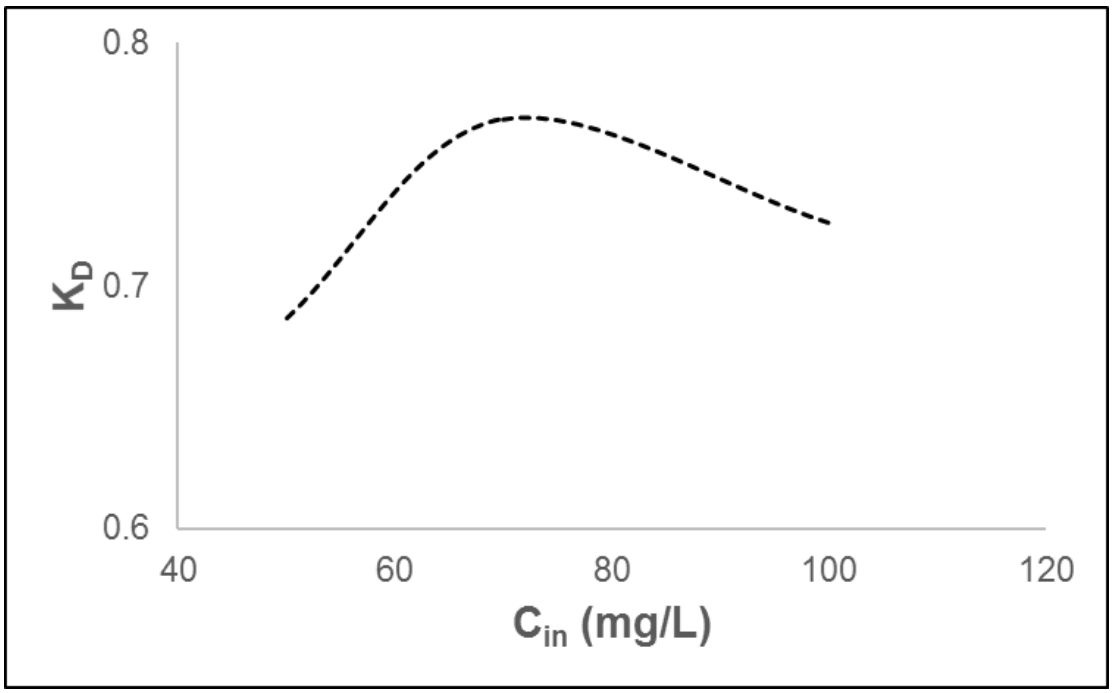

Figure 5.28: Distribution ratio versus initial zinc concentration at equilibrium at pH 6; zinc ion concentration: 50 – 100mg/L; agitation speed: 200rpm; at 21°C, 3h contact time, 5g/L alkali treated loofa dosage.

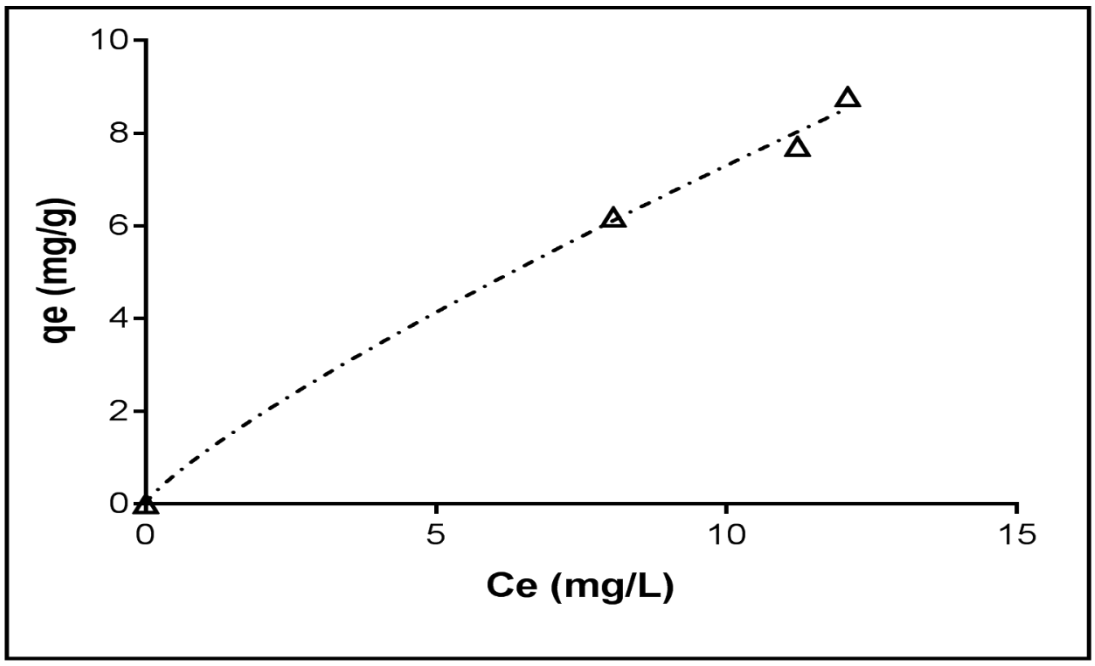

Figure 5.29: Zinc isotherm from pH 6.0 ± 0.1 at 21 °C at 3hr. contact time. Sips model fit shown by the dashed line (R^2 = 0.996).

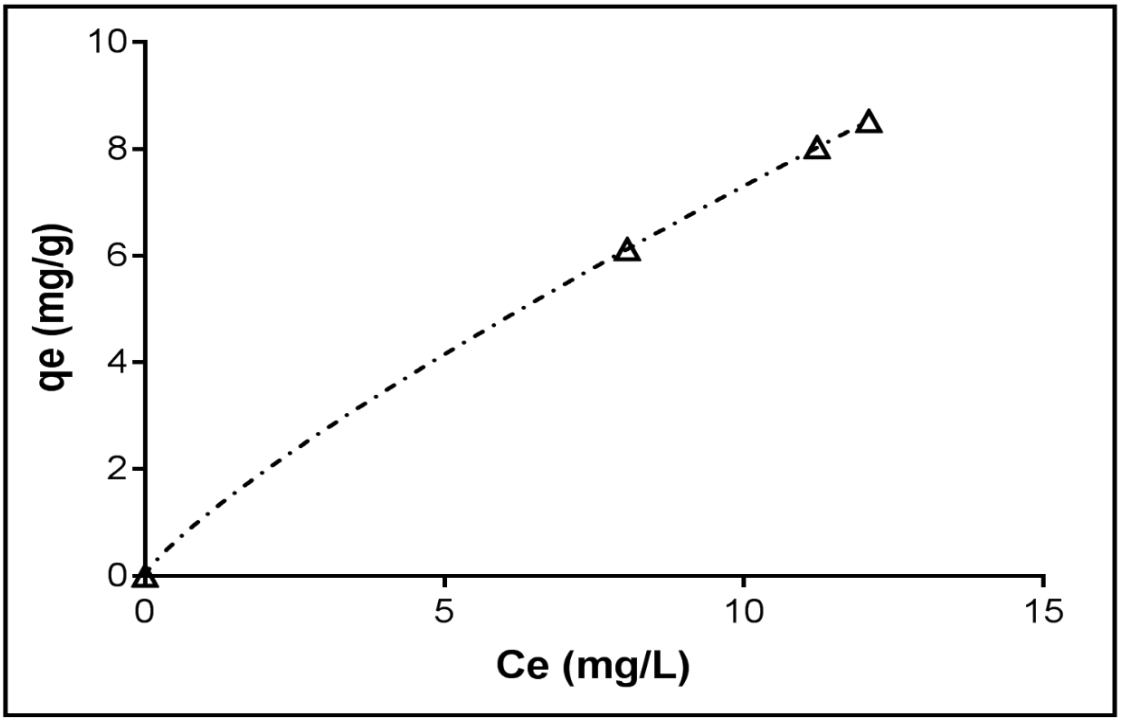

Figure 5.30: Zinc isotherm from pH 6.0 ± 0.1 at 21 °C at 3hr. contact time. Two-site Langmuir model fit shown by the dashed line (R^2 = 0.993; 0.991).

As reported by Areco *et al.* (2012), the Langmuir model indicates the availability of fewer active sites as the concentration of metal ion increases (Areco *et al*., 2012). Figure 5.28 gives an indication of the Langmuir model fitting which does not show a good fit. Additionally, the plot of K_D vs. zinc ion concentration (Figure 5.28 does not support the Langmuir model. The sips isotherm model (both by linear and non-linear regression) (Figure 5.29) gives the best fit for the zinc adsorption onto loofa with a correlation coefficient of 0.996. However, the two-site Langmuir model also shows the good fit at dual R^2 values of 0.993 & 0.991, which indicates that two types of adsorption site are available on the loofa for adsorption of zinc ions.

CHAPTER SIX

6.0 CADMIUM BIOSORPTION MECHANISM

6.1 Introduction

This chapter looks at the speciation of cadmium in aqueous solution and describes the effect of changes to experimental conditions on the adsorption of cadmium ions onto *Luffa cylindrica* (loofa). Sections 6.2 – 6.10 show plots of cadmium uptake with change in pH and initial cadmium ion concentration. Figures 6.11 – 6.21 show kinetic and isotherm models used to fit the sorption data obtained from the investigation of the interaction between the loofa and cadmium ions.

6.2 Batch experiments

The pH of solution is an important factor that affects the speciation of cadmium in aqueous solution. The formation of cadmium ions in aqueous solution is shown in the speciation plot (Figure 6.1). It shows the species of cadmium at different pH values. The effect of pH will be explained in the subsequent sections (Figure 6.2 -6.5). The FT-IR spectra of the cadmium loaded alkali treated loofa as compared to the untouched alkali treated loofa are shown in Figure 6.6. The distribution ratio versus the solution pH is described in Figure 6.7.

6.2.1 Speciation of cadmium in aqueous solution

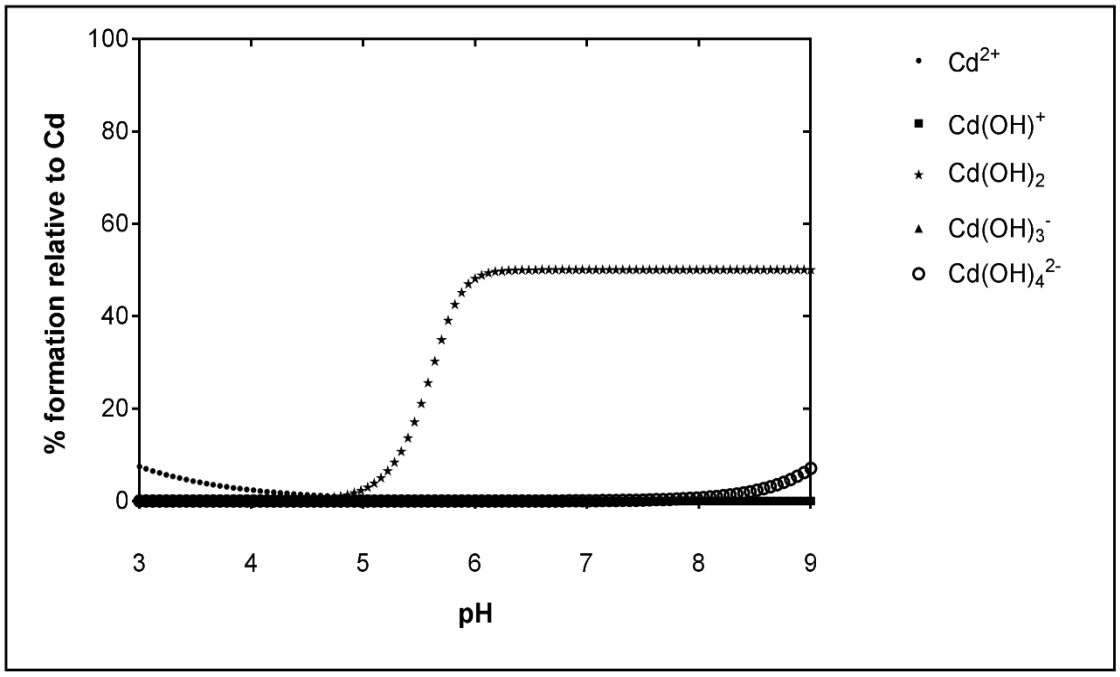

Figure 6.1: Speciation diagram of cadmium nitrate ions in aqueous solution at 21°C (Ekberg & Brown, 2016).

Interestingly, the dominant form of cadmium absorbed on the loofa surface is $Cd(OH)_2$ which only accounts for a maximum of 50% of the available metal from pH 6 – 8. In acidic medium, a low percentage of free cadmium ions are formed. A build-up of $Cd(OH)_4^{2-}$ is shown under alkaline conditions from pH 8. However, hydroxylation of the cadmium ions is indicated above a pH of 5 but there is no noticeable decrease in the formation of $Cd(OH)_2$ adsorbed onto the loofa surface over pH 8. Instead $Cd(OH)_4^{2-}$ is formed. A reduction in the adsorption capacity of the cadmium ions onto loofa at pH 9 (Figure 6.2) show the effect of the different forms of cadmium ions on its adsorption process. The species of cadmium ion that is attached to the loofa surface during adsorption at an optimum pH of 7, is $Cd(OH)_2$ (Amer *et al*., 2010; ElShafei *et al*., 2014).

6.2.2 pH effect

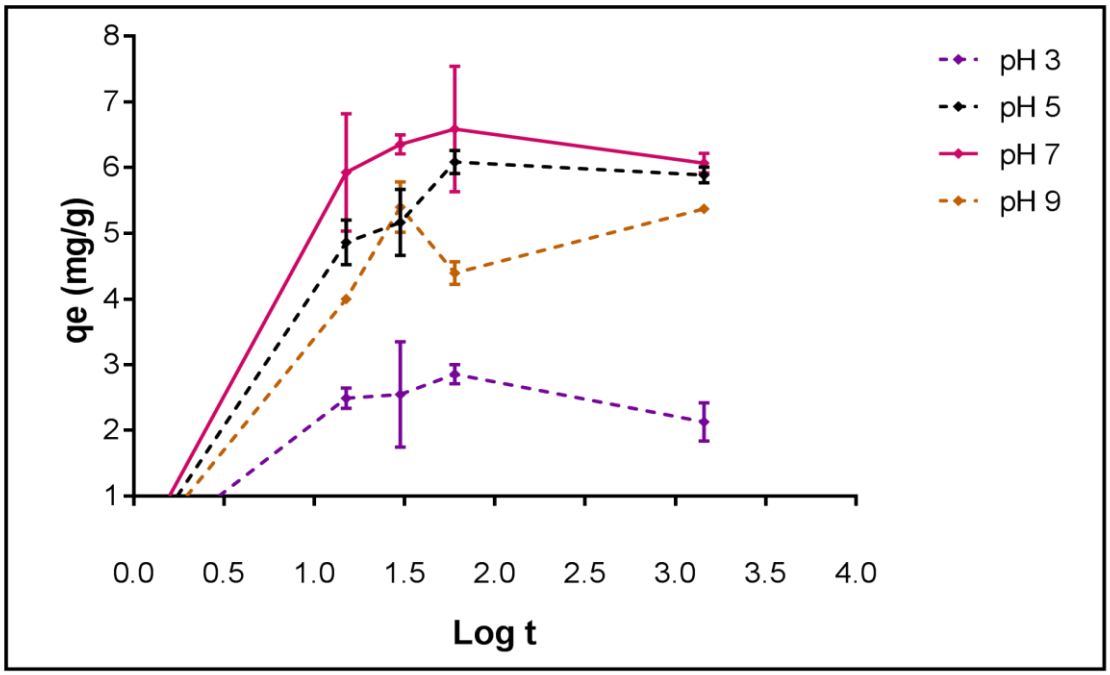

Figure 6.2: Uptake capacity (qe) of cadmium ion with time after 24hrs at pH range 3-9; cadmium ion concentration: 50mg/L; agitation speed: 200rpm; at 21°C, 24h contact time (represented by the log of time in mins [Log t]), 5g/L dosage of alkali treated loofa dosage. Data from 3 replicate measurements.

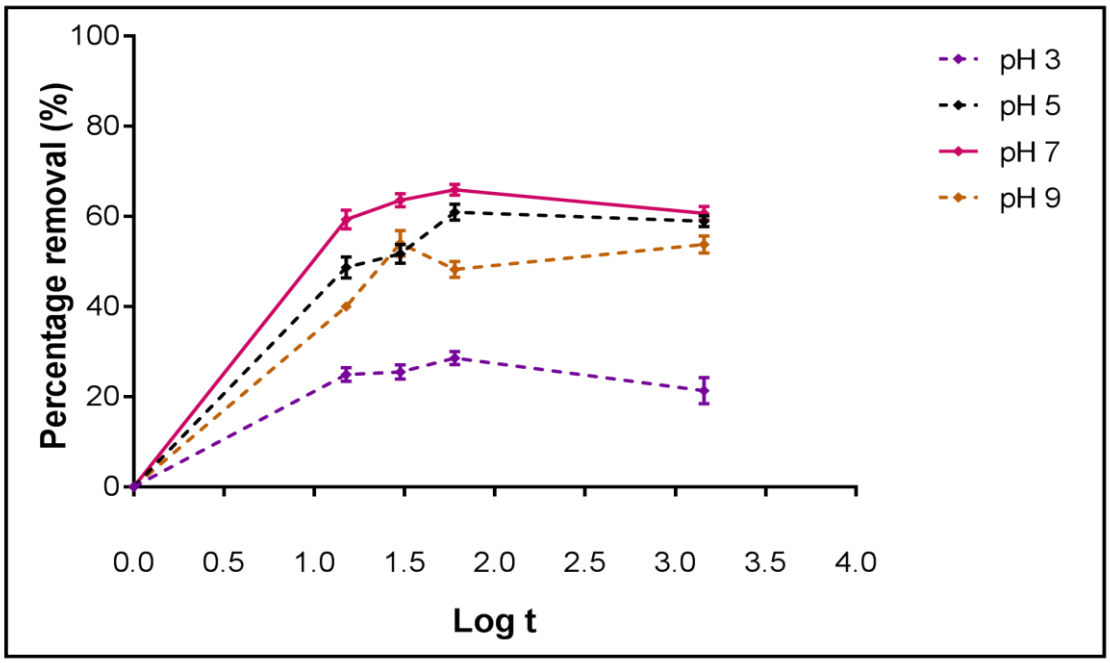

Figure 6.3: Percentage removal of cadmium ions with change in time after 24hrs at pH range 3-9; cadmium ion concentration: 50mg/L; agitation speed: 200rpm; at 21°C,24h contact time (represented by the log of time in mins [Log t), 5g/L dosage of alkali treated loofa dosage. Data from 3 replicate measurements.

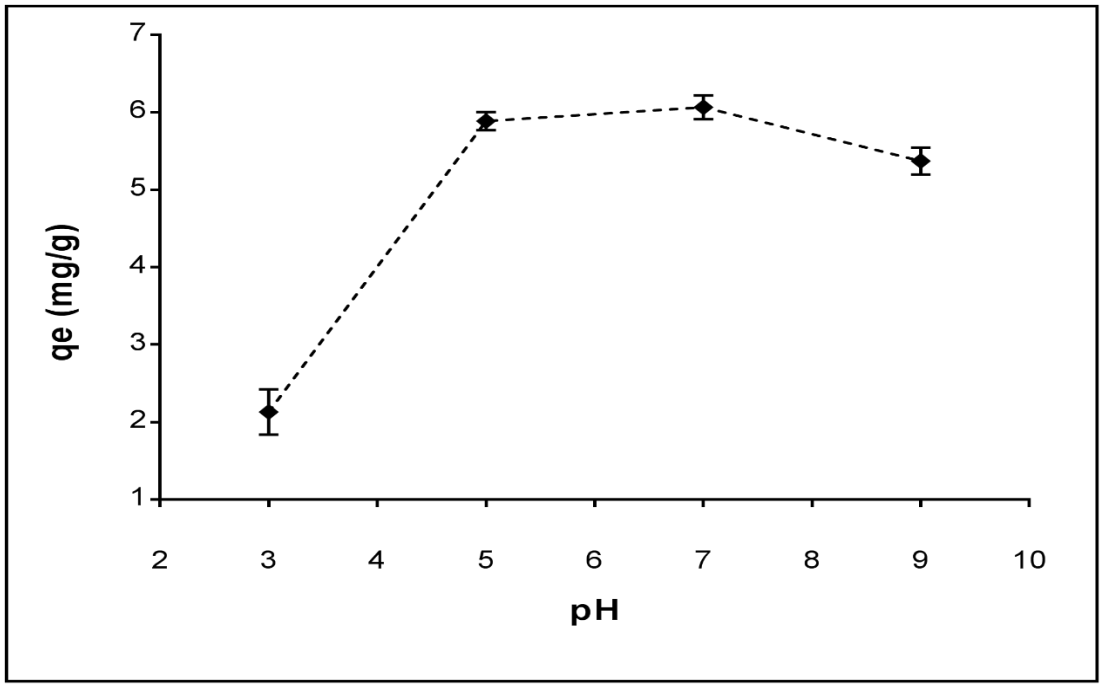

Figure 6.4: Cadmium uptake (q_e) at different pH values after 24hrs; cadmium ion concentration: 50mg/L; agitation speed: 200rpm; at 21^{o}C,24h contact time, 5g/L dosage of alkali treated loofa dosage. Data from 3 replicate measurements.

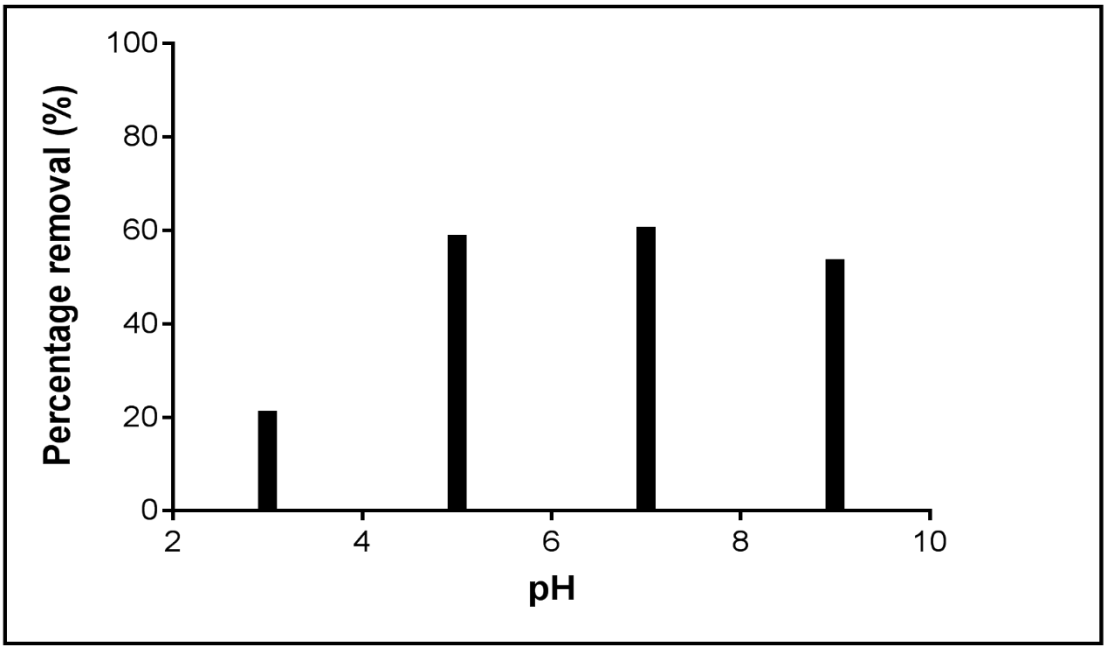

Figure 6.5: Percentage removal of cadmium ions (E%) with change in pH after 24hrs at pH range 3-9; lead ion concentration: 50mg/L; agitation speed: 200rpm; at 21^{o}C, 24h contact time, 5g/L dosage of alkali treated loofa dosage.

The rate of adsorption was fast, reaching a maximum in less than 30mins (Figure 6.2 & 6.3). At equilibrium, the adsorption of cadmium ions was found to be maximum at pH 7. As pH increased

from 3 - 7, the percentage removal of cadmium ions is shown to increase by 40% to give a maximum removal percentage of 60% at pH 7. Further increase in pH above 7 leads to a decrease in the adsorption capacity due to the formation of hydroxylated cadmium complexes that compete with the active sites on the loofa surface. The ionic interaction that occur at both acidic and alkaline pH medium play a dominant role in the adsorption process of cadmium ions (Shin & Rowell, 2005; Kulkarni *et al*., 2014). This maximum percentage removal is consistent with the speciation diagram of cadmium (Figure 6.1) that the $Cd(OH)_2$ species present becomes dominant at pH 7.

6.2.3 FT-IR spectra

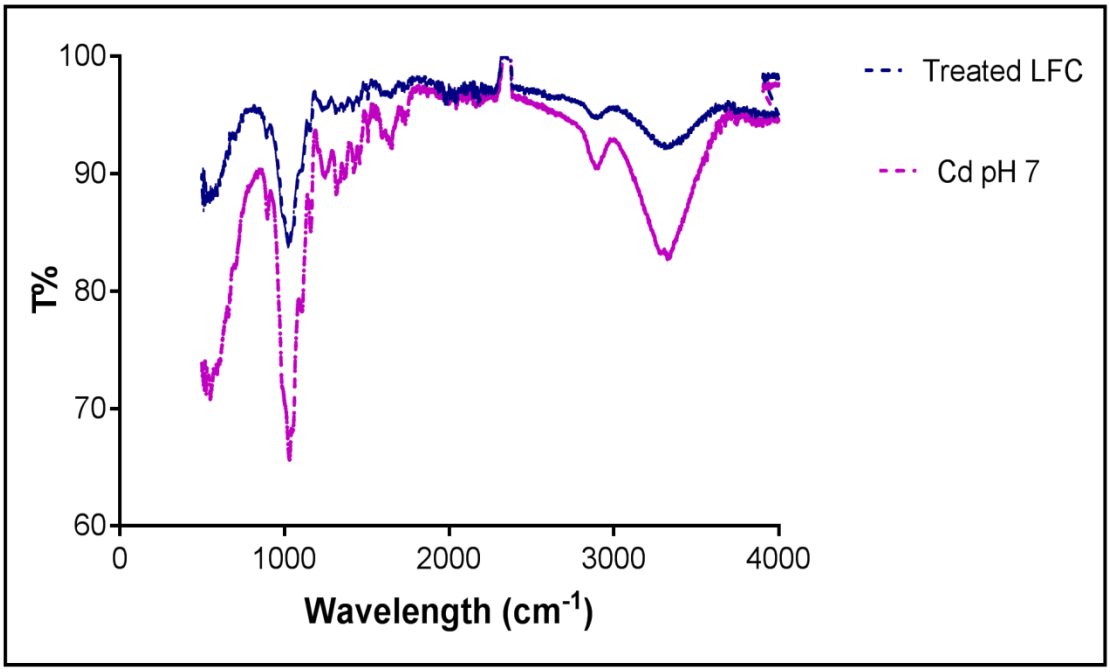

Figure 6.6: T% (transmittance percentage) versus wavelength FT-IR spectra of 4% NaOH treated loofa before exposure to Cd, Cd-loaded loofa at pH 7 (cadmium ion concentration: 50mg/L; agitation speed: 200rpm; at 21°C,24h contact time, 5g/L alkali treated loofa dosage.

The shift bands that occur at wavelength 1050cm^{-1} are attributed to O-H stretching (Lindino *et al*., 2014). This shift in the adsorption peaks as shown in figure 6.6 is attributed to the stretching of carboxyl groups present on the loofa surface (Kulkarni *et al*., 2014). The broad hydroxyl bands at wavelength at 3200cm^{-1} – 3400cm^{-1} show the O-H bonding. These changes in peak intensities

and binding energies occur as adsorption takes place and indicates the involvement of these groups in the mechanism of adsorption (Shin & Rowell, 2005; Sari & Tuzen, 2008; Najiah *et al*., 2014).

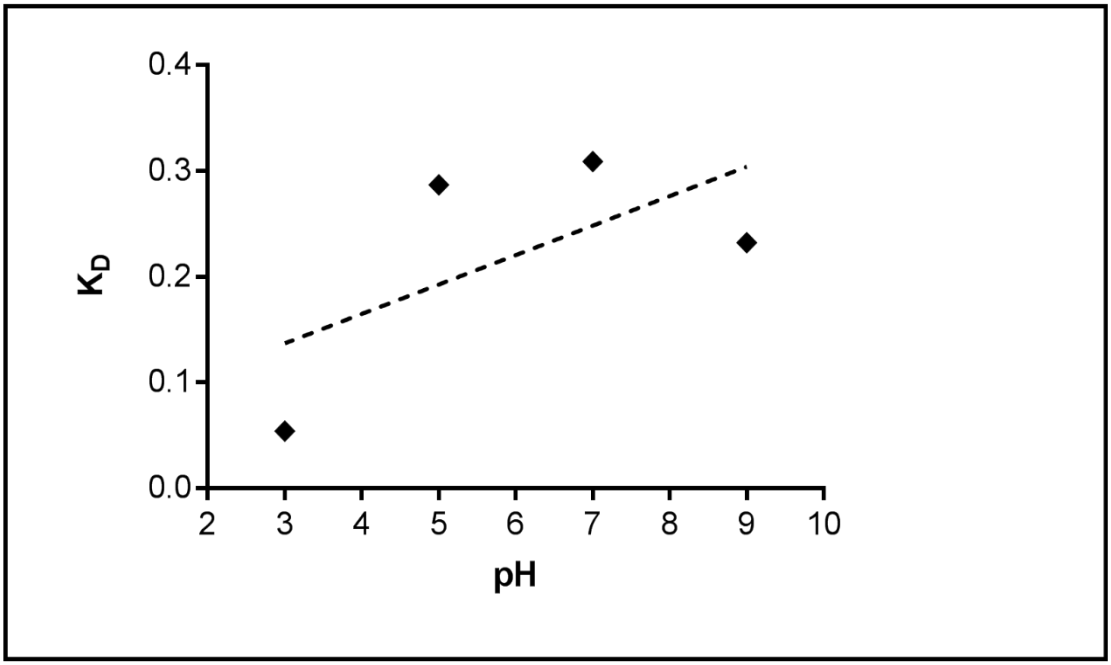

Figure 6.7: Distribution ratio versus pH at equilibrium at pH range 3-9; cadmium ion concentration: 50mg/L; agitation speed: 200rpm; at 21^{o}C,24h contact time, 5g/L alkali treated loofa dosage.

As the pH increases, the distribution ratio increases until a maximum value is obtained. This shows an increase in metal ion chelation, which is the binding of the ions in solution to the charged ions on the loofa surface, as the pH increases. The highest distribution ratio at pH 7 shows a strong chelation and thereby a maximum adsorption efficiency. Further increase in the pH leads to occurrence of hydroxylated cadmium ions thereby reducing the distribution ratio which in turn decreases the adsorption capacity (Ahamed *et al*., 2010).

6.2.4 Concentration effect

Figure 6.8- 6.10 shows the trend of cadmium ion adsorption at different initial concentrations.

As the initial concentration increases, the cadmium ion adsorption increases.

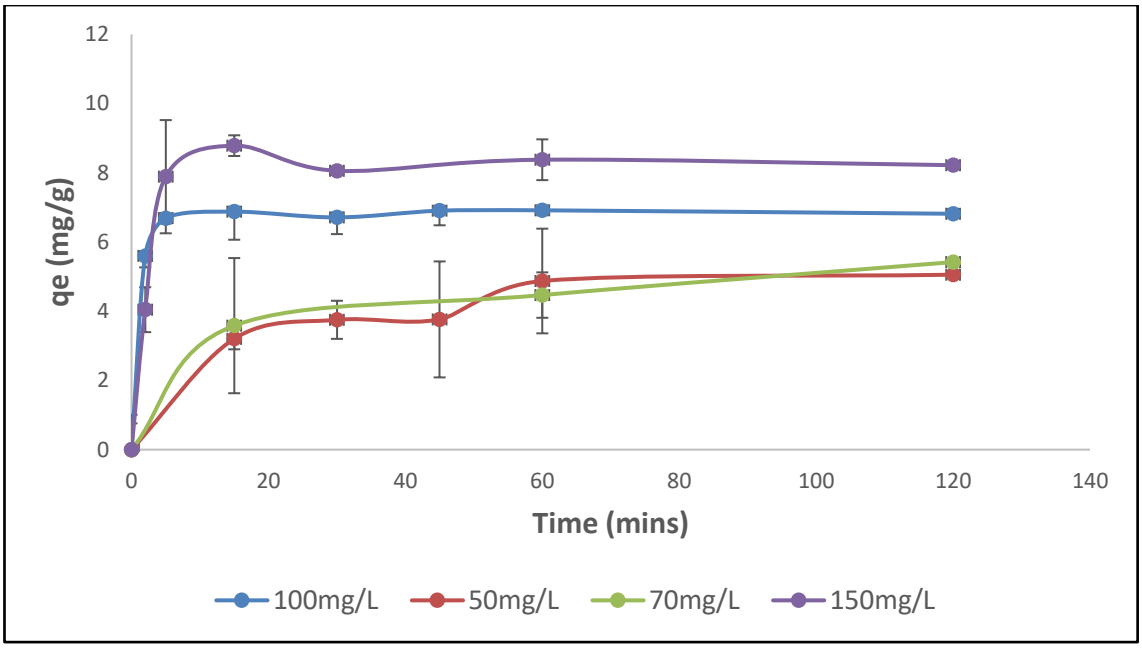

Figure 6.8: Uptake capacity (qe) of cadmium ions with time up to 2hrs at pH 6; cadmium ion concentration ranges of 50 – 150mg/L; agitation speed: 200rpm; at 21^{o}C,2h contact time, 5g/L alkali treated loofa dosage. Data from 3 replicate measurements.

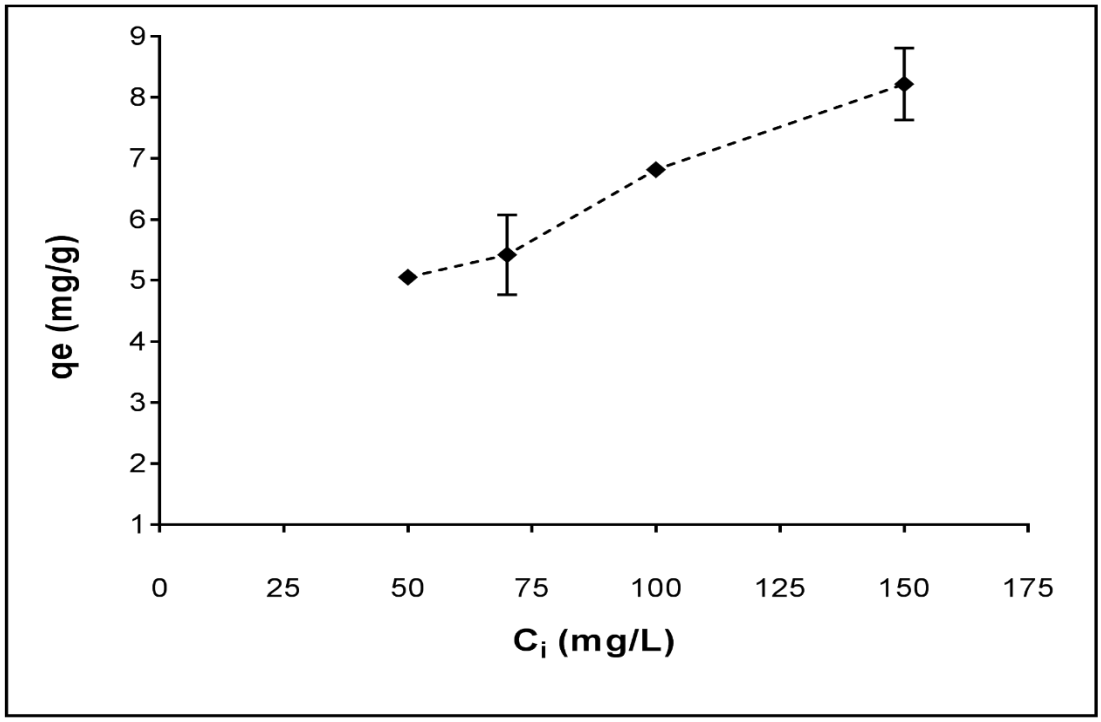

Figure 6.9: Uptake capacity (qe) of cadmium ions with change in initial concentration after 2hrs at pH 7; lead ion concentration ranges of 50 – 150mg/L; agitation speed: 200rpm; at 21^{o}C,24h contact time, 5g/L alkali treated loofa dosage. Data from 3 replicate measurements.

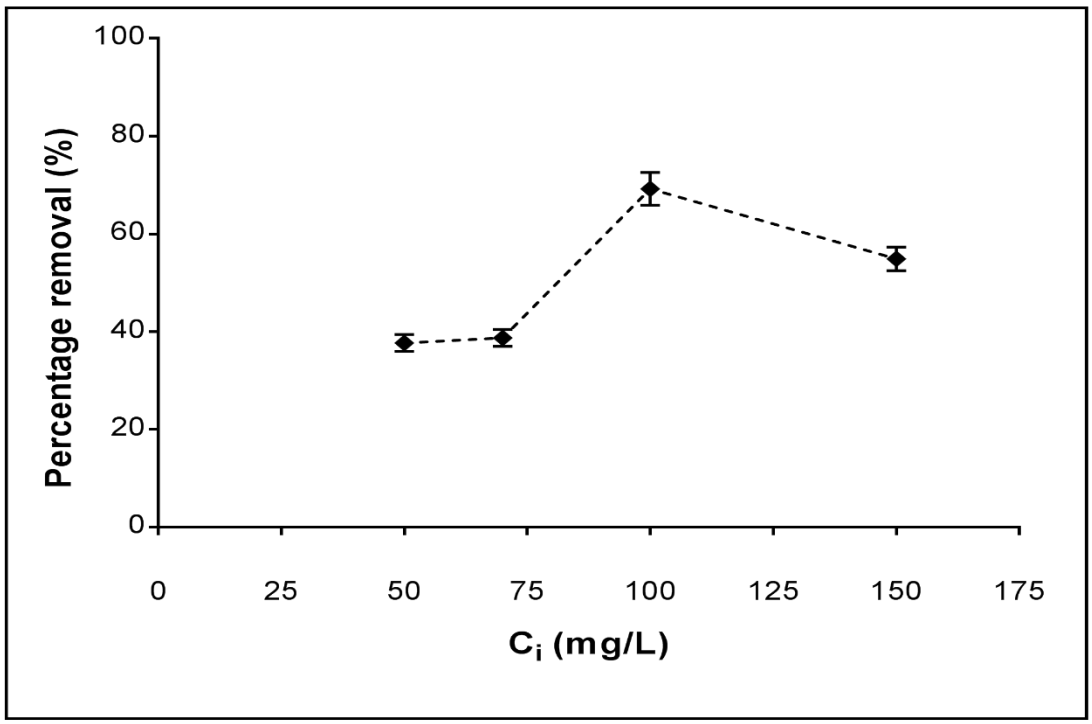

Figure 6.10: Percentage removal (E%) of cadmium ions with change in initial concentration after 2hrs at pH 7; lead ion concentration ranges of 50-150mg/L; agitation speed: 200rpm; at 21^{o}C,2h contact time, 5g/L alkali treated loofa dosage. Data from 3 replicate measurements.

As the concentration is increased, the uptake capacity increases due to the fact that, at higher concentration, more available sorption sites are being occupied. This explains the greater driving force as a result of a higher concentration gradient (Amer *et al*., 2010; Suguna & Kumar, 2013). Adsorption occurs fast at 15mins, bulk transport, and then becomes slower (intracellular uptake) till equilibrium is attained (Figure 6.8) (Akhtar *et al*., 2003). The percentage removal is increased by approximately 10% as concentration increases to 50 - 150mg/L.

6.2.5 Temperature

According to previous researchers, the effect of temperature could have a positive or negative effect on the adsorption process of metal ions. The physical adsorption features of metal ion adsorption depend on the effect of temperature. The increase in the adsorption capacity is influenced by the reactions that occur between the loofa and cadmium ions (Li *et al*., 2004; Amer *et al*., 2010). As reported in chapter 4, the damage to the actives sites as a result of a rise in temperature could be the reason for decreased adsorption of lead ions, therefore temperature may not be a dominant factor in the adsorption process onto to loofa nor have a positive effect in the adsorption mechanism of cadmium ions.

6.2.6 Kinetic modeling

The kinetic models predict the rate controlling step of the adsorption system. The validity of each model will be based on the fitness (R^2 values). Figures 6.11 – 6.15 show the different kinetic fits and figure 6.16 shows the best fit using non-linear regression. Table 6.1 & 6.2 show the obtained values from the best fit model as both linear and non-linear regression parameters. Figure 6.17 show the related values of the best fit rate constant as regards to change in initial concentration. The correlation coefficients of each model are depicted in the plots and the best fit shown.

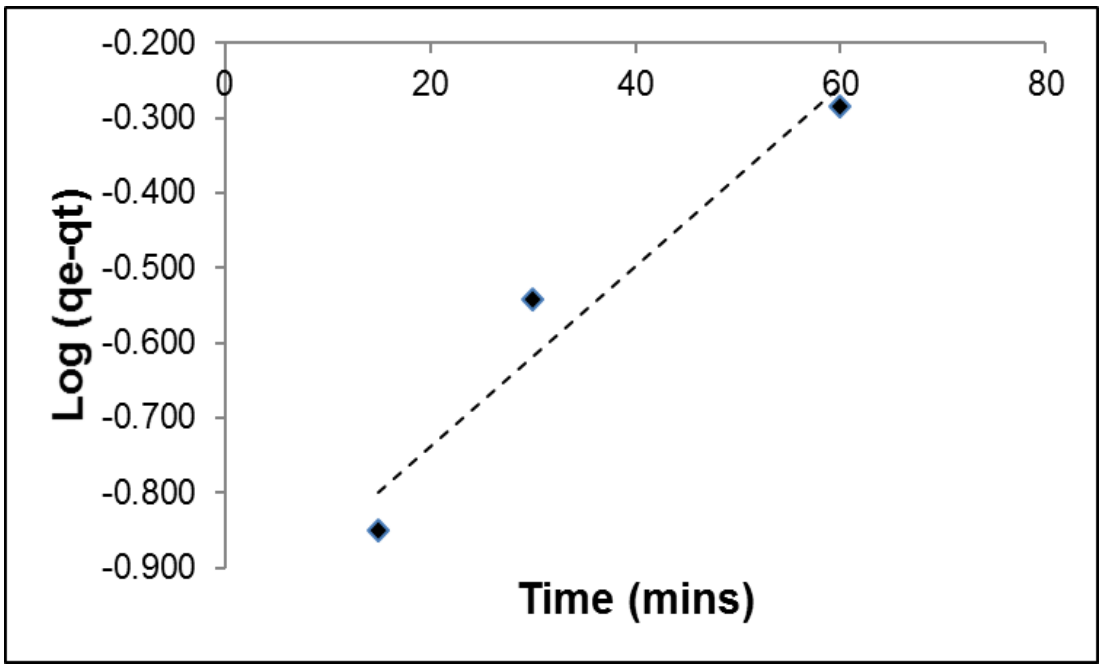

Figure 6.11: Pseudo first order (PFO) kinetic model at pH 7; cadmium ion concentration 50 mg/L; agitation speed: 200rpm; at 21°C, 2h contact time, 5g/L alkali treated loofa dosage (R^2 = 0.9437). PFO model fit shown by the dashed line.

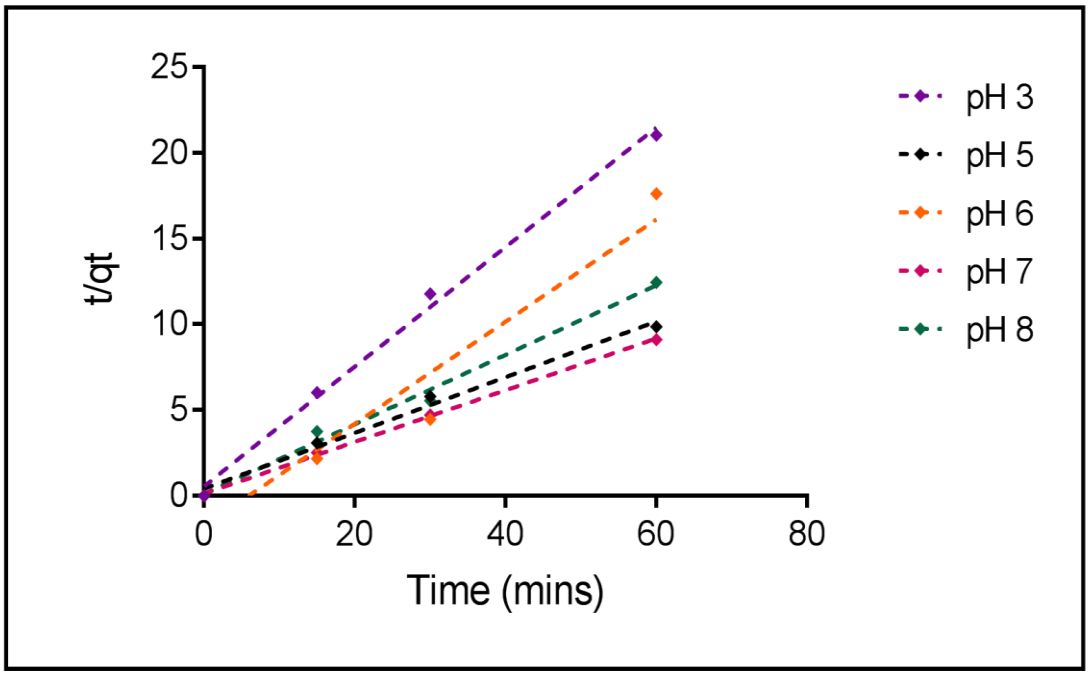

Figure 6.12: Pseudo second order (PSO) kinetic model at pH 3-9; cadmium ion concentration 50 mg/L; agitation speed: 200rpm; at 21°C, 2h contact time, 5g/L alkali treated loofa dosage (t/qt is the fraction of cadmium uptake at time t and the uptake capacity of cadmium at that time t). PSO model fit shown by the dashed line.

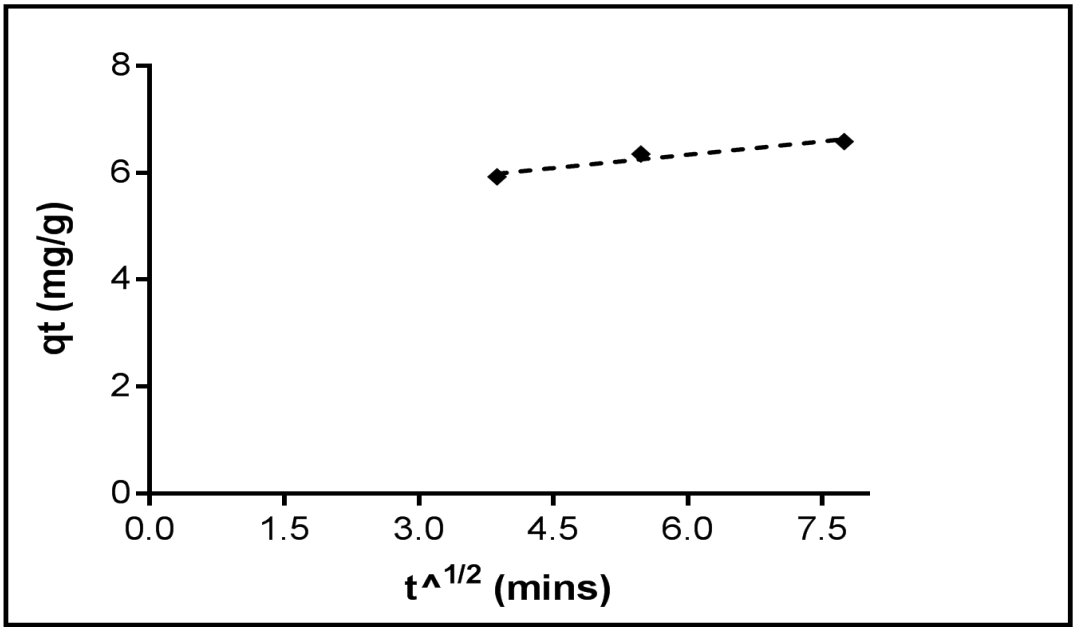

Figure 6.13: Intraparticle diffusion (IntraP) model at pH 7; cadmium ion concentration 50 mg/L; agitation speed: 200rpm; at 21^{o}C, 2h contact time, 5g/L alkali treated loofa dosage (qt and qe is the uptake capacity at time t and at equilibrium respectively) (R^2 = 0.9302). IntraP model fit shown by the dashed line.

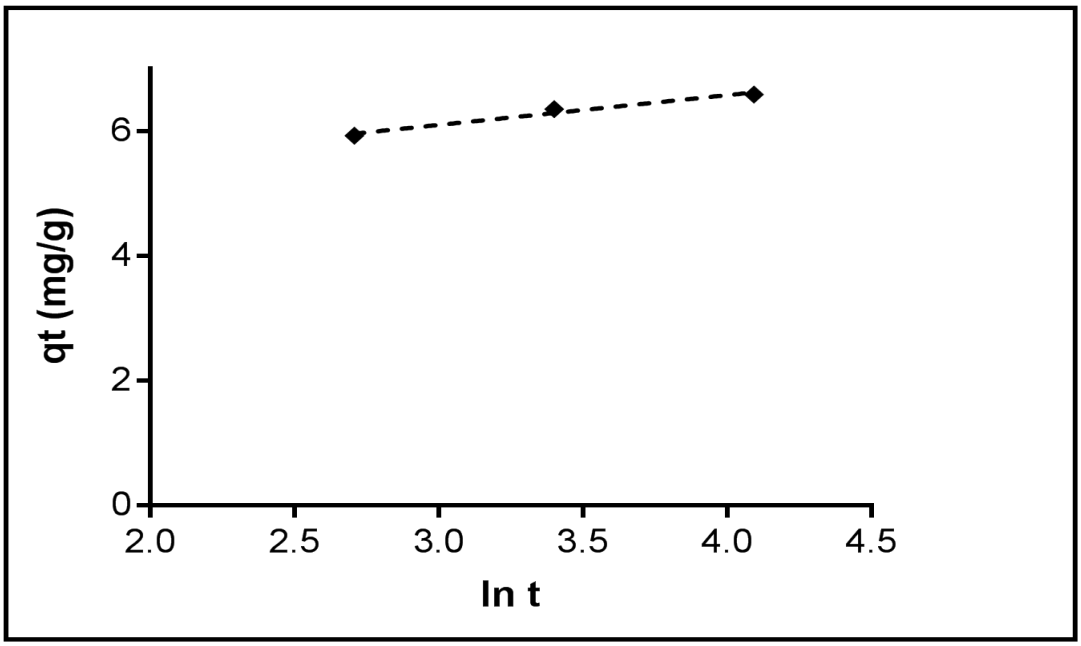

Figure 6.14: Elovich kinetic model at pH 7; cadmium ion concentration 50 mg/L; agitation speed: 200rpm; at 21^{o}C, 2h contact time, 5g/L alkali treated loofa dosage (R^2 = 09719). Elovich model fit shown by the dashed line.

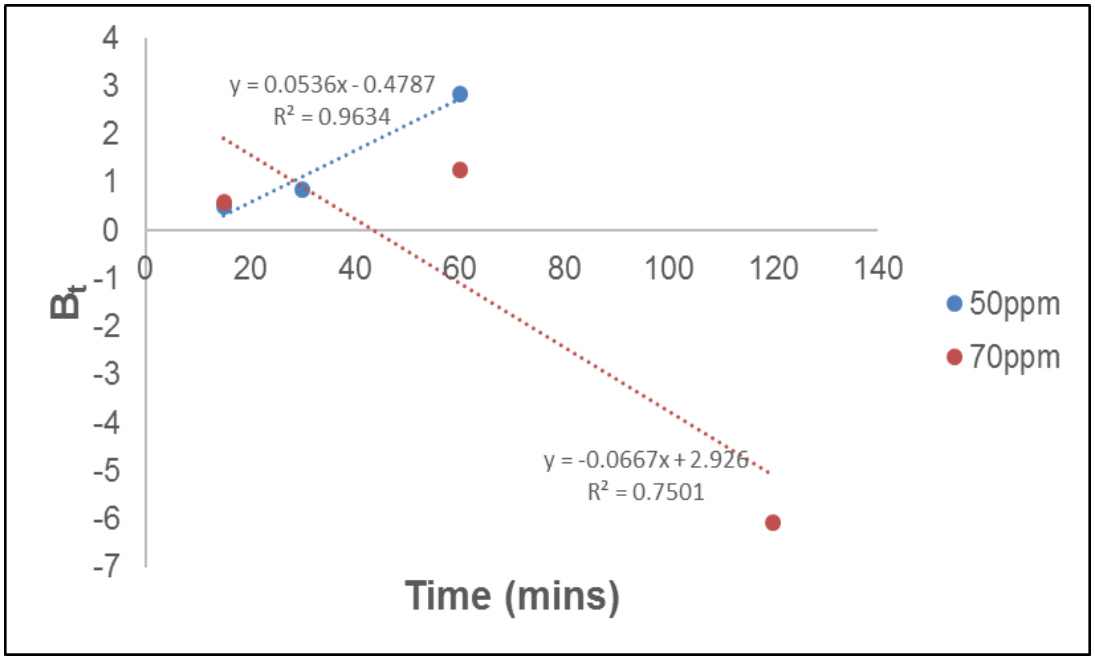

Figure 6.15: Boyd model at pH 7; lead ion concentration 50 mg/L & 70mg/L; agitation speed: 200rpm; at 21°C, 2h contact time, 5g/L alkali treated loofa dosage. Boyd model fit shown by the dashed line.

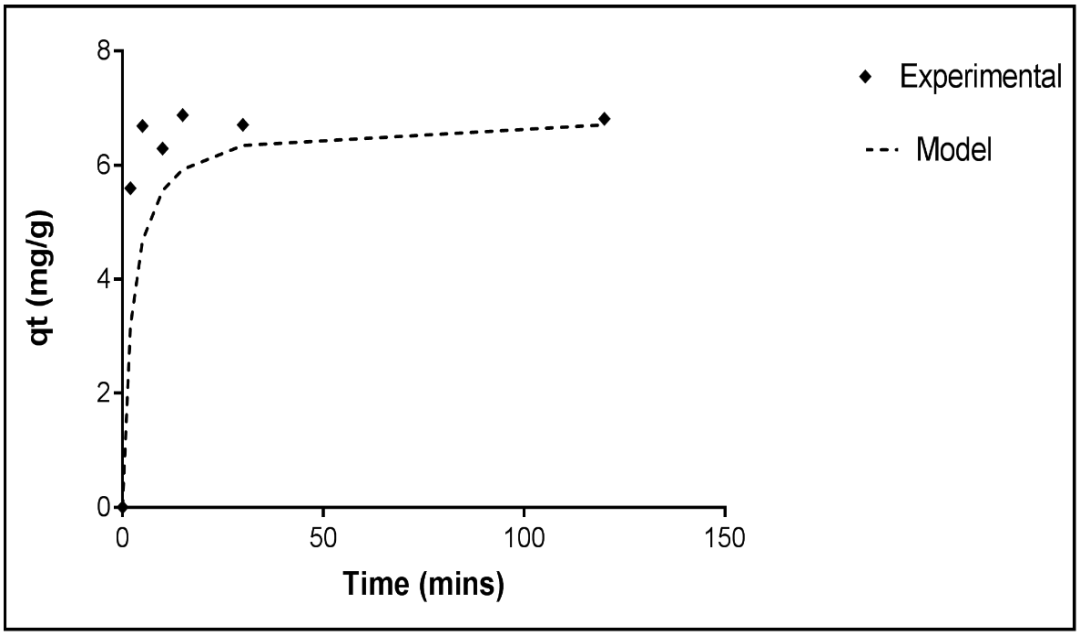

Figure 6.16: Pseudo second order kinetic model using non-linear regression. PSO model fit shown by the dashed line.

Table 6.1: Pseudo second order kinetic model parameters for linear regression (varying concentration).

Concentration (mg/L)	**qe_2**	**K_2**	**R^2**
50	5.672	0.012	0.985
70	5.896	0.013	0.990
100	6.845	1.906	0.999
150	8.292	0.255	0.994

Table 6.2: Pseudo second order kinetic model parameters for linear regression (varying pH values).

pH	**qe_2**	**K_2**	**h**	**R^2**
3	3.032	0.078	0.713	0.997
5	6.743	0.021	0.943	0.994
7	6.840	0.063	2.960	1.000
9	5.040	0.128	3.240	0.982

Pseudo second order models best describe the adsorption of divalent metal ions (Vilar *et al*., 2009). This is shown to have the best fit model compared to the all other kinetic models utilised. This further explains that there is an interaction between the loofa and the cadmium ions in solution. Pseudo second order successfully predicts the kinetics of adsorption at initial concentration from 50 -150mg/L and pH 3-9 (Table 6.1 & 6.2).

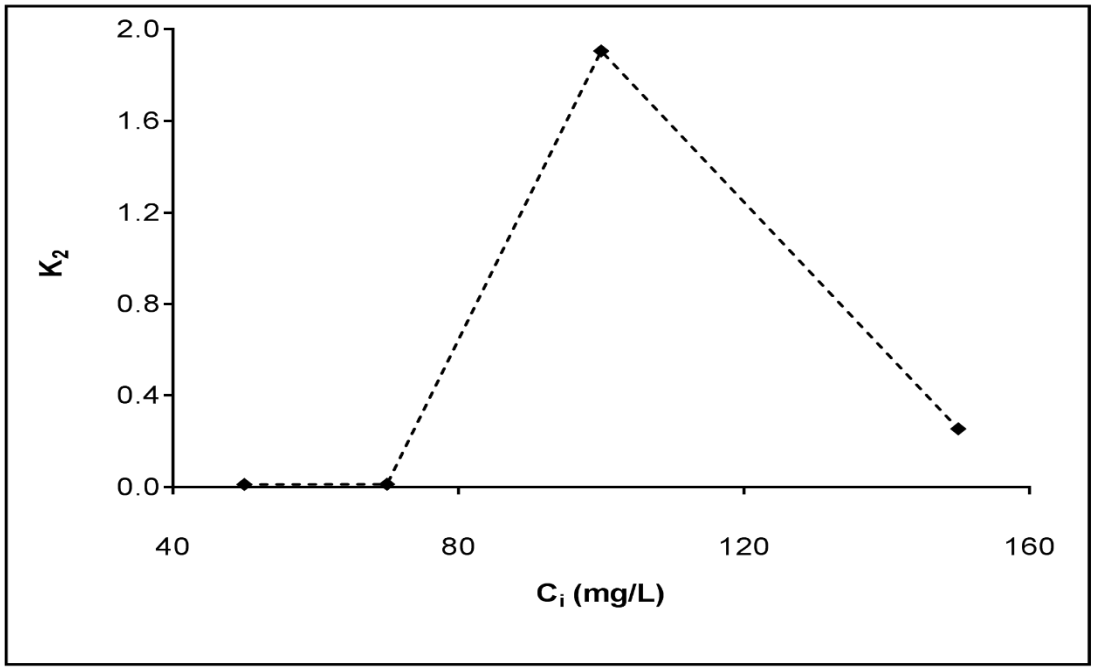

Figure 6.17: K_2 (pseudo second order constant) vs. initial metal ion concentration (50 - 150mg/L).

The Boyd model describes whether the sorption process is via film diffusion or intraparticle diffusion. As the Boyd model shows a good fit at 50mg/L (Figure 6.16), values recorded at 15, 30 & 60mins, the rate controlling step is predicted to be film diffusion. As the concentration increases the plot is closer to linearity, thereby not showing a fit and this is explained by film diffusion as the rate controlling step. This is consistent with the intraparticle diffusion plot (Figure 6.13) which describes a complex mechanism (intercept not equal to zero) that is not solely attributed to a single rate controlling step. The Elovich model, on the other hand, (Figure 6.14) which describes a chemisorption process, gives a good fit which predicts the experimental data (Suguna & Kumar, 2013; Madala *et al*., 2013; Martins *et al*., 2014).

As the pseudo second rate constant, (K_2) is increased, the initial concentration of cadmium ions is increased (Figure 6.17) till a maximum value is obtained. This gives a consistent report on the effect of experimental factors as it relates to the kinetics of the adsorption system. Furthermore, this explains the correlation between the number of available binding sites, based on the initial concentration of the cadmium ions and the loofa dosage, and the rate of adsorption.

6.2.7 Isotherm modelling

Two and three parameter isotherm models were used to predict the mechanism behaviour of cadmium adsorption onto loofa. Figure 6.18 – 6.21 show the different isotherm fitting models utilised using non-linear regression. Table 6.3 show the correlation coefficient values obtained for the utilised isotherm models.

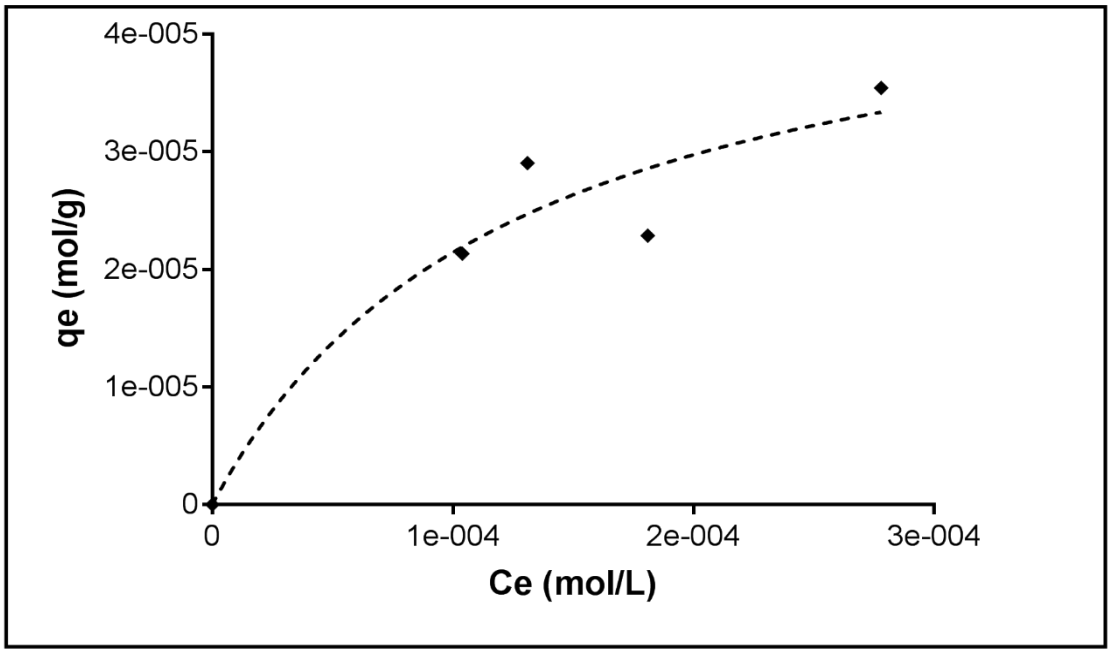

Figure 6.18: Cadmium isotherm from pH 6.0 ± 0.1 at 21 °C at 2hr. contact time. Langmuir model fit shown by the dashed line.

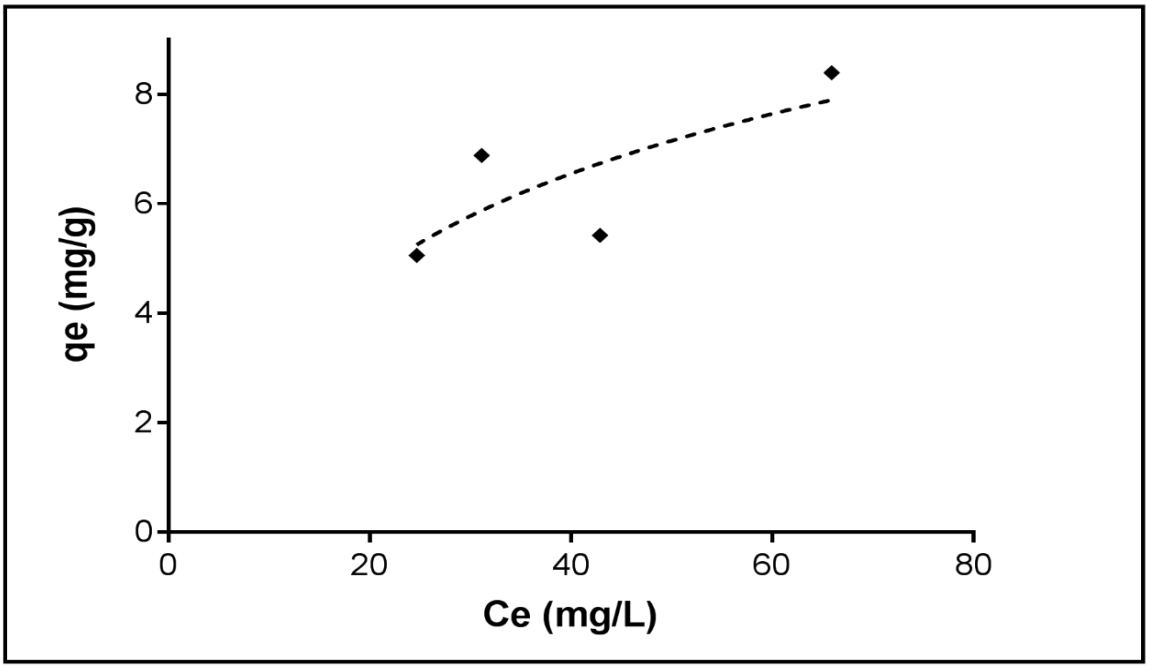

Figure 6.19: Cadmium isotherm from pH 6.0 ± 0.1 at 21 °C at 2 hr. contact time. Temkin model fit shown by the dashed line.

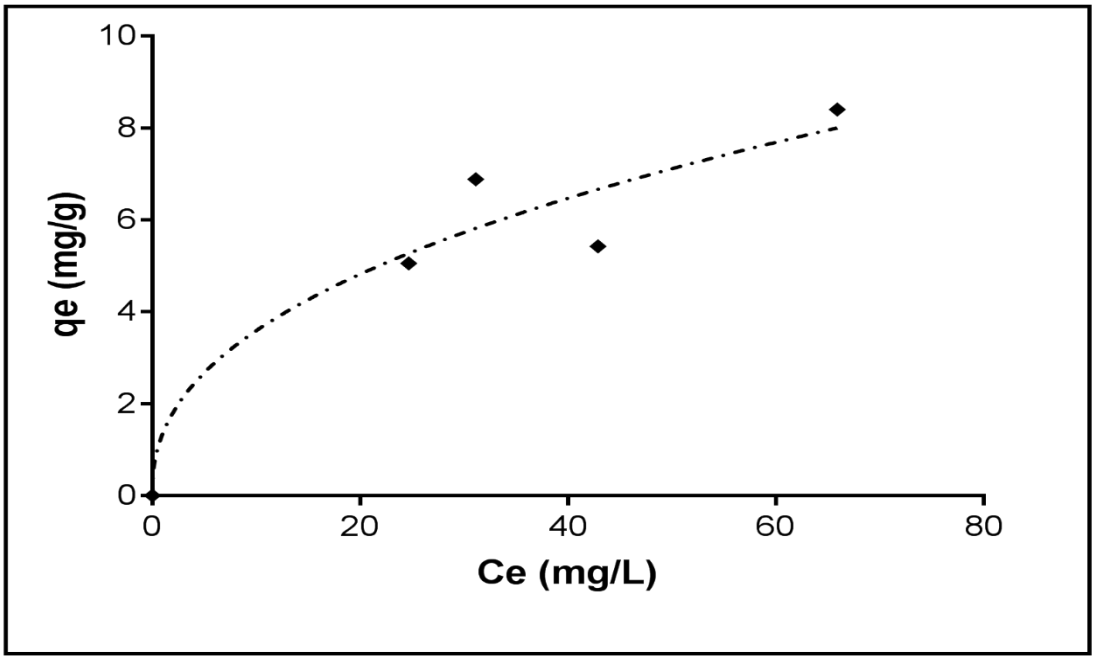

Figure 6.20: Cadmium isotherm from pH 6.0 ± 0.1 at 21 °C at 24 hr. contact time. Sips model fit shown by the dashed line.

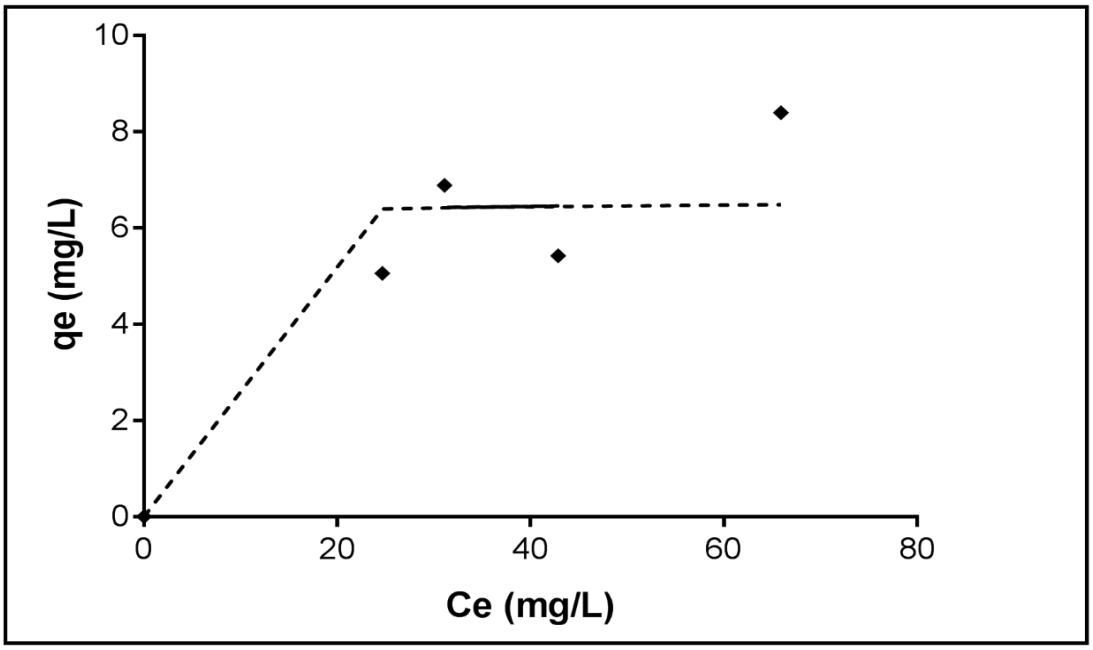

Figure 6.21: Cadmium isotherm from pH 6.0 ± 0.1 at 21 °C at 24 hr. contact time. Two-site Langmuir model fit shown by the dashed line. (R^2 = 0.930; no fit).

Table 6.3: Correlation coefficient of isotherm models

Isotherm models	**R^2**
Langmuir	0.922
Sips	0.928
Temkin	0.564
Two-site Langmuir	0.930,no fit

None of the utilised isotherm models satisfactorily predicted the experimental data but all fitted to a R^2 value over 0.9 expect the Temkin model. Figure 6.9 shows an increased adsorption capacity as the initial concentration increases and Figure 6.10 shows an increased percentage removal capacity that attains a maximum as initial concentration is increased. Further increase in initial concentration led to a decrease in percentage removal of the cadmium ions. The experimental data utilised to fit the isotherm models were at pH 6, which is shown in Figure 6.1 to give a maximum uptake capacity. However, the results for this fitting are inconclusive, as a higher correlation coefficient is needed to sufficiently explain the experimental data yet the best fit in comparison to the others is the Sips model (Shahidi *et al*., 2016). Furthermore, the data did not fit to the two-site Langmuir model which explains a single but heterogeneous adsorption site on the loofa surface (Onyango *et al*., 2004).

CHAPTER SEVEN

7.0 METHYLENE BLUE BIOSORPTION

7.1 Introduction

This chapter describes the effect of different experimental conditions on the adsorption of methylene blue (MB) onto *Luffa cylindrica* (loofa). The methylene blue dye, as explained in chapter one, acts as a model compound of an organic pollutant. Therefore, section 7.2 describes the characteristics of the loofa after methylene blue adsorption examined by the FT-IR technique and the speciation of MB in aqueous solution. It then presents the batch experimental results as regards to change in pH, initial methylene blue ion concentration, loofa treatment, temperature and mixed solutions of MB with metal ions. Also, it presents the kinetic and isotherm models used to investigate the adsorption reactions between the loofa and methylene blue. The effect of MB adsorption under dark and light conditions was investigated; and the intensity of light was also considered. UV-Vis spectra of the adsorption was used to study the interaction of the methylene blue structure during adsorption onto untreated and treated loofa.

7.2 Batch experiments

7.2.1 FT-IR spectra

The FT-IR spectra for both NaOH and HCl treated and untreated loofa loaded with MB is shown in Figures 7.1 to 7.4. The difference in the spectra is depicted by the change in the intensity of the functional groups present on the loofa surface.

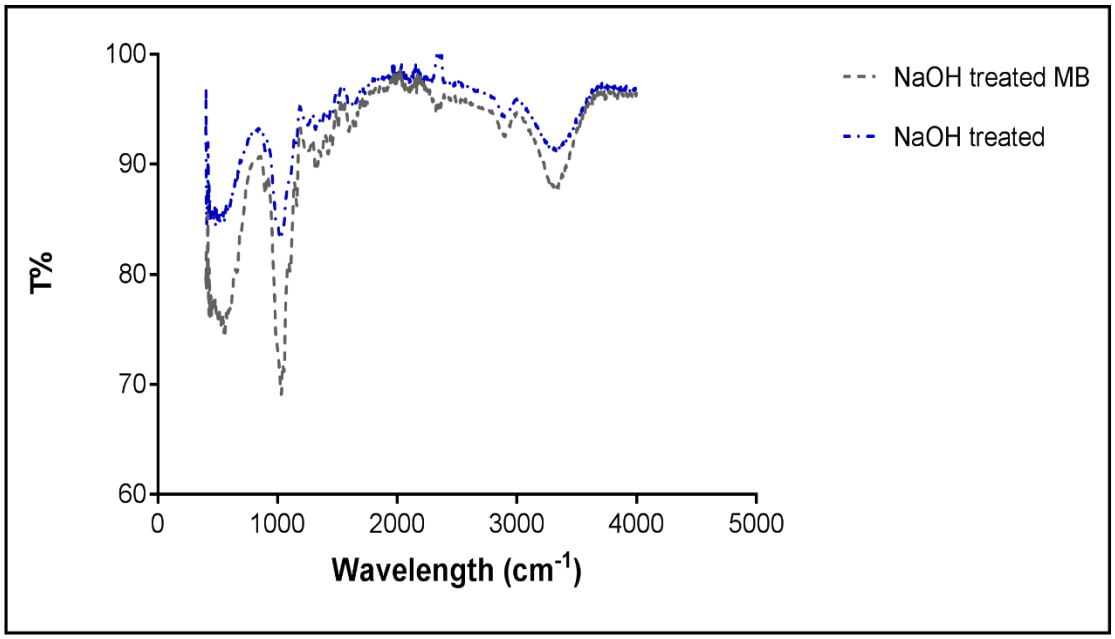

Figure 7.1: T% (percentage transmittance) versus wavelength FT-IR spectra of 4% NaOH treated and MB-loaded loofa at pH 7 (methylene blue concentration: 20mg/L; agitation speed: 200rpm; at 21°C, 1h contact time, 5g/L loofa dosage).

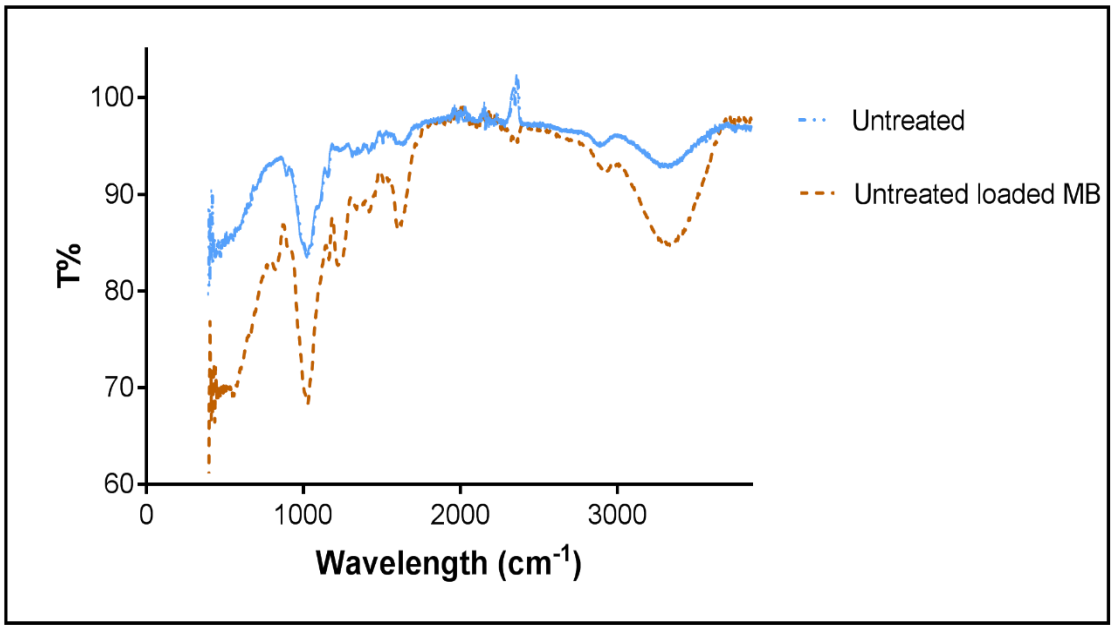

Figure 7.2: T% (percentage transmittance) versus wavelength FT-IR spectra of untreated and MB-loaded loofa at pH 7 (methylene blue concentration: 20mg/L; agitation speed: 200rpm; at 21°C, 1h contact time, 5g/L loofa dosage).

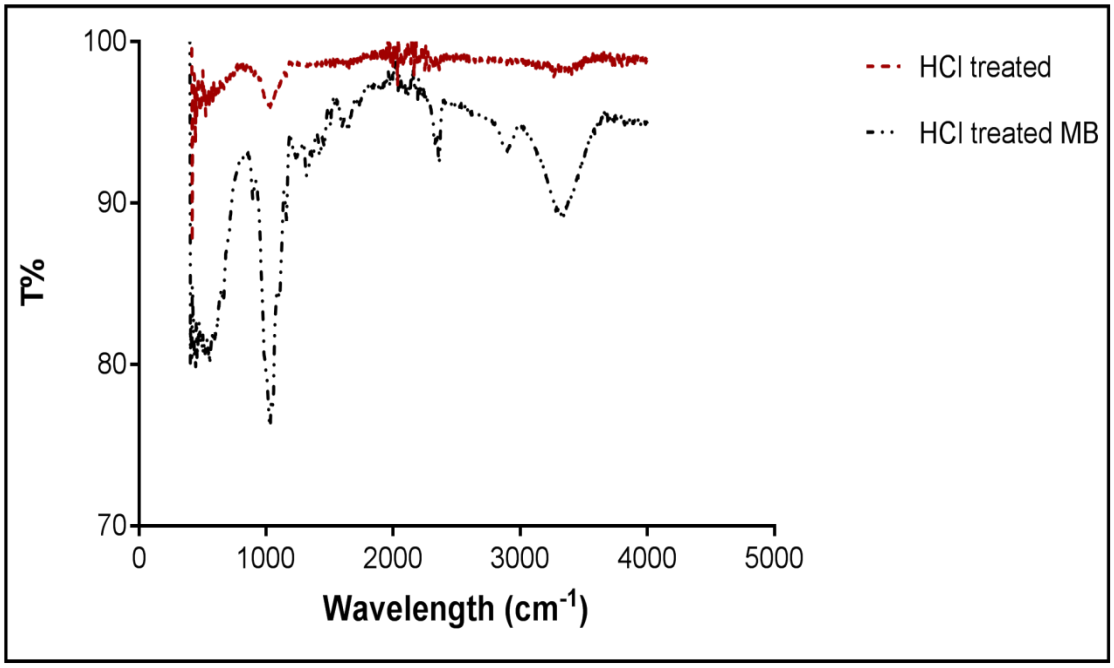

Figure 7.3: T% (percentage transmittance) versus wavelength FT-IR spectra of 4% HCl treated and MB-loaded loofa at pH 7 (methylene blue concentration: 20mg/L; agitation speed: 200rpm; at 21°C,1h contact time, 5g/L loofa dosage).

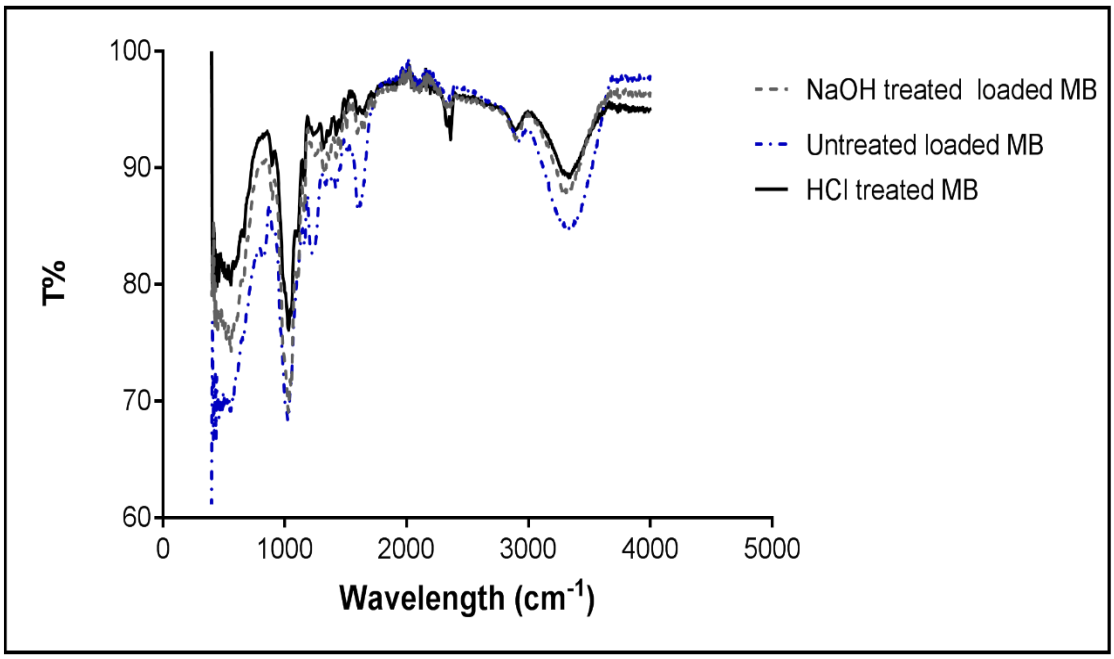

Figure 7.4: T% (percentage transmittance) versus wavelength FT-IR spectra of untreated, 4% NaOH treated and HCl treated MB-loaded loofa at pH 7; methylene blue concentration: 20mg/L; agitation speed: 200rpm; at 21°C, 1h contact time, 5g/L loofa dosage.

The broad band indicated by the FTIR spectra at 3300 cm^{-1} represents bonded OH^- groups. The bands observed at 2300cm^{-1} are assigned to C≡N group. The shift in the bond at 2800cm^{-1} is attributed to aliphatic C—H group in methyl group.

The peak intensity of adsorption bands, shown in Figure 7.1, have changed. This indicates the involvement of O-H, C-H and C-O bonds (wavelength range of 1000 – 3300cm^{-1}) in the adsorption of MB onto loofa. A similar change in peak intensity occurs with the untreated and HCl treated loofa (Figure 7.2 & 7.3). The new peaks formed at 1610cm^{-1} and 1235cm^{-1} bands after the adsorption of MB onto the untreated loofa attribute to the stretching of the carbonyl groups and bending vibrations of the C-H of the methyl group (Figure 7.2) (Peydayesh *et al*., 2015). For the HCl treated MB loaded loofa, the band shift is also at wavelength range of 1000 – 3300cm^{-1}. The FT-IR vibrations of all loofa used had been altered and both NaOH and HCl treated loofa loaded with MB show a significant change at 3300cm^{-1} which indicates the strong bond of the carboxylic group as the dominant group in adsorption leading to a higher adsorption capacity as compared to untreated loofa loaded with MB.

Furthermore, the highest pore volume and BET surface area was obtained for NaOH treated loofa (Chapter 3 - Table 3.5) which explains a pore volume diffusion process of MB adsorption onto NaOH treated loofa. The average pore diameter of > 2nm supports the adsorption of larger dye molecules. The mesopores (higher volume of pores per gram of loofa) lead to a greater adsorption process (Gusmao *et al*., 2013).

7.2.2 Speciation of methylene dye in aqueous solution

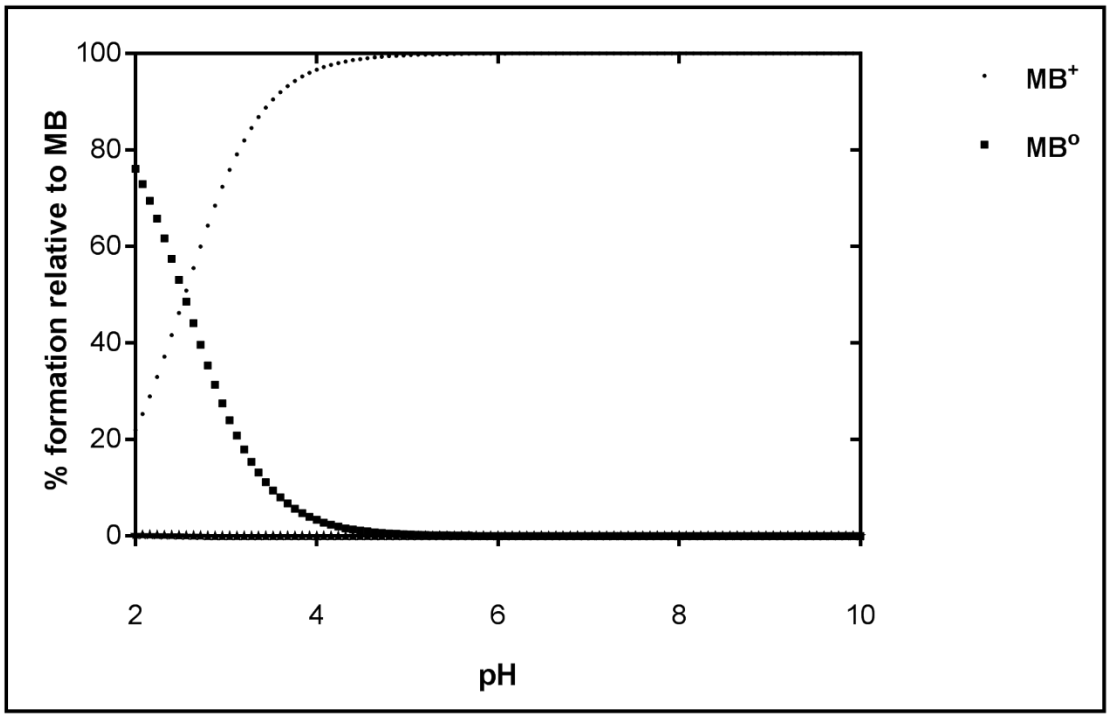

Figure 7.5: Speciation diagram of MB ions (MB^+ - cationic species; MB^o – molecules) in aqueous solution between pH 3 – 9 at 21°C.

The solution pH has a prominent effect on MB speciation in solution. MB exists as a cationic species (MB^+) and undissociated molecules (MB^o) in aqueous solution (Salazar-rabago *et al*., 2017). Different aggregation forms of MB occur when MB is dissolved in aqueous solutions. The aggregation constants have been calculated in the literature and the percentage of MB aggregate that forms as it relates to solution conditions can be described. Using the equilibrium aggregation constants derived from the aggregation constants, an attempt has been made to determine the speciation of MB in water solution as pH changes (Klika, 2007). As shown in figure 7.5, at a pH = 3, the MB cationic species and the undissociated MB molecules coexist. As pH increases the undissociated MB molecule decreases and the only available MB form is the cationic species which increases (Salazar-rabago *et al*., 2017). As pH increases to pH 7, the cationic species of MB are dominant in the adsorption process.

7.2.3 pH effect

pH is one of the most important factors that influence the adsorption of methylene blue.

The calibration plot of absorbance versus concentration (mg/L), derived from the experimental data of absorbance readings of known concentrations, is obtained from using the interpolation function of Mathematica software 10.1. The speciation diagram of MB is shown in Figure 7.5. Using equation (1) and (2) (Chapter two) to calculate the percentage removal and uptake capacity, the effect of pH is shown in figure 7.6 to 7.12 for NaOH treated loofa and Figure 7.13 & 7.14 for HCl treated loofa. The distribution ratio versus pH change is shown at the optimum pH 7. Figure 7.15 & 7.16 show the effect of pH for untreated loofa.

Methylene blue in aqueous solution exists as positively charged ions. The solution pH affects the surface charge on the adsorbent which in turn influences the degree of adsorption of the MB (Uddin *et al*., 2009). As shown in Figure 7.7, there is an increase in the percentage removal as pH is increased from 4 to 7. As the pH increases, the number of hydroxyl groups increased and the attraction occurs between the negatively charged loofa surface and the MB cations (Kim *et al*., 2013).

At pH 7, the optimum value is obtained above which there is a decrease in adsorption percentage. At low pH, protonation of carboxyl groups and high concentration of H^+ influences adsorption of positively charged methylene blue cations. The former by force repulsion and the latter by competition for available adsorption sites. At pH 8, the decreased percentage removal indicates that apart from electrostatic attraction and competition for active sites on the loofa, there are other factors that play a role in the adsorbent-adsorbate interactions.

❖ **NaOH treated MB loaded loofa**

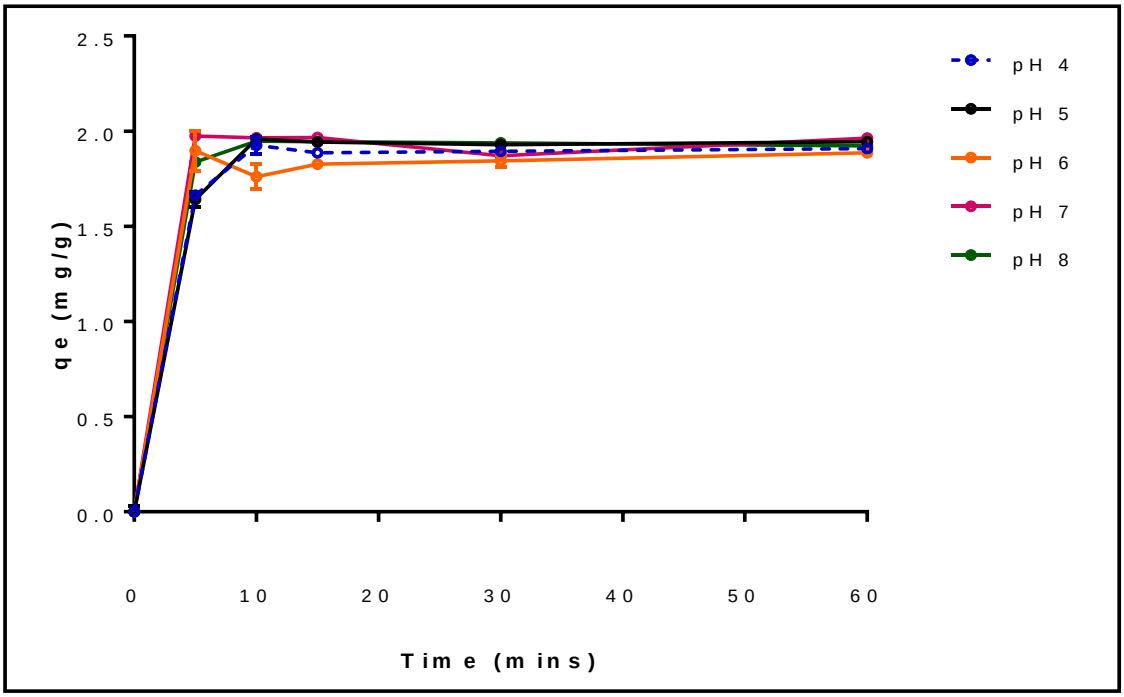

Figure 7.6: Uptake removal of MB with change in time after 60mins at pH range 4-8; MB ion concentration: 10mg/L; agitation speed: 200rpm; at 21^{o}C, 1h contact time, 5g/L alkali treated loofa dosage. Data from 3 replicate measurements.

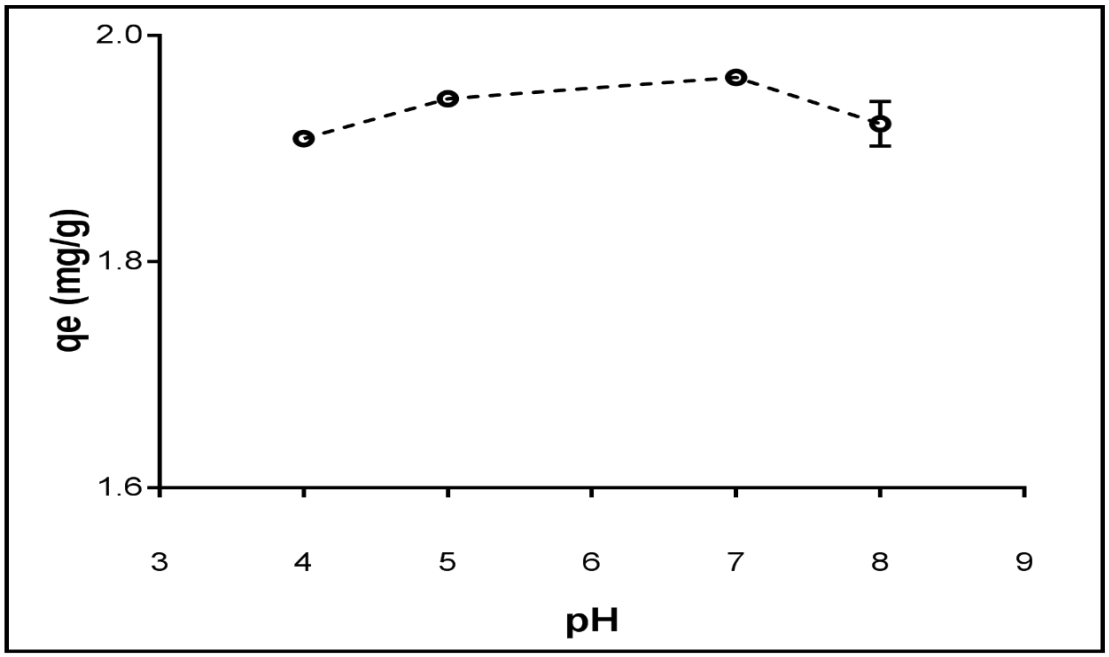

Figure 7.7: Effect of initial pH on the uptake capacity of MB onto loofa; MB ion concentration: 10mg/L; agitation speed: 200rpm; at 21^{o}C, 1h contact time, 5g/L alkali treated loofa dosage. Data from 3 replicate measurements.

As pH increases and decreases during the adsorption process, due to electrostatic attraction, an optimum pH value of 7 is reached. This further explains that as pH increases, a favoured alkali solution leads to negatively charged loofa surface which attracts the cationic species of MB.

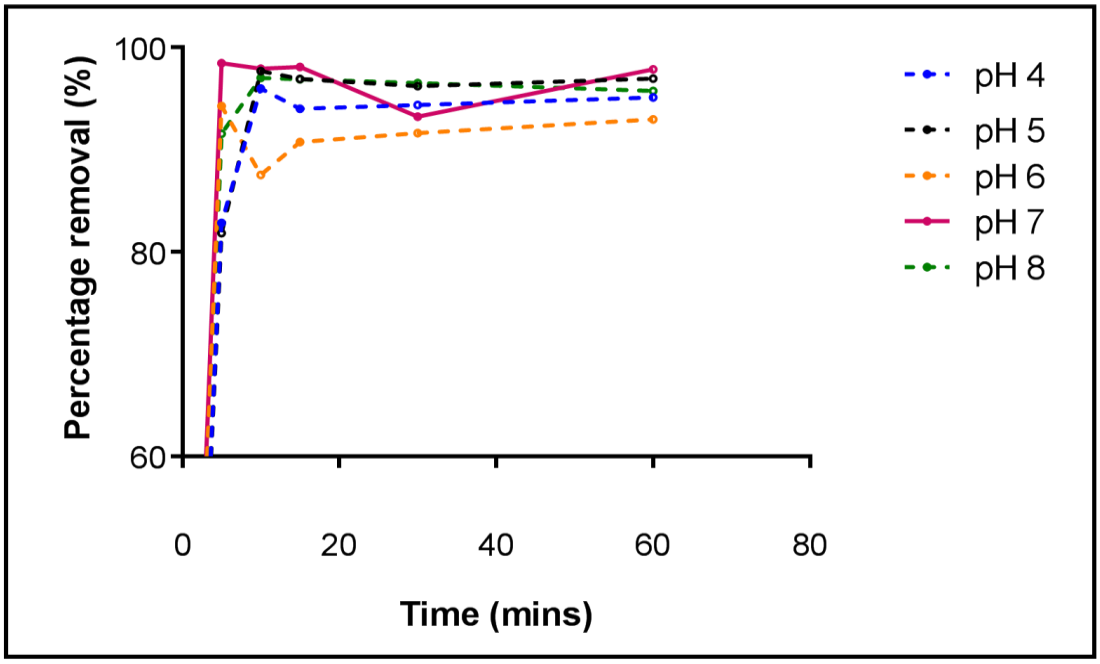

Figure 7.8: Percentage removal of MB with change in time after 60mins at pH range 4-8; MB concentration: 10mg/L; agitation speed: 200rpm; at 21^{o}C, 1h contact time, 5g/L alkali treated loofa dosage.

Maximum adsorption capacity is shown to occur in less than 15 mins and an equilibrium at 60 mins. At equilibrium, the adsorption of methylene blue ions was found to be maximum at pH 7. Over 80% removal is shown to occur at pH range from 4 to 8.

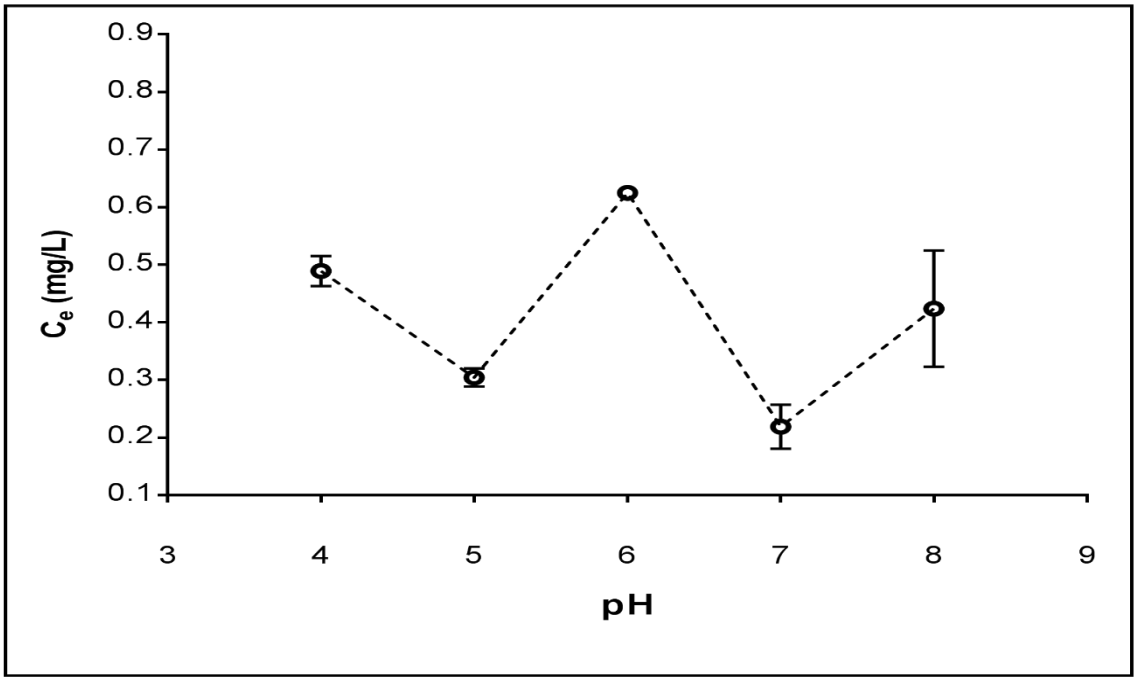

Figure 7.9: Adsorption pattern curve of methylene blue onto loofa at 60mins at pH range 4-8; MB concentration: 10mg/L; agitation speed: 200rpm; at 21^{o}C, 1h contact time, 5g/L alkali treated loofa dosage. Data from 3 replicate measurements. C_e is the final concentration of MB after adsorption.

Figure 7.9 shows the final concentration of MB in solution at different pH values. The lowest final concentration at pH 7 is 0.22mg/L and the highest final concentration is at pH 6 which supports the fact that the lowest percentage removal of MB occurs at this pH. The decrease and then increase in concentration as pH increases indicates protons in solution compete with the MB cations and the complex formation (formed aggregates of the MB forms) with MB on the loofa surface.

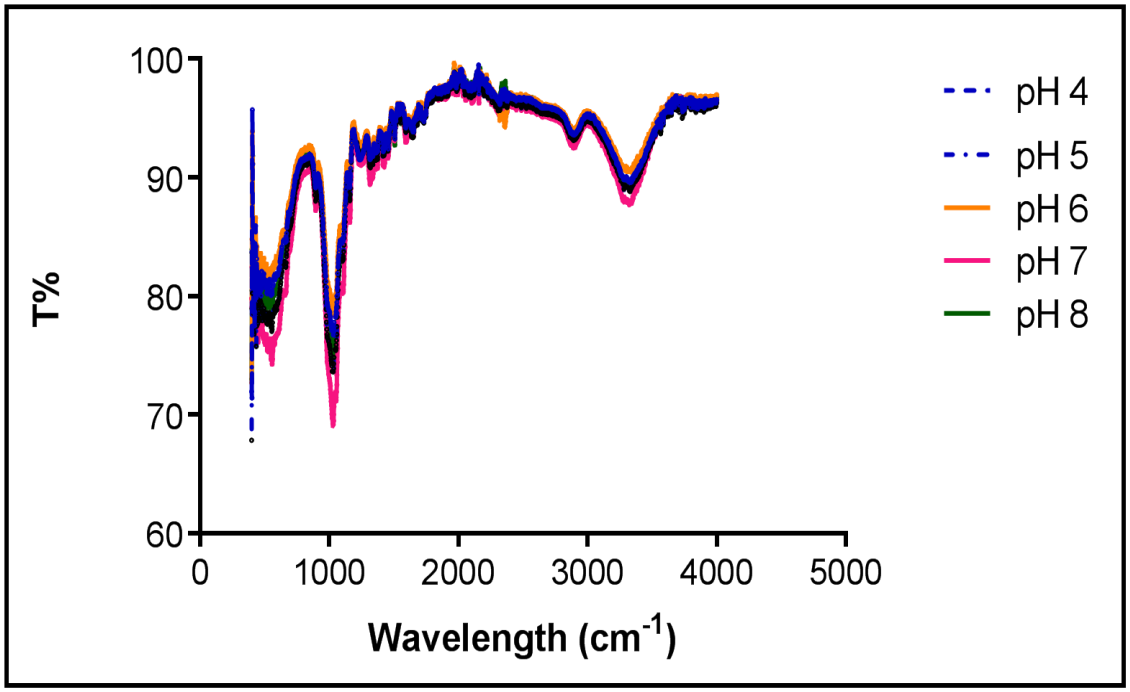

Figure 7.10: T% (percentage removal) versus wavelength FT-IR spectra of 4% NaOH treated MB loaded loofa at pH range 4-8; methylene blue concentration: 20mg/L; agitation speed: 200rpm; at 21°C, 24h contact time, 5g/L alkali treated loofa dosage.

FT-IR spectra in Figure 7.10 at pH 4, 5, 6 and 8, are respectively similar but at pH 7, the transmittance value is lower at the same wavelength of 3400cm^{-1} and also at wavelength at 1050cm^{-1} (Figure 7.10). This shows the formation of higher aggregates at the maximum adsorption capacity at pH 7. Generally, all peaks indicate the involvement of certain functional groups, and at pH 7 shows the lowest transmittance which means the highest absorbance occurs as a result of maximum adsorption of MB onto the loofa. This supports the data giving the maximum adsorption capacity at pH 7 (Figure 7.6 & 7.7).

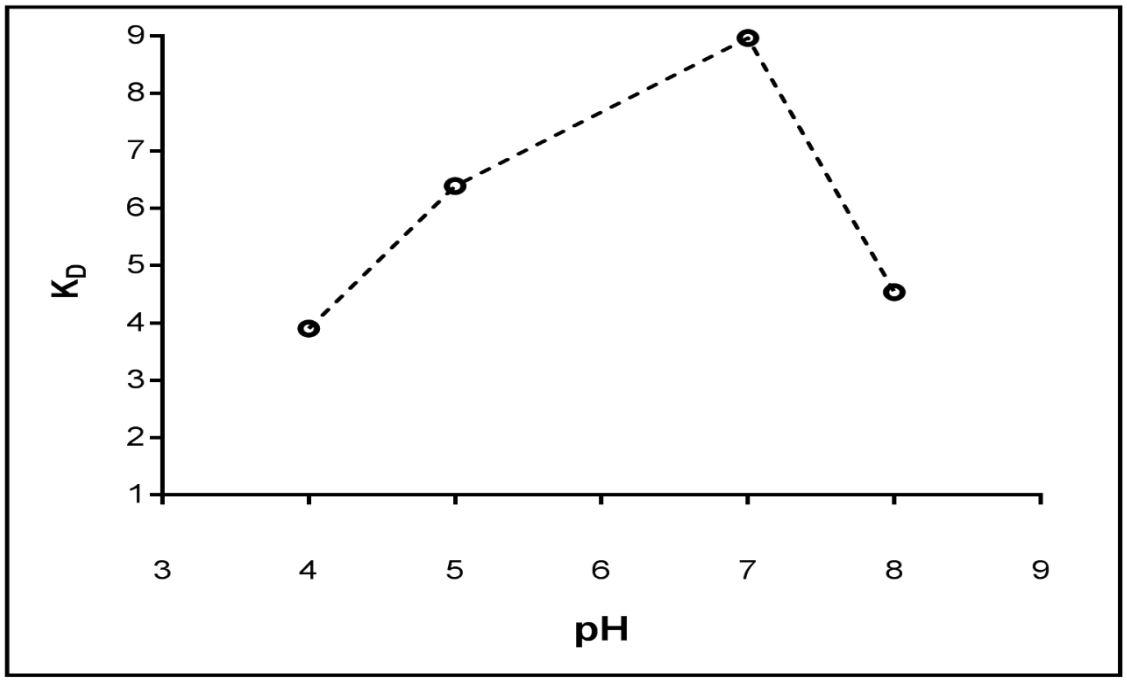

Figure 7.11: Distribution ratio versus pH at equilibrium at pH range 4-8; MB concentration: 10mg/L; agitation speed: 200rpm; at 21°C, 1h contact time, 5g/L alkali treated loofa dosage.

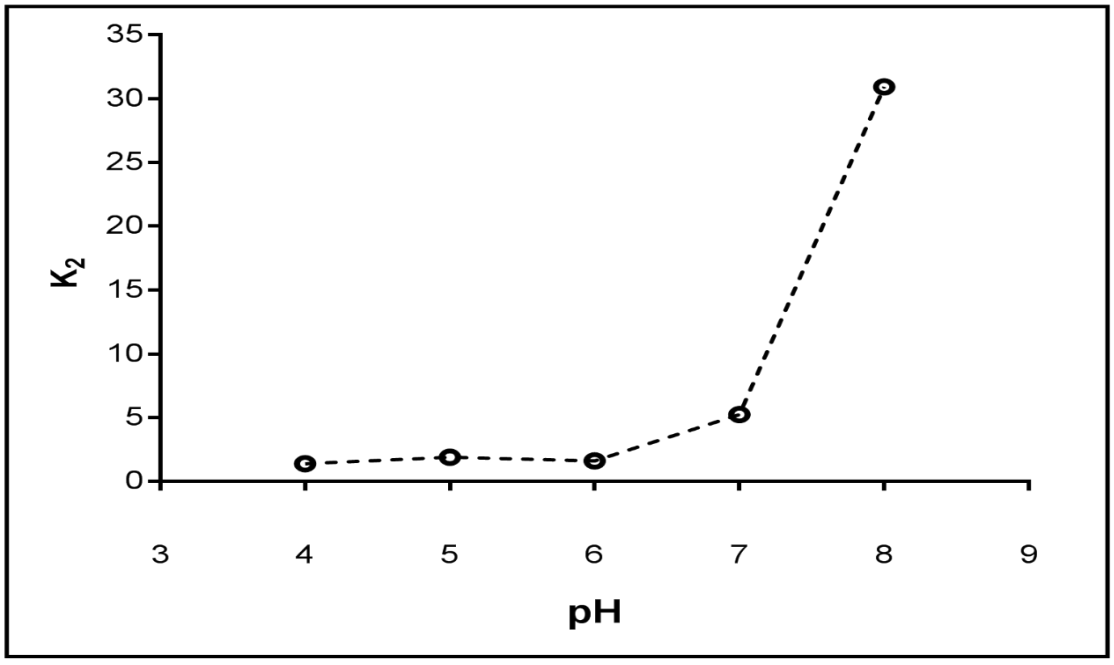

Figure 7.12: Pseudo second order constant versus pH of MB concentration at equilibrium at 10mg/L; pH concentration ranges of 4-8; agitation speed: 200rpm; at 21°C, 1h contact time, 5g/L alkali treated loofa dosage.

As the rate of MB adsorption increases, the amount of OH^- in solution is increased leading to an increase in pH. The rate of adsorption increases as pH increases over time (Figure 7.12).

❖ **HCl treated MB loaded loofa**

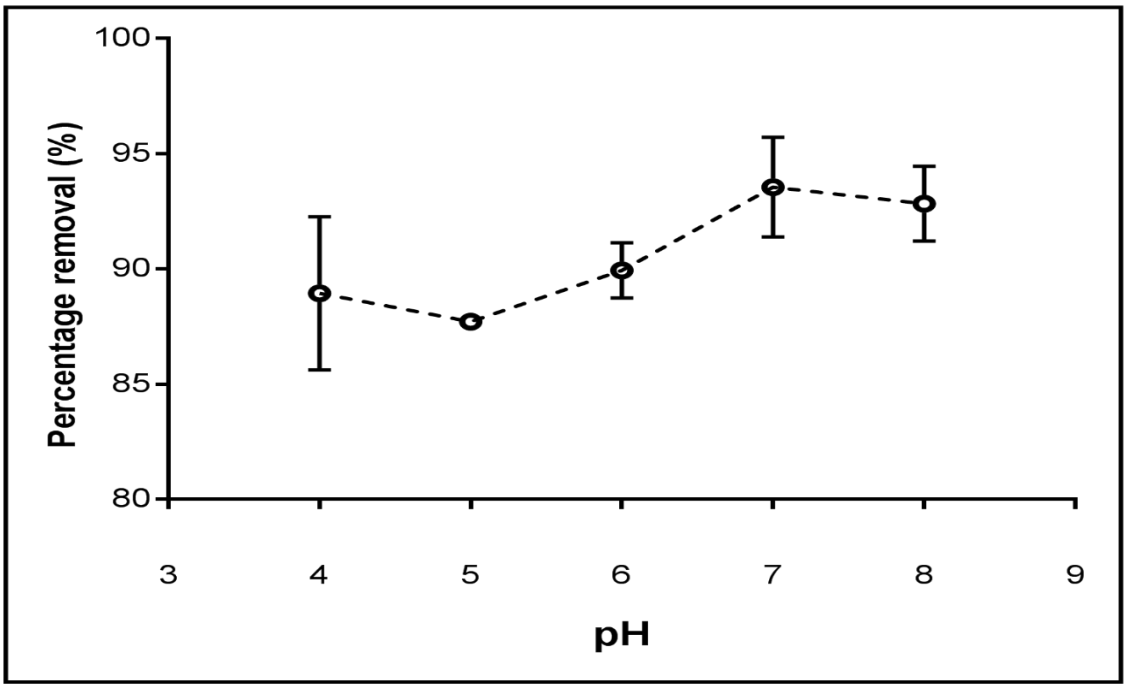

Figure 7.13: Percentage removal of MB with change in pH after 60mins; MB concentration: 10mg/L; agitation speed: 200rpm; at 21°C, 1h contact time, 5g/L HCl treated loofa dosage. Data from 3 replicate measurements.

The percentage removal capacity slightly decreases by 1.2% between pH 4 and 5 and then increases till an optimum value is reached at pH 7 (Figure 7.13). It would also be expected that the distribution ratio versus the change in pH shows a similar trend (Figure 7.14). However, HCl treated loofa and untreated loofa show a lower percentage removal capacity (93.5% and 93.7% respectively), than NaOH treated loofa at 99% (Figure 7.8, 7.13 & 7.16).

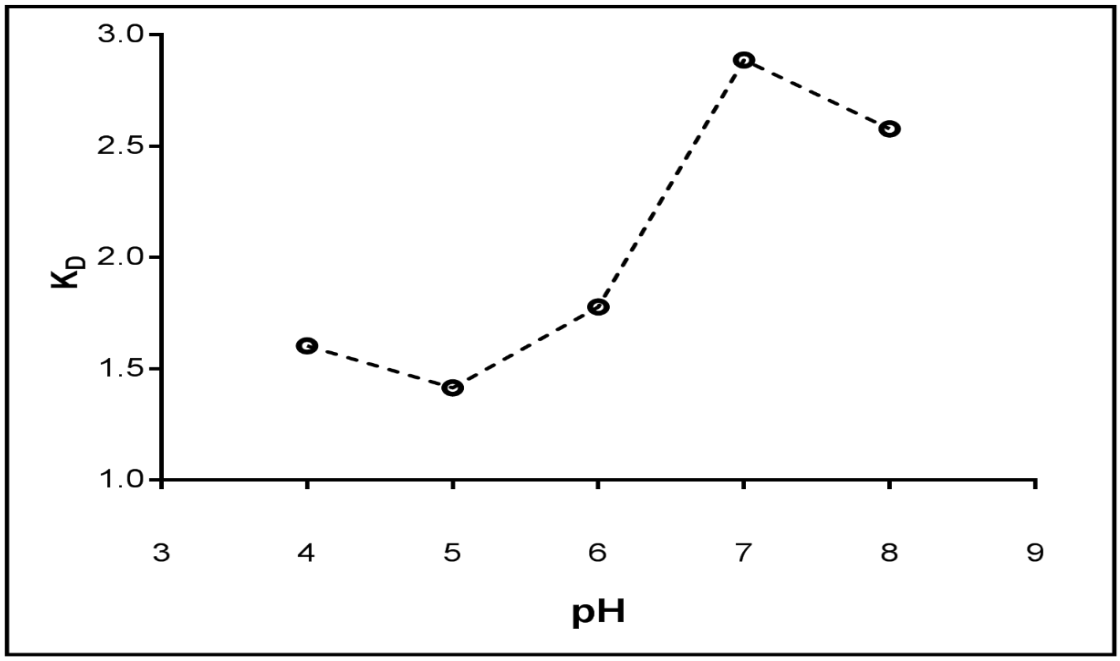

Figure 7.14: Distribution ratio versus pH at equilibrium at pH range 4-8; MB concentration: 10mg/L; agitation speed: 200rpm; at 21°C, 1h contact time, 5g/L HCl treated loofa dosage.

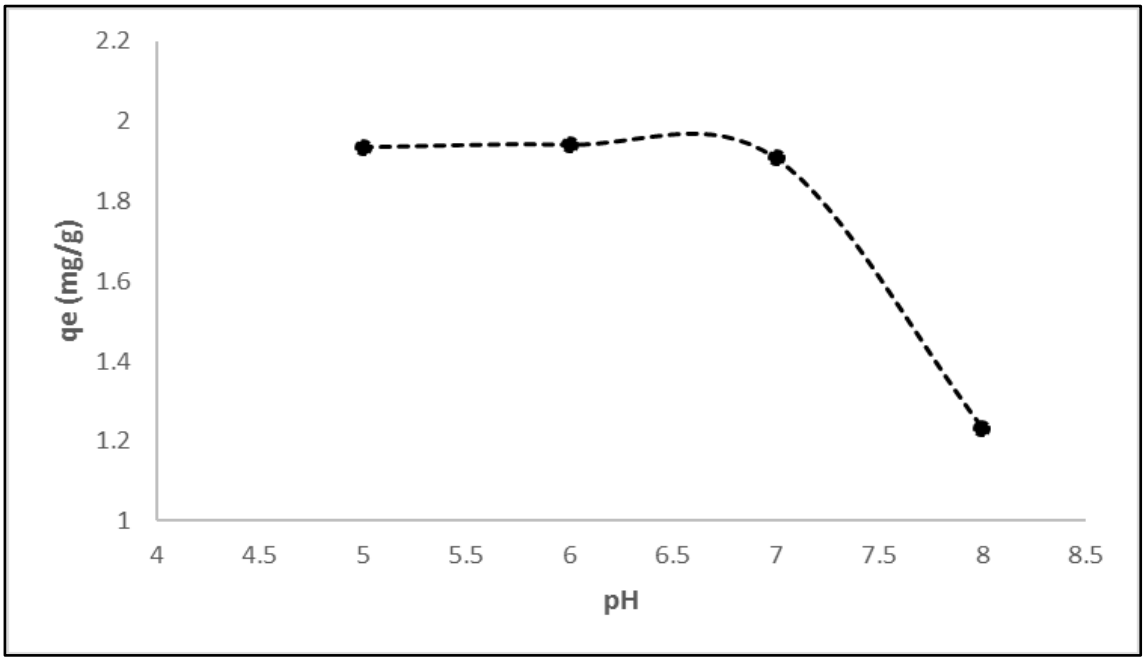

Figure 7.15: Effect of initial pH on the uptake capacity of MB onto loofa; MB ion concentration: 10mg/L; agitation speed: 200rpm; at 21°C, 1h contact time, 5g/L untreated loofa dosage. Data from 3 replicate measurements.

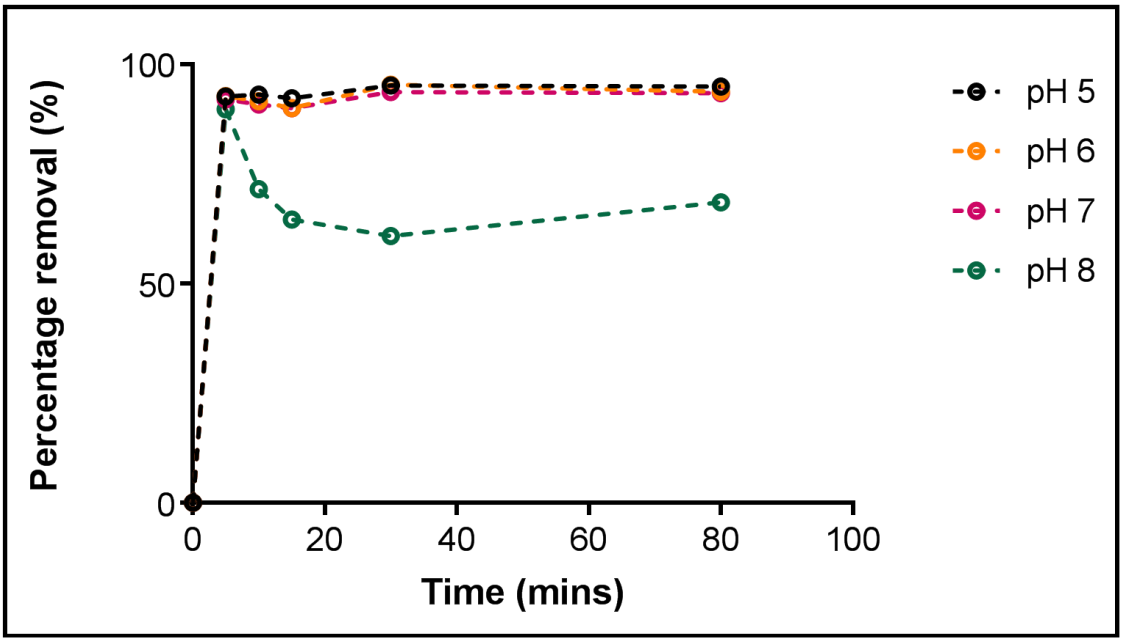

Figure 7.16: Percentage removal of MB with change in time over 60mins at pH range 4-8; MB concentration: 10mg/L; agitation speed: 200rpm; at 21°C, 1h contact time, 5g/L untreated loofa dosage. Data from 3 replicate measurements.

The optimum removal capacity is shown to occur at pH 5 & 6 (Figure 7.15) which then decreases as the pH increases. MB adsorption on untreated loofa binds differently compared to HCl and alkali treated loofa adsorbents.

7.2.4 Concentration effect

Figure 7.17 shows an increase in adsorption capacity as initial concentration increases. Figure 7.18 shows the percentage removal capacity to be similar as the adsorption process approaches equilibrium. Figure 7.19 shows the slight increase of less than 2% removal capacity of MB by untreated loofa when the initial concentration is increased from 10 – 40mg/L. Figure 7.20 shows the effect of increase in initial concentration of MB on adsorption capacity.

❖ **Untreated MB loaded loofa**

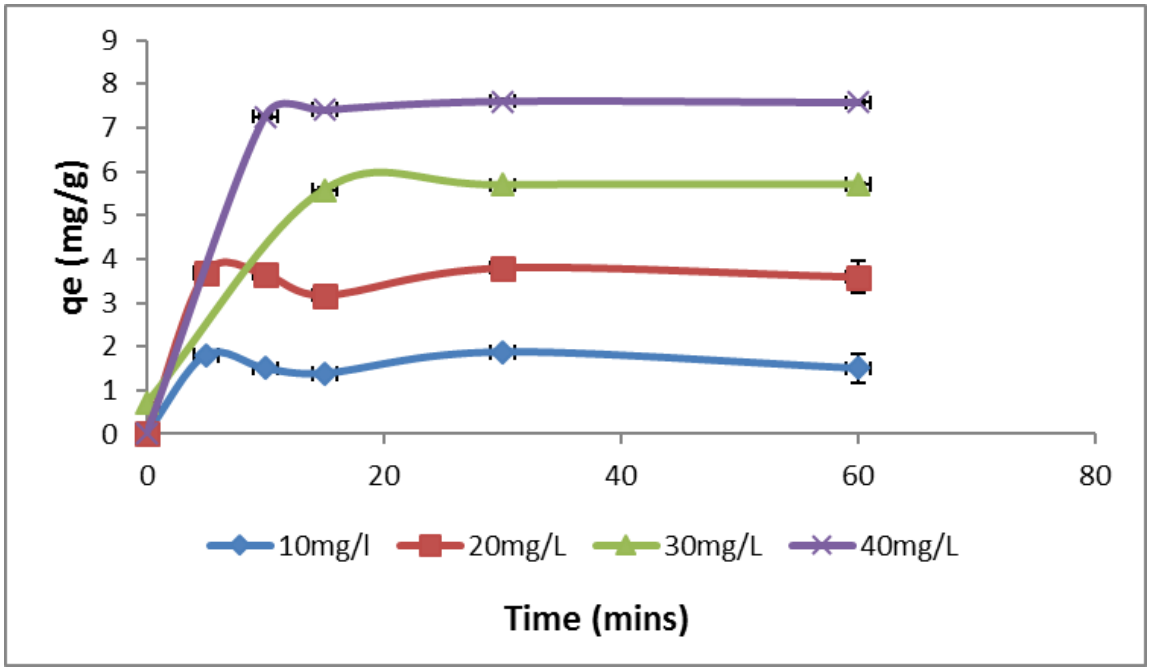

Figure 7.17: MB uptake capacity with change in time over 60 mins at pH 7; MB concentration ranges of 10-40mg/L; agitation speed: 200rpm; at 21°C, 1h contact time, 5g/L untreated loofa dosage. Data from 3 replicate measurements.

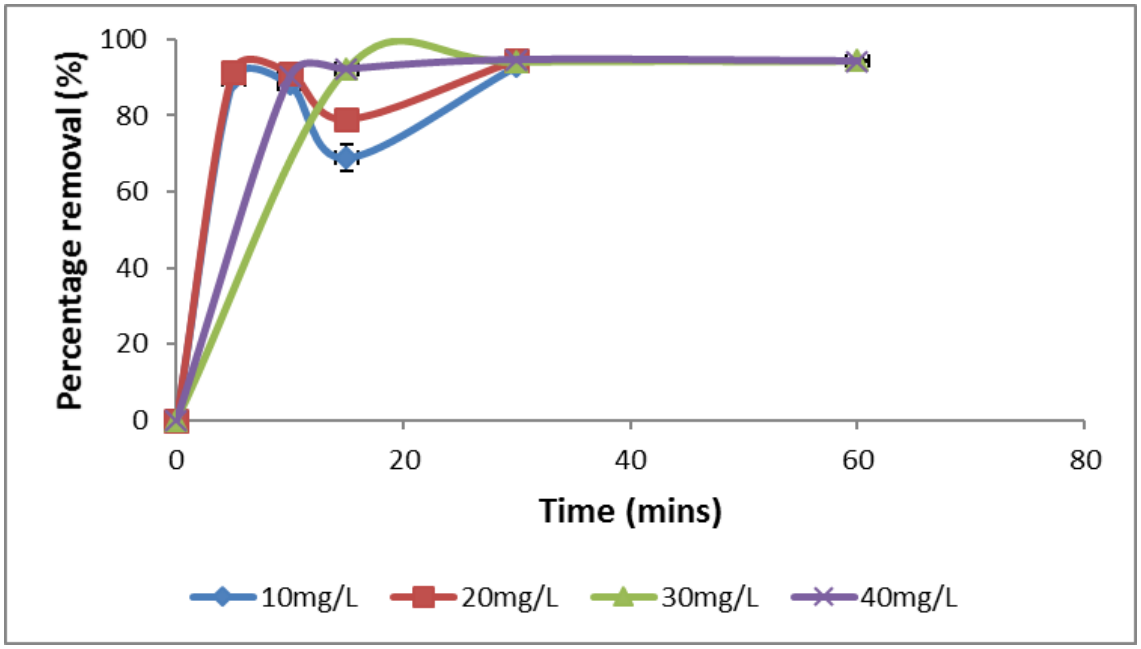

Figure 7.18: Percentage removal of MB with change in time over 60 mins at pH 7; MB concentration ranges of 10-40mg/L; agitation speed: 200rpm; at 21°C, 1h contact time, 5g/L untreated loofa dosage. Data from 3 replicate measurements.

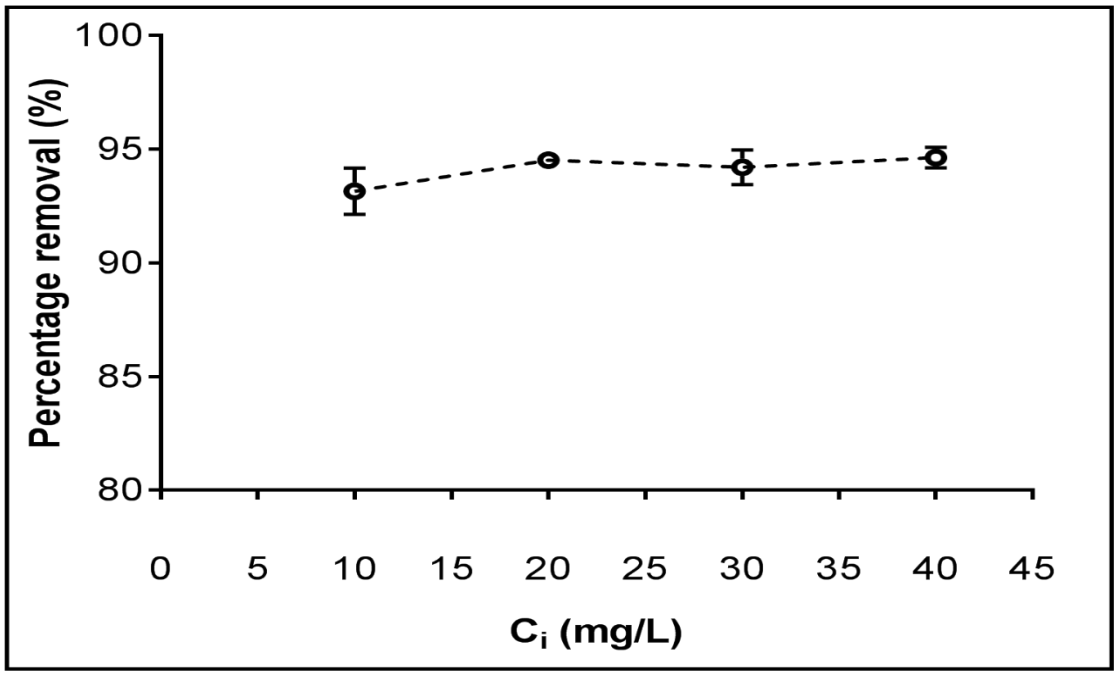

Figure 7.19: Percentage removal of MB after equilibrium at 60 mins at pH 7; MB concentration ranges of 10-40mg/L; agitation speed: 200rpm; at 21°C, 1h contact time, 5g/L untreated loofa dosage. Data from 3 replicate measurements.

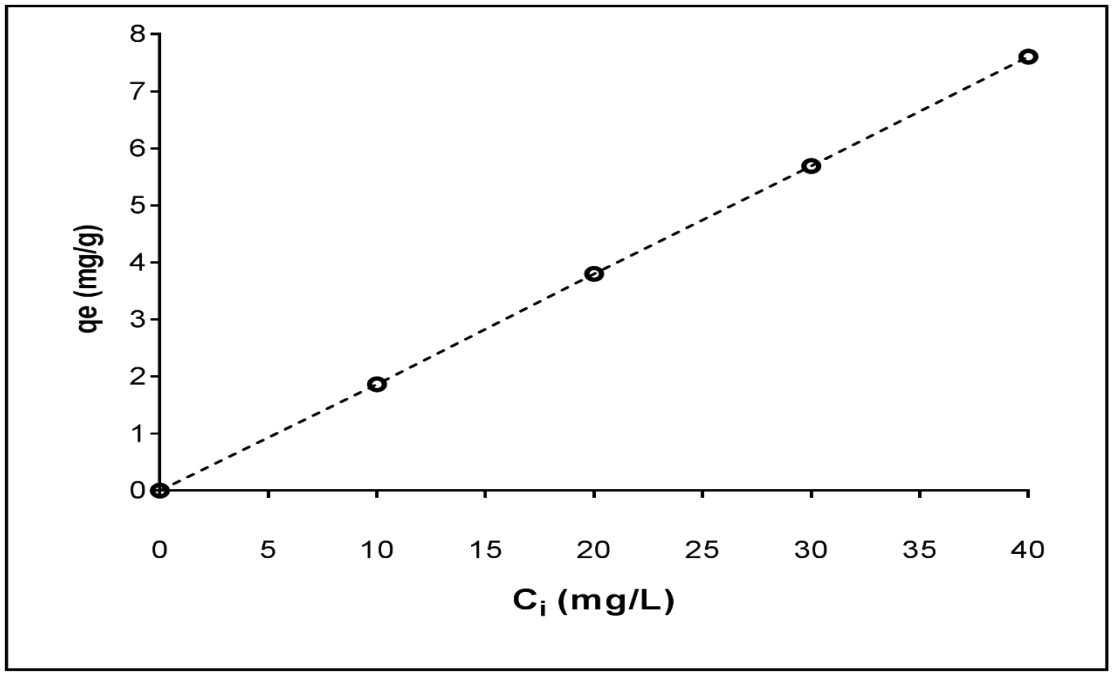

Figure 7.20: MB uptake capacity of MB versus MB initial concentration after equilibrium at 60 mins at pH 7; MB concentration ranges of 10-40mg/L; agitation speed: 200rpm; at 21°C, 1h contact time, 5g/L untreated loofa dosage. Data from 3 replicate measurements.

It is expected that as the initial concentration increases the uptake capacity increases (Figure 7.20) up to the point of saturation. Also, as the heterogeneous surface becomes occupied, the number of binding active sites is decreased, thereby leading to change in the percentage removal capacity over time as initial concentration increases (Figure 7.18 & 7.19).

- **NaOH treated MB loaded loofa**

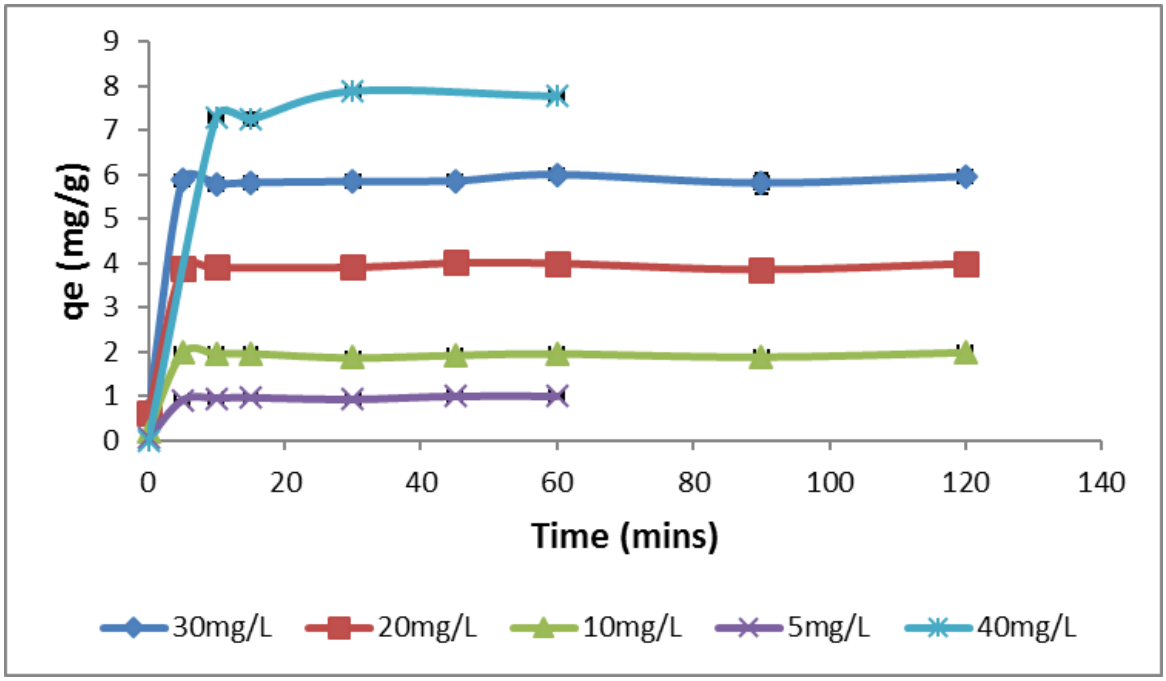

Figure 7.21: MB uptake capacity with change in time after 60 mins at pH 7; MB concentration ranges of 10-40mg/L; agitation speed: 200rpm; at 21°C, 1h contact time, 5g/L alkali treated loofa dosage. Data from 3 replicate measurements.

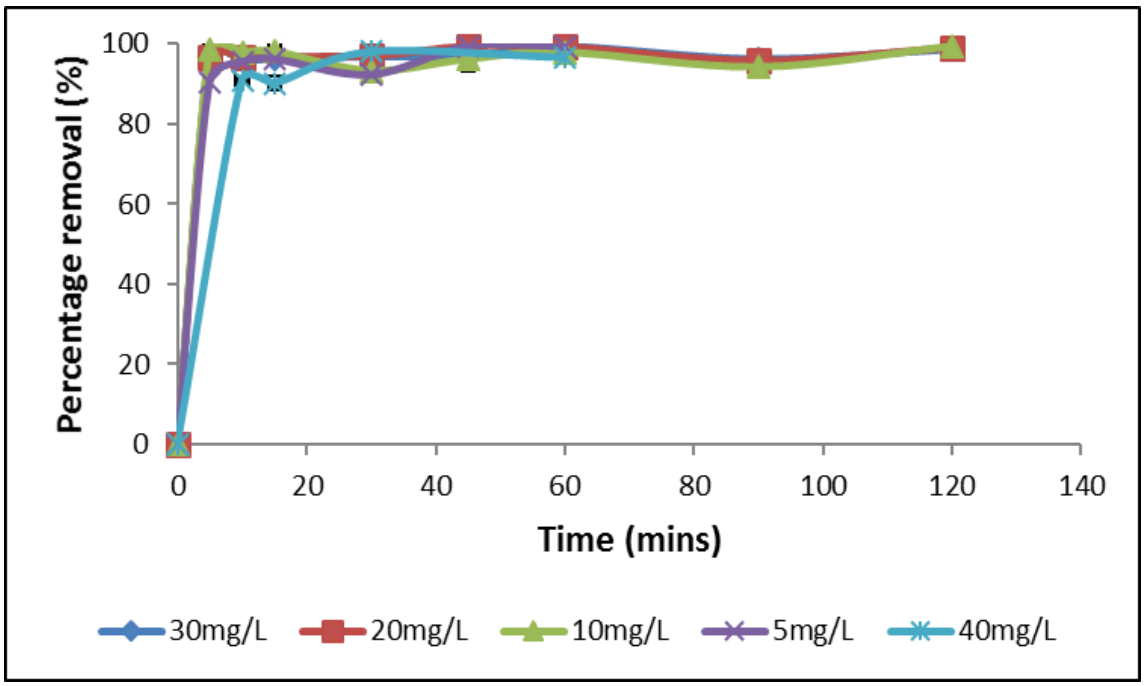

Figure 7.22: Percentage removal of MB with change in time after 60 mins at pH 7; MB concentration ranges of 10-40mg/L; agitation speed: 200rpm; at 21°C, 1h contact time, 5g/L alkali treated loofa dosage. Data from 3 replicate measurements.

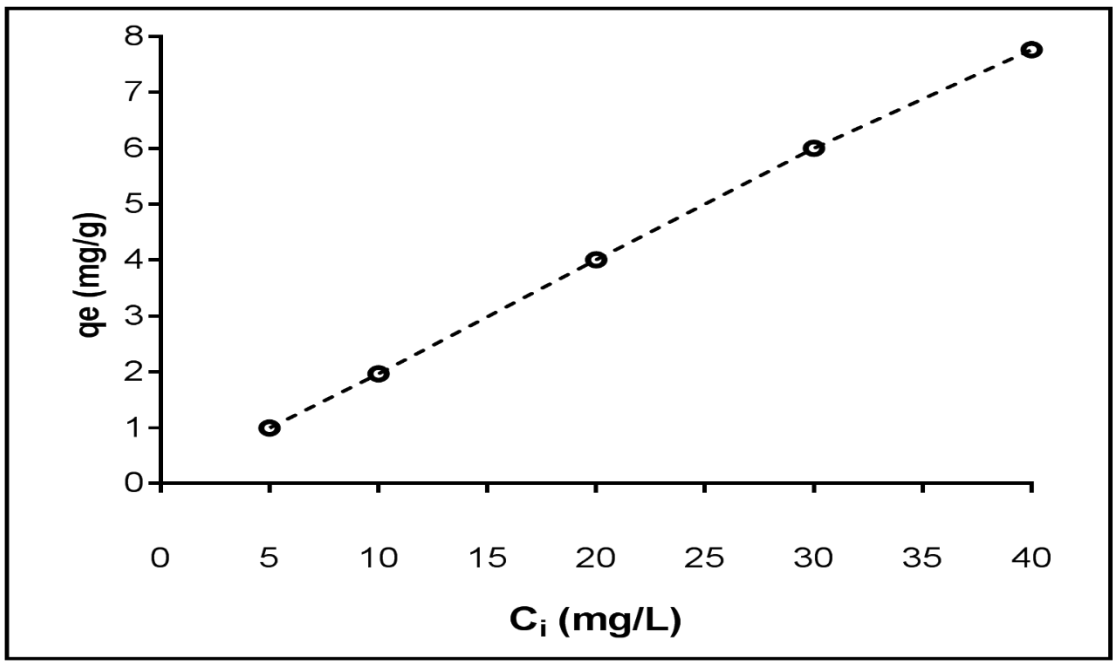

Figure 7.23: MB uptake capacity of MB versus MB initial concentration after equilibrium at 60 mins at pH 7; MB concentration ranges of 10-40mg/L; agitation speed: 200rpm; at 21°C, 1h contact time, 5g/L alkali treated loofa dosage.

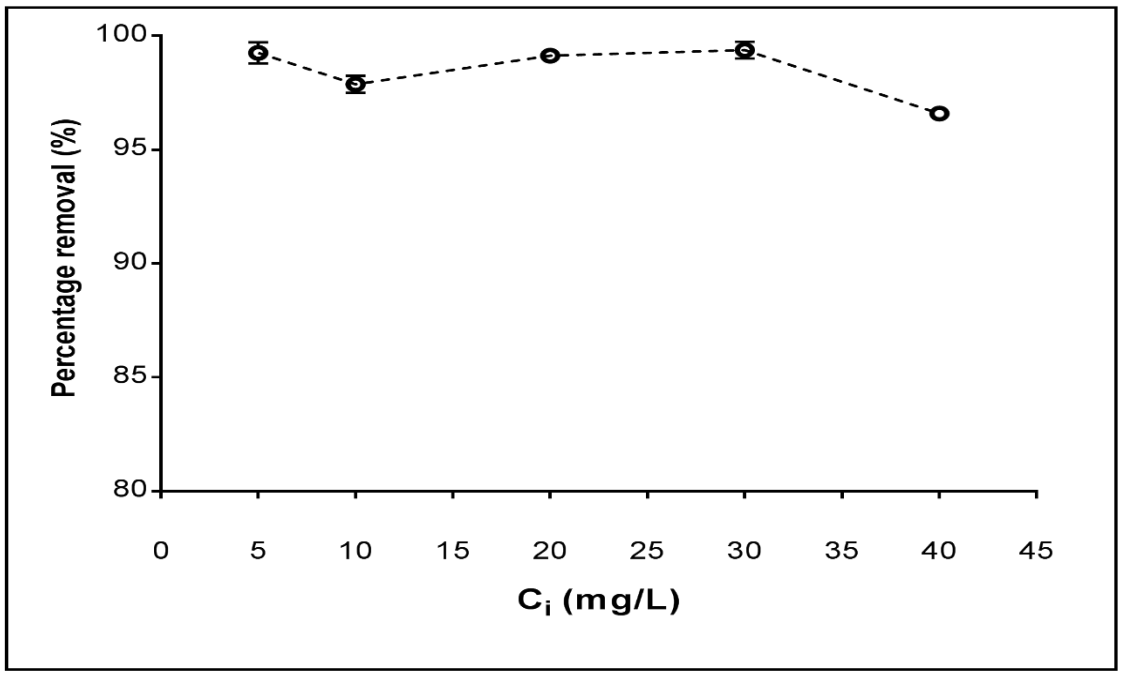

Figure 7.24: Percentage removal of MB after equilibrium at 60 mins at pH 7; MB concentration ranges of 10-40mg/L; agitation speed: 200rpm; at 21°C, 1h contact time, 5g/L alkali treated loofa dosage. Data from 3 replicate measurements.

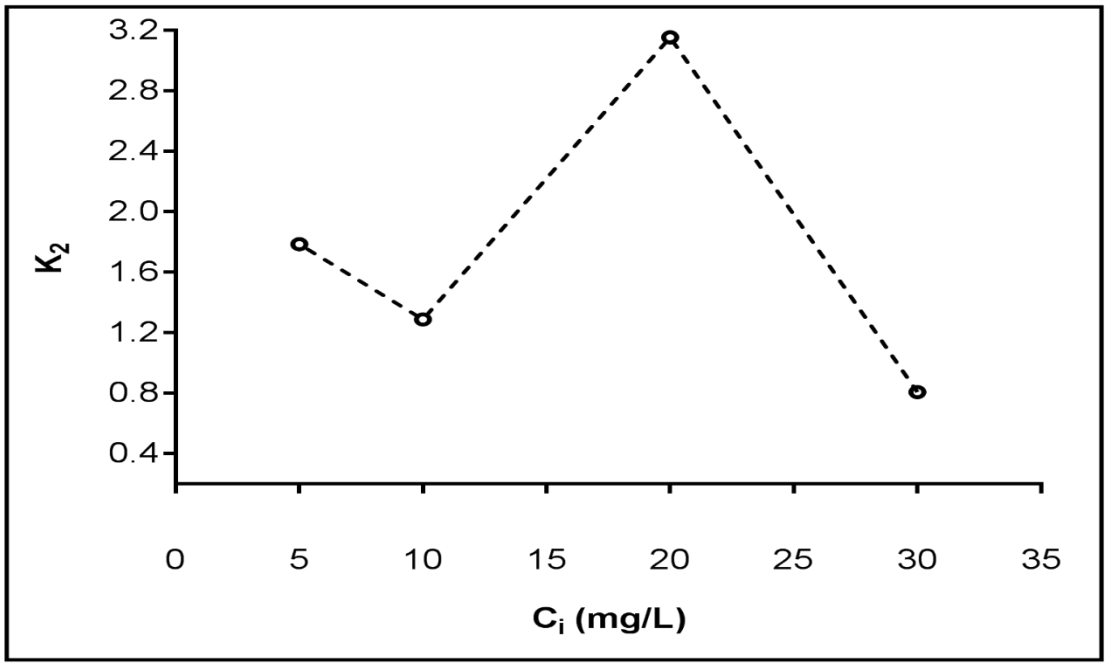

Figure 7.25: Pseudo second order constant versus initial MB concentration at equilibrium at pH 7; MB concentration ranges of 10-40mg/L; agitation speed: 200rpm; at 21°C, 1h contact time, 5g/L alkali treated loofa dosage.

Figures 7.21 – 7.23 show a similar trend in the adsorption capacity and percentage removal of MB as concentration increases. Figure 7.22, shows that methylene blue absorbs rapidly onto the active vacant sites of the NaOH treated loofa within 5 minutes, this is followed by slower adsorption which reaches equilibrium at 60 minutes. Figure 7.24 describes an overall decrease in the percentage removal capacity of MB by NaOH treated loofa as initial concentration increases. The overall rate of MB adsorption is increased till an optimum is reached (Figure 7.25). When all the active sites available have been saturated any further increase will lead to a slight desorption thereby giving a reduced rate of adsorption as shown in Figure 7.25.

- **HCl treated MB loaded loofa**

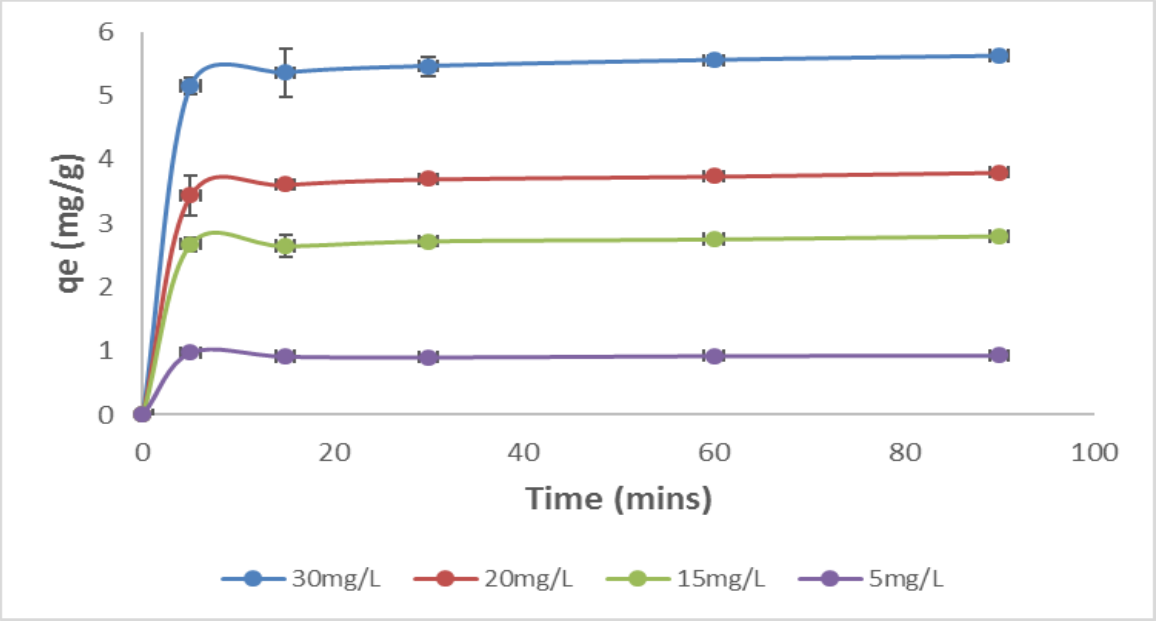

Figure 7.26: MB uptake capacity over 60 mins at pH 7; MB concentration ranges of 5-30mg/L; agitation speed: 200rpm; at 21°C, 1h contact time, 5g/L HCl treated loofa dosage. Data from 3 replicate measurements.

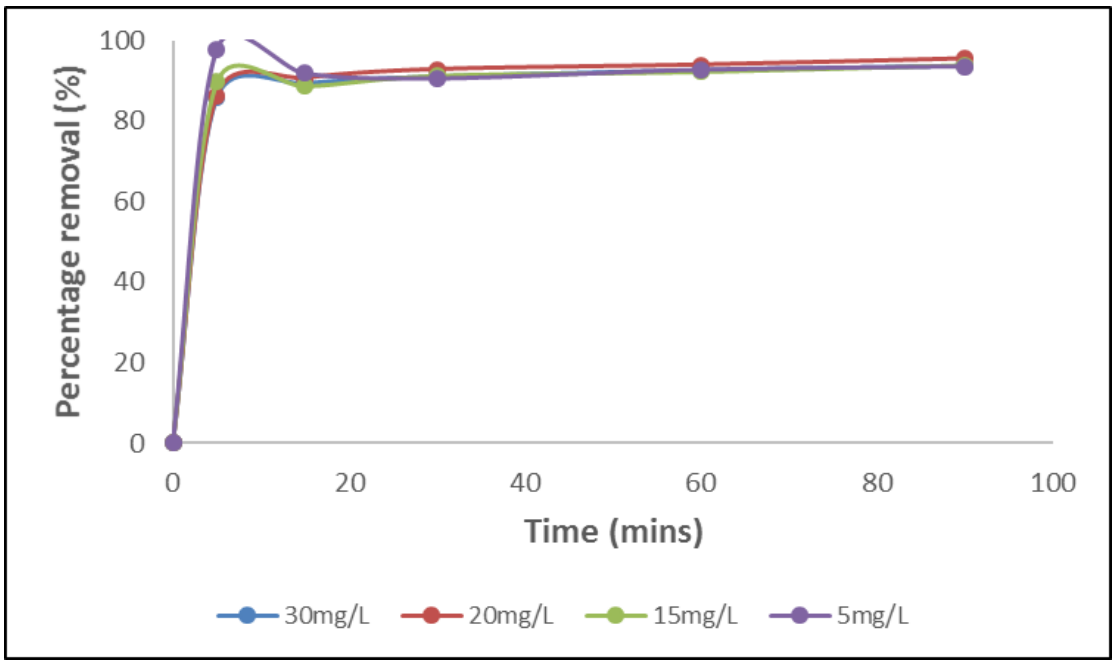

Figure 7.27: Percentage removal of MB over 60 mins at pH 7; MB concentration ranges of 5-30mg/L; agitation speed: 200rpm; at 21°C, 1h contact time, 5g/L HCl treated loofa dosage. Data from 3 replicate measurements.

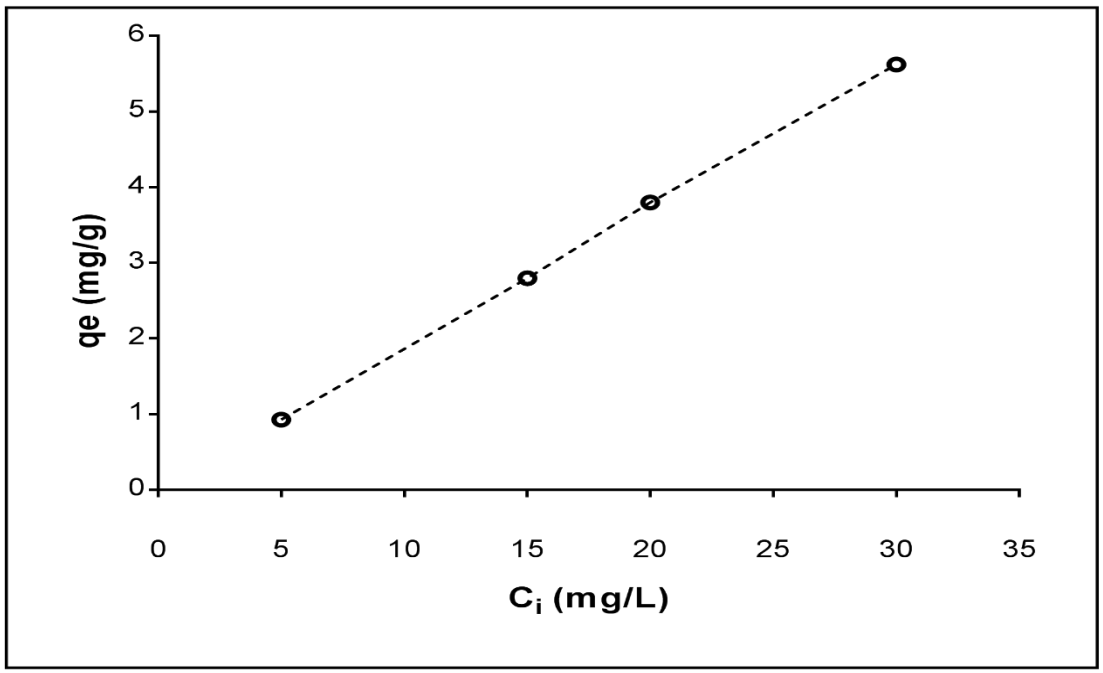

Figure 7.28: Uptake capacity of MB versus MB initial concentration after equilibrium at 60 mins at pH 7; MB concentration ranges of 5-30mg/L; agitation speed: 200rpm; at 21°C, 1h contact time, 5g/L HCl treated loofa dosage. Data from 3 replicate measurements.

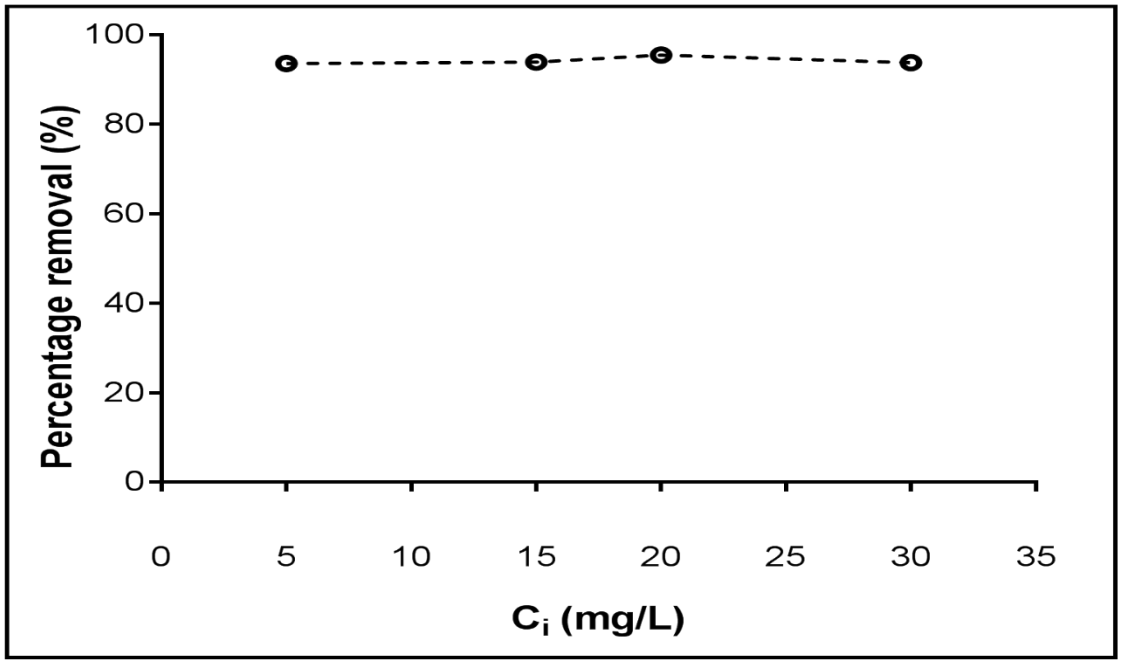

Figure 7.29: Percentage removal of MB after equilibrium at 60 mins at pH 7; MB concentration ranges of 5-30mg/L; agitation speed: 200rpm; at 21°C, 1h contact time, 5g/L HCl treated loofa dosage. Data from 3 replicate measurements.

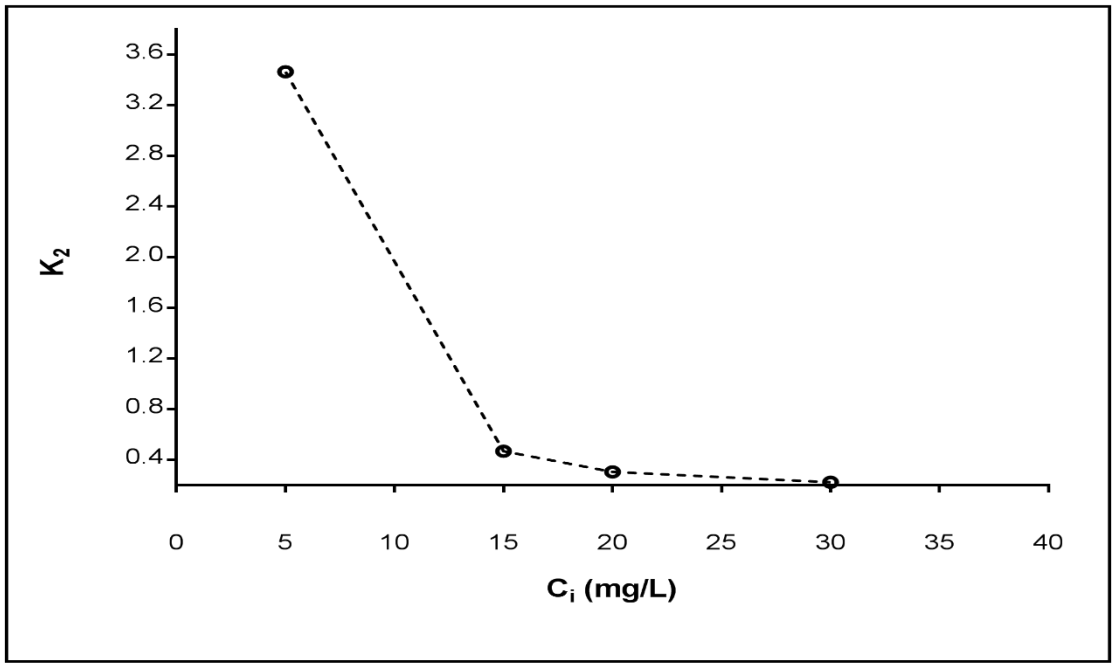

Figure 7.30: Pseudo second order constant versus initial MB concentration at equilibrium at pH 7; MB concentration ranges of 5-30mg/L; agitation speed: 200rpm; at 21°C, 1h contact time, 5g/L HCl treated loofa dosage.

Figures 7.26 – 7.29 show a similar trend in the adsorption capacity of percentage removal of MB by HCl treated loofa. Figure 7.30 indicates a decrease in the overall rate of adsorption as concentration increases. The active sites on the loofa surface decreases as the initial concentration increases due to the binding and occupying of the sites thereby leading to a slower process over time.

- **All three loofa**

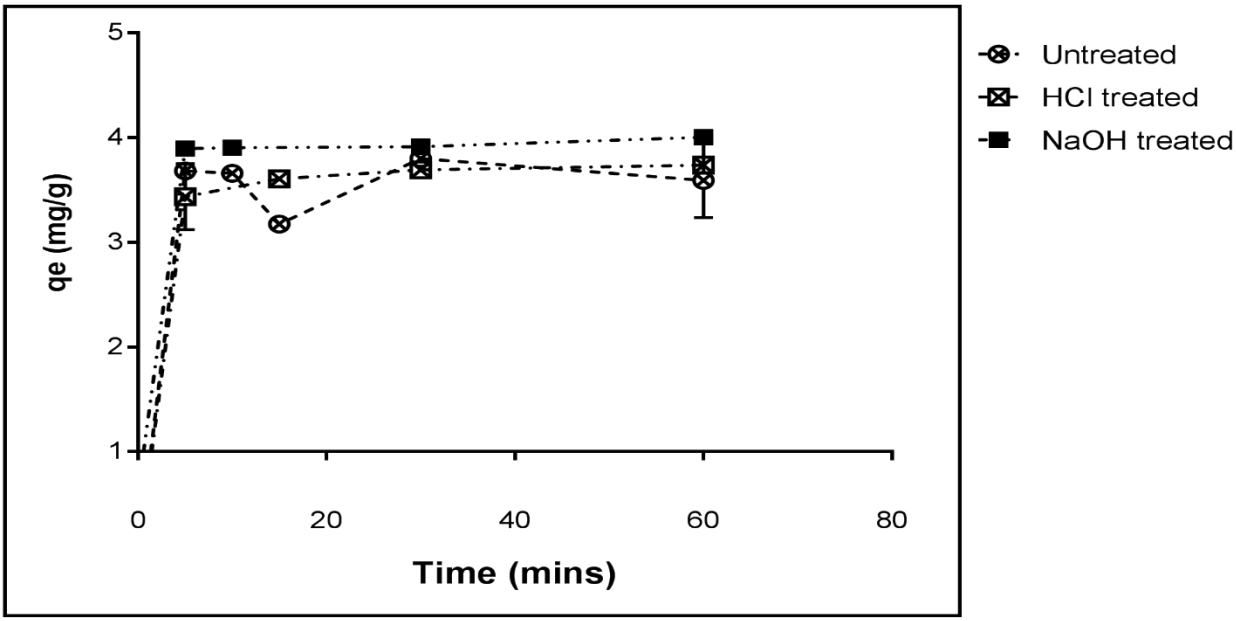

Figure 7.31: MB adsorption capacity with change in time after 60 mins at pH 7 onto untreated and treated loofa; MB concentration 20mg/L; agitation speed: 200rpm; at 21^{o}C, 1h contact time, 5g/L treated (both alkali and HCl) and untreated loofa dosage. Data from 3 replicate measurements.

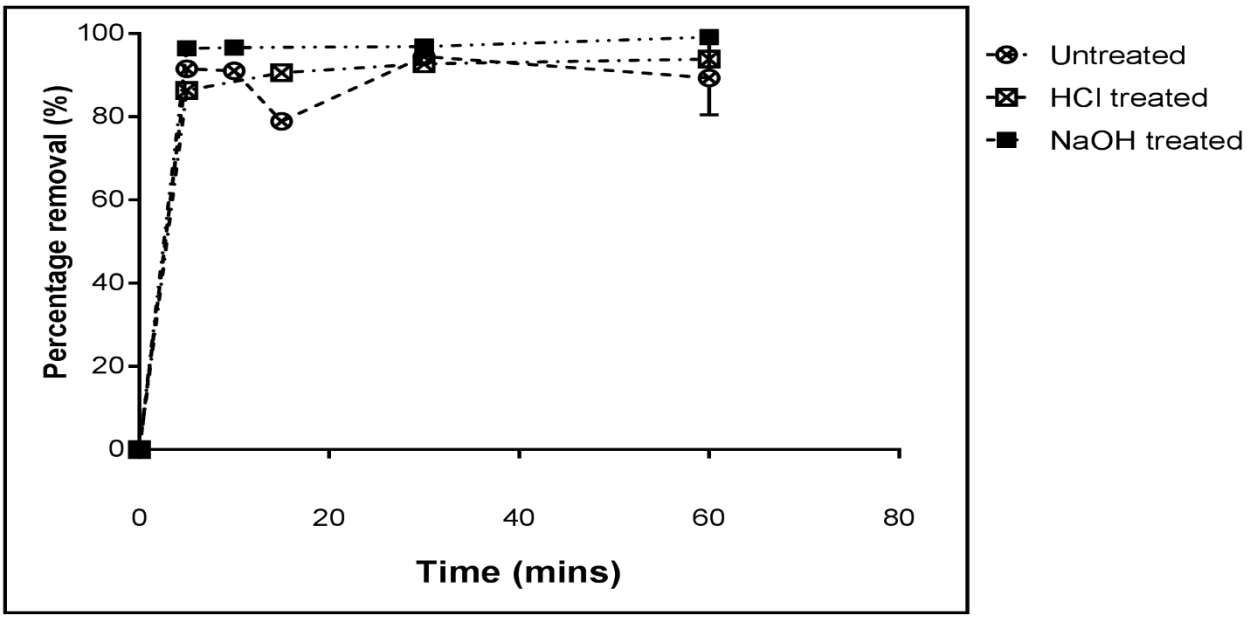

Figure 7.32: Percentage removal capacity of MB with change in time after 60 mins at pH 7 onto untreated and treated loofa; MB concentration 20mg/L; agitation speed: 200rpm; at 21^{o}C, 1h contact time, 5g/L treated (both alkali and HCl) and untreated loofa dosage. Data from 3 replicate measurements.

When compared to the untreated and HCl treated loofa (Figures 7.31 & 7.32), NaOH treated loofa shows the highest amount of uptake and percentage removal capacity over time.

7.2.5 Temperature

Figures 7.33 to 7.42 show the uptake trend of MB as temperature changes over time.

❖ **NaOH treated MB loaded loofa**

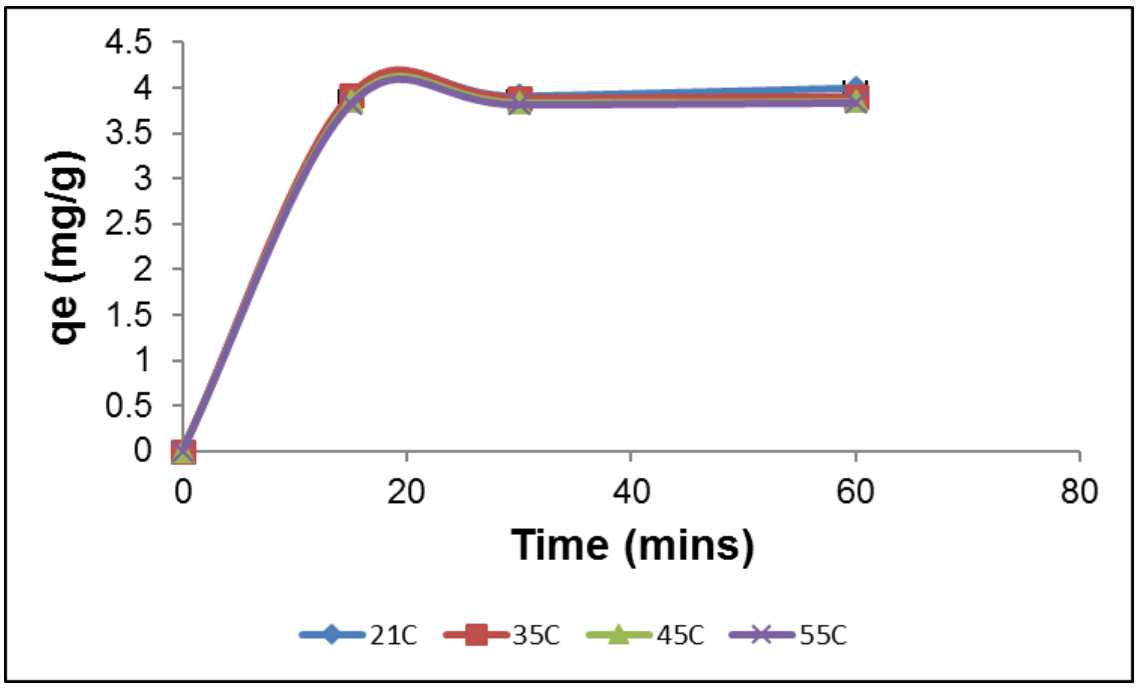

Figure 7.33: MB uptake capacity with change in time after 60 mins at pH 7; MB concentration at 10mg/L; agitation speed: 200rpm; temperature range 21°C – 55°C, 1h contact time, 5g/L alkali treated loofa dosage (C represents °C). Data from 3 replicate measurements.

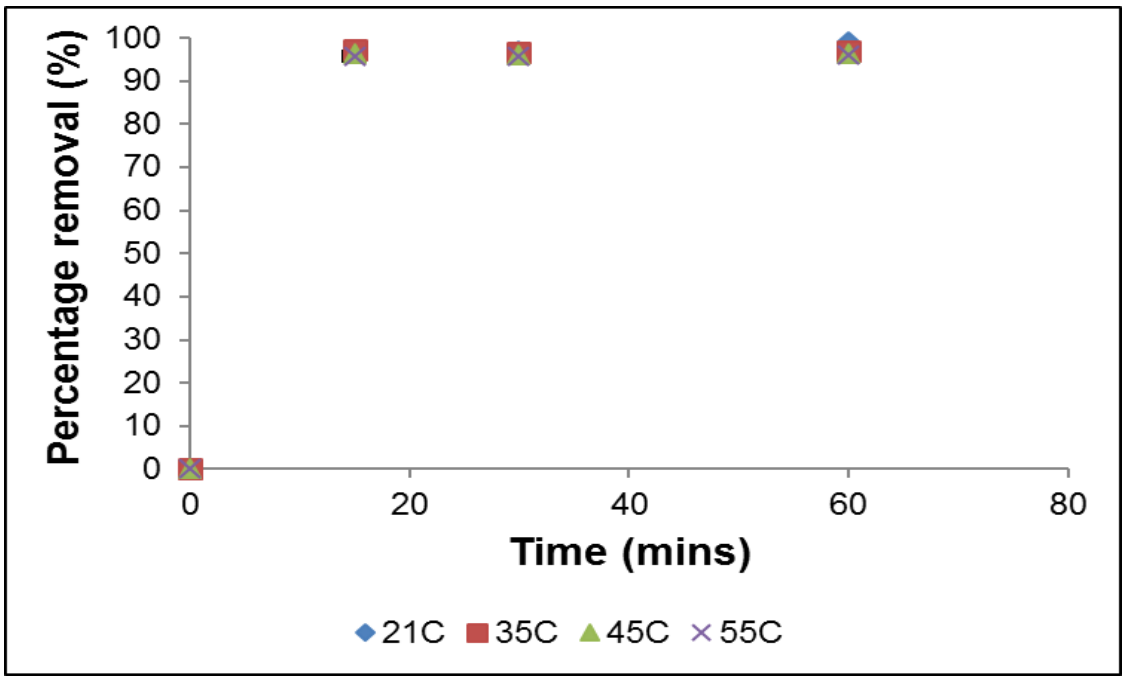

Figure 7.34: Percentage removal of MB with change in time after 60 mins at pH 7; MB concentration at 10mg/L; agitation speed: 200rpm; temperature range 21°C – 55°C, 1h contact time, 5g/L alkali treated loofa dosage (C represents °C). Data from 3 replicate measurements.

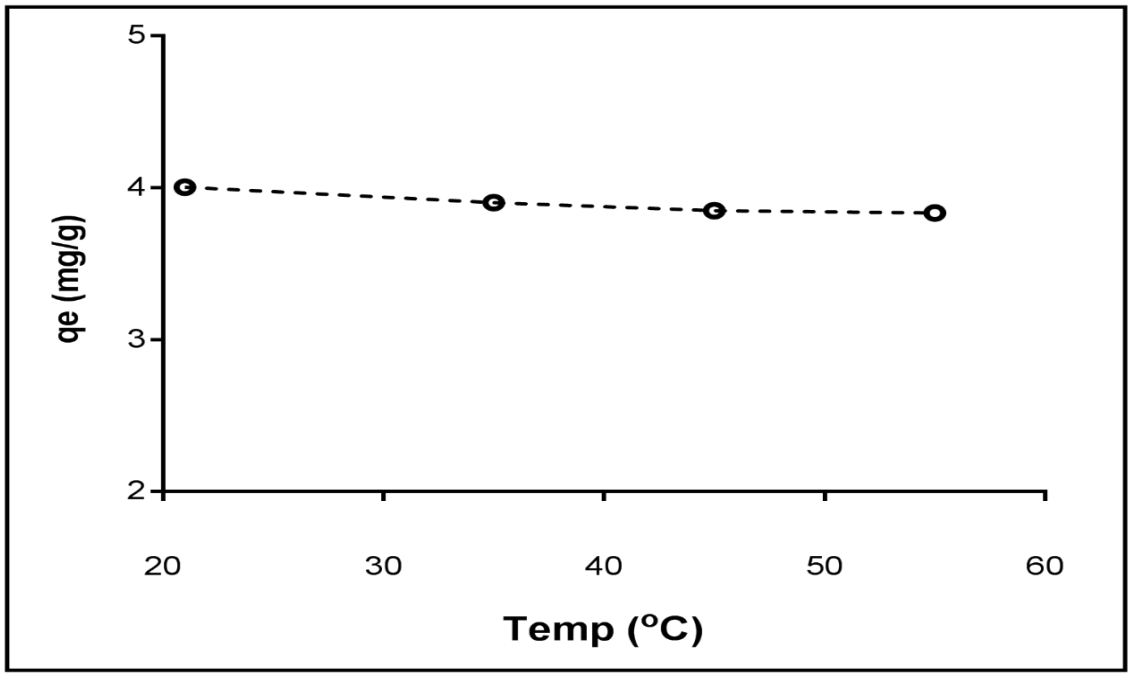

Figure 7.35: MB uptake capacity of MB versus temperature after equilibrium at 60 mins at pH 7; MB concentration 10mg/L; agitation speed: 200rpm; temperature range 21°C-55°C, 1h contact time, 5g/L alkali treated loofa dosage. Data from 3 replicate measurements.

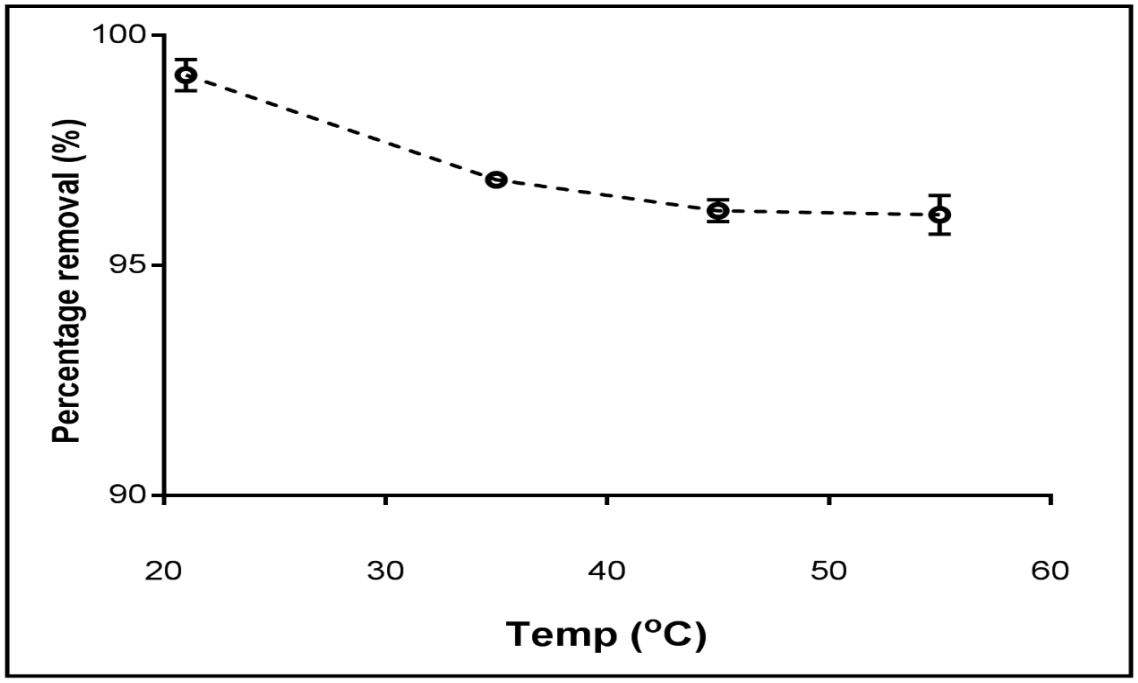

Figure 7.36: Percentage removal of MB after equilibrium at 60 mins at pH 7; MB concentration 10mg/L; agitation speed: 200rpm; at temperature range 21°C-55°C, 1h contact time, 5g/L alkali treated loofa dosage. Data from 3 replicate measurements.

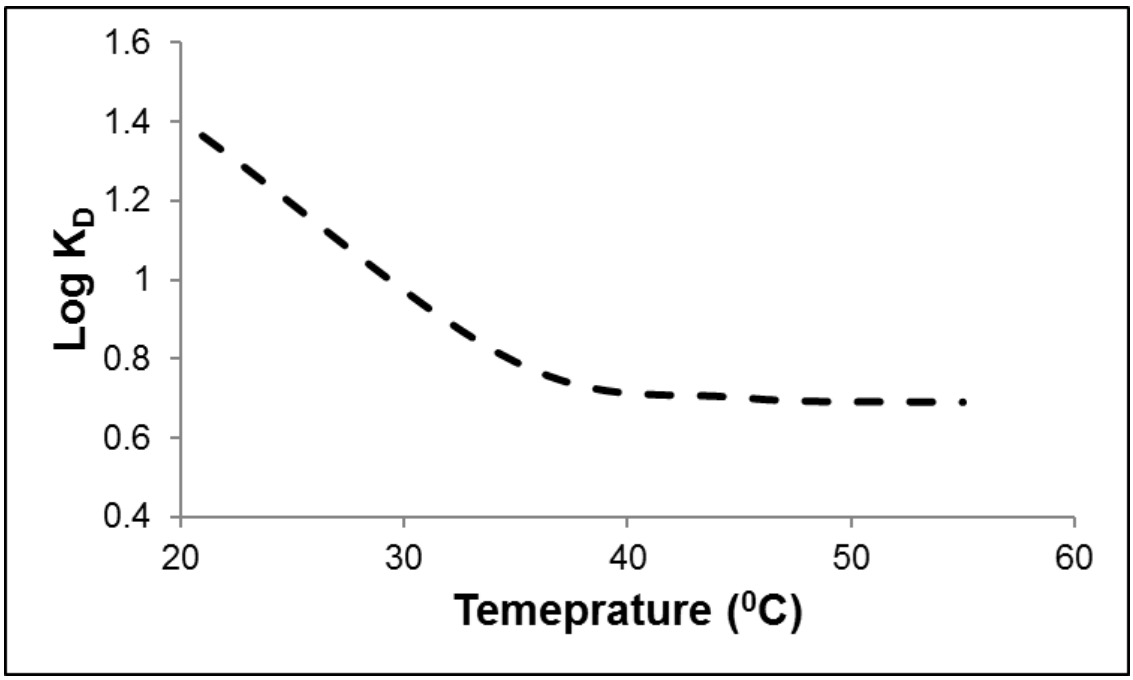

Figure 7.37: Log distribution ratio versus temperature at equilibrium at pH 7; MB concentration: 10mg/L; agitation speed: 200rpm; at temperature range 21°C – 55°C, 1h contact time, 5g/L alkali treated loofa dosage.

- **HCl treated MB loaded loofa**

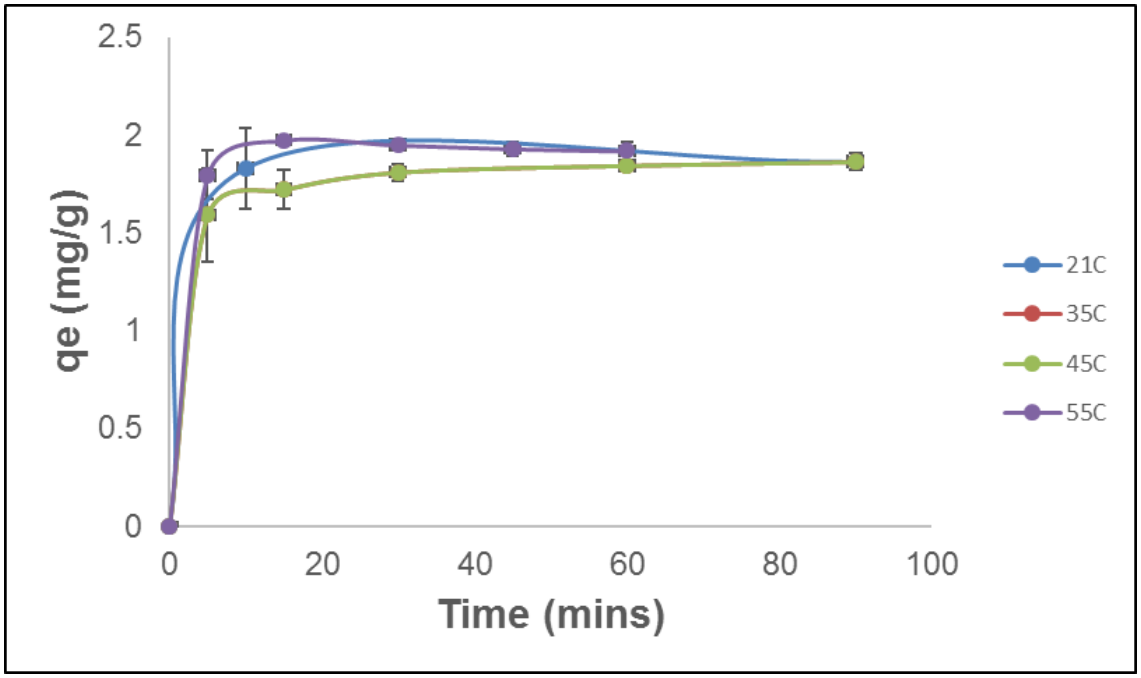

Figure 7.38: MB uptake capacity with change in time after 60 mins at pH 7; MB concentration at 10mg/L; agitation speed: 200rpm; at temperature range 21°C – 55°C, 1h contact time, 5g/L HCl treated loofa dosage (C represents °C). Data from 3 replicate measurements.

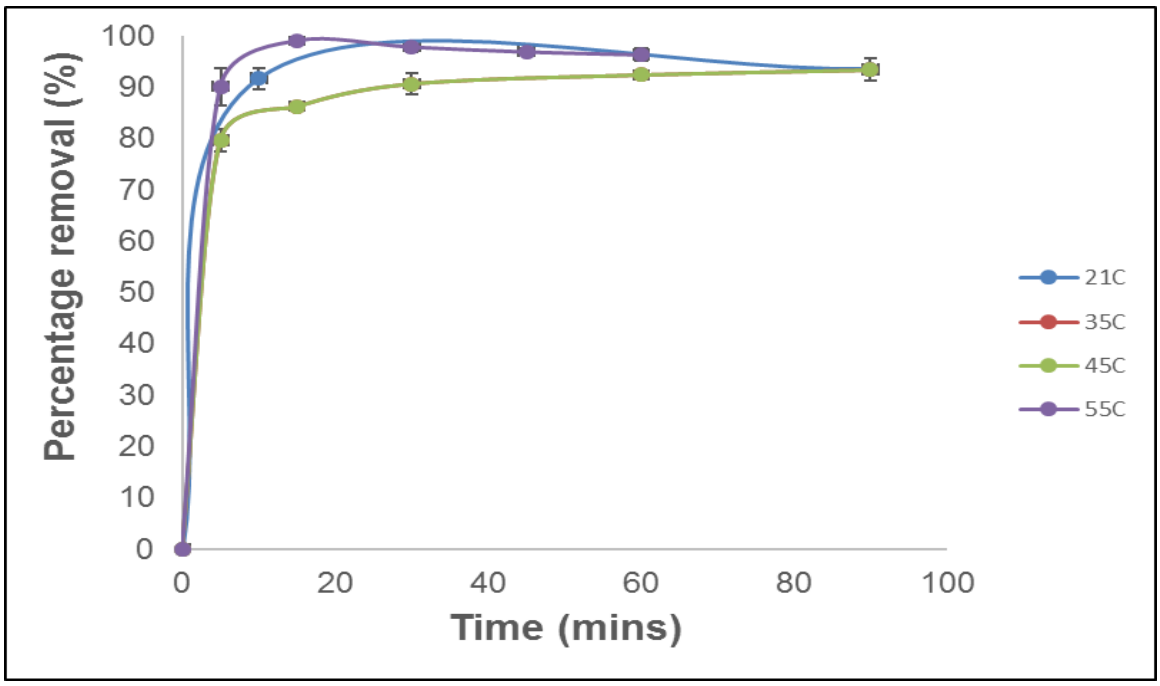

Figure 7.39: Percentage removal of MB over time at pH 7; MB concentration 10mg/L; agitation speed: 200rpm; at temperature range 21°C-55°C, 1h contact time, 5g/L HCl treated loofa dosage. Data from 3 replicate measurements.

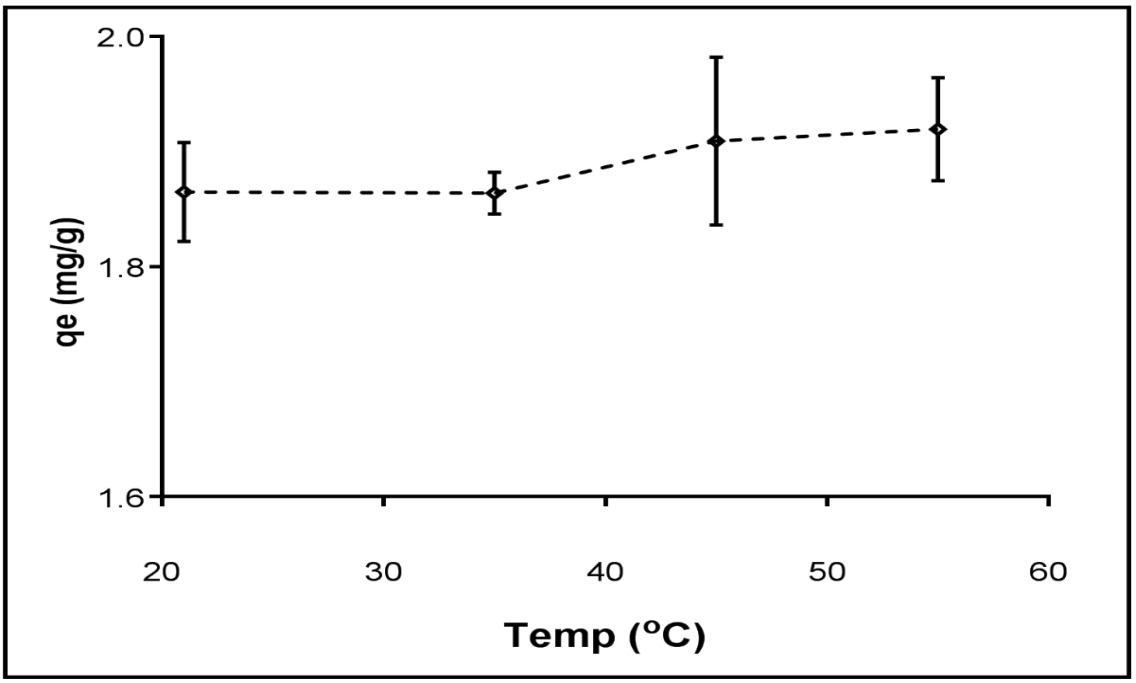

Figure 7.40: Uptake capacity of MB versus temperature after equilibrium at 60 mins at pH 7; MB concentration 10mg/L; agitation speed: 200rpm; at temperature range 21°C-55°C, 1h contact time, 5g/L HCl treated loofa dosage. Data from 3 replicate measurements.

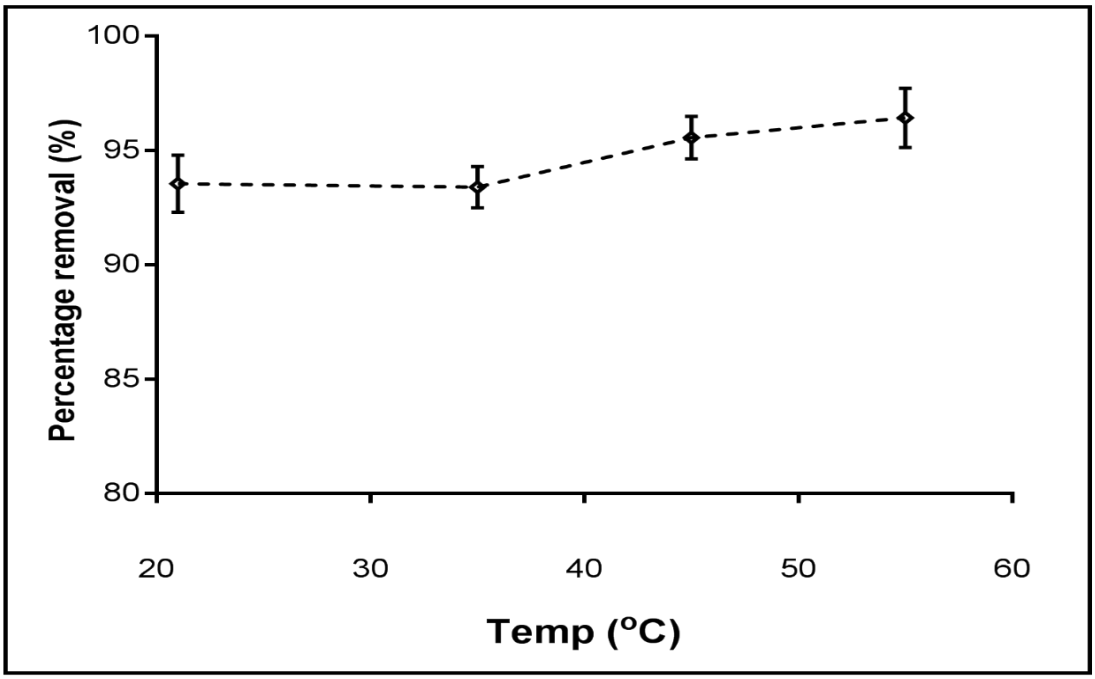

Figure 7.41: Percentage removal of MB after equilibrium at 60 mins at pH 7; MB concentration 10mg/L; agitation speed: 200rpm; at temperature range 21°C-55°C, 1h contact time, 5g/L HCl treated loofa dosage. Data from 3 replicate measurements.

For the NaOH treated loofa, the uptake capacity and percentage removal of methylene blue adsorption shows a similar trend at each temperature over time before equilibrium. As temperature increases from 21^{o}C to 55^{o}C, the uptake capacity (q_e)of MB is decreased by 5% and the percentage removal is decreased by approximately 3% at equilibrium (60mins). The distribution ratio shows a similar trend to the uptake capacity and percentage removal with temperature increase. Adsorption on alkali treated loofa is not favoured by an increase in temperature. For HCl treated loofa, the uptake capacity as well as percentage removal of MB shows an increase as temperature increases from 21^{o}C to 55^{o}C, the uptake capacity and percentage removal is increased by approx. 3%. This also shows that temperature has a little effect on MB adsorption and that the increase in temperature favours the adsorption mechanism on acid treated loofa. Furthermore, it confirms that there is a difference in the binding behaviour of MB for the two different treatments.

7.2.6 Mixed metal ions and MB

Figures 7.42 – 7.47 show the effect of MB uptake capacity in mixed metal solutions. The individual metal ions are shown to affect the MB adsorption differently due to the level of interaction with the MB cations in aqueous solution.

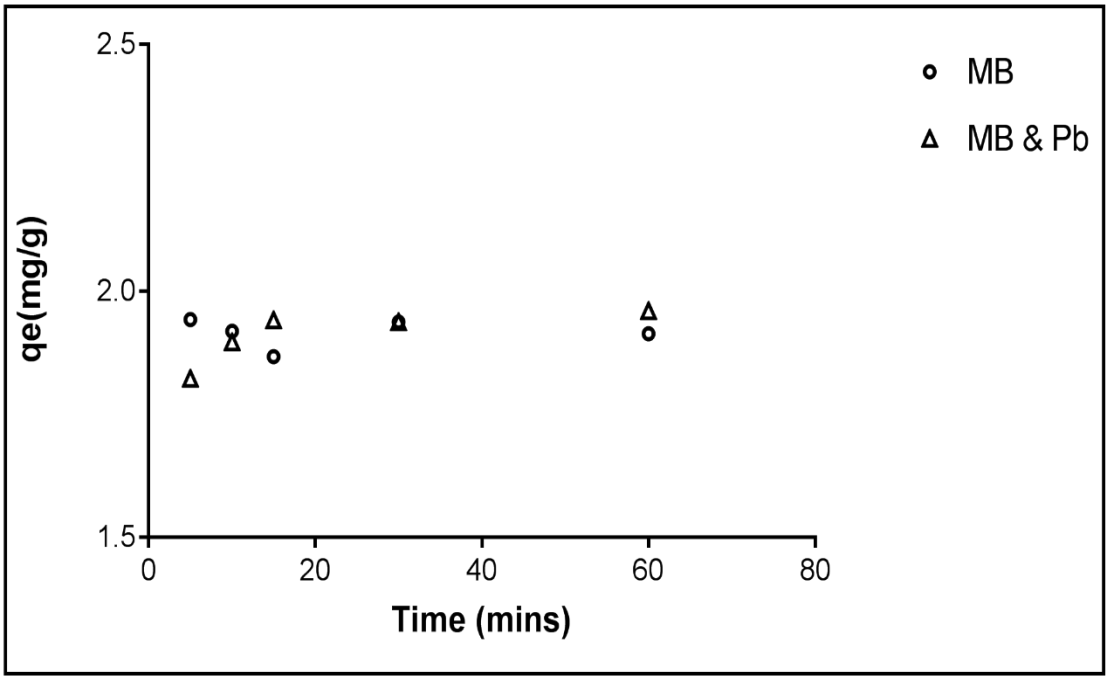

Figure 7.42: Uptake capacity of MB in mixed solution with lead ions over in time at pH 7; MB concentration at 10mg/L; agitation speed: 200rpm; at 21^{o}C, 1h contact time, 5g/L alkali treated loofa dosage.

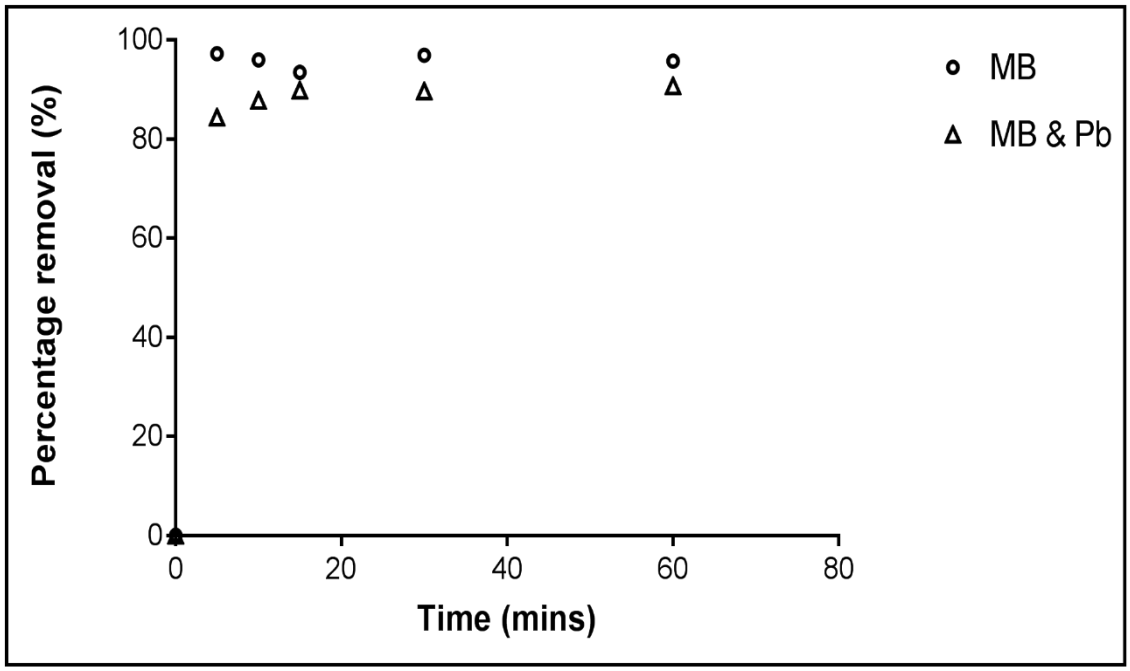

Figure 7.43: Percentage removal of MB in mixed solution with lead ions over in time at pH 7; MB concentration at 10mg/L; agitation speed: 200rpm; at 21^{o}C, 1h contact time, 5g/L alkali treated loofa dosage.

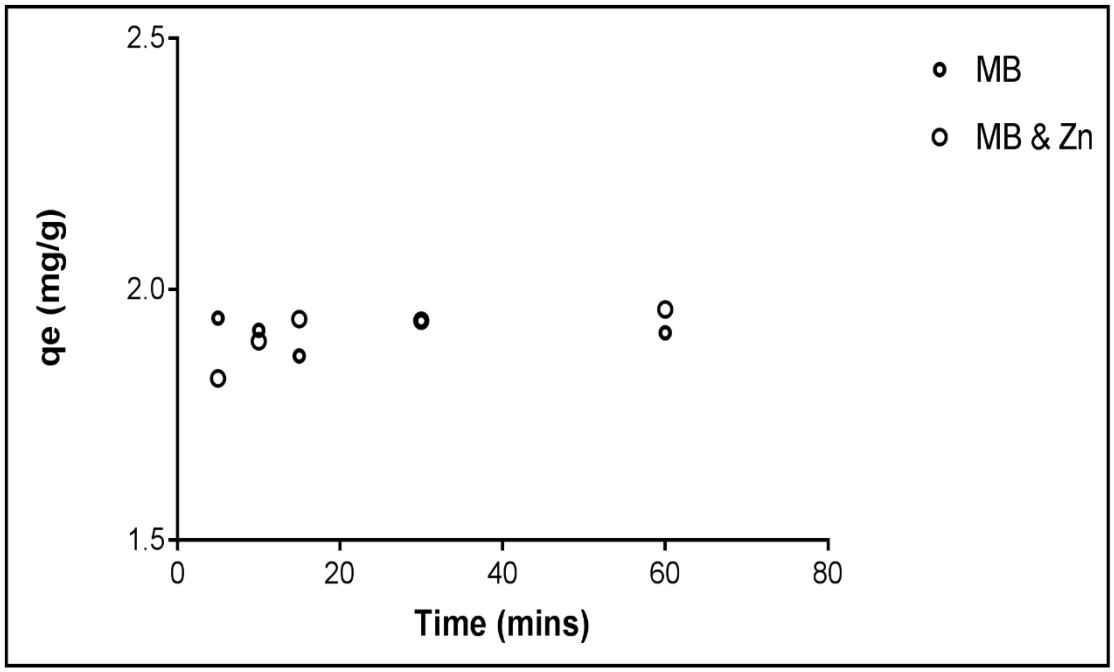

Figure 7.44: Uptake capacity of MB in mixed solution with zinc ions over in time at pH 7; MB concentration at 10mg/L; agitation speed: 200rpm; at 21^{o}C, 1h contact time, 5g/L alkali treated loofa dosage.

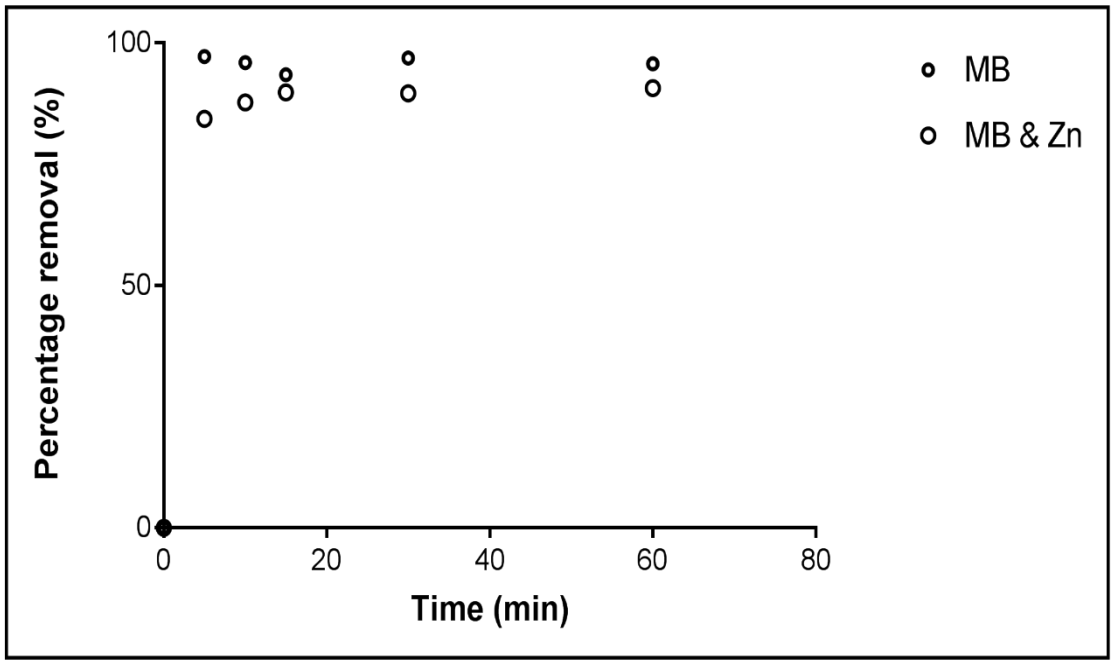

Figure 7.45: Percentage removal of MB in mixed solution with zinc ions over in time at pH 7; MB concentration at 10mg/L; agitation speed: 200rpm; at 21^{o}C, 1h contact time, 5g/L alkali treated loofa dosage.

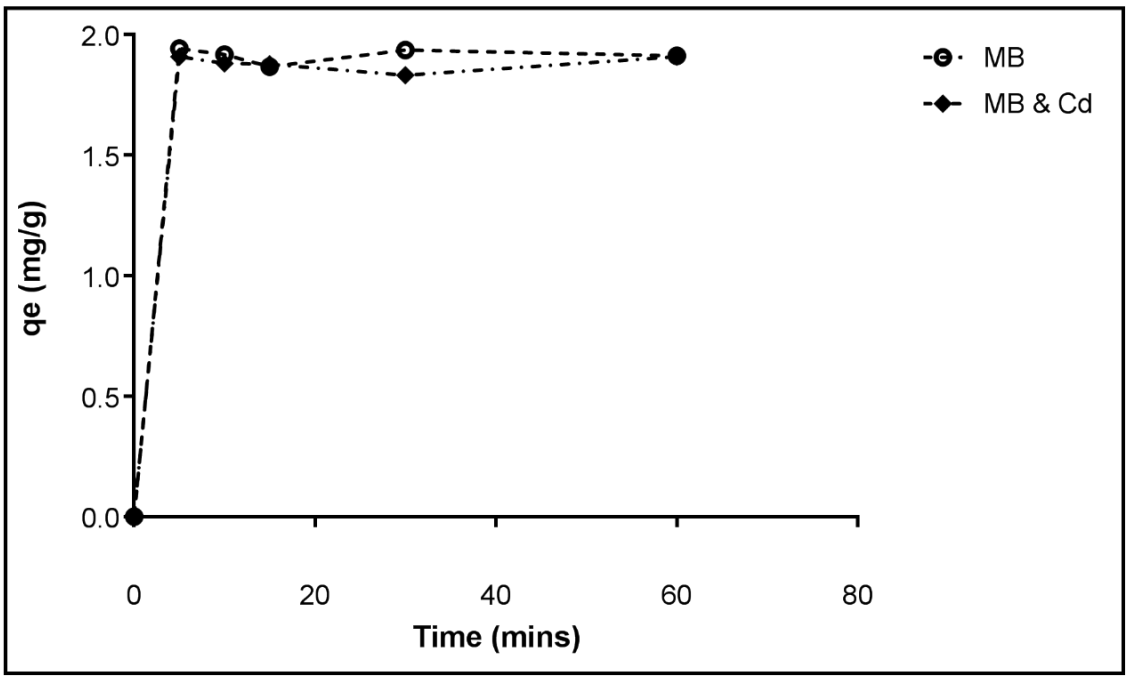

Figure 7.46: Uptake capacity of MB in mixed solution with cadmium ions over in time at pH 7; MB concentration at 10mg/L; agitation speed: 200rpm; at 21°C, 1h contact time, 5g/L alkali treated loofa dosage. Data from 3 replicate measurements.

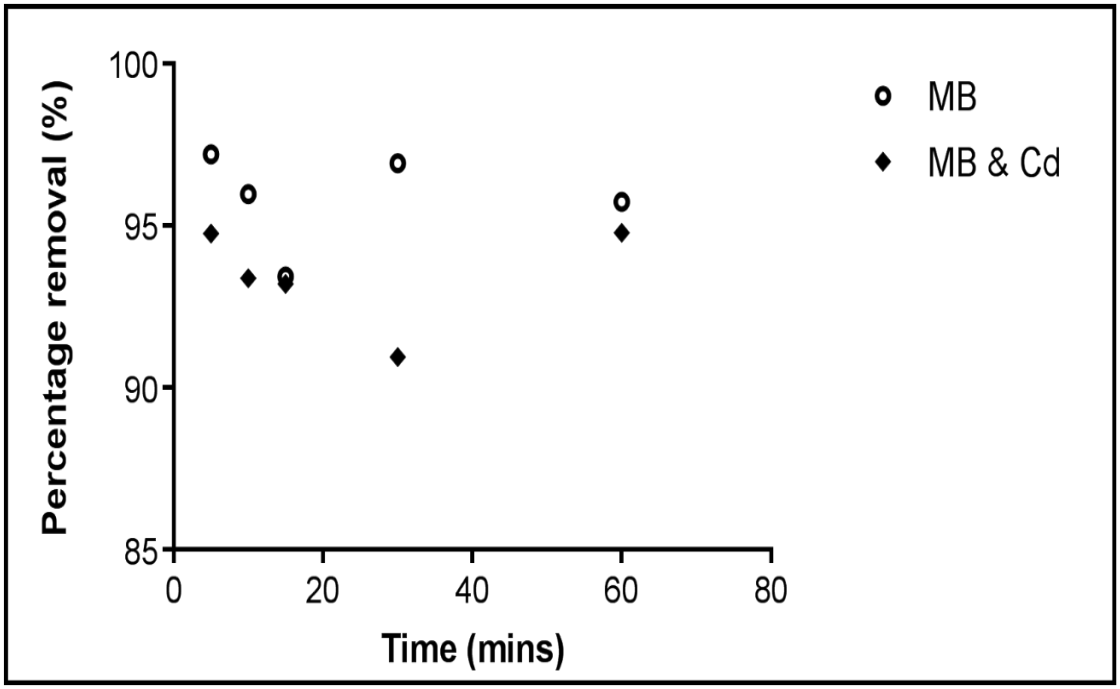

Figure 7.47: Percentage removal of MB in mixed solution with cadmium ions over in time at pH 7; MB concentration at 10mg/L; agitation speed: 200rpm; at 21°C, 1h contact time, 5g/L alkali treated loofa dosage. Data from 3 replicate measurements.

There is a small change in the uptake capacity of MB with each metal ion as compared to MB adsorption alone (Figures 7.42 ,7.44 & 7.46). On the other hand, percentage removal shows a significant decrease when MB is mixed with other metal ions in aqueous solution. MB and zinc ions show the smallest difference in the percentage removal. Zinc has the lowest effect on the adsorption of MB on alkali treated loofa.

7.2.7 Kinetics modeling

Figure 7.48 – 7.50 show the kinetics of MB adsorption on loofa. The pseudo second order model gives the best fit model for all the variations of loofa. Table 7.1 shows the pseudo first and second order models, intra particle diffusion model, Elovich, liquid film diffusion and Boyd model correlation coefficient values (R^2 values) of the MB adsorption on untreated, NaOH treated and HCl treated loofa.

Figures 7.48 – 7.50 show the pseudo second order model at constant pH, concentration and temperature.

Table 7.1: Kinetic model fitting R^2 values – linear regression (MB initial concentration 20mg/L; pH 7; at 21^{o}C, 5g/L loofa dosage.

Loofa	**PFO**	**PSO**	**Intra-particle diffusion**	**Elovich**	**Liquid film diffusion**	**Boyd**
Untreated	0.106	0.997	0.475	0.632	0.106	0.824
4% NaOH	0.215	0.999	0.357	0.203	0.327	0.412
4% HCl	0.667	0.999	0.116	0.697	0.685	0.763

Where, PFO – Pseudo first order model; PSO – Pseudo second order model.

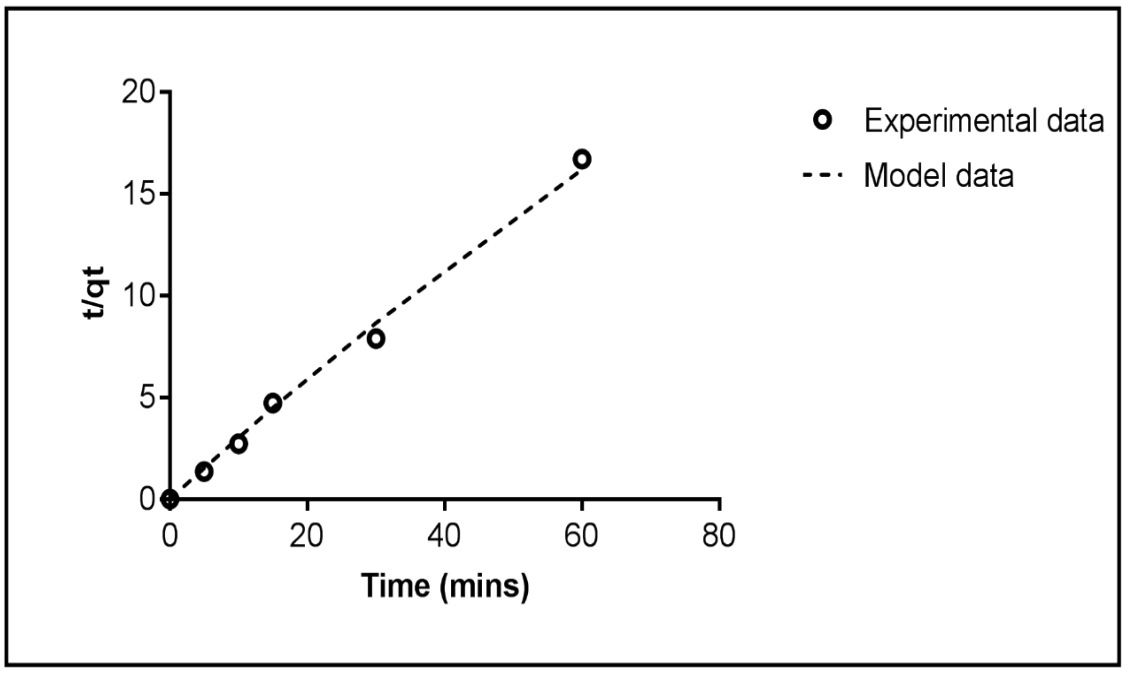

Figure 7.48: Pseudo second order (PSO) model; Non- linear regression - R^2 = 0.995 (pH 7; MB concentration at 20mg/L; agitation speed: 200rpm; at 21^{o}C, 1h contact time, 5g/L untreated loofa). PSO model fit shown by the dashed line.

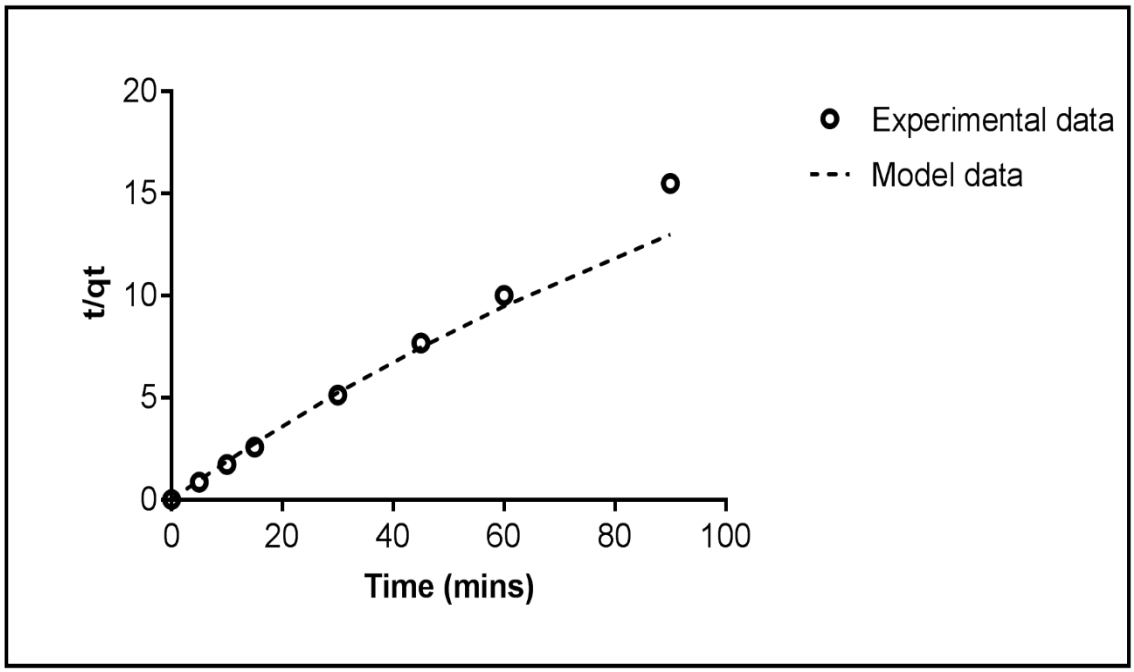

Figure 7.49: Pseudo second order (PSO) model; Non- linear regression - R^2 = 0.997 (pH 7; MB concentration at 20mg/L; agitation speed: 200rpm; at 21^{o}C, 1h contact time, 5g/L 4% NaOH treated loofa). PSO model fit shown by the dashed line.

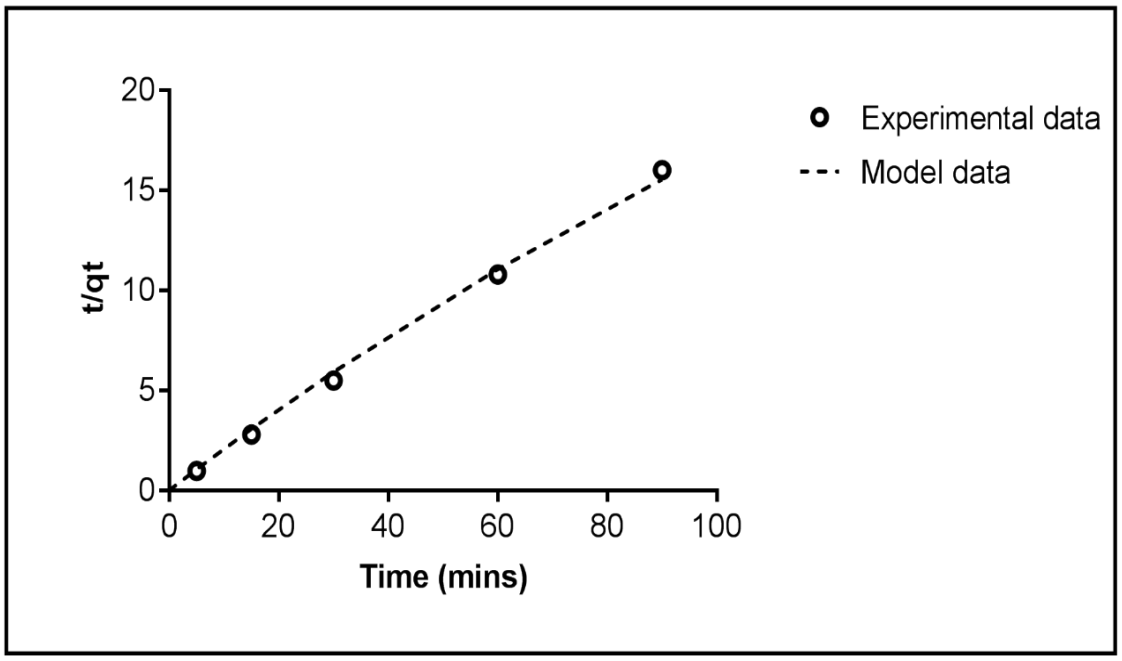

Figure 7.50: Pseudo second order (PSO) model; Non- linear regression - R^2 = 0.997 (pH 7; MB concentration at 20mg/L; agitation speed: 200rpm; at 21^{o}C, 1h contact time, 5g/L 4% HCl treated loofa). PSO model fit shown by the dashed line.

The intra particle diffusion model is not suitable to describe the MB adsorption behaviour on untreated, NaOH treated and HCl treated loofa, $R^2 < 0.5$, therefore the boundary layer effect cannot be applied to further explain the adsorption process. The Boyd model gives an $R^2 > 0.5$ for untreated and acid treated loofa, thereby indicates that particle diffusion could be the rate controlling step. The alkali treated loofa results cannot be explained by Boyd model kinetics.

7.2.8 Isotherm modeling

Table 7.2 shows the isotherm model correlation coefficient values (R^2 values) of MB adsorption on untreated, NaOH treated and HCl treated loofa (linear regression values). Figure 7.51 – 7.53 show the different isotherm model fits for MB adsorption on alkali treated loofa. Figure 7.55 shows the thermodynamics parameters obtained for the MB adsorption process. The non-linear regression values calculated for the four isotherm models are shown in Table 7.3.

Table 7.2: Isotherm model fitting R^2 values – linear regression (MB initial concentration 20mg/L; pH 7; temperature 21°C, 5g/L loofa dosage).

Loofa	Langmuir	Freundlich	Sips	Temkin
Untreated	0.557	0.987	0.981	0.975
4% NaOH	0.388	0.716	0.851	0.671
4% HCl	No fit	0.954	0.984	0.942

At room temperature (21°C) the binding constant of MB on untreated loofa is 1.99L/mg, for NaOH treated loofa it is 10.28L/mg and for HCl treated loofa it is 3.86L/mg (obtained from the Temkin model). This indicates that MB adsorption by alkali modified loofa has the highest binding constant and therefore shows the highest adsorption capacity. For MB adsorption on alkali treated loofa, the non-linear regression plots and values were obtained, using EXCEL solver, and the Freundlich and Dubinin-Radushkevich model was found to be the best fit (R^2 = 0.998) which predicts the heterogeneous distribution of active sites on the loofa surface for the adsorption of methylene blue (Table 7.3) Dubinin-Radushkevich shows a lower sum of squares at 3.33×10^{-5}. Figure 7.51 – 7.54 shows the non-linear regression values using Graphpad Prism. Sips model gives the best fit (R^2 = 0.689) which also predicts a heterogeneous surface.

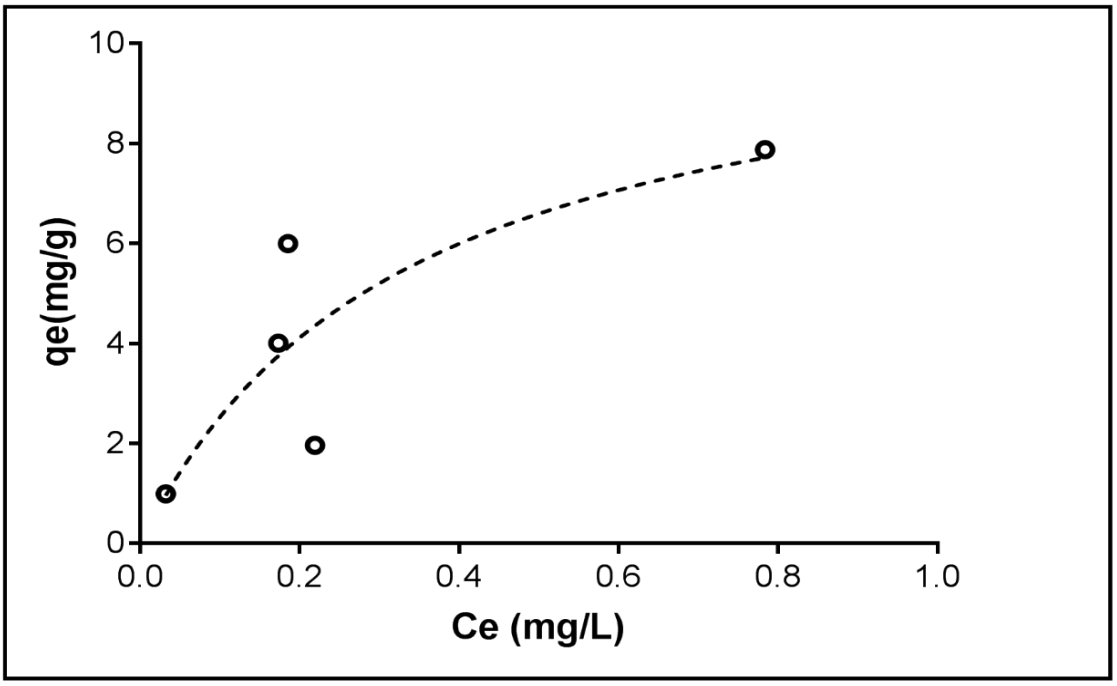

Figure 7.51: MB isotherm from pH 7.0 ± 0.1 at 21 °C at 1hr. contact time. Langmuir model fit shown by the dashed line. R^2 = 0.684 (MB concentration at 20mg/L; 4% NaOH treated loofa).

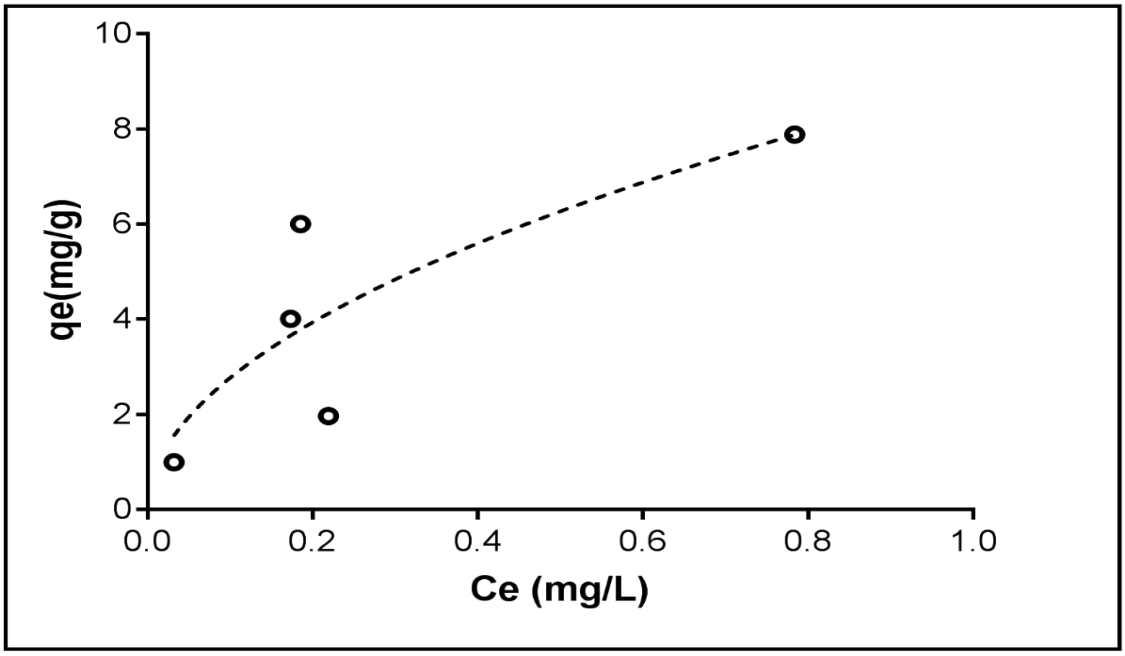

Figure 7.52: MB isotherm from pH 7.0 ± 0.1 at 21 °C at 1hr. contact time. Freundlich model fit shown by the dashed line. R^2 = 0.689 (MB concentration at 20mg/L; 4% NaOH treated loofa).

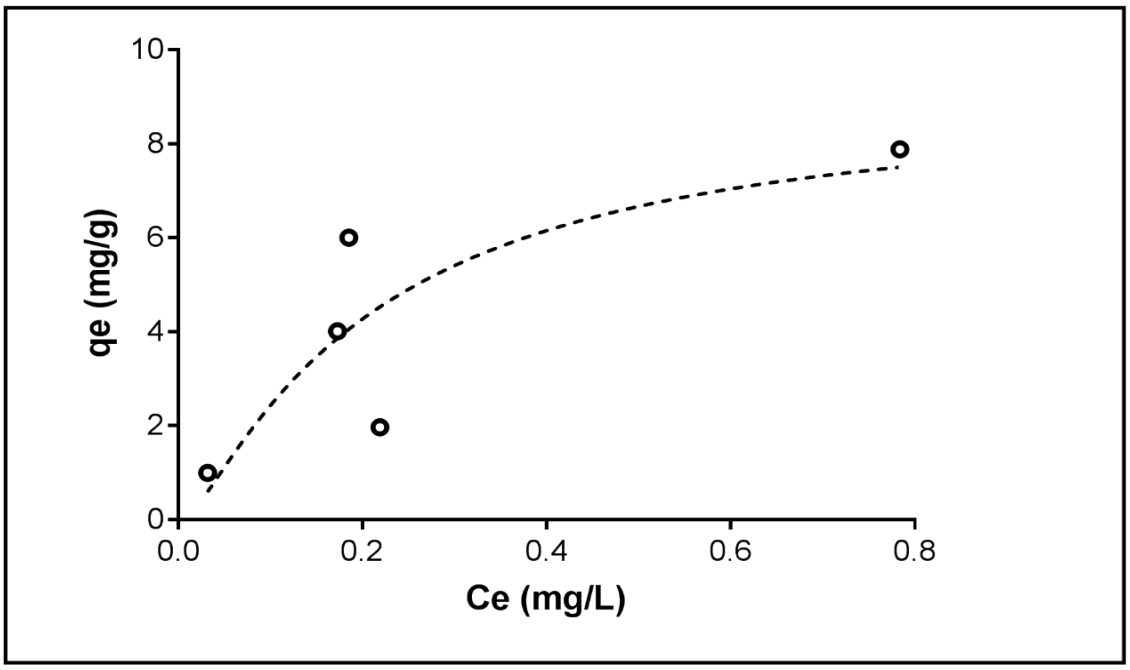

Figure 7.53: MB isotherm from pH 7.0 ± 0.1 at 21 °C at 1hr. contact time. Dubinin-Radushkevich model fit shown by the dashed line. R^2 = 0.667 (MB concentration at 20mg/L; 4% NaOH treated loofa).

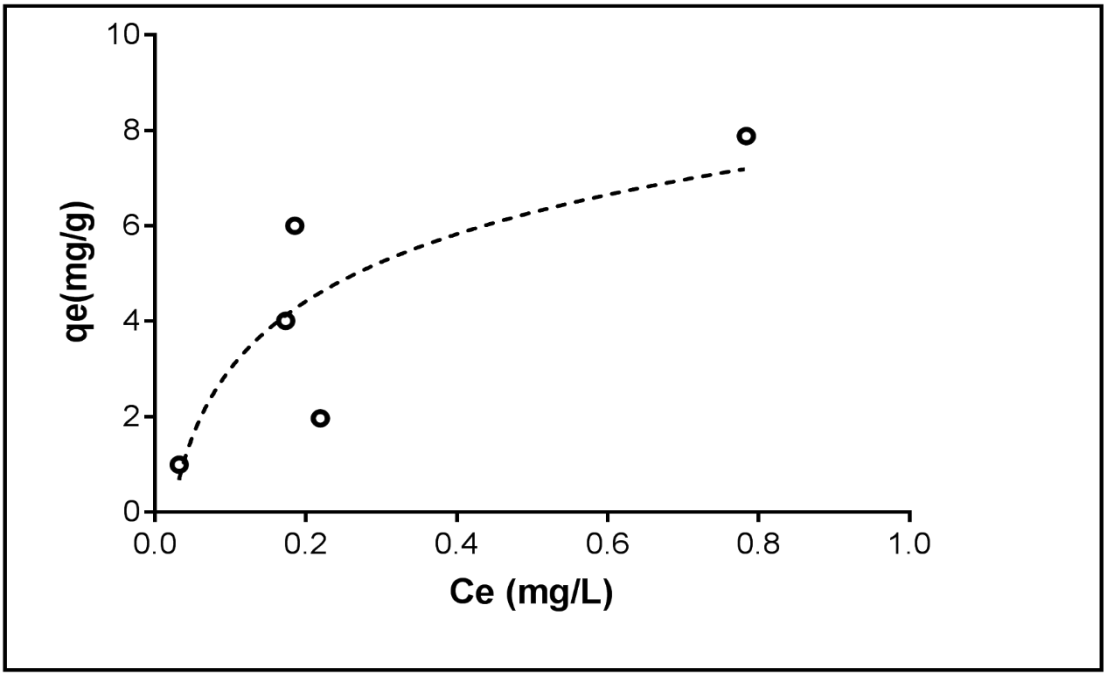

Figure 7.54: MB isotherm from pH 7.0 ± 0.1 at 21 °C at 1hr. contact time. Temkin model fit shown by the dashed line. R^2 = 0.671 (MB concentration at 20mg/L; 4% NaOH treated loofa).

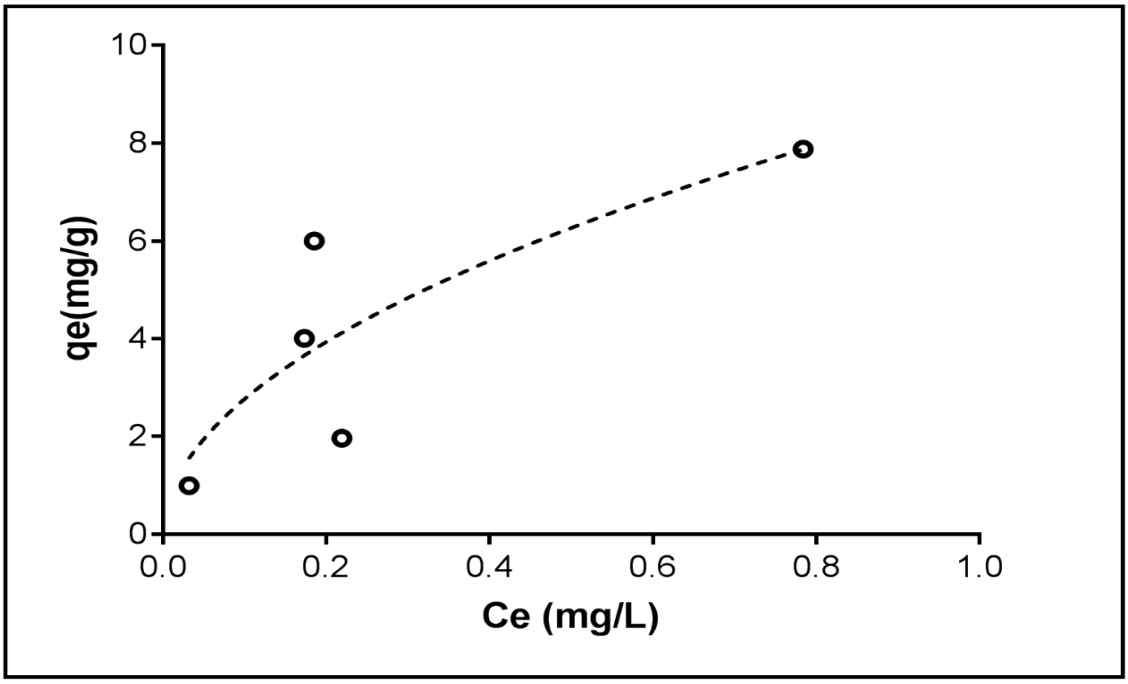

Figure 7.55: MB isotherm from pH 7.0 ± 0.1 at 21 °C at 1hr. contact time. Sips model fit shown by the dashed line. R^2 = 0.689 (MB concentration at 20mg/L; 4% NaOH treated loofa).

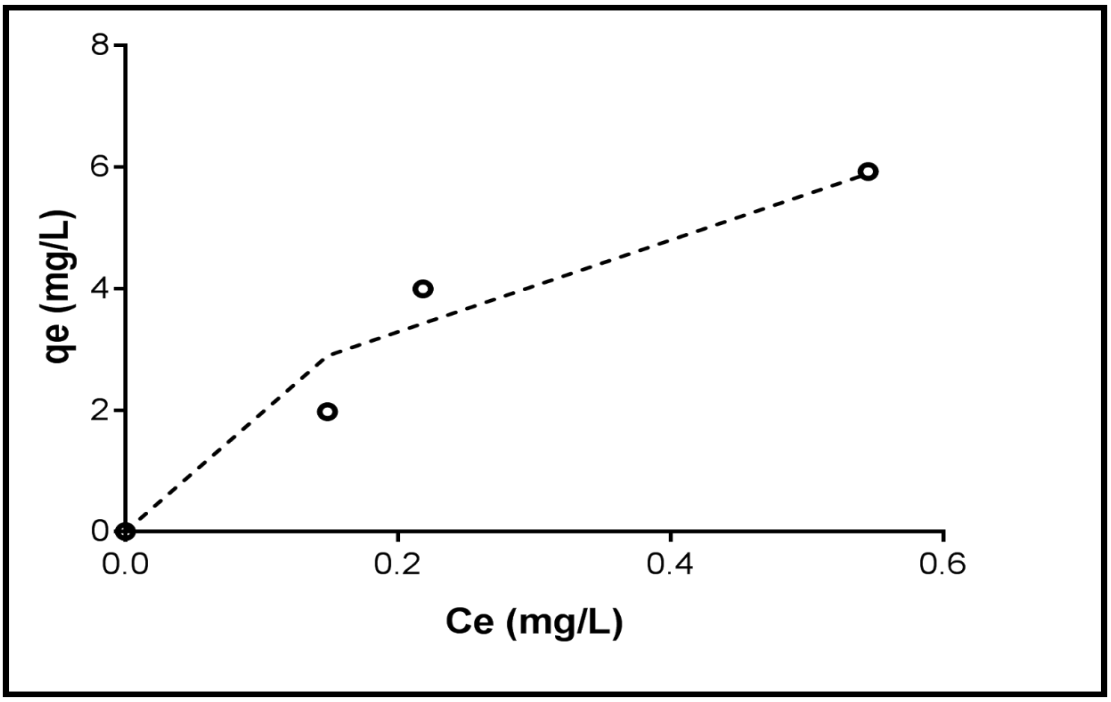

Figure 7.56: MB isotherm from pH 7.0 ± 0.1 at 21 °C at 24 hr. contact time. Two-site Langmuir model fit shown by the dashed line. (R^2 = 0.683; 0.979).

Table 7.3: Non- linear regression and linear regression constant values of isotherm models (MB initial concentration 20mg/L; pH 7; temperature 21^{o}C, 5g/L alkali treated loofa).

Sips		**Freundlich**	
Constant	Value	Constant	Value
K_L	2.8 ± 0.01	K_F	8.9 ± 0.2
n	0.5 ± 0.02	n_F	1.9 ± 0.05
q_m (mg.g^{-1})	4.2 ± 0.05	R^2	0.998
R^2	0.689		
Dubinin-Radushkevich		**Temkin**	
Constant	Value	Constant	Value
B_D (x10^{-9})	2.0 ± 0.1	A_T	10.3 ± 0.05
q_D (mg·g^{-1}) (x10^{-4})	3.8 ± 0.1	b_T (x10^{8})	2.0 ± 0.5
E_D (kJ·mol^{-1})	15.8 ± 0.5	R^2	0.671
R^2	0.998		

Equilibrium occurs faster for MB adsorption with the use of untreated loofa at 30mins compared to the use of 4% NaOH treated loofa at 60mins.

Table 7.4: Heat of sorption values (B_T) obtained from Temkin model fit for alkali and acid treated loofa.

Concentration (mg/L)	4% NaOH treated (J/mol)	4% HCl treated (J/mol)
20mg/L	0.976	2.275
30mg/L	1.510	2.627

Table 7.4 shows a stronger bond required on the surfaces of both treated loofas with an increase in initial MB concentration during adsorption.

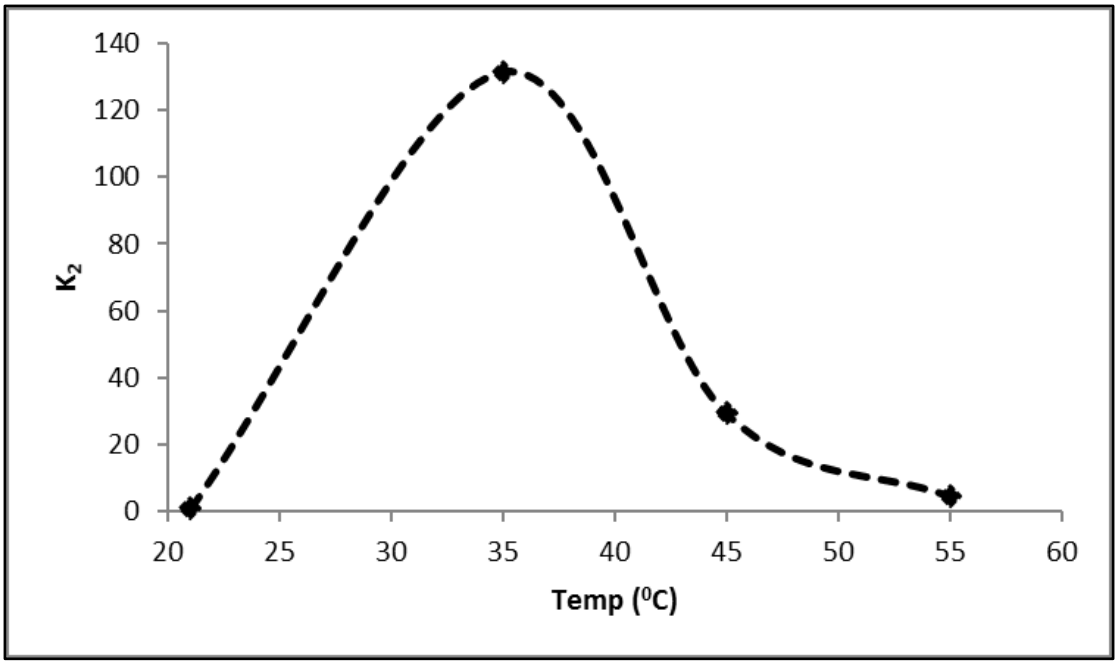

Figure 7.57: Pseudo second order constant (K^2) versus the temperature (pH 7; MB concentration at 20mg/L; agitation speed: 200rpm; 1h contact time, 5g/L 4% NaOH treated loofa dosage).

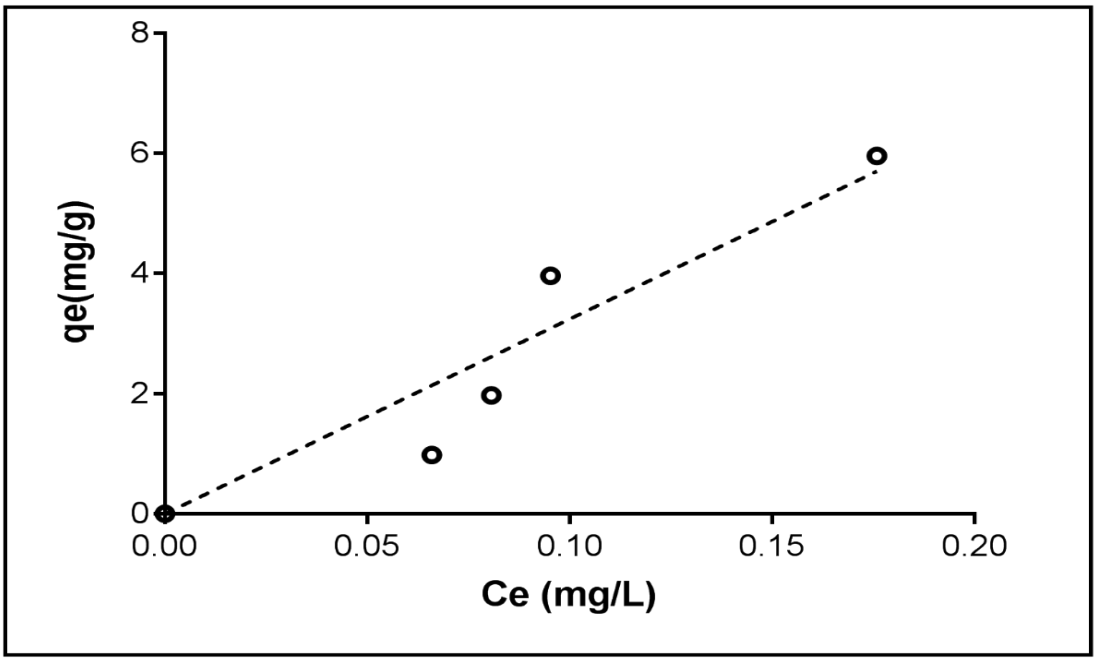

Figure 7.58: MB isotherm from pH 7.0 ± 0.1 at 35 °C at 1hr. contact time. Temkin model fit shown by the dashed line. R^2 = 0.887 (MB concentration at 20mg/L; 4% NaOH treated loofa dosage).

Figure 7.57 shows that the rate of adsorption reaches an optimum at 35°C. At this temperature, the binding constant is reduced at 21°C from 10.28L/mg to 7.25L/mg (Figure 7.58). Furthermore, there is an adsorption – desorption process at this point leading to a lower MB uptake on the NaOH treated loofa.

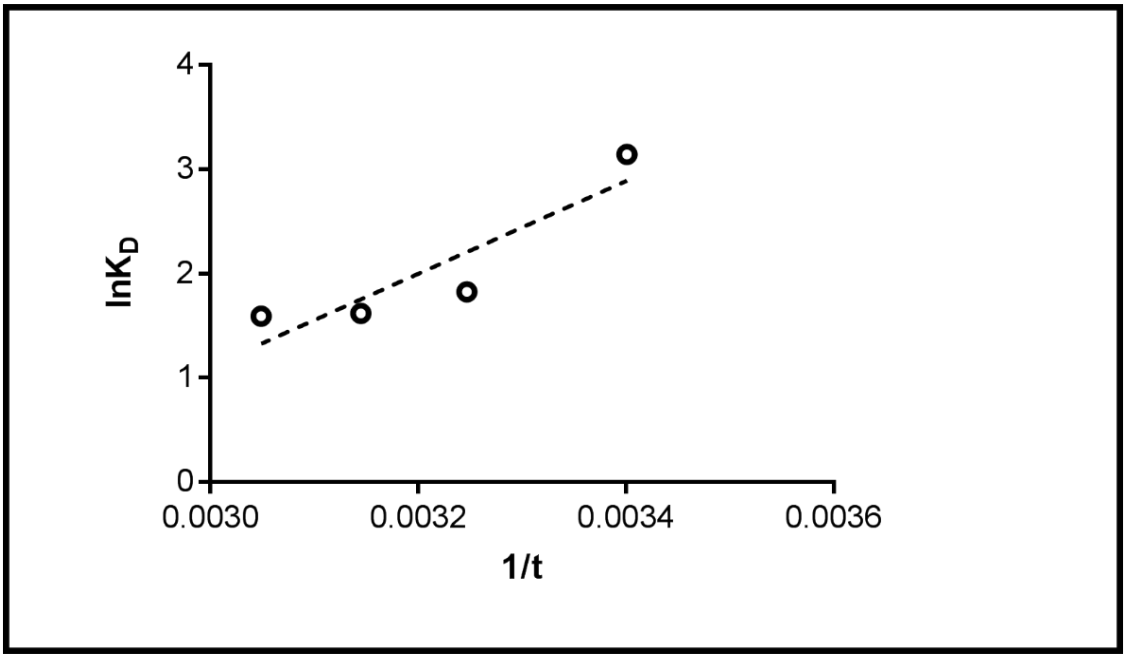

Figure 7.59: Estimation of thermodynamic parameters showing a plot of InK_D versus 1/T.

The thermodynamic behaviour of MB adsorption on loofa can be described by the ΔG, ΔS & ΔH values. The negative values ΔG (Gibb free energy) (-7.7kJ/mol, -4.7kJ/mol, -4.3kJ/mol & -4.3kJ/mol) at each temperature (294K, 308K, 318K & 328K) shows the thermodynamic feasibility and spontaneous nature of the adsorption process. The values ΔS and ΔH (-0.1kJ/mol &-36.9kJ/mol) were both negative (obtained from Figure 7.59) which identifies an exothermic reaction (Liu & Lee, 2014; Sharma & Tiwari, 2016). The ΔS (entropy change) determines the randomness at the solid/solution interface. The negative value obtained for ΔS shows a decrease in the randomness. The activation energy at 15.8 kJ/mol describes a chemisorption adsorption process.

7.2.9 UV-Vis spectra

Figures 7.60 – 7.62 show the UV-Vis spectra of MB adsorption on NaOH, HCl and untreated loofa at specific times. Also, the adsorption of mixed MB & lead ions on NaOH treated loofa is depicted.

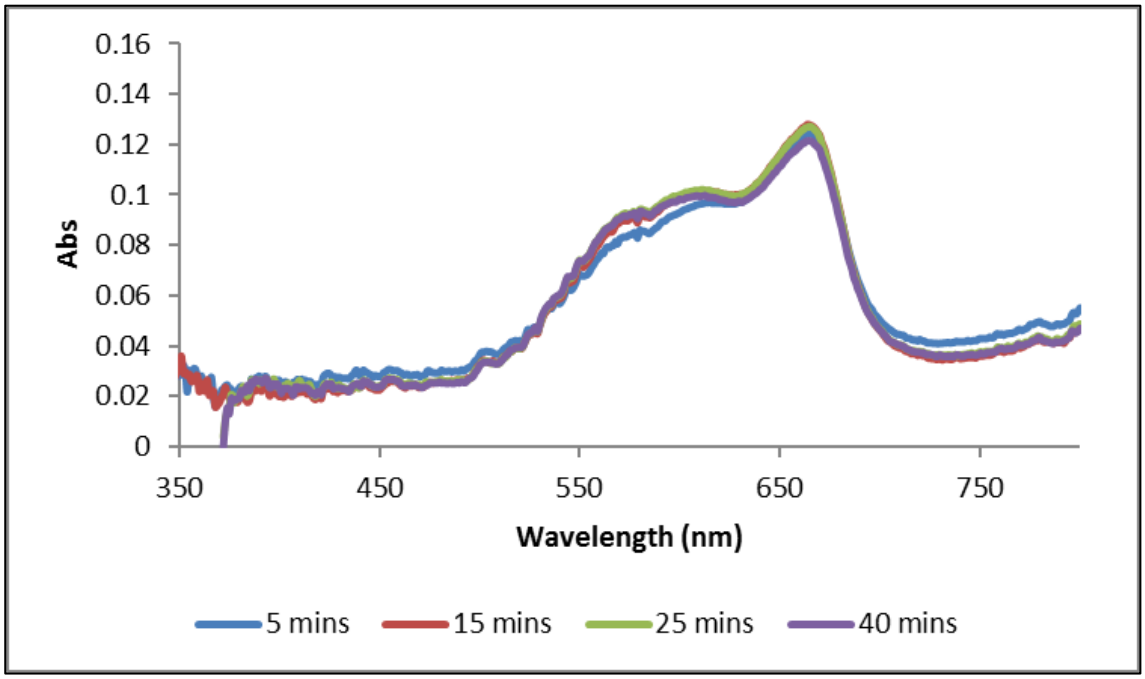

Figure 7.60: UV-Vis spectra of MB adsorption onto alkali treated loofa at different times (pH 7; MB concentration at 20mg/L; agitation speed: 200rpm; at temperature 21°C, 1h contact time, 5g/L alkali treated loofa dosage). Data from 3 replicate measurements.

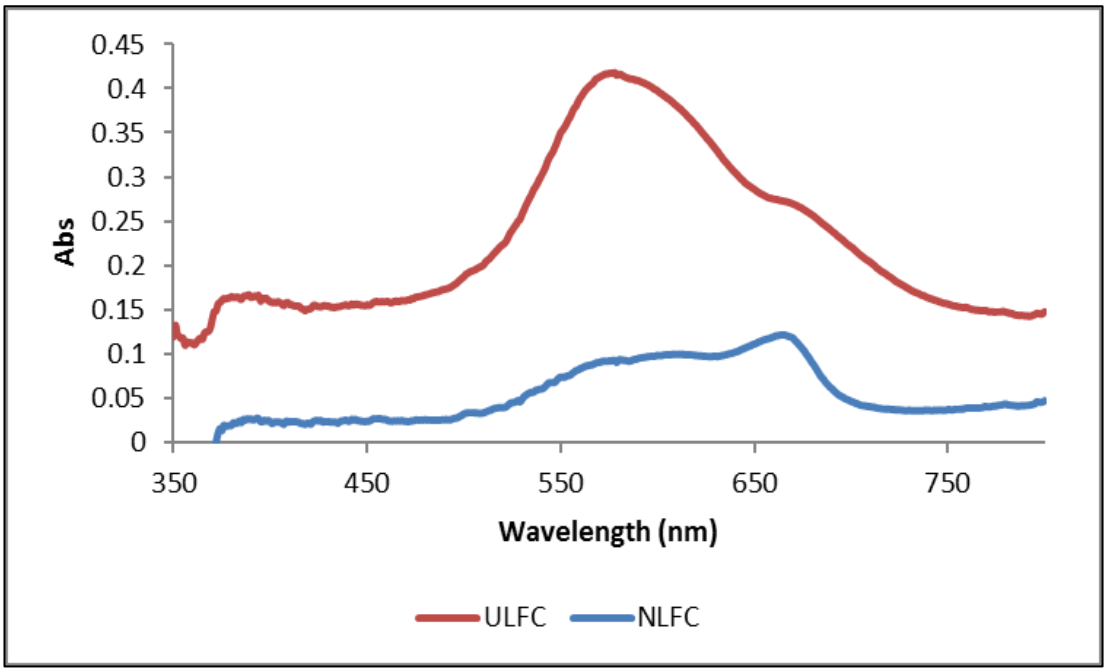

Figure 7.61: UV-Vis spectra of MB adsorption onto alkali treated loofa (NLFC) & untreated loofa (ULFC) at 40mins (pH 7; MB concentration at 20mg/L; agitation speed: 200rpm; at temperature 21°C, 1h contact time, 5g/L alkali treated and untreated loofa dosage). Data from 3 replicate measurements.

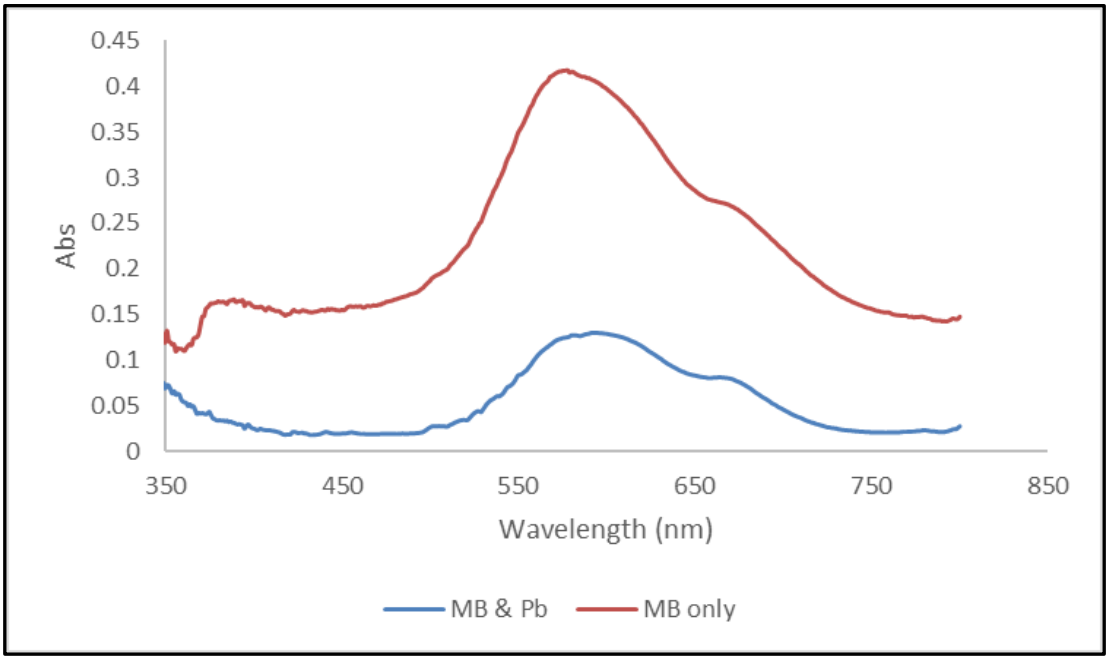

Figure 7.62: UV-Vis spectra of MB and mixed MB & Pb adsorption on untreated loofa (NLFC) at 40mins (pH 7; MB concentration at 20mg/L; agitation speed: 200rpm; at temperature 21°C, 1h contact time, 5g/L untreated loofa dosage). Data from 3 replicate measurements.

Figure 7.60 shows no significant difference in the absorbance values of MB in aqueous solution after 5mins. This indicates that a high percentage of MB has been rapidly absorbed.

The complex formation of methylene blue with untreated loofa and NaOH treated loofa differ over time. This complexation mechanism is explained on the basis of steric hindrance which leds to change in color. Discoloration of MB that occurs with NaOH treated loofa is from blue to colorless which involves the formation of the reduced form of MB cations. For untreated loofa, the discoloration occurs from blue to violet and then colorless. This can be explained by chemical variations of MB. Figure 7.61 shows that there is an intermediate product that is formed during the adsorption process for untreated loofa at an absorbance at 580nm wavelength at 40 mins (Wainwright & Amaral, 2005; Tabbara & El Jamal, 2012). The higher binding constant of NaOH treated loofa indicates the involvement of monomer forms of MB molecules. A lower binding constant as calculated for untreated loofa indicates the utilisation of dimer forms of MB molecules. Furthermore, the adsorption of MB dimers, trimers or tetramers leads to the appearance of MB molecules, which can be observed as a change in colour in aqueous solution, and formation with OH^- groups (Samiey & Ashoori, 2012). For an increasing MB concentration, higher aggregates are formed. MB cations form dimer, trimers and tetramers and may possibly form higher aggregate in aqueous solution. Adsorption at 666-668nm relates to MB monomer while at 580-582nm relates to a possible MB trimer aggregation (Klika, 2007). The shift of the maximum wavelength of MB in aqueous solution from 666nm to 582nm during adsorption by untreated loofa leads to the formation of MB aggregates which were induced by the complexes formed between the MB cations and untouched loofa surface (Fradj *et al*., 2014). Figure 7.62 shows that the effect of lead ions on the adsorption spectra of MB on untreated loofa, which gives a lower absorbance (decreased concentration of MB). Furthermore, the lead ions present in the aqueous solution, do not seem to have an effect on the binding complexes formed between the MB molecules and the untreated loofa (Figure 7.62). Figure 7.4 corresponds with the data shown in Figure 7.61 by showing a lower transmittance percentage due to a higher absorbance value as the MB molecule forms a stronger bond with the dimer forms of MB.

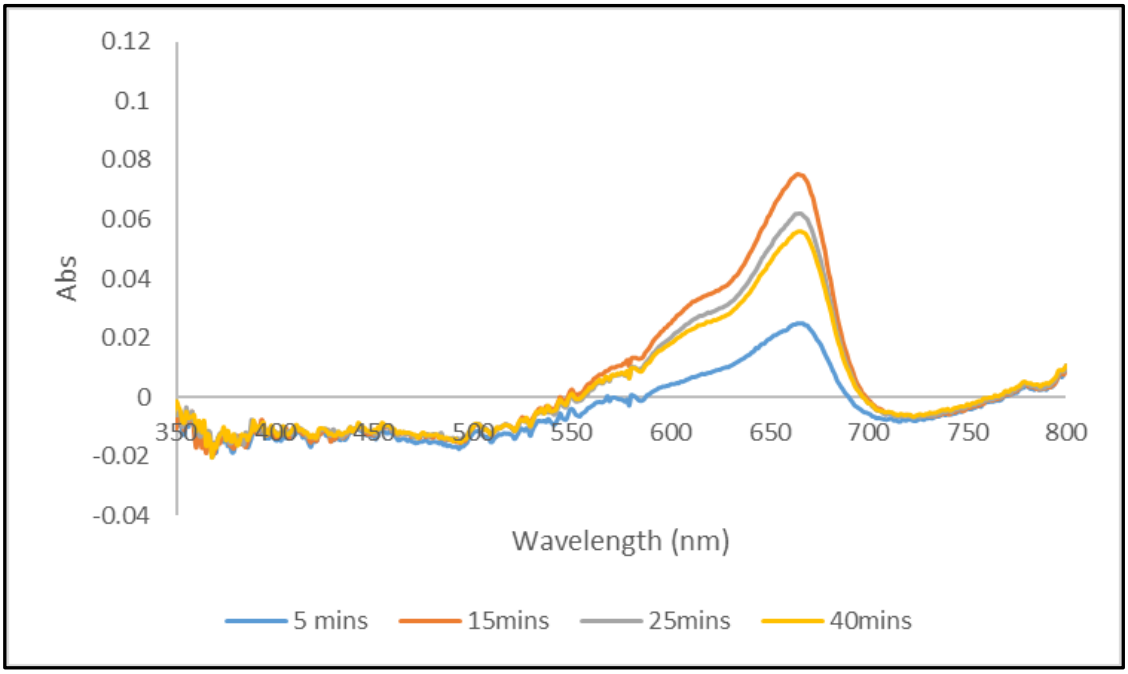

Figure 7.63: UV-Vis spectra of MB adsorption on acid treated loofa at different times (pH 7; MB concentration at 30mg/L; agitation speed: 200rpm; at 21^{o}C, 1h contact time, 5g/L HCl treated loofa).

The UV-Vis spectra of MB adsorption on HCl treated loofa shows a lower absorbance value over 40mins than with alkali treated loofa (Figure 7.60 & 7.63). Yet, the overall uptake capacity and percentage removal is lower than with alkali treated loofa (Figure 7.31 & 7.32). This is further explained by the solid-liquid ratio of MB cations and loofa active sites available in aqueous solution. Figures 7.24 & 7.29 show a lower percentage removal with HCl treated loofa than with NaOH treated loofa but with little or no difference in the uptake capacity at an initial MB concentration of 30mg/L.

7.2.10 Light intensity

Figure 7.64 to 7.69 show the effect of light intensity of 0.17 lux and 820 lux on MB adsorption on acid and alkali treated loofa. Figure 7.64 shows the calculated uptake capacity under the different light conditions. The UV-Vis spectra data as compared with the initial absorbance value at the set concentration is shown in figure 7.65. Figure 7.66 to 7.69 compare the absorbance of MB on acid treated loofa (HCl treated) at 820 and 0.17 lux light intensity.

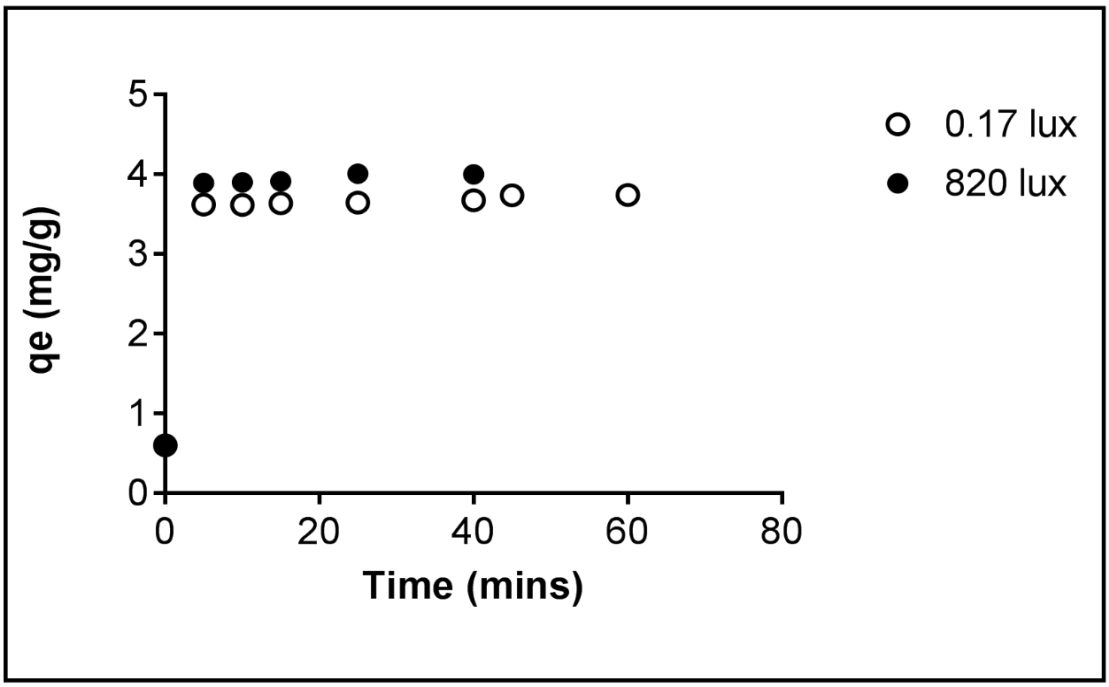

Figure 7.64: MB adsorption capacity on alkali treated loofa at different light intensities over time (pH 7; MB concentration at 20mg/L; agitation speed: 200rpm; at 21°C, 1h contact time, 5g/L alkali treated loofa dosage).

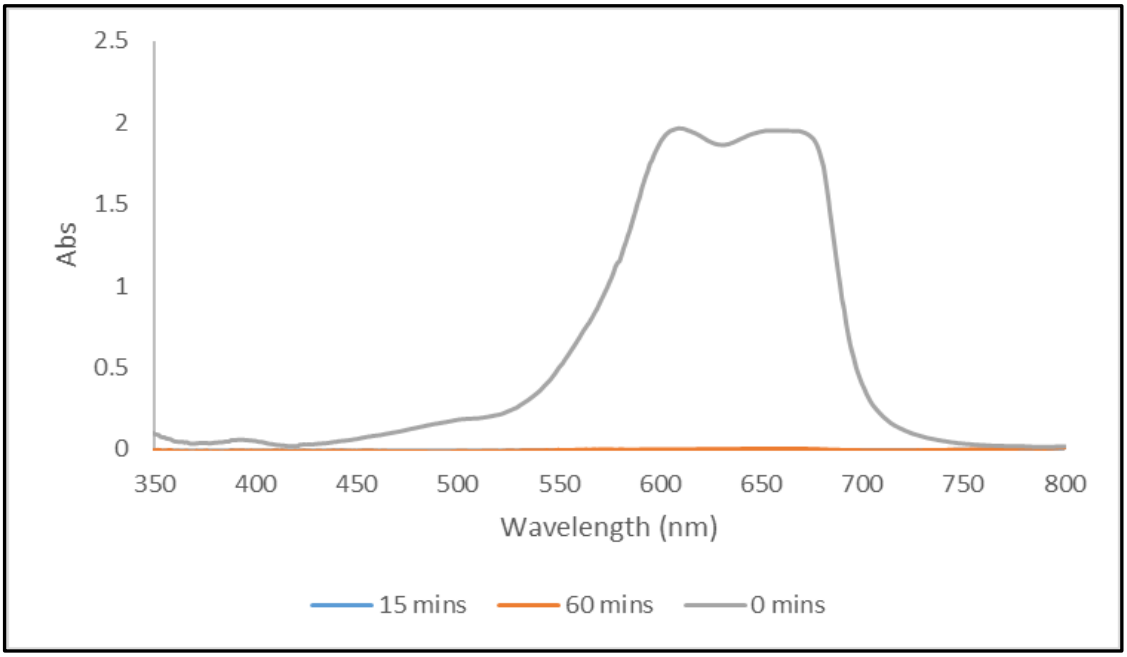

Figure 7.65: UV-Vis spectra of MB adsorption on acid treated loofa over time as compared at 0mins; set at 820 lux (pH 7; MB concentration at 20mg/L; agitation speed: 200rpm; at 21°C, 1h contact time, 5g/L HCl treated loofa dosage).

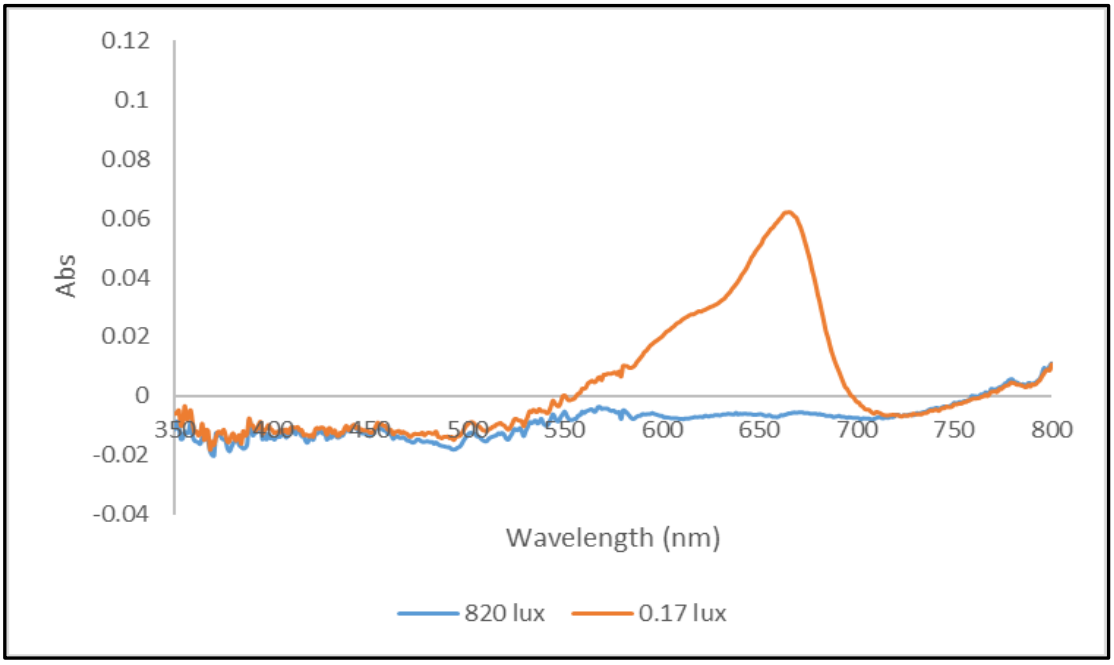

Figure 7.66: UV-Vis spectra of MB adsorption on acid treated loofa at different light intensities at 25 mins (pH 7; MB concentration at 20mg/L; agitation speed: 200rpm; at 21^{o}C, 1h contact time, 5g/L HCl treated loofa dosage).

Figure 7.64 shows that an increase in light intensity leads to a higher uptake of MB over time for alkali treated loofa. No absorbance values were observed when the MB solution was exposed to a higher light intensity of 820 lux. This explains that light intensity has an effect on MB adsorption and shows that MB adsorption capacity increases as the light intensity is increased (absorbance peak disappears as light intensity is increased (Figure 7.65 & 7.66).

7.2.11 Light and dark conditions

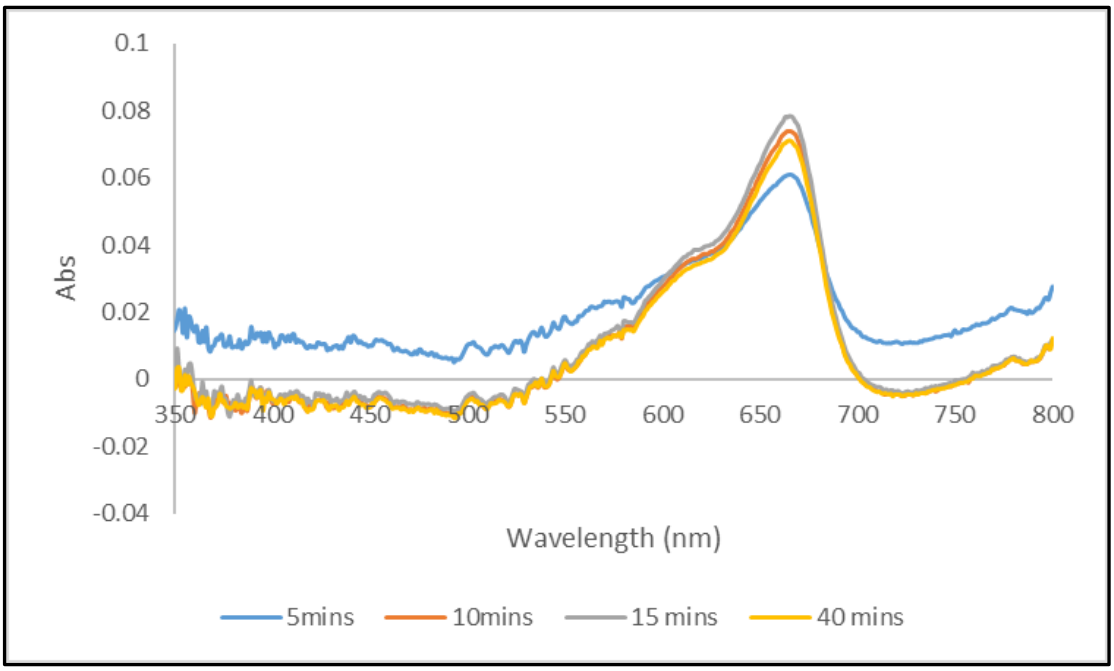

Figure 7.67: UV-Vis spectra of MB adsorption on acid treated loofa at different times under dark conditions (pH 7; MB concentration at 20mg/L; agitation speed: 200rpm; at 21^{o}C, 1h contact time, 5g/L HCl treated loofa dosage). Data from 3 replicate measurements.

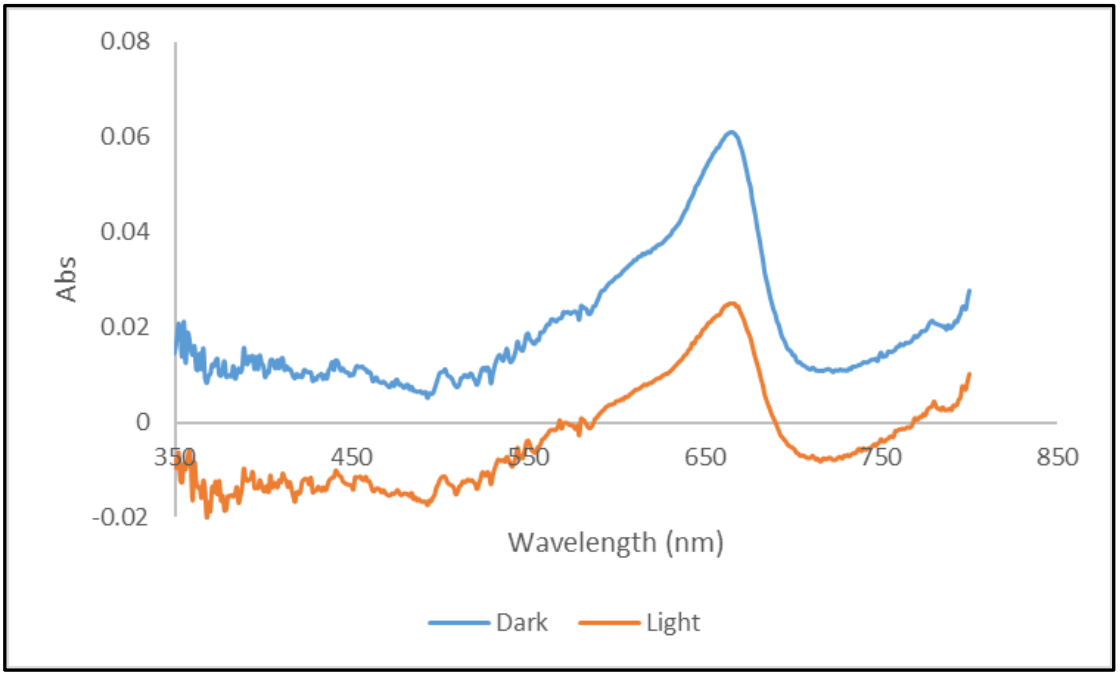

Figure 7.68: UV-Vis spectra of MB adsorption on acid treated loofa at 5 mins under dark and light conditions (pH 7; MB concentration at 20mg/L; agitation speed: 200rpm; at 21°C, 1h contact time, 5g/L HCl treated loofa dosage).

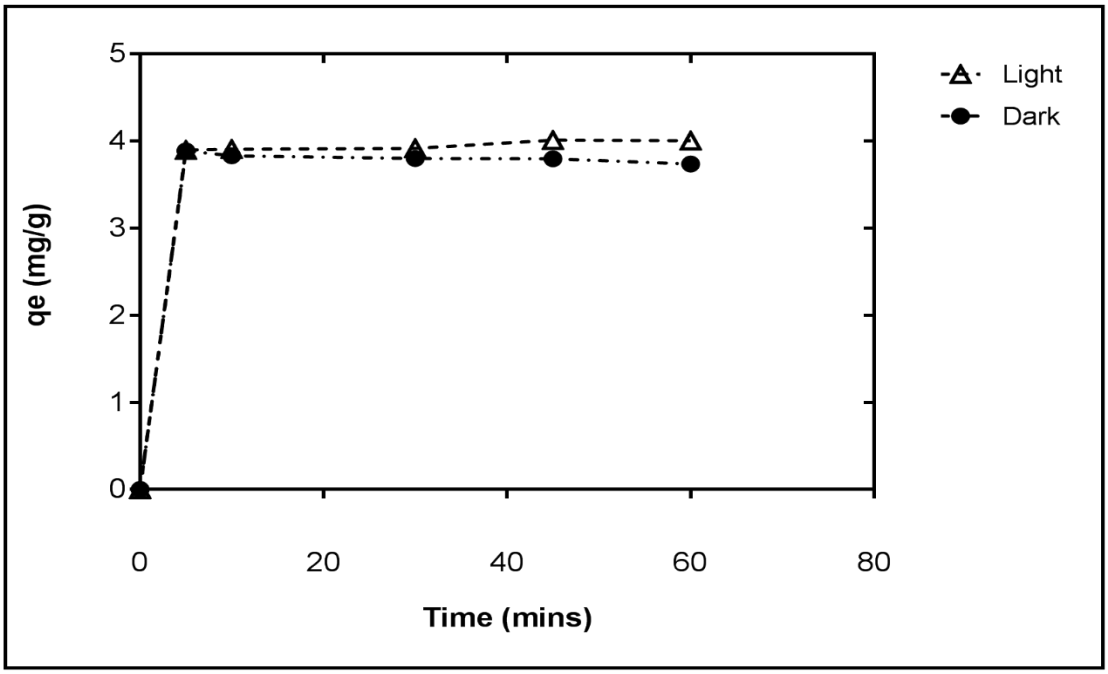

Figure 7.69: MB adsorption unto alkali treated loofa under dark and light (0.17 lux) conditions over time (pH 7; MB concentration at 20mg/L; agitation speed: 200rpm; at 21°C, 1h contact time, 5g/L alkali treated loofa dosage). Data from 3 replicate measurements.

Figures 7.67 – 7.69 confirm the effect of light on MB adsorption onto loofa. A lower MB adsorption capacity was shown under dark conditions as compared to light conditions. A 2.8% difference of adsorption capacity occurred under dark and light conditions at equilibrium.

The kinetics of the methylene blue adsorption onto to alkali treated loofa in the dark is best correlated by the pseudo second model (R^2 = 1) and Elovich model (R^2 = 0.93) (Figure 7.70) and this exhibits a highly heterogeneous nature which involves the different energies of the binding sites in the adsorption process (Madala *et al*., 2013; Shanthi *et al*., 2014).

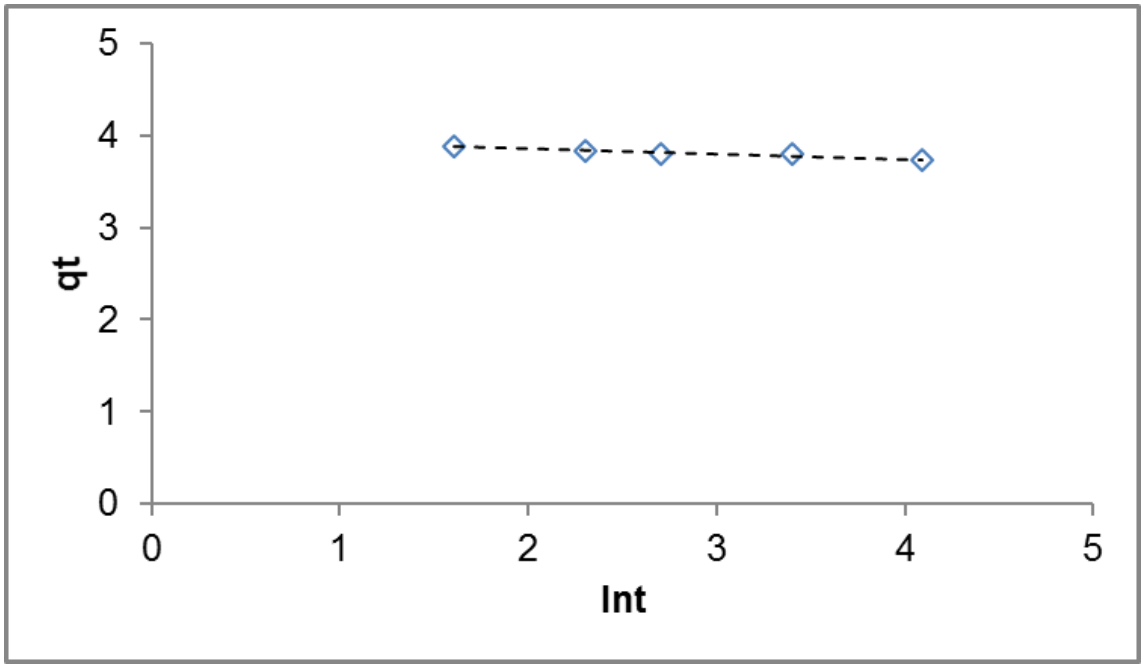

Figure 7.70: MB isotherm from pH 7.0 ± 0.1 at 21 °C at 1hr. contact time. Elovich model fit shown by the dashed line. R^2 = 0.934 (Under dark conditions; pH 7; MB concentration at 20mg/L; agitation speed: 200rpm; at 21°C, 1h contact time, 5g/L alkali treated loofa dosage.

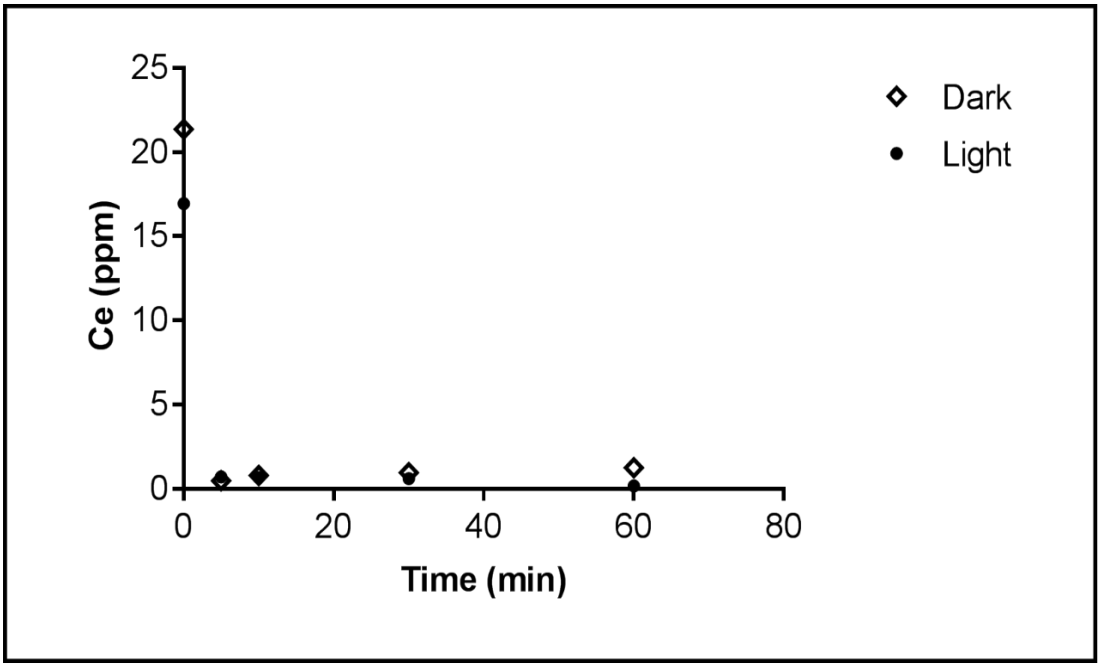

Figure 7.71: Degradation of MB during adsorption on alkali treated loofa under dark and light conditions (0.17 lux) over time (pH 7; MB concentration at 20mg/L; agitation speed: 200rpm; at 21^{o}C,1h contact time, 5g/L alkali treated loofa dosage). Data from 3 replicate measurements.

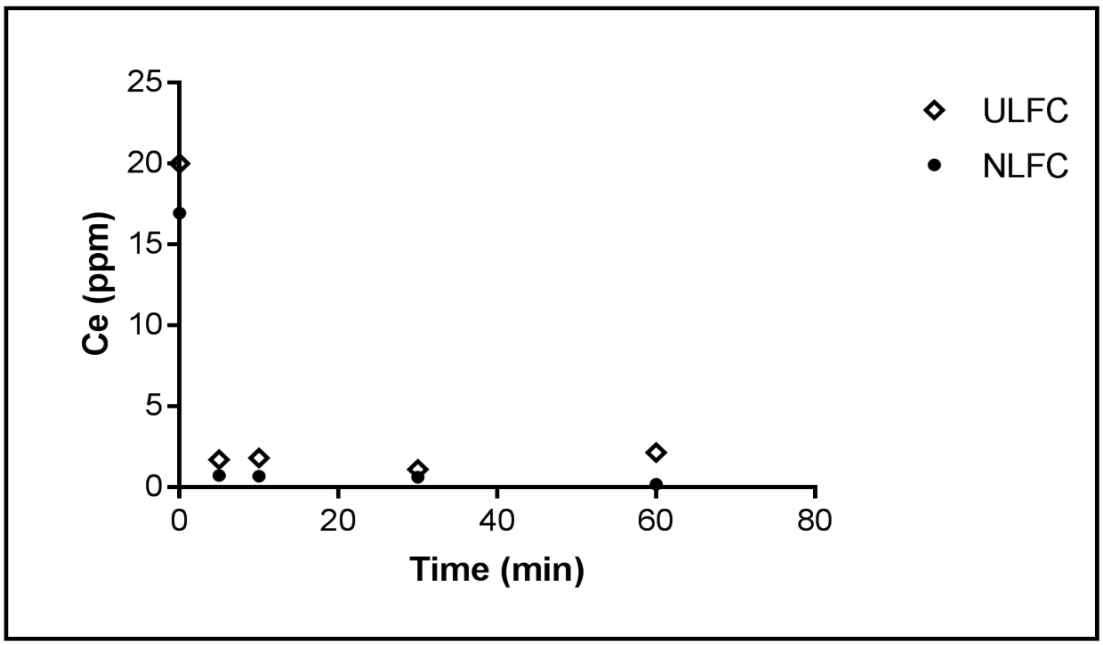

Figure 7.72: Degradation of MB during adsorption on alkali treated loofa (NLFC) & untreated loofa (ULFC) under light conditions (0.17 lux) over time (pH 7; MB concentration at 20mg/L; agitation speed: 200rpm; at 21^{o}C,1h contact time, 5g/L alkali treated and untreated loofa dosage). Data from 3 replicate measurements.

The experiments carried out under dark conditions show the actual loading capacity of the loofa. The degradation of MB starts to occur at 0 mins during light conditions (Figure 7.65). This confirms that photodegradation of MB has an effect on the MB adsorption (Figure 7.71). Further degradation occurs over time and shows a slightly lower final MB concentration at equilibrium (60 mins) under light conditions. As compared with untreated loofa under light conditions, degradation of MB from NaOH treated loofa is lower (Figure 7.72). This confirms the difference in the interaction between the MB molecules and the loofa material during adsorption. The Elovich model gives a good fit and indicates a highly heterogeneous adsorbent surface with a desorption constant of 3.97g/mg (Figure 7.69). K_2 values of the pseudo second order constant are lower in the dark than in the light under the same conditions of concentration, temperature and pH. A lower distribution coefficient was calculated for the dark condition than for the light conditions. Therefore, K_D and K_2 rates of adsorption increase in the light conditions, which indicates more uptake capacity for MB adsorption.

CHAPTER EIGHT

8.0 MIXED METAL BIOSORPTION

8.1 Introduction

This chapter describes how mixed metal ions (previously discussed metal ions – chapter 4, 5 & 6) have an effect on the adsorption of each other onto *Luffa cylindrica* (loofa). Section 8.2 describes the batch experiments run with mixed metal ion solutions and investigates the effect that different experimental factors, such as pH, time and initial metal ion concentration, have on the uptake of each of these metal ions. Covered in this chapter are the kinetic and isotherm models used to understand the behavioural pattern of each of the metal ions, in the presence of other metal ions, and the loofa.

8.2 Batch experiments

8.2.1 pH and concentration effect

The adsorption of mixed lead, cadmium and zinc ions with change in pH over time is shown in Figure 8.1.

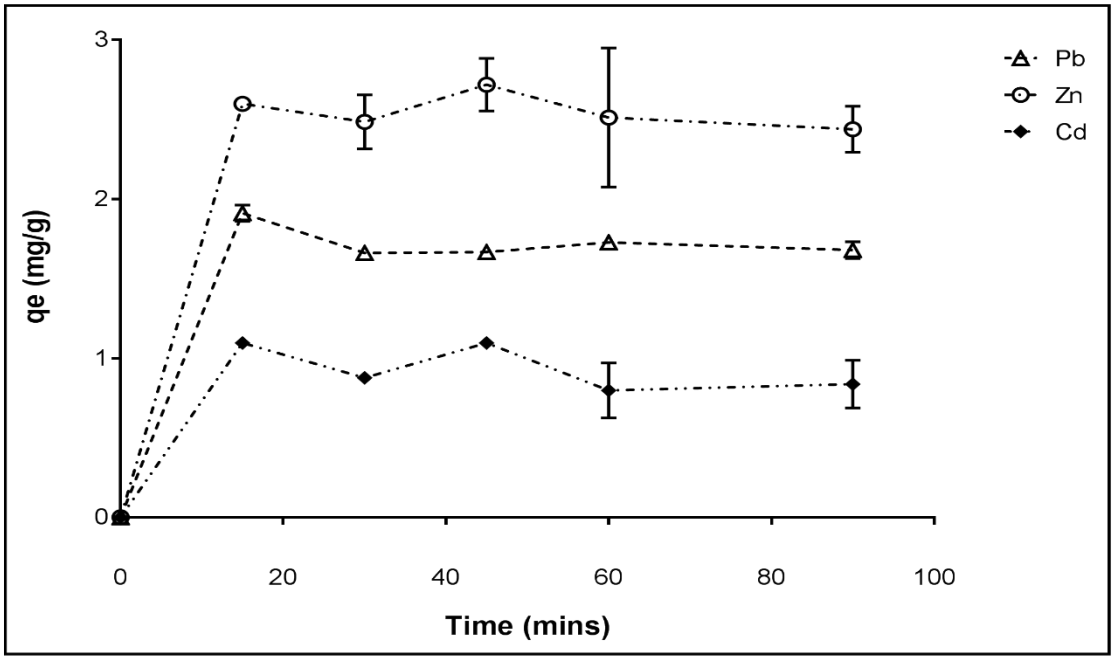

Figure 8.1: Uptake capacity (q_e) of lead, zinc and cadmium ions at pH 5 after 1.5hrs; mixed metal ion concentration: ratio 6:3:1- 50mg/L (zinc- 30mg/L, lead- 15mg/L & cadmium- 5mg/L); agitation speed: 200rpm; at 21^{o}C,1.5h contact time, 5g/L dosage of alkali treated loofa dosage. Data from 3 replicate measurements.

Weak chelates are formed by lead and zinc ions with other ions in solution, compared to cadmium ions, which can explain the higher uptake by the loofa (Ahamed *et al*., 2010). The weak chelates are as a result of the weak bonding energy for the formation of ions in solution and the charged surface of the loofa based on the distribution ratio of the metal ions. Therefore, the ratio of concentration of the individual metals was chosen to investigate how the effect of co-ions formed by increased concentration of lead and zinc ions as compared to cadmium will make a difference to the adsorption capacity. The initial concentration is highest for zinc, followed by lead and then cadmium.

Zinc ions have the highest uptake capacity (qe) (which is also known as the uptake capacity is the adsorption onto the loofa which leads to the unit adsorbate sorption capacity of the loofa adsorbent) compared to lead and cadmium. This shows an impact on the lead adsorption. This is followed by lead ions and then cadmium ions having the least uptake. Figure 8.1 shows that

equilibrium is attained after 60 mins. The fastest adsorption rate for all three metals is in the first 15 mins (as described individually in chapters 4, 5 & 6).

As explained in chapter 4, pH 5 is the optimum pH for maximum lead ion adsorption onto loofa. The different binding capacities at pH 5 change in mixed metal solution are due to the solution chemistry, the competition of each metal ion and the availability of active sites on the loofa surface for adsorption (Lee *et al*., 2002).

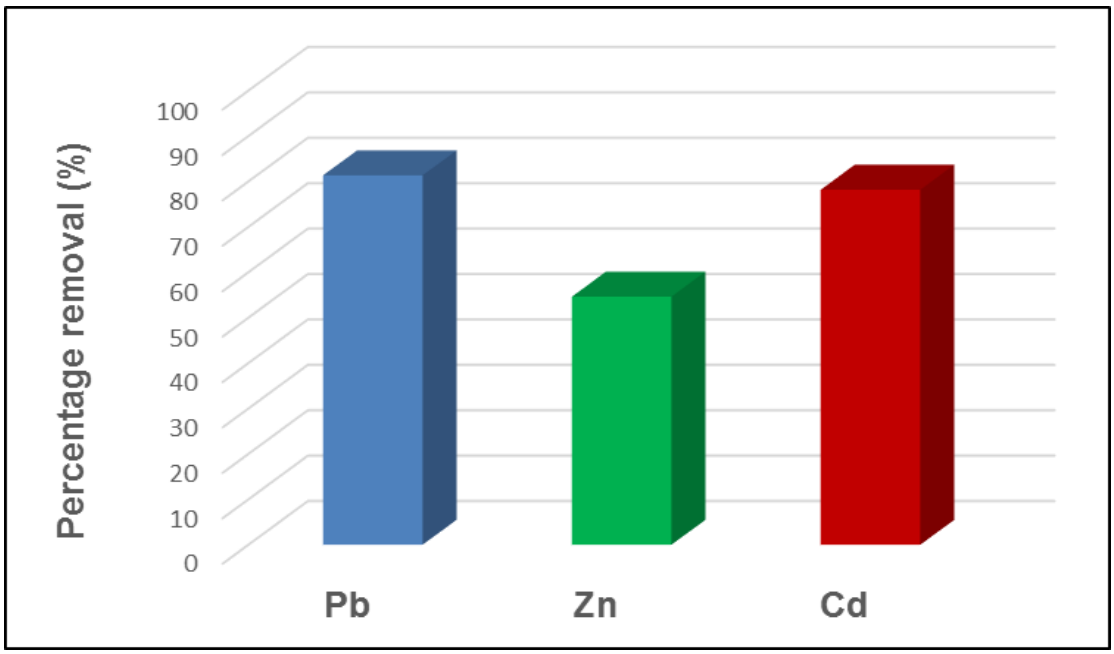

Figure 8.2: Percentage removal of lead, zinc and cadmium ions at pH 5 after 24hrs; mixed metal ion concentration: 6:3:1- 50mg/L (zinc- 15mg/L, lead- 30mg/L & cadmium- 5mg/L); agitation speed: 200rpm; at 21^{o}C, 24h contact time, 5g/L dosage of alkali treated loofa dosage.

The percentage removal is highest for lead ions at 78%, followed by the cadmium ions at 74% and then zinc ions at 51%. Compared to the single metal (Chapters 4, 5 & 6), the percentage removal of zinc ions shows the greatest decrease in removal at 20% decrease, lead ions by 17% while cadmium ion removal actually increased by 15%. Lead and cadmium ions in mixed solution show the greatest decrease in adsorption capacity (q_e) as compared to each of its single solutions; and zinc shows the lowest decrease in adsorption capacity (q_e). Zinc thus shows the largest decrease in the percentage removal (%) and the lowest decrease in its adsorption

capacity (q_e) as compared to its single solution. The percentage removal represents the loofa to metal ions ratio which leads to the difference in the concentration of adsorbate before and after adsorption and the uptake capacity is the adsorption onto the loofa which leads to the unit adsorbate sorption capacity of the loofa adsorbent. This shows the negative effect co-ions have on adsorption of all three metal ions. The zinc ions show the highest adsorption capacity due to having the highest initial concentration present in the mixed solution but the lowest percentage removal due to competition for sites by lead and cadmium ions. This is explained by the displacement of the zinc ions by the lead and cadmium ions. Also, the percentage removal of lead ions is highest which is explained by the highest affinity of lead ions to loofa. The cadmium ion increase is an example of the positive effect of lead and zinc ions on the percentage removal of cadmium (Liu, *et al*., 2004). The total removal of cadmium from a mixture of all three ions is better than for cadmium alone but shows a lower percentage removal for lead and zinc compared to single lead and zinc ions (each metal ion 50mg/L) (Figure 8.3).

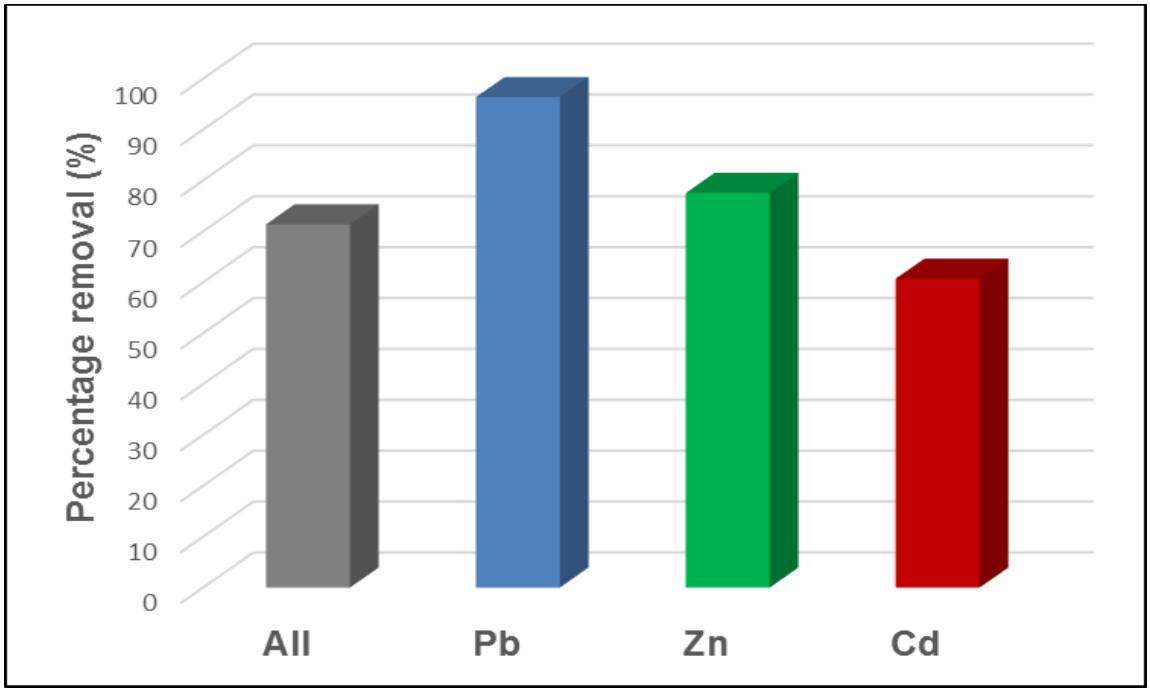

Figure 8.3: Percentage removal of all three metal ions, single lead, zinc and cadmium ions at each optimum pH range 5-7 after 24hrs; agitation speed: 200rpm; at 21°C, 24h contact time, 5g/L dosage of alkali treated loofa dosage.

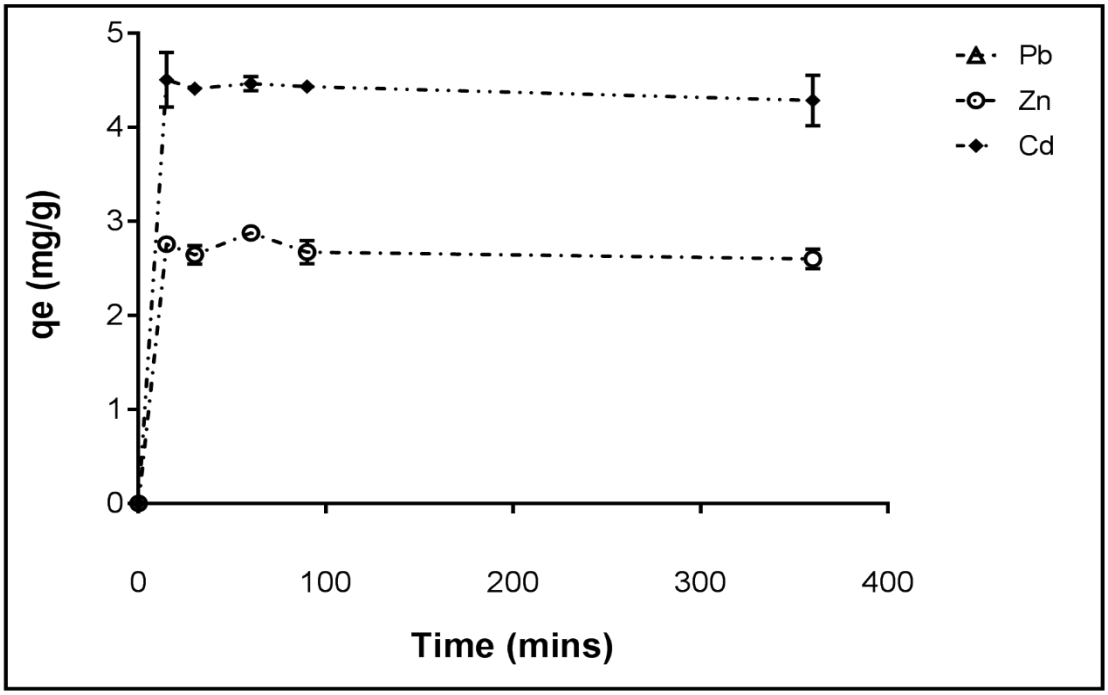

Figure 8.4: Uptake of lead, zinc and cadmium ions at pH 6 over 6hrs; mixed metal ion concentration: ratio 1:1:1 (50mg/L); agitation speed: 200rpm; at 21^{o}C,6h contact time, 5g/L dosage of alkali treated loofa dosage. Data from 3 replicate measurements.

At pH 6, equilibrium is reached at 90mins for both zinc and cadmium ions. Lead ions were not detected in solution which means that all lead is either precipitated out of solution or absorbed. This is explained by the precipitation of lead ions by further increase in pH. The adsorption capacity is approximately 4.5mg/g and 2.5mg/g for cadmium and zinc respectively but could not be determined for lead. pH 6 is the optimum pH value for zinc ion adsorption in single metal solution and does not show the highest uptake capacity in a mixed metal solution (figure 8.4) but this is still a 46% decrease compared to the single solution. Cadmium uptake is decreased by approximately 15%. This shows that the affinity of zinc and cadmium ions to loofa is highly affected by co-ions in mixed metal solutions (Kim, 2003).

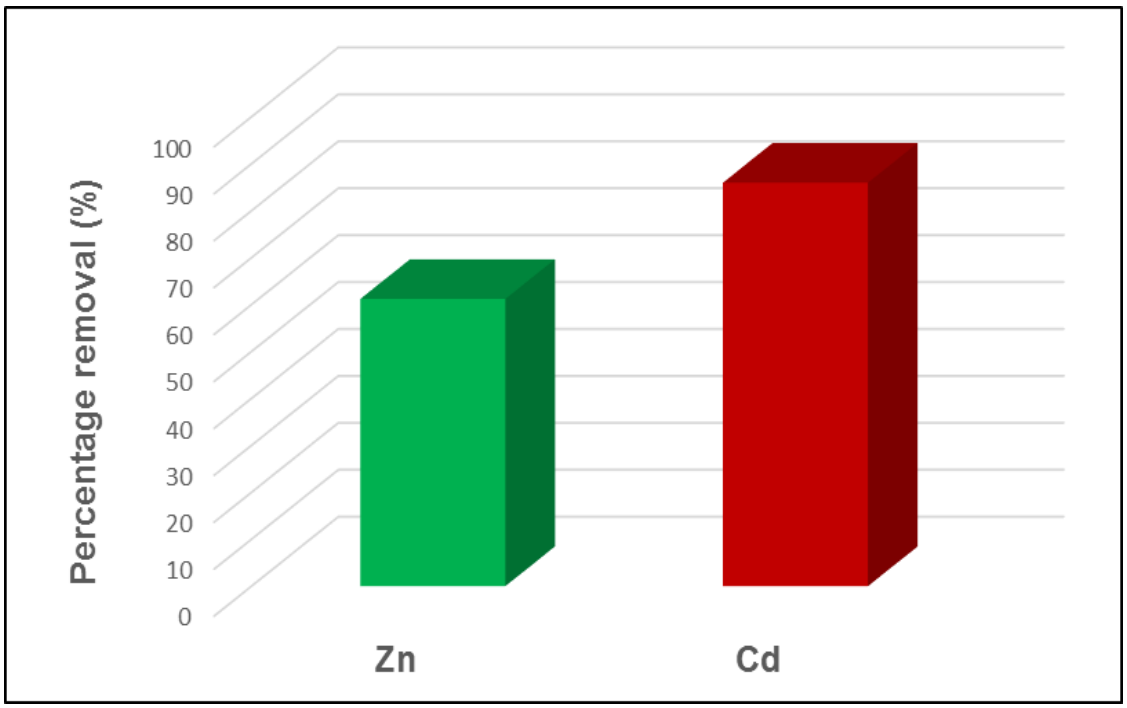

Figure 8.5: Percentage removal of zinc and cadmium ions at pH 6 after 6hrs; mixed metal ion concentration: ratio 1:1:1 (50mg/L); agitation speed: 200rpm; at 21°C, 6h contact time, 5g/L dosage of alkali treated loofa dosage.

The percentage removal of cadmium ions was higher at 80% than that of zinc ions at 65%. When compared to single ion solutions, cadmium uptake is increased by approximately 20% and zinc is decreased by approximately 15%. This further supports the co-ions effect.

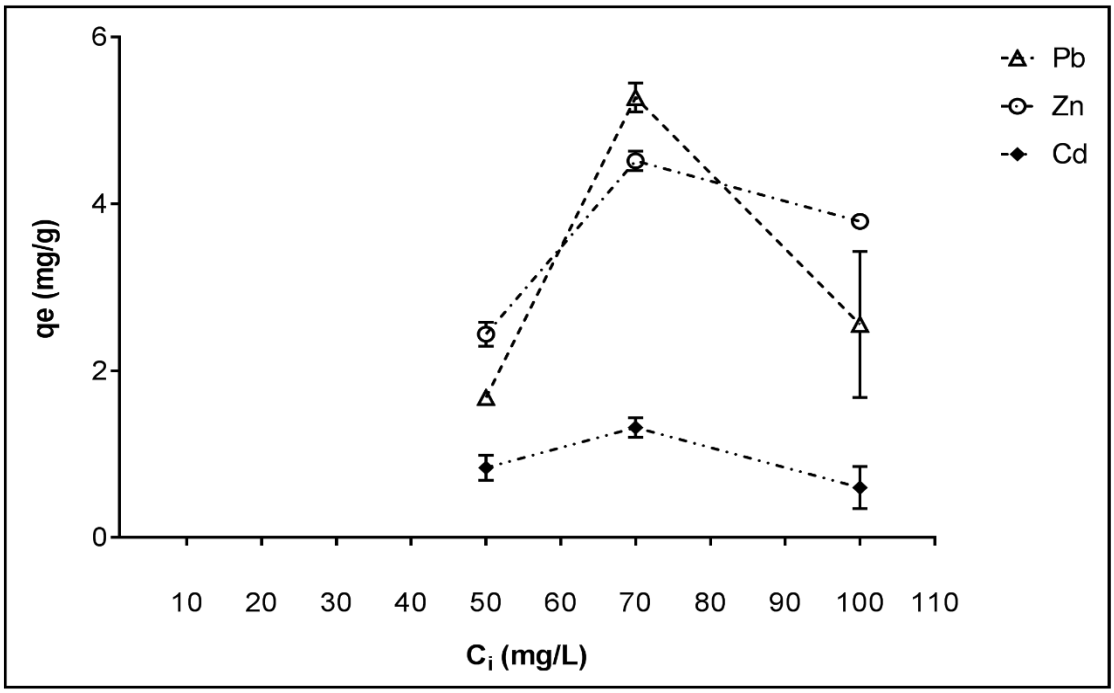

Figure 8.6: Uptake capacity of lead, zinc and cadmium ions at pH 5 after 1.5hrs; mixed metal ion concentration: (50 - 100mg/L); agitation speed: 200rpm; at 21^{o}C,1.5h contact time, 5g/L dosage of alkali treated loofa dosage. Data from 3 replicate measurements.

The uptake capacity of lead, zinc and cadmium ions are shown to increase as initial concentration increases till a maximum value is attained and then decrease as further initial concentration increases (Figure 8.6) Cadmium shows the lowest adsorption capacity (q_e) at all initial concentrations studied. This indicates that cadmium ions have the lowest affinity to loofa at pH 5. Figure 8.6 further shows the competition between the zinc and lead ions in mixed solution over an increase in initial concentration.

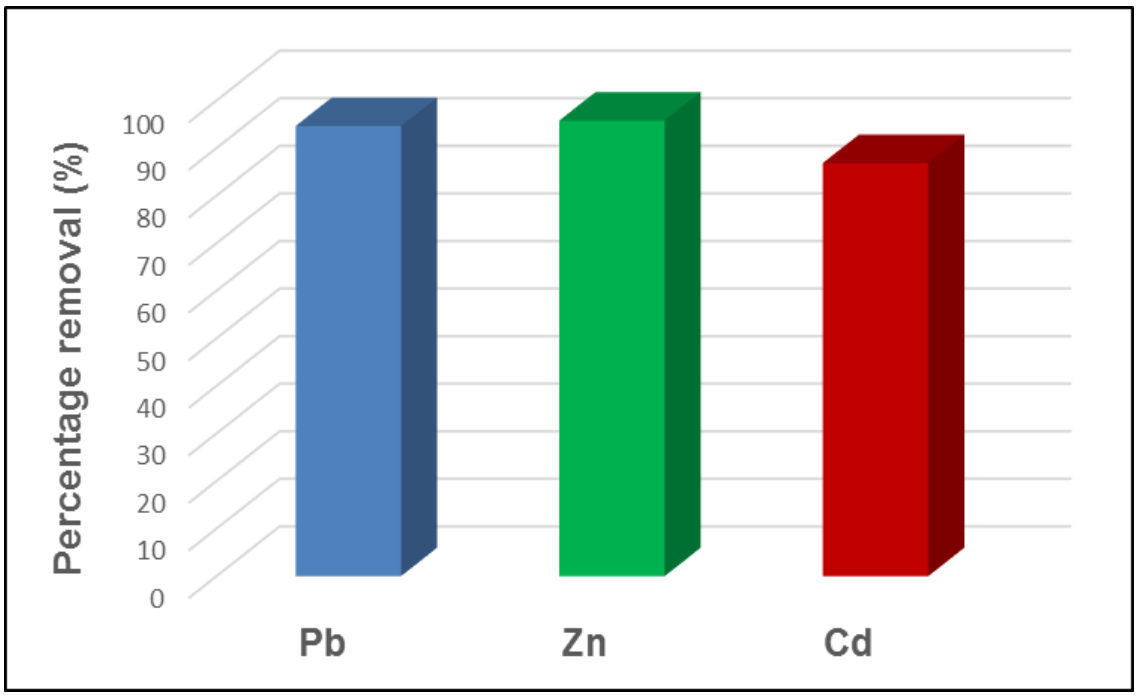

Figure 8.7: Percentage removal of zinc, lead and cadmium ions at pH 6 after 3hrs; mixed metal ion concentration: ratio 4:3:1 (70mg/L – Pb, Zn & Cd); agitation speed: 200rpm; at 21^{o}C, 3h contact time, 5g/L dosage of alkali treated loofa dosage.

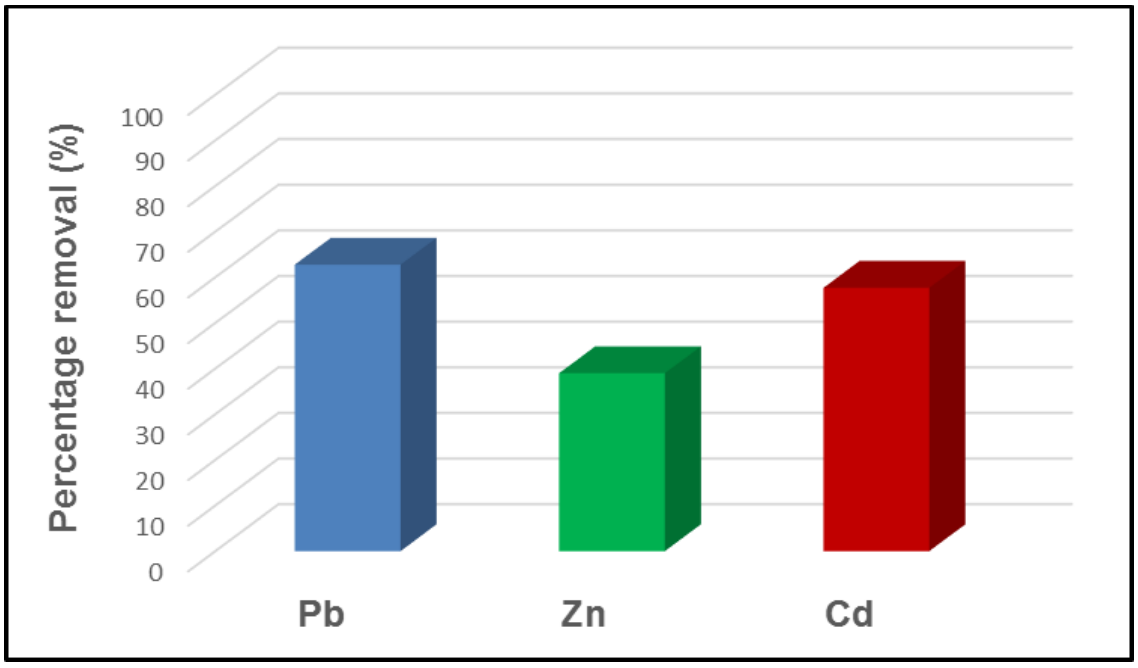

Figure 8.8: Percentage removal of lead, zinc and cadmium ions at pH 6 after 3hrs; mixed metal ion concentration: ratio 1:6:2 (100mg/L- Pb, Zn & Cd); agitation speed: 200rpm; at 21^{o}C, 3h contact time, 5g/L dosage of alkali treated loofa dosage.

As the total concentration is increased, the percentage removal decreases. This is explained by the saturation of the adsorption sites on the loofa surface leading to a decrease in the amount capable of being removed by the loofa (Figures 8.7 & 8.8). The change in the ratio of the initial concentration of each metal ion shows the varied effects of co-ions on adsorption in mixed solution. Figure 8.8 shows the lowest ratio of lead ions in the mixed solution (lower initial concentration compared to the other ions) but the highest percentage removal for all metal ions studied with cadmium showing the lowest percentage removal. This shows that lead ions have the least effect on the percentage removal of other ions in mixed solutions.

The effect of pH was studied since the pH is known to be the most sensitive factor in the adsorption process. The batch experimental results were not obtained beyond pH 6 to limit the effect of precipitation which is expected to occur over pH 6 for these metal ions. However, the maximum adsorption capacity of both lead and zinc was at pH 5 & 6 respectively and the speciation of cadmium (Figure 6.1) shown to have the dominant form of cadmium ($Cd(OH)_2$) absorbed on the loofa surface which accounts for a maximum uptake capacity to be reached between pH 6 - 8 was therefore considered sufficient in explaining the maximum uptake capacity of cadmium at pH 6 in comparison to mixed metal solution.

8.2.2 Kinetic modeling

The rate controlling step of the adsorption process was determined by the use of kinetic models as shown in Figures 8.9 & 8.10. The values of the best fit kinetic model are tabulated in Table 8.1. The pseudo second rate constants versus initial concentration of lead ions in mixed solution is shown in Figure 8.11.

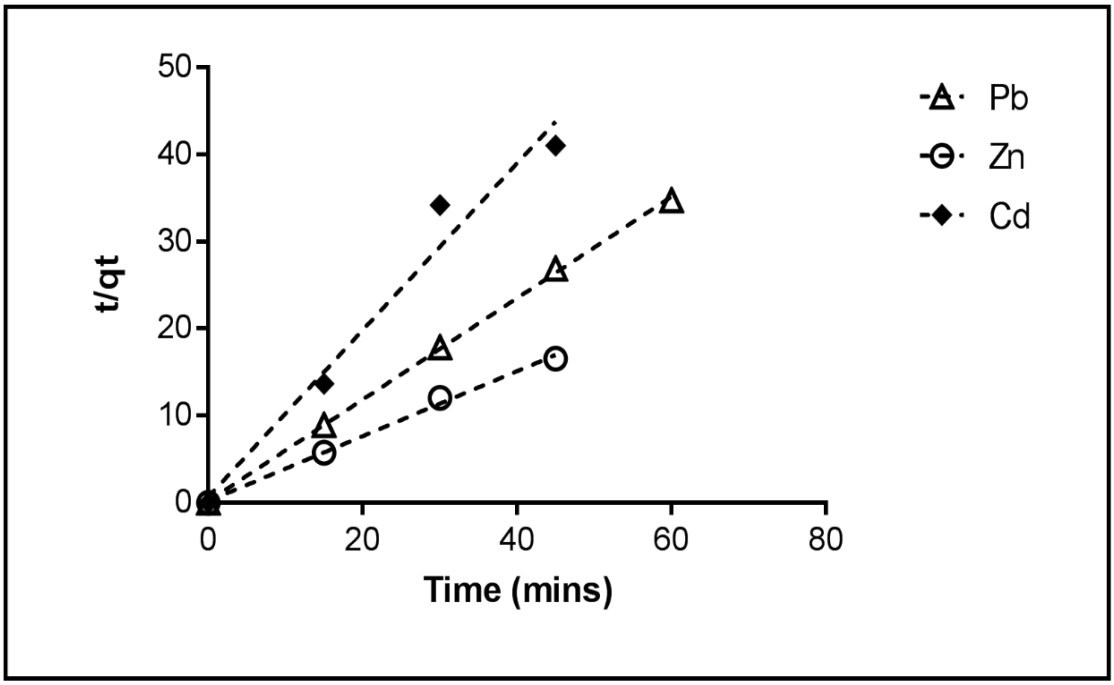

Figure 8.9: Pseudo second order (PSO) kinetic model at pH 5; lead, zinc and cadmium ion concentration: ratio 6:3:1 (50mg/L – lead, zinc & cadmium); agitation speed: 200rpm; at 21^{o}C, 1.5h contact time, 5g/L alkali treated loofa dosage. PSO model fit shown by the dashed line.

Table 8.1: Pseudo second order kinetic model parameters for linear regression (mixed metal ions: ratio 6:3:1 (50mg/L – zinc, lead & cadmium; pH 5).

	qe_2	K_2	h	R^2
Pb	1.738	0.632	1.908	0.999
Zn	2.782	0.189	1.464	0.991
Cd	1.097	0.365	0.439	0.923

The q_e values of zinc, lead and cadmium are close in value to that of the experimental data obtained for the uptake capacity of zinc, lead and cadmium in mixed solution.

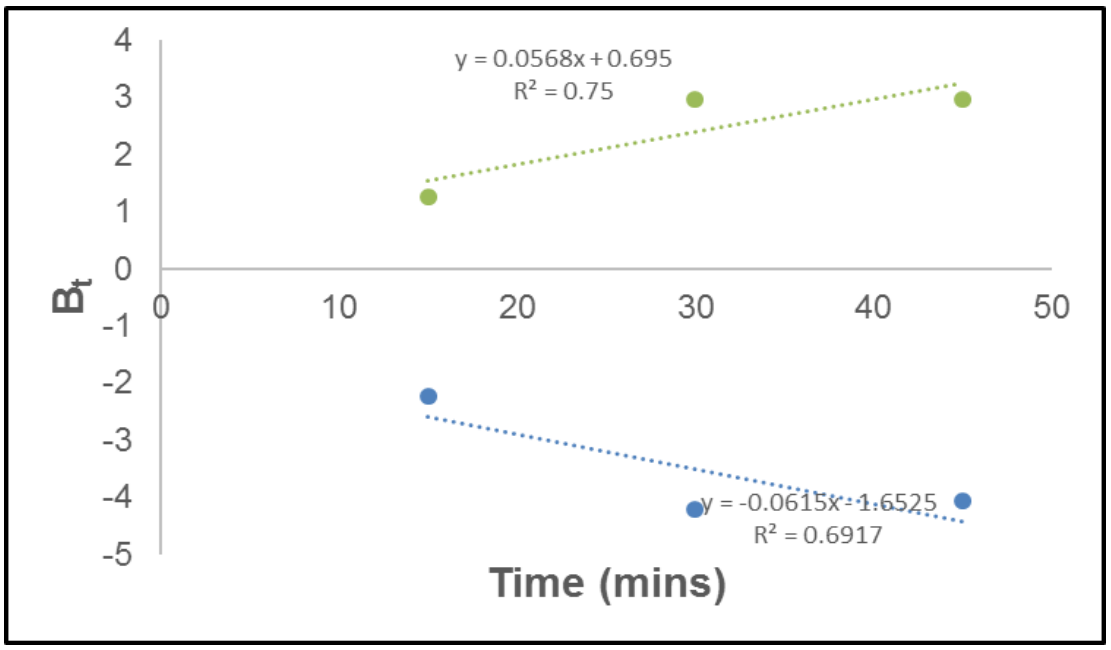

Figure 8.10: Boyd model at pH 5; lead ion concentration in mixed metal solution 50 mg/L; agitation speed: 200rpm; at 21°C, 3h contact time, 5g/L alkali treated dosage. Boyd model fit is shown by the dashed line.

Figure 8.10 shows the Boyd model of lead ion adsorption in mixed solutions. The correlation coefficient moves towards linearity as the concentration increases. This shows the rate is controlled by film diffusion. Zinc and cadmium adsorption does not show a good fit to the Boyd model.

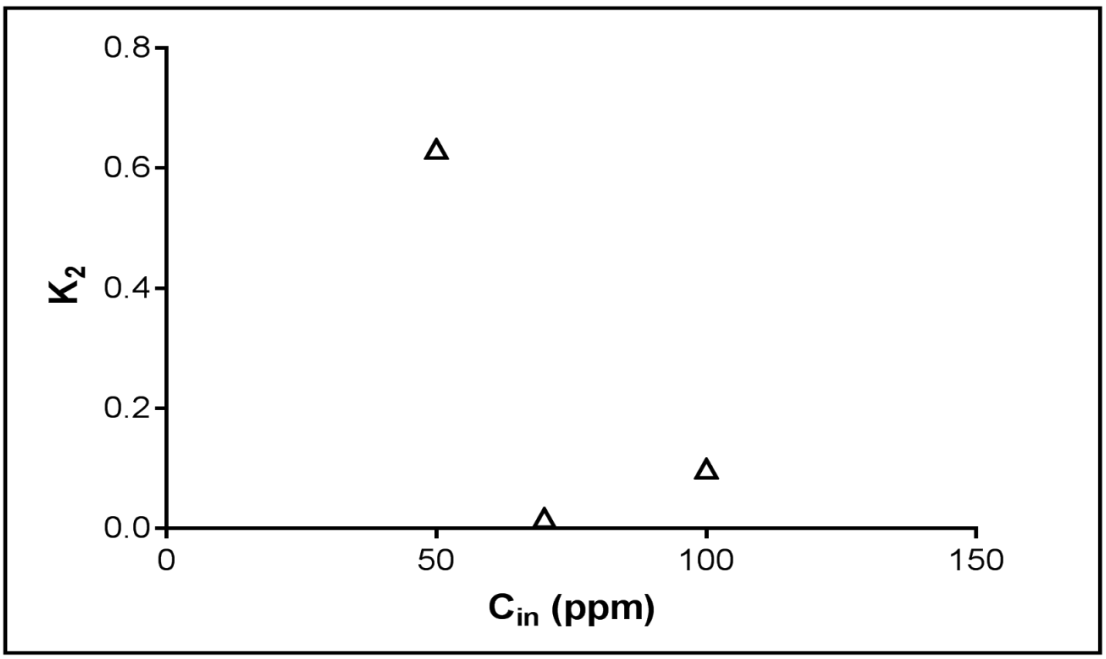

Figure 8.11: K_2 (pseudo second order constant) vs. initial lead ion concentration (50 - 100mg/L) in mixed solution at pH 5; agitation speed: 200rpm; at 21°C, 1.5h contact time, 5g/L alkali treated loofa dosage.

The pseudo second order rate constant (k_2) decreases as concentration increases. This shows the rate of uptake to increase and resistance in the mesopores to decrease and is explained by the change in the ratio of binding interactions and also implies that diffusion plays an important role in the kinetic process of adsorption in mixed solutions (Chi *et al*., 2013).

8.2.3 Isotherm modeling

Table 8.2 shows the correlation coefficient values of two and three parameter isotherm models used to predict the behavioural pattern of the mixed metal ions in solution, obtained from linear regression.

Table 8.2: Correlation coefficient of isotherm models fitting (linear regression).

Isotherm models	Pb	Zn	Cd
Langmuir	0.951	0.848	0.999
Freundlich	No fit	0.842	0.925
Sips	No fit	0.600	0.996

For lead, zinc and cadmium ion adsorption in mixed metal solution, the best fit model gives a R^2 value of 0.951, 0.848 and 0.999 respectively. A monolayer adsorption is predicted for each metal in the mixed solution, therefore resulting in competition of the metal ions for adsorption sites and thus the competitive effect on each other during the adsorption process.

CHAPTER NINE

9.0 COLUMN ADSORPTION MECHANISMS

9.1 Introduction

In this chapter, the column testing results are presented for a set pH, concentration range, temperature and loofa dosage (Section 9.2). Section 9.3 presents the breakthrough curves, the point at which saturation occurs, for adsorption of each metal ion (lead, zinc and cadmium) and methylene blue onto the loofa. The desorption of the metal ion and MB loaded loofa are also shown. The plots indicate the time taken to attain saturation of the loofa during adsorption, where the inlet concentration in the range 10-100mg/L is equal to the outlet concentration. Also, the breakthrough curve is plotted based on the time and bed volume required. This further applies to the dynamic testing of the desorption process. The parameters and values for a column design for a scale up process is also discussed.

9.2 Column experimental conditions

Bed volume is the minimum volume required to wet a defined quantity of loofa within the column. For the operational parameters of this experiment, a bed height of 5cm and loofa mass of 2.0g, the amount of solvent required to wet the loofa completely before it is released into the collection tubes was calculated. Firstly, with a flow rate of 0.5mL/min, 4ml of solvent is required before it reaches the column (i.e. reaches the loofa from the reservoir), then another 4.75ml is required before drops reach the first collection tube (total of 8.75mL is eluted). However, approximately 4.75ml is required to wet the loofa in the column hence the 1BV (one bed volume) is found to be the quantity of metal solution that completely immerses the loofa in column which is measured at 5ml. At a flow rate of 0.5mL/min, the solution was released into the column for approximately 8 minutes prior to sample collection.

The design of the fixed bed adsorption system is based on the laboratory batch experiments and column data. The following points were considered in the laboratory column design:

- The wall effects did not affect the experimental work because the column was designed to release fluid flowing through the tube from the centre of the packed bed column.
- Formation of voids in the column were prevented by tightly packing the loofa. The tube diameter to particle size should be in a certain range to overcome void spaces and make wall effects negligible. For this experiment, ratio of the column to particle diameter was 10:1, therefore the wall effects were deemed negligible.
- Inconsistency in the final concentration of solution may be that the fluid does not fully pass through the entire bed. However, when the flow rate was increased to 2mL/min or 2.5mL/min, the column was waterlogged and there was a pressure drop. The flow rate for adsorption and desorption was thus set at values below 2mL/min.
- The axial dispersion effect was minimised by a bed length to particle diameter ratio of 25 (> 15).

9.3 Lead

9.3.1 Adsorption

Figure 9.1 and 9.2 show the breakthrough curves for adsorption of lead on loofa as it relates to bed volume and time. At a flow rate of 0.5mL/min, there is a long contact time between the loofa and lead ions. Saturation is observed to occur at over 3hrs at a set BV of over 60mL.

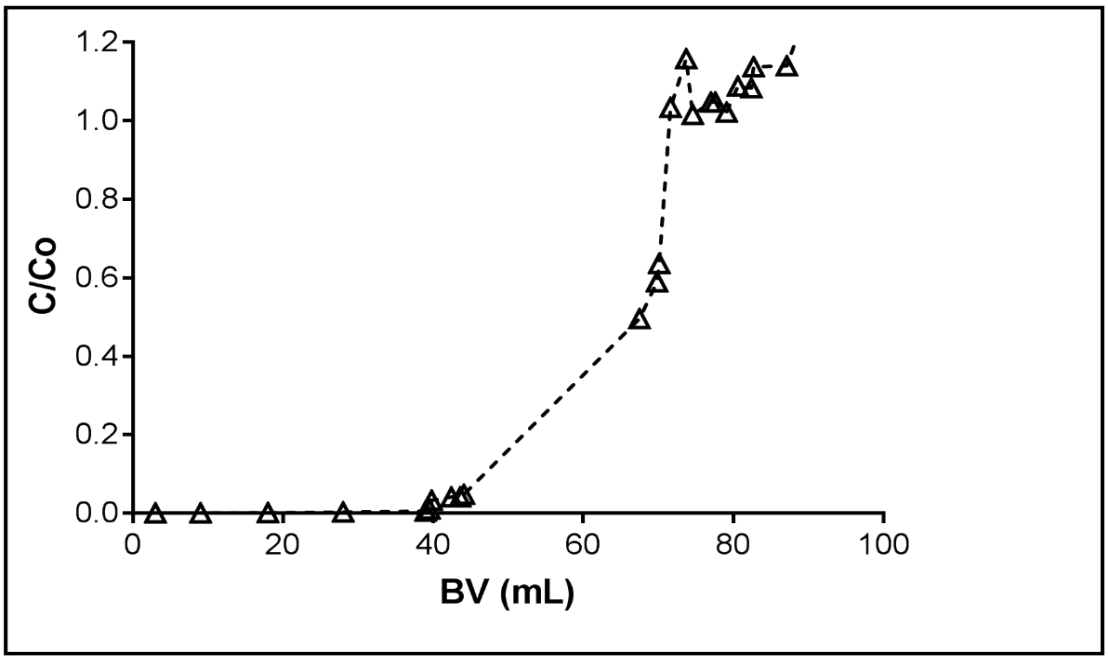

Figure 9.1: Breakthrough curve of lead ion adsorption based on bed volume, lead ion concentration 50 mg/L; flow rate 0.5mL/min; at 21°C, loading capacity 2g; particle size 2mm; column height 9.5cm.

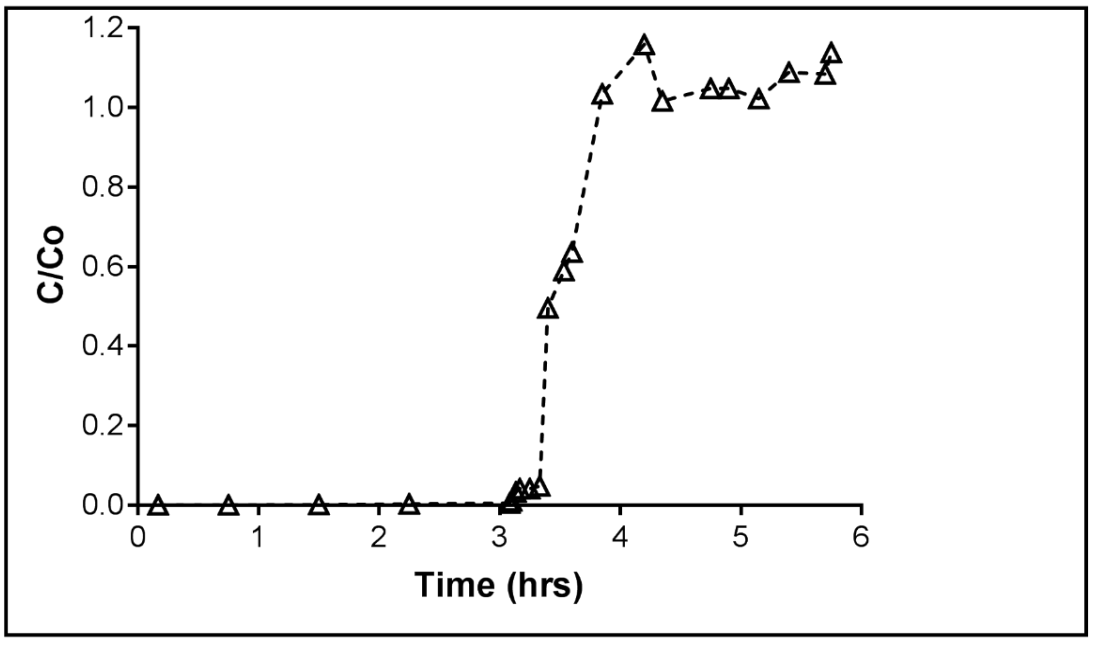

Figure 9.2: Breakthrough curve of lead ion adsorption based on time, lead ion concentration 50 mg/L; flow rate 0.5mL/min; at 21°C, loading capacity 2g; particle size 2mm; column height 9.5cm.

A steep curve, indicating the breakthrough point, was observed at a bed volume of 40mL and at approximately 3.5hrs. An increased flow rate will reduce the adsorption capacity due to more limited interaction between the loofa and lead ions. On the other hand, a decrease in the inlet concentration will lead to an extended breakthrough time, thereby allowing the adsorption of a higher volume of lead ions by the loofa (Chowdhury *et al*., 2013; Chung *et al*., 2015).

9.3.2 Desorption

Figure 9.3 shows the time taken for desorption of lead ions, from the lead-loaded loofa, using 0.1M HCl as eluent.

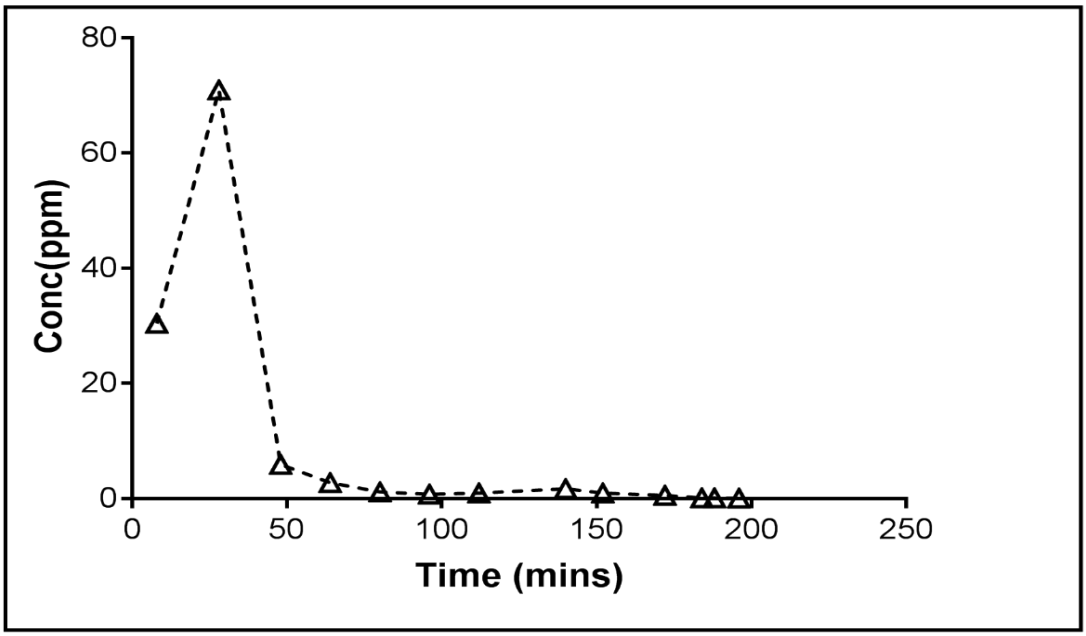

Figure 9.3: Desorption curve of lead ions from loofa based on time, 0.1M HCl; flow rate 0.5mL/min; at 21^{o}C, loading capacity 2g; column height 9.5cm.

Complete desorption is shown to occur after 65mins with a rapid desorption rate of less than 50mins.

9.3.3 Scale-up procedure

The scale-up of the fixed bed column data determines the design of a column (pilot-scale) for the dynamic analysis of removal of lead ions from aqueous solution by loofa. Parameters obtained from the experiments will enable the design of a pilot plant (Okewale *et al*., 2015; Abdolali *et al*., 2017). With a flow rate of 0.5mL/min (0.5cm^3/min) and column diameter of 2cm, the filtration rate was calculated (equation 23) to be 0.16cm/min. Using equation (25) the area of the packed column can be calculated by substituting the same filtration rate as obtained from a laboratory scale to a pilot plant.

Using the same filtration rate, Empty bed contact time (EBCT) and packed bed column, equations (23) – (33) were utilised to obtain the results as shown in table 9.2. Table 9.1 shows the experimental parameters used to calculate the dimensions required for the scale –up process.

Table 9.1: Set laboratory and pilot scale parameters

	Laboratory scale	Pilot scale
Flow rate (cm^3/min)	0.5	**12**
Diameter (cm)	2	Refer to table 9.2
Volume of packed column (cm^3)	12	Refer to table 9.2
Filtration rate (cm/min)	0.16	0.16
Column height(cm)	9.5	Refer to table 9.2
Bed height(cm)	5	5

Table 9.2: Calculated parameters of the column for scale up of the pilot plant for lead sorption

Diameter (cm)	9.8
EBCT (mins)	86
Height (cm)	13.7
Volume of packed column (cm^3)	1032
Total volume capacity (cm^3)	207000
Mass Transfer Zone (MTZ)(cm)	1.5
Area of the packed column(cm^2)	75.4
Mass of adsorbent in column (g)	41.3

Table 9.2 gives the calculated values to be used in a scale up design for lead adsorption.

9.3.4 Column design conditions

The same filtration rate, which is the amount of metal ions solution pumped downward through the loofa column per unit time, as the laboratory scale applies to the column design. The EBCT obtained from the laboratory scale applies to the column dimensions as well. The fraction of volume capacity left unused is calculated to be 36.8%.

9.3.5 Modeling

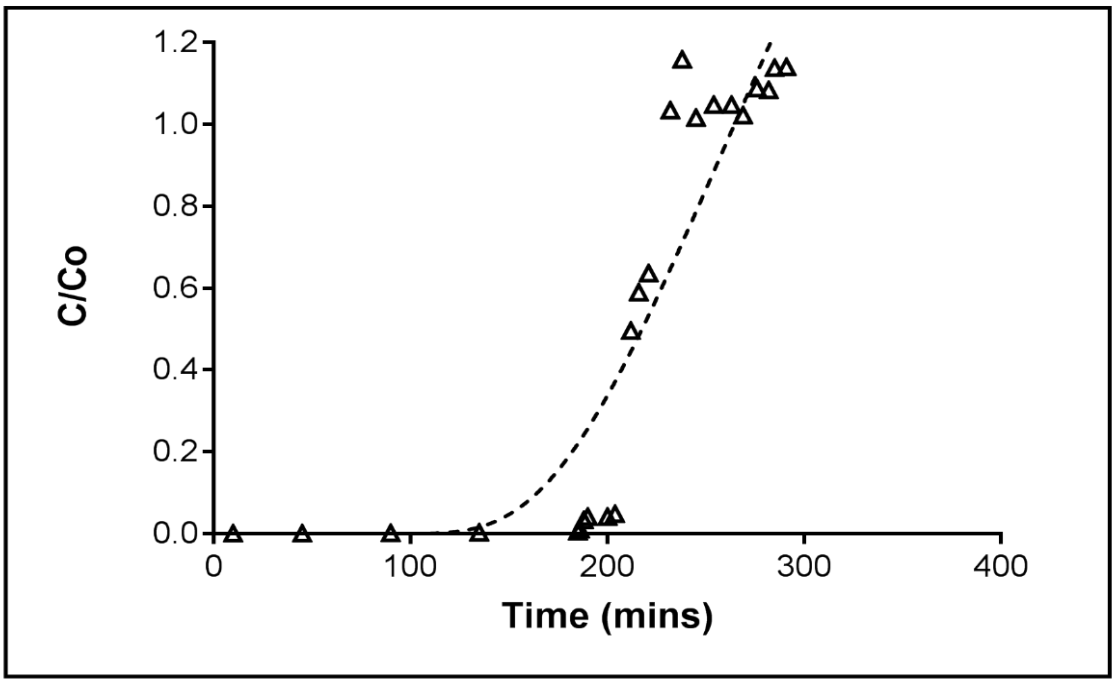

Figure 9.4: Thomas model of a fixed bed column adsorption of lead ions; lead ion concentration 50 mg/L; flow rate 0.5mL/min; at 21^{o}C, loading capacity 2g; column height 9cm, total volume 600ml. Thomas model fit is shown by the dashed line.

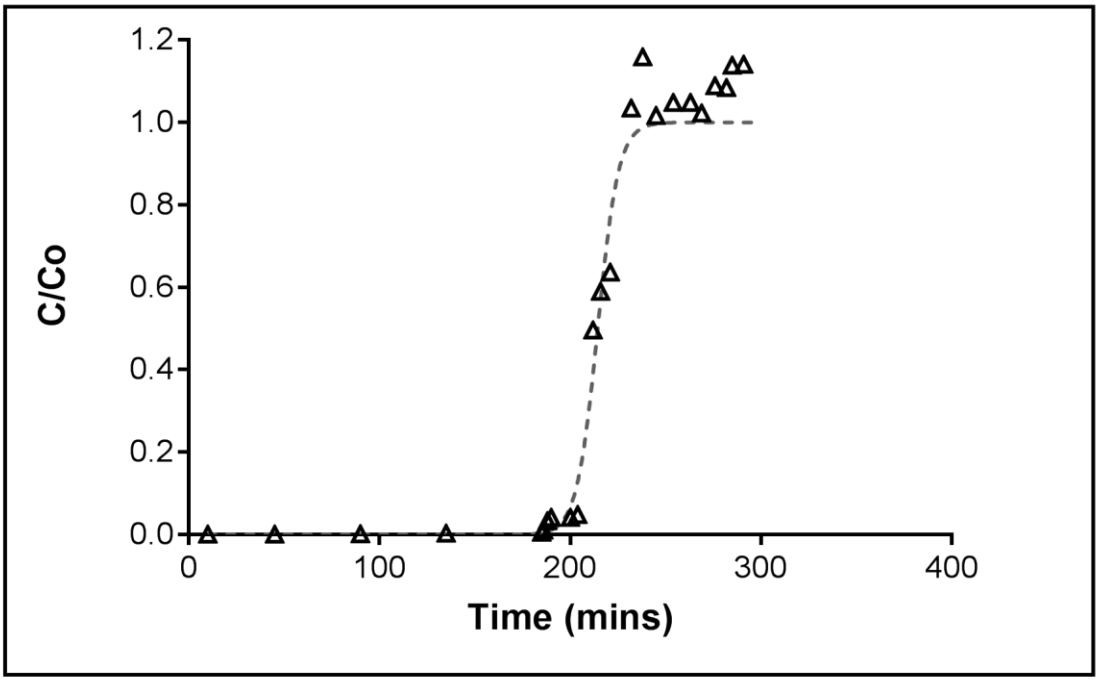

Figure 9.5: Yoon-Nelson model of a fixed bed column adsorption of lead ions; lead ion concentration 50 mg/L; flow rate 0.5mL/min; at 21^{o}C, loading capacity 2g; column height 9cm, total volume 600ml. Yoon-Nelson model fit is shown by the dashed line.

The Thomas model (Figure 9.4) was used to define part of the dynamic behaviour of the packed bed column. Within the range of 0 – 0.5 breakthrough, the Thomas model was not a good fit (R^2 = 0.64), as compared to the Yoon –Nelson model, R^2 = 0.97. This indicates that the external and internal mass diffusion steps may be rate limiting steps of the adsorption process and the 50% breakthrough data can describe the adsorption process (Abdolali *et al*., 2017). Since adsorption and saturation occur from layer to layer in the downward movement, the loofa at the bottom layer of the column may not have fully adsorbed the lead ions to optimum capacity.

9.4 Zinc

9.4.1 Adsorption

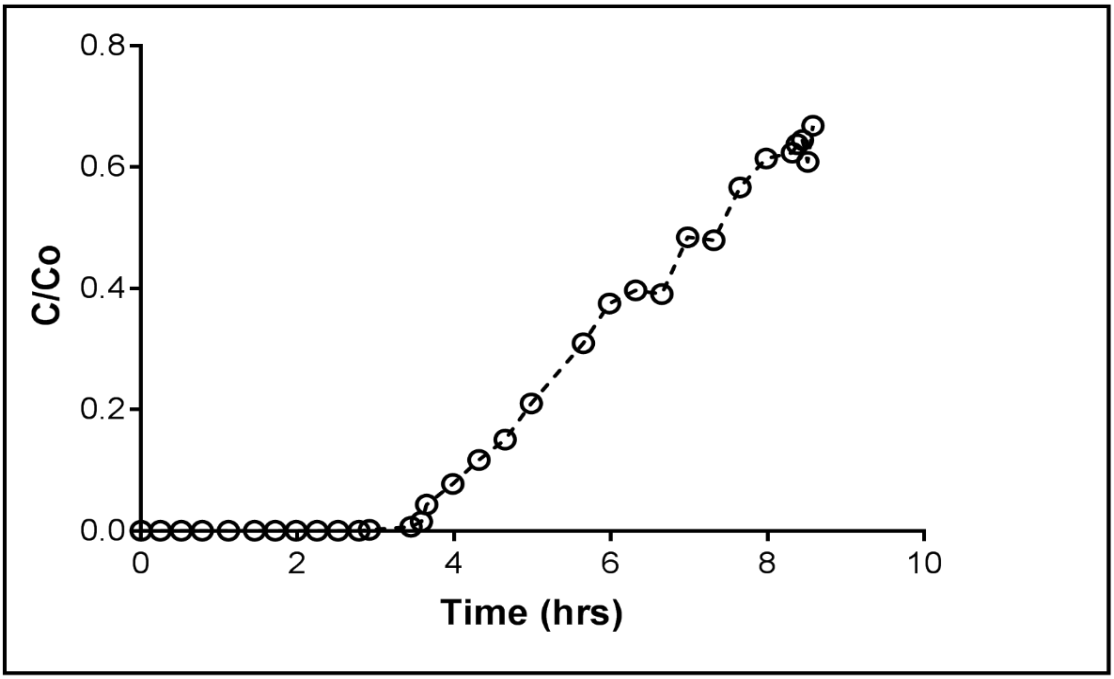

Figure 9.6: Breakthrough curve of zinc ion adsorption based on time, zinc ion concentration 20 mg/L; flow rate 0.5mL/min; at 21^{o}C, loading capacity 2g; particle size 2mm; column height 9.5cm.

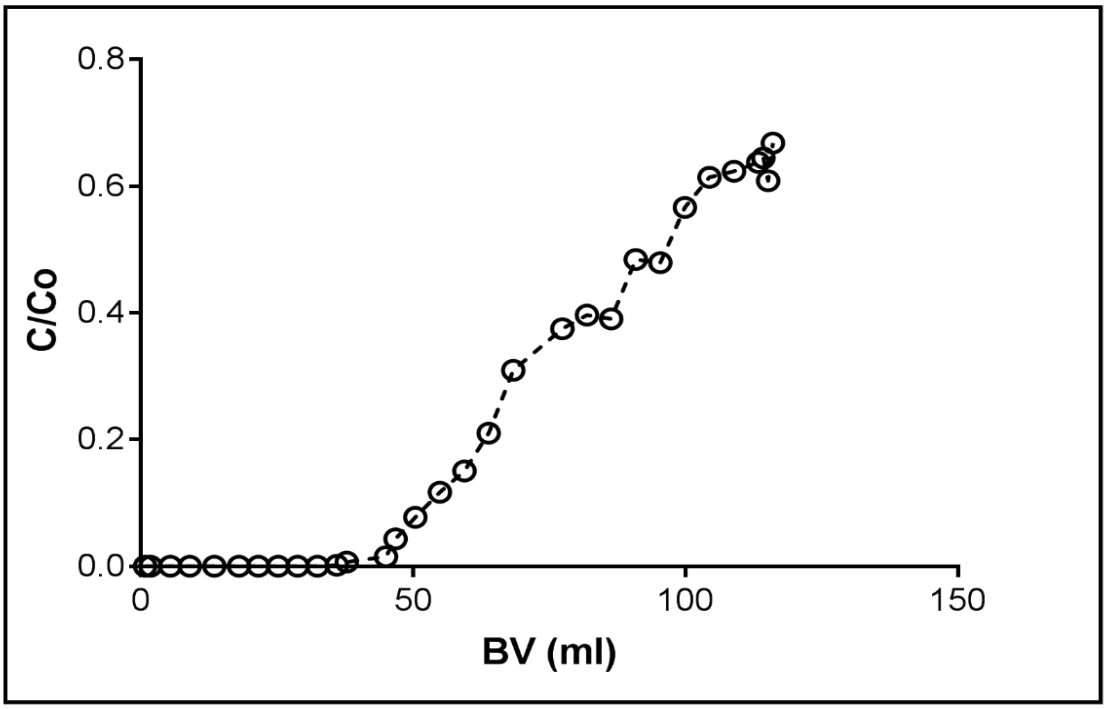

Figure 9.7: Breakthrough curve of zinc ion adsorption based on time, zinc ion concentration 20 mg/L; flow rate 0.5mL/min; at 21^{o}C, loading capacity 2g; particle size 2mm; column height 9.5cm.

9.4.2 Desorption (20mg/L)

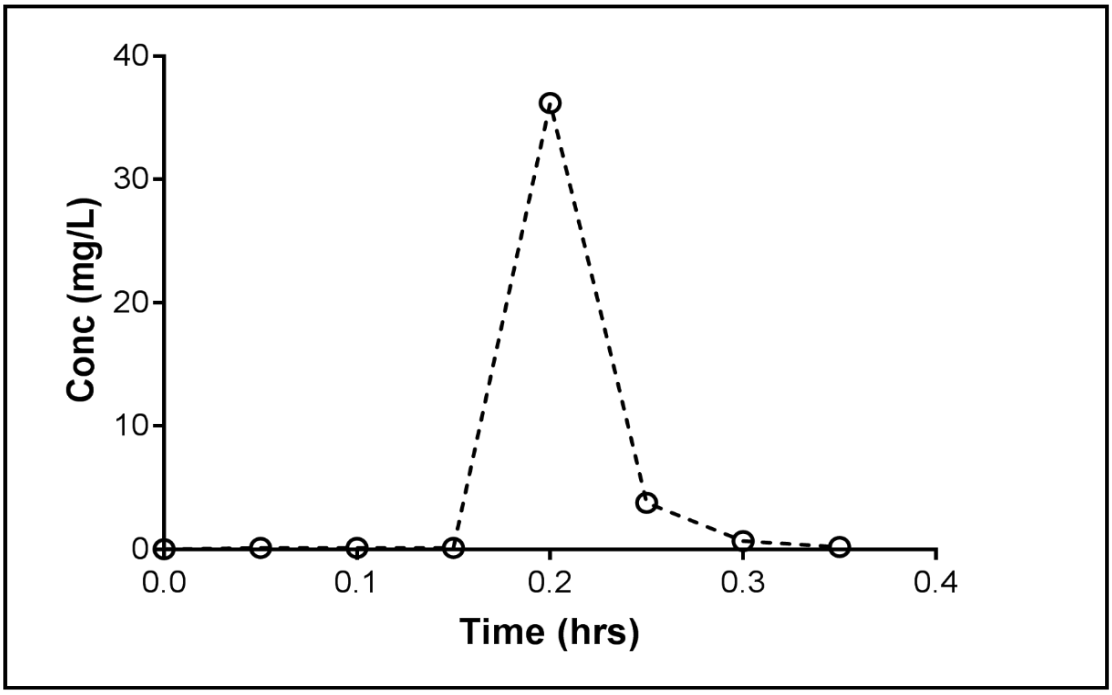

Figure 9.8: Desorption curve of zinc ions from loofa based on time, 0.1M HCl; flow rate 0.5mL/min, zinc ion concentration 20 mg/L; at 21^{o}C, loading capacity 2g; column height 9.5cm.

Figures 9.6 & 9.7 show that the column capacity, for zinc adsorption under the experimental parameters is 3.8hrs. As shown in Figure 9.6, the time required to reach 50% breakthrough is approximately 7 hrs. A breakthrough point was not reached at the initial concentration of 20mg/L. Therefore, a higher concentration of zinc ions can be adsorbed by the loofa material since saturation had not been attained. The desorption rate is rapid and occurs within 20mins of passing the eluent through the column at approximately 2.5BV. 53mL is the total volume required to elute the zinc ions loaded on the loofa. The scale up procedure for adsorption of zinc differs from the lead uptake parameters as shown in Table 9.3.

9.4.3 Scale up procedure

Table 9.3: Calculated parameters of the column for scale up of the pilot plant (Zinc 20mg/L)

EBCT (mins)	94
Height (cm)	14.95
Volume of packed column (cm^3)	1128
Mass of adsorbent in column (g)	45.12

The reduced inlet concentration of 20mg/L as compared to lead shows a higher breakthrough time and increased bed volume required to reach the breakthrough point. This is as a result of the reduced mass transfer flux of zinc ions from bulk solution to the adsorbent surface due to a weaker driving force (Nwabanne & Igbokwe, 2012). The maximum adsorption capacity (q_{max}), obtained from batch experimental results of zinc ions is lower than that of lead ions therefore, under the same experimental column conditions (loofa dosage, flow rate etc.), a higher inlet concentration of zinc can be adsorbed by the loofa before saturation is reached. Increased inlet concentrations of zinc were analysed (see below). Table 9.3 gives the calculated values of the scale–up process for zinc adsorption at 20mg/L initial concentration.

9.4.4 Modeling

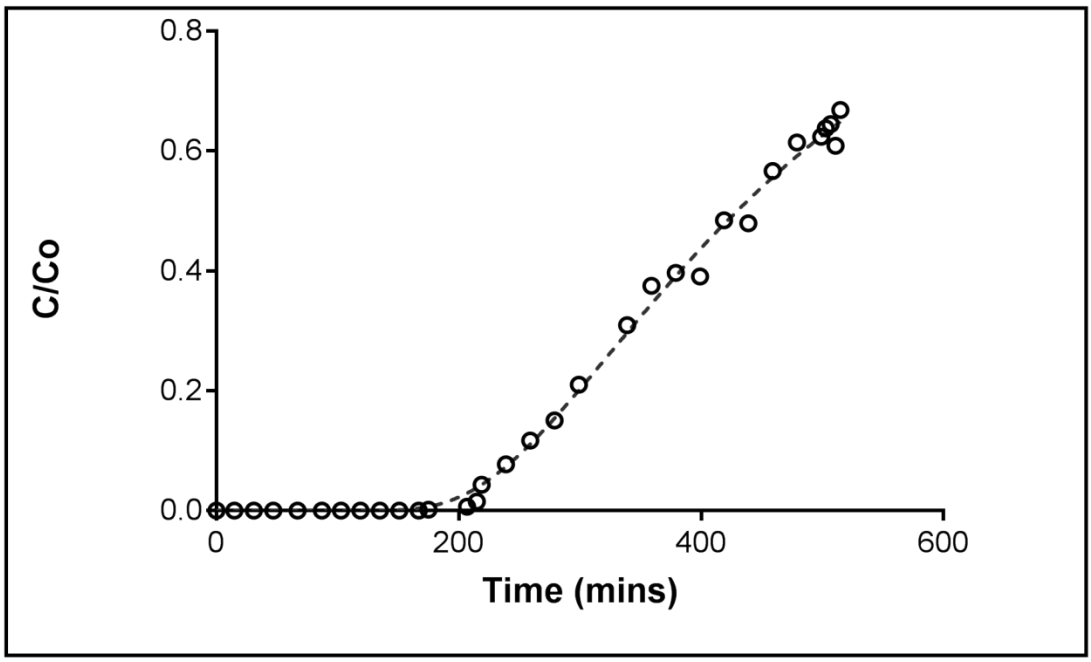

Figure 9.9: Thomas model of a fixed bed column adsorption of zinc ions; lead ion concentration 20 mg/L; flow rate 0.5mL/min; at 21^{o}C, loading capacity 2g; column height 9.5cm, total volume 600ml. Thomas model fit is shown by the dashed line.

The Thomas model (Figure 9.9) shows a good fit for the zinc adsorption data, R^2= 0.90. This indicates that external and internal diffusion are not the rate limiting step. The rate of adsorption is attributed to the surface reaction between the loofa and zinc ions. The Yoon model shows an R^2 of 0.63 (linear regression) and no correlation fit. The initial concentration of zinc was increased to 50 & 100mg/L and the adsorption desorption process was repeated.

9.4.5 Adsorption (50mg/L)

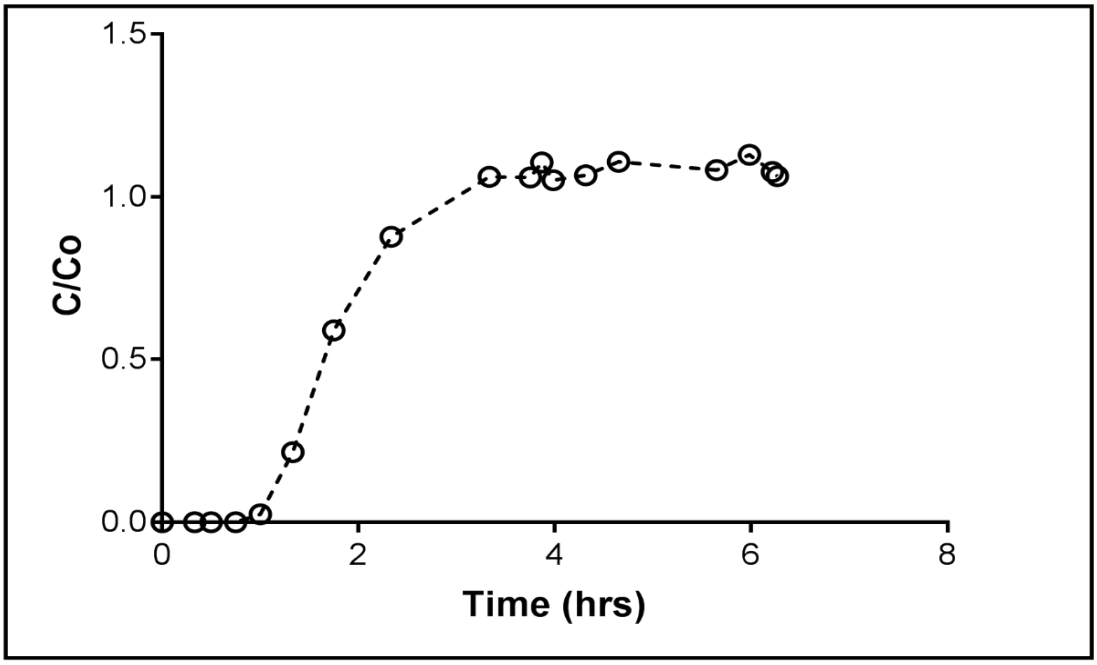

Figure 9.10: Breakthrough curve of zinc ion adsorption based on time, zinc ion concentration 50 mg/L; flow rate 0.5mL/min; at 21^{o}C, loading capacity 2g; particle size 2mm; column height 9cm.

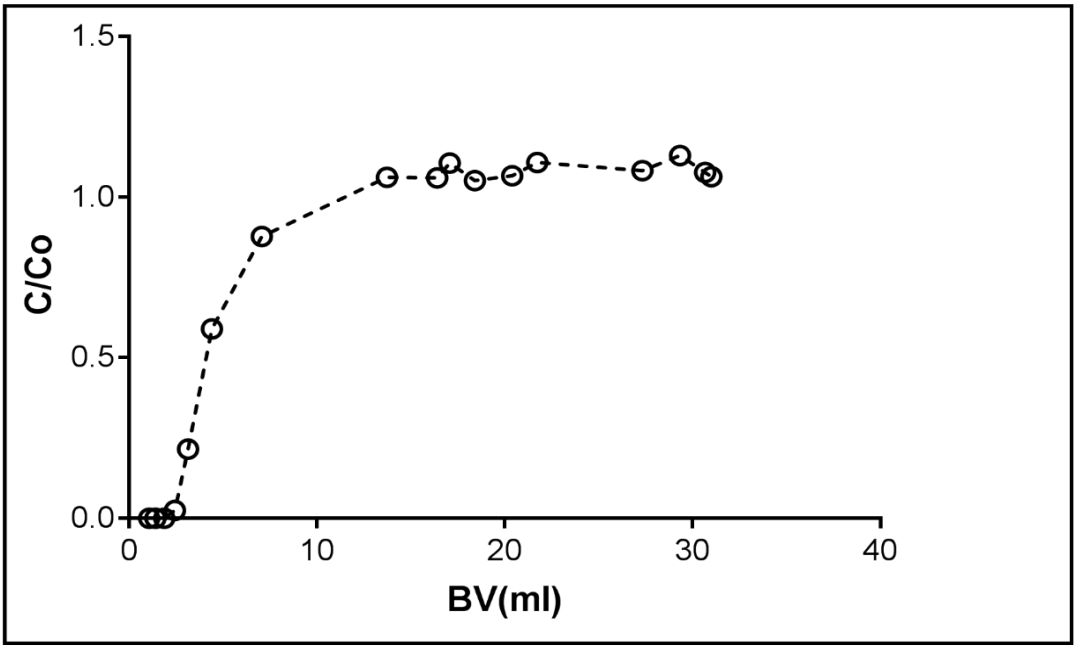

Figure 9.11: Breakthrough curve of zinc ion adsorption based on time, zinc ion concentration 50 mg/L; flow rate 0.5mL/min; at 21^{o}C, loading capacity 2g; particle size 2mm; column height 9cm

9.4.6 Desorption (50mg/L)

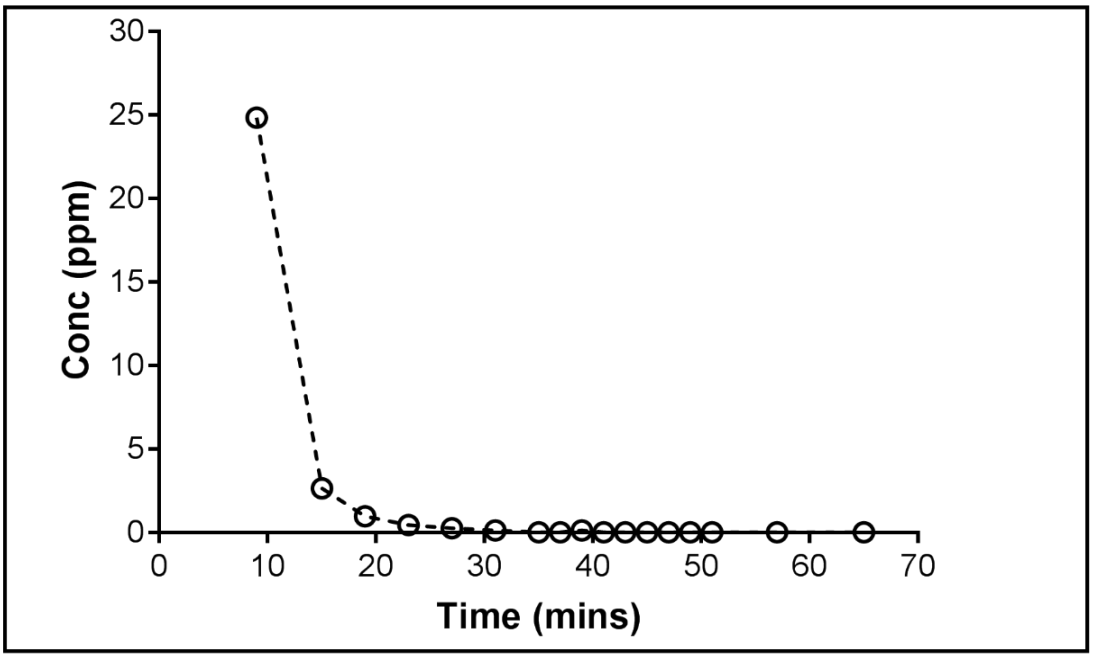

Figure 9.12: Desorption curve of zinc ions from loofa over on time, 50mg/L 0.1M HCl; flow rate 0.5mL/min; at 21^{o}C, loading capacity 2g; column height 9cm.

Increasing the inlet concentration of zinc to 50mg/L, it can be seen in figures 9.10 & 9.11 that the breakthrough time reduced to less than 2hrs and the BV was less than half the BV as compared to the 20mg/L concentration of zinc (Figure 9.7). Figure 9.10 & 9.11 show the breakthrough curves of zinc adsorption versus time and bed volume. The breakthrough point was at 1hr 15mins and saturation occurred at just over 2hrs. At a bed volume of 2.4ml, the breakthrough point is reached. An increase in the initial concentration leads to a decreased breakthrough time and bed volume. Therefore a faster breakthrough and saturation is observed (Chen *et al.*, 2014). Complete rapid desorption occurred at 27 mins (Figure 9.12).

9.4.7 Models

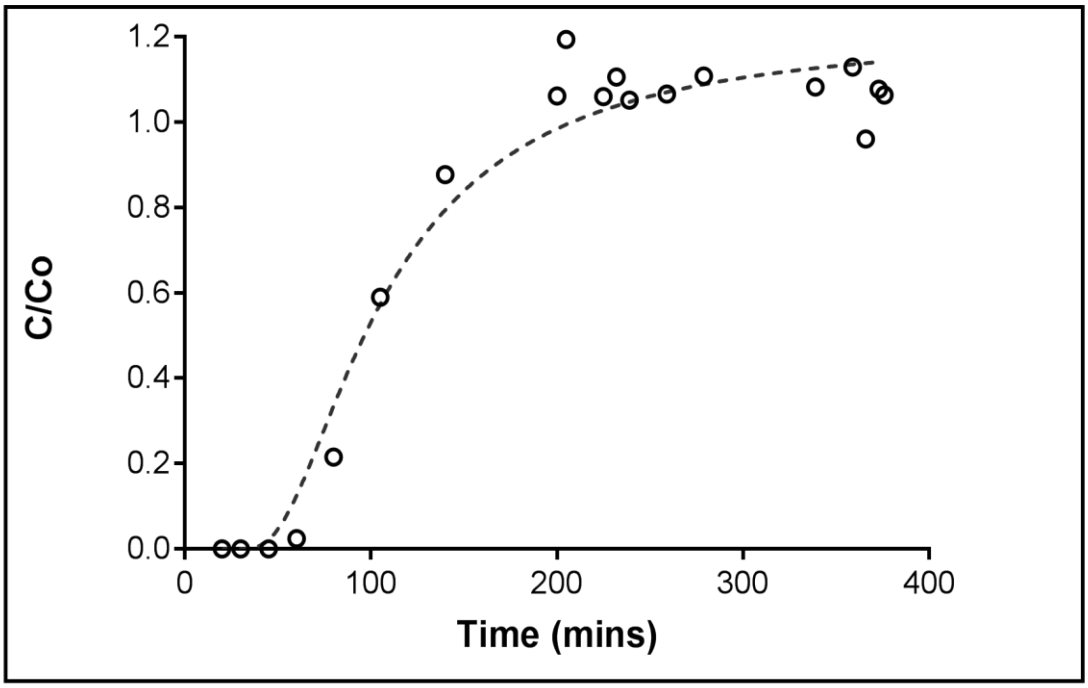

Figure 9.13: Thomas model of a fixed bed column adsorption of zinc ions; lead ion concentration 50 mg/L; flow rate 0.5mL/min; at 21°C, loading capacity 2g; column height 9cm, total volume 600ml. Thomas model fit is shown by the dashed line.

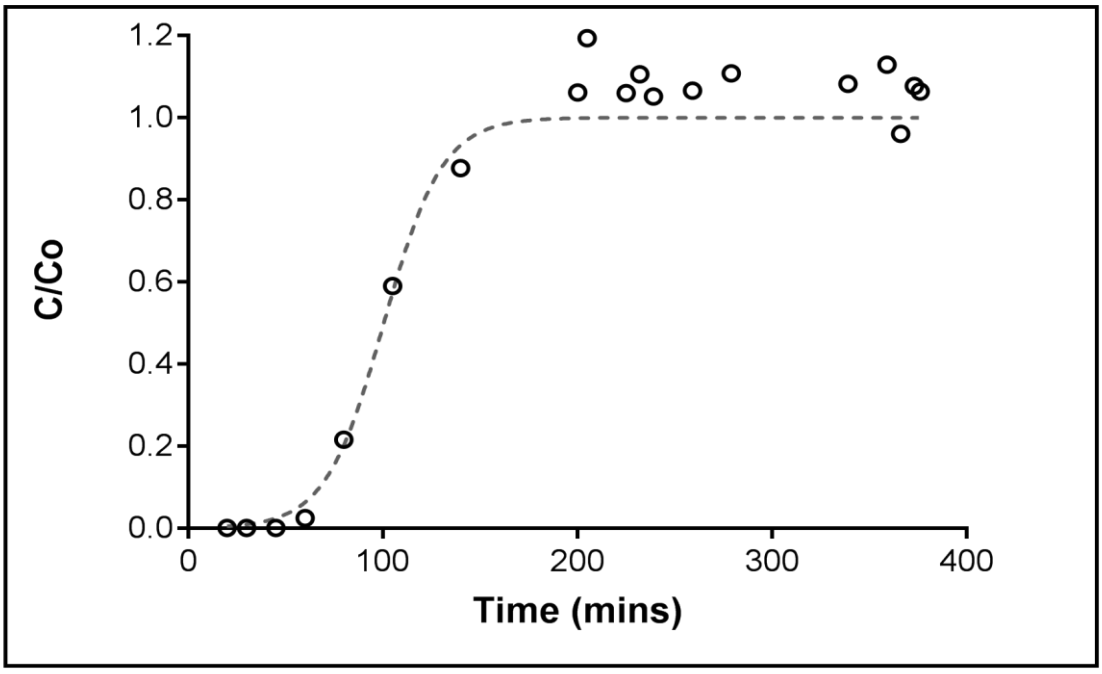

Figure 9.14: Yoon-Nelson model of a fixed bed column adsorption of zinc ions; zinc ion concentration 50 mg/L; flow rate 0.5mL/min; at 21°C, loading capacity 2g; column height 9cm, total volume 600ml. Yoon-Nelson model fit is shown by the dashed line.

Both models, Thomas and Yoon-Nelson, show a good fit in explaining the adsorption process of the zinc ions. The Yoon-Nelson model shows a better fit (R^2 = 0.970) than Thomas model (R^2= 0.726) and best describes the adsorption process by the 50% breakthrough saturation point data (Long *et al*., 2014). This data is derived under the set conditions of flow rate, influent concentration and bed height, and is the calculated time required to reach the 50% breakthrough point.

9.4.8 Adsorption (100mg/L)

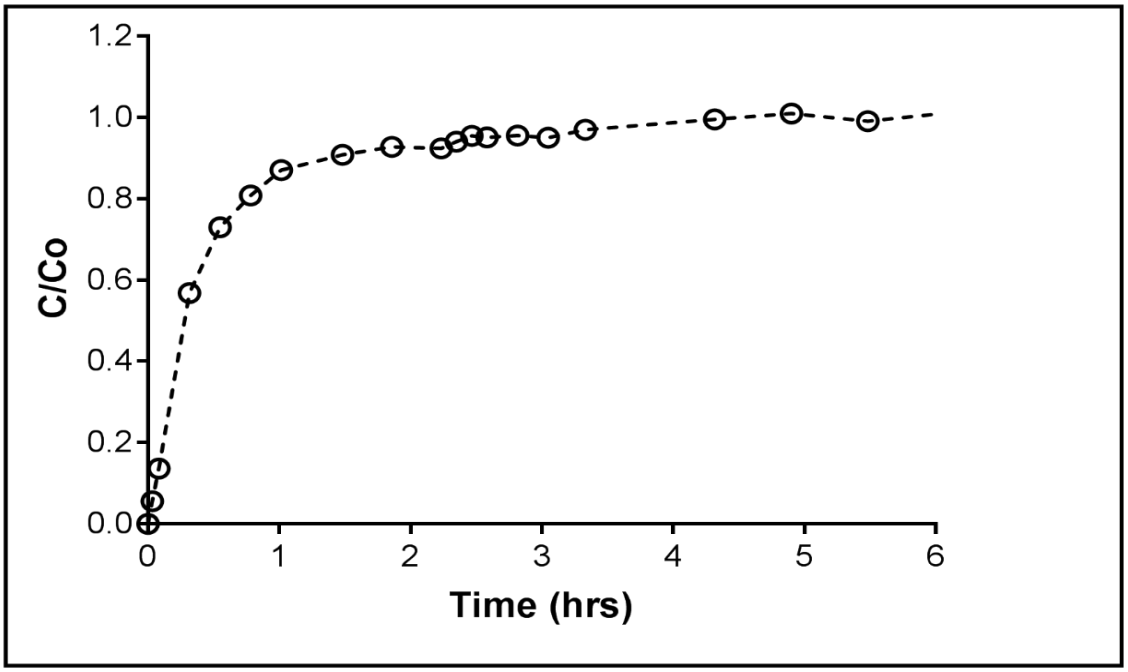

Figure 9.15: Adsorption curve of zinc ion adsorption over on time, zinc ion concentration 100 mg/L; flow rate 0.5mL/min; at 21^{o}C, loading capacity 2g; particle size 2mm; column height 9cm.

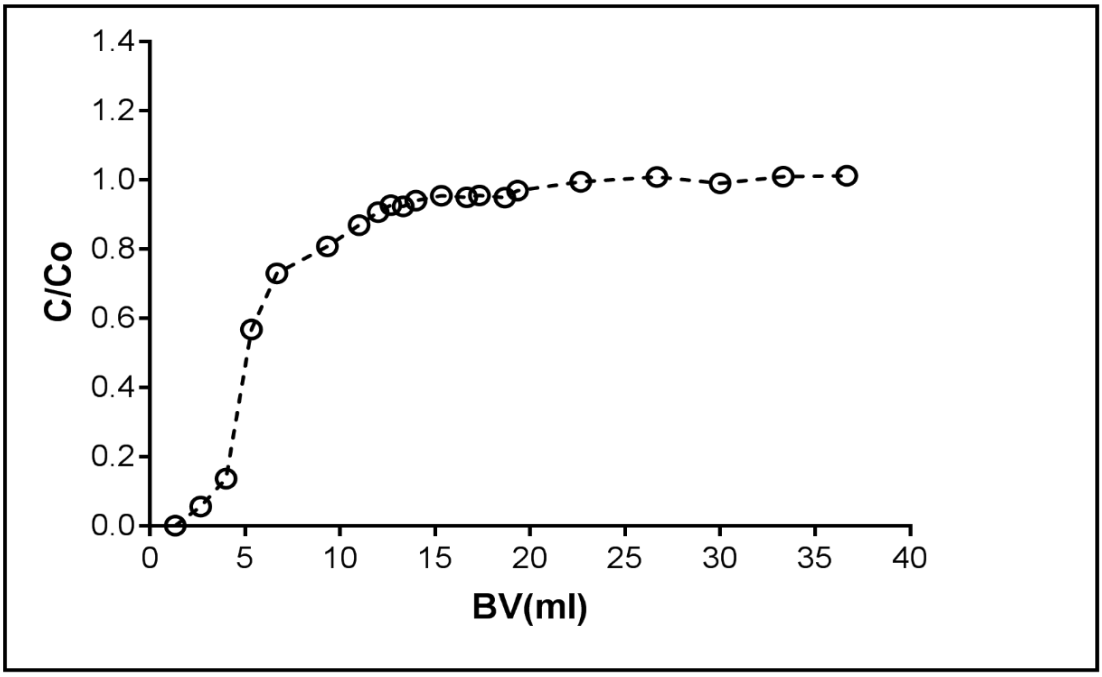

Figure 9.16: Breakthrough curve of zinc ion adsorption based on time, zinc ion concentration 100 mg/L; flow rate 0.5mL/min; at 21^{o}C, loading capacity 2g; particle size 2mm; column height 9 cm.

9.4.9 Desorption (100mg/L)

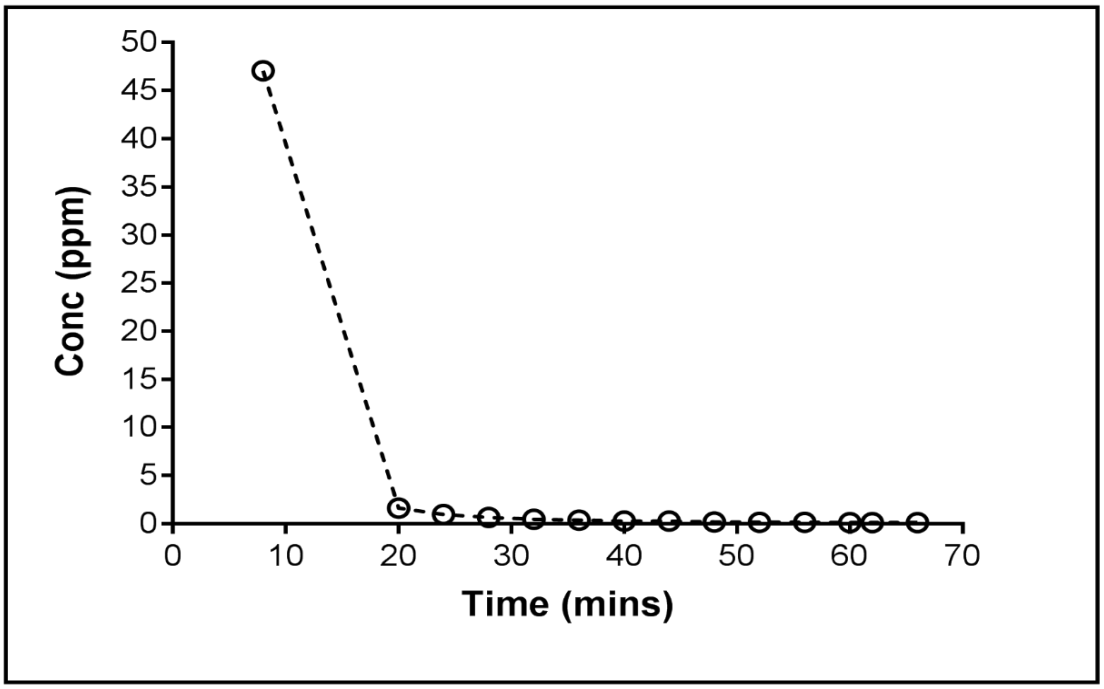

Figure 9.17: Desorption curve of zinc ions from loofa over on time, 0.1M HCl; zinc ion concentration 100mg/L; flow rate 0.5mL/min; at 21^{o}C, loading capacity 2g; column height 9.5cm.

The plot of breakthrough curves as related to time and bed volume for 100mg/L zinc are shown in Figure 9.15 & 9.16. The breakthrough point was less than an hour and at a bed volume of less than 5mL. An increase in the initial concentration leads to a decreased breakthrough time and bed volume. This gives a faster breakthrough and saturation, which is explained by lower mass transfer resistance that occurs as concentration increases (Aksu & Gönen, 2004). This is further explained by the effect of initial concentration of metal ions on the adsorption process (Chen *et al*., 2014; García-Mateos *et al*., 2015; Abdolali *et al*., 2017; Burkert *et al*., 2011). Complete rapid desorption occurred in 20mins.

9.4.10 Scale-up procedure

Table 9.4: Calculated parameters of the column for scale up of the pilot plant (Zinc 100mg/L).

EBCT (mins)	74
Height (cm)	11.78
Volume of packed column (cm^3)	1110
Mass of adsorbent in column (g)	44.4

Table 9.4 shows the reduced EBCT time which corresponds with a decreased bed volume when the initial concentration of zinc is increased from 20mg/L to 100mg/L.

9.4.11 Modeling

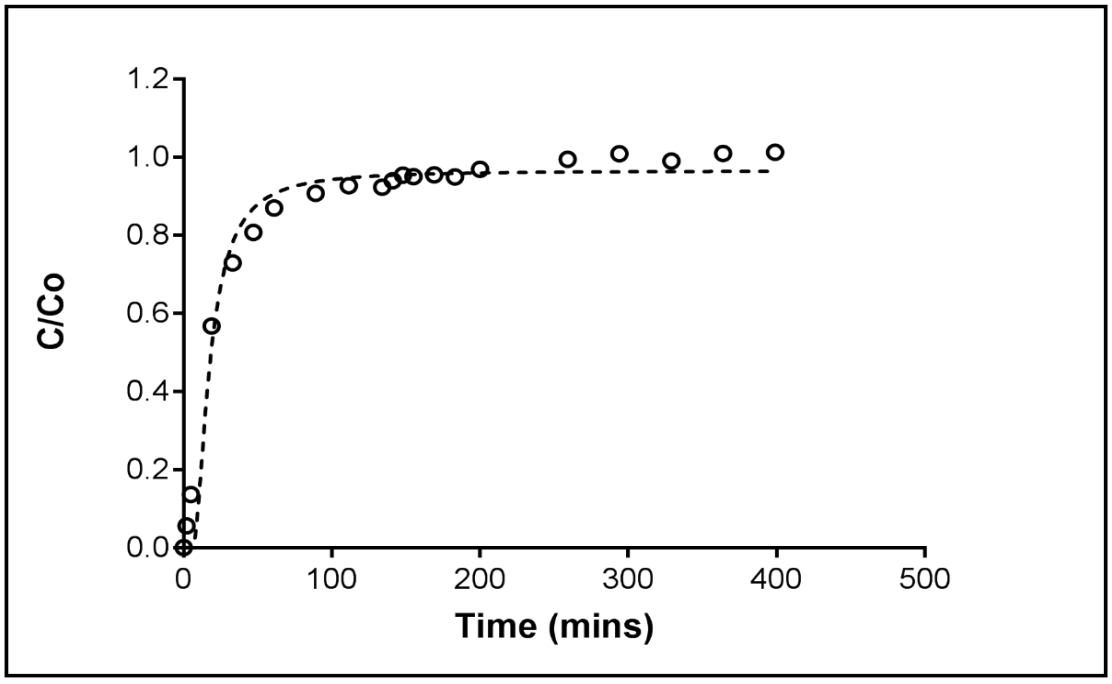

Figure 9.18: Thomas model of a fixed bed column adsorption of zinc ions; zinc ion concentration 100 mg/L; flow rate 0.5mL/min; at 21°C, loading capacity 2g; column height 9 cm, total volume 600ml. Thomas model fit is shown by the dashed line.

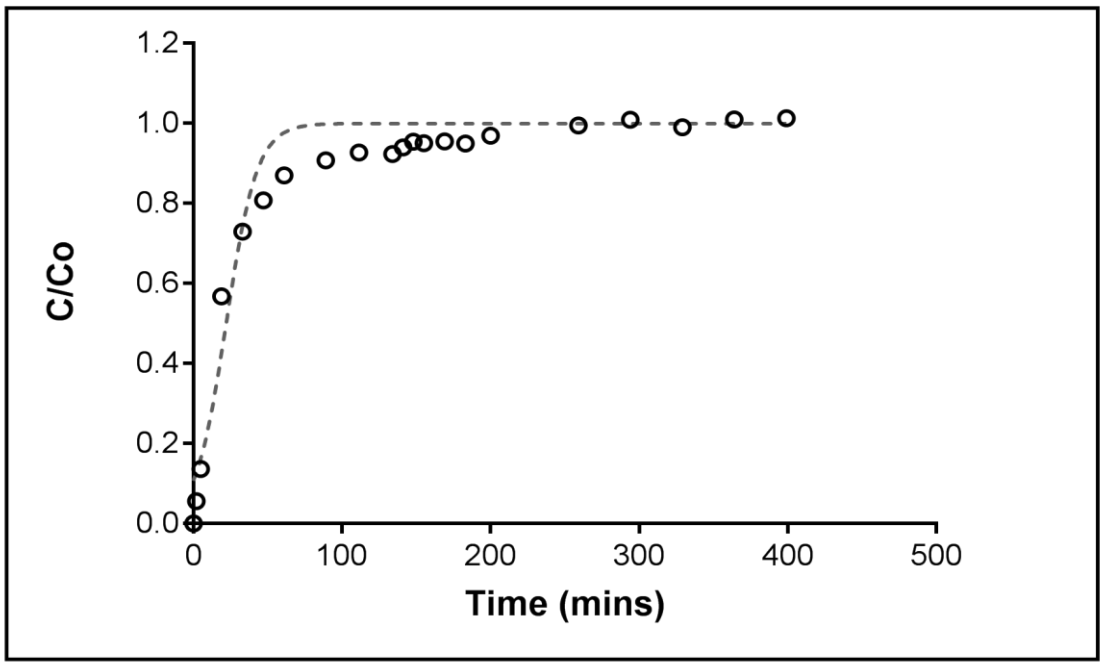

Figure 9.19: Yoon-Nelson model of a fixed bed column adsorption of zinc ions; zinc ion concentration 100 mg/L; flow rate 0.5mL/min; at 21^{o}C, loading capacity 2g; column height 9 cm, total volume 600ml. Yoon-Nelson model fit is shown by the dashed line.

The Thomas and Yoon-Nelson models (Figures 9.18 & 9.19) were used to describe the dynamic behaviour of the packed bed column experiment for the 100mg/L zinc ion adsorption. Both models show a good fit of 0.979 and 0.955. This indicates that the external and internal mass diffusion steps may not be the rate limiting steps of the adsorption process and the 50% retention breakthrough data can sufficiently describe the adsorption process (Abdolali *et al*., 2017).

9.5 Cadmium

9.5.1 Adsorption (10mg/L)

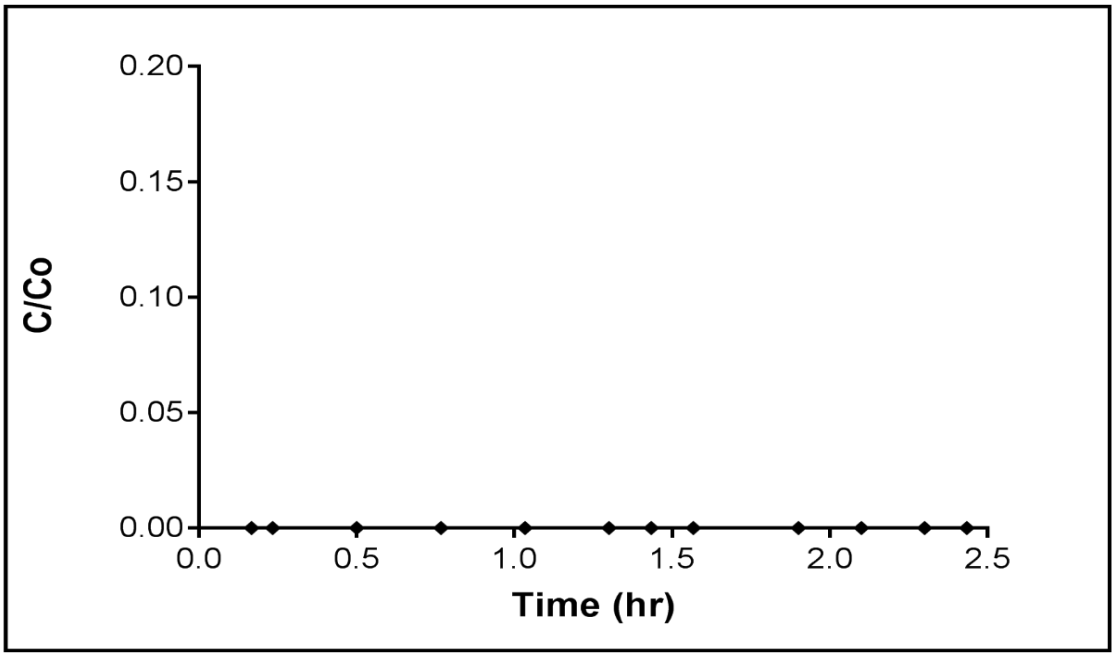

Figure 9.20: Adsorption curve of cadmium ion adsorption based on time, cadmium ion concentration 10 mg/L; flow rate 0.5mL/min; at 21^{o}C, loading capacity 2g; particle size 2mm; column height 9 cm.

9.5.2 Desorption (10mg/L)

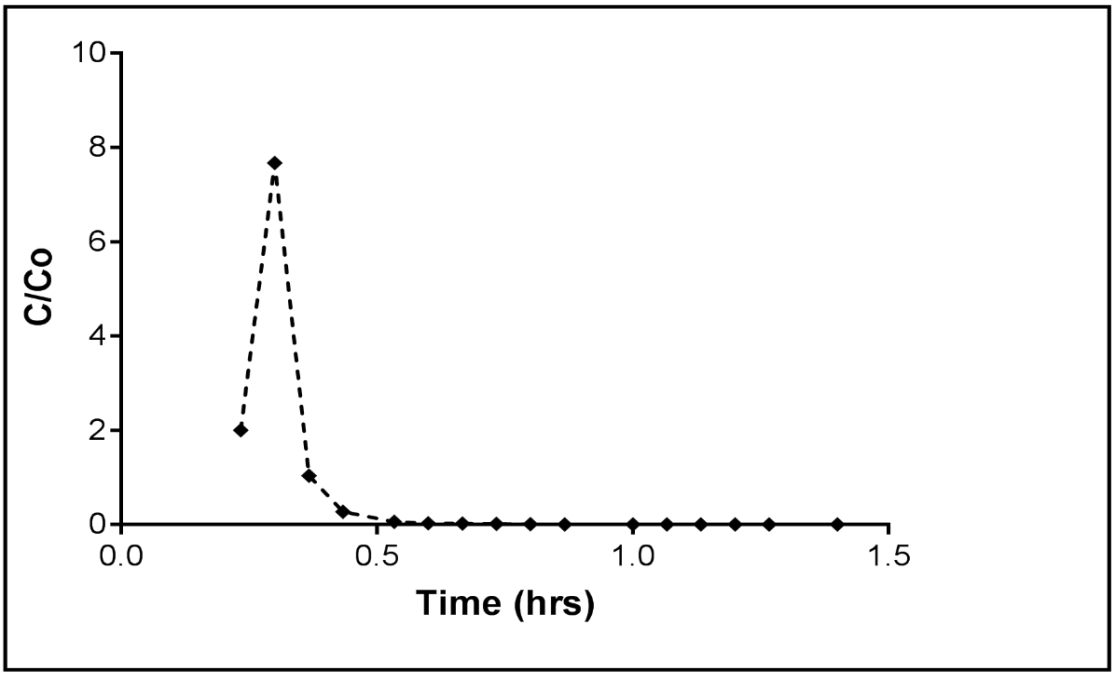

Figure 9.21: Desorption curve of cadmium ions from loofa over on time, 0.1M HCl; flow rate 0.5mL/min; at 21^{o}C, loading capacity 2g; column height 9.5cm.

At a low concentration of 10mg/L, no breakthrough point was reached for cadmium adsorption onto loofa (Figure 9.20 & 9.21). This means that saturation has not occurred and further uptake capacity of cadmium ions by the loofa is possible. Desorption of the cadmium ions adsorbed on the loofa was completed within 30mins. A higher concentration of cadmium was run under the same experimental conditions to ascertain the effect of the initial concentration and determine the breakthrough point.

9.5.3 Adsorption (50mg/L)

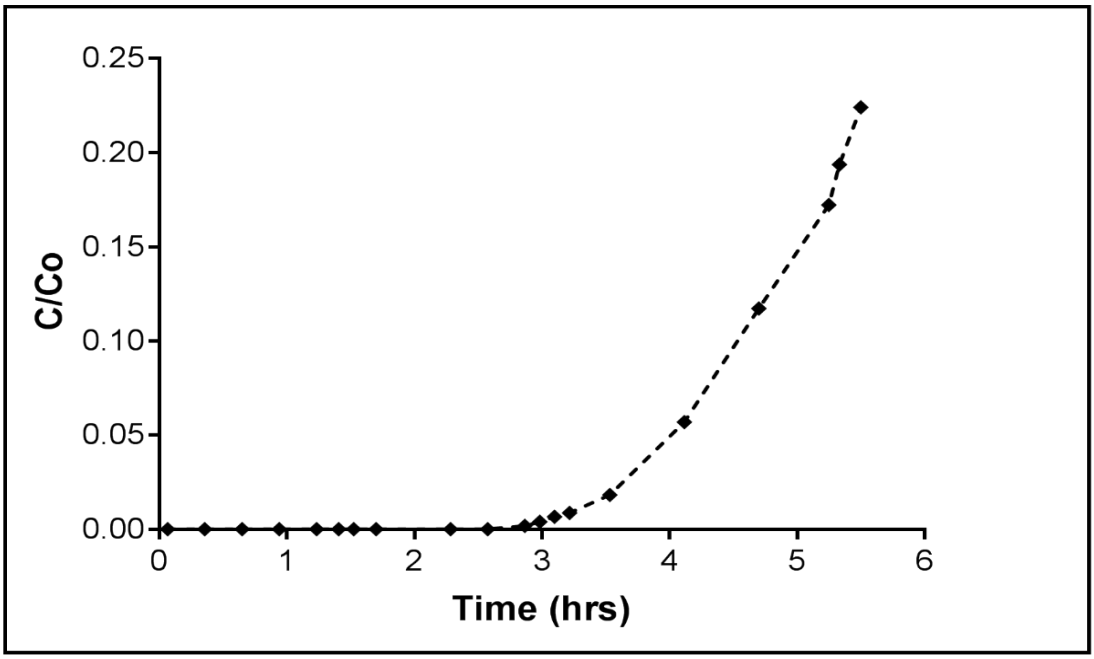

Figure 9.22: Adsorption curve of cadmium ion adsorption over on time, cadmium ion concentration 50 mg/L; flow rate 0.5mL/min; at 21^{o}C, loading capacity 2g; particle size 2mm; column height. 9cm.

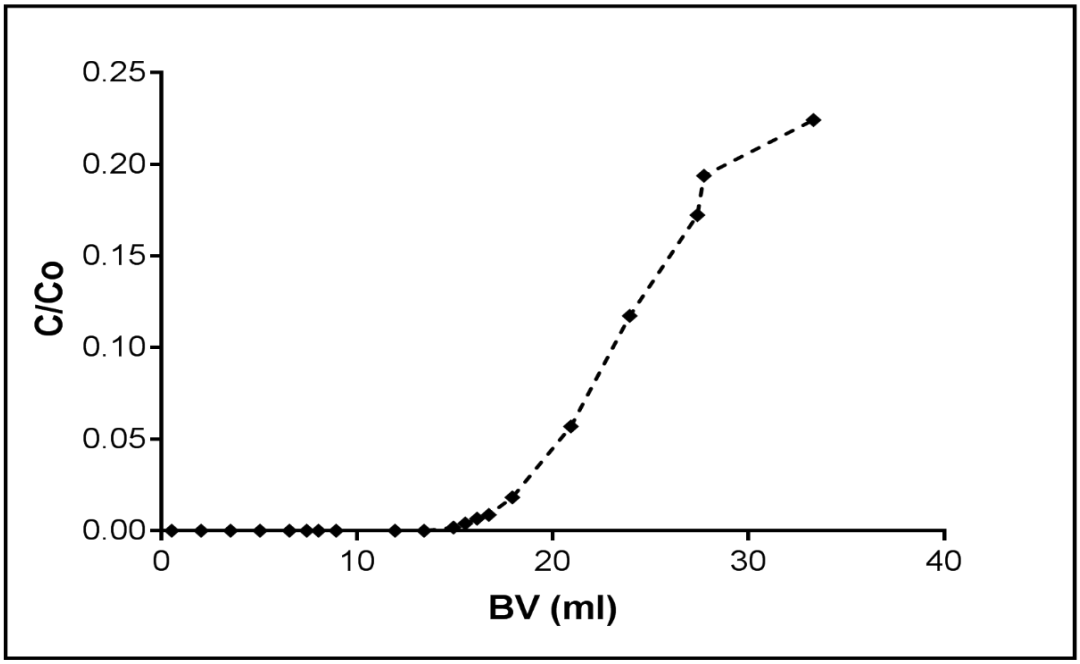

Figure 9.23: Breakthrough curve of cadmium ion adsorption based on time, cadmium ion concentration 50 mg/L; flow rate 0.5mL/min; at 21^{o}C, loading capacity 2g; particle size 2mm; column height 9cm.

9.5.4 Desorption (50mg/L)

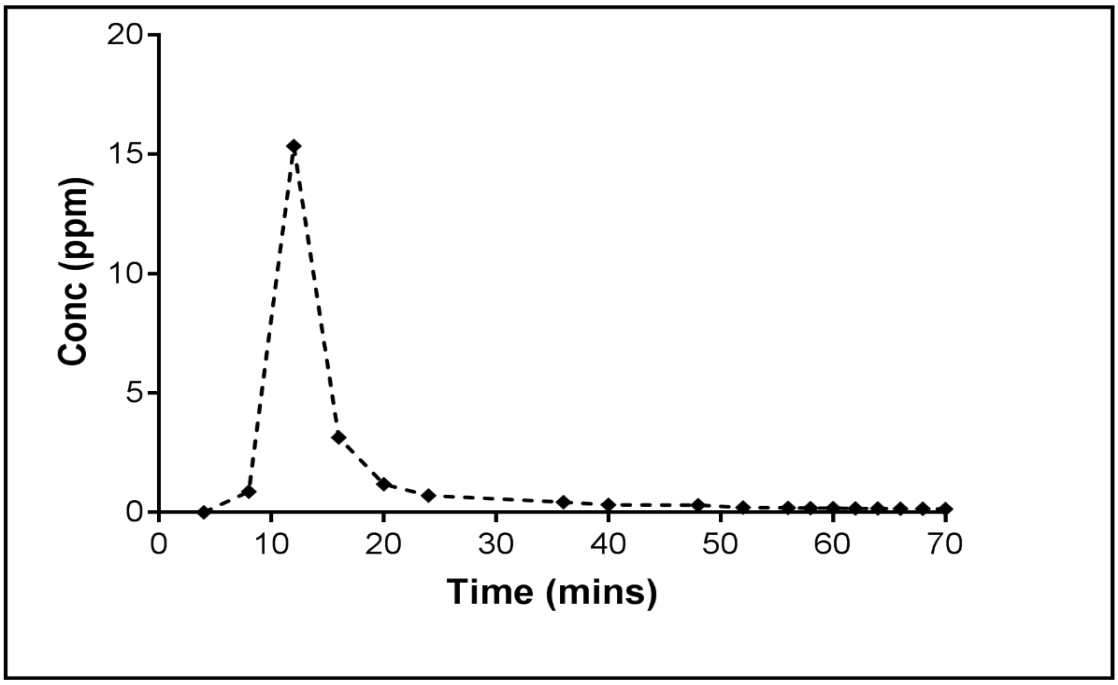

Figure 9.24: Desorption curve of cadmium ions from loofa over on time, initial cadmium ion concentration 50mg/L, 0.1M HCl; flow rate 0.5mL/min; at 21^{o}C, loading capacity 2g; column height 9cm.

Figures 9.22 & 9.23 show that a breakthrough point has been reached for the adsorption of cadmium ions when the initial concentration was increased to 50mg/L. However, a saturation point had not been obtained. The breakthrough time occurred at approximately 3hrs and at a bed volume of 16ml. Complete desorption occurred at 40mins (Figure 9.24), which is an increase on the 30 min for 10mg/L. This indicates that a higher amount of cadmium ions has been adsorbed.

9.5.5 Models

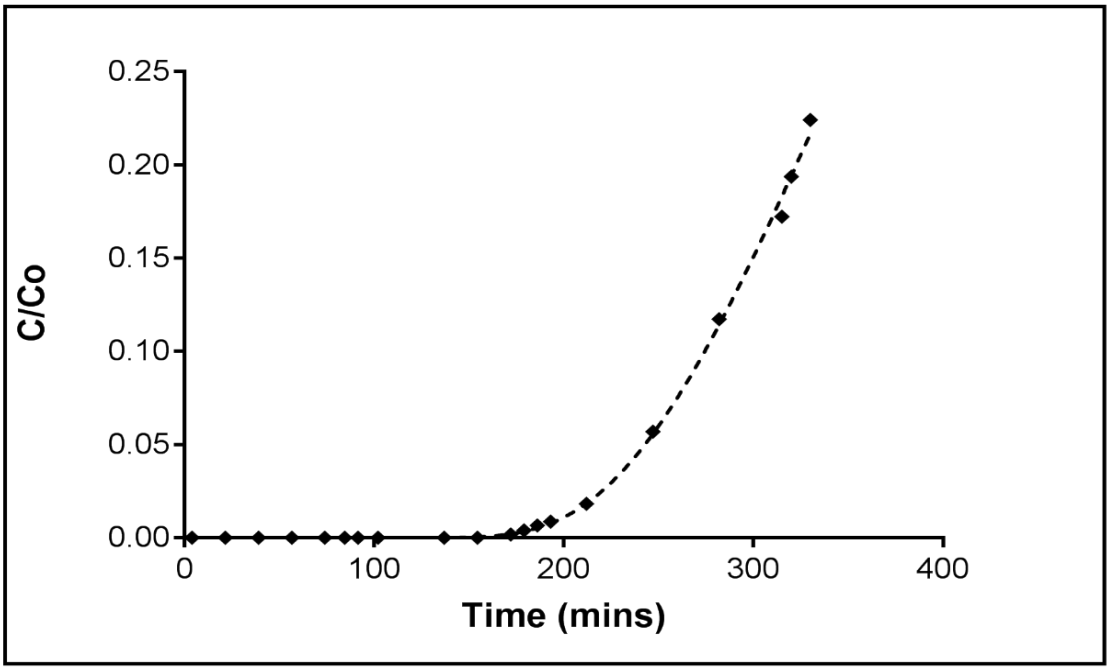

Figure 9.25: Thomas model of a fixed bed column adsorption of cadmium ions; cadmium ion concentration 50 mg/L; flow rate 0.5mL/min; at 21^{o}C, loading capacity 2g; column height 9cm, total volume 600ml. Thomas model fit is shown by the dashed line.

The Thomas model shows a fit of R^2 value of 0.673 which does not well describe the column performance of the mechanism of cadmium ion adsorption. Yoon-Nelson shows no fit (Long *et al*., 2014).

9.6 Mixed metal ions

9.6.1 Adsorption

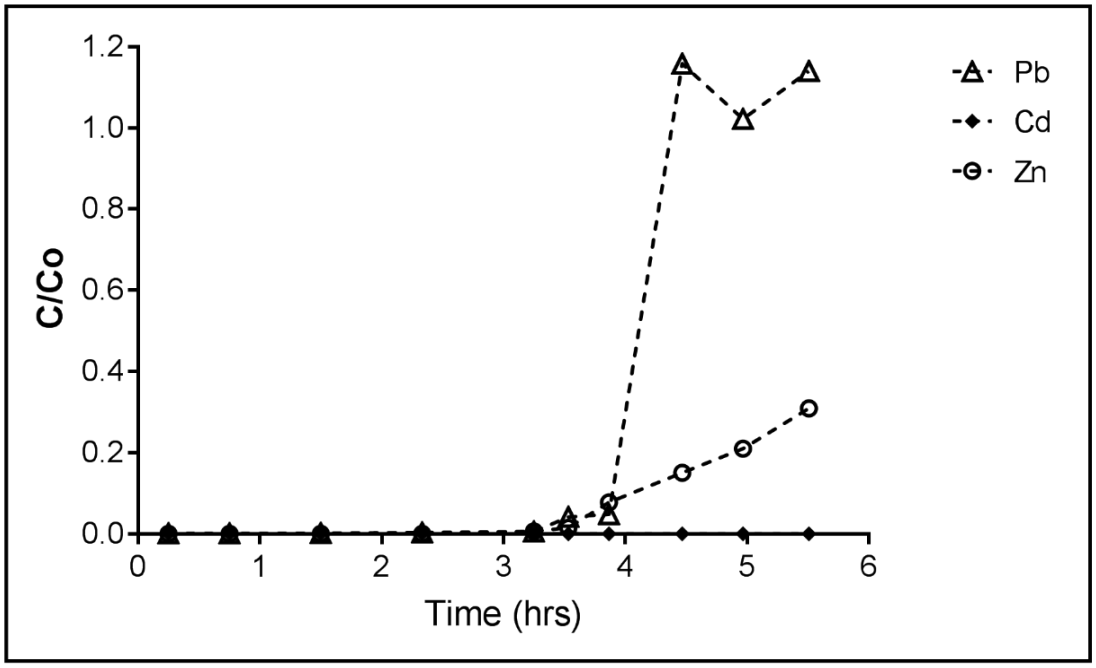

Figure 9.26: Breakthrough curve of all three metal ions adsorption over on time, Pb, Zn & Cd ion concentration (50, 20 & 10mg/L); flow rate 0.5mL/min; at 21^{o}C, loading capacity 2g; particle size 2mm; column height 9.5cm.

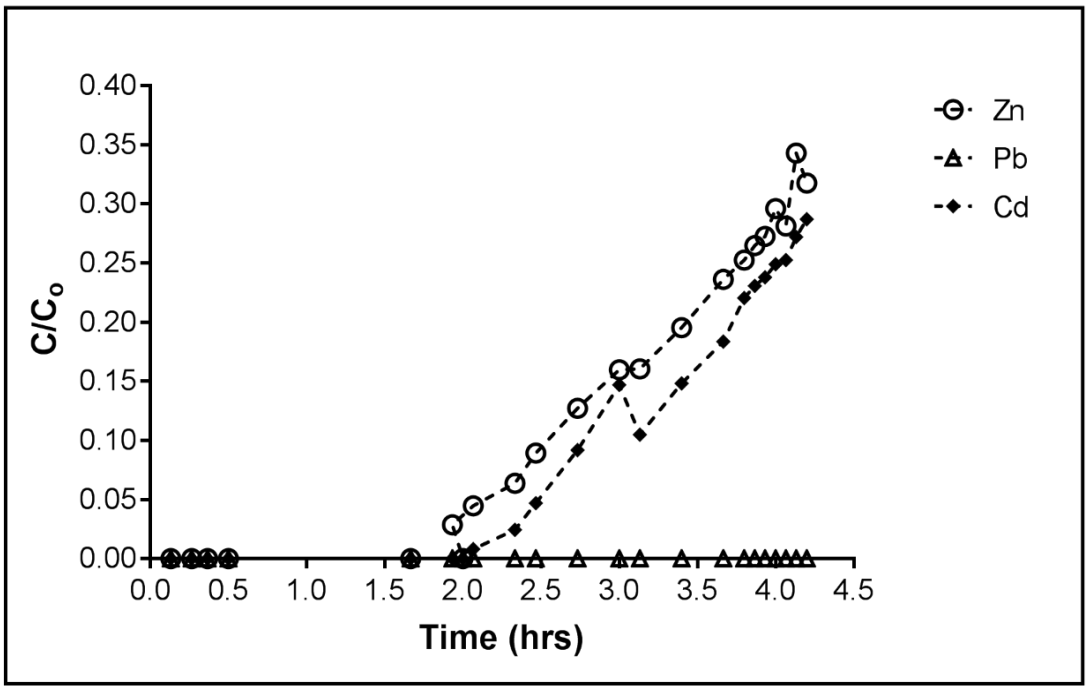

Figure 9.27: Breakthrough curve of mixed metal ions adsorption over on time, mixed metal ion concentration (ratio 2:1:1 – 50mg/L Zn, Pb & Cd); flow rate 0.5mL/min; at 21^{o}C, loading capacity 2g; particle size 2mm; column height 9 cm.

Figure 9.27 show the breakthrough point obtained over time for the mixed metal ions during the adsorption column process. Figure 9.27 shows no breakthrough point had been obtained for the lead ions in solution, while the single solution at the same concentration had a breakthrough point at 3.5hrs. After 4.2hrs, it is observed that lead ions were still not detected in the mixed solution. For the zinc adsorption, the breakthrough point time interval had increased to 1.6hrs (by 37.5% as compared to the single solution at the same concentration). Cadmium, on other hand, showed decrease to 2hrs. The lead adsorption capacity was the highest compared to zinc and cadmium ions due to a better affinity of the lead ions to the loofa surface (Abdolali *et al*., 2017).

9.6.2 Desorption

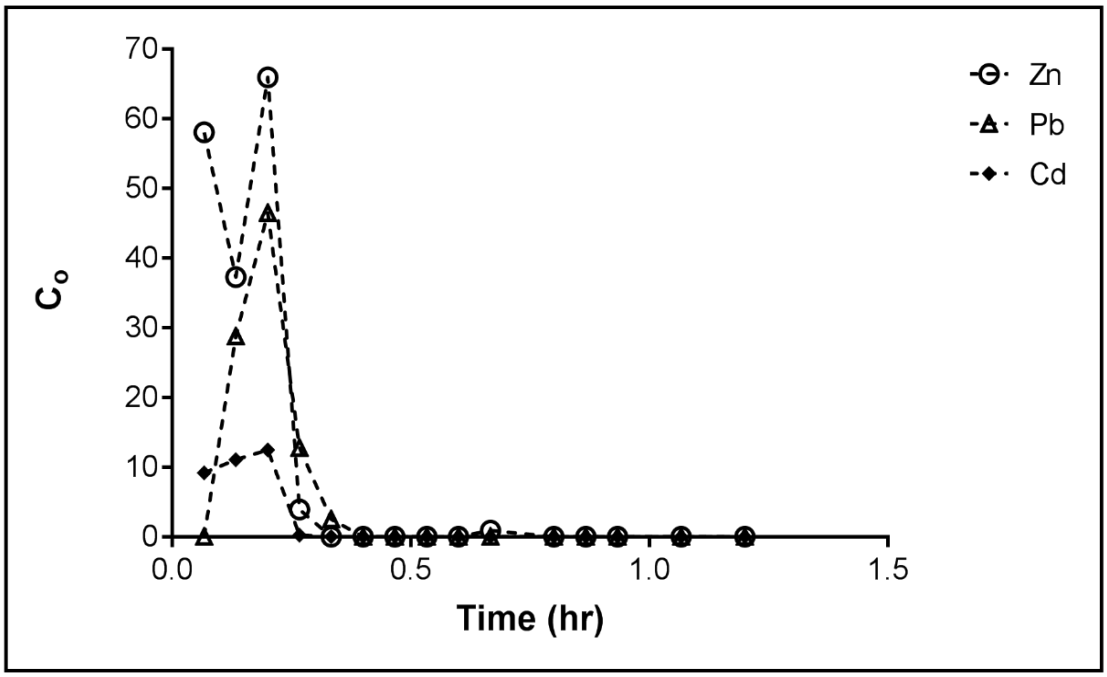

Figure 9.28: Desorption curve of mixed metal ions over time, mixed metal ion concentration (ratio 2:1:1 – Zn, Pb & Cd); flow rate 0.5mL/min; at 21^{o}C, loading capacity 2g; particle size 2mm; column height 9 cm.

Complete desorption occurs for all three metal ions in less than 30mins (Figure 9.28). No actual preference was observed for any metal in the desorption process.

9.6.3 Models

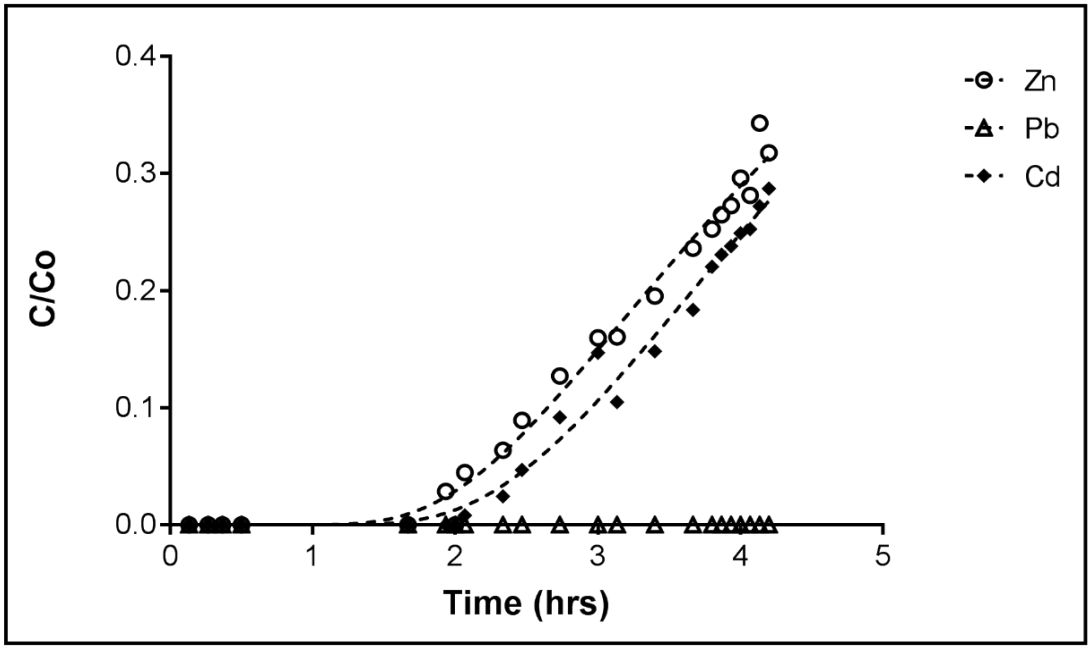

Figure 9.29: Thomas model of a fixed bed column adsorption of mixed metal ions; mixed metal ion concentration (ratio 2:1:1 – 50mg/L Zn, Pb & Cd); flow rate 0.5mL/min; at 21^{o}C, loading capacity 2g; column height 9cm, total volume 600ml. Thomas model fit is shown by the dashed line.

The Thomas model (Figure 9.29) gives a R^2 value of 0.862 and 0.810 for zinc and cadmium respectively. This shows that a better fit is obtained for all the metal ions in single solutions and further explains that the adsorption of metal ions in mixed solution may be moving closer to external and internal diffusion as the rate limiting step. The Yoon model shows no correlation fit to the experimental data and the 50% breakthrough curve is therefore not sufficient to describe the adsorption process of the whole system. As the initial concentration increases, the experimental data is less adequately explained by the Yoon-Nelson model because saturation is rapidly achieved in higher concentrations which decreases the time required to reach 50% retention.

Low concentrations were initially used in the experiments in order to mimic concentrations that are close to those found in industrial electroplating processes but since no breakthrough point

was obtained after several hours of running the experiment, higher concentrations were used to attain a breakthrough curve and ascertain the adsorption capacity of the loofa material.

9.7 Methylene blue

9.7.1 Adsorption

Figure 9.30 shows the adsorption cycle of methylene blue onto loofa in the column.

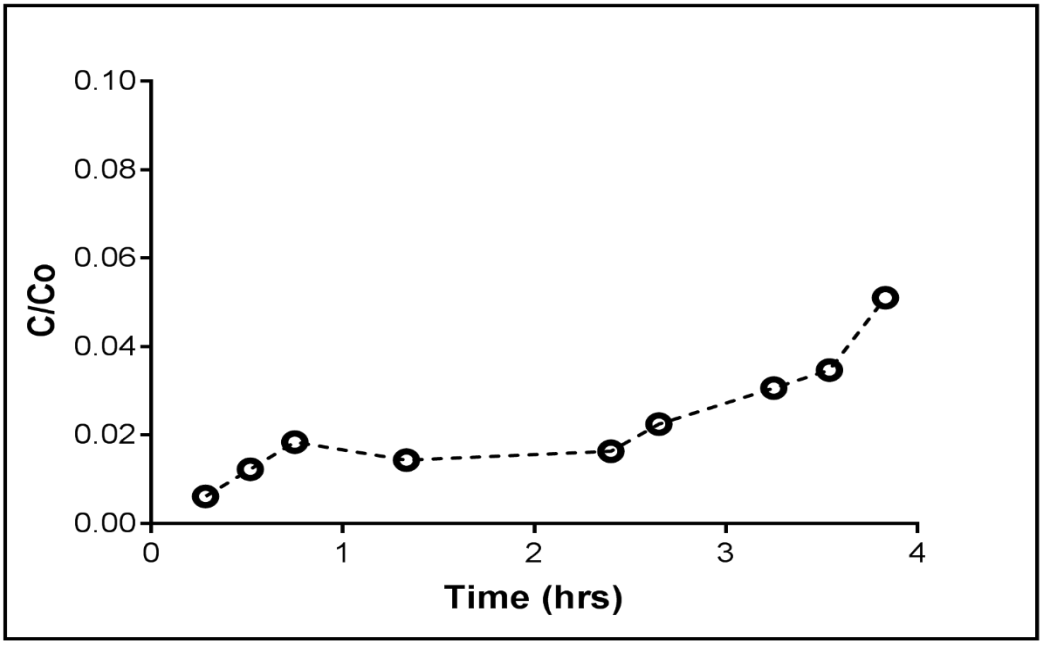

Figure 9.30: Adsorption curve of methylene blue adsorption over on time, methylene blue concentration 10 mg/L; flow rate 0.5mL/min; at 21^{o}C, loading capacity 2g; particle size 2mm; column height 9cm.

It is observed that an equilibrium was not reached after 4 hrs. This is the result of a low feed concentration of methylene blue at 10mg/L. The behaviour pattern shows an irregular curve. This explains a change in the adsorption layer at different column levels, where saturation had occurred at that specific column layer level and then moves on to the next layer of the column for further adsorption. During the experimental procedure, it was observed that, after 25 mins, only the top layer of the column was adsorbed with MB at a 0.5cm bed height. After 60mins, the next layer of approximately 0.7cm bed height was adsorbed with MB. This shows a slow process

of adsorption of MB onto the loofa in the column and therefore a longer breakthrough point is expected.

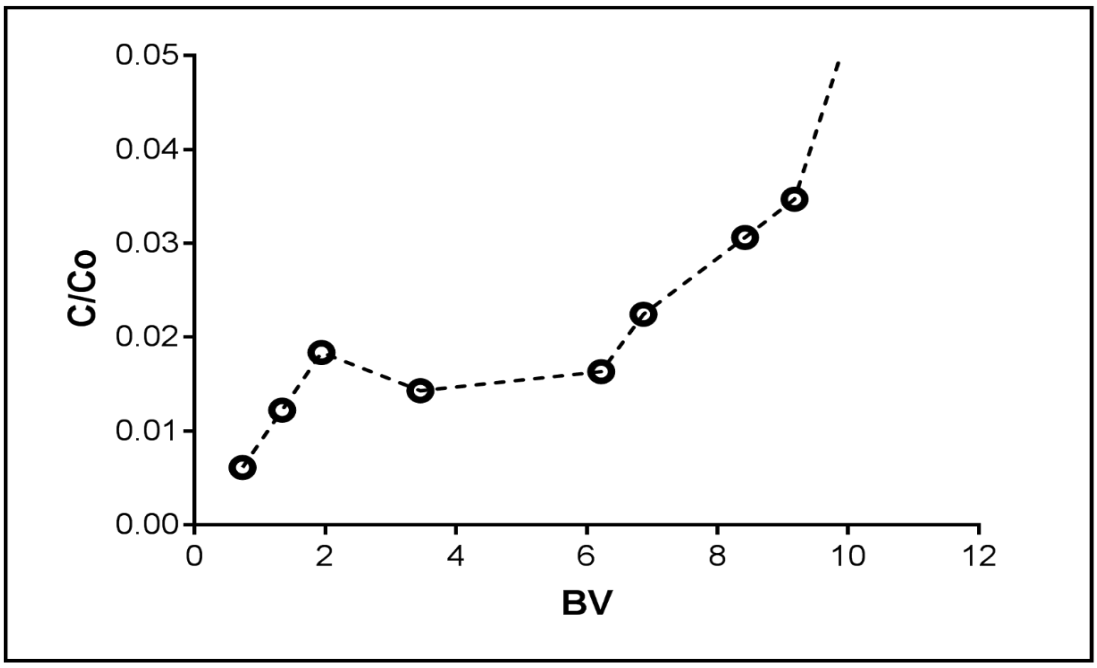

Figure 9.31: Adsorption curve of methylene blue adsorption over BV, methylene blue concentration 10 mg/L; flow rate 0.5mL/min; at 21^{o}C, loading capacity 2g; particle size 2mm; column height 9cm.

The change in the concentration ratio as a result of the saturation of the top layer of the loofa column occurs at approximately 4BV. It is observed that no breakthrough point was obtained at the studied BVs.

9.7.2 Desorption

Figure 9.32 shows the desorption curve of methylene blue after 60mins. Methylene blue was not completely desorbed from the loofa as can be seen in the graph.

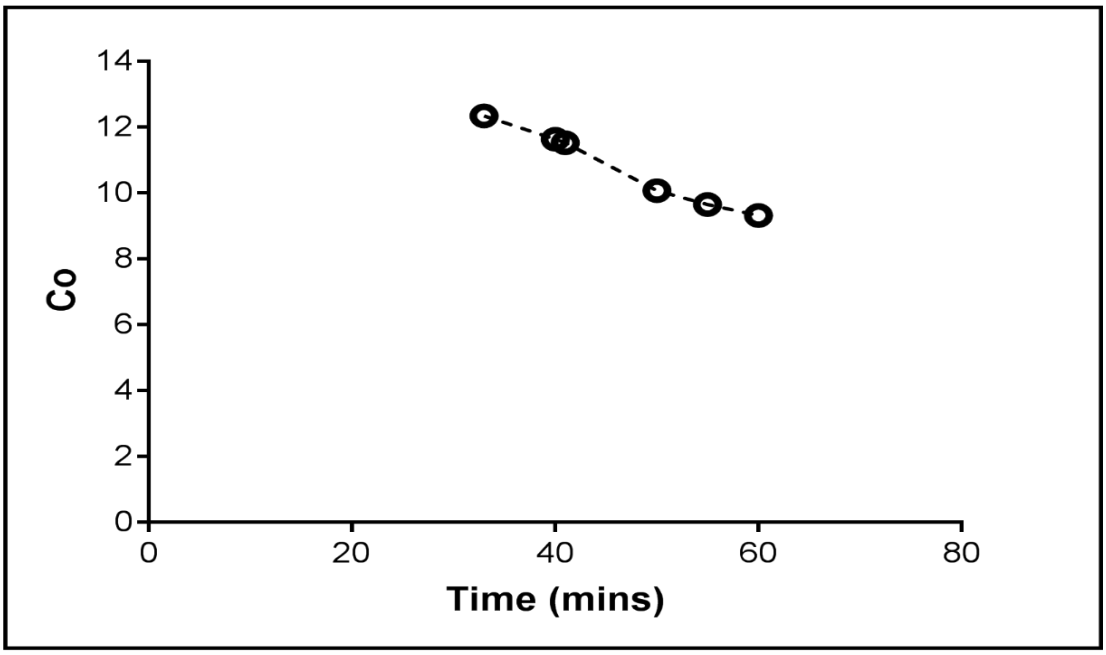

Figure 9.32: Desorption curve of methylene blue adsorption, methylene blue concentration 10 mg/L; flow rate 0.5mL/min; at 21^{o}C, loading capacity 2g; particle size 2mm; column height 9cm.

9.7.3 Models

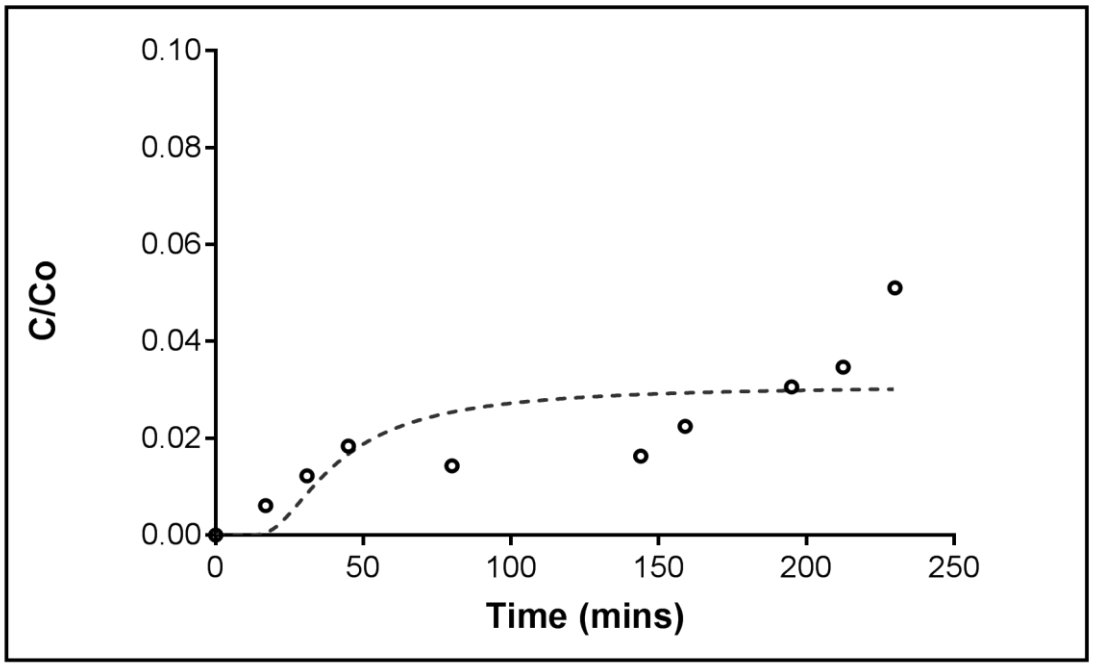

Figure 9.33: Thomas model of a fixed bed column adsorption of methylene blue; methylene blue concentration 10mg/L; flow rate 0.5mL/min; at 21^{o}C, loading capacity 2g; column height 9cm. Thomas model fit is shown by the dashed line.

The Thomas model shows a R^2 value 0.579 in describing the column mechanism of cadmium ion adsorption. This means that the external and internal mass diffusion steps may be rate limiting steps in the MB adsorption process. Yoon-Nelson showed no fit therefore no plot was obtained (Long *et al*., 2014).

9.8 Effect of methylene blue stained loofa on adsorption

9.8.1 Adsorption

Figure 9.34 shows the effect of stained MB loofa on adsorption of MB and mixed metal ions. The comparison is based on the concentration of methylene in the influent since at such a low concentration of 10mg/L, the breakthrough point of the metal ions could not be reached and the metal ions could not be detected.

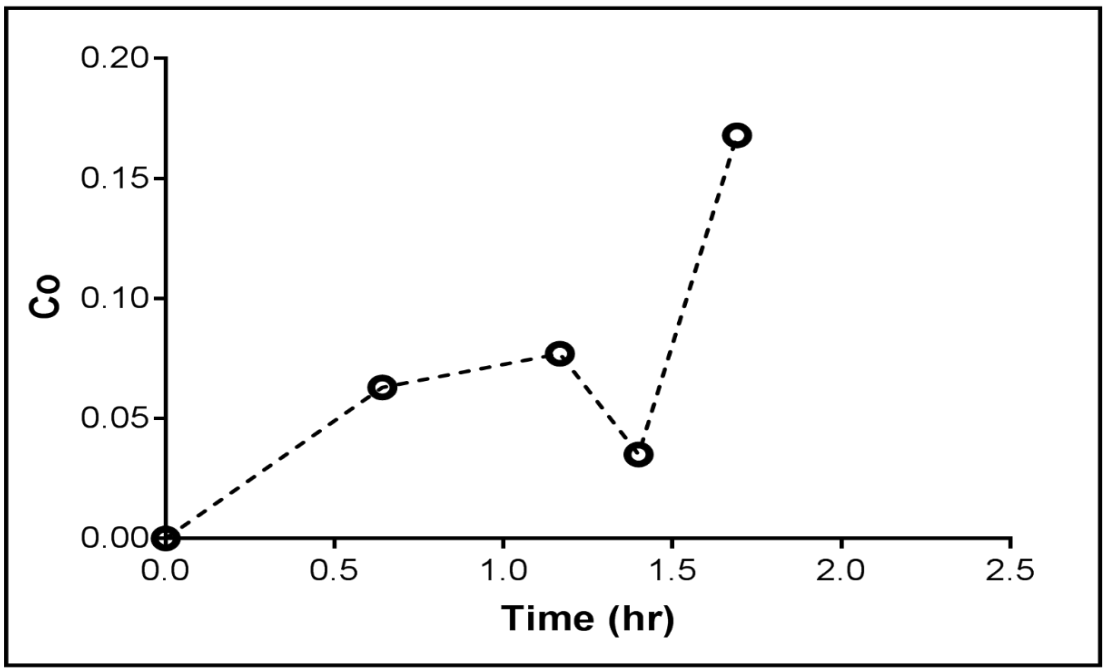

Figure 9.34: Effect of MB stained loofa on the adsorption curve of methylene blue adsorption over time, methylene blue initial concentration unknown; flow rate 0.5mL/min; at 21^{o}C, loading capacity 2g; particle size 2mm; column height 9cm.

Figure 9.34 shows a dip in the concentration of MB at approximately 1hr 30mins. This shows that the MB still on the loofa is washed out, through the column layers, by the mixed metal ions in solution.

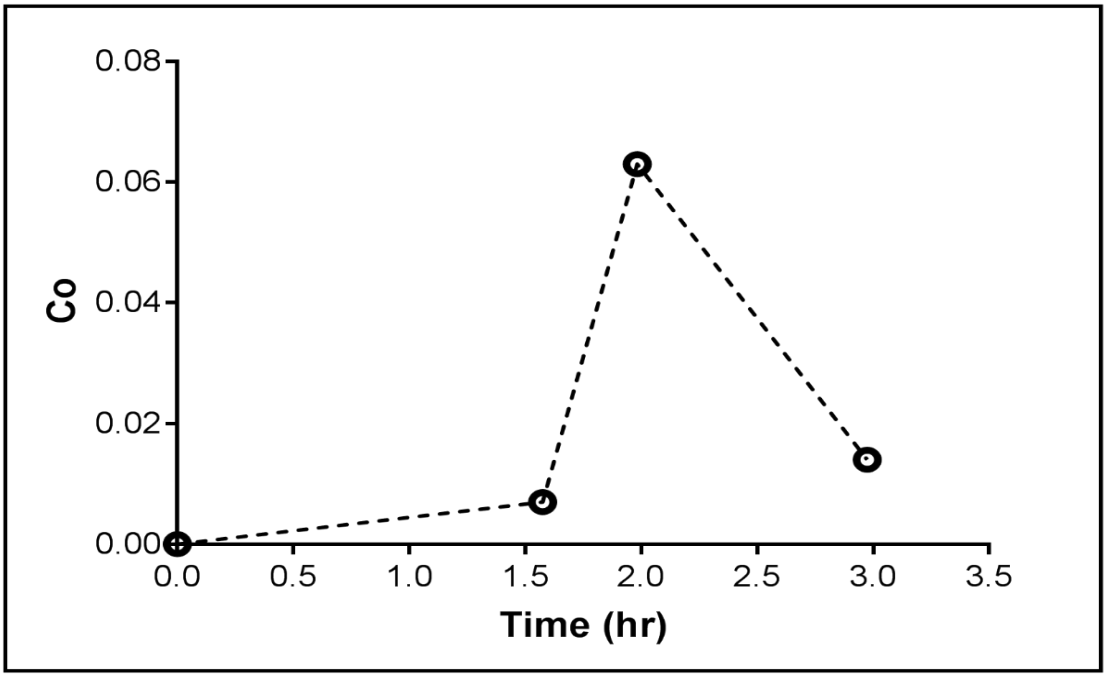

Figure 9.35: Adsorption curve of methylene blue adsorption over time, methylene blue concentration 10 mg/L; flow rate 0.5mL/min; at 21°C, loading capacity 2g; particle size 2mm; column height 9cm.

The pattern of adsorption for MB onto the loofa as shown in the previous plots is not repeated in Figure 9.35. There is an effect of the mixed metal ions on the MB adsorption onto loofa in the column system.

CHAPTER TEN

10.0 ION EXCHANGE CAPACITY

10.1 Introduction

This chapter investigates the ion exchange process that occurs during the adsorption mechanism of heavy metals onto loofa biosorbent. Ion exchange is one of the dominant reversible mechanisms and the adsorbed metals can be recovered by acid-base washing (Han *et al*., 2006). Sections 10.2 to 10.4 show how the characterisation of the alkali treated loofa relates to the ion exchange process. Section 10.5 highlights the difference in both percentage removal and adsorption capacity of lead ions onto alkali treated loofa as compared to loofa that has been treated through the exchange of ions. Section 10.6 explains the results obtained using the titration method. The ion exchange capacity (IEX) of the adsorption mechanism of lead ions was studied by use of hydrochloric acid and sodium hydroxide solutions. The strong acid and base was used to completely convert the cation exchanger loofa material to its H^+ form, to evaluate its optimum performance capacity. Ion exchange capacity (IEX) loofa is loofa mixed for 24 hrs in both NaOH and HCl solutions to determine the extent of exchange of ions (Chapter 2: 2.9). The loofa was first mixed with an aqueous solution of 0.1M NaOH, then the filtered loofa was rinsed with distilled water (to a neutral pH) and contacted with 0.1M HCl. To ensure sufficient time for complete contact between the loofa and the aqueous solutions of sodium hydroxide and hydrochloric acid, the mixtures were stirred magnetically for 24hrs. After this, the filtered loofa was used in the experiments whose results are shown in Figures 10.1 to 10.3. In the next part of the analysis, the filtered loofa was further mixed with 1M NaCl for 24hrs. The filtrate obtained was titrated against 0.1M NaOH and the pH was recorded at each point. The results are shown in section 10.5. The percentage removal and uptake capacity were expressed as E% and q_e (the percentage removal is determined by the loofa to lead ions ratio which leads to the difference in the concentration of adsorbate before and after adsorption and the uptake capacity is the

adsorption onto the loofa which leads to the unit adsorbate sorption capacity of the loofa adsorbent) respectively. IEX loofa is loofa that has been treated with NaOH and HCl consecutively while alkali treated loofa is loofa solely treated with NaOH. The IEX loofa was prepared to determine the exchange capacity of ions from the aqueous solution and from the loofa charged surface.

10.2 Point of zero charge

The pKa (deprotonation constant) determines the ionic state of the active binding sites on the loofa. For the COOH group it has a pKa value of 3.8 - 5.4 and the ion exchange reaction occurs with the dissociated COOH group at pH above 5 (Ngwenya *et al*., 2009). This explains the adsorption mechanism of Pb^{2+} ions onto loofa which has a pH_{pzc} of 7.2 (Chapter 3, figure 3.8). Positively charged surfaces are present when the pH is less than pH_{pzc}, however, maximum adsorption capacity occurs at pH 5-6. Carboxyl groups in cellulose are able to act as sources of ion exchange capacities. This implies that the quantity of accessible reactive end groups of the carboxyl groups can be tracked in order to determine the ion exchange capacity of the cellulose fibers. (Fras *et al*., 2000; Liu & Lee, 2014). This process of exchange of ions determines the adsorption mechanism.

10.3 Adsorption mechanism

Diffusion controlled mechanisms are accelerated by decreasing the particle size while the chemically controlled exchange does not depend on the particle size of the biosorbent (Rieman, 1961). As shown in figure 10.1, there is no significant difference in the percentage removal of lead ions as the particle size of the alkali treated (4% NaOH treated) loofa is changed from 45µm to 2mm. This describes a chemically controlled exchange involved in the adsorption process since the change in the particle size does not necessarily accelerate the adsorption process. Another factor that describes the exchange process is the adsorbent composition.

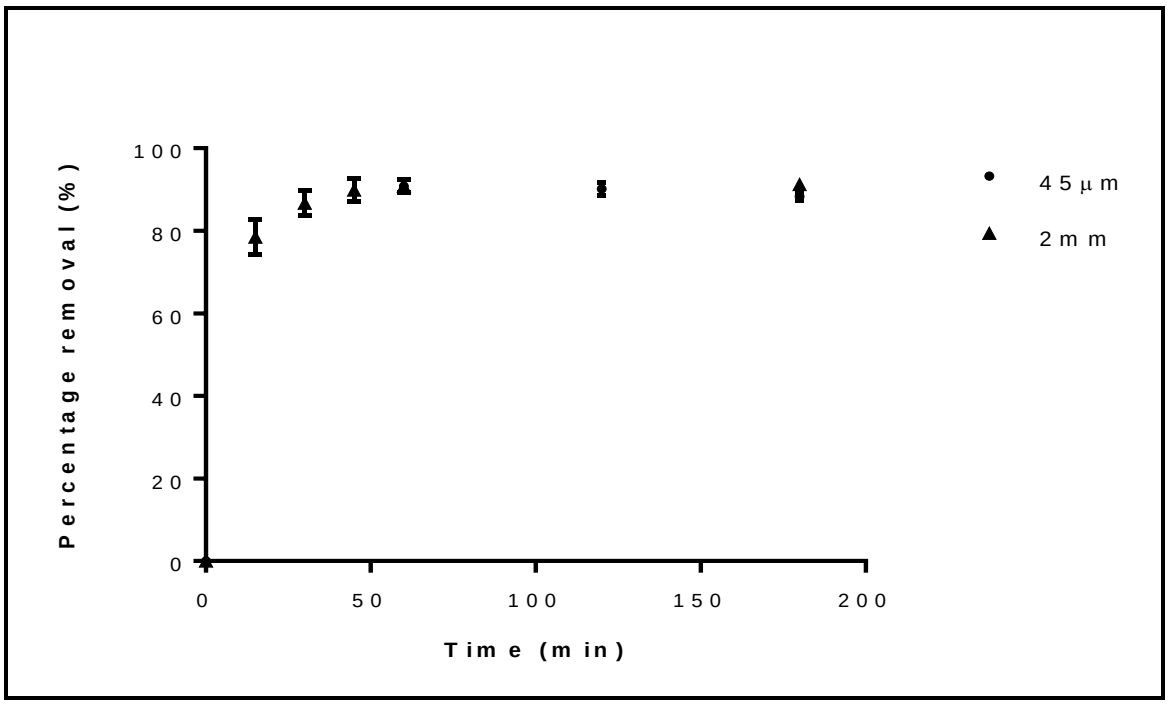

Figure 10.1: Percentage removal of lead ions at pH 5 after 3hrs contact time; lead ion concentration: 50mg/L; agitation speed: 200rpm; at 21^{o}C, 5g/L dosage of alkali treated loofa, particle size 45µm & 2mm. Data from 3 replicate measurements.

10.4 CHNS analysis

As shown in Table 3.3 (Chapter 3), the low percentage of hydrogen (3.68%) and high O/C ratio of 1.20 in the loofa, indicates that hydrogen ions are exchanged for lead ions on the IEX loofa and are present in solution, this explains the low pH of 3.85. The exchange of ions relates to the uptake capacity and percentage removal of lead ions in solution.

10.5 Uptake capacity and percentage removal (E%) of lead ions

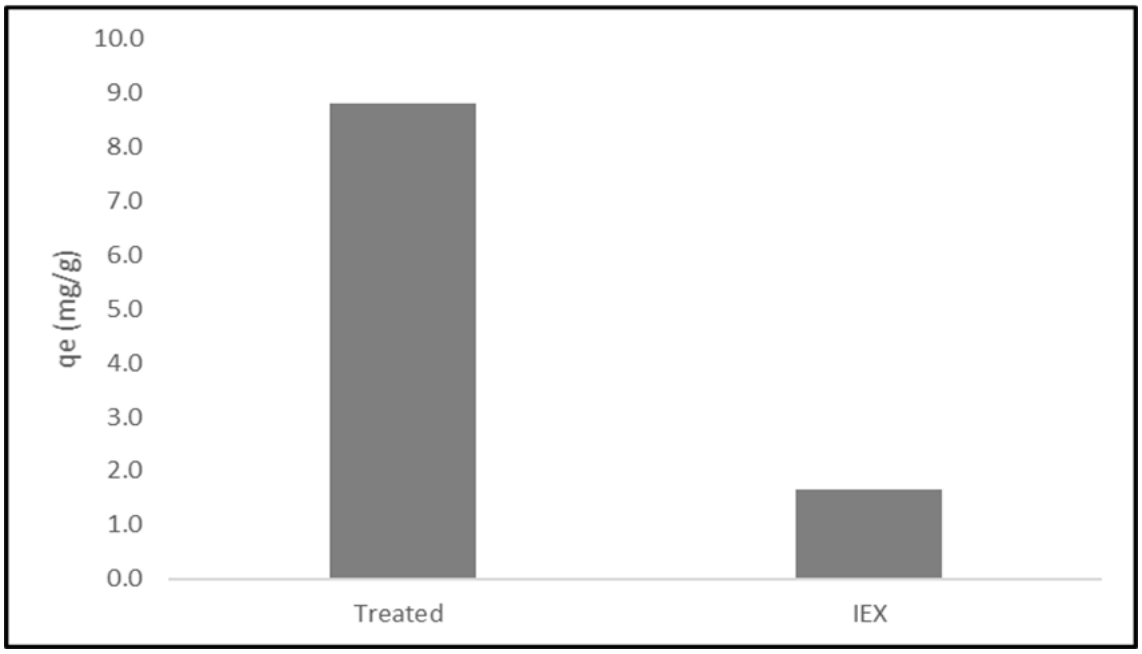

Figure 10.2: Uptake capacity of lead ions at pH 3 after 24hrs contact time; lead ion concentration: 50mg/L; agitation speed: 200rpm; at 21^{o}C, 5g/L dosage of alkali treated loofa & IEX (ion exchange capacity) loofa.

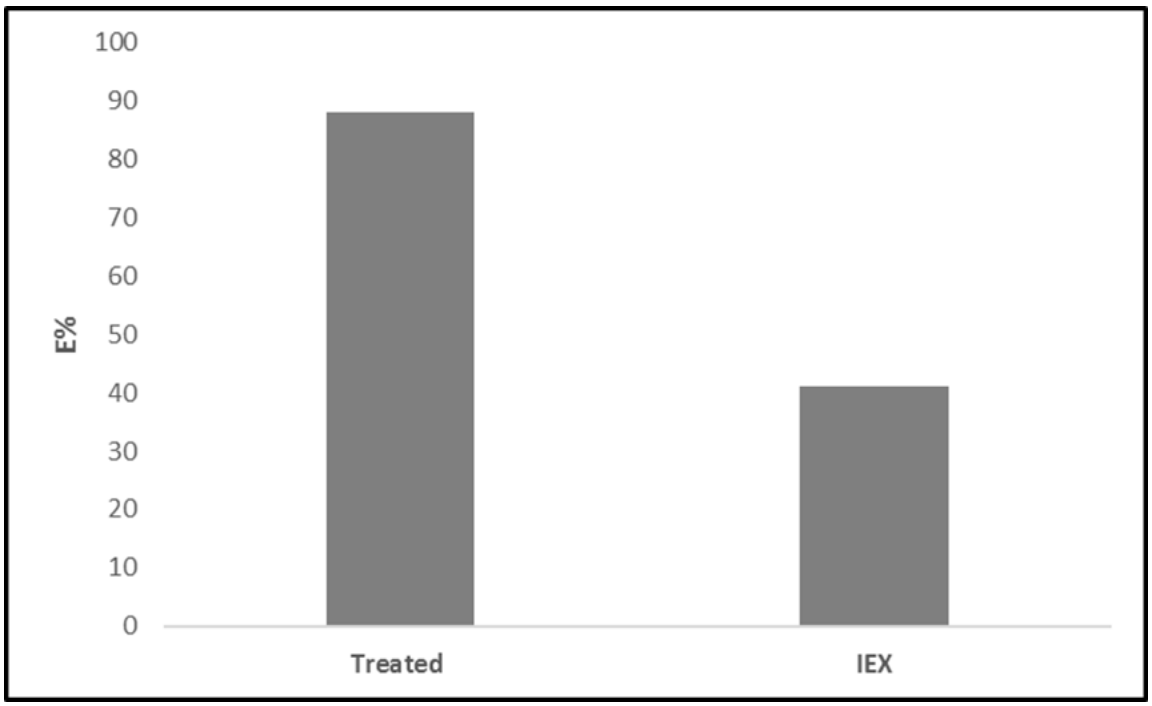

Figure 10.3: Percentage removal of lead ions at pH 3 after 24hrs contact time; lead ion concentration: 50mg/L; agitation speed: 200rpm; at 21^{o}C, 5g/L dosage of alkali treated loofa & IEX (ion exchange capacity) loofa.

Once the untreated loofa is mixed in NaOH solution the pH decreases over time, which shows the binding and exchange of H^{+} ions with Na^{2+} ion leading to a decrease in solution pH. Once the loofa is further mixed with HCl solution, the pH decreases to 1. The concentration of hydrogen ions can be calculated and the IEX loofa utilised in adsorption experiments for lead ion uptake. Figure 10.2 shows the decrease in the adsorption capacity of lead ions by approximately 80% when IEX loofa is utilised as compared to alkali treated loofa. The lower adsorption capacity of the IEX loofa (Figure 10.2) is as a result of more protons competing with the lead ions for the active binding sites in the acidic medium as compared to the protons available for ion exchange. When the percentage removal at pH 3 (acidic medium) of lead ions (Figure 10.3) by the IEX loofa (41.1%) is compared to the alkali treated loofa (88.2%), there is an approx. 47% decrease which shows that the ion exchange capacity of the metal ions is influenced by the solution pH (Holmberg, 2006).

Adsorption of metal ions is induced by hydrogen bonding and ion exchange (Liu & Lee, 2014b). This means that the exchange of hydrogen ions and metal ions in aqueous solution as well as the presence of hydrogen ions in the aqueous solution due to the acidic pH are the main factors that influence the adsorption capacity of metal ions onto loofa. Also, the fastest exchange rate, shown previously to occur in less than 20mins, indicates that the exchange positions are on the surface**.** Furthermore, for every 0.0081meq of H^+ (2 moles), present on the loofa surface, 0.04959meq of Pb^{2+} is absorbed. This shows that more lead ions are adsorbed than H^+ ions released into solution. This is explained by the fact that many factors contribute to the adsorption of metal ions onto loofa and the adsorption process cannot solely be an ion exchange mechanism (Burgess, 1999; Brinza *et al*., 2007). To support this data, the supernatant solution was also analysed to determine the exchange of hydrogen ions.

10.6 Titration

The concentration of hydrogen ions was determined by performing a NaOH titration of the supernatant solution from the IEX loofa. This is to show that the hydrogen ions contained in the hydrochloric acid solution were adsorbed onto the loofa surface. The actual concentration of HCl present was calculated and the ion exchange capacity measured. The concentration of NaOH was determined by the volume of NaOH needed to reach the equivalent equilibrium point and the pH was recorded. Using the relationship between pH and pOH, the actual concentration of HCl can be calculated. The ion exchange capacity was measured based on the concentration of hydrogen ions (Harland, 1994).

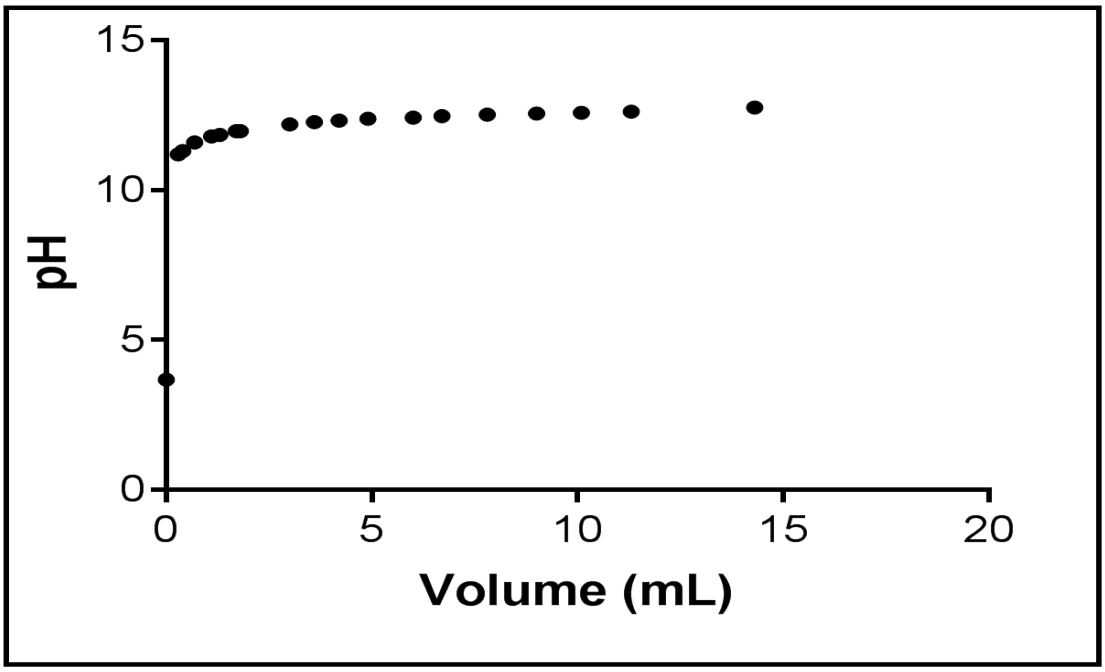

Figure 10.4: Titration of NaOH against IEX filtrate solution: agitation speed: 200rpm; at 21^{o}C, 5g/L IEX (ion exchange capacity) loofa.

As shown in Figure 10.4, 3.6ml of NaOH was required to reach equilibrium during the titration process. The pH at the equivalent point was 12.27 (pK_b = 12.27) and the pK_a calculated to be 1.3. The concentration of hydrogen ions present in the solution was determined to be 0.05M, therefore a 50% ion exchange capacity occurred. This indicates the exchange of 50% of the concentration of hydrogen ions onto the loofa which accounts for ion exchange of hydrogen ions and lead ions. As described in previous results, the lead adsorption capacity of the alkali treated loofa (88.2%) as compared to the IEX loofa (41.1%) is decreased by approximately 47%. Thus approx. 9% of the H^+ ions (IEX loofa) were not exchanged and were predominantly competing with the lead ions for adsorption onto the active binding sites of the loofa. The presence of other cations could also be the reason for the 41.1% exchange of ions. Therefore, the remaining 38.2% of the adsorbed lead ions (alkali treated loofa - 88.2%) were attributed to other adsorption mechanisms (Holmberg, 2006 ; Arshadi *et al.*, 2014).

CHAPTER ELEVEN

11.0 COMPARISON OF THE ANALYSIS OF METAL IONS USING DIFFERENT EQUIPMENT

11.1 Introduction

This chapter gives an analytical analysis of any differences in the values of lead, zinc and cadmium ions as measured by three different pieces of analytical equipment: Induced Coupled Plasma Mass Spectroscopy (ICP-MS); Induced Coupled Plasma Optical Emission Spectroscopy (ICP-OES) and Atomic Absorptive Spectroscopy (AAS). The discussion highlights any difference in measurement and the accuracy of the data obtained. Section 11. 1 considers the initial lead ion concentration values at 50 – 100mg/L, expressed as C_o. Sections 11.2 and 11.3, consider cadmium and zinc ion initial concentration values respectively. The final concentration values, as previously mentioned, is denoted by C_i, the adsorption capacity in mg/g is expressed by q_e, and the concentration ratio is the ratio of the final concentration in solution to the initial concentration in solution, which is expressed as C_i/C_o. The results discussed in this chapter form the basis of similarity and difference in the utilised experimental analysis and the choice of analytical methods used throughout the research work.

11.2 Lead

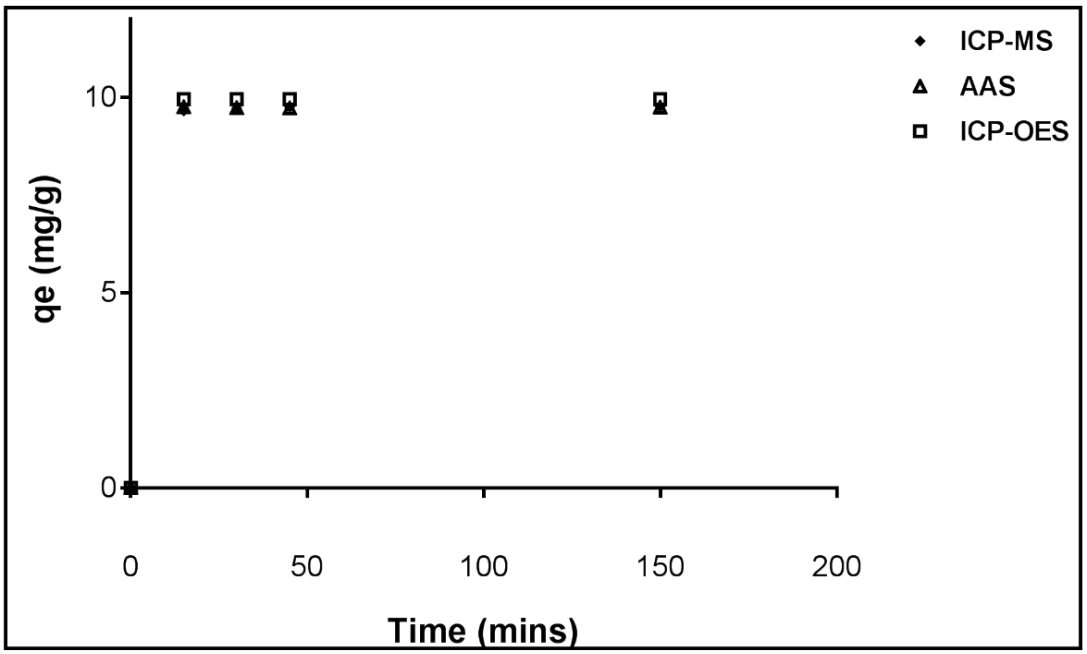

Figure 11.1: Uptake capacity of lead ions at pH 4 after 2.5hrs as measured by AAS, ICP-MS and ICP-OES; 50mg/L; agitation speed: 200rpm; at 21^{o}C,2.5h contact time, 5g/L of alkali treated loofa dosage.

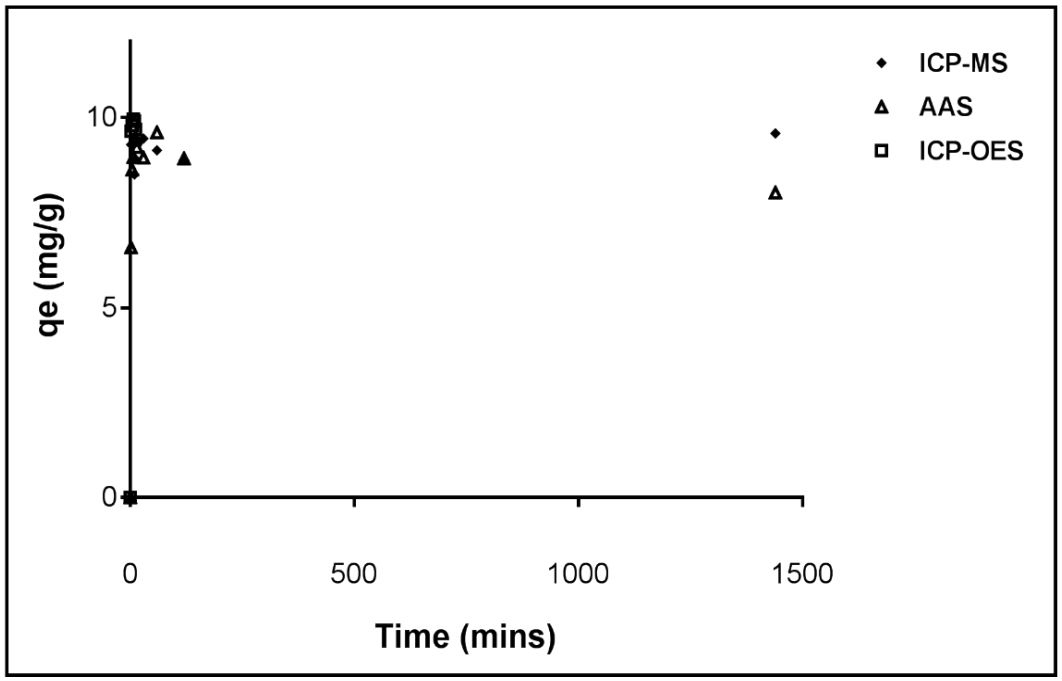

Figure 11.2: Uptake capacity of lead ions at pH 5 after 24hrs as measured by AAS, ICP-MS and ICP-OES; 50mg/L initial concentration; agitation speed: 200rpm; at 21^{o}C,24h contact time, 5g/L of alkali treated loofa dosage.

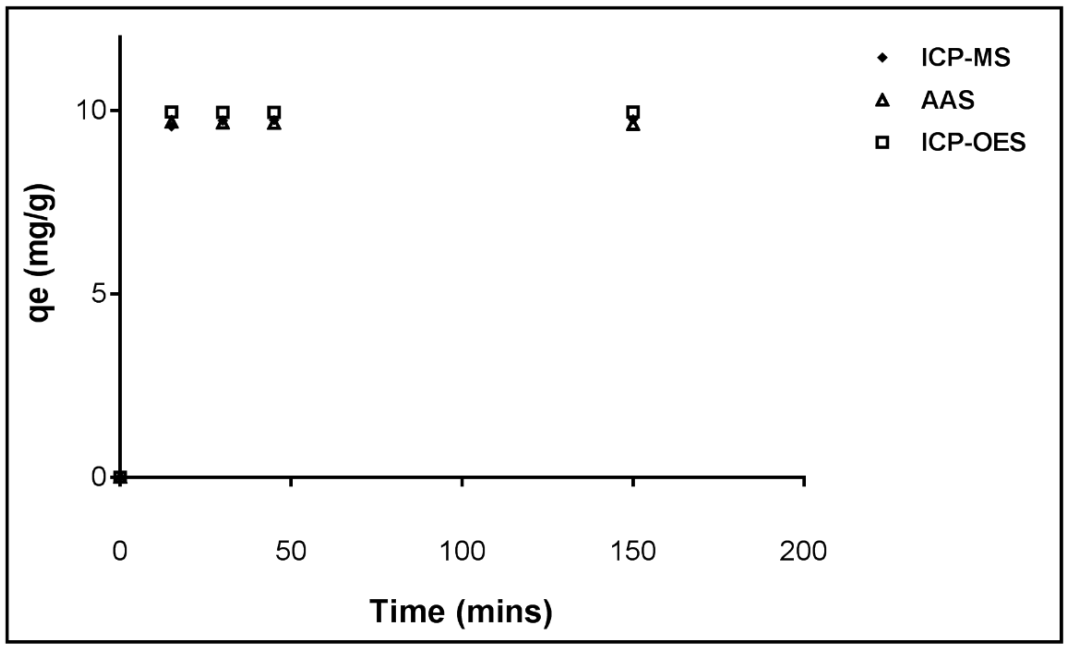

Figure 11.3: Uptake capacity of lead ions at pH 8 after 2.5hrs as measured by AAS, ICP-MS and ICP-OES; 50mg/L initial concentration; agitation speed: 200rpm; at 21^{o}C, 2.5h contact time, 5g/L of alkali treated loofa dosage.

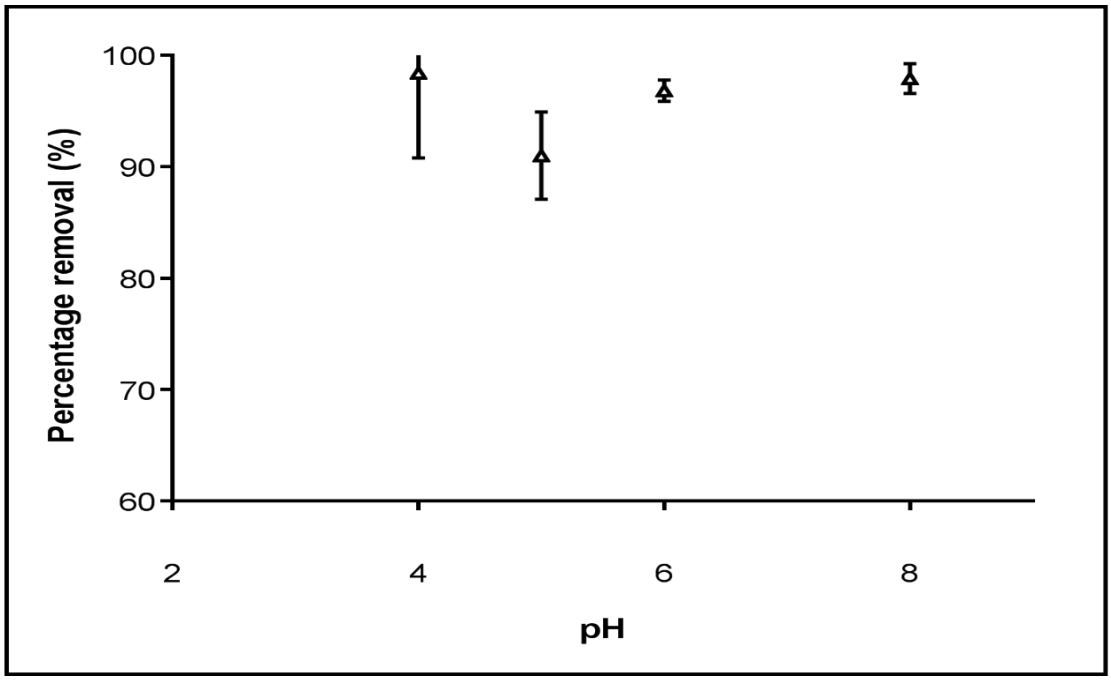

Figure 11.4: Percentage uptake (mean and standard deviation) of lead ions at pH range 4 - 8 after 2.5hrs as measured by AAS, ICP-MS and ICP-OES; 50mg/L initial concentration; agitation speed: 200rpm; at 21^{o}C, 2.5h contact time, 5g/L of alkali treated loofa dosage.

The differences in lead as measured by ICP-MS, ICP-OES and AAS are within 5-10% (Figures 11.1 – 11.4). As explained in chapter 4, the uptake of lead ions by loofa increases as pH increases to an optimum pH of 5, therefore at pH < 5, the lead ion concentration in the supernatant solution is high (over half of the initial concentration of 50mg/L) and can be detected by all three methods. This explains the close values of detection shown in Figure 11.1. At pH > 5, the accuracy of the AAS is increased (concentration found in solution increased due to lower uptake capacity and is found to be close to the other methods (Figure 11.3). At the optimum pH of 5, the uptake on the loofa is greatest and therefore the supernatant concentration is lowest and the AAS is not as accurate (Figure 11.2). The ICP-MS and ICP-OES show similar results for all pH values. Figure 11.4 shows the results for percentage uptake using the three types of analytical equipment. These are the mean results of all three measurements. The error bars indicate the smallest differences are at pH 6 and 8. At lower concentrations, there is a similarity between the measured values of lead ions for all three analytical equipment but at higher concentrations, the AAS differs from the ICP-MS and ICP-OES, which show a close similarity in measured values.

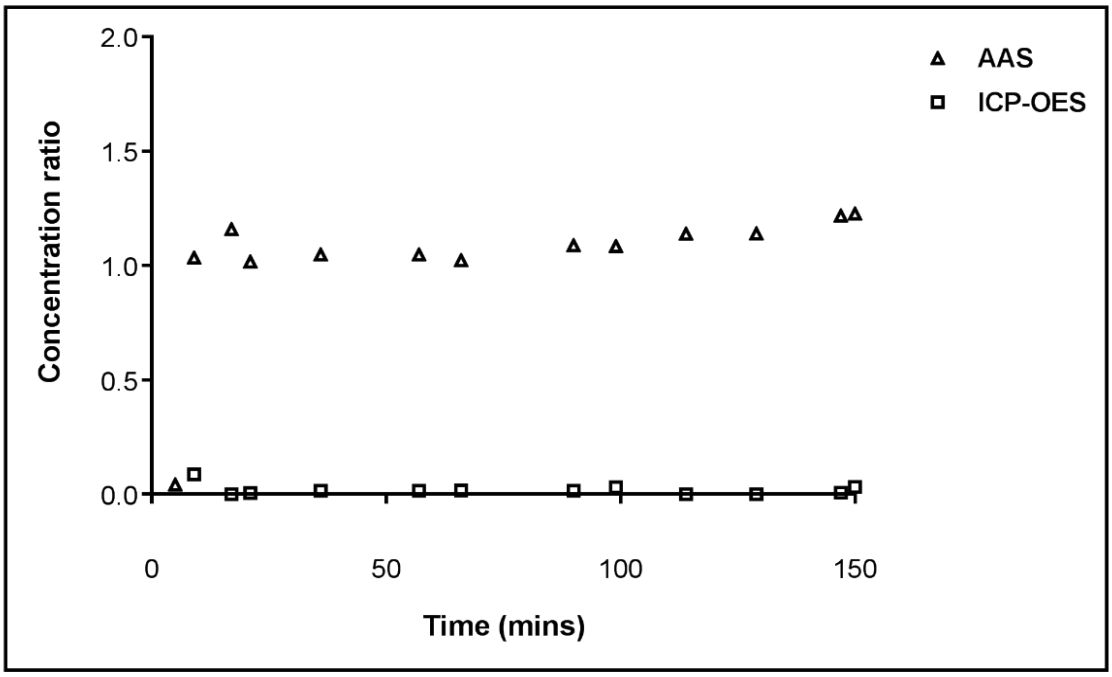

Figure 11.5: Concentration ratio of lead ions at pH 5 after 2.5hrs as measured by AAS and ICP-OES; 50mg/L initial concentration; agitation speed: 200rpm; at 21^{o}C,2.5h contact time, 5g/L of alkali treated loofa dosage.

Figure 11.5, shows the concentration ratio of lead in the supernatant as measured by AAS and ICP-OES after column experiments. As explained in Chapter 2, the low concentration values obtained were measured by the ICP-OES. This further supports the data shown in Figures 11.1 to 11.3 of the accuracy and detection standard of the ICP-OES.

11.3 Cadmium

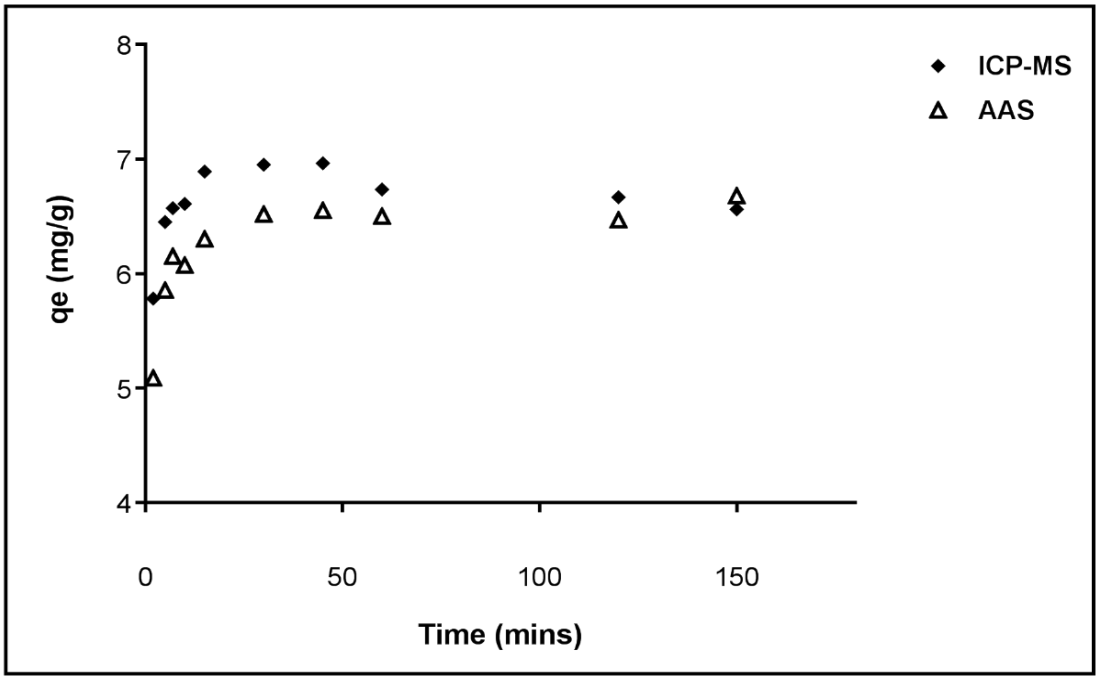

Figure 11.6: Uptake of cadmium ions at pH 6 after 2.5hrs as measured by ICP-MS and AAS; 10mg/L initial concentration; agitation speed: 200rpm; at 21^{o}C, 2.5h contact time, 5g/L of alkali treated loofa dosage.

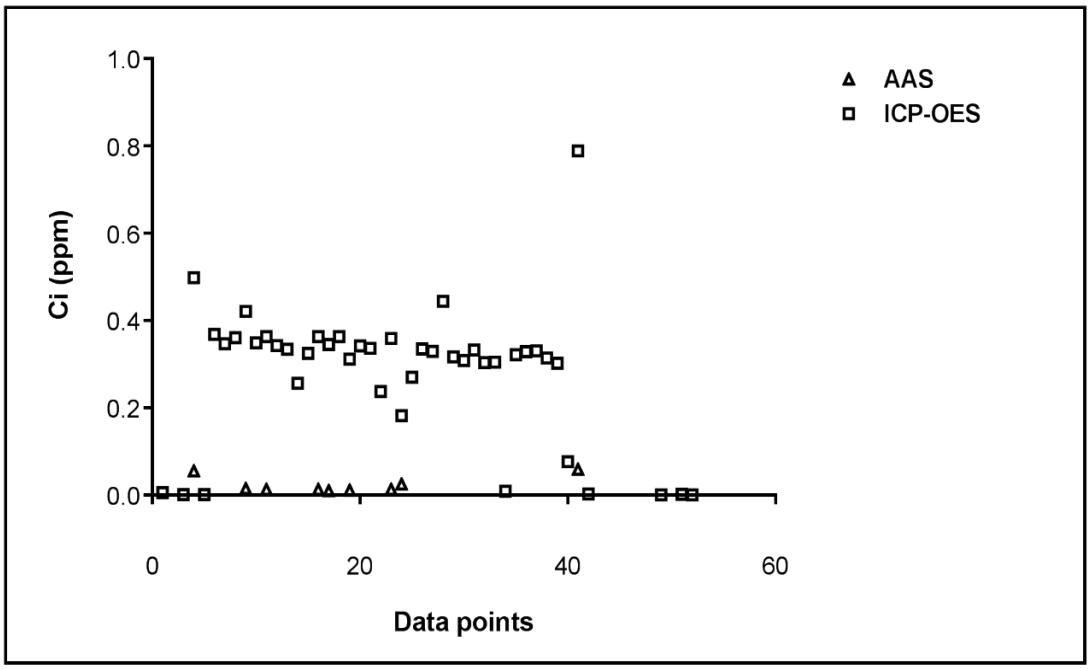

Figure 11.7: Comparison of cadmium ions adsorption in column experiments (see chapter 9) as measured by AAS and ICP-OES, cadmium ion concentration 10 mg/L; flow rate 0.5mL/min; at 21^{o}C, mass of loofa 2g; particle size 2mm; column height 9cm. Samples stored for three months.

Figure 11.6, shows only a 1.8% difference at equilibrium between the ICP-MS and AAS measured values. The values are close but the ICP-MS measures lower values and thus a higher uptake capacity is determined. Figure 11.7 shows that very low values of cadmium can be detected after storing the samples (1% HNO_3 acidified) for 3 months. The AAS cannot measure these low values at or close to 0mg/L. This shows the greater detection standard of the ICP-OES method.

11.4 Zinc

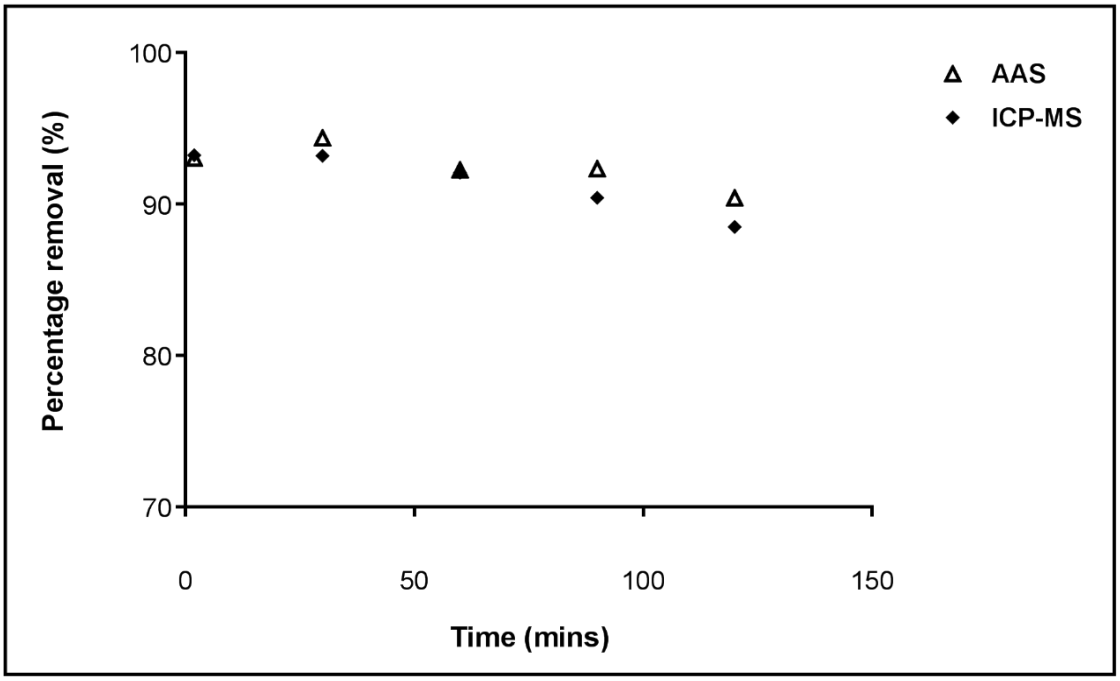

Figure 11.8: Percentage uptake of zinc ions at pH 6 after 2hrs as measured by AAS and ICP-MS; 20mg/L initial concentration; agitation speed: 200rpm; at 21^{o}C, 2h contact time, 5g/L of alkali treated loofa dosage.

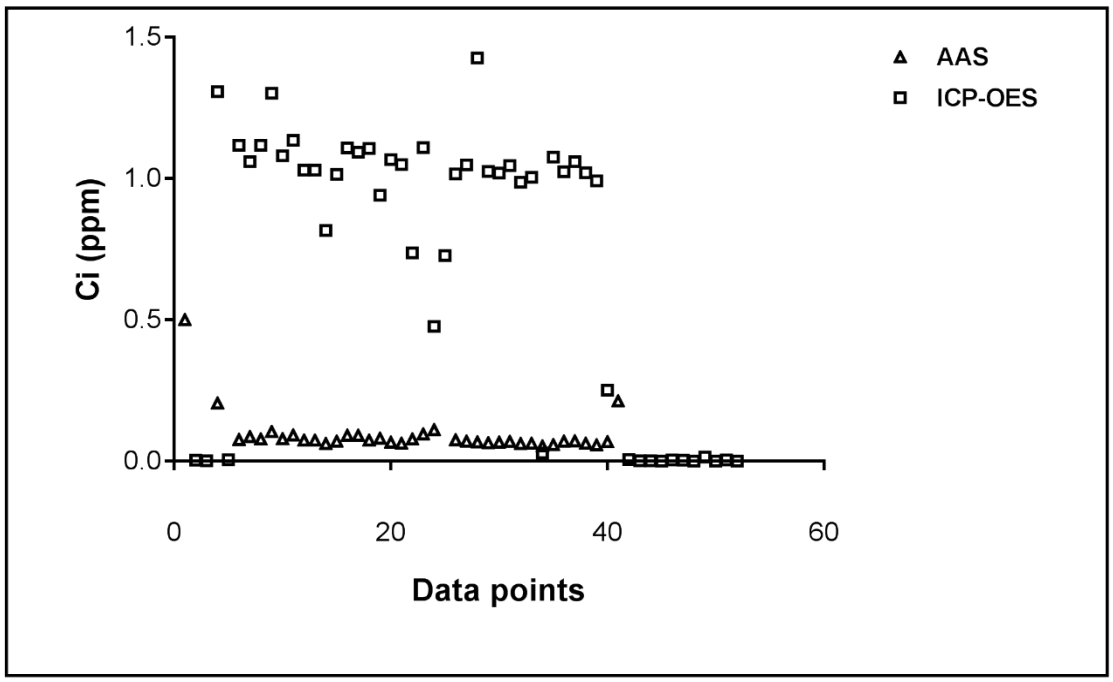

Figure 11.9: Comparison of zinc ions adsorption AAS and ICP-OES; zinc ion concentration 20 mg/L; flow rate 0.5mL/min; at 21^{o}C, loading capacity 2g; particle size 2mm; column height 9cm.

Figure 11.8 shows that the percentage uptake measured by ICP-MS is slightly lower (at 30, 90 & 120mins) than that measured by AAS (< 0.5% difference) thus the ICP-MS and AAS are sufficient in measuring low levels of zinc in the supernatant solution. Therefore, although the ICP-MS is considered more accurate than AAS, in the case of zinc, the AAS is performing remarkably well at low levels of zinc showing good consistency between the techniques. The column experimental analysis measurements in Figure 11.9, show a more accurate final concentration values (C_i) by the ICP-OES as compared to the AAS that indicates values around 0mg/L. The batch experiments are run at an initial range of 50 – 150mg/L and the column experiments run at a range of 10-50mg/L of metal ions. After contact with the loofa, the concentration of the supernatant solution is reduced, leaving a low concentration of metal ions (or a concentration of metal ions that is decreasing with time) that is, in most cases, more accurately measured by the ICP-MS and ICP-OES rather than the AAS. Also, the results show that after storing the samples (1% $HN0_3$ acidified) for 3 months, the low values could still be detected by the ICP-OES

but not by the AAS. Although the percentage difference (between 0.5 – 10%) is low and gives confidence in the results, these results justify the utilisation of the ICP-MS and in a few cases, the ICP-OES, as the most suitable techniques to gather all the experimental data. As compared in the results shown, lead and cadmium ions at low concentrations were accurately measured by the ICP-MS and ICP-OES, which were the preferred option to the AAS. Zinc ions at low concentrations, on the other hand, were accurately measured by the ICP-MS, ICP-OES and AAS. Therefore, there was no actual preferred option for analytical analysis of zinc ions but the experimental measurements were conducted on the basis of equipment availability.

CHAPTER TWELVE

12.0 GENERAL DISCUSSION

12.1 Introduction

This chapter gives a general discussion of the results reported in the previous chapters and looks to possible applications and further considerations of a treatment technology based on loofa biosorption.

The World Health Organisation recommended levels for pollutants in effluents released from industries have made it imperative to develop a sustainable and low cost means of wastewater treatment. While such treatments are applicable to all countries, developing countries now take on the highest proportion of basic, potentially highly polluting, industry. Biosorption, which has been studied for over 30 years, forms the basis of a promising technology for such applications (Bhatnagar & Minocha, 2006).

Lead, cadmium, zinc and an organic pollutant, methylene blue, representing some of the most detrimental pollutants to human health and the environment, were studied in this work and each pollutant was found to have a strong affinity to the biosorbent, loofa (*Luffa cylindrica*) which is a readily available and cheap biomaterial in many tropical and subtropical countries. The dominant functional groups, hydroxyl, carboxyl groups and carbonyl group of ketone, are the main groups involved in the adsorption process mechanism. These functional groups and the zeta potential values support the fact that an alkali treatment improves adsorption onto the loofa. The different adsorption behavioural patterns of each of the pollutants to this modified loofa indicate the availability of more free functional groups on the loofa surface, increased surface area and pore size distribution; and an increase in the magnitude of the negatively charged surface. Also, the availability of two sites, (strong and weak adsorption sites) enables differences in bonding requirements of each pollutant to be met by the loofa.

The experimental parameters, such as pH, temperature, initial concentration and time interval all have an effect on the equilibrium time and maximum uptake capacity of each cationic pollutant adsorbed. An alteration in ionic strength enables the lead and zinc ions to bind differently to the loofa by forming complexation on one site and showing competition with the Na^+ ions on the other sites. Alteration of the pH may increase adsorption of one species of a metal and suppress another. Also, different metal ions inhibit each other but there is still a considerable amount of uptake for each metal ion depending on the initial metal ion concentration in the mixed metal solution and also the solution pH and affinity of the metal ions for the loofa. Lastly, methylene blue uptake is affected by the presence of metal ions as well (≤ 5% difference).

12.2 Modification of loofa

The loofa fibres were modified to enhance adsorption capacity. The treatment of the loofa is regarded as a surface clean-up and preparation process. The functional groups and the surface charge on the loofa are involved in the adsorption processes. Therefore, enhancement of both the functional groups and surface charge should improve adsorption. The surface morphology was observed to have changed after treatment. The elemental composition showed no significant difference that could be considered to have an effect on the adsorption process (< 5%). However, in the case of IEX-HCl, which differs from the alkali treated by being mixed in NaOH for a longer period of 24hrs and also being mixed in HCl, the hydrogen composition of alkali treated loofa was a little over half that of the natural loofa (50% decrease). This may be explained by the release of H^+ ions during treatment to create more active bonding sites for adsorption. The surface of the NaOH treated loofa was also shown to be broken up thus exposing more pores to support adsorption. Asuquo & Martin (2016) reported that cervices seen on the surface of treated sweet potato peel to aid in the transport and adsorption of cadmium. Ghali *et al*. (2009) reported alkali treatment of loofa gives a higher crystalline structure and changes the surface morphology by removing gummy substances in order to improve adsorption. The

change in morphology shown in this report is a key indication of the enhancement of the surface for increased adsorption. The different changes in the surface of each treated loofa (before and after adsorption) are shown in Appendix 1. The breakup of the surface increases the surface area and pore volume as shown by the BET results. Feng and Guo (2012), using BET analysis to measure the surface changes of modified orange peel, reported a higher adsorption capacity of copper, lead and zinc ions. Apart from surface area, porosity is also important to the adsorption properties. Saygili and Guzel (2016) report that the porosity of carbon adsorbents is an important factor affecting adsorption capacity. Molecules of different sizes and shapes define the classification of pores into groups which determine the differences in adsorption capacity. Asuquo *&* Martin (2016) report that pore size, particularly the distribution of mesopores and macropores, control diffusion of the adsorbate into the adsorbent structure. When compared to untreated and HCl treated loofa, a higher surface area and pore size was found for the alkali treated loofa which leads to a better adsorption capacity for the studied pollutants. It was found that the number of mesopores on the loofa increased after alkali treatment, thereby showing the involvement of mesopores in the adsorption of pollutants. For loofa there is no significant change in the degradation profile and volatile matter after treatment and the loofa surface remained negatively charged (which is needed to adsorb cations from aqueous solutions). However, the point of zero charge changed after treatment, shifting the adsorption spectra slightly and changing the pH adsorption factor. The FT-IR analysis after treatment shows a stronger hydrogen bond (observed by a shift in the adsorption peak at $3340cm^{-1}$ – $3355cm^{-1}$). The alterations to the functional groups creates more active bonding sites for adsorption (Ghali *et al*., 2009; Asuquo & Martin, 2016; Feng & Guo, 2012). Modification of the loofa with 4% 0.1M NaOH improved the adsorption capacity of lead and methylene blue by 8.1% and 9.8% respectively. Compared to other adsorbents, such as *Luffa* charcoal, *Phanerochaete chrysosporium*, *Portulaca plant* and *Pongamia pinnata*, modified loofa (*Luffa cylindrica*) shows a higher percentage removal of lead, cadmium and zinc ions over a short period of time (Umpuch *et al*., 2011; Li *et al*., 2004; Dubey and Shiwani, 2012; Mamatha *et al*., 2012).

12.3 Adsorption mechanism of metal ions

12.3.1 pH

Lead, cadmium and zinc ions are adsorbed differently onto the loofa surface at different pH values. This is related to the strength of affinity of the bonding sites for each species of metal ion. This speciation depends on the solution pH. Also, the amount of cations present in solution determines the electrostatic attraction or repulsion between the ions in solution and the ionisation state of the carboxyl and hydroxyl groups on the loofa surface; and this influences the uptake mechanism of each metal ion. These factors result in an optimum pH for maximum adsorption. The speciation diagrams (Figures 4.5, 5.1,5.2,6.1 & 7.5 in Chapters 4, 5, 6 & 7 respectively) show the dominant species of a metal ion at any pH. At a certain pH, one or more metal species may exist and the quantity of these species adsorbed can be measured. Free lead ions, that do not form any complexes with other ions present in solution, have an optimum pH of 5-6, and while above pH 6 hydroxylated lead ions begin to increase. The latter is an insoluble form and precipitation occurs leading to a decrease in adsorption. Free lead ions are completely absent at pH 8.5 and only 30% of the hydroxylated lead ions are still present in solution while 70% of the hydroxylated lead ions have already precipitated from solution. In acidic media with low pH (below 5), hydrogen ions compete with the lead ions thereby decreasing the amount of lead adsorbed onto the loofa. Pagnanelli *et al*. (2003) reported the maximum adsorption of lead ions by *Sphaerotilus natans* biomass to occur at pH 5. This was attributed not only to the acidic properties of the lead ions but also to the properties of the active sites on the adsorbent. Iqbal *et al*. (2009) attributed the uptake of lead ions by mango peel waste over a range of pH values to the point of zero charge (pH_{pzc}) of the adsorbent. The report pointed out that the maximum pH for lead adsorption occurs at pH 5; and the lead species were positively charged at pH > pH_{pzc} in the presence of a negatively charged adsorbent surface which led to an electrostatic attraction between the two. Also, at pH < pH_{pzc}, higher concentrations of hydrogen ions compete with the positively charged ions for active sites on the adsorbent which are positively charged

leading to electrostatic repulsion forces. At a pH over 5, the free lead ions are decreasing in percentage as hydroxylated lead ions increase. There is a possible effect of different species of lead ions in solution at pH 5-6 and the hydroxylated lead ions may have occupied sites on the loofa surface or may have a negative effect on the adsorption of the free lead ions onto the loofa.

Zinc ions show an optimum adsorption at pH 6. Similar to lead, zinc ion uptake is influenced by the electrostatic attraction or repulsion of ions, the presence of hydroxylated zinc ions and the speciation that occurs at the maximum uptake point. The zinc speciation diagram shows that, at pH 6, 100% of the zinc is present as free zinc ions in solution and are thus expected to be adsorbed onto the loofa surface. However, only about 80% of zinc ion uptake occurs. This could be related to the complex stability properties of the two species. In this case, there is an absence of the hydroxylated zinc ions as these only occurs under alkaline conditions. Iqbal and Edyvean (2004) reported pH to be the most important factor in adsorption and describe the effect of acidity and alkalinity of the solution on the adsorption of zinc ions.

The maximum uptake of cadmium ions occurs at pH 7 and the uptake capacity shows a decrease in both acidic and alkaline media due to the presence of competing hydrogen ions and the precipitation of the hydroxylated cadmium ions respectively. Furthermore, it shows a possible uptake of 50% of the hydroxylated cadmium ions present in solution. However, as hydroxylated forms of cadmium are expected to precipitate, the loss of cadmium ions from solution cannot be ascertained to be all due to adsorption onto the loofa surface. Amer *et al*. (2010) reported 55% adsorption of cadmium ions onto polyphosphate-modified kaolinite clay from aqueous solutions. This is similar to the percentage uptake of cadmium ions of 60.7% in this report. The speciation diagram of cadmium ions shows that, at pH 4.8, free cadmium ions are disappearing as the $Cd(OH)_2$ start to form. El Shafei *et al*. (2014) report that the maximum adsorption capacity of cadmium ions occurs at pH 8 and show free cadmium ions as the only dominant species up to pH 10 (as do Srivastava & Angove, 2004). Iqbal and Edyvean (2004) support the findings that

complexation on the surface of the biosorbent is an important factor in the adsorption mechanism of heavy metals. In the present research, in the adsorption of cadmium ions ($Cd(OH)_2$ dominant form), complexes are formed with the dominant active charged sites on the loofa surface. Desorption studies show that not all the cadmium is released back into solution therefore there is either a permanent bonding to sites on the loofa or some of the cadmium has been precipitated out of solution. Optimum removal of cadmium ($Cd(OH)_2$) is at pH 7 with 60.7% removal. This is a lower adsorption capacity than that of lead and zinc. However, different bonding patterns are indicated during the process (Figure 6.15 & 6.17) and the quantity absorbed does not always reflect the strength of attachment. This can be further described by extended x-ray adsorption fine structure (EXAFS) spectroscopy. The K_D values obtained from each metal ion adsorption relate to the adsorption process with a smaller K_D value indicating better removal efficiency (greater binding affinity), which is shown by the optimum pH values. The dominant effect of pH on the adsorption of metal ions onto loofa is described in this report and supported by previous researchers (Pagnanelli *et al*., 2003; Iqbal *et al*., 2009; Amer *et al*., 2010; ElShafei *et al*., 2014; Iqbal & Edyvean, 2004; Srivastava & Angove, 2004).

12.3.2 Concentration

The concentration of each metal solution determines the uptake capacity of the loofa for the metal pollutant. Lead ions quickly occupy binding sites and, as these become saturated as the lead concentration increases, the percentage removal of lead ions is decreased. Zinc ions bind to two available sites on the loofa surface. Therefore, when the concentration is increased from 50mg/L to 70mg/L, the percentage removal increases until no further increase was observed (at a concentration greater than 70mg/L). Eventually, both specific and exchange sites are fully occupied and no further uptake capacity can be achieved. Naijah *et al.* (2014) report an increase in the amount of lead and zinc ions adsorbed onto selected agricultural wastes and also a decrease in the adsorption efficiency as the initial concentration is increased. They further report that all lead and zinc ions were completely removed from aqueous solution at low initial

concentrations of 10 and 25mg/L. For cadmium ions, the uptake capacity is attributed to the bonding of the cadmium ions to the active sites of the loofa. The uneven increase and then decrease in percentage removal of cadmium may be as a result of precipitation of cadmium from solution which shows, on analysis, as an increase in the percentage removal of cadmium ions from solution. The decrease can be attributed to all the bonding sites becoming occupied. A steady state of adsorption does not occur and maximum uptake is at 100mg/L. Further increases from 100mg/L to 150mg/L lead to an actual decrease (by 14.3%) in the absolute uptake (Figure 6.10 in chapter 6). The uncertainty of cadmium ion adsorption shows the need for further analysis for understanding the adsorption process. Suguna and Kumar (2013) reported the adsorption of cadmium ions onto woody pore fungi biomass to increase over time till a constant value was attained at equilibrium for the initial concentrations of 100 to 400mg/L.

While this shows a similar trend to the adsorption of cadmium ions onto loofa at the first stage of adsorption, no further explanation was given. Akhtar *et al.* (2003) showed rapid uptake to occur from 10 – 25mg/L but report a slight decrease in the absolute adsorption level, attributed to fewer available binding sites as a result of saturation as the cadmium concentration increases. This gives an insight into the adsorption that occurs as concentration increases and means that the adsorption of cadmium can be controlled and predicted at lower concentrations but not at high initial cadmium concentrations. In fact, low concentrations of all the metal ions will be sufficiently and predictably adsorbed onto the loofa surface. This finding is supported by Amuda *et al*. (2007) for the adsorption of heavy metals onto modified activated coconut shell carbon (see also Suguna & Kumar, 2013; Najiah *et al.*, 2014).

12.3.3 Temperature

Temperature is one of the factors affecting the adsorption of lead ions. The removal capacity is decreased as the temperature is increased from 21^{o}C to 55^{o}C.

Sari and Tuzen (2008) demonstrated the exothermic nature of lead adsorption onto *U.lactuca* biomass as the temperature was increased from 20 – 50^{o}C. The reason being the increasing

tendency for desorption of lead ions to occur and possible damage to active bonding sites on the biomass. As found by a number of researchers for other biomasses (Sari & Tuzen, 2008b), the negative value of ΔH, found in the present work, identifies an exothermic reaction for lead ion adsorption onto loofa .

12.3.4 Ionic strength

There is an antagonist effect that occurs in the uptake of lead when the ionic strength of the solution is increased. This alteration leads to saturation of the lead ions with no further increase in adsorption capacity with time. This is a gradual process that peaks at approximately 2hrs and then shows no further increase or decrease as there is saturation of the ions in the solution shows that all the available adsorption sites are occupied. Chlorine ions form complexes with lead ions and sodium ions compete with lead ions for bonding sites. Zhao *et al*. (2016) report the effect of ionic strength on the adsorption of pharmaceuticals onto multi-walled carbon nanotubes. This showed the effect of ionic strength on the adsorption mechanism process involving functional groups (Zhao *et al*., 2016). Ouyang *et al*. (2014) showed that the effect of sodium chloride on the adsorption efficiency of lead ions onto peanut shell is very small when less than 0.1M but has a significant effect at more than 0.1M. They explain that complexes are formed and there is competition due to the Na^+ ions. The addition of NaCl (a strong base and strong acid) is expected to produce a neutral solution when added to water. The change in the ionic strength changes the activity of the ions in solution and therefore drifts the pH towards neutrality (depending on the pH of the solution). After an increase in ionic strength (from 0.1M to 0.5M NaCl), the percentage removal of lead ions from aqueous solution decreases from 96% to 91%, which is similar to the percentage removal at pH 6 – 7. Also, the pH increased from pH 5 to 5.69 after the addition of NaCl. The adsorption of zinc ions decreases by about 15% when the ionic strength is increased by 0.5M NaCl, and this is similar to the decrease that occurs at pH 7 (Zhao *et al*., 2016).

12.3.5 FT-IR observations

Comparing alkali treated loofa alone and lead loaded alkali treated loofa, the presence of intermolecular forces of hydrogen bonding is shown to change after lead adsorption resulting in a small, sharper, peak indicating less bonding of hydrogen bonds from a-hydrogen bonded O-H bond. This means that the hydrogen bond has been broken down and hydrogen ions released into solution. The metal ion adsorption is attributed to the stretching vibrations of free and intermolecular bonded O-H groups (Van Thuan *et al*., 2017). This involvement of intermolecular interactions in adsorption leads to the formation of chemical bonds (Thommes *et al*., 2015). Jayamani *et al*. (2014) report the involvement of the COO-H and O-H groups as shown by a decrease in the peak intensity due to the vibrations, stretching and bending that occurs during treatment (Jayamani *et al*., 2014). The major changes that occur at the O-H and C-H groups are shown by the change in frequencies during adsorption of lead or zinc ions. There is a shift and stretching in the O-H bonding at 1000 – 1500cm^{-1} and 3330 - 3340 cm^{-1}. A small sharp absorption peak shows non hydrogen bonding of the O-H bond. Altinisik *et al*. (2010) report the presence of a sharper band denoting a stretching vibration of the O-H bond after adsorption of malachite green onto *Luffa cylindrica*. For Cd-loaded loofa, a sharper band is seen for the O-H bond group at 3200cm^{-1} – 3400cm^{-1} and also a new peak at 1650cm^{-1} which can be attributed to carbonyl group interactions with the cadmium ions (Altinişik *et al*., 2010). The change in frequency and peak intensity shows the involvement of functional groups in the adsorption process.

12.3.6 Models

12.3.6.1 Kinetic modelling

- **Pseudo second order model**

Pseudo second order models best describe the adsorption of divalent metal ions. The kinetic model fit confirms the interaction between lead ions and ions on the loofa surface. The pseudo second order constant for lead ion adsorption shows an uneven increase and then decrease as

the initial concentration is increased. This indicates that the interaction between the lead ions and the loofa surface is different throughout the adsorption process. The adsorption capacity does not correlate with the defined rate of adsorption. The maximum adsorption values of lead ions estimated from the PSO were shown to be very close at concentrations of 100mg/L & 150mg/L. This indicates that saturation is reached between 100 and 150mg/L and therefore the point where the model best applies. The uptake of zinc ions also fits a PSO kinetic model. Zinc adsorption follows the same saturation process as lead ion adsorption. There is an initial fast adsorption rate in the first 15 minutes and then adsorption gradually increases until equilibrium, and these equilibrium values were calculated to obtain the adsorption capacity which was compared with the PSO values. Again, the PSO model does not fit the initial stages but does fit at the equilibrium stage of adsorption. As for the cadmium ions, the calculated and actual adsorption values were not close for each concentration studied but show a maximum at pH 7 where the calculated and experimental values were closest. Zinc and cadmium ions have a similar adsorption process and fit the pseudo second order (PSO) model best. PSO models indicate that the rate limiting step is not a boundary layer resistance mechanism for these metal ions. Yi-Yang *et al*. (2012) found the maximum adsorption capacity of reactive black 5 onto fungal biomass to be in accord with the PSO q_{max} values. Also, Lasheen *et al*. (2012) found the maximum adsorption capacity of cadmium, copper and lead onto chemically modified orange peel to fit the PSO model. While PSO shows a good fit, further explanation of the adsorption process was investigated by using the Elovich model.

- **Elovich model**

The Elovich model does not explain lead and zinc adsorption behaviour but gives a good fit for cadmium adsorption and an adsorption rate of 34.4 mg/g/min and a significant surface coverage of 6 g/mg. Martins *et al.* (2014), using the Elovich equation, showed the adsorption of lead and cadmium ions onto aquatic moss to be different when the concentration was increased from 10mg/L to 100mg/L. Different behaviour was shown to occur at different pH values, having an

optimum adsorption rate at pH 7. The mass transfer steps were further analysed by utilising the intraparticle diffusion model.

- **Intraparticle diffusion model**

The intraparticle diffusion model is shown to play a significant role only in the adsorption of cadmium ions but this was not the only rate-limiting step in the adsorption process as further described by other models. The change between the initial and final slopes indicates that cadmium ions bond to the external surface and then diffuse into the loofa particle. Blazquez *et al*. (2014) report a similar two-step mechanism for the adsorption of lead onto native and chemically treated olive stone. They did not fit a model but the intraparticle diffusion plots showed two-step and single step mechanisms for lead and zinc ions respectively. Rahmand and Sathasivam (2015) report that the adsorption of lead and zinc ions onto *Kappaphycus sp.* fit both the Elovich and intraparticle diffusion models (R^2 = 0.79 – 1) due to adsorption on both the external surface and interior of the particle.

- **Boyd model**

The Boyd model shows film diffusion as the rate controlling step for lead, zinc and cadmium adsorption at 50mg/L. However, as the concentration increases, the values shift away from linearity and follow a different pattern of diffusion. Zinc ion adsorption showed no correlation to the Boyd model at 100mg/L which describes a shift from film diffusion to particle diffusion as the rate-controlling step at a higher concentration (Yang *et al*., 2012; Martins *et al*., 2014; Blázquez *et al*., 2014).

12.3.6.2 Isotherm modelling

- **Langmuir and Freundlich models**

The adsorption properties were further described under constant temperature by using isotherm models. The isotherm model fit indicates the loofa to have a heterogeneous surface with two different bonding sites available for lead ion adsorption. As initial concentration is

increased, the bonding pattern changes from film diffusion to pore diffusion until a peak is reached (Figure 4.28 & 4.30 - Chapter 4). Machida *et al* (2004) report the adsorption of lead ions onto activated carbon fits the Langmuir, Freundlich and two-site model, which means that adsorption occurs on a heterogeneous surface with two adsorption sites. One site gives a higher adsorption equilibrium constant than the other, which classifies the sites as strong or weak. The adsorption of lead ions onto loofa shows a good linearity fit to the two-site Langmuir model (modified Langmuir model), again indicating a two site adsorption process. As the process progresses and the initial concentration is increased, one type of site becomes fully occupied followed by the other (Machida *et al*., 2004). Zinc adsorption showed no fit to the Langmuir model and thus a homogenous surface bonding mechanism is not indicated. The high bonding capacity of lead and zinc ions was described by a good fit to the Freundlich model which indicates the involvement of different adsorption intensities. However, this model did not fit cadmium ion adsorption which shows low bonding capacity having only one site involved in the adsorption process. Cadmium and lead ions show a good fit to the experimental adsorption data for a monolayer covering on the loofa surface (correlation coefficients above 0.90) indicating a homogeneous surface adsorption. Foo and Hameed (2010) found each metal ion to differ in its adsorption affinity to loofa, which means that higher affinity sites are occupied first, therefore they utilised a two site Langmuir model. Lead and zinc ion adsorption showed a good fit to the two site Langmuir model but cadmium adsorption could not be explained. Onyango *et al.* (2004) reported the removal of fluoride by trivalent cation-exchanged zeolite to fit the two site Langmuir model. This explained the competitive nature and difference in the bonding process and also the difference in the capacity values of each trivalent ion during the adsorption process.

- **Dubinin-Radushkevich and Sips models**

The nature of the biosorption process of lead ions is described by the Dubinin-Radushkevich (DBR) model to be chemical. The temkin model, which can explicitly describe the interaction between the loofa and metal ions in terms of the heat of sorption that occurs at maximum bonding energy, gives a good fit only for lead ions. Bonding energies for the adsorption of zinc

and cadmium ions could not be estimated. Madala *et al*. (2013) described the adsorption of cadmium ions onto composite chitosan biosorbent to fit the Langmuir, Freundlich, DBR and temkin isotherm models with Langmuir as the best fit describing a homogeneous surface adsorption. The sips model was a good fit for lead, zinc and cadmium ions, which is a combined Langmuir and Freundlich model and predicts a heterogeneous adsorption system. (Madala *et al*., 2013; Foo & Hameed, 2010; Onyango *et al*., 2004). The adsorption of lead, zinc and cadmium show that there is a difference in the adsorption onto the loofa sites and competition as each ion binds onto loofa in multi- metal solutions.

12.4 Adsorption mechanism of methylene blue

12.4.1 Modification

Methylene blue (MB) is a cationic dye, due to its positively charged surface. The degree of ionization of the dye will depend on the solution pH. Maximum percentage removal of 99% is found at an optimum pH of 7. The surface chemistry of loofa can be modified to improve adsorption. At a constant pH of 7 and initial concentration of 20mg/L, the optimum percentage removal was found on alkali treated loofa, which has the highest pore size distribution.

MB shows a different bonding mechanism when binding to untreated loofa as compared to alkali treated loofa. A higher adsorption capacity is observed for the alkali treated loofa which shows that the complexation formed on the loofa surface optimises the adsorption process of MB. Increased light intensity has a positive effect on MB adsorption. Degradation of MB loaded untreated loofa and MB loaded alkali treated loofa is shown to increase in the presence of light with MB degraded greatest for the alkali treated loofa (Figure 7.71 & 7.72).

12.4.2 Experimental conditions

An absorbance versus concentration plot (appendix B) was generated to obtain all concentration values used to analyse the experimental data obtained. The optimum pH for MB adsorption onto loofa is pH 7. At a lower pH, the number of hydrogen ions increases and these compete with the

MB cations for sites leading to reduced adsorption. As the pH increases over pH 7, the adsorption capacity also decreases which shows that factors apart from electrostatic attraction and the competitive behaviour of hydrogen ions affect the adsorption process. MB cations exist at 100% over pH 6 but not all are adsorbed on the loofa since the adsorption capacity decreases with increasing pH. This applies to both NaOH and HCl treated loofa as well as untreated loofa. However, there is no significant difference in the adsorption capacity of MB onto any of the loofa types at pH 7 (a less than 10% difference in percentage removal and less than 5% difference in uptake (Figure 7.31 & 7.32).

In the present work, the effect of the initial concentration on adsorption of MB onto untreated, alkali treated and acid treated loofa was studied. The untreated loofa showed an initial rapid adsorption within 15 minutes and then a fairly constant uptake with time at each concentration in the range 10 – 40mg/L. The alkali and acid treated loofa showed similar behaviour but with an initial rapid adsorption in the first 5 minutes and then a fairly constant uptake with time for the same range of concentrations. This shows that treatment of the loofa decreases the time needed for MB adsorption to occur and also increases the percentage removal by creating larger amount of active sites for adsorption. It is expected that the available bonding sites of the loofa would decrease as the concentration increases until saturation occurs but saturation was not reached in the MB concentrations used in this experiment. Hamed *et al.* (2014) also reported a rapid increase in MB adsorption onto marble dust in less than 10mins and also an increase in uptake as initial MB concentration increased up to 180mg/L. with no saturation. The percentage removal for all three types of treated/untreated loofa show an uneven plot of increase and decrease in the percentage removal as the initial MB concentration is increased. This can be explained by an uneven distribution of MB cations on the surface and pores of the loofa. The pores are first occupied followed by the loofa surface.

Altenor *et al.* (2009) report that porosity as well as the chemical surface characteristics contribute to the adsorption of MB onto activated carbon. However, in the present work, while

there is some increase in percentage removal with an increase in initial concentration, the difference was small (below 10%). The alkali treated loofa showed the highest adsorption. There is a decrease in MB adsorption onto alkali treated loofa as temperature increases from 21 – 55^{o}C. Acid treated loofa shows a gradual, slight, increase in adsorption capacity as temperature increases from 21 – 55^{o}C. This indicates an endothermic reaction process, but the increase was very small.

Nasuha *et al.* (2010) report that the adsorption process of MB onto tea waste is endothermic in nature and that an increase in temperature increases the diffusion rate of the adsorbate molecules across the external boundary layer of the adsorbent particle into the internal pores. The slight positive and negative effects found for the two loofa treatments shows that the effect of the treatments on the loofa differs. It has been established that the pores and surface of the loofa play a part in the adsorption process. The pore diameter of the alkali treated loofa is less than that of the acid treated loofa which means that an increase in temperature expands the acid treated pores thereby increasing mobility of the MB cations and enhancing complex formation on the surface. However, as the alkali treatment creates smaller pore widths and an increase in temperature shows no effect on adsorption and even a decrease in adsorption capacity. The change in the FT-IR analysis of loofa after adsorption of MB shows the involvement of functional groups in the adsorption process. The broad adsorption peak of the untreated and treated loofa at wavelengths between 3100 – 3300cm^{-1} corresponds to O-H stretching which changes into a sharper peak after adsorption, and thus indicates the involvement of this functional group in the process. The peak at 1100cm^{-1} for the untreated and treated loofa represents a bending vibration of the C-O groups. The shift of the adsorption peak at wavelength 2900cm^{-1} is attributed to the stretching vibration of the C-H bond of the methyl group. Peydayesh and Rahbar-Kelishami (2015) showed the involvement of functional groups O-H, C-H and C-O-C bonds in the adsorption of MB onto *Platanus orientalis* leaf powder. A new peak was observed for untreated loofa after adsorption of MB at 1235cm^{-1} and 1610cm^{-1} which corresponds to the C-N bond and the C=O bond of the carbonyl group of ketone. This indicates

a change in the MB structure (from the change in the optimal wavelength observed by the UV-Vis spectra) during it's adsorption onto the untreated loofa.

12.4.3 Models

The pseudo second order model shows a good fit in describing the kinetic process of MB adsorption. The other kinetic models (Table 7.1) could not sufficiently describe the adsorption mechanism indicating that diffusion and boundary layer processes do not have a dominant effect on the MB adsorption mechanism. In mixed solutions with metals, MB has the greatest influence on the percentage removal capacity of lead when compared to MB/cadmium and MB/zinc aqueous solutions. This can be attributed to the larger boundary effect of lead adsorption onto loofa thereby creating an extra resistance for adsorption of lead ions on the surface. MB molecules are absorbed faster onto the loofa as there is no boundary layer effect but, once adsorbed, may provide a boundary layer for lead ions to overcome, thereby decreasing the adsorption capacity of lead. Sharma and Tiwari (2016) reported a boundary effect of MB onto *Sapindus* and *Camelina* seed-derived adsorbent as a mixed adsorption mechanism of surface and intraparticle diffusion. Manna *et al*. (2017) reported the involvement of functional groups in the adsorption of MB onto modified lignocellulose materials and also highlighted the importance of diffusion rate (good fit to the intraparticle diffusion model) as it plays a significant role in the adsorption mechanism. Chi *et al*. (2013) explain the adsorption of MB onto chemically modified loofa to be governed by intraparticle diffusion as the rate- limiting step and also showed a two-step process which was supported by Ofomaja *et al*. (2010). In contrast Demir *et al*. (2008) reported that the intraparticle diffusion model did not fit the adsorption of MB onto natural loofa. In the present work, the adsorption mechanism of MB onto alkali treated loofa could not be ascertained. The adsorption of MB onto untreated and treated loofa (table 7.2) could not be defined by the Langmuir model, unlike Demir *et al*. (2008) and Boudechiche *et al*. (2016) whom described the adsorption of MB onto natural loofa to be well defined by the Langmuir model. The Sips model shows a good fit for all three loofas indicating a heterogeneous

surface with two different bonding sites for the MB adsorption. The adsorption behaviour of MB in the present work best fits the pseudo second order kinetic model. Diffusion is not regarded as the rate-limiting step since MB adsorption does not fit well to the other kinetic models. (Reddy *et al*., 2015). A greater effect on the percentage removal of MB is shown when MB is mixed with lead ions than with cadmium and zinc. This is explained by the nature of the bonding sites available where lead ions inhibit the uptake of MB (involvement of the two different bonding sites for the high removal capacity of lead ions) but the uptake of cadmium and zinc show little effect due to their lower percentage adsorption and, in the case of zinc, having another bonding site available for further MB adsorption. It means that zinc bonds at different sites on the loofa thus reducing the competition between zinc and MB. Complexation explains the selective uptake of both methylene blue and metal ions. Alkali treated loofa shows the highest adsorption capacity for MB and shows an increase in adsorption capacity with an increase in light intensity. However, light acts as a catalyst which degrades MB and this affects the measurement of adsorption. The interaction of lead, zinc and cadmium in a ternary solution also shows an effect on each metal ion adsorption mechanism.

12.5 Mixed metal ions

pH and initial concentration are the main factors in the adsorption of mixed metal ions from aqueous solution. Competition for active ion exchange and complexation sites on the loofa explains the decrease in the amount of metal uptake. Other factors that have an effect are competition when adsorption occurs on two different sites and the behavioural pattern of the ions involved. That the behavioural pattern of mixed metals is altered is indicated by there being no relationship to the isotherm models that previously described the adsorption mechanism of single solutions. Also, competition adsorption via electrostatic forces and preferential adsorption is shown in the adsorption of each metal ion irrespective of their optimum pH and initial concentration (Chapter 8). This is further explained by the displacement of weakly adsorbed ions by more strongly adsorbed ions (Figure 8.4 & 8.5).

In some cases, where the initial concentration of one metal ion was increased, the percentage removal decreased while adsorption capacity was shown to be enhanced when the initial concentration of other was increased. In other cases, the pH altered the adsorption capacity irrespective of the initial concentration of the ions. Although, a change in the concentration ratio of the metal ions showed an effect based on the higher affinity and selectivity of the metal ions onto the loofa and also the properties of the ions present, solution pH was shown to be the most dominant factor. The kinetic mechanism of each metal ion adsorption process differs, as explained by the kinetic models, in mixed solutions. Hui *et al*. (2005) reported the removal of mixed heavy metal ions in wastewater by zeolite 4A and residual products from recycled coal fly ash to depend on the initial concentration of metal ions and the solution pH. In the present work, the high percentage removal of mixed metal ions at 78% at a rapid removal rate between pH 5-7 can be considered an effective process. The good fit of mixed solutions of lead, zinc and cadmium ions to the PSO model shows an adsorbate- adsorbent involvement of the loofa and metal ions, either considered as a single or as multi metal ions. Kim (2003) reported a change in the removal of single heavy metal ions compared to multi metal ions in adsorption onto crab shell. The affinity and inhibitory effects of the ions interchange under different conditions of single and binary systems. This can be explained by a strong affinity of lead ions for the crab shell in single ion solution which is inhibited by cadmium in a binary solution of cadmium and lead. In the present work, the fitting of the Boyd model to the lead ions in mixed solution indicates a greater boundary layer effect, which explains the extra resistance to be overcome for adsorption to occur. Lead ions are shown to have the least effect of the three ions in solution. The isotherm adsorption models predict a heterogeneous type of adsorption for zinc and cadmium with a different mechanism process of monolayer adsorption for lead.

12.6 Scale-up process – Column studies

A plant design will depend on the column experimental results of the adsorption of the pollutants onto the modified loofa (chapter 9). The concentration of the pollutants determines

the diffusion rate. As would be expected, the breakthrough time of lead, zinc and cadmium ions is decreased with increases in initial concentration. Exhaustion occurs faster and the mass transfer process is enhanced. The breakthrough point occurs when the maximum limit of the effluent solute concentration is reached. The loofa becomes saturated at this point and cannot adsorb any more pollutants. This was reached between 1-4hrs at a flow rate of 0.5ml/min, bed height of 9cm and at a concentration range of 20-40mg/L of the studied pollutants. At a lower concentration of 10mg/L, a breakthrough point was not reached after 6-8 hrs, the maximum experimental time. The time to reach a breakthrough depends on the concentration, bed height and flow rate. The Thomas and Yoon-Nelson models were used to explain the mass transfer process which is related to the initial concentration of the metal ions. Abdolali *et al*. (2017) reported the effect of initial concentration of heavy metals, which is related to the mass transfer process, of cadmium, copper, lead and zinc removal by a metal bonding biosorbent. The flow rate, bed depth and metal ion concentration were altered to obtain the optimal process. This was demonstrated to be highly dependent on the initial concentration.

These design data are important in developing an adsorption process in an industrial system. They determine the process stages that may be adopted to efficiently remove the desired pollutants from wastewater. Each metal ion studied has a different optimum pH for maximum adsorption capacity onto loofa. Therefore, the pH will need to be altered at each stage and the initial concentration taken into consideration. In the case of an initial concentration of all three metal ions of 50mg/L at pH 5, a total of 70% removal capacity can be achieved in the laboratory, leading to a projection of the need for several stages for optimum removal in industrial treatment. A diluted effluent, with lower initial concentration, will be more efficiently treated in fewer stages. Therefore, it would be economical to have the initial metal concentration at a low level (by dilution, or more preferably, by suitable pre-treatment, to enhance optimisation of the adsorption process (see below).

For MB, exhaustion occurs faster at a low concentration but no actual breakthrough point has been found. The description of the adsorption process of MB could not be explained since the diffusion of MB onto the loofa in the column was not evenly distributed. In industrial wastewater, the removal of each pollutant depends on the presence of other pollutants, therefore, further work on the MB adsorption mechanism process would assist in the design of a full scale adsorption process.

12.7 Industrial and economic impact of loofa utilisation in Nigeria

Pilot-plant scale studies, including the design and development of industrial scale columns, should be undertaken to check the feasibility at the industrial level and more research is required into the total cost evaluation in designated areas of the country in order to make full-scale implementation of a loofa based biosorption system possible (Wang & Peng, 2010; Mezohegyi *et al*., 2012; Tang *et al*., 2014).

In a densely populated country like Nigeria, the capital cost, installation costs and operational costs are expected to be high in terms of building, availability of land and the proximity of wastewater plants to the sources of pollution. Establishing an industry to produce loofa and to develop and run loofa based wastewater treatment systems will generate jobs and revenue for the Nigerian economy. Most importantly, it will curb environmental pollution, help meet UN and WHO targets and create a cleaner and healthier environment for the rising population in Nigeria.

12.8 Spent loofa

The recovery and reuse of the loofa is important in order to maximise its industrial application.

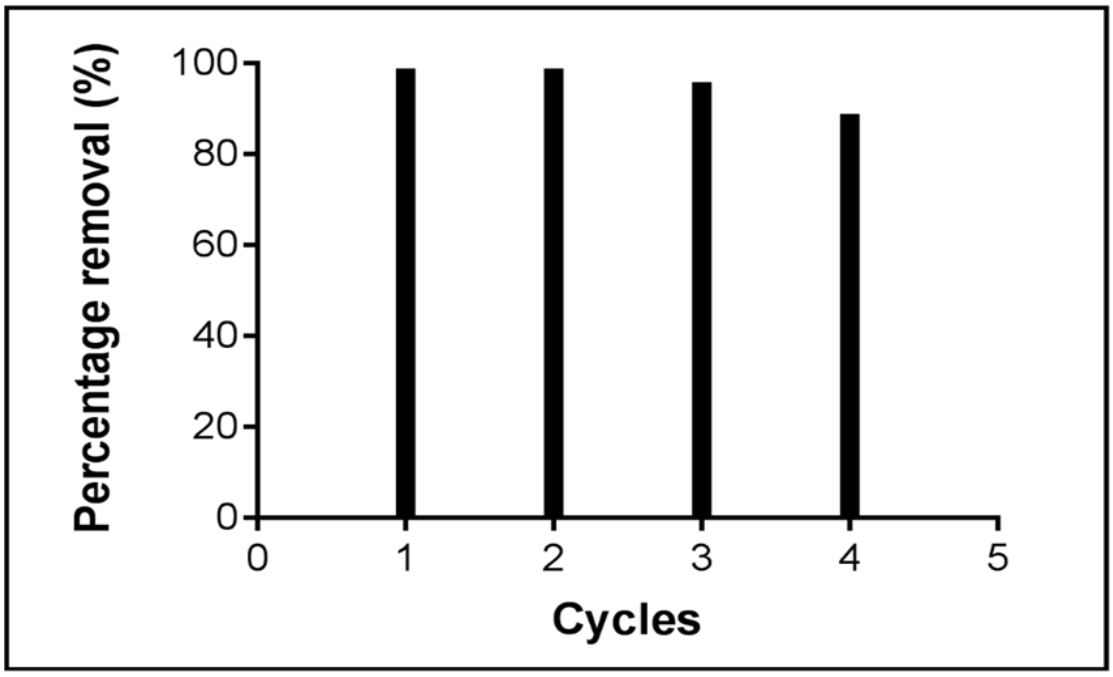

Figure 12.1: The percentage removal of lead ions over several cycles of adsorption with regeneration of the loofa with 0.1M HCl as eluent between each cycle at pH 5; lead ion concentration 50mg/L; flow rate 1mL/min; temperature 21^{o}C, loading capacity 2g; particle size 2mm; column height 9.5cm (obtained from Chapter 4, Figure 4.4).

Loofa regenerated and recycled four times for lead adsorption was found to give 98.9%, 98.8%. 95.8% & 88.8% removal in column studies for cycles 1, 2, 3 & 4 respectively. Bhatnagar *et al*. (2015) reported the regeneration and recycling of spent adsorbent to be effective at 89% in column studies. This shows an economically and environmentally sound use of loofa material. Once used for several cycles the loofa has to be disposed of. When looking for ways to dispose of the spent loofa, the cost of the loofa should be taken into consideration, in terms of its availability, treatment conditions, lifetime issues and country of production.

12.9 Summary

The contribution of this research to science was first to determine the reason the pollutants studied have a strong affinity for the loofa and under what optimum conditions this occurs. The

adsorbent properties of the loofa, why it binds differently to each of the pollutants and the factors that enhance or inhibit the adsorption process were ascertained. The results indicate the availability of multiple bonding sites on the loofa, how each pollutant binds differently to the surface and pores of the loofa and the mechanisms of adsorption involved. Thus a better understanding of the adsorption processes has been achieved.

CHAPTER THIRTEEN

13.0 CONCLUSION

- *Luffa cylindrica* (loofa) is a suitable biosorbent material that can be utilised in the treatment of wastewater containing metal ions such as lead, cadmium and zinc and also cationic dyes and similar organic compounds. It shows a high removal capacity under optimum experimental conditions.

- Loofa biosorbent has a stronger affinity for metal ions and the cationic dye, methylene blue, after modification by treatment with alkali which enhances its surface properties and thus improves its adsorption capacity. Its structural characteristics possess active binding sites having multiple binding energies which enable the pollutant ions to bind and be removed. The dominant functional carboxyl and hydroxyl groups play an important role in the adsorption process of all the pollutants studied.

- In solution the pollutants exist in different forms (speciation) at different pH values. The pH at which a pollutant optimally binds to the loofa indicates the species of the pollutant that is involved in this binding. Other factors, such as temperature, time interval, adsorbent dosage, initial concentration, ionic strength and the presence of other pollutants, positively or negatively affect the binding process and need to be controlled to achieve optimal adsorptive performance.

- The adsorption of pollutants onto loofa can be described by a number of models (chapters 4 – 9) that help explain the adsorption process. The adsorption mechanism was found to be a combination of ion exchange and complexation.

- The ion exchange mechanism of adsorption onto loofa can enable it to replace ion exchange resins in adsorption plant designs. Also, incorporation of the loofa column design into wastewater treatment plants is likely to deliver good results as highlighted in the study.

- Compared to many other biosorbents, loofa shows a significant uptake capacity that requires no extensive technological development. The loofa material is economically viable, available in large quantities and requires no expensive modification of its properties. These properties, together with a relatively green modification strategy for improvement of adsorption and potentially environmentally friendly disposal, make it a suitable candidate for use in the removal of pollutants from wastewater.

13.1 Recommendations for future work

Different species of metal ions occur in solution and the proportion of each species that actually binds to the active sites on the loofa should be determined (Asuquo *et al*., 2017). The complexes formed, based on the metal speciation on the loofa, due to the different available binding sites can be determined by Extended X-ray absorption fine structure (EXAFS) studies (Kirpichtchikova *et al*., 2006). Understanding the structural coordination of the complexes will further explain the nature of the binding of metal ions and organic molecules to alkali treated loofa. A greater understanding of the adsorption mechanisms and capacity at this level will assist in enhancing the performance of such biosorbents. A molecular level understanding of the uptake processes that will be able to optimise the loofa biosorbent systems efficiently was considered during this work, and a bid for time at the Diamond Light Source, B18 beamline at Harwell Campus in South Oxfordshire was made with the aim of using EXAFS to identify the metal species taken up and to determine the effect of chemical modification of the loofa surface on surface complexation. This would further explain the nature of bonding (metal speciation and proportion of carboxyl and hydroxyl groups) and also the effect of chemical changes, such as solution pH and basic surface modification, and their effects on the relative proportions of surface complexes formed. This would allow for the generation of surface complexation models which can be used to predict the physiochemical parameters of the most efficient and effective loofa biosorption process.

The EXAFS study would determine the speciation of both metals in model wastewater solutions and as surface adsorbed species on loofa by using Zn, Cd K-edge XAS and Pb LIII-edge XAS. The

speciation variability, due to the competitive effects between mixed metals and the pH would be determined. The expected results would describe the coordination environment about the metal centres under different conditions. A direct comparison of these results with those of established water treatment solutions in industrialised countries could lead to a cheap and sustainable water treatment process. Furthermore, a continuation of tests on the adsorption of real effluents onto loofa should be undertaken to allow an easier implementation of this adsorption process on a larger scale in developing countries such as Nigeria, giving a deep understanding on how to optimise a loofa biosorption process system. The stages of treatment could then be adopted based on the efficiency of the loofa in recovery and reuse. Further work could also focus on improving the adsorption capacity of metal ions and organic pollutants onto loofa by altering the structural bonding of the loofa and changing the speciation of the pollutants in solution whilst ensuring a cost-effective and sustainable process.

Considering the spent loofa material, one way to deal with this may be to incorporate it as a binding agent in tiles, bricks, concrete and cement like materials etc. Ramrakhiani *et al*. (2017) suggest glass matrix preparation to be most appropriate for immobilising tannery industrial waste sludge biosorbents. They show an environmentally stable product with a slow dissolution rate for glass immobilised tannery sludge spent biosorbent containing toxic metal ions. The addition of 25% of this biosorbent for glass manufacture showed no leaching for an incubation period of 35 days at 75^{o}C (Ramrakhiani *et al*., 2017). However, extensive work should be done on the capabilities of loofa for this process, it showed no sign of decomposition for an incubation period of 3 years at room temperature and the loofa was found to burn off at over 200^{o}C (Chapter 3). Combustion of the metal loaded loofa to ashes, by controlled incineration or pyrolysis, could be the first step to its utilisation in glass manufacturing. The disposal of the spent loofa to landfill will have a negative impact and is therefore not suitable because of potential contamination and pollution of water via leaching. Also, burning the biomass will lead to air pollution and should not be adopted (Bhatnagar & Minocha, 2006). The recovery and reuse of the loaded metals is also an industrial application that needs further investigation. Acid washing

could be considered as this is a non-destructive chemical method that removes concentrated metal solutions from the adsorbents without destructive effect to the adsorbent. The valuable metal ions can then be processed and re-used.

References

Abdelwahab, O. (2008). Evaluation of the Use of Loofa Activated Carbons as Potential Adsorbents for Aqueous Solutions Containing Dye. *Desalination*, 222(1–3), 357–367.

Abdolali, A., Hao, H., Guo, W., Zhou, J. L., Du, B., Wei, Q., et al. (2015). Bioresource Technology Characterization of a Multi-Metal Binding Biosorbent : Chemical Modification and Desorption Studies. *Bioresource Technology*, 193, 477–487.

Abdolali, A., Hao Ngo, H., Guo, W., Zhou, J. L., Zhang, J., Liang, S., et al. (2017). Application of a Breakthrough Biosorbent for Removing Heavy Metalsfrom Synthetic and Real Wastewaters in a Lab−scale Continuous Fixed−bed Column. *Bioresource Technology*, 229, 78–87.

Abdolali, A., Ngo, H. H., Guo, W., Lu, S., Chen, S. S., Nguyen, N. C., et al. (2016). A Breakthrough Biosorbent in Removing Heavy Metals: Equilibrium, Kinetic, Thermodynamic and Mechanism Analyses in a Lab-Scale Study. *Science of the Total Environment*, 542, 603–611.

Adewumi and Oguntuase. (2016). Planning of Wastewater Reuse Programme in Nigeria. , 15, 1–33.

Adewuyi, A. & Pereira, V. F. (2017). Underutilized Luffa Cylindrica Sponge : A Local Bio-Adsorbent for the Removal of Pb (II) Pollutant from Water System. *Beni-Suef University Journal of Basic and Applied Sciences*, 6(2), 118–126.

Ahamed, M. R., Azarudeen, R. S., Karunakaran, M. & Burkanudeen, A. R. (2010). Synthesis, Characterization, Metal Ion Binding Capacities and Applications of a Terpolymer Resin of Anthranilic acid/Salicylic acid/Formaldehyde. , 19(8), 635–646.

Ahmad, R. & Haseeb, S. (2015). Kinetic, Isotherm and Thermodynamic Studies for the Removal of Lead Ion by a Novel Adsorbent Luffa Acutangula (LAPR). *Desalination and Water Treatment*.

Ahmad, R. & Haseeb, S. (2015). Desalination and Water Treatment Kinetic , Isotherm and Thermodynamic Studies for the Removal of Pb 2 + Ion by a Novel Adsorbent Luffa Acutangula (LAPR) Kinetic , Isotherm and Thermod ... Kinetic , Isotherm and Thermodynamic Studies for the Removal of P. , (January 2016).

Ajuru, M. & Nmom, F. (2017). A Review on the Economic Uses of Species of Cucurbitaceae and Their Sustainability in Nigeria. *American Journal of Plant Biology*, 2(1), 17–24.

Akhtar, N., Iqbal, J. & Iqbal, M. (2003). Microalgal-Luffa Sponge Immobilized Disc : A New Efficient Biosorbent for the Removal of Ni (II) from Aqueous Solution. , (Ii), 149–153.

Aksu, Z. (2005). Application of Biosorption for the Removal of Organic Pollutants: A Review. *Process Biochemistry*, 40(3–4), 997–1026.

Aksu, Z. & Gönen, F. (2004). Biosorption of Phenol by Immobilized Activated Sludge in a Continuous Packed Bed: Prediction of Breakthrough Curves. *Process Biochemistry*, 39(5), 599–613.

Albadarin, A. B., Mangwandi, C., Walker, G. M., Allen, S. J., Ahmad, M. N. M. & Khraisheh, M. (2013). Influence of Solution Chemistry on Cr(VI) Reduction and Complexation onto Date-Pits/tea-Waste Biomaterials. *Journal of Environmental Management*, 114, 190–201.

Ali, I., Asim, M. & Khan, T. a. (2012). Low Cost Adsorbents for the Removal of Organic Pollutants from Wastewater. *Journal of Environmental Management*, 113, 170–183.

Altenor, S., Carene, B., Emmanuel, E., Lambert, J., Ehrhardt, J.-J. & Gaspard, S. (2009). Adsorption Studies of Methylene Blue and Phenol onto Vetiver Roots Activated Carbon Prepared by Chemical Activation. *Journal of hazardous materials*, 165(1–3), 1029–39.

Altenor, S., Carene, B., Emmanuel, E., Lambert, J., Ehrhardt, J. & Gaspard, S. (2009). Adsorption Studies of Methylene Blue and Phenol onto Vetiver Roots Activated Carbon Prepared by Chemical Activation. , 165, 1029–1039.

Altinişik, A., Gür, E. & Seki, Y. (2010). A Natural Sorbent, Luffa Cylindrica for the Removal of a Model Basic Dye. *Journal of hazardous materials*, 179(1–3), 658–64.

Álvarez-Ayuso, E., Garcia-Sanchez, A. & Querol, X. (2003). Purification of Metal Electroplating Waste Waters Using Zeolites. *Water Research*, 37(20), 4855–4862.

Amali, Z., Ramli, C., Asim, N., Isahak, W. N. R. W., Emdadi, Z., Ahmad-ludin, N., et al. (2014). Photocatalytic Degradation of Methylene Blue under UV Light Irradiation on Prepared Carbonaceous TiO 2. , 2014(C), 13–15.

Amer, M. W., Ahmad, R. A. & Awwad, A. M. (2015). Biosorption of Cu (II), Ni (II), Zn (II) and Pb (II) Ions from Aqueous Solution by Sophora Japonica Pods Powder. , 67–75.

Amer, M. W., Khalili, F. I. & Awwad, A. M. (2010). Adsorption of Lead , Zinc and Cadmium Ions on Polyphosphate-Modified Kaolinite Clay. , 2(1), 1–8.

Ameta, A., Ameta, R. & Ahuja, M. (2013). Photocatalytic Degradation of Methylene Blue over Ferric Tungstate. , 3(3), 172–180.

Amuda, O. S., Giwa, a. a. & Bello, I. a. (2007). Removal of Heavy Metal from Industrial Wastewater Using Modified Activated Coconut Shell Carbon. *Biochemical Engineering Journal*, 36(2), 174–181.

Anyakora, C., Nwaeze, K., Awodele, O., Nwadike, C., Arbabi, M. & Coker, H. (2011). Concentrations of Heavy Metals in Some Pharmaceutical Effluents in Lagos , Nigeria. , 3(February), 25–31.

Areco, M. M., Hanela, S., Duran, J. & Afonso, M. D. S. (2012). Biosorption of Cu(II), Zn(II), Cd(II) and Pb(II) by Dead Biomasses of Green Alga Ulva Lactuca and the Development of a Sustainable Matrix for Adsorption Implementation. *Journal of hazardous materials*, 213–214, 123–32.

Arshadi, M., Amiri, M. J. & Mousavi, S. (2014). Kinetic , Equilibrium and Thermodynamic Investigations of Ni (II), Cd (II), Cu (II) and Co (II) Adsorption on Barley Straw Ash. *Water Resources and Industry*, 6, 1–17.

Asuquo, E. D. & Martin, A. D. (2016). Sorption of Cadmium (II) Ion from Aqueous Solution onto Sweet Potato (Ipomoea Batatas L.) Peel Adsorbent: Characterisation, Kinetic and Isotherm Studies. *Journal of Environmental Chemical Engineering*, 4(4), 4207–4228.

Asuquo, E., Martin, A., Nzerem, P., Siperstein, F. & Fan, X. (2017). Adsorption of Cd(II) and Pb(II) Ions from Aqueous Solutions Using Mesoporous Activated Carbon Adsorbent: Equilibrium, Kinetics and Characterisation Studies. *Journal of Environmental Chemical Engineering*, 5(1).

Ayenimo, J. G., Adeeyinwo, C. E. & Amoo, I. A. (2005). Heavy Metal Pollutants in Warri River, Nigeria. , 27, 43–50.

Bach, M. T. (2007). Impact of Surface Chemistry on Adsorption : Tailoring of Activated Carbon. , 1–132.

Banerjee, S. & Chattopadhyaya, M. C. (2013). Adsorption Characteristics for the Removal of a Toxic Dye , Tartrazine from Aqueous Solutions by a Low Cost Agricultural by-Product. *Arabian Journal of Chemistry*.

Barakat, M. a. (2011). New Trends in Removing Heavy Metals from Industrial Wastewater. *Arabian Journal of Chemistry*, 4(4), 361–377.

Bhatnagar, A., Hogland, W., Marques, M. & Sillanpää, M. (2013). An Overview of the Modification Methods of Activated Carbon for Its Water Treatment Applications. *Chemical Engineering Journal*, 219.

Bhatnagar & Minocha, A. K. (2006). Conventional and Non-Conventional Adsorbents for Removal of Pollutants from Water – A Review. , 13(May), 203–217.

Bismarck, A., Aranberri-Aksargorta, I. & Springer, J. (2002). Surface Characterization of Flax , Hemp and Water Uptake Behavior. , 23(5).

Blázquez, G., Calero, M., Ronda, A., Tenorio, G. & Martín-Lara, M. A. (2014). Study of Kinetics in the Biosorption of Lead onto Native and Chemically Treated Olive Stone. *Journal of Industrial and Engineering Chemistry*, 20(5), 2754–2760.

Blázquez, G., Calero, M., Ronda, A., Tenorio, G. & Martín-Lara, M. A. (2014). Study of Kinetics in the Biosorption of Lead onto Native and Chemically Treated Olive Stone. *Journal of Industrial and Engineering Chemistry*, 20(5), 2754–2760.

Borbely, G. & Nagy, E. (2009). Removal of Zinc and Nickel Ions by Complexation-Membrane Filtration Process from Industrial Wastewater. *Desalination*, 240(1–3), 218–226.

Boudechiche, N., Mokaddem, H. & Sadaoui, Z. (2016). Biosorption of Cationic Dye from Aqueous Solutions onto Lignocellulosic Biomass (Luffa Cylindrica): Characterization , Equilibrium , Kinetic and Thermodynamic Studies. *International Journal of Industrial Chemistry*.

Brinza, L., Dring, M. J. & Gavrilescu, M. (2007). Marine Micro and Macro Algal Species as Biosorbents for Heavy Metals. , 6(3), 237–251.

Brouers, F. (2014). Statistical Foundation of Empirical Isotherms. , (October), 687–701.

Brouers, F. & Al-musawi, T. J. (2015). On the Optimal Use of Isotherm Models for the Characterization of Biosorption of Lead Onto Algae. , 1–14.

Burgess, J. (1999). Ions in Solution.

Burkert, C. A. V, Barbosa, G. N. O., Mazutti, M. A. & Maugeri, F. (2011). Mathematical Modeling and Experimental Breakthrough Curves of Cephalosporin C Adsorption in a Fixed-Bed Column. *Process Biochemistry*, 46(6), 1270–1277.

Cai, Q. Y., Mo, C. H., Wu, Q. T., Zeng, Q. Y. & Katsoyiannis, A. (2007). Concentration and Speciation of Heavy Metals in Six Different Sewage Sludge-Composts. *Journal of Hazardous Materials*, 147(3), 1063–1072.

Charerntanyarak, L. (1999). Heavy Metals Removal by Chemical Coagulation and Precipitation. *Water Science and Technology*, 39(10–11).

Chen, B., Chen, C., Guo, W., Chang, H., Chen, W., Lee, D., et al. (2014). Fixed-Bed Biosorption of

Cadmium Using Immobilized Scenedesmus Obliquus CNW-N Cells on Loofa (Luffa Cylindrica) Sponge. *Bioresource Technology*, 160, 175–181.

Chen, X. (2015). Modeling of Experimental Adsorption Isotherm Data. *Information*, 6(1), 14–22.

Chi, R., Yu, J., Wang, L., Zhang, Y., Xu, Z. & Guo, J. (2013). Removal of Cationic Dyes : Basic Magenta and Methylene Blue from Aqueous Solution by Adsorption on Modified Loofah. , 3775–3790.

Chowdhury, S. & Saha, P. Das. (2012). Biosorption of Methylene Blue from Aqueous Solutions by a Waste Biomaterial: Hen Feathers. *Applied Water Science*, 2(3), 209–219.

Chowdhury, Z. Z., Zain, S. M., Rashid, A. K., Rafique, R. F. & Khalid, K. (2013). Breakthrough Curve Analysis for Column Dynamics Sorption of Mn(II) Ions from Wastewater by Using Mangostana Garcinia Peel-Based Granular-Activated Carbon. *Journal of Chemistry*.

Christov, L. ., van Driessel, B. & du Plessis, C. . (1999). Fungal Biomass from Rhizomucor Pusillus as Adsorbent of Chromophores from a Bleach Plant Effluent. *Process Biochemistry*, 35(1–2), 91–95.

Chung, T., Loganathan, P., Vinh, T. & Vigneswaran, S. (2015). Simultaneous Adsorption of Cd , Cr , Cu , Pb , and Zn by an Iron-Coated Australian Zeolite in Batch and Fixed-Bed Column Studies. *Chemical Engineering Journal*, 270, 393–404.

Correa, R. C., Otto, T. & Kruse, A. (2017). Biomass and Bioenergy In Fl Uence of the Biomass Components on the Pore Formation of Activated Carbon. *Biomass and Bioenergy*, 97, 53–64.

Dahri, M. K., Kooh, M. R. R. & Lim, L. B. L. (2015). Application of Casuarina Equisetifolia Needle for the Removal of Methylene Blue and Malachite Green Dyes from Aqueous Solution. *Alexandria Engineering Journal*, 54(4), 1253–1263.

Defra UK. (2002). What Do the Measurements Tell Us ? Key Points. , 155–183.

Demir, H., Top, a, Balköse, D. & Ulkü, S. (2008). Dye Adsorption Behavior of Luffa Cylindrica Fibers. *Journal of hazardous materials*, 153(1–2), 389–94.

Derakhshan, Z., Baghapour, M. A. & Ranjbar, M. (2013). Adsorption of Methylene Blue Dye from Aqueous Solutions by Modified Pumice Stone : Kinetics and Equilibrium Studies. , 2(3).

Doss, V. R. & Kodolikar, S. P. (2012). Heavy Metal Adsorption by Ligand Loaded Granular Activated Carbon : Thermodynamics and Kinetics. , 2(4), 2126–2142.

Doyle, F. M. & Liu, Z. (2003). The Effect of Triethylenetetraamine (Trien) on the Ion Flotation of Cu2+ and Ni2+. *Journal of Colloid and Interface Science*, 258(2), 396–403.

Drweesh, S. A., Fathy, N. A., Wahba, M. A., Hanna, A. A., Akarish, A. I. M., Elzahany, E. A. M., et al. (2016). Journal of Environmental Chemical Engineering Equilibrium , Kinetic and Thermodynamic Studies of Pb (II) Adsorption from Aqueous Solutions on HCl-Treated Egyptian Kaolin. *Biochemical Pharmacology*, 4(2), 1674–1684.

Dubey, A.Shiwani, S. (2012). Adsorption of Lead Using a New Green Material Obtained from Portulaca Plant. , 15–20.

Edris, G., Alhamed, Y. & Alzahrani, A. (2012). 2 . Materials and Methods. , (II), 1–12.

Ehi-Eromosele, C. O. & Okiei, W. O. (2012). Heavy Metal Assessment of Ground, Surface and Tap Water Samples in Lagos Metropolis Using Anodic Stripping Voltammetry. *Resources and Environment*, 2(3), 82–86.

Ekberg, C. & Brown, P. L. (2016). *Hydrolysis of Metal Ions*.

ElShafei, G. M. S., ElSherbiny, I. M. a., Darwish, A. S. & Philip, C. a. (2014). Silkworms' Feces-Based Activated Carbons as Cheap Adsorbents for Removal of Cadmium and Methylene Blue from Aqueous Solutions. *Chemical Engineering Research and Design*, 92(3), 461–470.

Esan, O. S., Abiola, O. N., Owoyomi, O., Aboluwoye, C. O. & Osundiya, M. O. (2014). Adsorption of Brilliant Green onto Luffa Cylindrica Sponge: Equilibrium, Kinetics, and Thermodynamic Studies. *ISRN Physical Chemistry*, 1–12.

Escudero, R., Espinoza, E. & Tavera, F. J. (2013). Precipitation of Lead Species in a Pb – H 2 O System. , 2(9), 1–4.

Fan, H., Zhou, L., Jiang, X., Huang, Q. & Lang, W. (2014). Adsorption of Cu2+ and Methylene Blue on Dodecyl Sulfobetaine Surfactant-Modified Montmorillonite. *Applied Clay Science*, 95, 150–158.

Fan, J., Okyay, O. & Rodrigues, D. F. (2014). The Synergism of Temperature, pH and Growth Phases on Heavy Metal Biosorption by Two Environmental Isolates. *Journal of hazardous materials*, 279C, 236–243.

Febrianto, J., Kosasih, a, Sunarso, J., Ju, Y., Indraswati, N. & Ismadji, S. (2009). Equilibrium and Kinetic Studies in Adsorption of Heavy Metals Using Biosorbent: A Summary of Recent Studies. *Journal of Hazardous Materials*, 162(2–3), 616–45.

Feng, N. C. & Guo, X. Y. (2012). Characterization of Adsorptive Capacity and Mechanisms on Adsorption of Copper, Lead and Zinc by Modified Orange Peel. *Transactions of Nonferrous Metals Society of China (English Edition)*, 22(5), 1224–1231.

Fernando, Q. (1995). Metal Speciation in Environmental and Biological Systems. , 13–16.

Filatova, E. G., Pozhidaev, Y. N. & Pomazkina, O. I. (2016). Investigation of Adsorption of Heavy Metal Ions by Natural Aluminosilicate. , 52(3), 438–442.

Fomina, M. & Gadd, G. M. (2014). Biosorption: Current Perspectives on Concept, Definition and Application. *Bioresource technology*, 160, 3–14.

Foo, K. Y. & Hameed, B. H. (2010). Insights into the Modeling of Adsorption Isotherm Systems. *Chemical Engineering Journal*, 156(1), 2–10.

Fradj, A. Ben, Hamouda, S. Ben, Ouni, H., Lafi, R., Gzara, L. & Hafiane, A. (2014). Removal of Methylene Blue from Aqueous Solutions by Poly (Acrylic Acid) and Poly (Ammonium Acrylate) Assisted Ultrafiltration. *Separation and Purification Technology*, 133(October), 76–81.

Fras, L., Stana-kleinschek, K., Ribitsch, V., Sfiligoj-smole, M. & Kreze, T. (2000). Quantitative Determination of Carboxyl Groups in Cellulose by Complexometric Titration. , 80–88.

García-Mateos, F. J., Ruiz-Rosas, R., Marqués, M. D., Cotoruelo, L. M., Rodríguez-Mirasol, J. & Cordero, T. (2015). Removal of Paracetamol on Biomass-Derived Activated Carbon: Modeling the Fixed Bed Breakthrough Curves Using Batch Adsorption Experiments. *Chemical Engineering Journal*, 279.

Ghali, L. (2011). Effects of Fiber Weight Ratio, Structure and Fiber Modification onto Flexural Properties of Luffa-Polyester Composites. *Advances in Materials Physics and Chemistry*, 1(3), 78–85.

Ghali, L., Msahli, S., Zidi, M. & Sakli, F. (2009). Effect of Pre-Treatment of Luffa Fibres on the Structural Properties. *Materials Letters*, 63(1), 61–63.

Gimba, C. E., Ndukwe, G. I., Paul, E. D., Habila, J. D. & Madaki, L. A. (2015). Heavy Metals (Cd , Cu , Fe , Mn and Zn ,) Assessment of Groundwater , In. *international journal of Science and Technology*, 4(2), 49–56.

Gimenez, G. G., Ruiz, S. P., Caetano, W., Peralta, R. M. & Matioli, G. (2014). Biosorption Potential of Synthetic Dyes by Heat-Inactivated and Live Lentinus Edodes CCB-42 Immobilized in Loofa Sponges. *World journal of microbiology & biotechnology*, 30(12),

3229–44.

Gongden, J. J., Nnebedum, J. & Mafuyai, G. M. (2016). Equilibrium , Kinetic and Thermodynamic Study on the Removal of Cadmium (Ii) from Aqueous Solutions Using Sponge Gourd (Luffa Cylindrica) Fibers. , 5(1), 1–11.

Gordon, B., Callan, P. & Vickers, C. (2008). WHO Guidelines for Drinking-Water Quality. *WHO chronicle*, 38(3), 564.

Gouamid, M., Ouahrani, M. R. & Bensaci, M. B. (2013). Adsorption Equilibrium, Kinetics and Thermodynamics of Methylene Blue from Aqueous Solutions Using Date Palm Leaves. *Energy Procedia*, 36, 898–907.

Guerrero-Coronilla, L., Morales-Barrera, L. & Cristiani-Urbina, E. (2015). Kinetic, Isotherm and Thermodynamic Studies of Amaranth Dye Biosorption from Aqueous Solution onto Water Hyacinth Leaves. *Journal of Environmental Management*.

Guiza, S. (2017). Biosorption of Heavy Metal from Aqueous Solution Using Cellulosic Waste Orange Peel. *Ecological Engineering*, 99.

Gupta, V. K. & Rastogi, A. (2008). Biosorption of lead(II) from Aqueous Solutions by Non-Living Algal Biomass Oedogonium Sp. and Nostoc sp.—A Comparative Study. *Colloids and Surfaces B: Biointerfaces*, 64(2), 170–178.

Gusmao, K. A. G., Gurgel, L. V. A., Melo, T. M. S. & Gil, L. F. (2013). Adsorption Studies of Methylene Blue and Gentian Violet on Sugarcane Bagasse Modified with EDTA Dianhydride (EDTAD) in Aqueous Solutions: Kinetic and Equilibrium Aspects. *Journal of Environmntal Management*, 118, 135–143.

Han, X., Shan, Y., Fung, N. & Tam, Y. (2006). Surface Complexation Mechanism and Modeling in Cr (III) Biosorption by a Microalgal Isolate , Chlorella Miniata. , 303, 365–371.

Harland, C. E. (1994). *Ion Exchange: Theory and Practice*.

He, J. & Chen, J. P. (2014). A Comprehensive Review on Biosorption of Heavy Metals by Algal Biomass: Materials, Performances, Chemistry, and Modeling Simulation Tools. *Bioresource technology*, 160, 67–78.

Hernandez-Soriano, M. C. & Jimenez-Lopez, J. C. (2012). Effects of Soil Water Content and Organic Matter Addition on the Speciation and Bioavailability of Heavy Metals. *Science of the Total Environment*, 423, 55–61.

Ho, Y. S., Porter, J. F. & Mckay, G. (2002). Equilibrium Isotherms Studies for the Sorption of

Divalent Metal Ions onto Peat : Copper, Nickel and Lead Single Components Systems. , 1–33.

Holmberg, J. P. (2006). Competitive Adsorption and Displacement Behaviour of Heavy Metals on Peat.

Huang, E., Scales, F. & Copper, I. (2007). Use of Fish Scales as Biosorbent for the Removal of Copper in Water Esther Huang. , 1–14.

Hui, K. S., Chao, C. Y. H. & Kot, S. C. (2005). Removal of Mixed Heavy Metal Ions in Wastewater by Zeolite 4A and Residual Products from Recycled Coal Fly Ash. , 127, 89–101.

Hussain, S., Farooqui, M. & Rahim, S. A. (2013). Studies of Binary Complexes of Transition Metal Ions with Gallic Acid by Potentiometry. *International Journal of Emerging Technolgies in Computational and Applied Sciences(IJETCAS)*, 276–279.

Iqbal, M. & Edyvean, R. G. J. (2004). Biosorption of Lead, Copper and Zinc Ions on Loofa Sponge Immobilized Biomass of Phanerochaete Chrysosporium. *Minerals Engineering*, 17(2), 217–223.

Iqbal, M., Saeed, A. & Iqbal, S. (2009). FTIR Spectrophotometry , Kinetics and Adsorption Isotherms Modeling , Ion Exchange , and EDX Analysis for Understanding the Mechanism of Cd 2 + and Pb 2 + Removal by Mango Peel Waste. , 164, 161–171.

Jayamani, E., Hamdan, S., Heng, S. K., Rahman, M. R., Bakri, M. K. & Kakar, A. (2014). The Effect of Natural Fibres Mercerization on Natural Fibres / Polypropylene Composites : A Study of Thermal Stability , Morphology and Infrared Spectrum. *Australian Journal of Basic and Applied Science*, 8(15), 332–340.

Juang, R.-S. & Shiau, R.-C. (2000). Metal Removal from Aqueous Solutions Using Chitosan-Enhanced Membrane Filtration. *Journal of Membrane Science*, 165(2), 159–167.

Kapur, M. & Mondal, M. K. (2014). Journal of the Taiwan Institute of Chemical Engineers Competitive Sorption of Cu (II) and Ni (II) Ions from Aqueous Solutions : Kinetics , Thermodynamics and Desorption Studies. *Journal of the Taiwan Institute of Chemical Engineers*, 45(4), 1803–1813.

Khosravi, R., Fazlzadehdavil, M., Barikbin, B. & Taghizadeh, A. A. (2014). Removal of Hexavalent Chromium from Aqueous Solution by Granular and Powdered Peganum Harmala. *Applied Surface Science*, 292, 670–677.

Kim, D. S. (2003). The Removal by Crab Shell of Mixed Heavy Metal Ions in Aqueous Solution. ,

87, 355–357.

Kim, G., Igunnu, E. T. & Chen, G. Z. (2014). A Sunlight Assisted Dual Purpose Photoelectrochemical Cell for Low Voltage Removal of Heavy Metals and Organic Pollutants in Wastewater. *Chemical Engineering Journal*, 244, 411–421.

Kim, J. & Lawler, D. F. (2005). Characteristics of Zeta Potential Distribution in Silica Particles. , 26(7), 1083–1089.

Kirpichtchikova, T. A., Manceau, A., Spadini, L., Marcus, M. A. & Jacquet, T. (2006). Speciation and Solubility of Heavy Metals in Contaminated Soil Using X-Ray Microfluorescence , EXAFS Spectroscopy , Chemical Extraction , and Thermodynamic Modeling. , 70, 2163–2190.

Klika, Z. (2007). Composition , Structure , and Luminescence of Montmorillonites Saturated with Different Aggregates of Methylene Blue. , 311, 14–23.

Kulkarni, R. M., Shetty, K. V. & Srinikethan, G. (2014). Cadmium (II) and Nickel (II) Biosorption by Bacillus Laterosporus (MTCC 1628). *Journal of the Taiwan Institute of Chemical Engineers*, 45(4), 1628–1635.

Kurniawan, T. A., Chan, G. Y. S., Lo, W. H. & Babel, S. (2006). Physico-Chemical Treatment Techniques for Wastewater Laden with Heavy Metals. *Chemical Engineering Journal*, 118(1–2), 83–98.

Laidani, Y. (2012). Study of Fibrous Annual Plant, Luffa Cylindrica for Paper Application.Part 1: Characterization of the Vegetal. , 31(4), 119–129.

Lasheen, M. R. & Ammar, N. S. (2009). Assessment of Metals Speciation in Sewage Sludge and Stabilized Sludge from Different Wastewater Treatment Plants , Greater Cairo , Egypt. , 164, 740–749.

Lasheen, M. R., Ammar, N. S. & Ibrahim, H. S. (2012). Adsorption/desorption of Cd(II), Cu(II) and Pb(II) Using Chemically Modified Orange Peel: Equilibrium and Kinetic Studies. *Solid State Sciences*, 14(2), 202–210.

Lazaridis, N. ., Matis, K. . & Webb, M. (2001). Flotation of Metal-Loaded Clay Anion Exchangers. Part I: The Case of Chromates. *Chemosphere*, 42(4), 373–378.

Lee, M., Lim, J. & Kam, S. (2002). Biosorption Characteristics in the Mixed Heavy Metal Solution by Biosorbents of Marine Brown Algae. , 19(2).

Lesmana, S. O., Febriana, N., Soetaredjo, F. E., Sunarso, J. & Ismadji, S. (2009). Studies on

Potential Applications of Biomass for the Separation of Heavy Metals from Water and Wastewater. *Biochemical Engineering Journal*, 44(1), 19–41.

Li, Q., Wu, S., Liu, G., Liao, X., Deng, X., Sun, D., et al. (2004). Simultaneous Biosorption of Cadmium (II) and Lead (II) Ions by Pretreated Biomass of Phanerochaete Chrysosporium. *Separation and Purification Technology*, 34(1–3), 135–142.

Li, Q., Wu, S., Lui, G., Liao, X., Deng, X. U., Sun, D., et al. (2004). Simultaneous Biosorption of Cadmium (II) and Lead (II) Ions by Pretreated Biomass of Phanerochaete Chrysosporium. *Seperation Purification Technology*, 34, 135–142.

Li, X., Liao, D., Xu, X., Yang, Q., Zeng, G., Zheng, W., et al. (2008). Kinetic Studies for the Biosorption of Lead and Copper Ions by Penicillium Simplicissimum Immobilized within Loofa Sponge. , 159, 610–615.

Lindino, C. A., Marciniak, A. A. & Strey, L. (2014). Adsorption of Cadmium in Vegetable Sponge (Luffa Cylindrica). , 9.

Liu, X. & Lee, D.-J. (2014a). Thermodynamic Parameters for Adsorption Equilibrium of Heavy Metals and Dyes from Wastewaters. *Bioresource Technology*, 160(0), 24–31.

Liu, X. & Lee, D.-J. (2014b). Thermodynamic Parameters for Adsorption Equilibrium of Heavy Metals and Dyes from Wastewaters. *Bioresource technology*, 160, 24–31.

Liu, X., Yang, Y., Shi, X. & Li, K. (2015). Fast Photocatalytic Degradation of Methylene Blue Dye Using a Low-Power Diode Laser. *Journal of Hazardous Materials*, 283, 267–275.

Long, Y., Lei, D., Ni, J., Ren, Z., Chen, C. & Xu, H. (2014). Packed Bed Column Studies on lead(II) Removal from Industrial Wastewater by Modified Agaricus Bisporus. *Bioresource Technology*, 152, 457–463.

Luo, Y. & Millero, F. J. (2007). Stability Constants for the Formation of Lead Chloride Complexes as a Function of Temperature and Ionic Strength. , 71(2), 326–334.

Machida, M., Kikuchi, Y., Aikawa, M. & Tatsumoto, H. (2004). Kinetics of Adsorption and Desorption of Pb(II) in Aqueous Solution on Activated Carbon by Two-Site Adsorption Model. *Colloids and Surfaces A: Physicochemical and Engineering Aspects*, 240(1–3), 179–186.

Madala, S., Nadavala, S. K., Vudagandla, S., Boddu, V. M. & Abburi, K. (2013). Equilibrium, Kinetics and Thermodynamics of Cadmium (II) Biosorption on to Composite Chitosan Biosorbent. *Arabian Journal of Chemistry*.

Mahmood, T., Saddique, M. T., Naeem, A., Westerhoff, P., Mustafa, S. & Alum, A. (2011). Comparison of Different Methods for the Point of Zero Charge Determination of NiO. *Industrial & Engineering Chemistry Research*.

Mamatha, M., Aravinda, H. B., Manjappa, S. & Puttaiah, E. T. (2012a). Kinetics and Mechanism for Adsorption of Lead in Aqueous and Industrial Effluent from Pongamia Pinnata Tree Bark. , 2(3), 1–9.

Mamatha, M., Aravinda, H. B., Manjappa, S. & Puttaiah, E. T. (2012b). Kinetics and Mechanism for Adsorption of Lead in Aqueous and Industrial Effluent from Pongamia Pinnata Tree Bark. *Journal of Environmental Science*, 2(2), 1–9.

Mancy, T. B., Mathew, M. M. & Stanley, S. A. (2013). Comparative Analysis of Cost Effective Biosorbents in the Removal of Chromium and Iron from Aqueous Solution. , 12(12), 1–5.

Martins, R. J. E., Vilar, V. J. P. & Boaventura, R. A. R. (2014). Kinetic Modelling of Cadmium and Lead Removal by Aquatic Mosses. , 31(1), 229–242.

Mazali, I. O. & Alves, O. L. (2005). Morphosynthesis: High Fidelity Inorganic Replica of the Fibrous Network of Loofa Sponge (Luffa Cylindrical). *Anais da Academia Brasileira de Ciencias*, 77(1), 25–31.

Mazmanci, M. A. & Ünyayar, A. (2005). Decolourisation of Reactive Black 5 by Funalia Trogii Immobilised on Luffa Cylindrica Sponge. *Process Biochemistry*, 40(1), 337–342.

Merdan et al., 2012. (2012). Effect of Applied Different Surface Modification Processes with Cellulose Enzyme on Properties of Luffa Fibres. *Asian Journal of Chemistry*, 24(3), 975–980.

Mezohegyi, G., Zee, F. P. Van Der, Font, J., Fortuny, A. & Fabregat, A. (2012). Towards Advanced Aqueous Dye Removal Processes : A Short Review on the Versatile Role of Activated Carbon. *Journal of Environmental Management*, 102, 148–164.

Mohammed, M. A., Shitu, A. & Ibrahim, A. (2014). Removal of Methylene Blue Using Low Cost Adsorbent : A Review. , 4(1), 91–102.

Mohsen, M. S. & Jaber, J. O. (2002). Potential of Industrial Wastewater Reuse. , 9164(2).

Montazer-Rahmati, M. M., Rabbani, P., Abdolali, A. & Keshtkar, A. R. (2011). Kinetics and Equilibrium Studies on Biosorption of Cadmium, Lead, and Nickel Ions from Aqueous Solutions by Intact and Chemically Modified Brown Algae. *Journal of hazardous materials*, 185(1), 401–7.

Muhammad, I. & Edyvean, R. G. J. (2007). Ability of Loofa Sponge-Immobilised Fungal Biomass to Remove Lead Ions from Aqueous Solution. *Pak. J. Bot. (special issue)*, 39(1), 231–238.

Munoz, R., Alvarez, M. T., Munoz, A., Terrazas, E., Guieysse, B. & Mattiasson, B. (2006). Sequential Removal of Heavy Metals Ions and Organic Pollutants Using an Algal-Bacterial Consortium. *Chemosphere*, 63(6), 903–911.

Mussarat, M., Bhatti, A. U. & Khan, F. U. (2007). Concentration of Metals in Sewage and Canal Water Used for Irrigation in Peshwar. *Sarhad Journal of Agriculture*, 23(2), 335–338.

Naeem, A., Saddique, M. T., Mustafa, S., Kim, Y. & Dilara, B. (2009). Cation Exchange Removal of Pb from Aqueous Solution by Sorption onto NiO. *Journal of Hazardous Materials*, 168(1), 364–368.

Nagy, B., Maicaneanu, A., Indolean, C., Manzatu, C., Majdik, C. & Silaghi-Dumitrescu, L. (2014). Comparative Study of Cd (II) Biosorption on Cultivated Agaricus Bisporus and Wild Lactarius Piperatus Based Biocomposites . Linear and Nonlinear Equilibrium Modelling and Kinetics. *Journal of the Taiwan Institute of Chemical Engineers*, 45, 921–929.

Nagy, B., Măicăneanu, A., Indolean, C., Mânzatu, C., Silaghi-Dumitrescu, L. & Majdik, C. (2014). Comparative Study of Cd(II) Biosorption on Cultivated Agaricus Bisporus and Wild Lactarius Piperatus Based Biocomposites. Linear and Nonlinear Equilibrium Modelling and Kinetics. *Journal of the Taiwan Institute of Chemical Engineers*, 45(3), 921–929.

Najiah, S., Yusoff, M., Kamari, A., Putra, W. P., Ishak, C. F., Mohamed, A., et al. (2014). Removal of Cu (II), Pb (II) and Zn (II) Ions from Aqueous Solutions Using Selected Agricultural Wastes : Adsorption and Characterisation Studies. , (March), 289–300.

Namieśnik, J. & Rabajczyk, A. (2010). The Speciation and Physico-Chemical Forms of Metals in Surface Waters and Sediments. *Chemical Speciation and Bioavailability*, 22(1), 1–24.

Nasuha, N., Hameed, B. H. & Din, A. T. M. (2010). Rejected Tea as a Potential Low-Cost Adsorbent for the Removal of Methylene Blue. , 175, 126–132.

Ngwenya, B. T., Tourney, J., Magennis, M., Kapetas, L. & Olive, V. (2009). A Surface Complexation Framework for Predicting Water Purification through Metal Biosorption. *Desalination*, 248(1–3), 344–351.

Njoku, V. O. (2014). Biosorption Potential of Cocoa Pod Husk for the Removal of Zn(II) from Aqueous Phase. *Journal of Environmental Chemical Engineering*, 2(2), 881–887.

Nwabanne, J. T. & Igbokwe, P. K. (2012). Adsorption Performance of Packed Bed Column for

the Removal of Lead (Ii) Using Oil Palm Fibre. , 2(5), 106–115.

Oboh, I., Aluyor, E. & Audu, T. (2009). Biosorption of Heavy Metal Ions from Aqueous Solutions Using a Biomaterial. *Leonardo Journal of Sciences*, (14), 58–65.

Oboh, I., Aluyor, E. & Audu, T. (2016). Kinetic Modelling for Zinc (II) Ions Biosorption Onto Luffa Cylindrica. , 20079(1653).

Oboh, I. O. & Aluyor, E. O. (2009). Luffa Cylindrica. , 4(August), 684–688.

Oboh, I. O., Aluyor, E. O. & Audu, T. O. K. (2009). Application of Luffa Cylindrica in Natural Form as Biosorbent to Removal of Divalent Metals from Aqueous Solutions - Kinetic and Equilibrium Study. , 546.

Oboh, I. O., Aluyor, E. O. & Audu, T. O. K. (2013). Mathematical and ANN Models of the Effect of Dosage on Cu2+ Sorption Capacity of Luffa Cylindrica. , 2(2), 23–30.

Occelli, M., Olivier, J. P., Petre, A. & Auroux, A. (2003). Determination of Pore Size Distribution , Surface Area , and Acidity in Fluid Cracking Catalysts (FCCs) from Nonlocal Density ... , (April).

Okewale, A. O., Igbokwe, P. K. & Babayemi, K. A. (2015). Design of Pilot Plant Packed Column for the Dehydration of Water from Ethanol-Water Mixtures. , (April), 152–157.

Okunola, O. J., Uzairu, A., Ndukwe, G. I. & Adewusi, S. G. (2008). Assessment of Cadmium and Zinc in Roadside Surface Soils. *Research Journal of Environmental Sciences*, 2(4), 266–274.

Olu-owolabi, B. I. & Unuabonah, E. I. (2010). Kinetic and Thermodynamics of the Removal of Zn 2 + and Cu 2 + from Aqueous Solution by Sulphate and Phosphate-Modified Bentonite Clay. *Journal of Hazardous Materials*, 184(1–3), 731–738.

Onyango, M. S., Kojima, Y., Aoyi, O. & Bernardo, E. C. (2004). Adsorption Equilibrium Modeling and Solution Chemistry Dependence of Fluoride Removal from Water by Trivalent-Cation-Exchanged Zeolite F-9. , 279, 341–350.

Ouajai, S. & Shanks, R. A. (2005). Composition , Structure and Thermal Degradation of Hemp Cellulose after Chemical Treatments. , 89, 327–335.

Oushabi, A., Sair, S., Oudrhiri Hassani, F., Abboud, Y., Tanane, O. & El Bouari, A. (2017). The Effect of Alkali Treatment on Mechanical, Morphological and Thermal Properties of Date Palm Fibers (DPFs): Study of the Interface of DPF–Polyurethane Composite. *South African Journal of Chemical Engineering*, 23, 116–123.

Ouyang, X., Yang, L. & Wen, Z. (2014). Adsorption of Pb(II) from Solution Using Peanut Shell as

Biosorbent in the Presence of Amino Acid and Sodium Chloride. , 9(Ii), 2446–2458.

Özkaya, B. (2006). Adsorption and Desorption of Phenol on Activated Carbon and a Comparison of Isotherm Models. *Journal of Hazardous Materials*, 129(1–3), 158–163.

Pagnanelli, F., Esposito, a., Toro, L. & Vegli??, F. (2003). Metal Speciation and pH Effect on Pb, Cu, Zn and Cd Biosorption onto Sphaerotilus Natans: Langmuir-Type Empirical Model. *Water Research*, 37(3), 627–633.

Parida, C., Dash, S. K. & Chaterjee, P. (2016). The Thermal and Crystallization Studies of Luffa Fiber Reinforced Poly Lactic Acid Composites. , (January), 1–7.

Park, D., Yun, Y. & Park, J. M. (2010). The Past , Present , and Future Trends of Biosorption. , 86–102.

Pavan, F. a, Lima, E. C., Dias, S. L. P. & Mazzocato, A. C. (2008). Methylene Blue Biosorption from Aqueous Solutions by Yellow Passion Fruit Waste. *Journal of hazardous materials*, 150(3), 703–12.

Plazinski, W., Dziuba, J. & Rudzinski, W. (2013). Modeling of Sorption Kinetics : The Pseudo-Second Order Equation and the Sorbate Intraparticle Diffusivity. , 1055–1064.

Plazinski, W., Rudzinski, W. & Plazinska, A. (2009). Theoretical Models of Sorption Kinetics Including a Surface Reaction Mechanism : A Review. *Advances in Colloid and Interface Science*, 152(1–2), 2–13.

R.Leyva-Ramos , L.A. Bernal-Jacome, I. A.-R. (2005). Adsorption of Cadmium (II) from Aqueous Solution on Natural and Oxidized Corncob. , 45, 41–49.

Rafatullah, M., Sulaiman, O., Hashim, R. & Ahmad, A. (2010). Adsorption of Methylene Blue on Low-Cost Adsorbents: A Review. *Journal of hazardous materials*, 177(1–3), 70–80.

Rahman, M. M., Choudhury, F. A., Hossain, D. & Islam, N. (2012). A Comparative Study on the Photocatalytic Degradation of Industrial Dyes Using Modified Commercial and Synthesized TiO 2 Photocatalysts. , C(2).

Ramrakhiani, L., Halder, A., Majumder, A., Mandal, A. K., Majumdar, S. & Ghosh, S. (2017). Industrial Waste Derived Biosorbent for Toxic Metal Remediation: Mechanism Studies and Spent Biosorbent Management. *Chemical Engineering Journal*.

Rangabhashiyam, S., Anu, N., Nandagopal, M. S. G. & Selvaraju, N. (2014). Journal of Environmental Chemical Engineering Relevance of Isotherm Models in Biosorption of Pollutants by Agricultural Byproducts. *Journal of Environmental Chemical Engineering*,

2(1), 398–414.

Reddy, P. M. K., Verma, P. & Subrahmanyam, C. (2015). Bio-Waste Derived Adsorbent Material for Methylene Blue Adsorption. *Journal of the Taiwan Institute of Chemical Engineers*.

Rieman, W. M. (1961). Kinetics of Ion Exchange in a Chelating Resin. , (5), 5–8.

Saber-Samandari, S., Saber-Samandari, S., Nezafati, N. & Yahya, K. (2014). Efficient Removal of Lead (II) Ions and Methylene Blue from Aqueous Solution Using chitosan/Fe-Hydroxyapatite Nanocomposite Beads. *Journal of environmental management*, 146, 481–490.

Saeed, A., Iqbal, M. & Iqbal, S. (2009). Immobilization of Trichoderma Viride for Enhanced Methylene Blue Biosorption : Batch and Column Studies. , 168, 406–415.

Salazar-rabago, J. J., Leyva-ramos, R., Rivera-utrilla, J., Ocampo-perez, R. & Cerino-cordova, F. J. (2017). Biosorption Mechanism of Methylene Blue from Aqueous Solution onto White Pine (Pinus Durangensis) Sawdust : Effect of Operating Conditions. *Sustainable Environment Research*, 27(1), 32–40.

Samiey, B. & Ashoori, F. (2012). Adsorptive Removal of Methylene Blue by Agar : Effects of NaCl and Ethanol. , 1(c), 1–13.

Sangi, M. R., Shahmoradi, A., Zolgharnein, J., Azimi, G. H. & Ghorbandoost, M. (2008). Removal and Recovery of Heavy Metals from Aqueous Solution Using Ulmus Carpinifolia and Fraxinus Excelsior Tree Leaves. , 155, 513–522.

Sari, A. & Tuzen, M. (2008a). Biosorption of Pb(II) and Cd(II) from Aqueous Solution Using Green Alga (Ulva Lactuca) Biomass. *Journal of Hazardous Materials*, 152(1), 302–308.

Sari, A. & Tuzen, M. (2008b). Biosorption of cadmium(II) from Aqueous Solution by Red Algae (Ceramium Virgatum): Equilibrium, Kinetic and Thermodynamic Studies. *Journal of Hazardous Materials*, 157(2–3), 448–454.

Saueprasearsit, P., Nuanjaraen, M. & Chinlapa, M. (2010). Biosorption of lead(Pb2+) by Luffa Cylindrica Fiber...Saueprasearsit et Al., 2010.pdf.

Saw, S. K., Purwar, R., Nandy, S., Ghose, J. & Sarkhel, G. (2013). Fabrication, Characterization, and Evaluation of Luffa Cylindrica Fiber Reinforced Epoxy Composites. , 8, 4805–4826.

Shahidi, A., Jalilnejad, N. & Jalilnejad, E. (2016). A Study on Adsorption of Cadmium (II) Ions from Aqueous Solution Using Luffa Cylindrica. , 3994(June).

Shanthi, P., Tamilarasan, G., Anitha, K. & Karthikeyan, S. (2014). Film and Pore Diffusion

Modeling for Adsorption of Reactive Red-4 onto Sterculia Quadrifida Seed Shell Waste as Activated Carbon. *Rasayan J. Chem*, 7(3), 229–240.

Sharma, S. & Tiwari, D. P. (2016). Model-Fitting Approach for Methylene Blue Dye Adsorption on Camelina and Sapindus Seeds-Derived Adsorbents.

Shen, J., Min, Y., Huang, X., Zhou, S. & Ruan, D. (2012). Mechanical Properties of Luffa Sponge. , (July).

Shi, H. (2013). Industrial Wastewater- Types, Amounts and Effects. , I.

Shi, S., Gondal, M. a., Shen, K., Ali, M. a., Xu, Q. & Chang, X. (2014). Batch and Column Adsorption of Dye Contaminants Using a Low-Cost Sand Adsorbent. *Research on Chemical Intermediates*.

Shields, L., Thomas & Thommes. (2004). Characterization of Porous Materials and Powders: Surface Area, Pore Size and Density.

Shin, E. W. & Rowell, R. M. (2005). Cadmium Ion Sorption onto Lignocellulosic Biosorbent Modified by Sulfonation : The Origin of Sorption Capacity Improvement. , 60, 1054–1061.

Singh, R., Gautam, N. & Gupta, R. (2011). Heavy Metals and Living Systems: An Overview. *Indian Journal of Pharmacology*, 43(3), 246–253.

Siqueira, G., Bras, J. & Dufresne, A. (2010). Luffa Cylindrica as a Lignocellulosic Source of Fiber, Microfibrillated Cellulose, and Cellulose Nanocrystals. , 5, 727–740.

Smith, M. C., Crist, R. M., Clogston, J. D. & Mcneil, S. E. (2017). Zeta Potential : A Case Study of Cationic , Anionic , and Neutral Liposomes. , 5779–5787.

Šoštari, T., Petrovic, M., Stojanovic, M., Milojkovic, J., Mihajlovic, M., Stanojevic, M., et al. (2016). Removal of Pb2+ Ions by Raw Corn Silk (Zea Mays L .) as a Novel Biosorbent. *Journal of the Taiwan Institute of Chemical Engineers*, 58, 407–416.

Srivastava, P. & Angove, M. (2004). Competitive Adsorption of Cadmium (II) onto Kaolinite as Affected by pH. , (December 2004), 5–9.

Stana-Kleinschek, K., Ribitsch, V., Kreze, T. & Fras, L. (2002). Determination of the Adsorption Character of Cellulose Fibres Using Surface Tension and Surface Charge. *Materials Research Innovations*, 6(1), 13–18.

Suguna, M. & Kumar, N. S. (2013). Equilibrium , Kinetic and Thermodynamic Studies on Biosorption of Lead (II) and Cadmium (II) from Aqueous Solution by P Olypores Biomass. , 20(January), 57–69.

Suhas, Gupta, V. K., Carrott, P. J. M., Singh, R., Chaudhary, M. & Kushwaha, S. (2016). Cellulose: A Review as Natural, Modified and Activated Carbon Adsorbent. *Bioresource Technology*, 216.

Tabbara, M. A. & El Jamal, M. M. (2012). A Kinetic Study of Te Discoloration of Methylene Blue by Na2SO3, Comparison with NaOH..Tabbara and Jamal, 2012.pdf.

Tang, X., Li, Y., Chen, R., Min, F., Yang, J. & Dong, Y. (2014). Evaluation and Modeling of Methyl Green Adsorption from Aqueous Solutions Using Loofah Fibers. *Korean Journal of Chemical Engineering*, 32(1), 125–131.

Taty-Costodes, V. C., Fauduet, H., Porte, C. & Delacroix, A. (2003). Removal of Cd(II) and Pb(II) Ions, from Aqueous Solutions, by Adsorption onto Sawdust of Pinus Sylvestris. *Journal of Hazardous Materials*, 105(1–3), 121–142.

Thommes, M., Kaneko, K., Neimark, A. V, Olivier, J. P., Rodriguez-reinoso, F., Rouquerol, J., et al. (2015). Physisorption of Gases , with Special Reference to the Evaluation of Surface Area and Pore Size Distribution (IUPAC Technical Report).

Van Thuan, T., Quynh, B. T. P., Nguyen, T. D., Ho, V. T. T. & Bach, L. G. (2017). Response Surface Methodology Approach for Optimization of Cu2+, Ni2+ and Pb2+ Adsorption Using KOH-Activated Carbon from Banana Peel. *Surfaces and Interfaces*, 6.

Tong et al., 2014. (2014). Improving Cracking and Drying Shrinkage Properties of Cement Mortar by Adding Chemically Treated Luffa Fibres. , (June 2015).

Tran, H. N., You, S. J., Hosseini-Bandegharaei, A. & Chao, H. P. (2017). Mistakes and Inconsistencies Regarding Adsorption of Contaminants from Aqueous Solutions: A Critical Review. *Water Research*, 120, 88–116.

Tsai, W.-T. & Chen, H.-R. (2010). Removal of Malachite Green from Aqueous Solution Using Low-Cost Chlorella-Based Biomass. *Journal of hazardous materials*, 175(1–3), 844–9.

Tullin, C. J. & Amand, L. (2000). The Theory Behind FTIR Analysis. , (0).

Umpuch, C., Bunmanan, N., Kueasing, U. & Kaewsan, P. (2011). Adsorption of Lead from Synthetic Solution Using Luffa Charcoal. , 89–93.

Vijayaraghavan, K. & Yun, Y.-S. (2008). Bacterial Biosorbents and Biosorption. *Biotechnology advances*, 26(3), 266–91.

Vilar, V. J. P., Botelho, C. M. S., Pinheiro, J. P. S., Domingos, R. F. & Boaventura, R. a R. (2009). Copper Removal by Algal Biomass: Biosorbents Characterization and Equilibrium

Modelling. *Journal of Hazardous Materials*, 163(2–3), 1113–1122.

Vincent, K. & Passant, N. (2006). Assessment of Heavy Metal Concentrations in the United Kingdom. , (April 2006).

Volesky, B. (2003). Sorption and Biosorption.

Volesky, B. & Holan, Z. R. (1995). Biosorption of Heavy Metals.

Wainwright, M. & Amaral, L. (2005). Review : The Phenothiazinium Chromophore and the Evolution of Antimalarial Drugs. , 10(6), 501–511.

Wang, S. & Peng, Y. (2010). Natural Zeolites as Effective Adsorbents in Water and Wastewater Treatment. , 156, 11–24.

Watkins, D., Hosur, M., Tcherbi-narteh, A. & Jeelani, S. (2014). Extraction and Characterization of Lignin from Different Biomass Resources &. *Integrative Medicine Research*, 4(1), 26–32.

Whittaker, D. (2000). Interpreting Organic Spectra [Royal Society of Chemistry].

Williams, D. & Fleming, I. (2008). Spectroscopic Methods in Organic Chemistry.

Williams, T., Hosur, M., Theodore, M., Netravali, a., Rangari, V. & Jeelani, S. (2011). Time Effects on Morphology and Bonding Ability in Mercerized Natural Fibers for Composite Reinforcement. *International Journal of Polymer Science*, 2011, 1–9.

Wuana, R. a. & Okieimen, F. E. (2011). Heavy Metals in Contaminated Soils: A Review of Sources, Chemistry, Risks and Best Available Strategies for Remediation. *ISRN Ecology*, 2011, 1–20.

Yahaya, A., Adegbe, A. A. & Emurotu, J. E. (2012). Assessment of Heavy Metal Content in the Surface Water of Oke-Afa Canal Isolo Lagos , Nigeria. , 4(6), 2322–2326.

Yang, B., Zuo, J., Tang, X., Liu, F., Yu, X., Tang, X., et al. (2014). Effective Ultrasound Electrochemical Degradation of Methylene Blue Wastewater Using a Nanocoated Electrode. *Ultrasonics sonochemistry*, 21(4), 1310–7.

Yang, J. & Volesky, B. (1999). Biosorption of Uranium on Sargassum Biomass. *Water Research*, 33(15), 3357–3363.

Yang, Y.-Y., Li, Z.-L., Wang, G., Zhao, X.-P., Crowley, D. E. & Zhao, Y.-H. (2012). Computational Identification and Analysis of the Key Biosorbent Characteristics for the Biosorption Process of Reactive Black 5 onto Fungal Biomass. *PloS one*, 7(3), e33551.

Ye, C., Hu, N. & Wang, Z. (2013). Experimental Investigation of Luffa Cylindrica as a Natural Sorbent Material for the Removal of a Cationic Surfactant. *Journal of the Taiwan Institute of Chemical Engineers*, 44(1), 74–80.

Yu, J., Wang, L., Chi, R., Zhang, Y., Xu, Z. & Guo, J. Removal of Cationic Dyes: Basic Magneta and Methylene Blue from Aqueous Solution by Adsorption on Modified Loofah. *Research on Chemical Intermediates*, 39(8).

Yukselen, Y. & Kaya, A. (2003). Zeta Potential of Kaolinite in the Presence of Alkali, Alkaline Earth and Hydrolyzable Metal Ions. *Water Air and Soil Pollution*.

Zhao, H., Liu, X., Cao, Z., Zhan, Y., Shi, X., Yang, Y., et al. (2016). Adsorption Behavior and Mechanism of Chloramphenicols, Sulfonamides, and Non-Antibiotic Pharmaceuticals on Multi-Walled Carbon Nanotubes. *Journal of Hazardous Materials*, 310, 235–245.

Zhao, K., Liu, X., Xu, J. & Selim, H. M. (2010). Heavy Metal Contaminations in a Soil–rice System: Identification of Spatial Dependence in Relation to Soil Properties of Paddy Fields. *Journal of Hazardous Materials*, 181(1–3), 778–787.

Appendix A

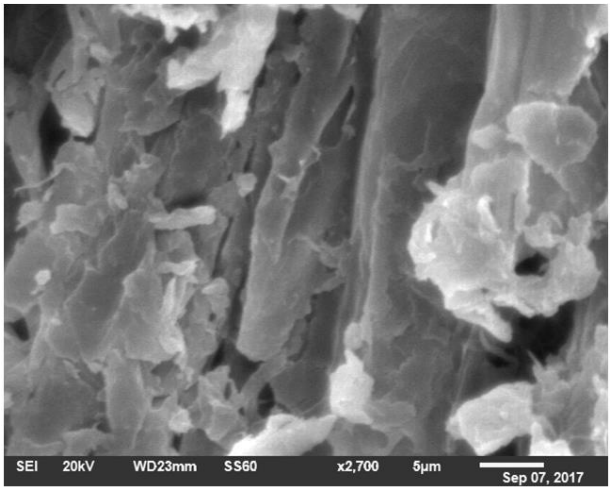

a

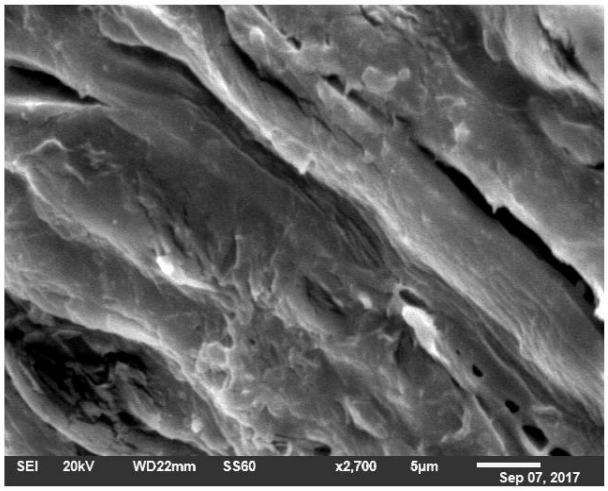

b

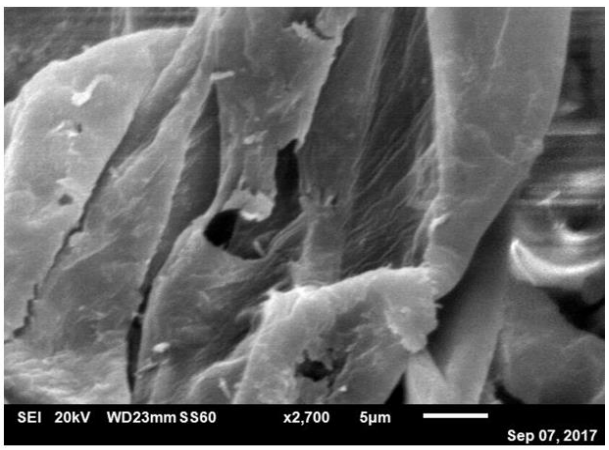

c

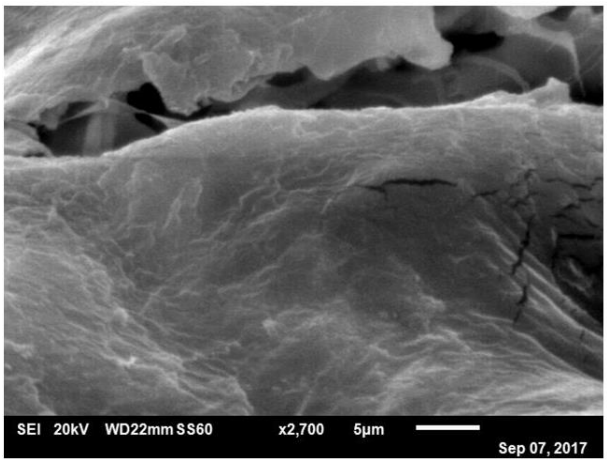
SEI 20kV WD22mm SS60 x2,700 5µm
Sep 07, 2017

d

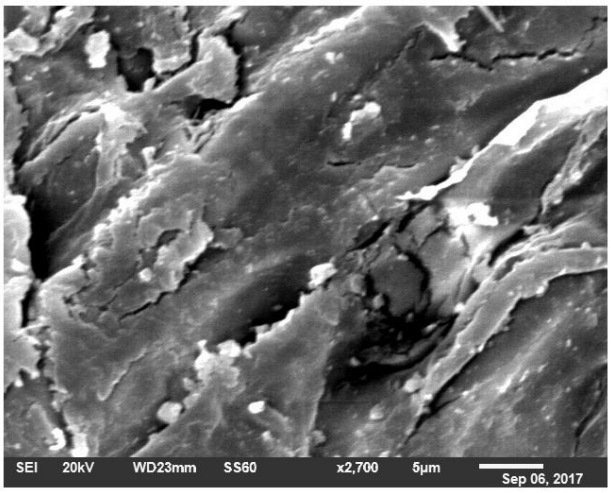
SEI 20kV WD23mm SS60 x2,700 5µm
Sep 06, 2017

e

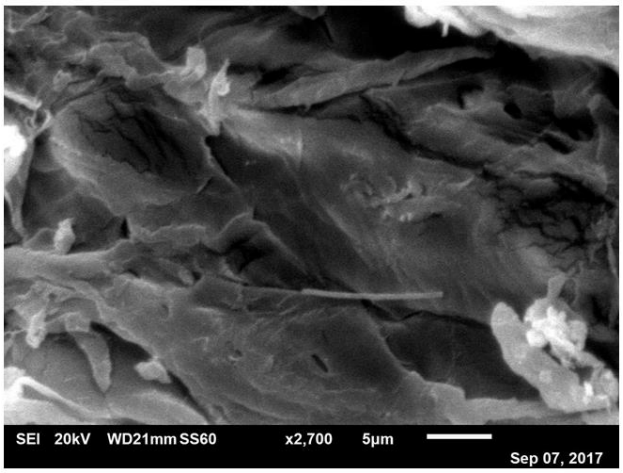
SEI 20kV WD21mm SS60 x2,700 5µm
Sep 07, 2017

f

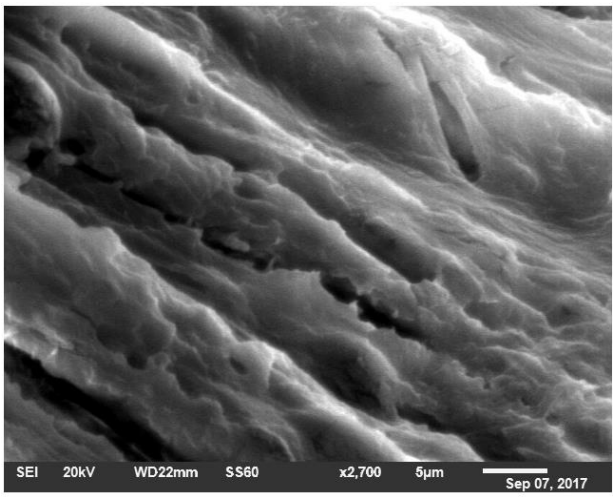

g

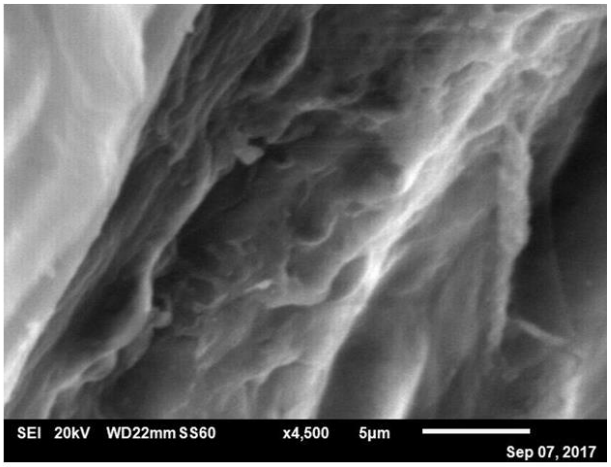

h

Appendix a-h: Images of Scanning Electron Miscrocopy (SEM) of loofa under certain conditions. **a –** Pb loaded alkali treated loofa**, b –** Zinc loaded alkali treated loofa, **c-** Cadmium loaded alkali treated loofa, **d –** Methylene loaded alkali treated loofa, **e-** HCl treated loofa, **f-** HCL IEX – Pb loaded loofa, **g -** NaCl- Zn loaded alkali treated loofa, **h-** Mixed metals loaded alkali treated loofa.

Appendix B

Please refer to CD disc for software data.

Appendix C

Removal of lead from solution using chemically modified *Luffa Cylindrica* as a method of sustainable water treatment in Nigeria.

Akanimo U. Emene[1], Robert Edyvean[1]

[1]Department of Chemical and Biological Engineering, University of Sheffield, Western Bank, Sheffield, S10 2TN, United Kingdom

Corresponding author email: cpp13aue@sheffield.ac.uk

Abstract

Luffa cylindrica, when chemically treated with 4% NaOH shows an increased amount of ion exchange functionality, thereby enhancing the adsorption capacity. Chemical modification of *Luffa cylindrica* also changes its structural characteristics by exposing its pores for enhanced adsorption and shows an increased BET surface area of 43.10m^2/g. From the FT-IR spectra an increase in protonated hydroxyl and carboxyl functional groups was observed. The adsorption of Pb^{2+} onto alkali treated *Luffa cylindrica* (ATLC) was investigated in batch experiments as a function of pH, temperature, initial metal ion concentration and ionic strength. Adsorption kinetic and isotherm models, pseudo second order, Boyd, Langmuir, two-site Langmuir, Dubinin-Radushkevich and Sips were utilized in understanding the adsorption mechanism and the ability of the adsorption system evaluated. The maximum adsorption capacity is 24.9mg/g as described by the Langmuir isotherm and the maximum percentage uptake (efficiency) is 96.4%. The Sips model fits better than the Langmuir, two site Langmuir and Dubinin-Radushkevich model using GraphPad. The film diffusion mechanism is described as feasible. The kinetics of the biosorption process was studied. A pseudo second order model shows a good correlation fit. In agreement with the literature, the optimum condition for the maximum adsorption capacity occurs at pH 5 at room temperature.

Keywords: Adsorption, ion exchange, lead, *Luffa cylindrica (L. cylindrica)*, Alkali treated *Luffa cylindrica* (*ATLC*).

1 Introduction

Lead is a heavy metal pollutant that contaminates water and soil environments. It is a global problem, affecting most industrialised nations, as well as developing nations (1). The release of lead into the environment, and its subsequent uptake by plants and animals causes serious health problems and environment issues. It is a major health risk, particularly in developing countries (2).

The prominence of environmental lead contamination results both from its persistence (3-5) and from its present and past numerous sources. Sources of lead contamination are typically anthropogenic: fuel burning (particularly incomplete combustion from vehicles), mining operations, lead-based paints, tyre wear, electroplating activities, plastic, smelting, paper manufacturing industries, pesticides, leakage of oils, metal mining and corrosion of batteries and metallic parts such as radiators, etc.(1, 6, 7). Lead contamination of surface waters is a particular problem in Nigeria: Leaching of lead pipes, run off from roads and extensive utilization of crude oil have resulted in wide spread contamination (8). The major source of contamination in Nigeria is from the large scale production, transport and disposal of petroleum products (9). Oil exploration in the Niger Delta (South of Nigeria) has been ongoing for decades and the United

Nations Environment Programme (UNEP) have set targets for clean-up and remediation of the area. Furthermore, poor industrial practice has resulted in some pharmaceutical companies in Nigeria discharging effluents that contain concentrations of lead above the WHO recommended maximum contaminant concentration level (10).

Lead has no known biological function in living organisms. If ingested or inhaled, lead and its compounds are poisonous to animals and humans. Lead is a neurotoxin that accumulates both in soft tissues and in bones, damaging the nervous system and causing brain disorders. Excessive lead also causes blood disorders in mammals (2).The maximum recommended safe daily intake, biomarker for lead toxicity, for humans is as low as 1.0 µg/g. Lead is also highly toxic to plants, restricting root elongation and plant growth, and impairs transpiration and chlorophyll production (11).

As the largest, and fastest growing economy in Africa, Nigeria is expected to lead by example and engage in the global drive to tackle environmental contamination and enhance the sustainability of the environment (12). With its rapid industrialization and population growth, it is critical for Nigeria to ensure that the effective treatment of wastewater is prioritised to reduce environmental and health impacts of contaminated waterways, and the subsequent negative impact on the socio-economic development of the country (1).

Studies carried out on the treatment of heavy metal pollution in wastewater have highlighted a pressing need to develop low cost, environmentally friendly and effective materials to tackle this issue (1, 13).

Biosorbents are biological materials with functionalised surfaces capable of removing trace metals and other contaminants from water. These materials are favoured for their renewable nature, and their ability to biodegrade. Current research has focused on plant materials that are by-products of other industries, such as sawdust, coconut husks or palm kernel shells (55, 36,14). Also of interest are plants that grow easily in, and are well suited to, the conditions found in the community that will actually make use of the biosorbent technology.

The loofa sponge, derived from the sub-tropical plant *Luffa cylindrica (LC),* is grown annually in China, Japan, Nigeria and many countries in South America (15). In Nigeria, the loofa fruit is commonly grown as a feed for poultry and also as a vitamin supplement for aqua feeds. The fibrous residue of the fruit (mature fruit) is used in producing gourds and loofa sponges, after which it is regarded as a waste material (16). The smooth and cylindrical shaped fruit is about 12cm long (15), the flesh of which is a sponge-like material that is comprised of a reticulate matrix consisting of various fibrous interwoven cords. The cellular structure of the cords is made up parenchyma cells that are responsible for the metabolic activities of the plant. The network of these cords comprises flexible and hollow cylindrical fibres (17, 18). These cords are composed of fibrils which are resinous lignocellulose material comprising of 55-90% cellulose, 10-23% lignin, 8-22% hemicellulose (the exact proportions depending on factors such as plant origin, weather conditions, nature of soil, etc.) (15). It is this inner part of the fruit which, when dried, forms the typical loofa sponge that has been employed for centuries as a sponge or scrubber for washing.

The high proportion of cellulose material in *LC* can be utilised in the removal of heavy metal ions from aqueous solution due to the presence of active functional groups within the molecular structure. Studies have shown that the *LC* material is able to remove both metal cations (6, 19) and organic pollutants (20, 21) from aqueous solutions. Furthermore, due to the type of functional groups present in the cellulosic structure, *LC* can be chemically modified to enhance its sorption properties (15, 22). *LC* has also been utilised as an immobilising medium to provide reliable support for the immobilisation of microalgae for the removal of toxic metal ions from wastewater (15, 23).

LC represents a low cost, renewable, biodegradable solution for sustainable water treatment in Nigeria (15). However, before it can be developed as a viable, large-scale process, it is necessary to gain a thorough understanding of the chemistry involved, so that the process can be optimized. This requires an understanding of the chemistry of the wastewater streams, the surface properties of *LC*, and the metal surface complexes formed during removal of lead from water.

Here, we investigate the efficiency of AT*LC* as an adsorbent in the removal of Pb (II) ions from aqueous solution, across the pH range 3-9. The methodology used to modify the *LC* requires little energy and presents a promising optimization strategy for a developing country like Nigeria. The results obtained contribute to the understanding of the surface properties of *LC*, as well as the *LC*-Pb biosorption mechanism.

2 Material and methods

2.1 Reagents and stock solutions

All chemicals utilised were of analytical grade. The stock solution, 1 g/L of Pb (II) was prepared by dissolving $PbCl_2$ salt, obtained from Sigma-Aldrich, United Kingdom, in deionised water. The desired concentrations were obtained by diluting the stock solution to set concentrations, varied from 50 to 200mg/L. 0.1 M HCl and NaOH solutions were used to alter the solution pH.

2.2 Chemical Modification of *Luffa Cylindrica (LC)*

Dried fruit of *LC* were purchased commercially in the United Kingdom. The pale yellow *cylindrica* fibre were washed several times with distilled water to remove surface impurities and seeds, then alkali treated by soaking in 4% NaOH at room temperature for 1h. It was repeatedly washed in distilled water until the pH was almost neutral, and then oven dried at 90 °C for 24h.The dried samples were ground and sieved to a 1 mm particle size fraction and stored for utilization in further experiments.

2.3 Characterisation of AT*LC*

2.3.1 Surface Analysis of ATLC and LC

The surface structure of loofa was analysed by an Analytical Scanning Electron Microscope (SEM) (Model JOEL JSM- 6010LA) coupled with energy dispersive X-ray (EDX) with an accelerating voltage of 10kV and at a magnification of x550 SS60. The chemical characteristics was analysed by using a Nicolet 6700 Fourier Transform Infra-red (FT-IR) Spectrometer to identify the functionality that interacts with lead ions. 50mg of dried *ATLC* (< 250µm thickness) were prepared for ATR- FTIR analysis. Measurements were made in transmittance mode using a spectral resolution of $4cm^{-1}$ by 256 scans and approximately 150 seconds per step across the range $4000cm^{-1}$ to 650 cm^{-1}. The surface area of each sample of loofa was determined from nitrogen adsorption at 77.2K in the range of relative pressure (p/p^0) of 0.05 – 1 by using a Micromeritics 3Flex instrument. The samples were degassed at 150°C for 24 hours. A three-parameter non-linear fitting procedure was used and the loofa samples were subjected to a 99-point BET surface analysis and a full adsorption isotherms were collected for all samples. The conventional single point method of relative pressure was used.2.3.2 Zeta potential measurementsThe electrophoretic mobility technique was conducted to measure the zeta potential by using a Malvern Zetasizer Nano Instrument. 0.1% concentration of *ATLC* in 0.01mol/L NaCl aqueous solution was stirred continuously with a magnetic stirrer. As desired, the pH was adjusted by addition of 0.1M of HCl and 0.1M NaOH over a range of pH 2-10. The pH of the sample solution was measured before each measurement. The samples were loaded into a capillary cell and measurements were performed at room temperature (21°C). An average of three measurements were recorded for each analysed sample (30, 31).

2.3.3 Ion exchange loading capacity

A single contact of 1g of 1mm sieve size *ATLC* was mixed with 100 mL of aqueous simulant feed of 0.1M NaOH using a magnetic stirrer for 24hrs. Then the filtered sample was rinsed off with distilled water until neutral pH and then contacted with 100ml of aqueous solution of 0.1M HCl and mixed for 24hrs. After which the filtered sample was used for further batch adsorption experiments. The filtered *ATLC* from step 1 was mixed with 1M NaCl for 24hrs, sufficient time for exchange of ions in the solution. Then the filtrate solution obtained, after the contact time of exchange of ions, was titrated against 0.1M NaOH. The pH was then recorded at each point (29)**.**

2.4 Batch adsorption experiments

All batch studies as a function of acid concentration were carried out as single contacts with the contact of 1g of 1mm sieve size 4% alkali treated *Luffa cylindrica* (*ATLC*) with 200 mL of aqueous solution. Experiments were carried out at Pb (II) concentrations of 50, 70,100, 150 and 200mg/L; and each at pH 3, 5, 7 and 9 at 50mg/L. The *ATLC* and aqueous solution were continuously mixed at an agitation speed of 200rpm for a period of 24 hrs at room temperature (21 °C) on a magnetic stirrer. Distribution behaviour was determined using the following;

$$q_e = \left(\frac{C_i - C_e}{C_e}\right) \times \frac{v}{m} \qquad (1)$$

q_e is the weighted distribution of the metal ions where C_i is the initial aqueous concentration of the metal ions before contact and C_e is the aqueous concentration of the metal ions after equilibration. *V* is the volume of the aqueous phase (mL) and *m* is the mass of the *ATLC* (g). The percentage removal (R%) was determined by difference (using eqn. 2) and the concentrations of the lead determined by ICP-MS.

$$R\% = \frac{C_i - C_e}{C_i} \times 100 \qquad (2)$$

Where C_i is the initial metal concentration before contact and C_e is the concentration of the metal ion in the aqueous phase after contact with the *ATLC*. pH measurements for solutions were determined using a silver/silver chloride reference electrode calibrated from pH 4-7 using buffers. Error was determined by triplicate measurement in aqueous solution concentrations prior to contact.

2.5 Ionic strength effect

All batch experiments were carried out as single contacts with the contact of 250mg of 1 mm sieve size *ATLC* with 50ml of both NaCl (0.1 M, 0.5 M and 1 M) and 50 mg/L lead chloride solution (100 mg/L Cl^-). The *ATLC* and binary solution were continuously mixed at an agitation speed of 200rpm for a period of 24hrs at pH 5 at room temperature (21^{o}C) on a magnetic stirrer. The distribution behaviour and percentage removal were determined using equation (1) and (2) and the concentrations of both lead and sodium ions were analysed by ICP-MS.

2.6 Determination of loading behaviour.

All loading isotherms were carried out as single contacts with the contact of 1 g of *ATLC* with 200 mL of aqueous solution. The *ATLC* and aqueous solution were continuously mixed at an agitation speed of 200rpm for a period of 24 hrs at room temperature (21°C). A widely researched and commonly used two parameter fitting model, was used to determine the fitting ability due to its quantitative criteria for evaluation (24, 25). The 3 parameter model which gives a clearer evaluation of the data was also utilised. The data were fitted to Langmuir, two site Langmuir, and Dubinin-Radushkevich (26) and Sips models, equations (3-8).

2.7 Calculations

The fitting was carried out by using linear regression and by non-linear least squares analysis using GraphPad (27).

Langmuir

$$q_e = \frac{K_L C_e}{1+a_L C_e} \quad (3)$$

The monolayer saturation capacity, q_m (mg L^{-1}), was calculated from the Langmuir equation using equation (4).

$$K_L = q_m a_L \quad (4)$$

Dubinin-Radushkevich

$$q_e = q_D \exp(-B_D \left[RTln\left(1+\frac{1}{C_e}\right)\right]^2) \quad (5)$$

Where the mean free energy of sorption, E, can be calculated using B_D in equation (6).

$$E = \frac{1}{\sqrt{2B_D}} \quad (6)$$

Two site Langmuir

$$q_e = \frac{Q_1 b_1 C_e}{1+b_1 C_e} + \frac{Q_2 b_2 C_e}{1+b_2 C_e} \quad (7)$$

Sips

$$q_e = \frac{K_s C_e^{\beta s}}{1+a_s C_e^{\beta s}} \quad (8)$$

Error in the isotherm constants was calculated from the linearized form of the model using the EXCEL calculated values using the deviations of the experimental data from this best fit line.

2.8 Determination of the kinetics of extraction

Batch kinetics was carried out with the contact of 1 g of *ATLC* with 200 mL of aqueous simulant feed. The *ATLC* and aqueous feed were continuously mixed for a period of 24 hrs at 21 °C and 5 mL samples were extracted at set time intervals. The data was fitted using a linear fit of pseudo second order models which do not take into account the mechanism of reaction.

The linear form of the pseudo-second-order kinetic model (28) is as follows;

$$\frac{t}{q_t} = \frac{1}{k_2 {q_e}^2} + \frac{1}{q_e} t \quad (9)$$

Where k_2 = pseudo second order reaction constant (hr^{-1}). The non-linear form for the pseudo second-order kinetics is given below;

$$q_t = \frac{k_2 q_e^2 t}{1+k_2 q_e t} \quad (10)$$

The non-linear form was fitted using the minimization of the sum of square errors (SSE) using SOLVER (28). The $t_{1/2}$ was calculated by the relationship;

$$t_{1/2} = \frac{1}{k_2 q_e} \quad (11)$$

The initial sorption rate h_0 (26) is given by;

$$h_0 = k{q_e}^2 \quad (12)$$

Boyd model

$$B_t = -0.4977 - In\left(1 - \frac{q_t}{q_e}\right) \quad (13)$$

3 Results and Discussion

3.1 Chemical modification of *Luffa cylindrica* (*LC*)
The morphology of *LC*, shown in Figure 1, appears dry and flaky with many loose particles on the surface. In Figure 2, the morphology of the NaOH treated loofa (*ATLC*) is more broken up with fewer loose particles on the surface. This may be as a result of exposure of the pores [47]. Ghali *et al*. (2009) showed that treating *L. cylindrica* fibres with 4 % NaOH leads to a higher crystallinity index and to the improvement in adhesion capacity [38].

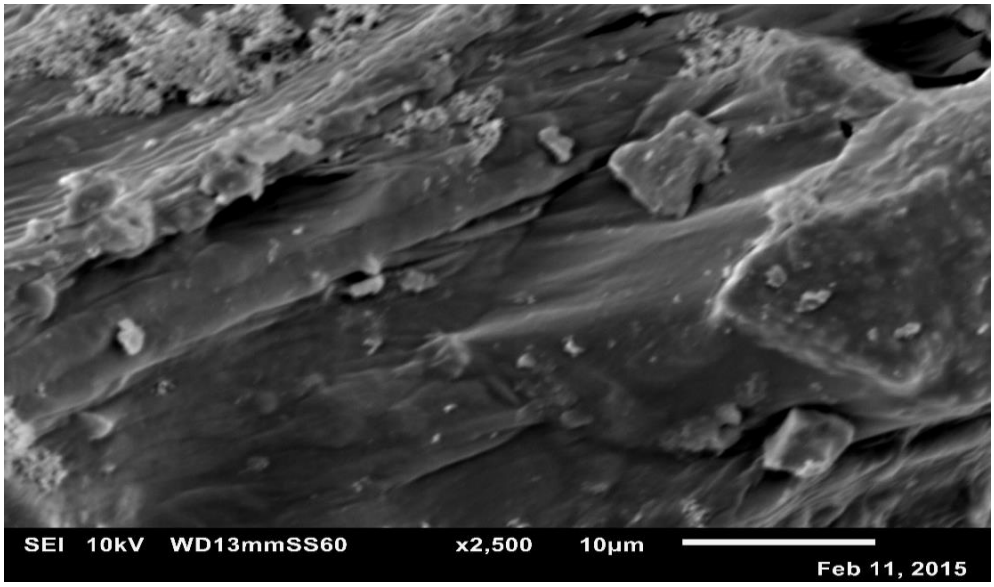

Figure 1: Surface morphology of untreated loofa (raw loofa)

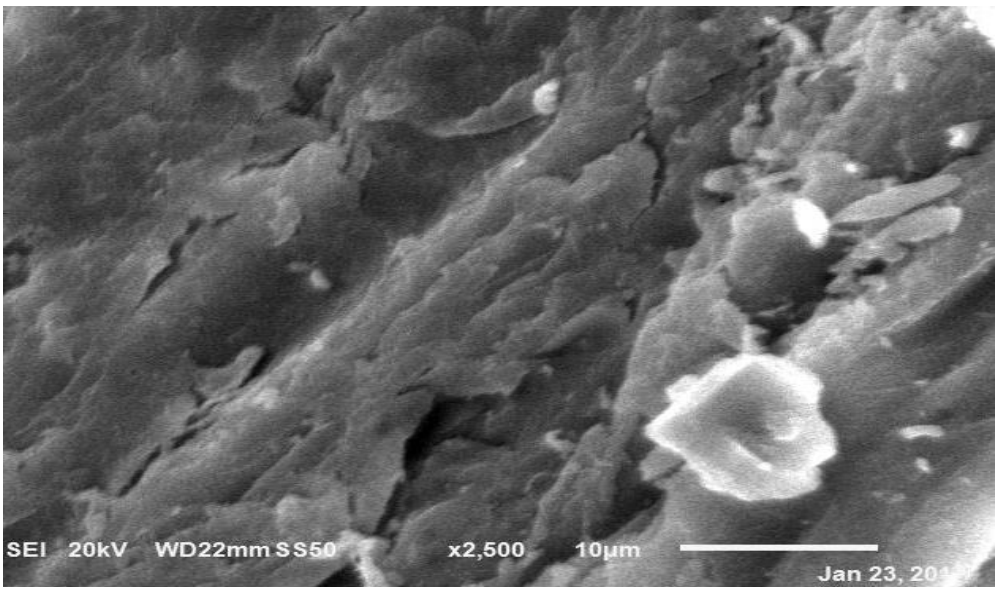

Figure 2: Surface morphology of treated loofa (4% NaOH)

Treatment with acids and alkali has been widely used to enhance the sorption properties of biomaterials. Alkali treatment has been used to enhance the properties of the *L. cylindrica* surface (32). The maximum percentage of NaOH to treat *L. cylindrica*, without damage to the crystalline region is reported to be 8% (42). Modification of *L. cylindrica* with 4% NaOH bestows additional functionality of OH^- groups added onto the surface area of *L. cylindrica* (33, 34). The higher the pKa (deprotonation constant) the greater the adsorption preference on the *ATLC* surface (35).

The surface characteristics of the NaOH treated loofa with a BET surface area of 43.096m^2/g is higher in value than the untreated at 25.322m^2 /g (Table 1). This shows an increased surface area which accounts for the broken up and rougher loofa surface. The increase in surface area and pore volume after alkali treatment by 41.3% and 29.4% respectively shows the involvement of the loofa surface and particle pores in enhancing the adsorption process.

Table 1. BET result values of ATLC and untreated *L. cylindrica*

Data	Untreated	NaOH treated
Surface area	25.322 m^2/g	43.096 m^2/g
Specific surface area	5.748 m^2	6.995 m^2
Total pore volume	0.012 cm^3/g	0.017 cm^3/g

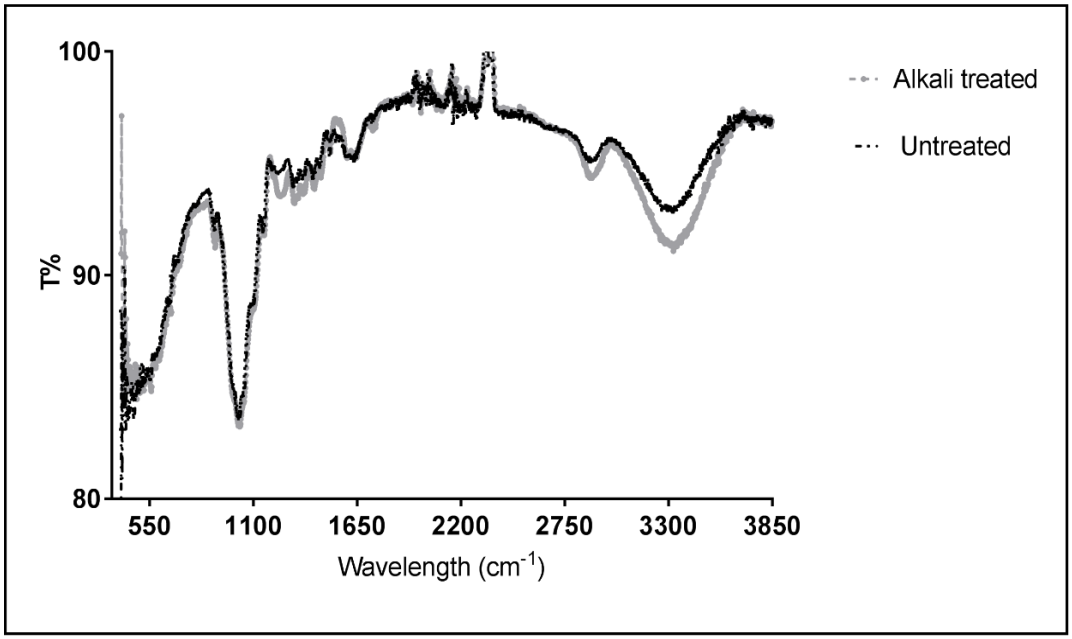

Figure 3: FT-IR spectra of *ATLC* and untreated loofa at 21°C, 256 scans

The change in the adsorption bands between untreated and treated loofa are shown in Figure 3 & 4. These indicate characteristic functional groups on the adsorbent and a change in the bands, across the range 800cm^{-1} to 4000cm^{-1}, and also a change in the surface chemistry of the *ATLC* following alkali treatment was observed at various points. The peak at 3340 cm^{-1} is attributed to the stretching vibration of the O-H group. A shift to 3323cm^{-1} and also to 1040cm^{-1}, including a decrease in peak intensity was observed, indicating a change in the binding energy pattern (21, 33, 36, 37). The band stretching at 1035cm^{-1} and 1250cm^{-1} are attributed to the cellulose and the characteristic bands at 1450cm^{-1} to 1600cm^{-1} indicate lignin. An alteration of the peak at 1735cm^{-1} and 1550cm^{-1} are attributed to the disappearance of the hemicellulose and lignin contents (29,(38). The majority characteristic adsorption bands are changed as shown in Table 2 which shows the effect of NaOH treatment focus on the various functional groups. The presence of a higher and stronger band at 3100cm^{-1} to 3600cm^{-1} may be as a result of the presence of exchangeable protons contained in the hydroxyl group which leaves room for adsorption to occur via ion exchange (39, 40). This stronger band exposes the hydroxyl groups for adsorption (36, 41). The broad band in the range 3545-3050cm^{-1} indicates strong intramolecular hydrogen bonds that gives rise to strong adsorption (42, 43).

Table 2: Change in transmission FTIR results at specific regions of absorbance.

Region	ΔT%	Corresponding absorbance	Reference
1265cm^{-1}-1460cm^{-1} (fingerprint region)	+0.6 - +1.1	O-H bending	(44, 45)
1540cm^{-1}	-0.85	N-H bending	(46)
1735cm^{-1}	+0.6	C=O stretching (carbonyl group of ketone)	(44)
2890cm^{-1}	+0.8	C-H stretching	(21, 47)
3340cm^{-1}	+1.6	O-H bonding	(21, 36, 44)

On the other hand, NaOH treatment disrupts the hydrogen bonding of OH^- functional groups thereby ripping off H^+ for adsorption to occur (34, 48). Carboxyl group are the dominant functional groups of *ATLC* in adsorption. Therefore, the difference in the binding energy of the functional groups as shown by the spectra peaks indicates the importance of the role of O-H in

the absorption of Pb^{2+} ions onto *ATLC* (49). The characteristic bands that indicate the functional groups on the loofa surface show the structure of the loofa to possess lignin, cellulose and hemicellulose.

Figure 4 shows an increase in the zeta potential values and an increase towards linearity when the loofa is treated with alkali. This change is explained by the change in the loofa structure after modification (50). The untreated cucumber peel, a biosorbent material that contain cellulose, hemicellulose and lignin, which possess carboxyl and hydroxyl groups, also show a negatively charged surface that increases in zeta potential as the pH is increased (pH 2-6) (51). Lower pH tends to cause the colloids in the system to coagulate and form more visible particles in solution. Therefore, the surface charge is expected to be lower at a lower zeta potential than at a higher zeta potential which occurs at a higher pH. The zeta potentials of *ATLC* over the pH range of 2 – 10 shows a negative surface charge on the loofa (52)**.** The increase in the magnitude of the negative zeta potential of *ATLC* shows the availability of free functional groups available for binding, which is responsible for the generated charge on the loofa surface (53). The zeta potential increases as pH increases, which suggest a potential stability for lead adsorption as pH increases. Since formation of hydroxylated lead ions are expected over pH 6 (shown in figure 7), pH 5 – 6 (optimum mV values) is determined as the appropriate pH for an effective adsorption process (54).

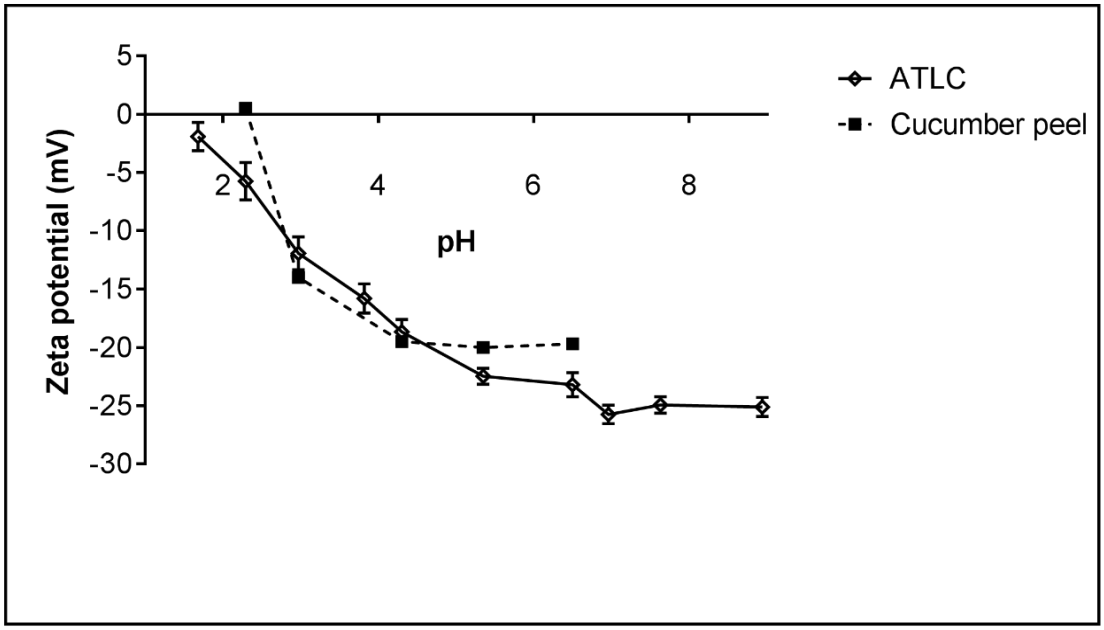

Figure 4: The zeta potential of *ATLC* and cucumber peel at constant ionic strength in aqueous solution as a function of pH.

As compared to the chitin-lignin material of high carbon content and the grafted loofa sponge, the presence of a negative zeta potential over a pH range of 1-12 is attributed to the presence of specific functional groups, such as -COOH and -OH, on the surface which aid adsorption of metal ions (53, 55)**.** The pH at which a colloid with an acidic functional group changes from uncharged to a negative charge is related to the pK_a of those groups.

3.2 Adsorption studies as a function of acid and anion concentration onto *ATLC*.

The effect of pH on the adsorption of lead onto *ATLC* is shown in Figure 5. It can be seen that the percentage removal has a maximum at pH 5. The effect of increasing ionic strength through the addition of NaCl at a constant pH of 5 is presented in Figure 6. Interestingly the increase of chloride has minimal impact on the uptake of Pb^{2+} onto the *ATLC* surface. Increasing NaCl up to 1 $mol \cdot L^{-1}$ concentration in solution supresses Pb^{2+} uptake by around 10%, with the highest extraction occurring at 0.002 $mol \cdot L^{-1}$ chloride.

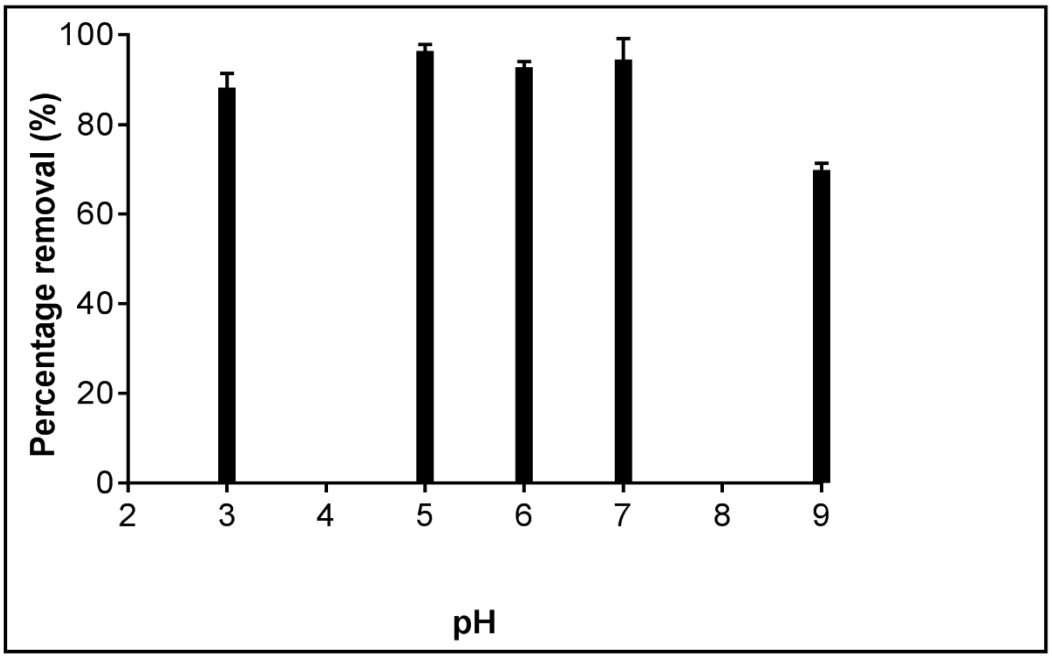

Figure 5: Effect of solution pH conditions on the percentage removal of Pb after 24hrs contact; lead ion concentration: 50mg/L; agitation speed: 200rpm; at temperature 21°C, 5g/l biosorbent dosage.

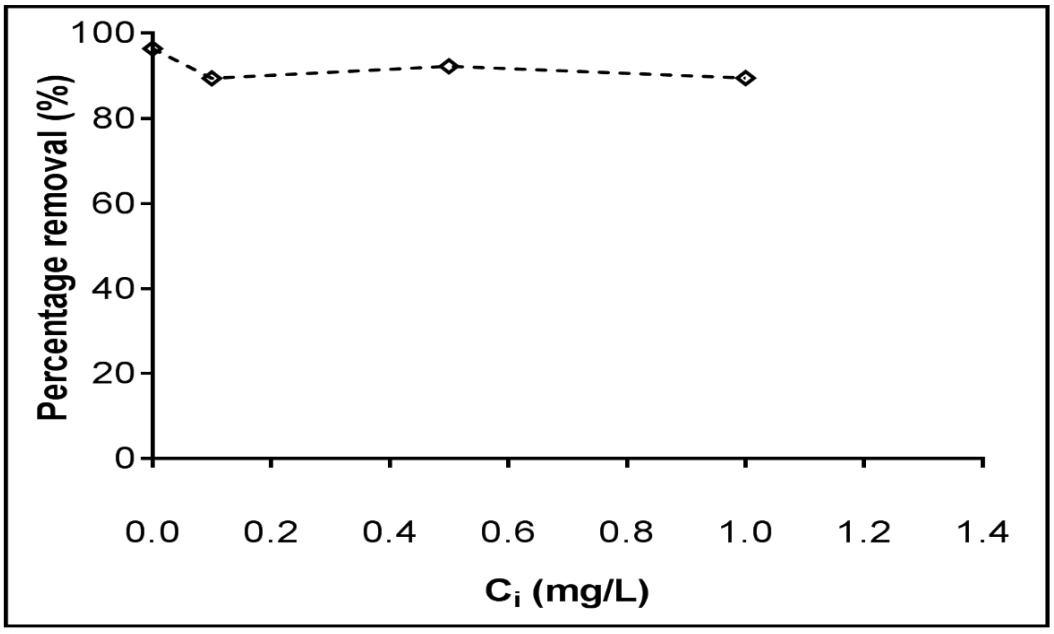

Figure 6: Effect of chloride concentration on the percentage removal of Pb after 24 hrs contact; lead ion concentration: 50mg/L; agitation speed: 200rpm; at temperature 21°C, 5g/l biosorbent dosage

pH is the most important controlling factor in the adsorption process of heavy metal ions (56). At equilibrium pH lower than 5 the lower adsorption was attributed to the competition of H^+ ions for the binding sites on *ATLC* thereby reducing the adsorption capacity. At pHs above 6 the decrease in Pb uptake is most likely due to the hydrolysis of the metal ion in solutions. This shows the difference in lead species and their ability to be adsorbed at different solution pH.

Furthermore, optimum adsorption of lead ions occurs below the point of zero charge (pH_{pzc} of 7.2). The ionic charge is positive at a lower pH and negative at a higher pH, the electrostatic attraction is opposite as the maximum uptake occurs between pH 5 – 6. Therefore, the adsorption process is dominated by ionic exchange of the ions present and other adsorption mechanisms (57). The optimum pH for adsorption of lead ions onto tree sawdust, coconut coir and palm empty fruit bunch was similarly found to be at pH 5-6 and decreases above pH 6 (13, 58-60). As shown in Figure 5, the lead species present at pH 5 gives 96.4% of the lead available for uptake. The potential effect of the metal ion speciation as a function of pH is presented in Figure 7 and carried out using Hyss2009 program and stability constants from the NIST database. The protonated complexes $Pb(OH)_2$, $PbOH^+$ and $Pb_3(OH)_4^{2+}$ occur in alkaline media and achieve a maximum of between 40% and 50% of hydroxylated Pb as it relates to free Pb ions. The attachment of lead ions onto the surface of loofa was highest at a pH of 5 and this indicates that the speciation of lead ions attaching are free lead ions. Furthermore, the adsorption of lead ions at over pH 7 indicates hydroxylation of the lead ions and therefore a reduction in the adsorption capacity of free lead ions to be adsorbed on the surface. The presence of free lead ions decreases as the pH increases (7, 13, 52, 54 -56). The values for the model are averages taken from low ionic strength concentrations (ClO_4^-, NO_3^- and Cl^-) from the literature.

The effect of ionic strength (Figure 6) is a dual effect of Na^+ and Cl^- ions. The tendency of Cl^- ions to form complexes with Pb^{2+} , thus decreasing the concentration of Pb^{2+} ions in solution by forming $PbCl_2$, allows for Na^+ ions to compete with remaining Pb^{2+} ions in solution for the active sites (62). Na^+ can also occupy the active sites on *LC* limiting the binding capacity for Pb^{2+} ions (27, 56). The binding of lead ions by *ATLC* is through both electrostatics and covalent inner and outer sphere complexes (63). The little effect of NaCl on the Pb^{2+} ion adsorption is indicative of an inner sphere, potentially chelating, sorption mechanism (13, 28, 49). Since, the adsorption mechanisms from the results show more than one mechanism process, the chelating adsorption indicates a fraction of the entire adsorption mechanism process is affected in the presence of ionic strength.

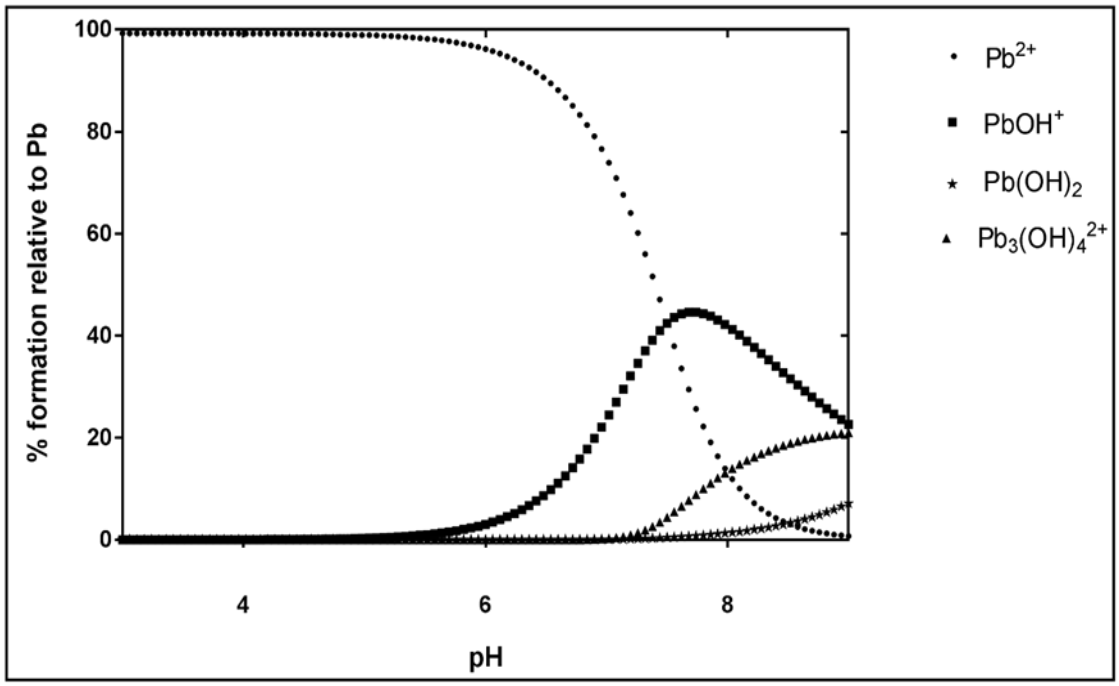

Figure 7: Distribution of lead (II) species in aqueous solution as a function of pH.

3.3 Isotherm behaviour of removal

The isotherm fitting parameters for all the isotherm models tested is given in Table 3 based on linear regression and non-linear regression using GraphPad (22, 65). The isotherms are used to determine the best fit in order to explain and suggest the model that best predicts the biosorption that occurs (64).

Table 3: Isotherm fitting parameter calculated using various models for lead adsorption onto *ATLC* at 21 °C and 24 hr contact time, using non-linear least squares fitting using GraphPad and SOLVER.

Langmuir		Sips	
Constant	Value	Constant	Value
K_L	0.16 ± 0.1	Ks	1.0E-01
R_L	0.09 ± 0.01	q_m	5.9 ± 0.1
q_m (mg·g^{-1})	24.9 ± 0.2	a_S	1.9 ± 0.2
R^2	0.861	R^2	0.983
Dubinin-Radushkevich		Two site Langmuir	
Constant	Value	Constant	Value
B_D (x10^{-9})	2.1 ± 0.1	K_L	0.003,1.740±0.02
q_D (mg·g^{-1})	9.6E-04	q_m (mol·g^{-1})	85.8, 12 ± 0.01
E_D (kJ·mol^{-1})	12.9 ± 0.2	R^2	0.984, 0.975
R^2	0.922		

The relationship between the equilibrium concentration and adsorption capacity is depicted in Figure 8. It shows a gradual increase in uptake capacity to a point where there is no significant change. This is a monolayer adsorption behavioural pattern. The adsorption behaviour of lead ions fitted both Langmuir, D-R and two site Langmuir models but the Sips model was shown (Figure 8) to give the best fit with a R^2 value of 0.983 (66).

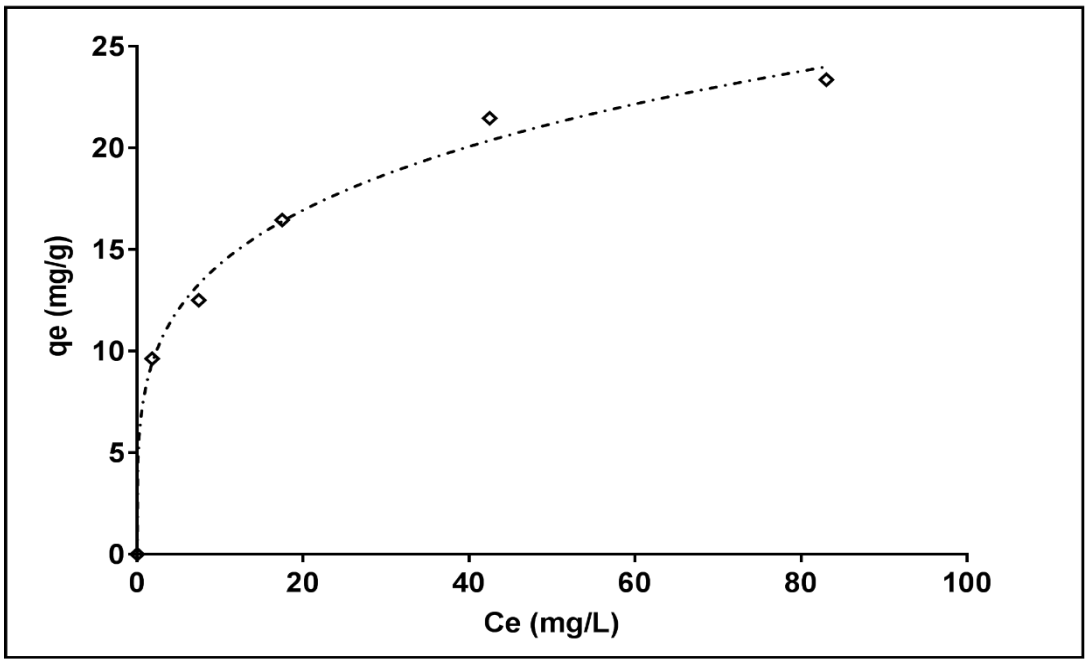

Figure 8: Lead isotherm from pH 5.0 ± 0.1 at 21 °C and 24 hr. contact time. Sips model fit shown by dashed line.

The model fittings to Sips and two site Langmuir show a heterogeneous surface which possesses both weak and strong sites. The Langmuir maximum loading capacity was 24.9 mg/g having a K_L

value of 0.160L/mg. As compared to results obtained by Li *et al*. (2008) which describes a Langmuir model fit, the q_{max} was lower but with a lower K_L value and according to Madala *et al*. (2013), q_{max} and Langmuir constant increased as temperature increased. The K_L values relate to a higher binding energy of adsorption which leads to higher adsorption capacity (67),50).The lead ion biosorption behaviour of *L. cylindrica* was termed a favourable adsorption. The value of 1/n at 0.245 measures the surface heterogeneity which becomes more heterogeneous with a value closer to 1 (26). Since the E value (15.6 kJ/mol) is in the range of 8-16kJ/moles, it shows an ion exchange chemisorption process (68, 69). However, this is taken at a lower compatibility compared to Sips model**.** The activation energy which indicates a chemisorption mechanism with the involvement of both the surface and pores of the loofa in the adsorption process is attributed to the presence of two different kinds of sites available for adsorption. The ion exchange capacity was calculated to be at 47%, where it accounts for every 0.0081meq of H^+ (2 moles), present on the loofa surface, 0.04959 meq of Pb^{2+} was absorbed. It further explains and supports the different mechanisms of the adsorption process that occur with the utilisation of loofa. However, the maximum loading capacity exceeds that of the ion exchange capacity which indicates the remaining adsorption mechanism to be a surface mechanism process.

Modification of the loofa with 4% NaOH improved the adsorption capacity of lead by 9.8%. Compared to other adsorbents, such as *Luffa* charcoal, *Phanerochaete chrysosporium*, *Portulaca plant* and *Pongamia pinnata*, modified loofa (*ATLC*) shows a higher percentage removal of lead over a short period of time at room temperature.

Table 4: Maximum uptake capacity (Langmuir isotherm) of lead ions by other biosorbents between pH 5-6.

Adsorbent	pH	q_{max} (mg/g)	Temp (^oC)	Percentage removal (%)	Reference
Phanerochaete chrysosporium		12.34	27	25	(44, 45)
Pinus slyvestris		22.22	21	98	Taty-Costodes *et al*., 2003
Low cost materials		4.50 – 7.56	25	99	Mishra and Patel, 2009
Portulaca plant		17.24	21	78	(7)
Pongamia pinnata		34.36	30	80	(60)
Luffa acutangula		47.39	30	98	(21, 47)
Luffa charcoal		51.02	25	80	(6)
ATLC (Luffa cylindrica)		24.90	21	96	This study

3.4 Kinetics of extraction

The modelling of batch kinetics is important in explaining the mechanism of adsorption and to determine the potential controlling steps in mass transport. The Boyd kinetic model expression, shown in figure 9, determines the mechanism of adsorption kinetics, was utilized in differentiating between film and intra-particle diffusion (70, 71).The better fit of the adsorption kinetics to the Boyd model emphasizes that film diffusion and not intra-particle diffusion dominates the adsorption of lead. The results (figure 9) show a linear relationship with a correlation coefficient of 0.959 at 50mg/L. As the concentration increases the correlation coefficient decreases. This shows that the further away the values are from linearity, the higher the pore diffusion coefficient, which gives an indication that the rate controlling step is not governed by pore diffusion. This can be explained as being film diffusion at lower

concentrations. Therefore, the initial stages have film diffusion as the rate-controlling step and particle diffusion as the diffusion path increases (72).

The results fit the pseudo-second order (PSO) better than the pseudo first order model (Figure 10) indicating the involvement of two species in the sorption process of metal ions. As agreed with the literature, a pseudo second order model best describes the adsorption of divalent metal ions (36). The rate constant of a pseudo second order model (k_2) increases as the concentration is increased till it reaches a peak. This shows that the uptake rate is decreased and resistance in the micropores is increased, till equilibrium is reached (73). This may be attributed to a change in the ratio of binding interactions. The maximum adsorption capacity values of the experiments were very close in value to the model qe values as shown in table 5. Also, the fastest exchange rate, shown to occur in less than 20mins in Figure 10, may mean that exchange positions are initially on the surface**.** The increase in initial concentration results in a decrease in k_2 (K_2) and then an increase in value had been reached, a further decrease in K_2 was seen as concentration further increased. This implies that other experimental factors, not solely diffusion, play an important role in the kinetic process of adsorption. Also, this further explains the relationship between the number of available binding sites and the rate of adsorption since availability of sites is related to the initial concentration of metal ions and the time at which equilibrium adsorption capacity is reached (74).

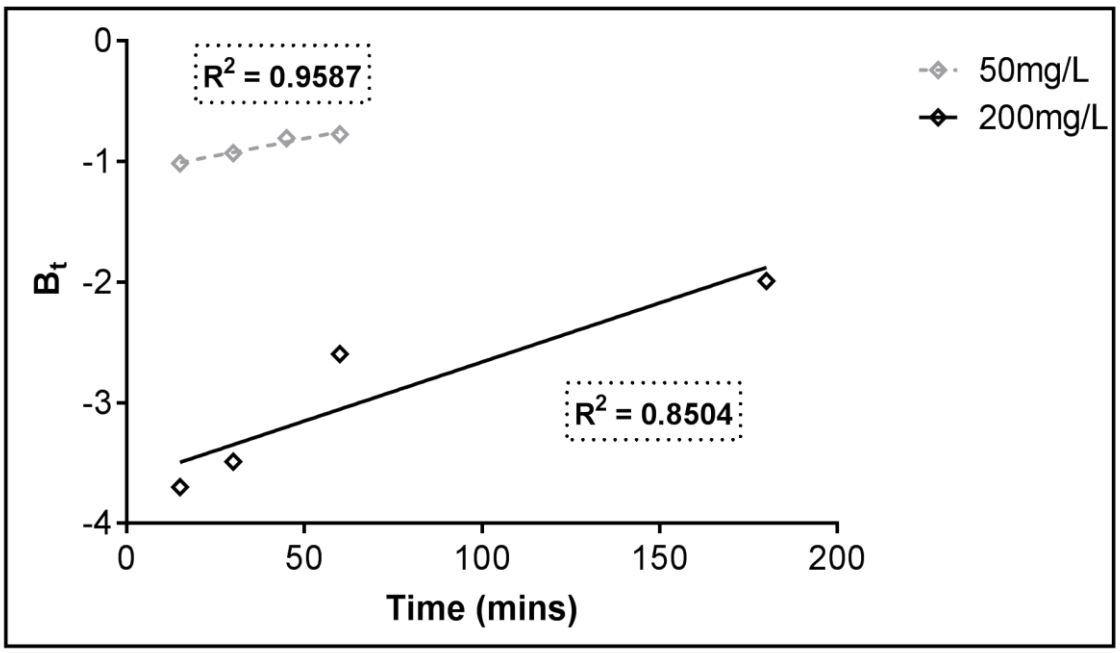

Figure 9: Lead isotherm from pH 5.0 ± 0.1 at 21 °C and 24 hr. contact time. Boyd model fit shown by line.

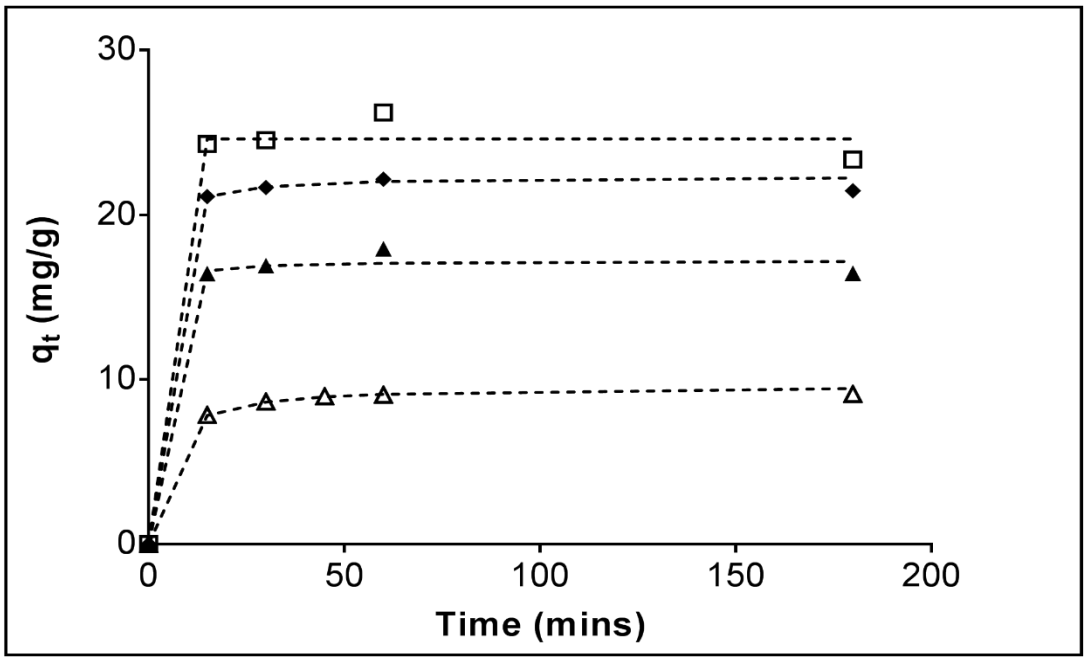

Figure 10: Pseudo second order kinetic using non-linear regression in SOLVER (65), Δ=50mg/L, ▲=100mg/L, ◆=150mg/L, □=200mg/L Pb^{2+} in solution at pH 5.0 ± 0.1 at 21 °C. PSO model shown with dashed line.

Model efficiency, which equates to the correlation coefficient R^2 value, is a good measure to avoid errors that occur as a result of experimental values and is the best indicator for model fitting data values. The non-linear chi square test values also confirm the best fit of the model to the experiment data of the adsorption system (64, 75). More accurate estimations are implied with smaller NSD values (76).

PSO k_2 values of 50mg/L is higher than that of 200mg/L, this shows that the sorption rate of lead ions reached a maximum value at 50mg/L, and then reduces. This indicates that the film diffusion controlling step in the mass transport process is not predominantly represented by an increase in concentration due to the involvement of other controlling mechanisms such as intra-particle diffusion, adsorbent-adsorbate interactions in solution etc. (77). This means at higher concentration the adsorption process is not governed by film diffusion.

Table 5: Kinetic parameters of pseudo second order (Linear regression) at pH 5.7 at 21 °C

Concentration (mg/L)	q_e (mg·g^{-1})	h_0 (mins)	k_2 (g·mg^{-1}·min^{-1})
50	9.630	3.88E-03	0.062
100	16.458	0.86E-03	0.031
150	21.458	0.10E-03	0.040
200	23.359	0.26E-03	0.016

Saueprasearsit *et al*. (2010) reported the use of untreated loofa for the adsorption of lead ions to be at 82.7% at a temperature of 40°C. The Langmuir model was not a good fit but it showed that the loofa surface is heterogeneous in nature by model fitting to the Freundlich model. Also, the adsorption capacity was recorded at 4.63mg/g (34). Compared to the 4% NaOH treated loofa used for this study, the percentage removal was higher (81.4% increase) and at a lower temperature which is preferable for a sustainable adsorption design process.

Table 6: Comparison of pseudo second order values obtained from lead ion (10-50mg/L) adsorption with other adsorbents.

Adsorbent	q_e (mg·g^{-1})	k_2 (g·mg^{-1}·min^{-1})	Reference
Pongamia pinnata	n/a	1.31E03	(60)
Palm kernel fiber	47.60	0.086	(45)
Portulaca plant	20.41	0.005	(7)
ATLC (Luffa cylindrica)	9.63	0.062	This study

5 Conclusions

The above results show that *L. cylindrica* is a good potential biosorbent for the removal of lead ions from aqueous solutions. Alkali treatment of *L. cylindrica* enhances the adsorption mechanism by producing additional free hydroxyl groups. The negative zeta potential shows a negatively charged loofa surface. The data show the feasibility of the modified *L. cylindrica* in the removal of lead ion from aqueous solution and also in the presence of NaCl. The change in frequency occurring due to vibrations at prominent peaks on the *L. cylindrica*, indicates the functional groups on the *L. cylindrica* that are involved in the adsorption process. The efficiency of Pb (II) uptake depicts a significant dependence on pH, metal ion concentration, temperature and ionic strength. The optimum pH of the adsorption of lead ions by *L. cylindrica* at room temperature (21^{o}C) was at pH 5-6 at equilibrium. The Sips isotherm model predicted the adsorption process better than the other models. The removal uptake of Pb (II) ions is hindered by the presence of high levels of NaCl in aqueous solution. The kinetics proved the pseudo second order model to be applicable and the adsorption rate was at 0.062g/mg/min at 50mg/L. The sorption processes of the lead ions by loofa were not solely controlled by one mechanism. The thermodynamics showed a feasible exothermic chemisorption reaction.

As compared to other recently used adsorbents in the adsorption of lead, some have been found to have a higher maximum loading capacity than loofa used in this report but because the loofa material is economically viable, requires no expensive modification of its properties, utilises no extensive technological application and can also be obtained in large quantities, it is sustainable on a global scale (78, 79).

Loofa is usually cultivated to make items such as cooking pots, bath sponges, in industrial filters and in sound insulation, it is easily grown in large quantities. The adoption of the design adsorption process with loofa will create revenue and jobs in Nigeria and also help to curb the environmental issues in the Niger Delta and other parts of the country (16, 80).

Conflict of interest

The authors declare no conflict of financial interests.

6 Acknowledgements

The authors would like to thank the Nigerian government for scholarship funding (Niger Delta Development Commission (NDDC)/DEHSS award). All ICP-MS analysis was carried out by Kroto Research Institute, Groundwater Protection and Restoration Group, The University of Sheffield. Thanks to Andrew Fairburn and Gabriella Kakonyi. All FT-IR analysis was carried out at Kroto Research Institute, The University of Sheffield. Thanks to Dr. Mark Ogden, Dr. Esther Karunakaran, Dr. Joe Lovett, Joseph Hufton, Mat Pringle and Keith Penny.

7 References

1. Okunola OJ, Uzairu A, Ndukwe GI, Adewusi SG. Assessment of Cd and Zn in roadside surface soild and vegetations along some roads of Kaduna metropolis, Nigeria. Research Journal of Environmental Sciences. 2008.
2. Flora G, Gupta D, Tiwari A. Toxicity of lead: A review with the recent updates. Interdisciplinary Toxicology. 2012;5(2):47-58.
3. Islam E, Liu D, Li T, Yang X, Jin X, Mahmood Q, et al. Effect of Pb toxicity on leaf growth, physiology and ultrastructure in the two ecotypes of Elsholtzia argyi. Journal of Hazardous Materials. 2008 6/15/;154(1–3):914-26.
4. Andra SS, Datta R, Sarkar D, Makris KC, Mullens CP, Sahi SV, et al. Induction of lead-binding phytochelatins in vetiver grass [Vetiveria zizanioides (L.)]. Journal of Environmental Quality. 2009;38(3):868-77.
5. Punamiya P, Datta R, Sarkar D, Barber S, Patel M, Das P. Symbiotic role of Glomus mosseae in phytoextraction of lead in vetiver grass [Chrysopogon zizanioides (L.)]. Journal of Hazardous Materials. 2010 5/15/;177(1–3):465-74.
6. Umpuch C, Bunmanan U, Kueasing U, Kaewsan P. Adsorption of lead from synthetic solution using luffa charcoal. World Academy of Science, Engineering and Technology. 2011;5(09):24.
7. Dubey A, Shiwani S. Adsorption of lead using a new green material obtained from *Portulaca* plant. International Journal of Environental Science and Technology. 2012;9:15-20.
8. Ayenimo JG, Adeeyinwo CE, Amoo IA. Heavy metal pollutants in Warri river, Nigeria. Kragujevac Journal of Science. 2005;27:43-50.
9. Olawale AM. Bioremediation of wastewater from an industrial effluent system in Nigeria using *Pseudomonas aeruginosa*: Effectiveness tested on albino rats. Journal of Petroleum and Environmental Biotechnology. 2014;5(1).
10. Anyakora C, Nwaeze K, Awodele O, Nwadike C, Arbabi M, Coker H. Concentrations of heavy metals in some pharmaceutical effluents in Lagos, Nigeria. Journal of Environmental Chemistry and Ecotoxicology. 2011;3(2):25-31.
11. Pourrut B, Shahid M, Dumat C, Winterton P, Pinelli E. Lead uptake, toxicity, and detoxitication in plants. Reviews of Environmental Contamination and Toxicology. 2011;213:113-36.
12. Adewumi JR, Oguntuase AM. Planning of wastewater reuse programme in Nigeria. The Journal of Sustainable Dvelopment. 2016;15(1):1-33.
13. Sangi MR, Shahmoradi A, Zolgharnein J, Azimi GH, Ghorbandoost M. Removal and recovery of heavy metals from aqueous solution using Ulmus carpinifolia and Fraxinus excelsior tree leaves. Journal of Hazardous Materials. 2008 7/15/;155(3):513-22.
14. Ali I, Asim M, Khan TA. Low cost adsorbents for removal of organic pollutants fromm wastewater. Journal of Environmental Management. 2012;113:170-83.
15. Emene A. Biosorption of certain selected toxic heavy metals and methylene blue by use of anionised Chlorella kesslerii and Phanerocheate chrysosporium loaded Luffa cylindrica. 2015.
16. Ajuru M, Nmom F. A Review on the Economic Uses of Species of Cucurbitaceae and Their Sustainability in Nigeria. American Journal of Plant Biology. 2017;2(1):17-24.
17. Laidani Y, Hanini S, Mortha G, Heninia G. Study of fibrous annual plant, luffa cylindrica for paper application .Part I: Charatcerization of the vegetal. Iran J Chem Chem Eng. 2012;31(4).
18. Chen Q, Shi Q, Gorb SN, Li Z. A multiscale study on the structural and mechanical properties of the *Luffa cylindrica* plant. Journal of Biomechanics. 2014;47(6):1332-9.
19. Iqbal M, Edyvean RGJ. Biosorption of lead, copper and zinc ions on loofa sponge immobilized biomass of *Phanerochaete chrysosporium*. Minerals Engineering 2004;17:217-23.
20. Abdelwahab O, Amin NK. Adsorption of phenol from aqueous solutions by Luffa cylindrica fibers: Kinetics, isotherm and thermodynamic studies. The Egyptian Journal of Aquatic Research. 2013 //;39(4):215-23.

21. Boudechiche N, Mokaddem H, Sadaoui Z, Trari M. Biosorption of cationic dye from aqueous soutions onto lignocellulosic biomass (*Luffa cylindrica*): charcaterisation, equilibrium, kinetic and thermodynamic studies. International Journal of Industrial Chemistry. 2016;7(2):167-80.
22. Benhima H, Chiban M, Sinan F, Seta P, Persin M. Removal of lead and cadmium ions from aqueous solution by adsorption onto micro-particles of dry plants. Colloids and Surfaces B: Biointerfaces. 2008 1/15/;61(1):10-6.
23. Akhtar N, Iqbal J, Iqbal M. Microalgal-luffa sponge immobilized disc: a new efficient biosorbent for the removal of Ni(II) from aqueous solution. Letters in Applied Microbiology. 2003;37:149-53.
24. Chen X. Modeling of Experimental Adsorption Isotherm Data. Information. 2015 (6):14-22.
25. Ozkaya B. Adsorption and desorption of phenol on activated carbon and a comparison of isotherm models. Journa of Hazardous materials. 2006;129(1-3):158-63.
26. Foo KY, Hameed BH. Insights into the modeling of adsorption isotherm systems. Chemical Engineering Journal. 2010 1/1/;156(1):2-10.
27. Arshadi M, Amiri MJ, Mousavi S. Kinetic, equilibrium and thermodynamic investigations of Ni(II), Cd(II), Cu(II) and Co(II) adsorption on barley straw ash. Water Resources and Industry. 2014 8//;6:1-17.
28. Yang B, Zuo J, Tang X, Liu F, Yu X, Tang X, et al. Effective ultrasound electrochemical degradation of methylene blue wastewater using a nanocoated electrode. Ultrasonics Sonochemistry. 2014 7//;21(4):1310-7.
29. Harland CE. Ion Exchange: Theory and Practice. 1994:100-30.
30. Yukselen Y, Kaya A. Zeta Potential of Kaolinite in the Presences of Alkali, Alkaline Earth and Hydrolyzable Metal ions. Water Air and Soil Pollution. 2003.
31. Kim J, Lawler DF. Chractersitics of Zeta Potential Distribution in Silica Particles. Bulletin of Korean Chemical Society. 2005;26(7).
32. Ghali L, Msahli S, Zidi M, Sakli F. Effect of pre-treatment of Luffa fibres on the structural properties. Materials Letters. 2009 1/15/;63(1):61-3.
33. Saueprasearsit P, Nuanjaraen M, Chinlapa M. Biosorption of Lead (Pb^{2+}) by Luffa cylindrica Fiber Environmental Research Journal. 2010;4(1):157-66.
34. Tang W-W, Zeng G-M, Gong J-L, Lang J, Xu P, Zhang C, et al. Impact of humic/fulvic acid on the removal of heavy metals from aqueous solutions using nanomaterials; A review. Science of the Total Environment. 2014;468-469:1014-27.
35. Ngwenya B, Tourney J, Magennis M, Kapetas L, Olive V. A surface complexation framework for predicting water purification through metal biosorption. Desalination. 2009;248(1-3):344-51.
36. Vilar VJP, Botelho CMS, Pinheiro JPS, Domingos RF, Boaventura RAR. Copper removal by algal biomass: Biosorbents characterization and equilibrium modelling. Journal of Hazardous Materials. 2009 4/30/;163(2–3):1113-22.
37. Lasheen MR, Ammar NS, Ibrahim HS. Adsorption/desorption of Cd(II), Cu(II) and Pb(II) using chemically modified orange peel: Equilibrium and kinetic studies. Solid State Sciences. 2012 2//;14(2):202-10.
38. Rodriguez Correa C, Otto T, Kruse A. Influence of the biomass components on the pore formation of activated carbon. Biomass and Bioenergy. 2017 2017/02/01/;97(Supplement C):53-64.
39. White J. Infrared studies of the hydroxyl groups in intercalated kaolinite complexes.
40. Hassan M. Quaternization and anion exchange capacity of sponge gourd (*Luffa cylindrica*). Applied Polymer. 2006;101(4):2495-503.
41. Bai RS, Abraham TE. Studies on enhancement of Cr(VI) biosorption by chemically modified biomass of Rhizopus nigricans. Water Research. 2002;36(5):1224-36.
42. Dudley, Williams FI. Spectroscopic methods in organic chemistry. 2008.
43. Whittaker D. Interpreting organic spectra Royal Society of Chemistry. 2000.

44. Jayamani E, Hamdan S, Heng SK, Rahman MR, Bakri MK, Kakar A. The Effect of Natural Fibres Mercerization on Natural Fibres/Polypropylene Composites: A Study of Thermal Stability, Morphology and Infrared Spectrum. Australian Journal of Basic and Applied Sciences. 2014 (1991-8178).
45. Shaikh T, Agrawal SA. Qualitative and Quantitative Characterization of Textile Material by Fourier Transform Infra-Red. International Journal of Innovative Research in Science, Engineering and Technology. 2014;3(1).
46. Anastopoulos I, Massas I, Ehaliotis C. Composting improves biosorption of $Pb^{2+}$and Ni^{2+} by renewable lignocellulosic materials. Characteristics and mechanisms involved. Chemical Engineering Journal. 2013;231:245-54.
47. Nong G, Zhou Z, Wang S. Generation of Hydrogen, Lignin and Sodium Hydroxide from Pulping Black Liquor by Electrolysis. 2015.
48. Saw SK, Purwar R, Nandy S, Ghose J, Sarkhel G. Fabrication, characterisation ad evaluation of *Luffa cylindrica* fiber reinforced epoxy composites. Bioresources. 2013;8(4).
49. OuYang X, Yang L, Wen Z. Adsorption of Pb(II) from solution using peanut shell as biosorbent in the presence of amino acid and sodium chloride Bioresources. 2014;9(2).
50. Stana-Kleinschek K, Ribitsch V, Kreze T, Lidija F. Determination of the adsorption character of cellulose fibres using surface tension and surface charge. Materials Research Innovations. 2002;6(1):13-8.
51. Basu M, Guha AK, Ray L. Adsorption of Lead on Cucumber Peel. Journal of Cleaner Production. 2017 2017/05/10/;151(Supplement C):603-15.
52. Wu S, Zhao X, Li Y, Du Q, Sun J, Wang Y, et al. Adsorption Properties of Doxorubicin Hydrochloride onto Graphene Oxide: Equilibrium, Kinetic and Thermodynamic Studies. Materials. 2013;6(5):2026-42.
53. Zdarta J, Klapiszewski L, Wysokowski M, Malgorzata N, Kolodzeiejczak-Radzimska A, Moszyinski D, et al. Chitin-Lignin Material as a Novel Matrix for Enzyme Immobilization. Marine drugs. 2015;13(4):2424-46.
54. Adewuyi A, Pereira FV. Isolation and surface modification of cellulose from underutilized Luffa cylindrica sponge: A potential feed stock for local polymer industry in Africa. Journal of the Association of Arab Universities for Basic and Applied Sciences. 2017 2017/10/01/;24(Supplement C):39-45.
55. Liu C, Yan C, Zhou S, Ge W. Fabrication of sponge biomass adsorbent through UV-induced surface-initiated polymerization for the adsorption of Ce(II) from wastewater. Water Science & Technology 2017.
56. Saeed A, Iqbal M, Zafar SI. Immobilization of Trichoderma viride for enhanced methylene blue biosorption: Batch and column studies. Journal of Hazardous Materials. 2009 8/30/;168(1):406-15.
57. Iqbal M, Saeed A, Zafar SI. FTIR spectrophotometry, kinetics and adsorption isotherms modeling, ion exchange, and EDX analysis for understanding the mechanism of Cd2+ and Pb2+ removal by mango peel waste. Journal of Hazardous Materials. 2009 5/15/;164(1):161-71.
58. Feng N, Guo X, Liang S, Zhu Y, Liu J. Biosorption of heavy metals from aqueous solutions by chemically modified orange peel. Journal of Hazardous Materials. 2011 1/15/;185(1):49-54.
59. Ahmad R, Haseeb S. Kinetic, isotherm and thermodynamic studies for the removal of lead ion by a novel adsorbent Luffa acutangula (LAPR). Desalination and Water Treatment. 2015.
60. Yusoff SNM, Kamari A, Putra WP, Ishak CF, Mohamed A, Hashim N, et al. Removal of Cu(II), Pb(II0 and Zn(II) ions from aqueous solutions using selected agricultural wastes: Adsorption and characterisation studies. Journal of Environmental Protection. 2014;5:289-300.
61. Smith RM, Martell AE. NIST Critically Slected Stability Constants of Metal Complexes Database. NIST Standard Reference Database 46. 2004;Version 8.0.
62. Volesky B. Sorption and biosorption. 2003.
63. Holmberg JP. Competitive adsorption and displacement behaviour of heavy metals on peat. 2006.

64. Oboh I, Aluyor E, Audu T. Biosorption of heavy metal ions from aqueous solutions using a biomaterial. Leonardo Journal of Sciences. 2009 (14):58-65.
65. Hossain MA, Ngo HH, Guo W. Introductory of Microsoft Excel SOLVER Function - Spreadsheet Method for Isotherm and Kinetics Modelling of Metals Biosorption in Water and Wastewater. Journal of Water Sustainability. 2013;3(4):223- 37.
66. Dada AO, Olalekan AP, Olatunya AM, Dada O. Langmuir, Freundlich, Temkin and Dubini-Radushkevich isotherms studies of equilibrium sorption of Zn2+ unto phosphoric acid modified rice husk. Journal of Applied Chemistry. 2012;3(1):38-45.
67. Li X-m, Liao D-x, Xu X-q, Yang Q, Zeng G-m, Zheng W, et al. Kinetic studies for the biosorption of lead and copper ions by Penicillium simplicissimum immobilized within loofa sponge. Journal of Hazardous Materials. 2008 11/30/;159(2–3):610-5.
68. Mamatha M, Aravinda HB, Manjappa S, Puttaiah ET. Kinetics and mechanism for adsorption of lead in aqueous and industrial effluent from Pongamia pinnata tree bark. Journal of Environmental Science. 2012;2(2):1-9.
69. Chowdbury S, Saha PD. Biosorption of methylene blue from aqueous solutions by waste biomaterial: hen feathers. Applied Water Science. 2012;2(3):209-19.
70. Banerjee S, Chattopadhyaya MC. Adsorption characteristics for the removal of a toxic dye, tartrazine from aqueous solutions by a low cost agricultural by-product. Arabian Journal of Chemistry. (0).
71. Madala S, Nadavala SK, Vudagandla S, Boddu VM, Abburi K. Equilibrium, kinetics and thermodynamics of Cadmium (II) biosorption on to composite chitosan biosorbent. Arabian Journal of Chemistry.
72. Suresh S, Sundaramoorthy S. Green Chemical Engineering: An introduction to Catalysis, Kinetics and Chemical Processes. 2014.
73. Yu J, Wang L, Chi R, Zhang Y, Xu Z, Guo J. Removal of cationic dyes: basic magneta and methylene blue from aqueous solution by adsorption on modified loofah. *Research on Chemical Intermediates*. 2013;39(8).
74. Plazinski W, Rudzinski W, Plazinska A. Theoretical models of sorption kinetics including a surface reaction mechanism: A review. Advances in Colloid and Interface Science. 2009 11/30/;152(1–2):2-13.
75. Ho Y-S, Ofomaja AE. Pseudo-second-order model for lead ion sorption from aqueous solutions onto palm kernel fiber. Journal of Hazardous Materials. 2006 2/28/;129(1–3):137-42.
76. Gholizadeh A, Kermani M, Gholami M, Farzadkia M. Kinetic and isotherm studies of adsorption and biosorption process in the removal of phenolic compounds from aqueous solutions : comparative study. Journal of Environmenttal Health Science and Engineering. 2013;11(29).
77. Kumar A, Jena HM. Removal of methylene blue and phenol onto prepared activated carbon from Fox nutshell by chemical actiavtion in batch and fixed -bed column. Journal of Cleaner Production. 2016;137:1246-59.
78. Barakat MA. New trends in removing heavy metals from industrial wastewater. Arabian Journal of Chemistry. 2011;4:361-77.
79. Tsibranka I, Hristova E. Comparison of different kinetic models for adsorption of heavy metals onton activated carbon from apricot stones. Bulgarian Chemical Communications. 2011;43(3):370-7.
80. Agbabiaka LA, Okorie KC, Ezeafulukwe CF. Plantain peels as dietary supplement in pratical diest for African catfish (Clarias gariepinus burchell 1822) fingerlings. Agricultural and Biology Journal of North America. 2013.